

Dissertation zur Erlangung des Doktorgrades
der Fakultät für Chemie und Pharmazie der
Ludwig-Maximilians-Universität München



**Tailor-Made Highly Nucleophilic Pyridines
for Organocatalysis**

von

Raman Tandon

aus

München

2013

Erklärung

Diese Dissertation wurde im Sinne von § 7 der Promotionsordnung vom 28. November 2011 von Herrn Prof. Dr. Hendrik Zipse betreut.

Eidesstattliche Versicherung

Diese Dissertation wurde eigenständig und ohne unerlaubte Hilfe erarbeitet.

München,

.....

Raman Tandon

Dissertation eingereicht am:

1. Gutachter: Prof. Dr. Hendrik Zipse

2. Gutachter: Prof. Dr. Sonja Herres-Pawlis

Mündliche Prüfung am: 24.04.2013

Danksagung

Die Zeit zur Anfertigung dieser Doktorarbeit ermöglichte es mir, mich nicht nur chemisch, sondern auch persönlich enorm weiterzuentwickeln. Das habe ich vor allem meinem Doktorvater Prof. Hendrik Zipse zu verdanken. Neben der Überlassung des interessanten Forschungsgebietes möchte ich ihm vor allem für die nette und freundschaftliche Art, mit der er nicht nur mir, sondern auch all den anderen Doktoranden begegnet, für die große Hilfsbereitschaft in allen Lebenslagen, die weit über die Beantwortung offener Fragen oder ein offenes Ohr hinausgeht, sowie für die sportlichen Arbeitskreisausflüge bedanken. Danke Hendrik für die tolle Zeit.

Frau Prof. Sonja Herres-Pawlis möchte ich herzlich für die Übernahme des Zweitgutachtens und die hilfreiche Unterstützung im Kollaborationsthema „Lactid Polymerisation“ danken.

Des Weiteren möchte ich mich bei Prof. Wolfgang Steglich für sein reges Interesse an meinem Forschungsgebiet während der praktischen Arbeiten dieser Dissertation und der Möglichkeit mein chemisches Wissen mit mehr „Anwendungsbezug“ innerhalb einer durch ihn ermöglichten Kollaboration mit der medizinischen Fakultät anwenden zu dürfen, bedanken.

Ich danke auch allen anderen Mitgliedern des Prüfungsausschusses für ihre Teilnahmebereitschaft. Prof. Herbert Mayr danke ich für die kritische Durchsicht einiger meiner Manuskripte und Prof. Heuschmann für die Hilfestellung bei Nomenklaturproblemen.

Meinen Kollegen, von denen viele auch zu guten Freunden wurden, möchte ich besonders für das tolle Arbeitsklima, deren teilweise grenzenlose Hilfsbereitschaft und die schöne und lustige Zeit danken. Danke Yinghao, Evgeny, Christoph, Johnny, Sven, Valerio, Tobias, Flo A., Flo B., Cong, Vossi, Martin, Julian, Michi, Kanchan, Boris, Sateesh, Ingmar, Yin, Elija, Gökcen, Regina, Flo Geittner, Ulla und meinen Praktikanten: Angi, Chen und Tesi. Pascal Patschinski danke ich für die akkurate Verbesserung meiner Dissertation.

Herr Mayer, Herr Stephenson, Frau Dubler, Herr Spahl und Frau Kosak aus der Analytikabteilung danke ich für die hervorragende und schnelle Bearbeitung abgegebener Proben. Ines dos Santos Vieira danke ich für die Gelpermeationschromatographiemessungen.

Meinen Freunden Michi Heider, Andi Stanzel, Niko Wiegand und Markus Spallek danke ich für Ihre Nachsicht, wenn ich das Öfteren keine Zeit hatte, da entweder ein Experiment länger gedauert hat oder Kinetiken gemessen werden mussten. Es freut mich, dass diese Freundschaften über die Jahre des Studiums und der Dissertation bestehen geblieben und gewachsen sind.

Zuletzt möchte ich mich bei meiner Familie bedanken, die mir letztendlich das Studium und einen erfolgreichen Abschluss erst ermöglichten und mir mit Leibeskräften stets auf jede erdenkliche Weise halfen und immer für mich da waren und sind. Danke Mama, Papa, Kai, Emma, Michi, Martin, Susi, Sebastian, Leni, Evi, Otmar, Rainer, Susanna und natürlich

Danksagung

meinem lieben Sohn Leon, der mir die Zeit immer durch sehr viel Lachen erheitert, und meiner wunderbaren Frau Daniela für ihre immerwährende Unterstützung.

Publikationsverzeichnis

- [1] **Annelated Pyridines as Highly Nucleophilic and Lewis-Basic Catalysts for Acylation Reactions**
R. Tandon, T. Unzner, T. A. Nigst, N. De Rycke, P. Mayer, B. Wendt, O. R. P. David, H. Zipse, *Chem. Eur. J.* **2013**, *19*, 6435 – 6442.
- [2] **Inductive Effects Through Alkyl Groups – How Long is Long Enough?**
R. Tandon, T. A. Nigst, H. Zipse, *Eur. J. Org. Chem.* **2013**, *accepted*.
- [3] **Platelet Inhibition by the Natural LXR Agonist 22(R)-OH-Cholesterol and its Fluorescence Labeling with Full Bioactivity**
S. Schaffer, R. Tandon, H. Zipse, W. Siess, A. Schmidt, W. Steglich, R. Lorenz, *Biochem. Pharmacol.* **2013**, *accepted*.
- [4] **Can Amination Reactions be Catalyzed by Pyridines?**
T. A. Nigst, R. Tandon, H. Zipse, H. Mayr, *manuscript in preparation*.
- [5] **The aza-Morita-Baylis-Hillman Reaction of Electronically and Sterically Deactivated Substrates**
C. Lindner, R. Tandon, Y. Liu, B. Maryasin, H. Zipse, *Org. Biomol. Chem.* **2012**, *10*, 3210 – 3218.
- [6] **Cation Affinity Numbers of Lewis Bases**
C. Lindner, R. Tandon, B. Maryasin, E. Larionov, H. Zipse, *Beilstein J. Org. Chem.* **2012**, *8*, 1406 – 1442.
- [7] **Synthesis, Magnetic Properties and X-ray Structure Analysis of a 1-D Chain Iron(II) Spin Crossover Complex with wide Hysteresis**
B. Weber, R. Tandon, D. Himsl, *Z. Anorg. Allg. Chem.* **2007**, *633*, 1159 – 1162.

Konferenzbeiträge

- 02/2013 Modeling Chemical and Biological (Re)Activity 3, Mohali, Indien, Vortrag, **“Carbo- and Hetero-Annulated Pyridines as Potent Lewis Bases and Nucleophiles”**.
- 02/2013 Modeling Chemical and Biological (Re)Activity 3, Mohali, Indien, Posterpräsentation, **“Highly Nucleophilic Pyridines as Potent Organocatalysts”**.
- 02/2013 Industry Day, München, Posterpräsentation, **“The aza-Morita-Baylis-Hillman Reaction of Electronically and Sterically Deactivated Substrates”**.
- 03/2012 Winterschool (Alexander-von-Humboldt-Linkage Program), München, *„Computational Life Sciences on Open Shell Intermediates“*.
- 10/2011 MolMod, Heidelberg, Posterpräsentation, **“Inductive Effects Through Alkyl Groups – How Long is Long Enough?”**
- 10/ 2009 Modeling Chemical and Biological (Re)Activity 2, Wildbad Kreuth, Organisationsassistentz.

TABLE OF CONTENTS

0. GENERAL COMMENTS AND CONVENTIONS	1
1. INTRODUCTION	4
2. SUMMARY	9
3. ANNELATED PYRIDINES AS HIGHLY NUCLEOPHILIC AND LEWIS-BASIC CATALYSTS FOR ACYLATION REACTIONS	33
3.1. Introduction	34
3.2. Results and Discussion	35
3.3. Conclusion	47
3.4. Experimental Part	48
3.5. References	114
4. CATION AFFINITY NUMBERS OF LEWIS BASES	117
4.1. Introduction	118
4.2. Results and Discussion	118
4.3. Conclusion	129
4.4. Experimental Part	129
4.5. References	143
5. INDUCTIVE EFFECTS THROUGH ALKYL GROUPS – HOW LONG IS LONG ENOUGH?	145
5.1. Introduction	146
5.2. Results	146
5.3. Discussion	157
5.4. Conclusion	160
5.5. Experimental Part	160
5.6. References	194
6. INDUCTIVE EFFECTS IN DMAP–POLYMERS	196
6.1. Introduction	197
6.2. Results and Discussion	197
6.3. Conclusion	201
6.4. Experimental Part	201
6.5. References	209

7. THE AZA-MORITA-BAYLIS-HILLMANN REACTION OF ELECTRONICALLY AND STERICALLY DEACTIVATED SUBSTRATES	210
7.1. Introduction	211
7.2. Results and Discussion	211
7.3. Conclusion	224
7.4. Experimental Part	225
7.5. References	246
8. POLYMERIZATION OF LACTIDES MEDIATED BY DMAP-DERIVATIVES	249
8.1. Introduction	250
8.2. Results and Discussion	252
8.3. Conclusion	259
8.4. Experimental Part	260
8.5. References	263
9. PLATELET INHIBITION BY THE NATURAL LXR AGONIST 22(R)-OH-CHOLESTEROL AND ITS FLUORESCENCE LABELING WITH FULL BIOACTIVITY	266
9.1. Introduction	267
9.2. Results	268
9.3. Discussion	274
9.4. Conclusion	277
9.5. Experimental Part	277
9.6. References	283
10. SYNTHETIC STUDIES TOWARDS DERIVATIVES OF 9-AZAJULOLIDINE	285
10.1. Introduction	286
10.2. Results and Discussion	286
10.3. Conclusion	294
10.4. Experimental Part	294
10.5. References	297

Chapter 0

General Comments and Conventions

As most parts of this thesis have already been published or have been submitted for publication my contributions to multi-author publications are explicitly mentioned at the beginning of every chapter. The contributions from other authors are always omitted in the Experimental Part. In addition to the general Introduction in Chapter 1 individual introductions will be given at the beginning of every chapter. The main parts of this thesis are structured as follows:

- synthesis and structure of catalysts (Chapter 3)
- quantification of catalyst characteristics (Chapters 4 – 5)
- application of highly nucleophilic pyridines as organocatalysts (Chapters 6 – 9)

The synthetic studies towards derivatives of 9-azajulolidine are mentioned in the end (Chapter 10) for completeness of contents. In order to avoid confusion, the used catalysts will be consecutively numbered throughout the chapters as they appear in this thesis, beginning from Chapter 3, and will be assigned with the same number in every chapter. In this way 4-dimethylaminopyridine (DMAP) *e.g.* is in every chapter number **1**, 4-(pyrrolidin-1-yl)pyridine (PPY) number **2**, and so on (compare Figure 0.1).

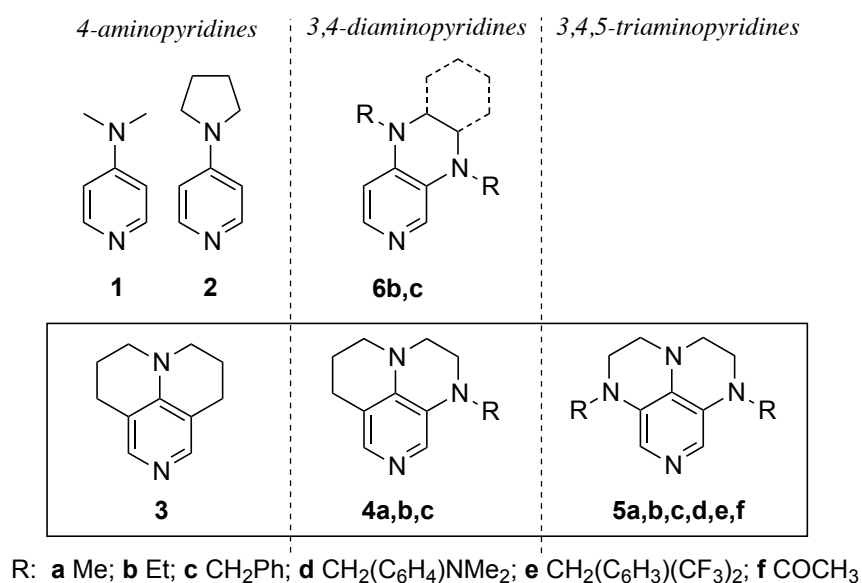
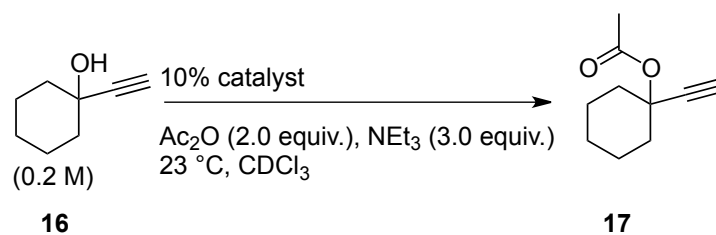


Figure 0.1. Structures of pyridine derivatives based on the DMAP motif used as nucleophilic organocatalysts.

In the same way the numbers for compounds connected to important benchmark reactions are treated. Thus *e.g.* 1-ethynylcyclohexanol appears in Chapter 3 the first time as compound number **16** and is therefore reserved throughout the thesis for this compound (compare Scheme 0.1).



Scheme 0.1. Acylation reaction in CDCl_3 .

The laminated inlay page shows (along with the numbering for the catalysts) the most important kinetic and thermodynamic data for common pyridine-based catalysts and can be used as a reference sheet.

Chapter 1

Introduction

Organocatalysis

Some of the most valuable chemical transformations are often energetically disfavored due to high barriers, which need to be overcome by lowering the activation energy. In nature specialized proteins, so called enzymes, catalyze virtually all chemical reactions within cells.^[1] The use of enzymes is often aspired not only because of their high activity, but also for reasons of ‘green chemistry’. But as these ‘biological catalysts’ are very often sensitive to heat or pH changes they are not always applicable under harsh reaction conditions. At this point organocatalysts can demonstrate their superior characteristics. The definition of an ‘organocatalyst’ was coined by MacMillan which is a “sub-stoichiometric amount of an organic compound which does not contain a metal atom”.^[2] They are usually designed by chemists to be insensitive to oxygen and moisture and easily accessible. The low toxicity and the easy immobilization compared to metal based catalysts make organocatalysts predominant. During the last few years a spectacular increase of interest in organocatalysis is obtained belonging now to the fastest growing areas in organic chemistry.^[3-6] Recently List *et al.* introduced a system for the classification of organocatalysts depending on the mechanism of catalysis.^[3] This system differentiates between Lewis acids/bases and Brønsted acids/bases. Lewis bases like phosphanes,^[7] sulfides^[8] or *e.g.* nitrogen-based catalysts such as pyridines^[7b,9-15] are commonly used and show outstanding catalytic activity. Regarding pyridines the pioneering work of Steglich and Höfle in 1969 paved the way for a new catalyst class that is still subject of current research: 4-dimethylaminopyridine (DMAP, **1**).^[10] DMAP (**1**) is a powerful acylating agent and more nucleophilic variations (**3 – 5**, see Figure 1.1) have recently been developed.^[12-16]

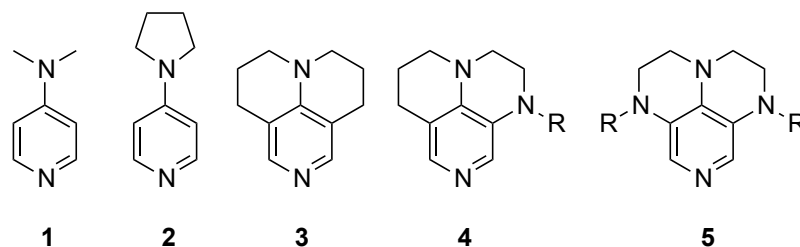
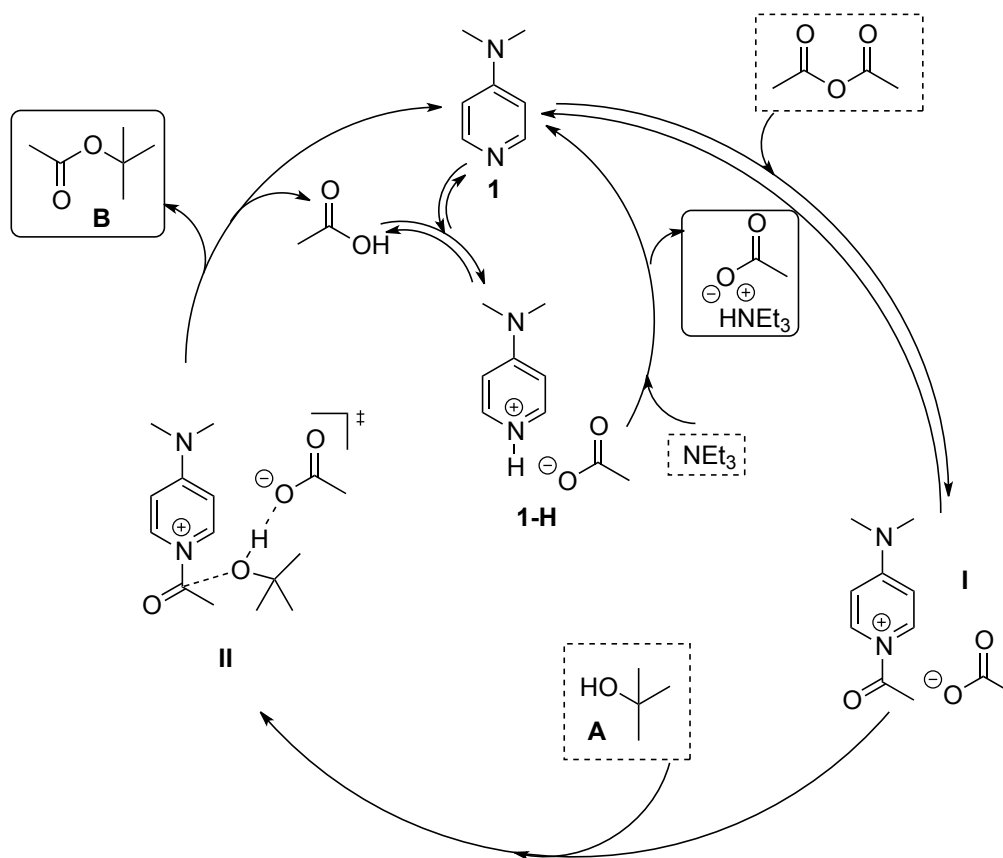


Figure 1.1. DMAP (**1**) and other commonly used Lewis base catalysts **2 – 5**.

Catalysts **1 – 5** can not only be employed in acylation reactions, but are also active in other transformations such as the Baylis Hillman reaction^[7c,17], macrolactonisations^[18] as well as in total-^[19] and polymer synthesis.^[20] Recently Christmann *et al.* showed the application of **3** and **5** in the isomerization of *Z*- α,β -unsaturated aldehydes.^[21] In the mechanism of the esterification of alcohols the catalyst plays a key role in the catalytic cycle. Scheme 1.1 shows that the catalyst is involved in every single step. The accepted mechanism^[22] starts with the formation of a pre-equilibrium of catalyst **1** and the acylating agent acetic anhydride to form a *N*-acylpyridinium salt (**I**). This intermediate is consumed in the rate-determining step by alcohol (**A**) to form ester (**B**) by passing through transition state (**II**). In this transition state the acetate anion coordinates to the alcohol proton in order to facilitate the nucleophilic attack of the alcohol to the *N*-acylpyridinium salt (**I**). In this way acetic acid is formed, which may

react as a Brønsted acid with catalyst (**1**) to yield the protonated species **1-H**. To regenerate catalyst **1** an auxiliary base is needed to deprotonate **1-H** and thus triethylammonium acetate is formed.



Scheme 1. Consensus mechanism for the DMAP-catalyzed acylation reaction.^[17]

Aside from the nucleophilic pathway shown in Scheme 1 a base-catalyzed pathway has been discussed previously. However, due to the lack of correlation of activity with pK_a values of the amines, this mechanism is considered to be less likely. Nevertheless the pK_a values of triethylamine ($pK_a = 10.7$) and DMAP ($pK_a = 9.2$)^[23] in water are not different enough to exclude a base catalyzed mechanism as concurrent reaction. Computational studies suggest that the nucleophilic pathway is favored over the base catalyzed.^[24]

As already outlined before the Lewis basicity and nucleophilicity of the catalysts play a crucial role for catalyst activity. The aim of this thesis was to develop synthetic strategies for tailor-made highly nucleophilic pyridines of selected nucleophilicity and Lewis basicity. The catalysts **1** – **5** of defined structure were quantified with respect to their Lewis basicity and nucleophilicity using established procedures.^[25,26] Moreover this thesis was devoted to the prediction of catalytic activity on basis of calculated ground state data and the subsequent use of highly nucleophilic pyridines in different applications such as fluorescence labeling of biological active molecules or ring opening polymerization.

References

- [1] Cooper GM. The Cell: A Molecular Approach. 2nd edition. Sunderland (MA): Sinauer Associates; **2000**. The Central Role of Enzymes as Biological Catalysts.
- [2] K. A. Ahrendt, C. J. Borths, D. W. C. MacMillan, *J. Am. Chem. Soc.* **2000**, *122*, 243–4244.
- [3] J. Seayad, B. List, *Org. Biomol. Chem.* **2005**, *3*, 719–724.
- [4] C. E. Müller, R. P. Schreiner, *Angew. Chem. Int. Ed.* **2011**, *50*, 6012 – 6042.
- [5] D. W. C. MacMillan, *Nature* **2008**, *455*, 304–308.
- [6] C. Grondal, M. Jeanty, D. Enders, *Nature Chem.* **2010**, *2*, 167– 178.
- [7] a) A. Marinetti, A. Voituriez, Synlett 2010, 174 –194. b) S. W. Smith, G. C. Fu, *J. Am. Chem. Soc.* **2009**, *131*, 14231 –14233. c) C. Lindner, R. Tandon, Y. Liu, B. Maryasin, H. Zipse, *Org. Biomol. Chem.* **2012**, *10*, 3210 – 3218. d) Y. Wei, M. Shi, *Acc. Chem. Res.* **2010**, *43*, 1005 –1018.
- [8] a) E. M. McGarrigle, E. L. Myers, O. Illa, M. A. Shaw, S. L. Riches, V. K. Aggarwal, *Chem. Rev.* **2007**, *107*, 5841 – 5883. b) V. K. Aggarwal, M. Crimmin, S. Riches, *Sci. Synth.* **2008**, *37*, 321 – 406. c) S. L. Riches, C. Saha, N. Fontan Filgueira, E. Grange, E. M. McGarrigle, V. K. Aggarwal, *J. Am. Chem. Soc.* **2010**, *132*, 7626 –7630. d) O. Illa, M. Arshad, A. Ros, E. M. McGarrigle, V. K. Aggarwal, *J. Am. Chem. Soc.* **2010**, *132*, 1828 –1830.
- [9] a) N. De Rycke, F. Couty, O. R. P. David, *Chem. Eur. J.* **2011**, *17*, 12852 – 12871. b) N. De Rycke, G. Berionni, F. Couty, H. Mayr, R. Goumont, O. R. P. David, *Org. Lett.* **2011**, *13*, 530 - 533.
- [10] W. Steglich, G. Höfle, *Angew. Chem.* **1969**, *81*, 1001. *Angew. Chem. Int. Ed. Engl.* **1969**, *8*, 981.
- [11] G. Höfle, W. Steglich, H. Vorbrüggen, *Angew. Chem.* **1978**, *90*, 602 - 615. *Angew. Chem. Int. Ed. Engl.* **1978**, *17*, 569 - 583.
- [12] M. R. Heinrich, H. S. Klisa, H. Mayr, W. Steglich, H. Zipse, *Angew. Chem.* **2003**, *115*, 4975. *Angew. Chem. Int. Ed.* **2003**, *42*, 4826 - 4828.
- [13] a) I. Held, S. Xu, H. Zipse, *Synthesis* **2007**, 1185-1196. b) H. Zipse, I. Held, Bayer Material Science LLC, US 2008/0176747A1, **2008**.
- [14] I. Held, E. Larionov, C. Bozler, F. Wagner, H. Zipse, *Synthesis* **2009**, 2267 - 2277.
- [15] E. Larionov, F. Achrainner, J. Humin, H. Zipse, *ChemCatChem* **2012**, *4*, 559 - 566.
- [16] R. Tandon, T. Unzner, T. A. Nigst, N. De Rycke, P. Mayer, H. Mayr, B. Wendt, O. R. P. David, H. Zipse, **2013**, *ASAP*.
- [17] Y.-L. Shi, M. Shi, *Eur. J. Org. Chem.* **2007**, *18*, 2905.
- [18] a) J. Inanaga, K. Hirata, H. Saeki, T. Katsuki, M. Yamaguchi, *Bull. Chem. Soc. Jpn.* **1979**, *52*, 1989. b) E. P. Boden, G. E. Keck, *J. Org. Chem.* **1985**, *50*, 2394.
- [19] a) D. R. Williams, L. A. Robinson, C. R. Nevill, J. P. Reddy, *Angew. Chem. Int. Ed.* **2007**, *46*, 915-918. b) T. Mita, N. Fukuda, F. X. Roca, M. Kanai, M. Shibasaki, *Org. Lett.* **2007**, *9*, 259. c) M. L. Maddess, M. N. Tackett, H. Watanabe, P. E. Brennan, C. D. Spilling, J. S. Scott, D. P. Osborn, S. V. Ley, *Angew. Chem. Int. Ed.* **2007**, *46*, 591.

- [20] a) R. L. Paddock, S. T. Nguyen, *J. Am. Chem. Soc.* **2001**, *123*, 11498. b) G. A. Luinstra, G. R. Haas, F. Molnar, V. Bernhart, R. Eberhardt, B. Rieger, *Chem. Eur. J.* **2005**, *11*, 6298.
- [21] D. Könnig, W. Hiller, M. Christmann, *Org. Lett.* **2012**, *14*, 5258–5261.
- [22] A. C. Spivey, S. Arseniyadis, *Angew. Chem. Int. Ed.* **2004**, *43*, 5436.
- [23] D. H. Ripin, D. A. Evans, http://daecr1.harvard.edu/pdf/evans_pKa_table.pdf
- [24] S. Xu, I. Held, B. Kempf, H. Mayr, W. Steglich, H. Zipse, *Chem. Eur. J.* **2005**, *11*, 4751.
- [25] a) C. Lindner, B. Maryasin, F. Richter, H. Zipse, *J. Phys. Org. Chem.* **2010**, *23*, 1036 – 1042. b) Y. Wei, G. N. Sastry, H. Zipse, *J. Am. Chem. Soc.* **2008**, *130*, 3473 -3477. c) Y. Wei, T. Singer, H. Mayr, G. N. Sastry, H. Zipse, *J. Comp. Chem.* **2008**, *29*, 291 – 297. d) C. Lindner, R. Tandon, B. Maryasin, E. Larionov, H. Zipse, *Beilstein J. Org. Chem.* **2012**, *8*, 1406 -1442.
- [26] a) H. Mayr, B. Kempf, A. R. Ofial, *Acc. Chem. Res.* **2003**, *36*, 66 -77. b) H. Mayr, M. Patz, *Angew. Chem., Int. Ed. Engl.* **1994**, *33*, 938 – 957. c) H. Mayr, M. Patz, M. F. Gotta, A. R. Ofial, *Pure Appl. Chem.* **1998**, *70*, 1993 – 2000. d) H. Mayr, A. R. Ofial, *Carbocation Chemistry*, G. A. Olah, G. K. S. Prakash, Wiley: Hoboken, NJ, 2004, Chapter 13, 331 – 358. e) H. Mayr, A. R. Ofial, *Pure Appl. Chem.* **2005**, *77*, 1807 – 1821. f) R. Lucius, R. Loos, H. Mayr, *Angew. Chem., Int. Ed.* **2002**, *41*, 91 – 95. g) M. Baidya, S. Kobayashi, F. Brotzel, U. Schmidhammer, E. Riedle, H. Mayr, *Angew. Chem., Int. Ed.* **2007**, *46*, 6176 - 6179. h) H. Mayr, J. Bartl, G. Hagen, *Angew. Chem., Int. Ed. Engl.* **1992**, *31*, 1613 - 1615.

Chapter 2

Summary

2.1 Annulated Pyridines as Highly Nucleophilic and Lewis-Basic Catalysts for Acylation Reactions

N,N-Dimethylaminopyridine (DMAP) is employed as a Lewis-base catalyst in a multitude of group transfer reactions and the development of more powerful Lewis-base catalyst is thus of significant synthetic interest.^[1,2] We explored the utility of annulated derivatives of DMAP such as 9-azajulolidine and its nitrogen-substituted derivatives (see Figure 2.1.1) as more potent Lewis bases.

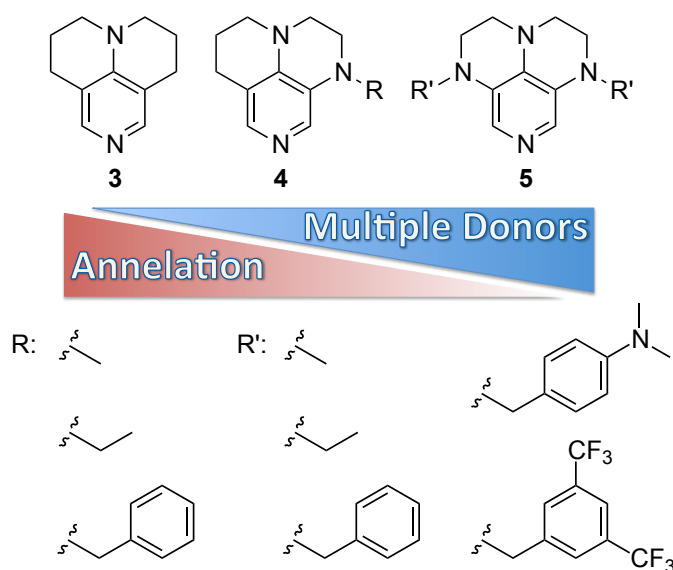
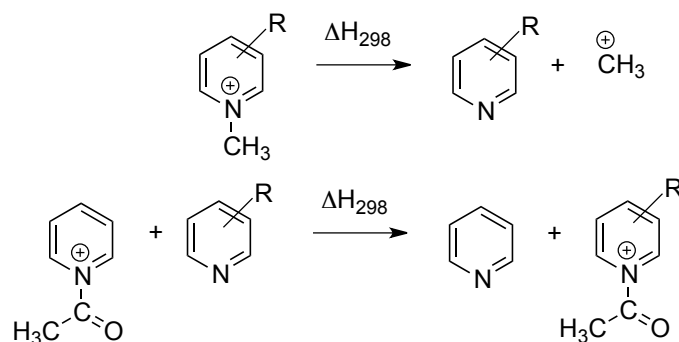


Figure 2.1.1. Carbo- and heteroannulated derivatives of DMAP.

Synthesis and Structure

The carbo- and heteroannulated derivatives of DMAP were synthesized in good to excellent yields. Due to the development of a purification protocol several of these compounds could be crystallized and analyzed by X-ray analysis. The Lewis basicity of amino-substituted pyridines depends, among others, on the alignment of the substituent nitrogen lone pair orbital with the pyridine π -system. Structural parameters connected to this orbital interaction are the 4-NC bond distance $\text{dist}_{\text{N-C}}$ (the distance between the pyridine carbon atom and the nitrogen at the 4-position) as well as the degree of pyramidalization of the nitrogen substituent (d_{abcd}). The 4-NC bond lengths in the crystal structures of mono-, di- and triaminopyridines are actually identical within experimental uncertainty (137.5 ± 0.2 pm), whereas the structures optimized at B98/6-31G(d) level (best conformer each) show slightly larger bond lengths in all cases. The calculated pyramidalisation angles (d_{abcd}) reflect the experimental results very well. It was further established that conformational reorientation of the annulated 6-membered rings and accompanying variations in the pyramidalization of the central nitrogen atom occurs with rather little increase in energy.

In order to match these structural properties to actual Lewis basicities, methyl cation affinities (MCA) and acylation enthalpies ΔH_{ac} as defined in Scheme 2.1.1 have been calculated for most of the synthesized pyridines at the MP2/6-31+G(2d,p)//B98/6-31G(d) level of theory in the gas phase. How solvent effects impact the Lewis basicity has been tested for the acylation enthalpies using the polarizable continuum model (PCM) in chloroform at the RHF/6-31G(d) level with UAHF radii. All three types of affinity data indicate quite clearly, that all tricyclic catalysts displayed in Figure 2.1.1 are stronger Lewis bases than the parent DMAP. The 3,4,5-triaminopyridines (**5**) are the strongest Lewis bases, irrespective of the choice of Lewis basicity indicator.



Scheme 2.1.1. Definitions of methyl cation affinities (up) and isodesmic acetyl transfer reaction (down).

Nucleophilicity

In how far the theoretically calculated Lewis basicities correlate well with reaction rates for reaction with reference electrophiles was next tested for additions to benzhydrylium cations. This type of addition reaction provides the basis for Mayr's comprehensive nucleophilicity scale according to the linear free energy relationship:

$$\log k_2 (20\text{ }^\circ\text{C}) = s_N(N + E)$$

The rate constants for nucleophile/electrophile combination reactions k_2 were studied under first-order conditions. Figure 2.1.2 shows, that the nucleophilic reactivities of 4-aminopyridines (**1–3**, black) and 3,4,5-triaminopyridines (**5**, red) correlate quite well (with $R^2=0.9022$) with acylation enthalpies in chloroform solution and even better with the gas phase acylation enthalpies ($R^2=0.9702$). We can thus conclude that the kinetic data for single-step addition to cationic electrophiles are related to the thermodynamic data for this structurally quite homogenous set of nucleophiles, thus providing evidence for a good correlation between Lewis basicity and nucleophilicity.

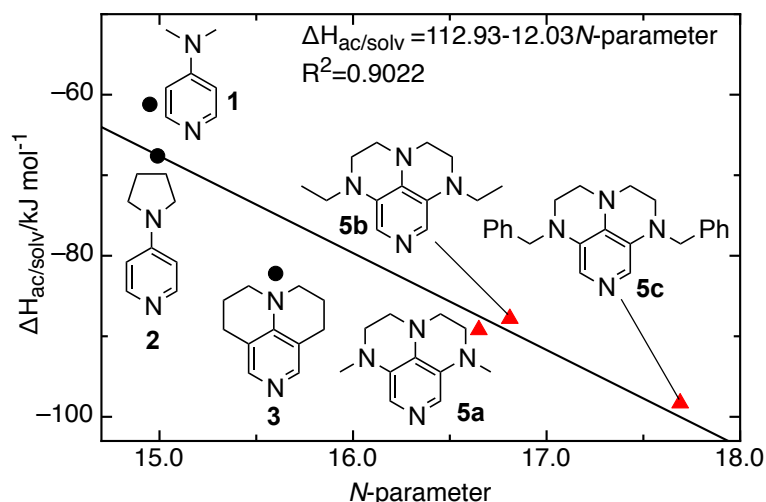
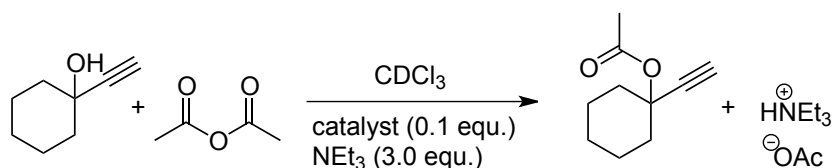


Figure 2.1.2. Correlation of acylation enthalpies ($\Delta H_{\text{ac/solv}}$) with *N*-parameters.

Catalytic Activity

The catalytic potential of the synthesized catalysts has been explored in the acetylation of 1-ethynylcyclohexanol. The reactions were followed by ^1H NMR spectroscopy in CDCl_3 as the solvent. All reactions eventually proceed to full conversion and the rates of the reactions can thus be characterized by the reaction half-life $t_{1/2}$ using an approach described previously.^[4] As expected from the calculated Lewis basicities and the experimentally measured *N*-parameters, all annelated donor-substituted pyridine derivatives are more reactive than DMAP (**1**).



Scheme 2.1.2. Aminopyridine-catalyzed acylation reaction of 1-ethynylcyclohexanol with acetic anhydride in CDCl_3 .

A comparison of the catalytic activities of the annelated catalyst systems shows that the conformationally constrained all-carbon analogue 9-azajulolidine (**3**) and the 3,4-diaminopyridines (**4**) are significantly more active than the 3,4,5-triaminopyridines (**5**). This is in remarkable contrast to the rather high Lewis basicities and *N*-parameters determined for this latter class of nucleophiles. In qualitative terms this implies that catalysts with higher and higher Lewis basicity will eventually slow down catalytic process due to the effort of detaching themselves from the substrate electrophiles. This general observation has recently also been made by Christmann *et al.* in the Lewis-base catalyzed isomerization of *Z*-allylic alcohols.^[5]

Due to the unexpectedly moderate catalytic activity of the strongly Lewis basic 3,4,5-triaminopyridines (**5**), investigations of the reaction rate on the catalyst concentration for the acetylation of 1-ethynylcyclohexanol were performed using catalyst **5c** revealing a clear first-order dependence as already found in the case of DMAP (**1**).^[6]

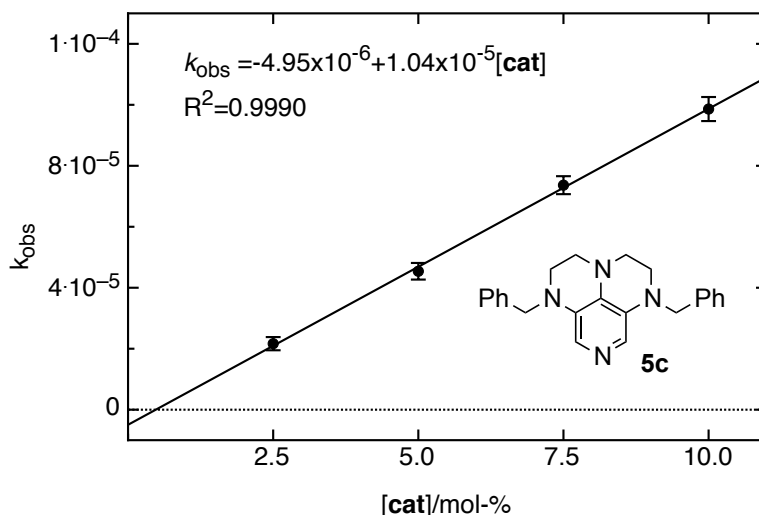


Figure 2.1.3. Variation of reaction rate as a function of the concentration of highly nucleophilic triaminopyridine **5c** in the acylation reaction of 1-ethynylcyclohexanol.

Since the catalytic performance of these compounds in acylation reactions of sterically hindered alcohols is found to be more complex, quantitative prediction of reaction rates requires a 3-component QSAR model including Lewis basicity, structural, and charge distribution parameters. The most important descriptors could be identified as the acylation enthalpies including solvation terms in chloroform ($\Delta H_{\text{ac/solv}}$, in kJ/mol), the charge of the *ortho*-hydrogen atom of the free catalyst ($q_{\text{ortho-H}}$, in units of elemental charge e) and the bond distance ($\text{dist}_{\text{N-C}}$, in Ångstroms) between the nitrogen atom in 4-position and the pyridine carbon atom at the same position. A QSAR model constructed with Sybyl X 2.0 yields good correlations between actual and predicted catalytic activity ($R^2=0.9320$, $Q^2=0.7880$, see Figure 2.1.4).

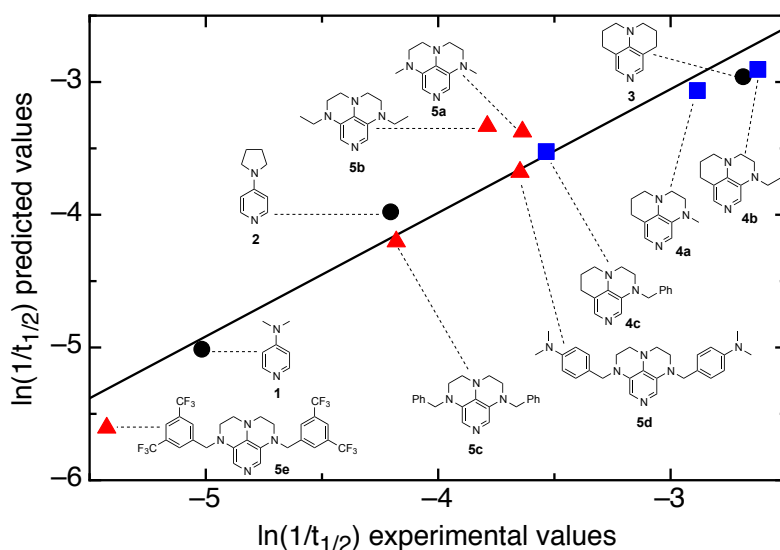


Figure 2.1.4. Experimental vs. predicted values for $\ln(1/t_{1/2})$ for the QSAR model described above involving $\Delta H_{ac/solv}$, $q_{ortho-H}$ and $dist_{N-C}$ for 4-aminopyridines (1–3, black circles), 3,4-diaminopyridines (4, blue squares), and 3,4,5-triaminopyridines (5, red triangles).

References

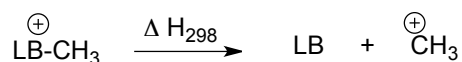
- [1] E. Larionov, F. Achraimer, J. Humin, H. Zipse, *ChemCatChem* **2012**, *4*, 559.
- [2] C. Lindner, R. Tandon, B. Maryasin, E. Larionov, H. Zipse, *Beilstein J. Org. Chem.* **2012**, *8*, 1406.
- [3] a) H. Mayr, B. Kempf, A. R. Ofial, *Acc. Chem. Res.* **2003**, *36*, 66 -77. b) H. Mayr, M. Patz, *Angew. Chem., Int. Ed. Engl.* **1994**, *33*, 938 - 957. c) H. Mayr, M. Patz, M. F. Gotta, A. R. Ofial, *Pure Appl. Chem.* **1998**, *70*, 1993 - 2000. d) H. Mayr, A. R. Ofial, *Carbocation Chemistry*, G. A. Olah, G. K. S. Prakash, Wiley: Hoboken, NJ, 2004, Chapter 13, 331 - 358. e) H. Mayr, A. R. Ofial, *Pure Appl. Chem.* **2005**, *77*, 1807 - 1821. f) R. Lucius, R. Loos, H. Mayr, *Angew. Chem., Int. Ed.* **2002**, *41*, 91 - 95. g) M. Baidya, S. Kobayashi, F. Brotzel, U. Schmidhammer, E. Riedle, H. Mayr, *Angew. Chem., Int. Ed.* **2007**, *46*, 6176 - 6179. h) H. Mayr, J. Bartl, G. Hagen, *Angew. Chem., Int. Ed. Engl.* **1992**, *31*, 1613 - 1615. i) H. Mayr, T. Bug, M. F. Gotta, N. Hering, B. Irrgang, B. Janker, B. Kempf, R. Loos, A. R. Ofial, G. Remennikov, H. Schimmel, *J. Am. Chem. Soc.* **2001**, *123*, 9500–9512.
- [4] I. Held, E. Larionov, C. Bozler, F. Wagner, H. Zipse, *Synthesis* **2009**, 2267 - 2277.
- [5] D. Könning, W. Hiller, M. Christmann, *Org. Lett.* **2012**, *14*, 5258–5261.
- [6] S. Xu, I. Held, B. Kempf, H. Mayr, W. Steglich, H. Zipse, *Chem. Eur. J.* **2005**, *11*, 4751 - 4757.

2.2 Cation Affinity Numbers of Lewis Bases

Due to the scarcity of accurate experimentally measured or theoretically calculated data, cation affinity values represent important guidelines for the reactivity of Lewis and Brønsted bases.^[1-3] This complements the limited amount of experimental affinity data and provides a quantitative guideline in catalyst development projects. Affinity data towards carbon electrophiles can be adopted as tools for the assessment of Lewis basicity.^[4]

Methyl Cation Affinities (MCA)

The methyl cation (CH_3^+) is the smallest carbocation useful as a chemical probe for Lewis bases. The respective methyl cation affinity (MCA) of a given Lewis base (LB) is obtained as the reaction enthalpy at 298.15 K and 1 bar pressure for the following reaction:



Pyridine, imidazole and pyrrolidine are comparatively weak nucleophiles (MCA=518–539 kJ/mol) as can be seen in the graphical overview in Figure 2.2.1. The introduction of an alkyl group into the pyridine ring gives a moderate increase in MCA value compared to the introduction of dialkylamino groups in DMAP (**1**) or in PPY (**2**). This is in accordance with the much higher catalytic efficiency of these compounds e.g. in acylation reactions.^[3,5-9] Conformational fixation is also accompanied by an increase in the MCA value (9-azajulolidine, **3**). Conformationally constrained pyridines with multiple nitrogen donors enhance the MCA dramatically. The commercially available triphenylphosphine is equal in Lewis basicity to the 3,4-diaminopyridines (**4** and **6**, blue boxes). The highest MCA values (618 – 661 kJ/mol) are obtained for the 3,4,5-triaminopyridines (**5**, red boxes in Figure 2.2.1).

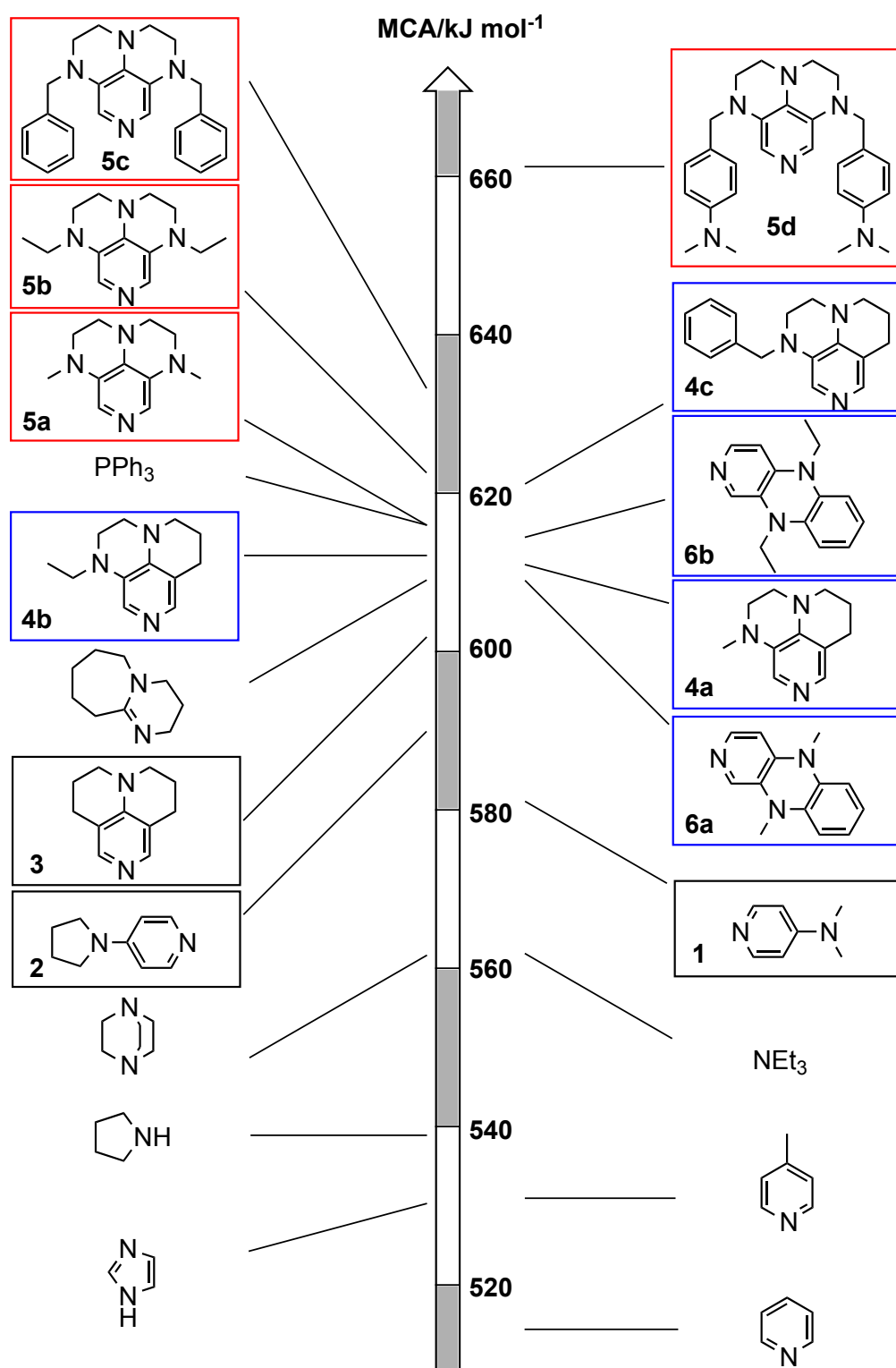
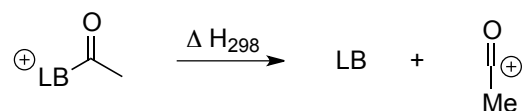


Figure 2.2.1. Overview of MCA values as descriptors for Lewis basicity for selected nitrogen-based organic compounds and triphenylphosphane.

Acetyl Cation Affinities (ACA)

The acyl transfer reaction catalyzed by pyridine bases, which involve acetylpyridinium cations as intermediates of the catalytic cycle, is well studied.^[10-26] The acetyl cation may be considered to be a representative cationic probe for this type of situation and the corresponding acetyl cation affinities (ACA) of neutral Lewis bases thus reflect the enthalpies for the reaction shown below:



The elongation of the alkyl substituents in *N,N*-dialkyl-4-aminopyridines leads to a rapid convergence of the ACA values towards 224 kJ/mol and is thus equal to that of PPY (**2**), which is also reflected in the similar catalytic performance. To raise the Lewis basicity of the parent compound DMAP (**1**) can be accomplished by different means:

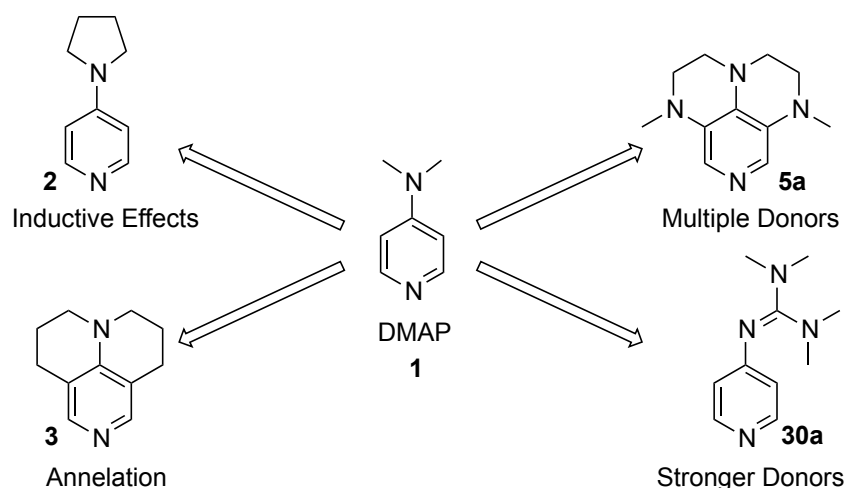


Figure 2.2.2. Increasing the Lewis basicity of DMAP (**1**).

In fact the same tendencies as already obtained for the MCA values as descriptors of Lewis basicity are also found for the acetyl cation as a probe (see Figure 2.2.3). Among the donor-substituted pyridines the 4-aminopyridines (**1–3**) are the least Lewis basic compounds with ACA values of 217–238 kJ/mol (see Figure 2.2.3). Guanidiny pyridines (**30**) have, in contrast, suprisingly low ACA values around 230 kJ/mol and are thus less Lewis basic than the 3,4-diaminopyridines (**4**) (233–246 kJ/mol) although guanidiny derivatives are from an experimental side quite challenging in terms of handling due to their great basicity. The same is true for the 3,4,5-triaminopyridines (**5**), which show the highest ACA values of all examined neutral Lewis bases with affinity values ranging from 243 to 263 kJ/mol.

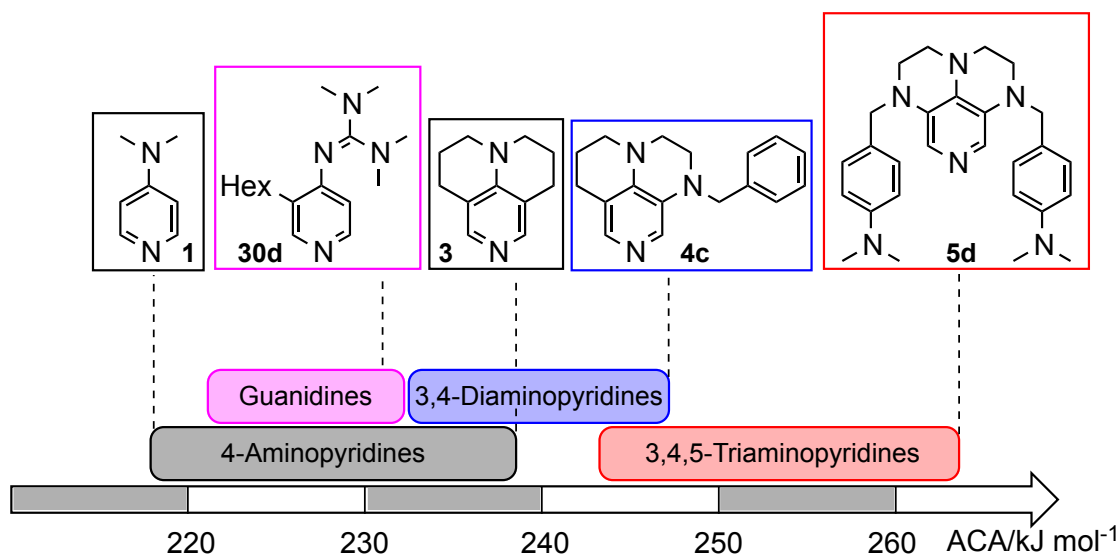


Figure 2.2.3. Overview of ACA values as descriptors for Lewis basicity for 4-aminopyridines (**1-3**, black), guanidinyl pyridines (**30**, magenta), 3,4-diaminopyridines (**4** and **6**, blue) and 3,4,5-triaminopyridines (**5**, red).

Finally a good correlation between MCA and ACA values can be obtained ($R^2=0.9374$, see Figure 2.2.4).

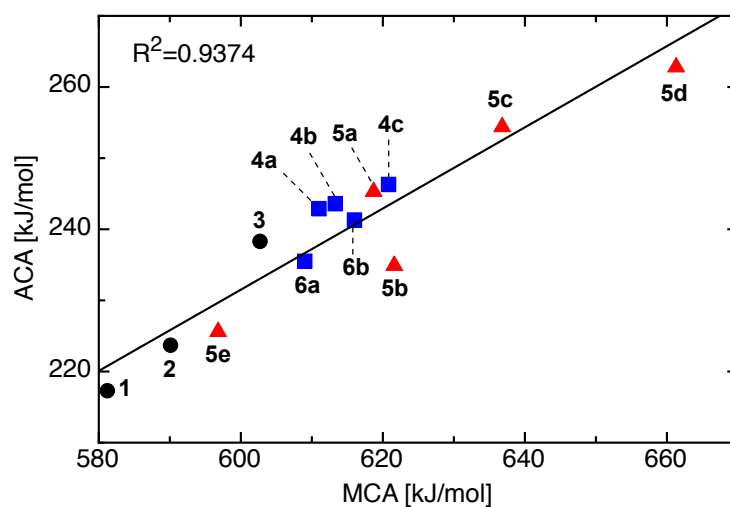


Figure 2.2.4. Correlation of MCA and ACA values for 4-aminopyridines (**1-3**, black), 3,4-diaminopyridines (**4** and **6**, blue) and 3,4,5-triaminopyridines (**5**, red).

References

- [1] E. Larionov, H. Zipse, *WIREs Comp. Mol. Sci.* **2011**, *1*, 601–619.
- [2] S.E. Denmark, G.L. Beutner, *Angew. Chem. Int. Ed.* **2008**, *47*, 1560–1638.
- [3] N. De Rycke, F. Couty, O.R.P. David, *Chem. Eur. J.* **2011**, *17*, 12852–12871.
- [4] Y. Wei, G.N. Sastry, H. Zipse, *J. Am. Chem. Soc.* **2008**, *130*, 3473–3477.

- [5] a) C. Lindner, R. Tandon, Y. Liu, B. Maryasin, H. Zipse, *Org. Biomol. Chem.* **2012**, *10*, 3210 – 3218; b) R. Tandon, T. Unzner, T. A. Nigst, N. De Rycke, P. Mayer, H. Mayr, B. Wendt, O.R.P. David, H. Zipse, **2012 submitted manuscript**; c) I. Held, S. Xu, H. Zipse, *Synthesis* **2007**, 1185–1196.
- [6] E. Larionov, F. Achrainger, J. Humin, H. Zipse, *ChemCatChem* **2012**, *4*, 559–566.
- [7] V. D'Elia, Y. Liu, H. Zipse, *Eur. J. Org. Chem.* **2011**, 1527–1533.
- [8] I. Held, P. von den Hoff, D.S. Stephenson, H. Zipse, *Adv. Synth. Catal.* **2008**, *350*, 1891–1900.
- [9] M.R. Heinrich, H.S. Klisa, H. Mayr, W. Steglich, H. Zipse, *Angew. Chem.* **2003**, *115*, 4975–4977. *Angew. Chem. Int. Ed.* **2003**, *42*, 4826–4828.
- [10] E. Vedejs, M. Jure, *Angew. Chem. Int. Ed.* **2005**, *44*, 3974–4001.
- [11] R. Wurcz, *Chem. Rev.* **2007**, *107*, 5570–5595.
- [12] A.C. Spivey, S. Arseniyadis, *Top. Curr. Chem.* **2010**, *291*, 233.
- [13] C.E. Müller, P.R. Schreiner, *Angew. Chem. Int. Ed.* **2011**, *50*, 6012–6042.
- [14] I. Held, A. Villinger, H. Zipse, *Synthesis* **2005**, 1425–1426.
- [15] Y. Wei, I. Held, H. Zipse, *Org. Biomol. Chem.* **2006**, *4*, 4223–4230.
- [16] I. Held, E. Larionov, C. Bozler, F. Wagner, H. Zipse, *Synthesis* **2009**, 2267–2277.

2.3 Inductive Effects Through Alkyl Groups – How Long is Long Enough?

The chain length dependence of inductive effects in alkyl substituents is not well documented. Thus the effects of chain elongation of the alkyl groups in 4-*N,N*-dialkylaminopyridines (see Figure 2.3.1) on the rates of pyridine-catalyzed acylations of alcohols, the benzylation of the pyridines, the reactions of *N*-benzoyl pyridinium ions with benzylamine, on their ¹H NMR properties, their theoretically calculated acetylation enthalpies and on electronic and geometric properties of the respective acylated intermediates were surveyed to provide a quantitative answer.

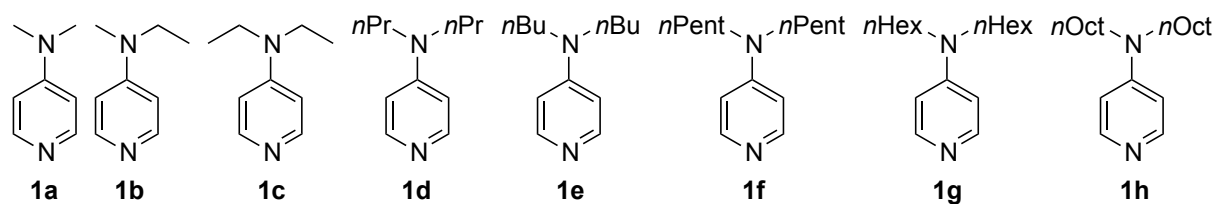
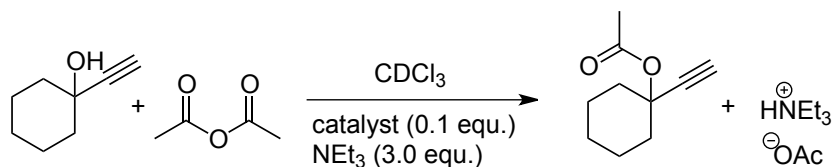


Figure 2.3.1. 4-*N,N*-dialkylaminopyridines used for the investigation of inductive effects.

In the acylation of 1-ethynylcyclohexanol with acetic anhydride (see Scheme 2.3.1) the catalytic activity increases with the chain length of the alkyl substituents on the 4-aminogroup by a factor of 2.6 from DMAP (**1a**) to 4-*N,N*-dioctylaminopyridine until saturation is observed starting with butyl groups.



Scheme 2.3.1. 4-*N,N*-dialkylaminopyridine-catalyzed acylation reaction of 1-ethynylcyclohexanol with acetic anhydride in CDCl_3 .

Other surveyed metrics (kinetic, thermodynamic or spectroscopic properties) of 4-*N,N*-dialkylaminopyridines show very similar saturation effects comparable to that obtained for the catalytic activity in the acetylation of 1-ethynylcyclohexanol. Assuming, that the increasingly large alkyl substituents influence the pyridine system only through electronic (inductive) effects and impart effectively no steric shielding on the reaction center (that is, the pyridine nitrogen atom) we tested the suitability of a model proposed by Galkin *et al.*^[1] in order to describe the chain length-dependent properties of the 4-*N,N*-dialkylaminopyridines in quantitative terms.

According to this model the effect of the 4-*N,N*-dialkylamino substituent can be expressed with a single substituent parameter σ^* , whose magnitude is derived using an inductive increment method.

$$\sigma^* = 7.840 \cdot \sum_i \chi_i \frac{R_i^2}{r_i^2}$$

These calculated σ^* values can subsequently be used together with a Hammett expression to quantitatively describe the influence of alkyl chain length on experimentally observed or theoretically calculated data.

$$\log \frac{k_X}{k_H} = \rho \sigma^*$$

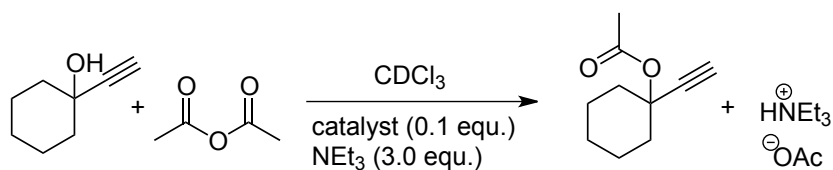
The fact that all observed saturation phenomena are well described with $R^2 = 0.80 - 0.99$ by a simple increment-based prediction of through-bond inductive effects can be seen as a proof for the existence of inductive effects of alkyl groups in situations lacking direct steric interactions between alkyl substituents and the respective reaction centers.

Reference

- [1] A.R. Cherkasov, V. I. Galkin, R. A. Cherkasov, *Russ. Chem. Rev.* **1996**, 65, 641–656.

2.4 Inductive Effects in DMAP-Polymers

The DMAP-derivative 4-*N,N*-dibutylaminopyridine (**1e**) was successfully immobilized on polystyrene support (1% crosslinked Merrifield resin) using a copper-catalyzed Huisgen reaction (see Figure 2.4.1). The catalytic potential of the synthesized immobilized catalyst as well as that of the soluble counterpart has been explored in the acetylation of 1-ethynylcyclohexanol (see Scheme 2.4.1), followed by ^1H NMR spectroscopy in CDCl_3 as the solvent.



Scheme 2.4.1. Aminopyridine-catalyzed acylation reaction of 1-ethynylcyclohexanol with acetic anhydride in CDCl_3 .

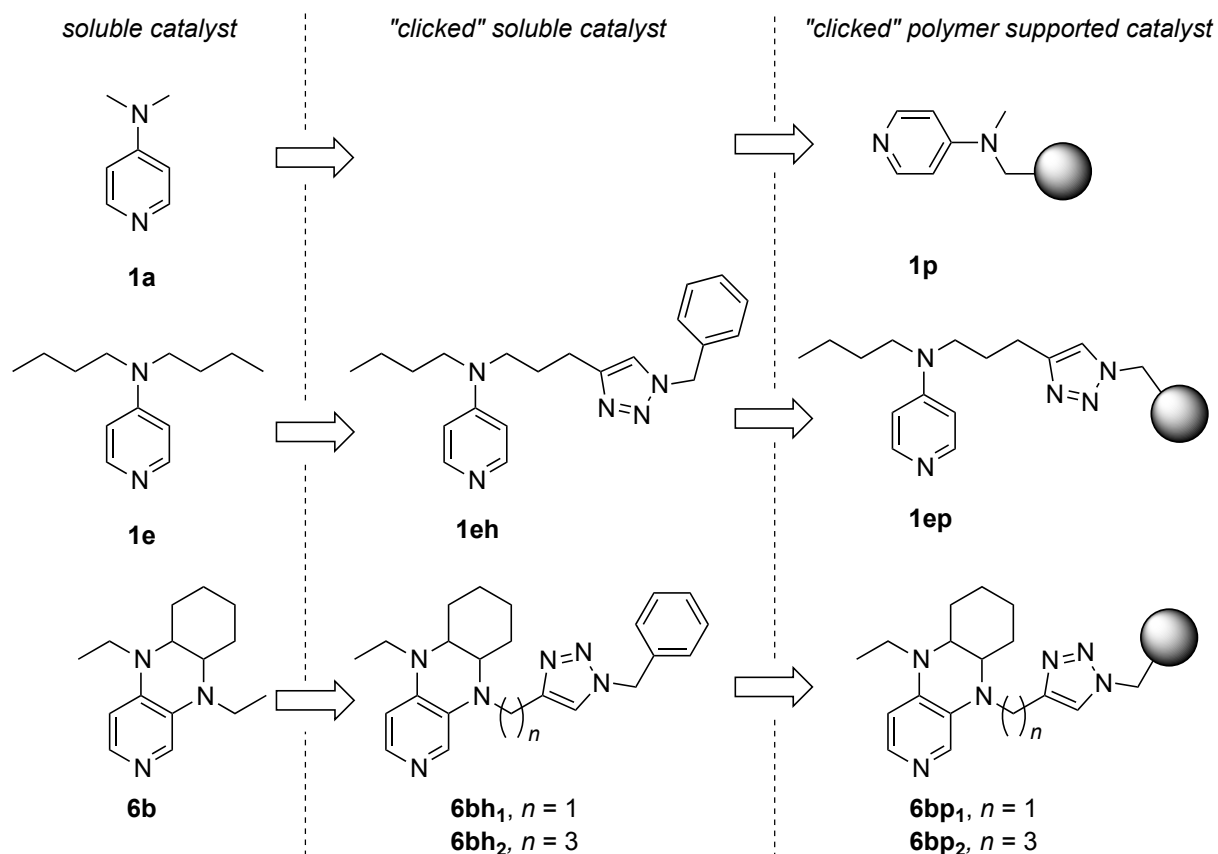


Figure 2.4.1. Polymer-supported DMAP and synthesized 4-*N,N*-dibutylaminopyridine polymer together with an immobilized 3,4-diaminopyridine derivative obtained by D'Elia *et al.*^[2]

Eventually, all immobilized catalysts are less reactive as compared to their soluble counterparts. This common phenomenon results from changes in the micro-environment of

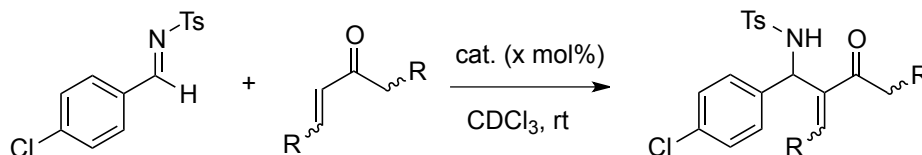
the catalyst and the increased difficulty for the reactants to diffuse to the reaction center.^[1] The supported variant of 4-*N,N*-dibutylaminopyridine (**1ep**) shows only a 0.1 fold increase in reactivity compared to commercially available DMAP polymer (**1p**) (kinetic half life time ($t_{1/2}$) = 500 min). In contrast, the soluble free catalyst 4-*N,N*-dibutylaminopyridine (**1e**) is 2.5 fold more reactive than the parent DMAP (**1a**) in the acetylation of tertiary alcohols. The additional inductive effects are thus not sufficient enough to obtain similar results like in the homogeneous catalysis, or diffusion control is too strongly restricted. The immobilized 3,4-diaminopyridines (**6pb**), which were obtained by D'Elia *et al.* (compare Figure 2.4.1) are the most active supported acylation catalysts obtained in this study with an 8-fold increase in reactivity as compared to the immobilized **1ep** and is three times more active than the free catalyst DMAP (**1a**).^[2]

References

- [1] I. Held, E. Larionov, C. Bozler, F. Wagner, H. Zipse, *Synthesis* **2009**, 2267 – 2277.
 [2] V. D'Elia, Y. Liu, H. Zipse, *Eur. J. Org. Chem.* **2011**, 1527 – 1533.

2.5 The Aza-Morita-Baylis-Hillmann Reaction of Electronically and Sterically Deactivated Substrates

A wide variety of Lewis-bases (LB) are known to catalyze the Morita-Baylis-Hillman (MBH) reaction and its aza-analogue (aza-MBH). In the latter transformation activated aldimines are condensed with Michael acceptors to yield densely functionalized β -aminocarbonyl compounds. Mechanistic studies reveal that Lewis base catalysts with increased carbon basicity will predictably lead to higher turnover rates.^[1–3] Using selected N- and P-based nucleophiles we showed that this is indeed the case.



Scheme 2.5.1. The azaMBH reaction of *para*-chlorotosylimine with different Michael acceptors in CDCl_3 .

In the group of nitrogen-based catalysts the reaction is rather sluggish with catalysts of low Lewis basicity such as DABCO. Significantly higher rates are observed for pyridine catalysts such as 4-*N,N*-dimethylaminopyridine (DMAP) or 4-pyrrolidinopyridine (PPY). Best results are obtained with the recently developed 3,4-diaminopyridine catalysts, with the annelated 9-azajulolidine, or with some of the phosphanes based on the PPh_3 motif. Using methyl vinyl ketone as a reference Michael acceptor of known high reactivity in all these latter cases,

complete turnover is achieved after 4 h. With respect to $t_{1/2}$ values the conformationally fixed 9-azajulolidine (**3**) and the 3,4-diaminopyridines (**4**) are found to be the fastest catalysts. Compared to that the highly nucleophilic, heteroannulated 3,4,5-triaminopyridines (**5**) perform substantially worse. This closely parallels recent results for the Lewis base-catalyzed acylation of tertiary alcohols.^[4] Triarylphosphanes carrying electron-donating substituents in *para* position are found to be equally active. Replacing one of the phenyl groups in PPh₃ by a cycloalkyl substituent enhances the catalytic activity, but also leads to a notable increase in phosphane oxidation (and thus deactivation).

Para-chlorotosylimine was also used in benchmark reactions with ethyl acrylate as the Michael acceptor. Due to the much lower reactivity of this latter compound, reasonable turnover times require higher substrate concentrations and a catalyst loading of 25 mol%. With the previously mentioned catalysts of high reactivity full conversion can be obtained after a maximum of five days. It should be mentioned that pyridine derivative 9-azajulolidine (**3**) and tri-*para*-tolylphosphane showed equal high activity.

In order to explore the effects of steric hindrance on the catalytic efficiency of pyridine and phosphane catalysts, the azaMBH reaction of cyclohexenone was studied under the same conditions used for ethyl acrylate. For the pyridine catalysts good turnover can be observed and full conversion can be achieved after 30 h reaction time. In surprising contrast there is practically no turnover when using any of the phosphane catalysts for the reaction with cyclohexenone. This unexpected result may indicate a generally larger sensitivity of triarylphosphanes to steric demands of the Michael acceptor, or may alternatively indicate the presence of stabilizing contacts between phosphane catalyst and the carbonyl oxygen atom in the zwitterionic enolates formed in the initial addition steps. This latter type of interaction is only possible in acyclic Michael acceptors for geometric reasons. In order to differentiate between these two effects, additional measurements have been performed for acyclic Michael acceptor *trans*-3-penten-2-one, in which the center of attack also carries an alkyl substituent. Whereas the pyridine catalysts show full conversion after 29 days, there is no significant turnover for triarylphosphanes. Since the acyclic nature of *trans*-3-penten-2-one does allow for contacts between carbonyl oxygen and phosphane catalysts in the zwitterionic intermediate, this latter result implies that triaryl phosphane catalysts are intrinsically more sensitive to the steric demands of Michael acceptors than pyridine catalysts.

An additional set of rate measurements was performed using *para*-chlorotosylimine at 0.25 M concentration in combination with 4.0 eq. Michael acceptor and 25 mol% of catalyst. The resulting conversion/time plots for 9-azajulolidine (top) and tri-*para*-tolylphosphane (bottom) are depicted in Figure 2.5.1.

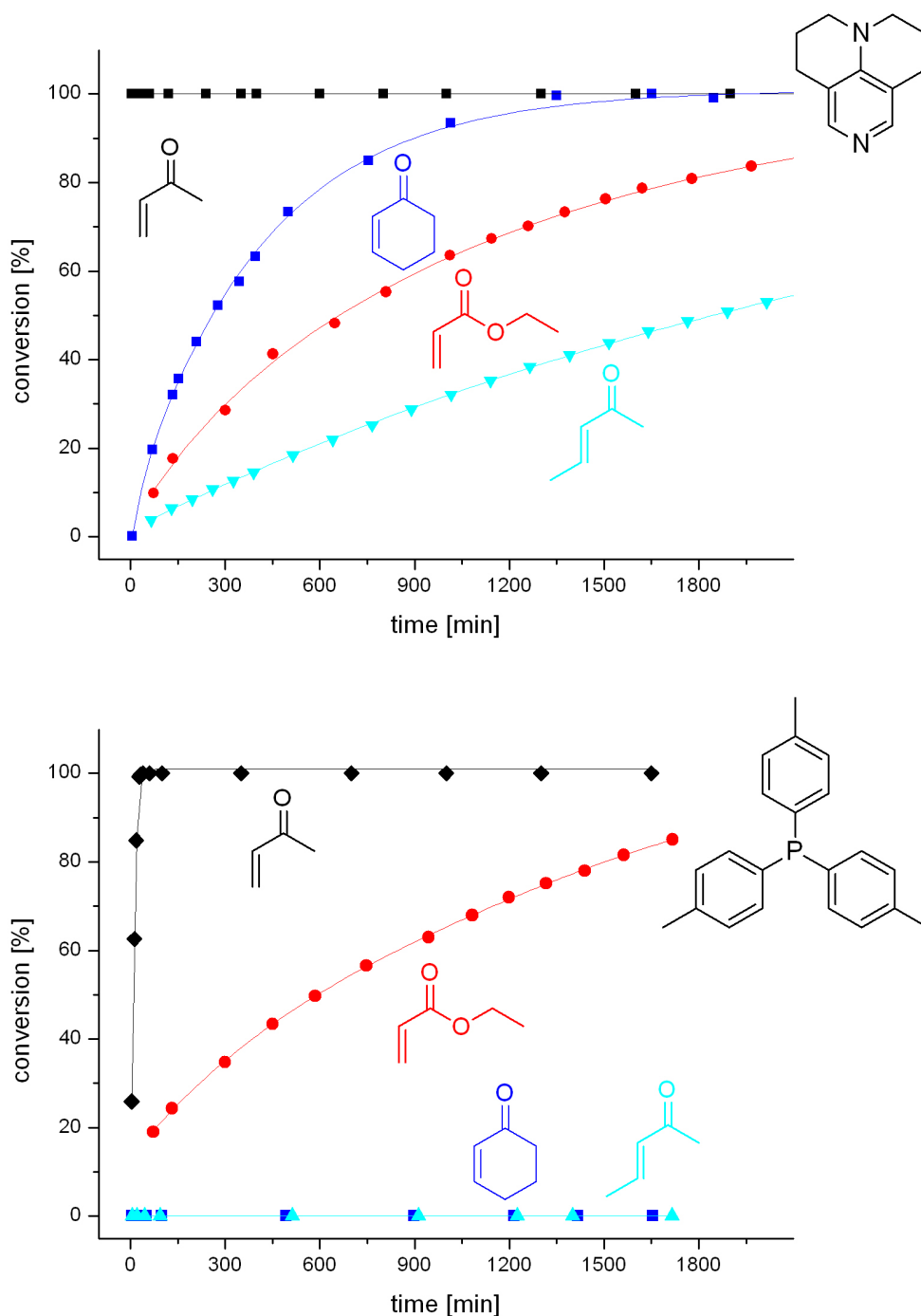


Figure 2.5.1. Turnover curves for 9-azajulolidine (top) and tri-*para*-tolylphosphane (bottom) for the azaMBH reactions of *para*-chlorotosylimine (0.25 M) with 4 eq. of MVK (black diamonds), ethyl acrylate (red circles), cyclohexenone (blue squares) or *trans*-3-penten-2-one (cyan triangles).

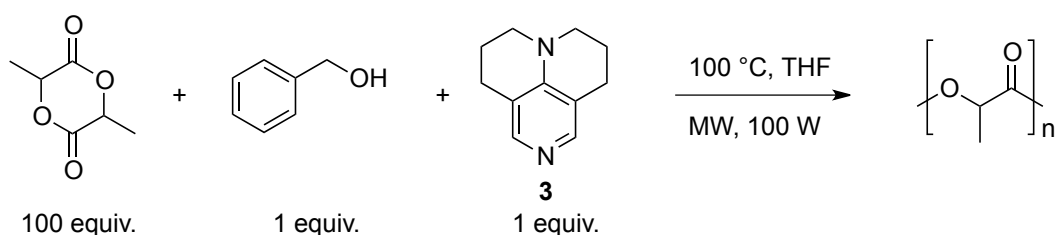
As already mentioned above, the phosphanes are not catalytically active in the case of sterically hindered Michael-acceptors. Investigations on the nature of the imine showed, that the substitution pattern appears to be of minor importance.

References

- [1] a) P. Buskens, J. Klankermayer, W. Leitner, *J. Am. Chem. Soc.* **2005**, *127*, 16762–16763. b) I. T. Raheem, E. N. Jacobsen, *Adv. Synth. Catal.* **2005**, *347*, 1701–1708.
- [2] T. Yukawa, B. Seelig, Y. Xu, H. Morimoto, S. Matsunaga, A. Berkessel, M. Shibasaki, *J. Am. Chem. Soc.* **2010**, *132*, 11988–11992.
- [3] V. K. Aggarwal, S. Y. Fulford, G. C. Lloyd-Jones, *Angew. Chem. Int. Ed.* **2005**, *44*, 1706–1708.
- [4] a) V. D'Elia, Y. Liu, H. Zipse, *Eur. J. Org. Chem.* **2011**, 1527–1533. b) I. Held, E. Larionov, C. Bozler, F. Wagner, H. Zipse, *Synthesis* **2009**, 2267–2277. c) I. Held, P. von den Hoff, D. S. Stephenson, H. Zipse, *Adv. Synth. Catal.* **2008**, *350*, 1891–1900. d) I. Held, S. Xu, H. Zipse, *Synthesis* **2007**, 1185–1196. e) M. R. Heinrich, H. S. Klisa, H. Mayr, W. Steglich, H. Zipse, *Angew. Chem. Int. Ed.* **2003**, *42*, 4826–4828.

2.6 Polymerization of Lactides Mediated by DMAP-Derivatives

Polylactide found already biomedical applications and is used in packaging or fibres. As a consequence the usually used tin compounds or metal-based catalysts have to be substituted by *e.g.* organocatalysts.^[1] 4-*N,N*-dimethylaminopyridine (DMAP, **1**) or 4-pyrrolidinopyridine (PPY, **2**) are already known to catalyze the ring opening polymerization (ROP) of lactide in the melt.^[2,3] In this study we tried to figure out, if another DMAP derivative, namely 9-azajulolidine (**3**) can show its superior catalytic behavior compared to DMAP (**1**) and PPY (**2**) (which was already demonstrated in different other reactions)^[4–6] also in the polymerization of lactide. Furthermore, we tried to utilize microwave technology as a source of heat. To the best of our knowledge no previous report exists yet on the ROP using microwave reactors and therefore we had to develop an optimized reaction protocol for the ROP using organocatalysts. Polymerization studies were conducted with sublimated lactide, benzyl alcohol (initiator) and 9-azajulolidine (**3**) in a ratio of 100:1:1 in dry THF using stock solutions to minimize errors (see Figure 2.6.1). The determination of yield was done by ¹H NMR, and number (*M_n*) and mass (*M_w*) averaged molar masses were analyzed by gel permeation chromatography (GPC).



Scheme 2.6.1. Standard reaction conditions for ring opening polymerization of lactide in the microwave using 9-azajulolidine (**3**) as nucleophilic organocatalyst in THF.

It was found, that 9-azajulolidine (**3**) indeed catalyzes the ring opening polymerization of lactide much faster than DMAP (**1**) or PPY (**2**) as Figure 2.6.1 shows.

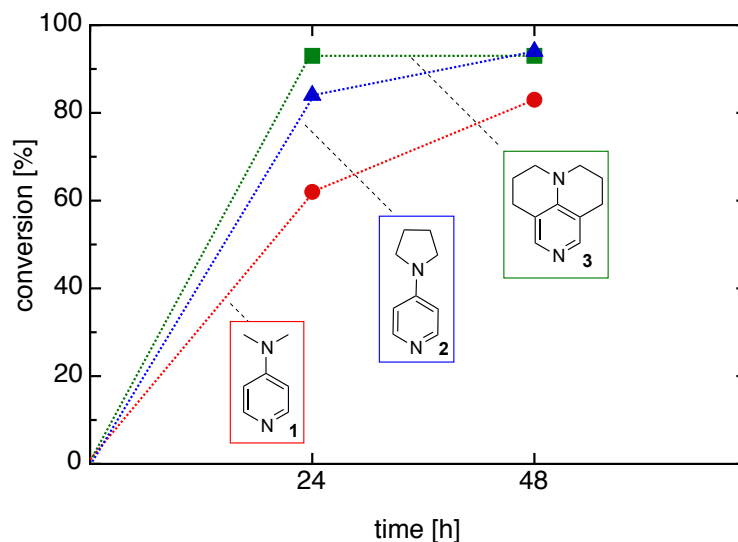


Figure 2.6.1. Conversion vs. time of DMAP (**1**, red circles), PPY (**2**, blue triangles) and 9-azajulolidine (**3**, green squares) for a reaction mixture of lactide/benzyl alcohol/catalyst 100:1:1.3 at 100 °C in THF in the microwave.

The GPC analysis of the reaction mixtures of DMAP (**1**), PPY (**2**) and 9-azajulolidine (**3**) revealed, that for longer reaction times the degree of polymerization is stable for DMAP (**1**) and PPY (**2**), but strongly decreases over time when 9-azajulolidine (**3**) is used as catalyst (see Figure 2.6.2).

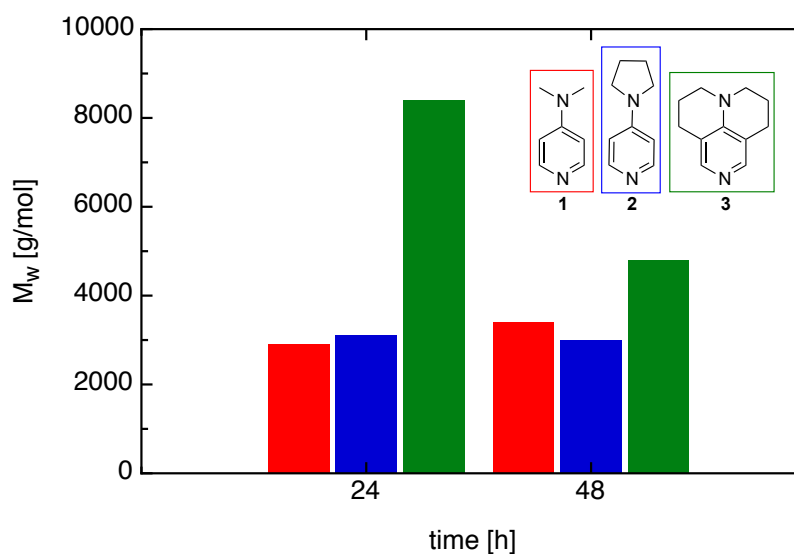


Figure 2.6.2. Conversion vs. time of **1** (red bar), **2** (blue bar) and **3** (green bar) for a reaction mixture of lactide/benzyl alcohol/catalyst 100:1:1.3 at 100 °C in THF in the microwave.

Detailed studies of the polymer length at different reaction times indicate that DMAP (**1**) keeps catalyzing the polymerization of lactide without transesterification of the polylactide backbone,^[1] but 9-azajulolidine (**3**) shows the strong tendency to catalyze not only the polymerization of lactide, but also the depolymerization of polylactide at longer reaction times (see Figure 2.6.3).

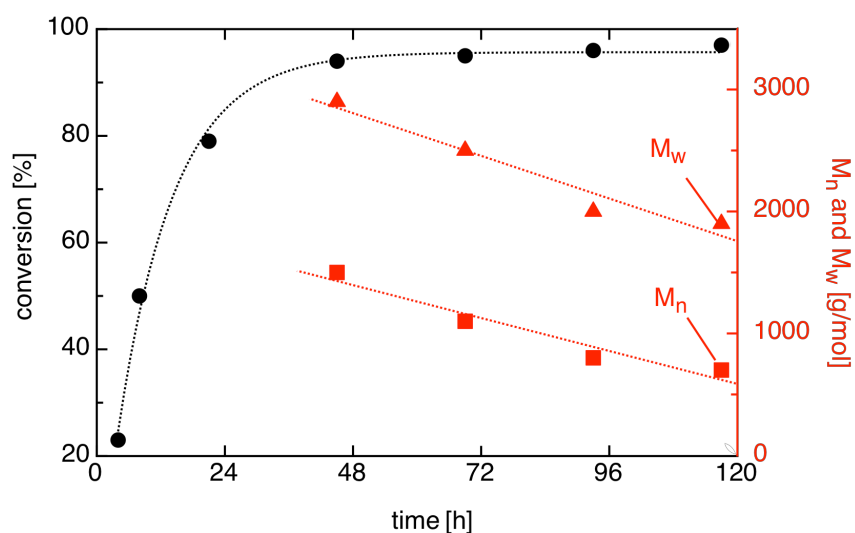


Figure 2.6.3. Conversion vs. time plot of 9-azajulolidine (**3**, black circles) for a reaction kinetic with lactide/benzyl alcohol/catalyst at a ratio of 100:1:1 at 100 °C in THF in the microwave combined with the number (M_n , red squares) and mass (M_w , red triangles) averaged molar masses vs. time plot of the same reaction.

The order of reaction for 9-azajulolidine in the ROP of lactide is found to be rather second order ($R^2 = 0.9824$) than first order ($R^2 = 0.9227$) when using a microwave reactor as the source of heat. Under similar reaction conditions with the exception of using an oil bath at 50 °C as the source of heat and CDCl_3 as solvent, a clear first order rate law was obtained, which is generally found according to mechanistic studies using DMAP (**1**) or PPY (**2**) as organocatalysts.^[1,3,7]

Utilizing microwave technology for the ROP using organocatalysts in melt, we encountered problems, most likely due to uneven heat distribution leading to decomposed material. For the ROP of lactide in solution microwave technology seems to be an attractive alternative to conventional heating in an oven due to dramatically reduced reaction times. Concerning the ratio of lactide/benzyl alcohol/organocatalyst 200:1:1 gave higher mass and number averaged molar masses and better polydispersity values as well. The addition of co-catalysts like 4-nitrophenol yields smaller averaged molar masses in the polymer. It can be stated that the usage of organocatalysts in combination with microwave technology could be a very powerful combination for the ROP of lactides but conditions still need to be improved and optimized.

References

- [1] a) A. Chuma, H. W. Horn, W. C. Swope, R. C. Pratt, L. Zhang, B. G. G. Lohmeijer, C. G. Wade, R. M. Waymouth, J. L. Hedrick, J. E. J. Rice, *J. Am. Chem. Soc.* **2008**, *130*, 6749–6754. b) M. Kieseewetter, E. Shin, J. Hedrick, R. Waymouth, *Macromolecules* **2010**, *43*, 2093–2107. c) F. Nederberg, E. Connor, M. Möller, T. Glauser, J. Hedrick, *Angew. Chem. Int. Ed.* **2001**, *40*, 2712–2715.
- [2] a) J. Kadota, D. Pavlovic, J.-P. Desvergne, B. Bibal, F. Peruch, A. Deffieux, *Macromolecules* **2010**, *43*, 8874–8879.
- [3] a) F. Nederberg, E. F. Connor, T. Glauser, J. L. Hedrick, *Chem. Commun.* **2001**, 2066–2067. b) F. Nederberg, E. F. Connor, M. Moller, T. Glauser, J. L. Hedrick, *Angew. Chem. Int. Ed.* **2001**, *40*, 2712–2715. c) H. R. Kricheldorf, N. Lomadze, G. Schwarz, *Macromolecules* **2008**, *41*, 7812–7816. d) H. R. Kricheldorf, N. Lomadze, G. Schwarz, *Macromolecules* **2007**, *40*, 4859–4864. e) H. R. Kricheldorf, C. Von Lossow, G. J. Schwarz, *Polym. Sci. Part A: Polym. Chem.* **2006**, *44*, 4680–4695.
- [4] M. R. Heinrich, H. S. Klisa, H. Mayr, W. Steglich, H. Zipse, *Angew. Chem.* **2003**, *115*, 4975; *Angew. Chem. Int. Ed.* **2003**, *42*, 4826–4828.
- [5] I. Held, S. Xu, H. Zipse, *Synthesis* **2007**, 1185–1196. b) H. Zipse, I. Held, Bayer Material Science LLC, US 2008/0176747A1, **2008**.
- [6] C. Lindner, R. Tandon, Y. Liu, B. Maryasin, H. Zipse, *Org. Biomol. Chem.* **2012**, *10*, 3210–3218.
- [7] a) L. Simon, J. M. Goodman, *J. Org. Chem.* **2007**, *72*, 9656–9662. b) A. Chuma, H. W. Horn, W. C. Swope, R. C. Pratt, L.;Zhang, B. G. G. Lohmeijer, C. G. Wade, R. M. Waymouth, J. L. Hedrick, J. E. Rice, *J. Am. Chem. Soc.* **2008**, *130*, 6749–6754. c) C.-L. Lai, H. M. Lee, C.-H. Hu, *Tetrahedron Lett.* **2005**, *46*, 6265–6270.

2.7 Platelet Inhibition by the Natural LXR Agonist 22(R)-OH-Cholesterol and its Fluorescence Labeling with Full Bioactivity

Two synthetic LXR agonists were recently shown to inhibit collagen-induced platelet aggregation and thrombus formation in mice by non-transcriptional interference with collagen receptor signalling.^[1] We studied herein whether also natural LXR agonists affect platelets and whether they can be fluorescence labelled preserving their bioactivity for LXR related functional imaging.

The fluorescence labelled 22-OH-cholesterols were synthesized utilising a slightly modified variant of the Steglich reaction.^[2] Initially the esterification reaction of 22(R)-OH-cholesterol and BODIPY[®] FL C3 resulted in just 4% yield under standard reaction conditions. As a

model system for optimising the reaction conditions, commercially available cholesterol and palmitic acid were used on a 100 mg scale. With prices of over 100 € for 1 mg 22(*R*)-hydroxycholesterol an effort was made to scale the reaction down to milligram quantities of substrate. Owing to the unusual small reaction scale a purpose-built microreactor allowed the handling of substrates on the 0.5 - 1 mg scale under inert gas conditions (Figure 2.7.1).

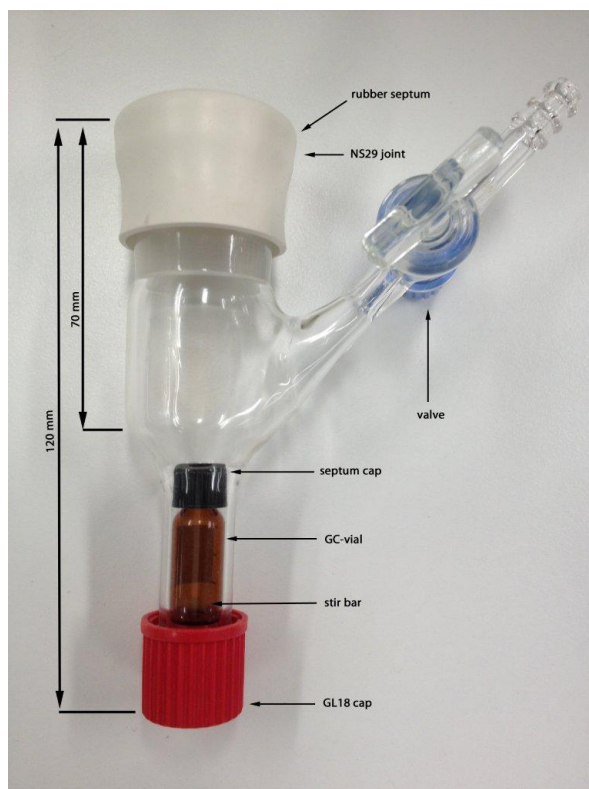
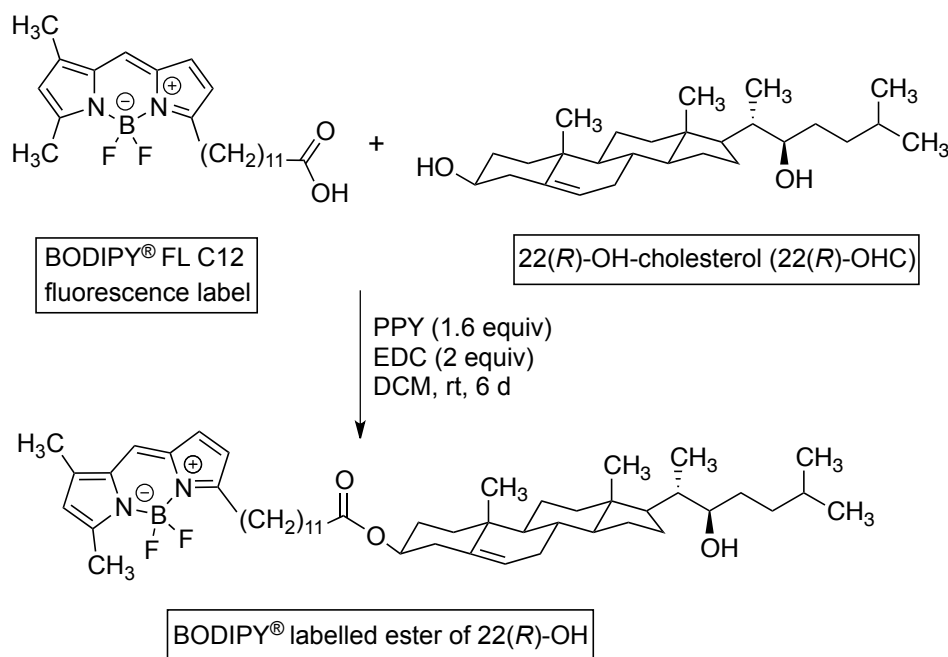


Figure 2.7.1. Microreactor for small scale esterification reactions under inert gas conditions.

Utilising this microreactor setup and the optimized reaction conditions, the 22(*S*)- as well as the 22(*R*)-OH-cholesterols could be fluorescence labelled by a Steglich-type esterification reaction with BODIPY[®] FL C12 with yields up to 90 % (determined by fluorescence spectrometry) on a 0.5 mg scale (Scheme 2.7.1).



Scheme 2.7.1. Reaction of BODIPY[®] FL C12 with 22(*R*)-OH-cholesterol under optimized reaction conditions in a purpose-built microreactor on a 0.5 mg scale.

When the labelled 22(*R*)- and 22(*S*)-OHC-BP esters were tested in platelets, we found that the stereospecific bioactivity of their unlabelled parent compounds was fully preserved. This fits well with the localization of intrinsic activity to the 22(*R*)-hydroxy configuration of the sterol side chain^[3,4] and demonstrates that the bulky fluorescence label esterified to the sterol 3-hydroxy group does not hinder LXR binding and activation. Incubation of macrophages with 22(*R*)- or 22(*S*)-OHC-BP showed characteristic differences in the time course, intracellular localization and structure of the staining. Whereas macrophage exposure to 22(*R*)-OHC-BP caused a sustained, diffuse, strictly nuclear localization of the label, 22(*S*)-OHC-BP resulted in a rapid but transient, granular, cytosolic accumulation of the label (see Figure 2.7.2). This parallels the well established lack of genomic LXRA agonistic effects of 22(*S*)-OHC in macrophages, hepatocytes and cells transfected with LXRA reporter gene constructs.^[3,4]

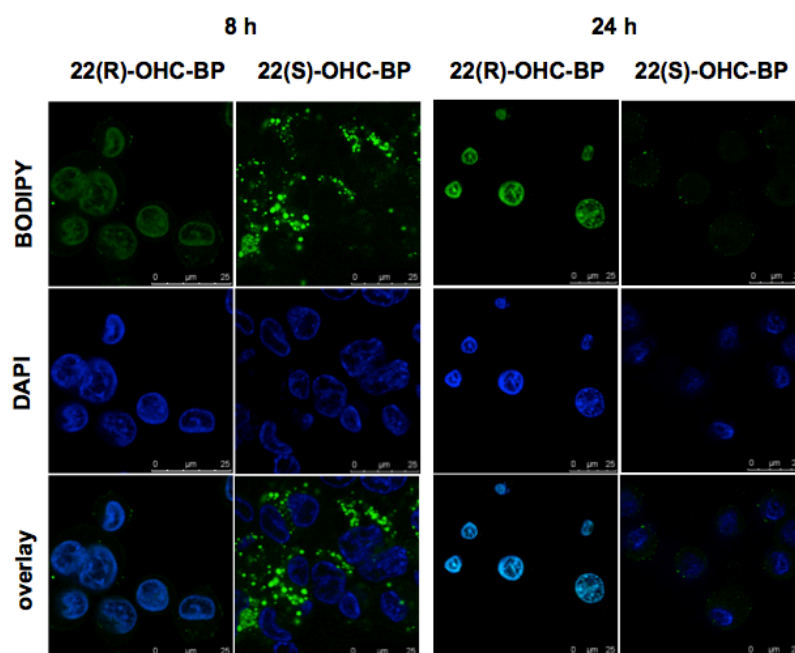


Figure 2.7.2. Confocal laser fluorescence microscopy of U937 cells incubated for 8 h (left) and 24 h (right) with 22(*R*)- or 22(*S*)-OHC-BP (1 μ M) as indicated and counterstained with DAPI. Top row: BODIPY (green). Middle row: DAPI (blue). Bottom row: overlay.

Consistent with preserved binding and intrinsic activity the fluorescence-labelled esters 22(*R*)- and 22(*S*)-OHC-BP showed stereospecific differences, too, when used for life cell staining in platelets and human macrophage cell lines. The natural LXR agonist 22(*R*)-OH-cholesterol (22(*R*)-OHC), but not its stereoisomer 22(*S*)-OHC (even at high concentrations), inhibited collagen induced platelet shape change and aggregation in a concentration- and time-dependent manner similar to synthetic LXR agonists. The stereospecificity of the 22(*R*)-OHC effect on collagen-induced platelet aggregation strongly supports LXR as the target molecule and argues against an undetected coincident mechanism of platelet inhibition by the synthetic compounds. The effects of 22(*R*)-OHC further demonstrate the potential of endogenous LXR ligands to modify platelet function. 22(*R*)-OHC-BP and 22(*S*)-OHC-BP can thus be versatile tools for combined functional and microscopic studies of LXR related pathomechanisms and for current drug development of LXR modulators.^[5]

References

- [1] M. Spyridon, L. A. Moraes, C. I. Jones, T. Sage, P. Sasikumar, G. Bucci, J. M. Gibbins, *Blood* **2012**, *117*, 5751–5761.
- [2] B. Neises, W. Steglich, *Angew. Chem. Int. Ed. Engl.* **1978**, *17*, 522–524.
- [3] B. A. Janowski, P. J. Willy, T. R. Devi, J. R. Falck, D. J. Mangelsdorf, *Nature* **1996**, *383*, 728–731.

- [4] T. A. Spencer, D. Li, J. S. Russel, J. L. Collins, R. K. Bledsoe, T. G. Consler, L. B. Moore, C. M. Galardi, D. D. McKee, J. T. Moore, M. A. Watson MA, D. J. Parks, M. H. Lambert, T. M. Willson, *J. Med. Chem.* **2001**, *44*, 886–897.
- [5] E. Viennois, K. Mouzat, J. Dufour, L. Morel, J. M. Lobaccaro, S. Baron, *Mol. Cell Endocrinol.* **2012**, *351*, 129–141.

Chapter 3

Annelated Pyridines as Highly Nucleophilic and Lewis-Basic Catalysts for Acylation Reactions

Raman Tandon, Teresa Unzner, Tobias A. Nigst, Nicolas De Rycke, Peter Mayer, Bernd Wendt, Olivier R. P. David, Hendrik Zipse, Chem. Eur. J. 2013, 19, 6435 – 6442.

Results obtained by co-authors are omitted in the Experimental Part. Catalysts **6a,b,c** are not included in the publication, but the data were added to Table 3.1 and the synthesis to the Experimental Part for completeness of contents.

3.1 Introduction

The catalytic potential of donor-substituted pyridines in acylation reactions is well established since the reports on 4-*N,N*-dimethylaminopyridine (DMAP, **1**) by Litvinienko *et al.* in 1967 and by Steglich *et al.* in 1969.^[1,2,3] A small improvement in catalytic activity was soon after documented for 4-(pyrrolidinyl)pyridine (PPY, **2**),^[4] but it took until 2003 that a larger increase in activity could be realized with annelated pyridines such as 9-azajulolidine (**3**).^[5] Pyridine derivative **3** is a powerful organocatalyst not only suitable for acylation reactions, but also for other transformations such as the aza-Morita Baylis Hillman reaction.^[6] Further development of this class of catalysts through modification of the attached ring systems thus seems desirable, but faces significant synthetic hurdles.

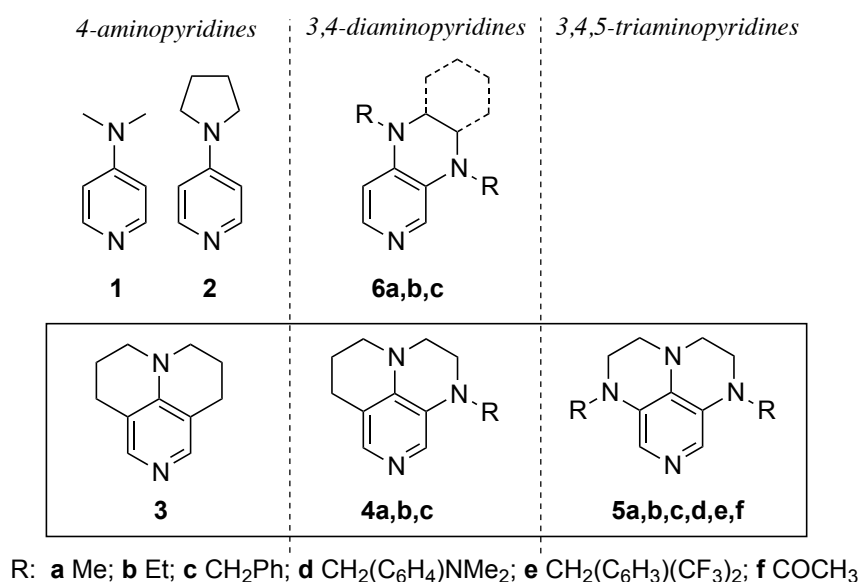


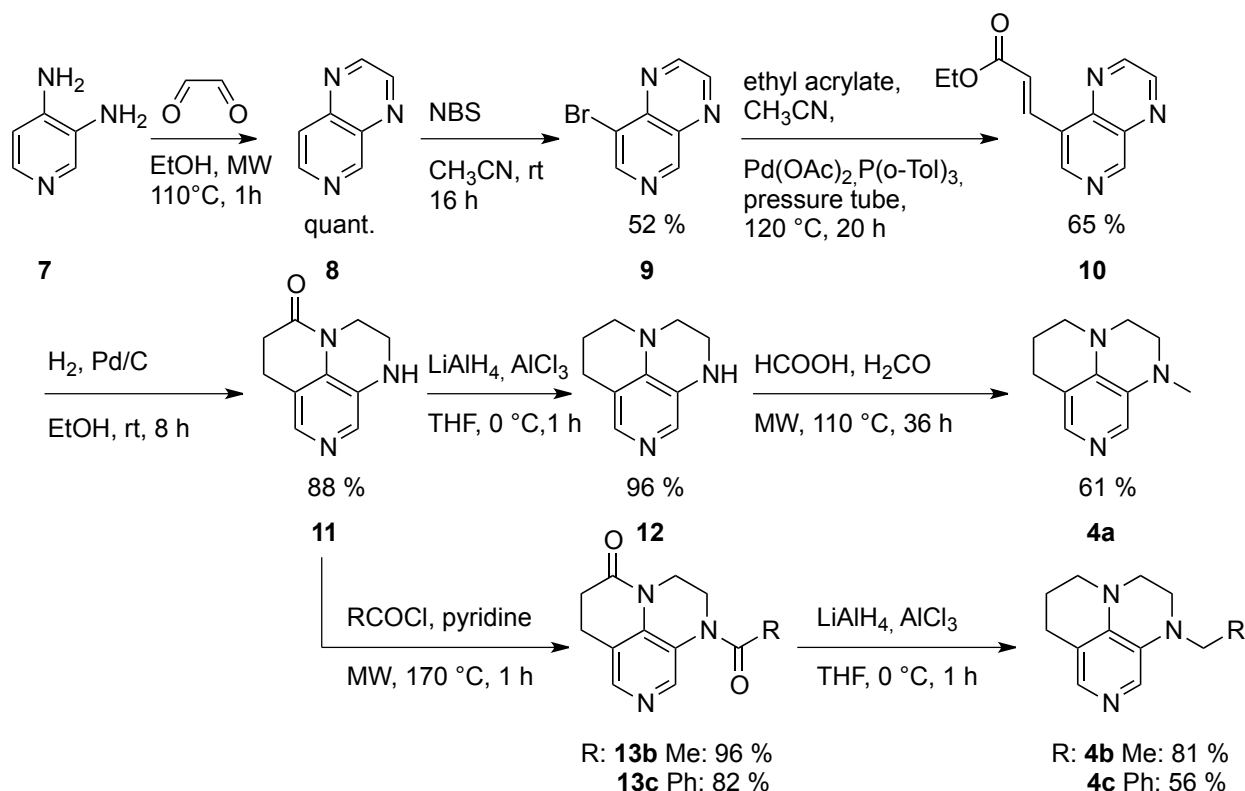
Figure 3.1. Structures of pyridine derivatives based on the DMAP motif used as nucleophilic organocatalysts.

We, therefore, explore here the potential of the respective di- and tri-nitrogen-substituted systems **4** and **5** (Figure 3.1). Selected members of this family were recently characterized with respect to their affinity towards carbocation electrophiles.^[7] These data show that the additional amino-substituents attached to the 3- and 5-position of pyridines **4** and **5** further increase the Lewis basicity relative to the all-carbon analogue **3**. Furthermore, for some derivatives of **5** it was recently shown in kinetic studies that the reaction rates for addition to benzhydryl cations correlate with theoretically calculated Lewis basicities.^[8] We now show here how the Lewis base properties of the tricyclic catalysts **3** - **5** depend on their particular substituent pattern, and also test the catalytic activity of these compounds using the acylation of 1-ethynylcyclohexanol as a benchmark reaction.

3.2 Results and Discussion

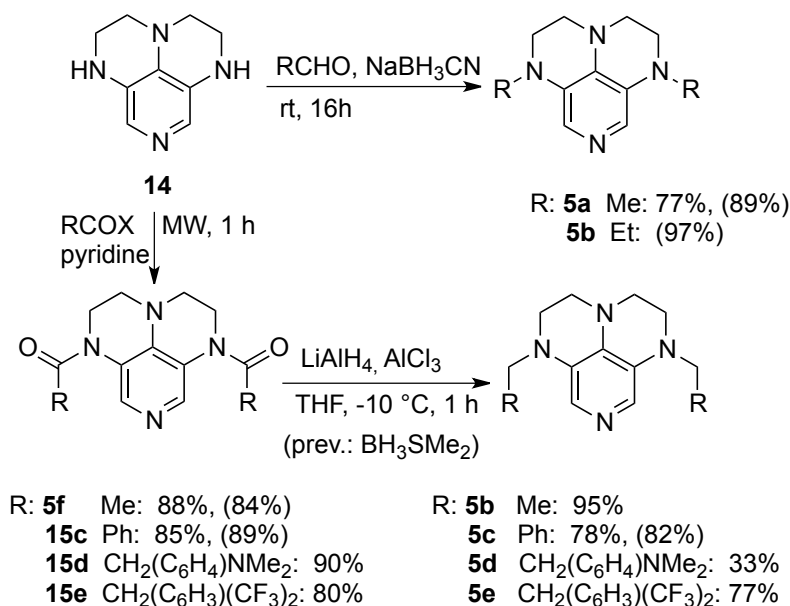
Synthesis and Structure

The synthesis of catalysts of general structure **4** follows the same strategy used to access pyridine derivatives **6**.^[9,10] This involves initial condensation of 3,4-diaminopyridine **7** with glyoxal and subsequent bromination at C5 position of the pyridine ring with NBS in acetonitrile at room temperature. Subsequent Heck reaction of **9** with ethyl acrylate worked best on larger scale with minimal solvent in a pressure tube. The reduction and immediate cyclization of **10** to core structure **11** was accomplished using palladium on charcoal in 88% yield. Catalysts **4a** - **4c** can all be synthesized starting from **11**. Synthesis of **4a** was accomplished through reduction with LiAlH₄/AlCl₃ to furnish 96% of **12** and subsequent Eschweiler-Clark reaction providing *N*-methylated product **4a** in 61% yield (Scheme 3.1). It should be added that the acidic reaction conditions used under Eschweiler-Clark conditions are significantly more effective than alkylation under basic conditions due to the intermediate protonation (and thus deactivation) of the pyridine nitrogen atom. Catalysts **4b** and **4c** were synthesized by microwave-induced acylation of the amino group with the appropriate acid chloride in pyridine. The acylated species **13b** (96 %) and **13c** (82 %) were obtained in good to excellent yields. Subsequent reduction of both amide groups in **13** with LiAlH₄/AlCl₃ furnished **4b** (81 %) and **4c** (56 %) in just one hour reaction time.



Scheme 3.1. Synthesis of compounds **4a,b,c** from 3,4-diaminopyridine **7** and glyoxal.

Catalysts **5a–e** were all synthesized starting from the 3,4,5-triaminopyridine derivative **14**, whose efficient synthesis was recently described by *David et al.*^[8] While catalyst **5a** was synthesized in 77% yield via reductive amination according to the originally proposed route (Scheme 3.2),^[8] minor modifications in workup procedures and the choice of reducing agents were introduced in the synthesis of **5b** and **5c**. Changes include the use of microwave irradiation (instead of conventional heating) in the respective acylation reactions, which reduces reaction times for the acylation of **14** from 6 hours (**5f**) or 3 days (**15c**) to just one hour (for both systems) without any detriment of yield. Final reduction of the bisamides **15** was accomplished with $\text{LiAlH}_4/\text{AlCl}_3$ (instead of $\text{BH}_3\cdot\text{SMe}_2$) in just one hour at $-10\text{ }^\circ\text{C}$ yielding **5b** and **5c** in comparable yields (Scheme 3.2). Following the same strategy additional derivatives of **5** bearing strongly electron donating groups in the aryl ring as in **5d** as well as electron withdrawing groups as in **5e** were synthesized in order to investigate different electronic effects on the catalyst reactivity. The acylation of **14** with four different acyl donors and subsequent reduction of the amide intermediates proceeded smoothly and in good to excellent yields in all cases, except for catalyst **5d**. Due to the high basicity of this latter compound the final product isolation and purification steps after reduction of amide **15d** could only be executed with substantial loss of material.

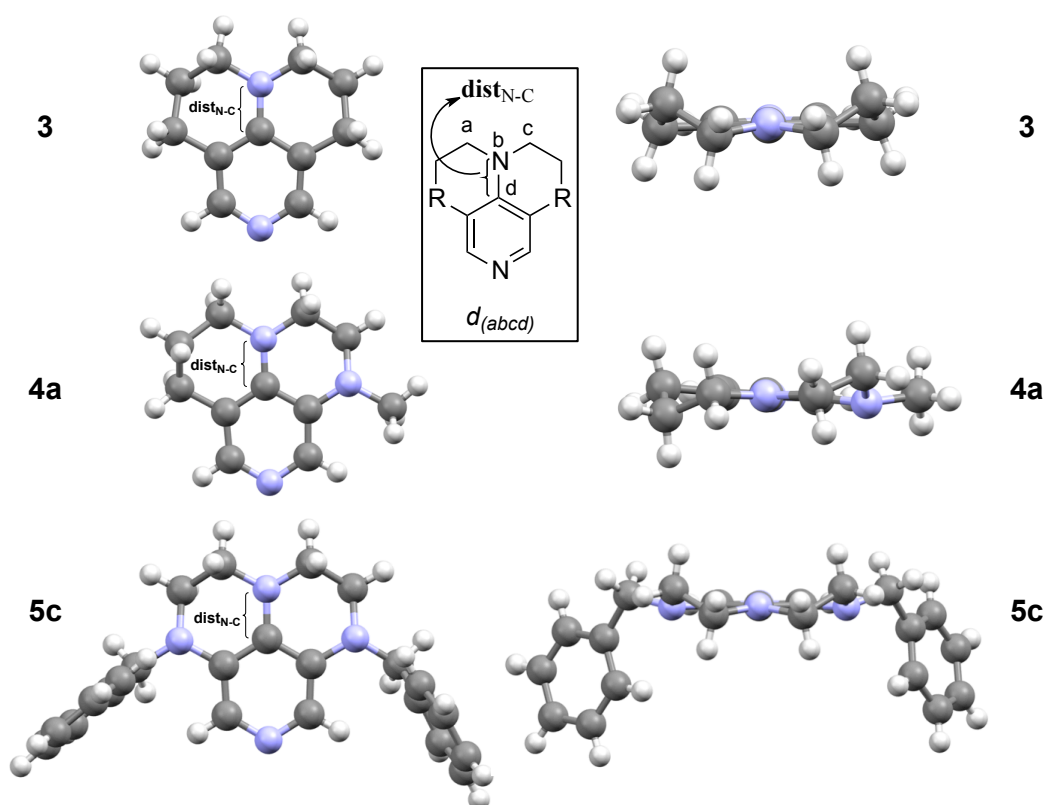


Scheme 3.2. Synthesis for catalysts **5a–e**. Previously obtained yields by *David et al.*^[8] are given in brackets.

It should be added at this point that purification of compounds of type **4** and **5** requires repeated chromatography on basic aluminum oxide^[11] (Brockmann 3) until ^1H NMR analytically pure material was obtained. Such material solidified on standing and was further purified through recrystallization from ethyl acetate under nitrogen and dried in high vacuum for at least 8 h and stored in an exsiccator in the dark at $-4\text{ }^\circ\text{C}$. The evaporation of solvent in all synthetic and purification steps of **4** and **5** was performed in a rotatory evaporator operated under nitrogen and at a water bath temperature not exceeding $30\text{ }^\circ\text{C}$. The catalytic activity of

4 and **5** depends significantly on their purity, and deviations from the purification protocol outlined above may thus lead to significant reduction of reaction rates.

The Lewis basicity of amino-substituted pyridines depends on the alignment of the substituent nitrogen lone pair orbital with the pyridine π -system. Structural parameters connected to this orbital interaction are the 4-NC bond distance **dist_{N-C}** (the distance between the pyridine carbon atom and the nitrogen at the 4-position) as well as the degree of pyramidalization of the nitrogen substituent ($d_{(abcd)}$). Shorter N-C bond distances and smaller pyramidalization angles are commonly considered to reflect better orbital alignment. These parameters are shown in Figure 3.2 in the crystal structures of pyridines **3**, **4a** and **5** as depicted in front (left) and top (right) view.



	3		4a		5c	
	dist_{N-C} /pm	$d_{(abcd)}$	dist_{N-C} /pm	$d_{(abcd)}$	dist_{N-C} /pm	$d_{(abcd)}$
crystal structure	137.5	12.7 °	137.3	1.0 °	137.7	11.4 °
best conformer ^[a]	138.8	12.9 °	139.4	2.1 °	140.4	21.1 °

[a] MP2/6-31+G(2d,p)/B98/6-31G(d) with PCM/UAHF/RHF/6-31G(d) solvation energies for chloroform.

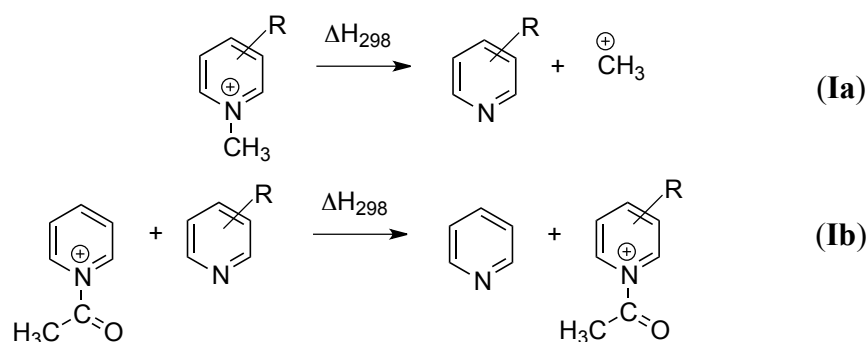
Figure 3.2. Crystal structures of **3**, **4a**, and **5c**. 4-NC bond distances (**dist_{N-C}** /pm) and pyramidalisation angles $d_{(abcd)}$ of crystal structure and best computed conformer.

The 4-NC bond lengths in the crystal structures of mono-, di- and triaminopyridines are actually identical within experimental uncertainty (137.5 ± 0.2 pm), whereas the structures optimized at B98/6-31G(d) level (best conformer each) show slightly larger bond lengths in all cases. For the pyramidalisation angles ($d_{(abcd)}$) the best conformers of **3** and **4a** reflect the

experimental results very well. For **5c** the best conformer shows a 10° higher pyramidalisation angle as compared to the crystal structure. For this latter system a second conformer exists only 1 kJ mol^{-1} higher in energy with a deformation angle of 10.7° , which is closely similar to the crystal structure. This implies that conformational reorientation of the annelated 6-membered rings and accompanying variations in the pyramidalization of the central nitrogen atom occurs with rather little increase in energy. From all structures analyzed it appears that catalysts **4a** and **5d** (Experimental Part) provide the best orbital alignment between the nitrogen lone pair electrons and pyridine π -system.

Cation Affinity Data

In order to match these structural properties to actual Lewis basicities, methyl cation affinities (MCA) and acylation enthalpies ΔH_{ac} as defined in equations **1a** and **1b** have been collected in Table 3.1 for most of the synthesized pyridines.



Scheme 3.3. Definitions of methyl cation affinities (**1a**) and isodesmic acetyl transfer reaction (**1b**).

The definition chosen here for methyl cation affinities follows the mass spectrometric definition of the gas phase proton affinity as recently applied to a larger number of Lewis bases.^[12,7] The acylation enthalpies as defined in eq. **1b** reflect relative acetyl cation affinities between the selected Lewis base and pyridine as the reference system. This latter definition was also used in previous studies matching the Lewis basicities of pyridines with the respective catalytic activity in acylation reactions. Both measures of Lewis basicity have been quantified here at the MP2/6-31+G(2d,p)//B98/6-31G(d) level of theory in the gas phase. How solvent effects impact the Lewis basicity has been tested for the acylation enthalpies using the polarizable continuum model (PCM) in chloroform at the RHF/6-31G(d) level with UAHF radii. All three types of affinity data indicate quite clearly, that all tricyclic catalysts displayed in Figure 3.1 are stronger Lewis bases than the parent DMAP. The triaminopyridine **5d** is the strongest Lewis base, irrespective of the choice of Lewis basicity indicator.

Table 3.1. Half-live times and affinity numbers for synthesized catalysts.

cat.	MCA [kJ/mol]	ΔH_{ac} MP2-5 ^[a] [kJ/mol]	$\Delta H_{ac/solv}$ MP2-5/solv ^[a] [kJ/mol]	$N(s_N)^{[b]}$	$t_{1/2}^{[c]}$ [min]
10 mol-% catalyst loading					
5d	661.3	-163.7	-106.7	-	38.4 ± 1.0
5c	636.8	-141.3	-98.3	17.69 (0.57) ^[e]	65.4 ± 3.1
5b	621.6	-120.6	-87.8	16.81 (0.60) ^[e]	44.2 ± 1.5
4c	620.8	-123.4	-90.2	-	34.3 ± 0.2
5a	618.7	-118.0	-89.2	16.65 (0.58) ^[e]	38.0 ± 1.5
6b	616.0	-118.2	-85.2	16.65 (0.64)	18.0 ± 0.5 ^[h]
4b	613.3	-113.5	-87.5	-	13.8 ± 0.4
4a	611.0	-111.0	-86.8	-	17.9 ± 0.9
6a	609.1	-108.2	-79.4	-	21.3 ± 1.1
3	602.7	-102.3	-82.2	15.60 (0.68)	14.7 ± 0.5 ^[g]
5e	596.8	-101.5	-69.5	-	227.3 ± 0.5
2	590.1	-87.5	-67.6	14.99 (0.68)	67 ± 0.1 ^[h]
1	581.2	-77.1	-61.2	14.95 (0.67) ^{[e],[f]}	151.0 ± 1.7 ^[h]
6c	-	-124.1	-81.4	-	94.0 ± 4.1 ^[i]
18	-	-90.1 ^[d]	-55.0 ^[d]	-	878.1 ± 59.9
5f	-	-71.6	-48.2	15.39 (0.60) ^[e]	≥ 2880 ^[j]
3 mol-% catalyst loading					
4b	613.3	-113.5	-87.5	-	45.9
4a	611.0	-111.0	-86.8	-	57.4
6b	616.0	-118.2	-85.2	16.65 (0.64)	57.7
6a	609.1	-108.2	-79.4	-	68.9
3	602.7	-102.3	-82.2	15.60 (0.68)	46.7

[a] Levels of theory: “MP2-5”: MP2/6-31+G(2d,p)/B98/6-31G(d), “MP2-5/solv”: MP2/6-31+G(2d,p)/B98/6-31G(d) with PCM/UAHF/RHF/6-31G(d) solvation energies for chloroform; [b] Nucleophilicity parameters in acetonitrile according to equation (II); [c] Kinetic half-life times for acylation reaction (III); [d] Extrapolated (for details Experimental Part); [e] Data from ref. [8]; [f] New measurements: 15.51 (0.62)^[14]; [g] Remeasured and in line with published data (15 ± 0.1)^[10]; [h] Data from ref. [10]; [i] Catalyst was resynthesized and remeasured. The obtained data are not in line with the published ones (116 ± 2.0)^[18]; [j] Extrapolated (13 % conversion after 12h).

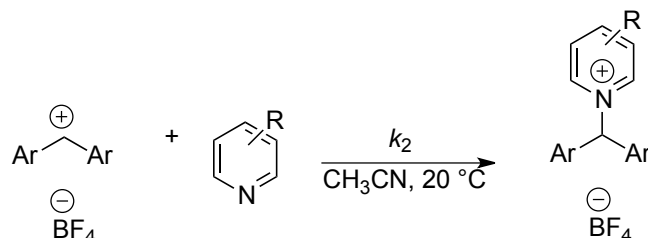
Nucleophilicity

In how far the theoretically calculated Lewis basicities correlate well with reaction rates for reaction with reference electrophiles was next tested for additions to benzhydrylium cations. This type of addition reaction provides the basis for Mayr's comprehensive nucleophilicity scale according to the linear free energy relationship (eq. II).

$$\log k_2 (20\text{ }^\circ\text{C}) = s_N(N + E) \quad (\text{II})$$

The rate constants for nucleophile/electrophile combination reactions k_2 were determined as described in the Experimental Part. The k_2 values were combined with the solvent independent electrophilicity parameter E for different cations (see SI) to yield the solvent dependent nucleophilicity parameter N (nucleophilicity) and s_N (nucleophile-dependent

sensitivity) as shown in Scheme 3.4 and Figure 3.3. These parameters are available for a variety of pyridines in several solvents such as CH_2Cl_2 and CH_3CN .^[13]



Scheme 3.4. Reactions of pyridines with benzhydrylium cations in CH_3CN at 20°C .

In order to compare the nucleophilic reactivities of **1** – **5** with the corresponding acylation enthalpies according to equation **1b** the nucleophilicity parameters of **2** and **3** were determined in acetonitrile (Figure 3.4).

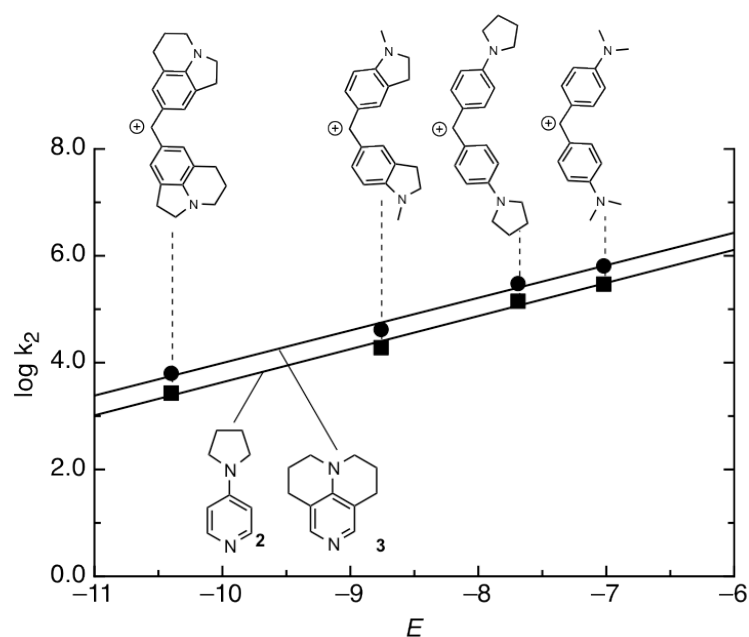


Figure 3.3. Determination of nucleophilicity parameters N and s_N (nucleophile-dependent sensitivity) through combination of rate constants k_2 with electrophilicity parameter E for different cations.

Figure 3.4 shows that the nucleophilic reactivities of pyridines **1-3**, **5** correlate quite well (with $R^2=0.9022$) with acylation enthalpies in chloroform solution and even better with the gas phase acylation enthalpies ($R^2=0.9702$) (see Experimental Part). We can thus conclude that the kinetic data for single-step addition to cationic electrophiles are related to the thermodynamic data for this structurally quite homogenous set of nucleophiles.

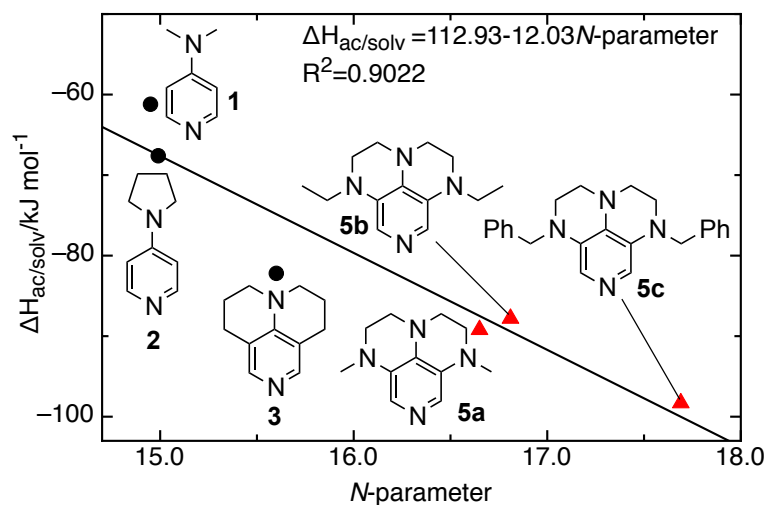
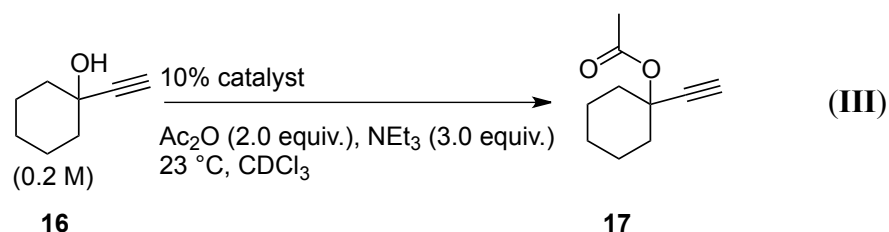


Figure 3.4. Correlation of acylation enthalpies ($\Delta H_{ac/solv}$) with *N*-parameters.

Catalytic Activity

The catalytic potential of the synthesized catalysts has been explored in the acetylation of tertiary alcohol **16** (reaction (III), Scheme 3.5). The reactions were followed by ¹H NMR spectroscopy in CDCl₃ as the solvent. All reactions eventually proceed to full conversion and the rates of the reactions can thus be characterized by the reaction half-life $t_{1/2}$ using an approach described previously.^[10] As expected from the calculated Lewis basicities and the experimentally measured *N*-parameters, all annelated pyridine derivatives are more reactive than DMAP (**1**) (Table 3.1, last column).



Scheme 3.5. Acylation reaction (III) in CDCl₃.

The substantial influence of conformational fixation on the reactivity is illustrated by the 60-fold decrease in activity going from catalyst **3** to **18** (compare Table 3.1, the structure of catalyst **18** is depicted in Figure 3.5). In catalyst **18** formally even more inductive effects than in the annelated **3** are present but without any conformational fixation.

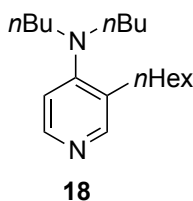


Figure 3.5. Conformationally unrestricted catalyst **18**.

A comparison of the catalytic activities of the annelated catalyst systems shows that the conformationally constrained 4-aminopyridine **3** and the 3,4-diaminopyridines **4** are significantly more active than the 3,4,5-triaminopyridines **5**. This is in remarkable contrast to the rather high Lewis basicities and *N*-parameters determined for this latter class of nucleophiles. The optimum balance between catalytic activity and nucleophilicity is thus achieved in pyridines **3** and **4**, where one or two nitrogen atoms are incorporated into conformationally restricted ring systems. The most active catalyst is the newly synthesized catalyst **4b**, which displays an even shorter half-life time than the most active catalyst **6b** in previous studies^[10] and is also slightly faster than the top performer 9-azajulolidine (**3**). These catalysts are more than 10 times more active than DMAP (**1**) (151 min) and thus very potent acyl transfer reagents. It is of note that in series **4** ethyl substituted compounds are slightly more efficient than methyl derivatives, whereas in the 3,4,5-triaminopyridine series the ethyl substituted compound **5b** is less effective than the methyl substituted **5a**. The benzylic compound **4c** is, in comparison, much less active than the alkyl substituted compounds **4a** and **4b**. This ordering is also found for the 3,4,5-triaminopyridines **5a,b,c**. Comparison of the benzylic compounds **5c**, **5d** and **5e** shows that electron-donating groups shorten the reaction half-life while electron-withdrawing groups decrease the catalytic activity tremendously (e.g. **5e** has a half-life time of 227 min whereas that of **5c** amounts to 65 min).

Reaction times are very short at 10% catalyst loading for some of the annelated pyridine derivatives, making precise measurements and an accurate comparison of the most active systems difficult. Reaction rates for these systems were therefore redetermined at 3% catalyst loading. From the conversion data shown in Figure 3.6 and reaction half-lives in Table 3.1 one can see that catalysts **4b** and **3** are equally active under these conditions. With reaction half-lives of 46-47 min they are more than three times faster at 3% catalyst loading than DMAP (**1**) at 10% loading and thus the fastest catalysts among the highly nucleophilic pyridines. With a half-life of 57.4 min catalyst **4a** is still somewhat less active than **3** and **4b**, but still more active at 3 mol-% than PPY (**2**) at 10 mol-%.

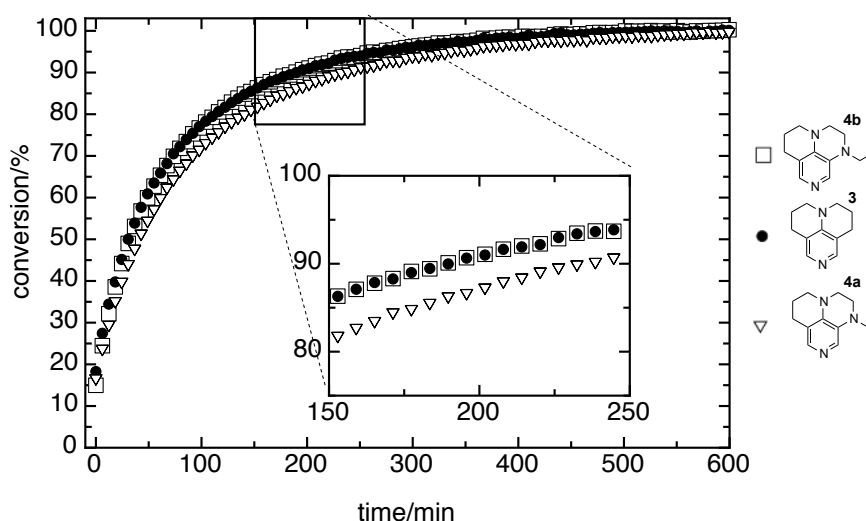


Figure 3.6. Conversion-time plots for catalysts **4b**, **3**, and **4a** at 3 mol% catalyst loading.

The unexpectedly moderate catalytic activity of the strongly Lewis basic 3,4,5-triaminopyridines **5** raises the question whether the reaction mechanism is the same for all aminopyridines studied here. One of the key questions concerns the dependence of the reaction rate on the catalyst concentration. Earlier studies had established a clear first-order dependence for aminopyridines such as DMAP (**1**) for benchmark reaction **III**.^[15] Using catalyst concentrations between 2.5 -10 mol% a first-order dependence can also be established for the triaminopyridine **5c** (Figure 3.7), which is one of the most Lewis basic candidates of series **5**. This excludes the possibility that a second catalyst molecule acts as general base in the rate limiting step. The rather small intercept of the correlation line with the ordinate axis also indicates a negligible background reaction and the reaction mechanism thus seems to be identical to that for DMAP (**1**).

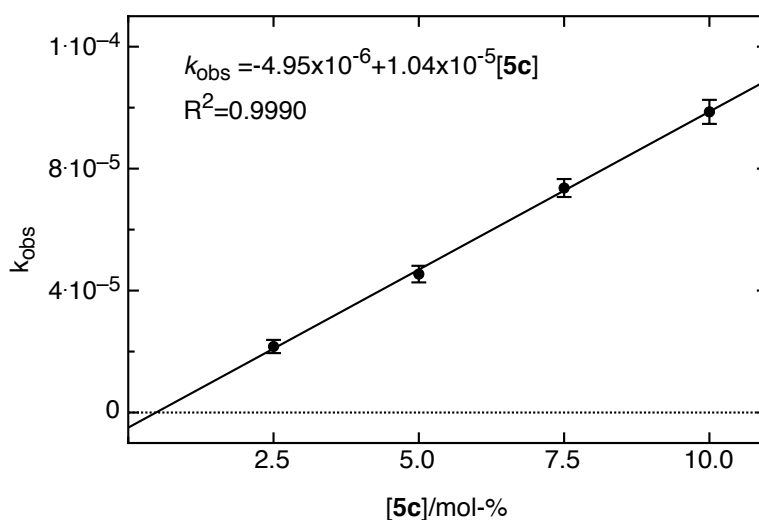
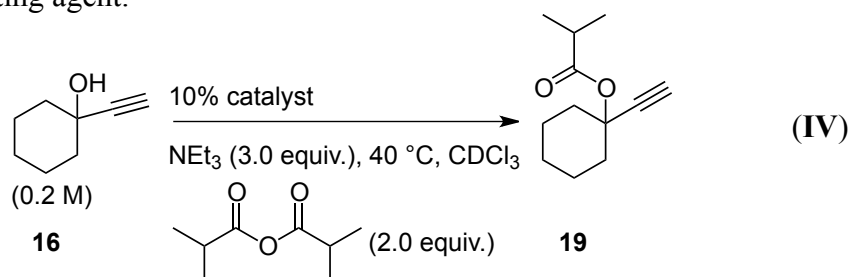


Figure 3.7. Variation of reaction rate as a function of the concentration of catalyst **5c** in acylation reaction **III**.

How annelated catalysts **5** respond to changes in the steric demand of the acylating reagent was subsequently tested by reacting alcohol **16** with isobutyric anhydride. These studies were performed at slightly elevated temperatures (40 °C) in deuteriochloroform (reaction **IV**). As reported earlier for simple aminopyridines such as PPY (**2**), the rates of reaction for this latter transformation are much lower as compared to that of benchmark reaction **III** (Table 3.2). The ratio of half-life times for these two transformations displays a distinct dependence on the absolute catalyst activity in that the most active catalyst **3** reacts most sensitively to the steric demand of the acylating agent.



Scheme 3.6. Isobutyrylation of alcohol **16** in CDCl₃ at 40 °C.

Table 3.2. Comparison of half-life times for benchmark reactions **III** ($t_{1/2}(\text{III})$) and **IV** ($t_{1/2}(\text{IV})$) and the ratio of these two reactivity parameters.

catalyst	$t_{1/2}(\text{IV})$	$t_{1/2}(\text{III})$	ratio
3	67 ^[a]	14.7 ± 0.5	4.56
5b	114	44.2 ± 1.5	2.56
2	171 ^[a]	67 ± 0.1 ^[b]	2.55
1	302 ^[a]	151 ± 1.7 ^[b]	2.00

[a] Data from ref. [9a]; [b] Data from ref. [10].

Previous studies have clearly established that Lewis-base catalyzed acylations work best in apolar organic solvents such as toluene, but can be quite slow in polar organic solvents.^[4,16] We therefore examined acylation reaction (**III**) in different solvents using commercially available **2** as the catalyst. Among all tested solvents the reaction was found to be fastest in CDCl₃ (for details see the Experimental Part). Also, earlier studies by Han *et al.* indicate that catalysts **3** and **5b** react with comparable rates with **16** according to Scheme 5 in CD₂Cl₂.^[17] As these results differ from our findings in CDCl₃ (Table 3.1) we have now reinvestigated benchmark reaction (**III**) in CD₂Cl₂ solution (Table 3.3).

Table 3.3. Half-life times for catalysts **2**, **3** and **5b** for reaction (**III**) in dichloromethane ($t_{1/2}(\text{CD}_2\text{Cl}_2)$) and chloroform ($t_{1/2}(\text{CDCl}_3)$), and the ratio of these kinetic parameters.

Catalyst	$t_{1/2}(\text{CD}_2\text{Cl}_2)$	$t_{1/2}(\text{CDCl}_3)$	ratio
3	20.8 ± 0.6	14.7 ± 0.5	1.42
5b	42.6 ± 0.6	44.2 ± 1.5	0.96
2	108.3 ± 0.9	67 ± 0.1 ^[a]	1.61

[a] Data from ref. [10].

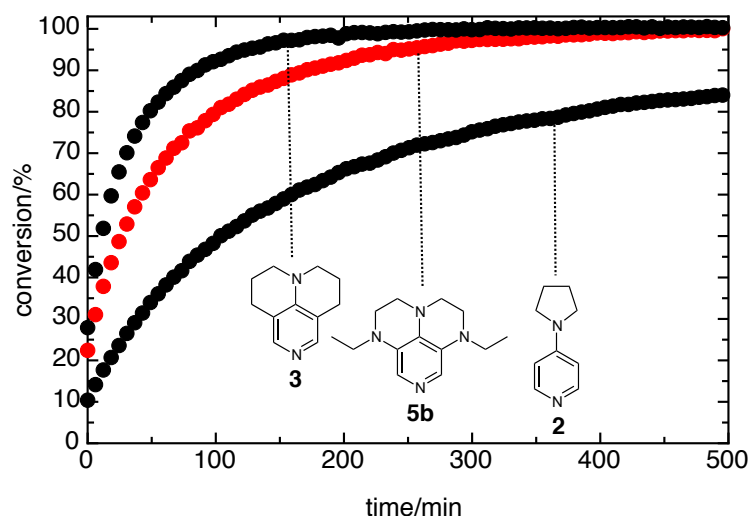


Figure 3.8. Conversion time plots for catalysts **2**, **3** and **5b** for reaction (III) in CD_2Cl_2 at 10 mol-% catalyst loading.

The results obtained at 10% catalyst loading (Figure 3.8, Table 3.3) indicate that reactions can indeed be slightly slower in CD_2Cl_2 than in CDCl_3 , but that the magnitude of the solvent effect depends on the nature of the catalyst. In both solvents, however, we find that catalyst **3** is clearly more effective than the 3,4,5-triaminopyridine catalyst **5b**. The lack of correlation between Lewis basicity and nucleophilicity parameters at one hand and catalytic performance in acylation reactions at different catalyst loadings at the other hand is thus clearly not an issue of solvent polarity.

The catalytic activities for the benchmark reaction (III) correlate poorly with the calculated acylation enthalpies ($R^2=0.2733$, Figure 3.9). This is in contrast to earlier studies for less Lewis basic catalysts,^[18] in which significantly better correlations were found. Could the nature of the one-step reaction underlying the quantification of Lewis basicities and nucleophilicities (as described above) in comparison to the multistep nature of catalytic processes be the reason for this discrepancy? As noted in previous studies, none of the ground state descriptors for the pyridine nitrogen atom (that is: the reaction center) has significant predictive value.^[18]

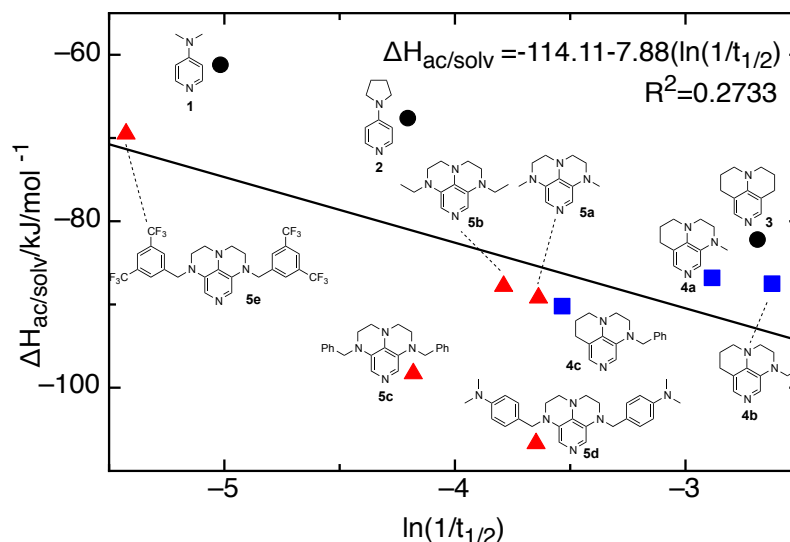


Figure 3.9. Correlation of acylation enthalpies ($\Delta H_{ac/solv}$) with kinetic data for acylation reaction (III) for 4-Aminopyridines (black circles), 3,4-diaminopyridines (blue squares), and 3,4,5-triaminopyridines (red triangles).

The possibility to predict catalytic rates using a multiparameter QSAR model was therefore tested, starting from an initial set of eight different parameters (see Experimental Part for details). The most important descriptors could be identified as the acylation enthalpies including solvation terms in chloroform ($\Delta H_{ac/solv}$, in kJ/mol), the charge of the *ortho*-hydrogen atom of the free catalyst ($q_{ortho-H}$, in units of elemental charge e) and the bond distance ($dist_{N-C}$, in Ångstroms) between the nitrogen atom in 4-position and the pyridine carbon atom at the same position. A QSAR model based on these three parameters for catalysts **1** – **5** (11 structures) constructed with Sybyl X 2.0 yields good correlations between actual and predicted catalytic activity ($R^2=0.9320$, $Q^2=0.7880$, see Figure 3.10). The QSAR equation (V) contains the acylation enthalpies $\Delta H_{ac/solv}$, in which more negative acylation enthalpies imply faster reaction rates. The *ortho*-hydrogen charge and the N-C distance parameters, in contrast, enter the QSAR equation as term 3 and 4 with negative sign, implying slower reaction rates for catalysts with more positively charged *ortho*-hydrogens and larger N-C bond distances.

$$\ln 1/t_{1/2} = \underbrace{85.867}_{\text{term 1}} - \underbrace{0.080 \cdot \Delta H_{ac/solv}}_{\text{term 2}} - \underbrace{162.8 \cdot q_{ortho-H}}_{\text{term 3}} - \underbrace{44.0 \cdot dist_{N-C}}_{\text{term 4}} \quad (\text{V})$$

As is readily seen from the data collected in Table 3.4 for catalysts **3**, **4a**, and **5a**, the last two terms are those relevant for predicting slower reactions for catalysts of higher Lewis basicity such as **5a**.

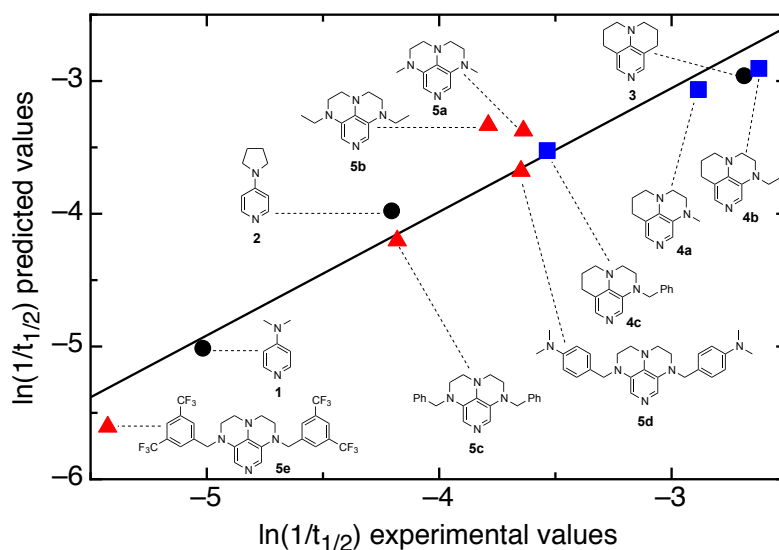


Figure 3.10. Experimental vs. predicted values for $\ln(1/t_{1/2})$ for the above described QSAR model involving $\Delta H_{ac/solv}$, $q_{ortho-H}$ and $dist_{N-C}$ for 4-Aminopyridines (black circles), 3,4-diaminopyridines (blue squares), and 3,4,5-triaminopyridines (red triangles).

Table 3.4. Comparison of QSAR parameters of annelated catalysts **3**, **4a** and **5a**.

Catalyst	$\Delta H_{ac/solv}$ [kJ/mol]	$q_{ortho-H}$	$dist_{N-C}$ [Å]	$\ln(1/t_{1/2})$ exp.	$\ln(1/t_{1/2})$ pred.	residual
3	-82.20	0.2108	1.3884	-2.6879	-2.9600	0.2722
4a	-86.80	0.2122	1.3939	-2.8848	-3.0640	0.1792
5a	-89.20	0.2137	1.3997	-3.6376	-3.3741	-0.2635

The value of this QSAR model, which is exclusively based on parameters available from theoretical data for the catalysts and their acylated intermediates, lies in the potential to further optimize the catalytic activity of pyridine catalysts.

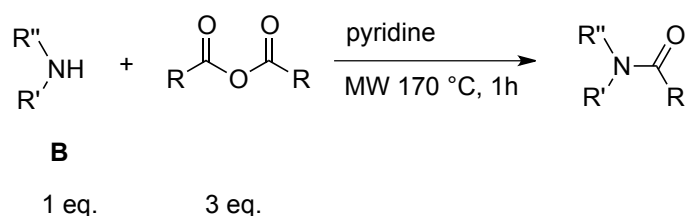
3.3 Conclusions

In conclusion we synthesized numerous new derivatives of 9-azajulolidine (**3**) and proved their structures by X-ray analysis. All new derivatives are strong Lewis bases as compared to the parent DMAP (**1**) system. The Lewis basicity correlates rather well with reaction rates for addition to cationic electrophiles, but not with rate data for the catalytic acylation of tertiary alcohol **16**. In qualitative terms this implies that catalysts with higher and higher Lewis basicity will eventually slow down the catalytic process due to the effort of detaching themselves from the substrate electrophiles. This general observation has recently also been made by Christmann *et al.* in the Lewis-base catalyzed isomerization of *Z*-allylic alcohols.^[19]

3.4 Experimental Part

All air and water sensitive manipulations were carried out under a nitrogen atmosphere using standard Schlenk techniques. Calibrated flasks for kinetic measurements were dried in the oven at 120 °C for at least 12 hours prior to use and then assembled quickly while still hot, cooled under a nitrogen stream and sealed with a rubber septum. All commercial chemicals were of reagent grade and were used as received unless otherwise noted. Acetonitrile (Acros >99.9%, extra dry), was purchased and used without further purification. CDCl₃ was refluxed for at least one hour over CaH₂ and subsequently distilled. ¹H and ¹³C NMR spectra were recorded on Varian 300 or Varian INOVA 400 and 600 machines at room temperature. All ¹H chemical shifts are reported in ppm (δ) relative to TMS (0.00); ¹³C chemical shifts are reported in ppm (δ) relative to CDCl₃ (77.16). ¹H NMR kinetic data were measured on a Varian Mercury 200 MHz spectrometer at 23 °C. HRMS spectra (ESI-MS) were carried out using a Thermo Finnigan LTQ FT instrument. IR spectra were measured on a Perkin-Elmer FT-IR BX spectrometer mounting ATR technology. Reactions utilizing microwave technology were conducted in a CEM Discover Benchmate microwave reactor (model nr. 908010). Analytical TLC's were carried out using aluminum sheets silica gel Si 60 F254. 9-Azajulolidine (**3**) was obtained from TCI China (CAS.nr.: 6052-72-8), purity: > 97.0 % (GC).

General procedure 1 (amino acylation)



In a flame dried 10 mL microwave-vial compound **B** (1 eq.) was dissolved in pyridine (2 mL/ mmol **B**) and the according anhydride (3-3.5 eq. per NH group) was added. For more nucleophilic compounds it is necessary to perform the handling under inert gas atmosphere, thus an arrangement that Figure 3.11 shows was invented. The tubing can be connected to a high vacuum pump. After stirring the solution for 10 min under nitrogen at room temperature the reaction mixture was heated for 1 h in a microwave reactor at 170 °C (200 W). After cooling the reaction mixture was quenched with methanol and the solvents were removed in vacuo (the usage of a big flask accelerates the removal of pyridine). The residue was taken up in DCM and washed with saturated K₂CO₃ solution. The aqueous phase was extracted three times with DCM and the combined organic extracts were dried over MgSO₄ and concentrated under vacuum. The crude mixture was purified by column chromatography.

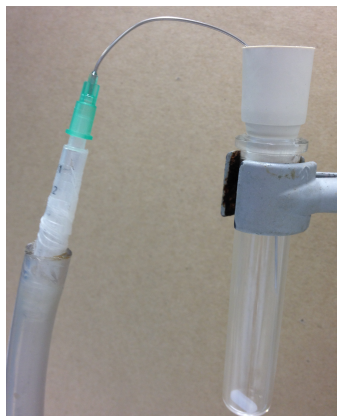
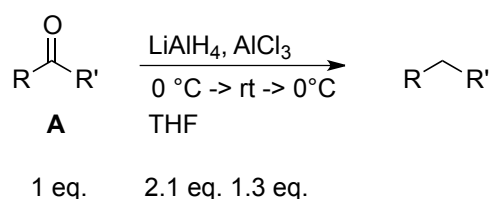


Figure 3.11. Arrangement for working under inert gas with 10 mL microwave-vials.

General procedure 2 (reduction with $\text{LiAlH}_4/\text{AlCl}_3$)



A flame dried Schlenk flask was charged with dry THF (5 mL/mmol substrate **A**). At 0 °C LiAlH_4 (2.1 eq. per carbonyl group) was added in portions and followed by the slow and portionwise addition of AlCl_3 (1.3 eq. per carbonyl group). The reaction mixture was stirred for 20 minutes at room temperature. To that solution the substrate **A** (1 eq.) in dry THF (5 mL/mmol substrate) was added dropwise at -10 °C. The reaction was stirred at -10 °C until the disappearance of starting material (TLC/GC) but for most compounds a reaction time of one hour was sufficient. For benzylic carbonyl groups elevated temperatures (room temperature or reflux) and longer reaction times (2.5 h to 8 h) sometimes turned out to be more efficient in terms of product yield but the exact conditions will be mentioned in detail in the experimental part. The reaction was quenched by pouring the mixture onto ice-cold water (5 mL/mmol substrate) and saturated K_2CO_3 (5 mL/mmol substrate) solution (it is important to adjust to pH=12-14, in case add more K_2CO_3). In that way the crude mixture was subjected to filtration over a Celite plug using vacuum (the optimized arrangement to obtain higher yields than previously published^[5] can be found in Figure 3.12, notice that a separation funnel can be attached directly with the NS 29 joint). The plug was washed with excess DCM and ethyl acetate. The resulting phases were separated by a separation funnel and the aqueous phase was washed three times with DCM and ethyl acetate. The combined organic phases were washed with saturated K_2CO_3 solution and dried over MgSO_4 . After evaporation of the organic solvent the crude product was purified by column chromatography.

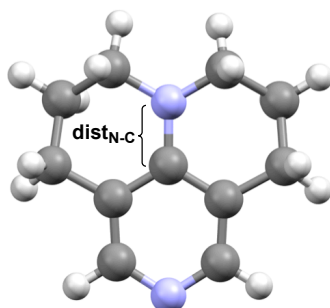


Figure 3.12. Optimized arrangement for filtration over Celite.

4-Aminopyridines

9-Azajulolidine (**3**)

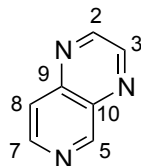
Since the discovery of 9-azajulolidine **3** (TCAP) in 2003 by *Steglich et al.*^[5] different methods for its synthesis were published yet.^[5,6,8,9] The different synthesis strategies are summarized in the recently published review by David *et al.*^[3] Nowadays **3** is also commercially available (TCI China). The crystal structure below was obtained after recrystallization (from ethyl acetate) of commercially available 9-azajulolidine.



	$\text{dist}_{\text{N-C}}/\text{pm}$	$d_{(\text{abcd})}$
crystal structure	137.5	12.7°
calculated best conf.	138.8	12.9°

3,4-Diaminopyridines

Pyrido[3,4-*b*]pyrazine (**8**)



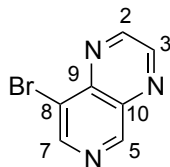
Under a constant nitrogen flow 2.50 g (22.9 mmol) 3,4-diaminopyridine **7** were dissolved in 40 mL ethanol. After the addition of 3.1 mL (27 mmol, $\rho = 1.256$ g/mL) glyoxal (40 wt.-% in water) the reaction mixture was submitted to a microwave reactor. After a reaction time of one hour at 110°C (70 W) the solvent was evaporated and the product **8** was obtained in quantitative yield (3.01 g) as a bright yellow solid.

¹H NMR (300 MHz, CDCl₃): δ = 7.91 (dd, $^4J = 0.83$ Hz, $^3J = 5.8$ Hz, 1 H, H-7), 8.81 (d, $^3J = 5.8$ Hz, 1 H, H-8), 8.92 (d, $^3J = 1.8$ Hz, 1 H, H-3), 8.99 (d, $^3J = 1.8$ Hz, 1 H, H-2), 9.53 (d, $^4J = 0.8$ Hz, 1 H, H-5).

¹³C NMR (75 MHz, CDCl₃): δ = 120.5 (CH, C-8), 137.5 (C_q, C-10), 144.3 (C_q, C-9), 145.6 (CH, C-7), 146.4 (CH, C-3), 148.4 (CH, C-2), 153.6 (CH, C-5).

In line with published data^[9]

8-Bromopyrido[3,4-*b*]pyrazine (**9**)



A solution of 6.90 g (52.6 mmol) **8** in 280 mL CH₃CN was stirred in the dark. To this solution 10.3 g (57.9 mmol) *N*-bromosuccinimide were added in portions under nitrogen atmosphere. After stirring the orange solution at room temperature over night cold Et₂O was added and it was filtered from the brown precipitation (for small scale synthesis). Evaporation of the solvent and repeated column chromatography (until the NMR shows no signal of the succinimide that was formed during the reaction) on silica gel (EtOAc/Isohexan/NEt₃/Et₂O, 20:15:1:1.5) yielded 5.74 g (52 %) of **9** as pale solid.

R_f: 0.53 (silica, EtOAc/Isohexan/NEt₃, 20:15:1).

mp: 110.9 - 111.8 °C.

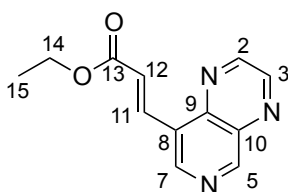
¹H NMR (300 MHz, CDCl₃): δ = 8.96 (d, $^3J = 1.8$ Hz, 1 H, H-3), 9.02 (s, 1 H, H-7), 9.08 (d, $^3J = 1.8$ Hz, 1 H, H-2), 9.44 (s, 1H, H-5).

^{13}C NMR (75 MHz, CDCl_3): δ = 120.5 (C_q , C-8), 139.7 (C_q , C-10), 144.1 (C_q , C-9), 148.0 (CH, C-3), 149.8 (CH, C-7), 150.4 (CH, C-2), 154.7 (CH, C-5).

IR (ATR): $\tilde{\nu}$ (cm^{-1}) = 1734 (w), 1578 (m, C=C stretching vibration), 1561 (w, C=C stretching vibration), 1548 (w, C=C stretching vibration), 1466 (m), 1428 (m), 1373 (m), 1256 (m), 1180 (m), 1103 (m), 1012 (m, C-Br), 969 (vs), 826 (m), 806 (m).

HRMS (EI): calculated for: $\text{C}_7\text{H}_4\text{N}_3\text{Br}$ [M^+] 208.9589, found: 208.9581.

(*E*)-Ethyl 3-(pyrido[3,4-*b*]pyrazin-8-yl)acrylate (**10**)



A flame dried pressure tube was charged with 10 mL dry CH_3CN , 46.9 mg (2.6 mol%, 0.21 mmol) $\text{Pd}(\text{OAc})_2$, 159 mg (6.5 mol-%, 0.53 mmol) $\text{P}(o\text{-tolyl})_3$, 0.76 mL (0.67 eq., 5.39 mmol, ρ = 0.72 g/mL) NEt_3 , 1.69 g (8.05 mmol) **9** and 1.48 mL (1.70 eq, 13.69 mmol, ρ = 0.924 g/mL) ethyl acrylate. The solution was heated for 20.5 h to 120 °C. After cooling to room temperature the solvent was evaporated and the crude mixture was purified by column chromatography on silica (gradient of Isohexan/EtOAc 1:1 to 1:9). The product **10** was obtained in 65 % yield (1.20 g) as yellow solid.

R_f : 0.43 (silica, Isohexane/EtOAc, 1:1).

mp: 147.9 - 150.6 °C.

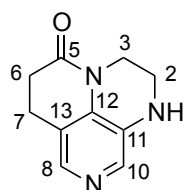
^1H NMR (300 MHz, CDCl_3): δ = 1.36 (t, 3J = 7.1 Hz, 3 H, H-15), 4.31 (q, 3J = 7.1 Hz, 2 H, H-14), 7.11 (d, 3J = 16.3 Hz, 1 H, H-12), 8.47 (dd, 3J = 16.3 Hz, 3J = 0.7 Hz, 1 H, H-11), 8.99 (d, 3J = 1.7 Hz, 1 H, H-3), 9.03 (s, 1 H, H-7), 9.07 (d, 3J = 1.7 Hz, 1 H, H-2), 9.52 (s, 1 H, H-5).

^{13}C NMR (75 MHz, CDCl_3): δ = 14.1 (CH_3 , C-15), 60.7 (CH_2 , C-14), 123.8 (CH, C-12), 126.6 (C_q , C-8), 136.3 (CH, C-11), 137.3 (C_q , C-10), 143.1 (C_q , C-9), 146.1 (CH, C-7), 146.6 (CH, C-3), 148.3 (CH, C-2), 155.3 (CH, C-5), 165.9 (CH, C-13).

IR (ATR): $\tilde{\nu}$ (cm^{-1}) = 3401 (w), 2956 (m, C-H stretching vibration), 2918 (s, C-H stretching vibration), 2850 (m, C-H stretching vibration), 1723 (vs, C=O), 1638 (m, C=N), 1566 (w, C=C stretching vibration), 1466 (w), 1442 (w), 1394 (w), 1375 (w), 1324 (s), 1275 (m), 1220 (vs), 1191 (s), 1178 (s), 1134 (w), 1028 (w), 979 (w), 912 (m, C-H deformation vibration (oop), alkene), 880 (w), 828 (w), 726 (w).

HRMS (EI): calculated for: $\text{C}_{12}\text{H}_{12}\text{O}_2\text{N}_3$ [$\text{M}+\text{H}$] $^+$ 230.0930, found: 230.0925.

2,3,6,7-Tetrahydropyrazino[3,2,1-*ij*][1,6]naphthyridine-5(1H)-on (**11**)



In a flame dried 2L Schlenk flask 1.91 g (8.33 mmol) of **10** were dissolved in 350 mL ethanol. To this solution 0.50 g of palladium on charcoal (10 %) were added. The flask was purged three times with hydrogen and the solution turned slowly purple. The reaction was conducted under hydrogen atmosphere at room temperature for 8 hours (too long reaction times will hydrogenate the pyridine ring and thus should be avoided). The black solution was filtered through Celite and the residue was washed with ethanol, ethyl acetate and dichloromethane. After removal of the solvents the crude product was purified twice by column chromatography using neutral aluminum oxide (CHCl₃/MeOH 40:1). The product **11** was obtained as brown solid in 88 % yield (1.39 g).

R_f: 0.50 (neutral aluminum oxide, CHCl₃/MeOH 40:1).

mp: 158.6 - 163.5 °C.

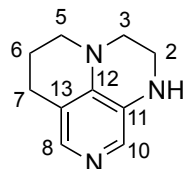
¹H NMR (300 MHz, CDCl₃): δ = 2.64 – 2.73 (m, 2 H, H-6), 2.88 (dd, ³*J* = 6.2 Hz, ³*J* = 8.7 Hz, 2 H, H-7), 3.33 – 3.42 (m, 2H, H-2), 3.90 – 3.99 (m, 2 H, H-3), 4.08 (s, br, 1 H, N-H), 7.77 (s, 1 H, H-9), 7.86 (s, 1 H, H-11).

¹³C NMR (75 MHz, CDCl₃): δ = 21.7 (CH₂, C-7), 30.6 (CH₂, C-6), 39.1 (CH₂, C-3), 39.3 (CH₂, C-2), 119.1 (C_q, C-8), 129.8 (C_q, C-12), 130.2 (C_q, C-13), 135.3 (CH, C-11), 138.2 (CH, C-9), 168.0 (C_q, C-5).

IR (ATR): $\tilde{\nu}$ (cm⁻¹) = 3323 (w, br, N-H stretching vibration), 2967 (w, C-H stretching vibration), 2934 (w, C-H stretching vibration), 2854 (w, C-H stretching vibration), 1659 (s, C=O), 1587 (s, C=C stretching vibration), 1496 (s), 1461 (m), 1378 (s), 1346 (s), 1304 (s), 1264 (m), 1233 (s), 1196 (s), 1153 (s), 1119 (m), 1090 (m), 1075 (m), 1032 (m), 908 (s), 865 (m), 842 (m), 776 (m), 690 (vs, C-H deformation vibration (oop), aromatic).

HRMS (EI): calculated for: C₁₀H₁₁ON₃ [M+H]⁺ 190.0980, found: 190.0975.

1,2,3,5,6,7-Hexahydropyrazino[3,2,1-*ij*][1,6]naphthyridine (**12**)



The reduction was conducted according to general procedure 2 applying 0.25 g (1.32 mmol) of starting material **11**. The crude mixture was purified by column chromatography on silica gel (EtOAc/NEt₃/MeOH 10:1:1) yielding the product as a yellow solid in 96 % yield (0.22 g).

R_f: 0.17 (silica, EtOAc/NEt₃/MeOH 10:1:1).

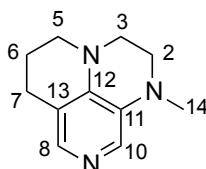
¹H NMR (300 MHz, CDCl₃): δ = 1.90 – 2.04 (m, 2H, CH₂), 2.66 (t, ³*J* = 6.4 Hz, 2H, CH₂), 3.10 – 3.23 (m, 2H, CH₂), 3.23 – 3.35 (m, 2H, CH₂), 3.34 (s, 2H, CH₂), 7.46 – 7.60 (m, 2H, CH_{Ar}).

¹³C NMR (75 MHz, CDCl₃): δ = 20.7, 23.7, 39.2, 48.1, 49.0, 115.0, 127.9, 129.2, 136.4, 139.5.

IR (ATR): $\tilde{\nu}$ (cm⁻¹) = 3191 (w, br, N-H stretching vibration), 3015 (w, C-H stretching vibration), 2923 (s), 2850 (s), 2754 (s), 2680 (s), 1704 (s), 1655 (s), 1628 (s), 1569 (vs), 1457 (s), 1333 (vs), 1250 (s), 1209 (s), 1169 (s), 1123 (s), 1070 (s), 1055 (s), 1026 (s), 958 (w), 942 (w), 905 (s), 869 (s), 853 (s), 741 (vs).

HRMS (EI): calculated for: C₁₃H₁₃N₃ [*M*]⁺ 175.1109, found: 175.1106.

1-Methyl-1,2,3,5,6,7-hexahydropyrazino[3,2,1-*ij*][1,6]naphthyridine (**4a**)



In a 80 mL microwave vial 0.88 g (5.03 mmol) of **12** were added to 12.54 mL of formic acid and 4.27 mL (37 % solution) of formaldehyde. The mixture was heated in a microwave reactor for 36 hours at 110 °C and 110 W. After completion the reaction mixture was quenched by careful addition of NaOH (32 %) at 0 °C until pH=12. The reaction mixture is stirred together with excess EtOAc for at least 20 min. The mixture is extracted three times with EtOAc and two times with DCM and the combined organic layers dried over MgSO₄. The crude reaction mixture was purified twice by column chromatography on basic Alox

(Brockmann 3) ($\text{CHCl}_3/\text{MeOH}$ 40:1) and recrystallized from ethyl acetate/isohehexane and yielded 61 % (0.58 g) of **4a** as white crystalline solid.

R_f : 0.45 (bas. Alox, EtOAc/ NEt_3/MeOH 10:1:1).

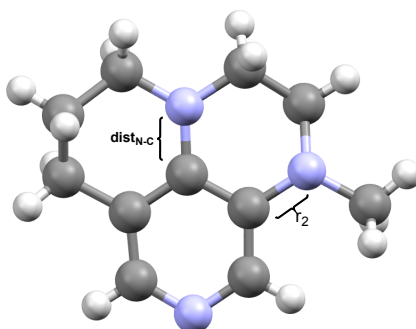
mp: 47.1 - 49.3 °C.

^1H NMR (300 MHz, CDCl_3): δ = 1.80 – 2.08 (m, 2H, CH_2), 2.66 (t, 3J = 6.4 Hz, 2H, CH_2), 2.83 (s, 3H, CH_3), 3.08 – 3.28 (m, 4H, $\text{CH}_2 \times 2$), 3.27 – 3.46 (m, 2H, CH_2), 7.53 (s, 1H, CH_{Ar}), 7.58 (s, 1H, CH_{Ar}).

^{13}C NMR (75 MHz, CDCl_3): δ = 21.1, 23.8, 39.1, 48.0, 48.5, 49.1, 114.3, 130.1, 130.8, 138.1, 140.9.

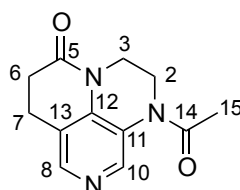
IR (ATR): $\tilde{\nu}$ (cm^{-1}) = 3255 (w, br), 3037 (w), 2942 (s), 2833 (s), 2810 (s), 2781 (w), 1578 (vs), 1522 (vs), 1469 (vs), 1430 (s), 1374 (s), 1358 (s), 1331 (vs), 1312 (vs), 1223 (vs), 1124 (vs), 1035 (vs), 986 (s), 906 (s), 869 (s), 852 (vs), 769 (vs), 745 (vs), 652 (s).

HRMS (EI): calculated for: $\text{C}_{11}\text{H}_{15}\text{N}_3$ $[\text{M}]^+$ 189.1266, found: 189.1262.



	dist _{N-C} /pm	r ₂ /pm	d _(abcd)
crystal structure	137.3	140.0	1.0°
calculated best conf.	139.4	140.6	2.1°

1-Acetyl-2,3,6,7-tetrahydropyrazino[3,2,1-ij][1,6]naphthyridin-5(1H)-one (**13b**)



The acylation of **11** was conducted following general procedure 1 with 0.70 g (3.70 mmol) of **11** and 1.23 mL (12.98 mmol, 3.5 eq.) acetic anhydride. The crude mixture was purified by column chromatography on silica (EtOAc/ NEt_3/MeOH 10:1:1) giving **13b** in 96 % (0.82 g) yield as yellow foam.

R_f: 0.17 (silica, EtOAc/NEt₃/MeOH 10:1:1).

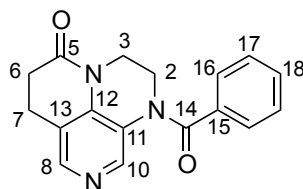
¹H NMR (300 MHz, CDCl₃): δ = 2.32 (s, 3H, CH₃), 2.75 (t, ³*J* = 7.6 Hz, 2H, CH₂), 2.99 (t, ³*J* = 7.6 Hz, 2H, CH₂), 3.92 (d, ³*J* = 5.0 Hz, 4H, CH₂ x 2), 8.17 (s, 1H, CH_{Ar}, H-8), 8.27 – 8.67 (m, 1H, CH_{Ar}, H-10).

¹³C NMR (75 MHz, CDCl₃): δ = 21.8, 22.4, 30.6, 42.5, 119.3, 123.3, 136.0, 144.0, 144.7, 168.5 (C=O), 168.6 (C=O).

IR (ATR): $\tilde{\nu}$ (cm⁻¹) = 3525 (w, br), 2960 (w), 2892 (w), 2359 (w), 2337 (w), 1679 (vs, C=O), 1584 (s), 1495 (s), 1366 (vs), 1325 (vs), 1195 (s).

HRMS (EI): calculated for: C₁₂H₁₃N₃O₂ [M]⁺ 231.1008, found: 231.1002.

1-Benzoyl-2,3,6,7-tetrahydropyrazino[3,2,1-*ij*][1,6]naphthyridin-5(1H)-one (**13c**)



The benzoylation of **11** was conducted according to general procedure 1 with 0.29 g (1.53 mmol) of compound **11** and 1.04 g (4.60 mmol, 3 eq.) benzoic anhydride. Purification of the crude product on basic aluminum oxide (DCM/MeOH 40:1) yielded the product in 82 % yield (0.37 g) as a light brown solid.

R_f: 0.78 (silica, EtOAc/NEt₃/MeOH 10:1:1).

mp: 171.8 - 175.9 °C.

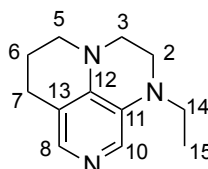
¹H NMR (300 MHz, CDCl₃): δ = 2.75 (t, ³*J* = 7.4 Hz, 2 H, H-6), 2.96 (t, ³*J* = 7.5 Hz, 2 H, H-7), 3.90 – 4.06 (m, 4 H, H-2, H-3), 7.28 – 7.51 (m, 5 H, H-16, H-17, H-18), 8.02 (s, 2 H, H-9, H-11).

¹³C NMR (75 MHz, CDCl₃): δ = 21.5 (CH₂, C-7), 30.3 (CH₂, C-6), 41.0 (CH₂), 41.9 (CH₂), 118.7 (C_q, C-13), 122.7 (C_q, C-11), 127.9 (CH, C-16, C-17, C-18), 128.3 (CH, C-16, C-17, C-18), 130.9 (CH, C-16, C-17, C-18), 133.6 (C_q, C-15), 134.4 (C_q, C-12), 143.4 (CH, C-8), 144.0 (CH, C-10), 168.1 (C_q, C-5), 168.5 (C_q, C-14).

IR (ATR): $\tilde{\nu}$ (cm⁻¹) = 3370 (w), 3059 (w), 2925 (w, C-H stretching vibration), 2852 (w, C-H stretching vibration), 1681 (s, C=O), 1648 (s, C=O), 1585(s, C=C stretching vibration), 1496 (s, C=C stretching vibration), 1458 (m, C-H deformation vibration), 1447 (m, C-H-deformation vibration), 1434 (m, C-H deformation vibration), 1372 (vs), 1329 (vs), 1260 (s), 1241 (s), 1195 (s), 1184 (s), 1160 (s), 1120 (s), 1086 (m), 1034 (m), 1006 (m), 968 (w), 913 (m), 888 (s), 843 (w), 789 (m), 717 (vs, C-H deformation vibration (oop), Aromat), 697 (vs), 666 (m).

HRMS (EI): calculated for: $C_{17}H_{15}O_2N_3 [M^+]$ 293.1164, found: 293.1158.

1-Ethyl-1,2,3,5,6,7-hexahydropyrazino[3,2,1-*ij*][1,6]naphthyridine (**4b**)



The reduction was done following general procedure 2 with 0.74 g (3.20 mmol) of **13b**. The crude mixture was purified by repeated column chromatography on silica gel (EA: NEt_3 10:1) and yielded the product **4b** as a white solid in 81 % (0.53 g) yield.

R_f : 0.45 (silica, EtOAc/ NEt_3 10:1).

mp: 63.2 – 64.5 °C.

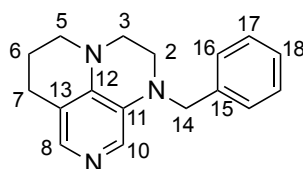
1H NMR (300 MHz, $CDCl_3$): δ = 1.16 (t, 3J = 7.1 Hz, 3H, CH_3), 2.01 – 2.91 (m, 2H, CH_2), 2.67 (t, 3J = 6.4 Hz, 2H, CH_2), 3.17 (dd, 3J = 6.9 Hz, 3J = 4.4 Hz, 2H, CH_2), 3.23 – 3.34 (m, 6H, $CH_2 \times 3$), 7.55 (s, 1H, CH_{Ar}), 7.59 (s, 1H, CH_{Ar}).

^{13}C NMR (75 MHz, $CDCl_3$): δ = 10.1, 21.2, 23.8, 45.0, 45.2, 47.7, 49.2, 114.8, 129.3, 130.2, 138.1, 140.2.

IR (ATR): $\tilde{\nu}$ (cm^{-1}) = 2954 (m), 2837 (m), 1578 (m), 1566 (m), 1513 (s), 1470 (s), 1429 (m), 1369 (m), 1343 (vs), 1316 (s), 1274 (m), 1204 (s), 1162 (s), 1091 (s), 938 (m), 879 (s), 795 (s), 766 (s), 747 (s).

HRMS (EI): calculated for: $C_{12}H_{17}N_3 [M]^+$ 203.1422, found: 203.1418.

1-Benzyl-1,2,3,5,6,7-hexahydropyrazino[3,2,1-*ij*][1,6]naphthyridine (**4c**)



According to general procedure 2 1.33 g (4.53 mmol) of **13c** was submitted to react. Purification of the crude mixture twice on basic aluminum oxide (EtOAc/ NEt_3 /MeOH 10:1:1) and once on silica gel (EtOAc/ NEt_3 /MeOH 10:1:1) yielded the product **4c** as a brown oily substance (0.67g, 56 %).

R_f : 0.67 (silica, EtOAc/ NEt_3 /MeOH 10:1:1).

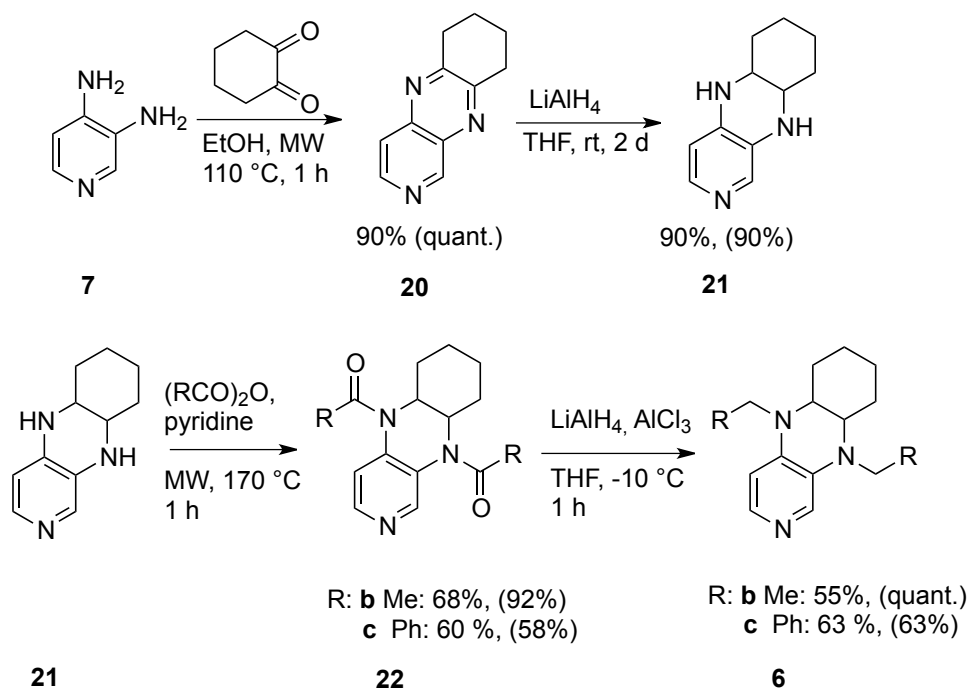
¹H NMR (400 MHz, CDCl₃): δ = 1.88 – 2.06 (m, 2 H, H-6), 2.67 (t, 3J = 6.4 Hz, 2 H, 7-H), 3.18 (dd, 3J = 6.8 Hz, 3J = 4.4 Hz, 2 H, H-5), 3.23 – 3.35 (m, 4 H, H-2, H-3), 4.36 (s, 2 H, H-14), 7.16 – 7.38 (m, 5 H, H-16, H-17, H-18), 7.56 (d, 3J = 5.7 Hz, 2 H, H-8, H-10).

¹³C NMR (100 MHz, CDCl₃): δ = 21.5 (CH₂, C-6), 24.2 (CH₂, C-7), 46.6 (CH₂, C-2), 48.1 (CH₂, C-3), 49.6 (CH₂, C-5), 55.5 (CH₂, C-14), 115.1 (C_q, C-13), 127.4 (CH, C-18), 127.6 (CH, C-16), 128.9 (CH, C-17), 130.4 (C_q, C-11), 130.6 (C_q, C-10), 138.1 (C_q, C-15), 138.3 (C_q, C-12), 140.6 (C_q, C-8).

IR (ATR): $\tilde{\nu}$ (cm⁻¹) = 3086 (w, C-H stretching vibration, aryl), 3060 (w, C-H stretching vibration, aryl), 3029 (w, C-H stretching vibration, aryl), 2930 (w, C-H stretching vibration), 2841 (w, C-H stretching vibration), 1647 (w), 1582 (m, C=C stretching vibration), 1515 (s, C=C stretching vibration), 1495 (m), 1469 (C-H deformation vibration), 1437 (C-H deformation vibration), 1452 (C-H deformation vibration), 1350 (s), 1325 (m), 1293 (m), 1255 (m), 1231 (m), 1196 (m), 1156 (s), 1109 (m), 1066 (m), 1038 (w), 1028 (w), 977 (w), 907 (s), 725 (vs, C-H deformation vibration (oop), aryl), 697 (vs, C-H deformation vibration (oop), aryl).

HRMS (EI): calculated for: C₁₇H₁₉N₃ [M⁺] 265.1579, found: 265.1568.

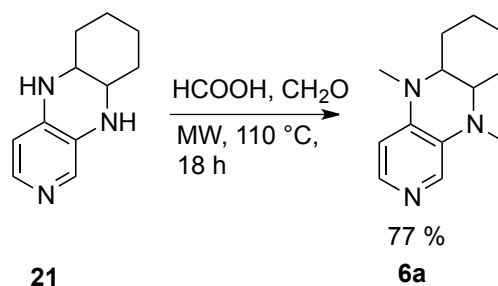
The catalysts **6b,c** were synthesized according to literature procedures.^[9,10,18] Scheme 3.7 outlines the synthesis (own yields are given in brackets).



Scheme 3.7. Synthesis of compounds **6a,b** according to literature known procedures (own yields are given in brackets).^[9,10,18]

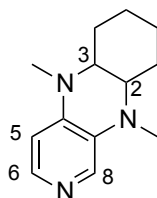
Applying general procedures 1 and 2 (optimized reaction conditions) the last two steps were dramatically increased in yield in case of compounds **22b** and **6b**.

Besides the published ones (**6b,c**) a new catalyst based on the same motif (**6a**) was synthesized through selective Eschweiler-Clark methylation of compound **21**. The advantage of the newly synthesized catalyst **6a** is the even easier accessibility (compared to **6b**) with a synthesis of just 3 steps instead of 4. Another benefit is the much easier handling of catalyst **6a** being a solid and easy to recrystallize from ethyl acetate/*iso*-hexane (instead of usually oily **6b**) but with similar catalytic activity. Scheme 3.8 shows the synthesis of **6a**.



Scheme 3.8. Synthesis of catalyst **6a** under Eschweiler-Clark conditions.

5,10-Dimethyl-5,10a,6,7,8,9,9a,10-octahydropyrido[3,4-*b*]quinoxaline (**6a**)



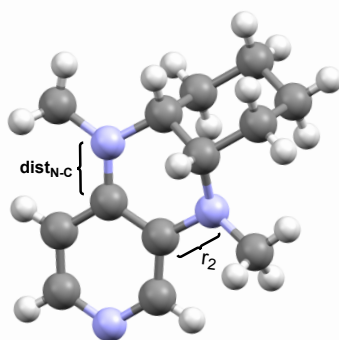
In a 10 mL microwave-vial 0.30 g (1.59 mmol) of **21** were added to 4.00 mL of formic acid and 2.80 mL (37 % solution) of formaldehyde. The mixture was heated in a microwave reactor for 18 hours at 110 °C and 110 W. After completion the reaction mixture was quenched by careful addition of NaOH (32 %) at 0 °C until pH=12. The reaction mixture is stirred together with excess EtOAc for at least 20 min. The mixture is extracted three times with EtOAc and two times with DCM and the combined organic layers dried over MgSO₄. The crude reaction mixture was purified twice by column chromatography on silica (EA/NEt₃/MeOH 10:1:1) and recrystallized from ethyl acetate/isohexane and yielded 77 % (0.13 g) of **6a** as pale yellow crystalline solid.

¹H NMR (600 MHz, CDCl₃): δ = 1.43 – 1.29 (m, 2H). 1.65 – 1.49 (m, 4H), 1.82 (d, ³J = 8.5 Hz, 2H), 2.81 (s, 3H), 2.86 (d, ³J = 3.8 Hz, 3H), 3.22 – 3.12 (m, 1H), 3.40 – 3.32 (m, 1H), 6.29 (d, ³J = 5.4 Hz, 1H), 7.66 (s, 1H), 7.80 (d, J=5.4, 1H),

^{13}C NMR (150 MHz, CDCl_3): δ = 21.6, 22.3, 26.1, 27.2, 34.4, 34.5, 56.2, 57.9, 104.2, 131.4, 132.1, 141.0, 141.9.

IR (ATR): $\tilde{\nu}$ (cm^{-1}) = 2933 (s), 2853 (m), 1578 (vs), 1515 (vs), 1471 (m), 1436 (s), 1368 (s), 1309 (s), 1244 (vs), 1264 (vs), 1223 (vs), 1059 (vs), 966 (m), 883 (w), 809 (vs), 746 (w)

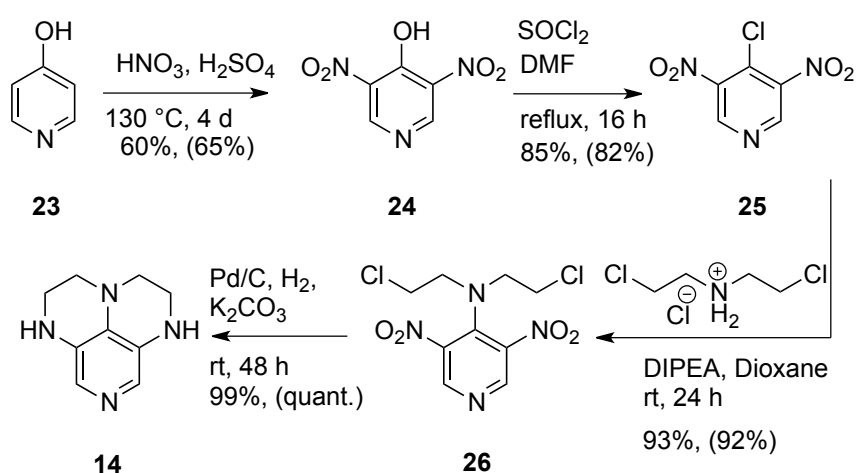
HRMS (EI): calculated for: $\text{C}_{13}\text{H}_{19}\text{N}_3$ $[\text{M}]^+$ 217.1579, found: 217.1575.



	$\text{dist}_{\text{N-C}}/\text{pm}$	r_2/pm	$d_{(abcd)}$
crystal structure	136.8	140.6	8.6°
calculated best conf.	138.9	140.5	12.8°

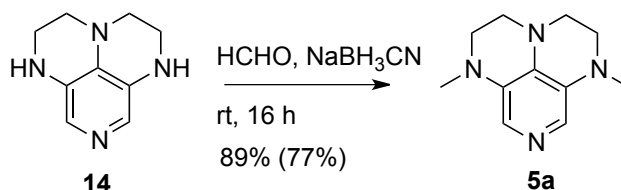
3,4,5-Triaminopyridines

The core structure **14** of the 3,4,5-triaminopyridines was synthesized from **23** according to the published procedures of *David et al.*^[8].



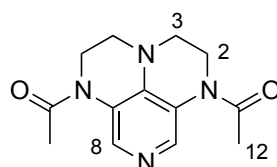
Scheme 3.9. Published synthesis of **14** starting with 4-hydroxypyridine **23**^[8] (own yields are given in brackets).

Catalyst **5a** was synthesized through established procedures by *David et al.*^[8] (own yields are given in brackets).



Scheme 3.10. Synthesis of **5a**.

1,1'-(2,3,4,5-Tetrahydro-1,3a,6,8-tetraazaphenalene-1,6-diyl)diethanone (**15b**)



The acylation was performed according to general procedure 1 with 0.36 g (2.04 mmol) of starting material **14**. After purification by column chromatography using silica gel (EtOAc/ NEt_3 /MeOH 10:1:1) the product was obtained as a pale brown solid in 88 % (0.47 g) yield.

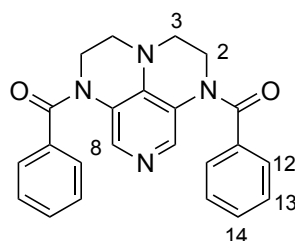
^1H NMR (200 MHz, CDCl_3): δ = 2.29 (s, 6H, $\text{CH}_3 \times 2$, H-12), 3.29 – 3.52 (m, 4H, $\text{CH}_2 \times 2$, H-3), 3.93 (t, 3J = 5.2 Hz, 4H, $\text{CH}_2 \times 2$, H-2), 8.01 (s, br, 2H, CH_{ar} , H-8).

^{13}C NMR (100 MHz, CDCl_3): δ = 22.4, 37.6, 45.8, 48.5, 121.2, 134.3, 140.6, 168.9.

HRMS (EI): calculated for: $\text{C}_{13}\text{H}_{16}\text{N}_4\text{O}_2$ $[\text{M}]^+$ 260.1273, found: 260.1267.

In line with published data.^[8]

(2,3,4,5-Tetrahydro-1,3a,6,8-tetraazaphenalene-1,6-diyl)bis(phenylmethanone) (**15c**)



The acylation was performed according to general procedure 1 with 1.50 g (8.51 mmol) of starting material **14** and 6 eq. of benzoic anhydride (11.6 g, 51.1 mmol) in a 80 mL microwave vial. After purification by column chromatography using basic Alox (Brockmann 3, EtOAc/ NEt_3 10:1) the product was obtained as an ocher colored solid in 85 % (2.76 g) yield.

R_f: 0.30 (basic Alox, EtOAc/NEt₃ 10:1).

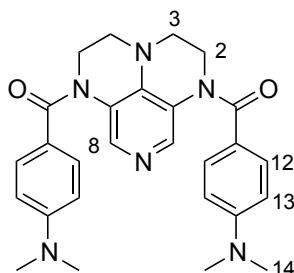
¹H NMR (300 MHz, CDCl₃): δ = 3.47 – 3.71 (m, 4H, CH₂ x 2, H-3), 3.98 – 4.22 (m, 4H, CH₂ x 2, H-2), 7.27 – 7.47 (m, 10H, CH_{ar}, H-12 x 4, H-13 x 4, H-15 x 2), 7.56 (dt, ³*J* = 4.4 Hz, ³*J* = 1.8 Hz, 1H), 7.89 – 8.21 (m, 1H).

¹³C NMR (75 MHz, CDCl₃): δ = 49.0, 121.4, 128.1, 128.2, 128.5, 130.9, 133.0, 134.5, 140.3, 169.0.

HRMS (EI): calculated for: C₂₃H₂₄N₄ [M]⁺ 356.2001, found: 356.1994.

In line with published data.^[8]

(2,3,4,5-Tetrahydro-1,3a,6,8-tetraazaphenalene-1,6-diyl)bis((4-(dimethylamino)phenyl) methanone) (**15d**)



The acylation was performed according to general procedure 1 with 0.25 g (1.42 mmol) of starting material **14** and 6 eq. of 4-(dimethylamino)benzoyl chloride (1.56 g, 8.51 mmol). After purification by column chromatography using basic Alox (Brockmann 3, EtOAc/NEt₃ 10:1) the product was obtained as brown solid in 90 % (0.60 g) yield.

R_f: 0.60 (basic Alox, EtOAc/NEt₃/MeOH 10:1:1).

mp: 243.2 -244.1 °C.

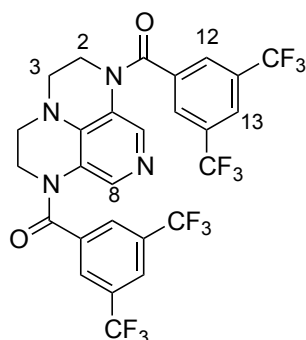
¹H NMR (600 MHz, CDCl₃): δ = 2.97 (s, 12H, CH₃ x 4, H-14), 3.53 (t, ³*J* = 5.2 Hz, 4H, CH₂ x 2, H-3), 4.02 – 4.10 (m, 4H, CH₂ x 2, H-2), 6.50 – 6.59 (m, 4H, CH_{ar}, H-13), 7.32 – 7.41 (m, 4H, CH_{ar}, H-12), 7.53 (³*J* = 19.7 Hz, 2H, CH_{ar}, H-8).

¹³C NMR (150 MHz, CDCl₃): δ = 40.0, 40.4, 40.1, 110.8, 120.8, 122.2, 130.8, 132.2, 139.8, 152.0, 162.1.

IR (ATR): $\tilde{\nu}$ (cm⁻¹) = 2871 (w), 1644 (s), 1629 (s), 1594 (vs), 1525 (s), 1444 (w), 1361 (vs), 1332 (vs), 1242 (s), 1123 (m), 946 (w), 887 (w), 819 (s), 764 (m).

HRMS (EI): calculated for: C₂₇H₃₀N₆O₂ [M]⁺ 470.2430, found: 470.2421.

(2,3,4,5-Tetrahydro-1,3a,6,8-tetraazaphenalene-1,6-diyl)bis((3,5-bis(trifluoromethyl) phenyl)methanone) (**15e**)



The acylation was performed according to general procedure 1 with 0.60 g (3.40 mmol) of starting material **14** and 6 eq. of 3,5-(bistrifluoromethyl)benzoyl chloride (5.65 g, 20.40 mmol) in 30 mL pyridine (80 mL microwave vial). After purification by column chromatography using basic Alox (Brockmann 3, EtOAc/NEt₃ 10:1 → EtOAc/NEt₃ 10:1) the product was obtained as beige powder in 80 % (1.80 g) yield.

mp: 239.8 – 240.2 °C.

¹H NMR (300 MHz, CDCl₃): δ = 3.67 (t, ³J = 5.2 Hz, 4H, CH₂ x 2, H-3). 4.11 (t, ³J = 5.2 Hz, 4H, CH₂, H-2), 7.49 (s, br, 2H, CH_{ar}, H-8), 7.88 (s, 4H, CH_{ar} x 4, H-12), 7.94 (s, 2H, CH_{ar} x 2, H-13).

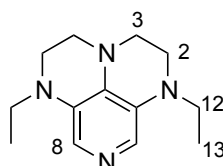
¹³C NMR (75 MHz, CDCl₃): δ = 48.8, 120.5 (d), 124.4, 124.5, 128.0, 128.6, 132.1 (q), 133.1, 136.7, 140.9, 165.4.

¹⁹F-NMR (282 MHz, CDCl₃): δ = - 63.1.

IR (ATR): $\tilde{\nu}$ (cm⁻¹) = 3016 (w), 1675 (m), 1663 (m), 1602 (m), 1543 (w), 1404 (w), 1366 (m), 1301 (vs), 1232 (m), 1163 (s), 1123 (vs), 902 (m), 681 (s).

HRMS (EI): calculated for: C₂₇H₁₆F₁₂N₄O₂ [M]⁺ 656.1082, found: 656.1060.

1,6-Diethyl-1,2,3,4,5,6-hexahydro-1,3a,6,8-tetraazaphenalene (**5b**)



The reduction was performed according to general procedure 2 with 0.18 g (0.69 mmol) of starting material **15b**. After purification by column chromatography using basic Alox (Brockmann 3, EtOAc/NEt₃ 20:1 → EtOAc/NEt₃/MeOH 10:1:3) the product was obtained as white solid in 95 % (0.15 g) yield.

mp: 258.2 – 260.3 °C.

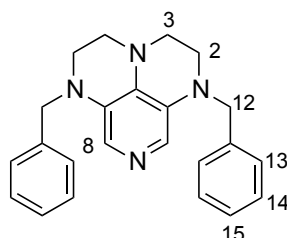
¹H NMR (600 MHz, CDCl₃): δ = 1.13 (t, ³J = 7.1 Hz, 6H, CH₃ x 2, H-13), 3.26 (q, ³J = 7.1 Hz, 4H, CH₂ x 2, H-12), 3.29 – 3.33 (m, 4H, CH₂ x 2, H-3), 3.47 (dt, ³J = 8.1 Hz, 3.6 Hz, 4H, CH₂ x 2, H-2), 7.18 (s, 2H, CH_{ar}, H-8).

¹³C NMR (150 MHz, CDCl₃): δ = 10.0, 43.5, 45.4, 47.7, 113.7, 128.7, 132.6.

HRMS (EI): calculated for: C₁₃H₂₀N₄ [M]⁺ 232.1688, found: 232.1682.

In line with published data.^[8]

1,6-Dibenzyl-1,2,3,4,5,6-hexahydro-1,3a,6,8-tetraazaphenalene (**5c**)



The reduction was performed according to general procedure 2 with 2.20 g (5.72 mmol) of starting material **15c**. After purification by column chromatography using basic Alox (Brockmann 3, EtOAc/NEt₃ 20:1 → EtOAc/NEt₃/MeOH 10:1:3) and recrystallization in EtOAc/Isohexane the product was obtained as white crystals in 78 % (1.59 g) yield.

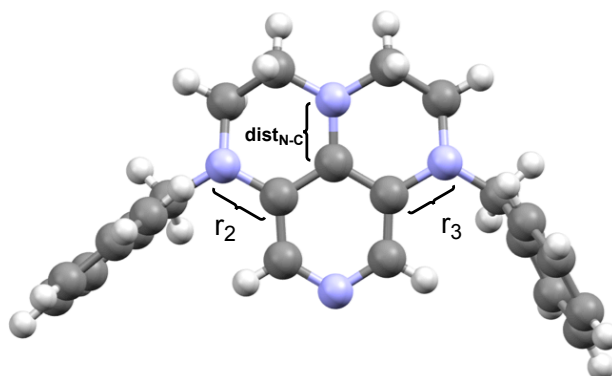
R_f: 0.66 (silica, EtOAc/NEt₃/MeOH 10:1:1).

¹H NMR (300 MHz, CDCl₃): δ = 3.20 – 3.33 (m, 4H, CH₂ x 2, H-3), 3.37 (dt, ³J = 8.1 Hz, 5.0 Hz, 4H, CH₂ x 2, H-2), 4.41 (s, 4H, CH₂ x 2, H-12), 7.18 – 7.38 (m, 10H, CH_{ar} x 10, H-13, H-14, H-15), 7.44 (s, 2H, CH_{ar} x 10, H-8).

¹³C NMR (75 MHz, CDCl₃): δ = 46.7, 47.6, 55.5, 125.6, 126.7, 127.1, 127.3, 128.6, 130.3, 138.2.

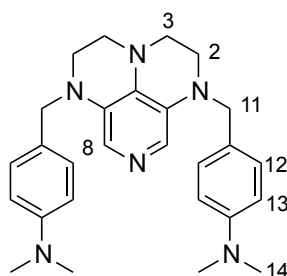
HRMS (EI): calculated for: C₂₃H₂₄N₄ [M]⁺ 356.2001, found: 356.1994.

In line with published data.^[8]



	dist _{N-C} /pm	r ₂ /pm	r ₃ /pm	d _(abcd)
crystal structure	137.7	140.2	141.7	11.4°
calculated best conf.	140.4	141.0	141.0	21.1°

4,4'-((2,3,4,5-Tetrahydro-1,3a,6,8-tetraazaphenalene-1,6-diyl)bis(methylene))bis(*N,N*-dimethylaniline) (**5d**)



The reduction was performed according to general procedure 2 at room temperature over night with 0.23 g (0.49 mmol) of starting material **15d**. After repeated purification by column chromatography using basic Alox (Brockmann 3, EtOAc/NEt₃ 20:1 → EtOAc/NEt₃/MeOH 10:1:1) the product was obtained as pale yellow solid in 33 % (0.07 g) yield.

R_f: 0.40 (basic Alox, EtOAc/NEt₃ 10:1).

mp: 100.1 – 100.9 °C.

¹H NMR (300 MHz, CDCl₃): δ = 2.93 (s, 12H, CH₃ x 4, H-14). 3.25 (td, ³J = 5.5 Hz, ³J = 2.7 Hz, 8H, CH₂ x 4, H-2, H-3), 4.30 (s, 4H, CH₂, H-11), 6.55 – 6.81 (m, 4H, CH_{ar}, H-13), 7.18 (d, ³J = 8.8 Hz, 4H, CH_{ar}, H-12), 7.53 (s, 2H, CH_{ar}, H-8).

¹³C NMR (75 MHz, CDCl₃): δ = 40.7, 45.8, 47.6, 54.8, 112.8, 125.5, 125.6, 127.0, 128.6, 130.4, 149.9.

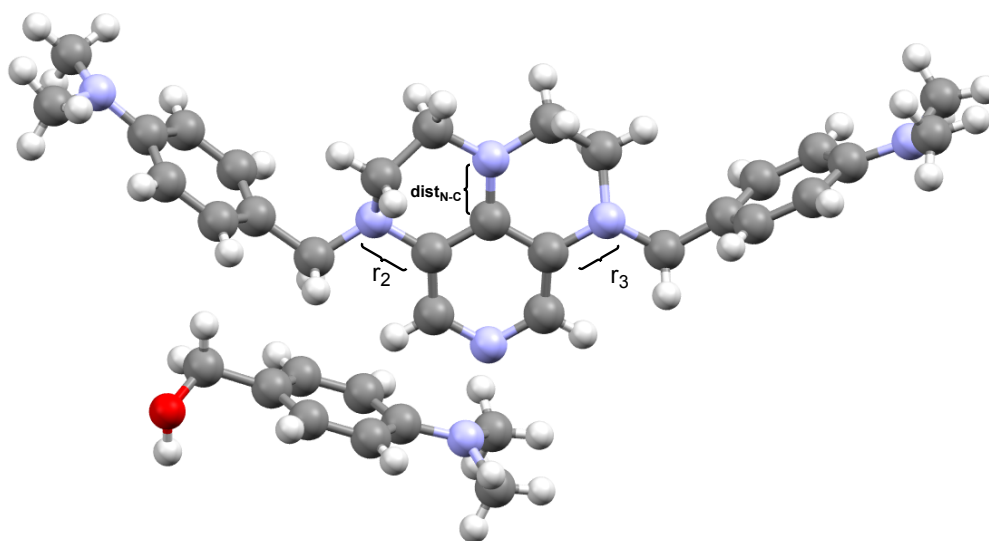
IR (ATR): $\tilde{\nu}$ (cm⁻¹) = 2820 (br, m), 1612 (s), 1565 (s), 1521 (vs), 1441 (m), 1341 (vs), 1222 (s), 1156 (vs), 1125 (s), 1063 (m), 1041 (w), 945 (m), 920 (w), 798 (vs), 743 (m).

HRMS (EI): calculated for: C₂₇H₃₄N₆ [M]⁺ 442.2845, found: 442.2831.

A recrystallization with EtOAc/Isohexane yielded bright yellow crystals. The crystal structure contains the catalyst with a benzylalcohol adduct.

^1H NMR (300 MHz, CDCl_3): δ = 2.93 (d, 3J = 3.4 Hz, 18H, $\text{CH}_3 \times 6$), 3.12 – 3.40 (m, 8H, $\text{CH}_2 \times 4$), 4.28 (s, 4H, $\text{CH}_2 \times 2$), 4.57 (s, 2H, CH_2), 6.62 – 6.83 (m, 6H, CH_{ar}), 7.29 – 7.06 (m, 6H, CH_{ar}), 7.50 (s, 2H, CH_{ar}).

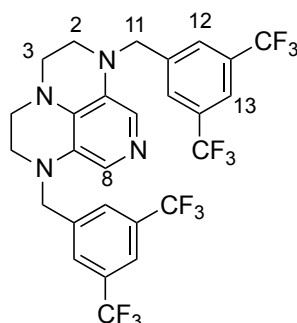
^{13}C NMR (100 MHz, CDCl_3): δ = 40.7, 40.7, 45.7, 47.6, 54.7, 65.2, 112.6, 112.8, 125.2, 127.1, 128.6, 128.7, 129.1, 130.4, 149.9, 150.3.



	dist _{N-C} /pm	r ₂ /pm	r ₃ /pm	d _(abcd)
crystal structure	136.8	141.4	141.5	1.76°
calculated best conf.	140.5	141.0	141.0	21.0°

In the calculated best conformer both benzylic substituents point downwards whereas in the crystal structure they point up. This could be due to packing effects in the crystal. Conformation **7** shows the same orientation for the benzylic substituents and is 1.6 kJ/mol higher in energy. Conformation **16** shows a pyramidalisation angle of 0.2° but a different orientation of the benzylic substituents and is 11.4 kJ/mol higher in energy.

1,6-Bis(3,5-bis(trifluoromethyl)benzyl)-1,2,3,4,5,6-hexahydro-1,3a,6,8-tetraazaphenalene (**5e**)



The reduction was performed according to general procedure 2 applying 1.38 g (2.10 mmol) of starting material **15e**. After purification by column chromatography using basic Alox (Brockmann 3, EtOAc/NEt₃ 10:1) the product was obtained as skin colored powder in 77 % (1.02 g) yield.

R_f: 0.67 (silica, EtOAc/NEt₃/MeOH 10:1:1).

mp: 207.1 – 208.3°C.

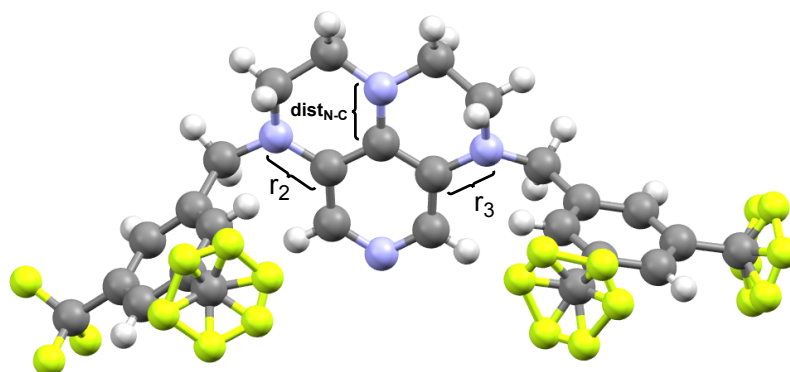
¹H NMR (600 MHz, CDCl₃): δ = 3.43 (m, 8H, CH₂ x 4, H-2, H-3), 4.50 (s, 4H, CH₂ x 2, H-11), 7.30 (s, 2H, CH_{ar}), 7.75 (s, 4H, CH_{ar}, H-12), 7.78 (s, 2H, CH_{ar}).

¹³C NMR (100 MHz, CDCl₃): δ = 47.3, 47.4, 55.5, 119.1, 121.4, 121.8, 124.6, 125.8, 127.1, 127.8, 129.6, 132.1 (q), 141.2.

¹⁹F-NMR (282 MHz, CDCl₃): δ = -62.9.

IR (ATR): $\tilde{\nu}$ (cm⁻¹) = 2857 (w), 1622 (w), 1571 (s), 1525 (m), 1443 (w), 1370 (m), 1352 (s), 1274 (vs), 1236 (m), 1162 (s), 1120 (vs), 1094 (vs), 1004 (w), 907 (s), 825 (s), 707 (s), 681 (s).

HRMS (EI): calculated for: C₂₇H₂₀F₁₂N₄ [M]⁺ 628.1496, found: 628.1492.

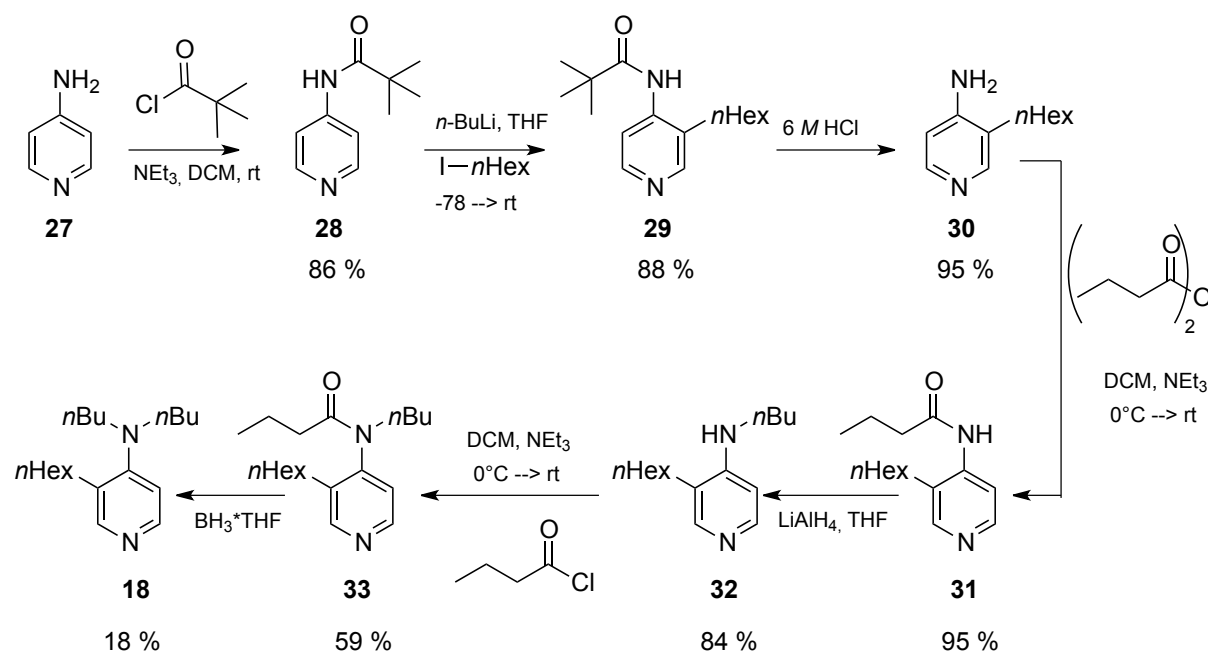


	dist _{N-C} /pm	r ₂ /pm	r ₃ /pm	d _(abcd)
crystal structure	138.5	140.4	138.9	20.3°
calculated best conf.	140.2	141.1	140.3	18.0°

In the best conformer of the calculated structure the substituents in 3- and 5- position are not the same like the crystal structure. One substituent directs to the back and one to the front.

The conformer found to be most similar to the crystal structure is conformer 5, in which both benzylic substituents point to the front. The $d_{(abcd)}$ angle is 20.6° and it is just 1 kJ/mol higher in energy.

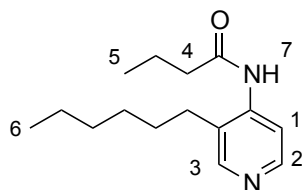
Synthesis of catalyst **18**



Scheme 3.11. Synthesis of catalyst **18**.

Compound **30** was synthesized according to a previously published strategy by *Held et al.*^[10]

N-(3-Hexylpyridin-4-yl)butyramide (**31**)



Compound **30** 0.60 g (3.37 mmol) was dissolved in NEt₃ 0.70 mL (1.5 eq., 5.01 mmol) and 8 mL DCM. At 0 °C butyric anhydride 0.55 mL (3.37 mmol) in 2 mL DCM was added slowly via a dropping funnel. After stirring for one hour at 0°C the reaction mixture was stirred at room temperature over night. The reaction mixture was washed three times with sat. NaHCO₃ and three times with DCM. The combined organic layers were dried over MgSO₄ and the solvent was distilled off at reduced pressure. Column chromatography (silica, EtOAc/iH 9:1) gave **31** as a pale brown solid in 95 % (0.80 g).

R_f: 0.47 (silica, EtOAc/IH 9:1).

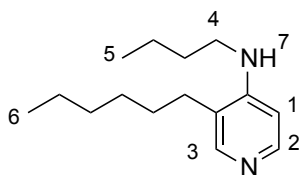
¹H NMR (200 MHz, CDCl₃): δ = 0.89 (s, 3H), 1.02 (t, ³*J* = 7.4 Hz, 3H), 1.24 – 1.49 (m, 6H), 1.50 – 1.71 (m, 2H), 1.77 (dd, ³*J* = 14.9 Hz, ³*J* = 7.4 Hz, 2H), 2.40 (t, ³*J* = 7.4 Hz, 2H), 2.48 – 2.64 (m, 2H), 7.20 (s, br, 1H, NH, H-7), 8.16 (d, ³*J* = 5.6 Hz, 1H, H-1), 8.33 (s, 1H, H-3), 8.39 (d, ³*J* = 5.6 Hz, 1H, H-2).

¹³C NMR (100 MHz, CDCl₃): δ = 13.6, 13.9, 18.8, 22.5, 28.5, 29.0, 39.1, 29.2, 29.3, 29.6, 31.5, 31.9, 39.9, 114.5, 124.7, 142.6, 148.9, 150.6, 171.4.

IR (ATR): $\tilde{\nu}$ (cm⁻¹) = 3252 (w, br, NH), 2957 (m), 2924 (s), 2854 (m), 1672 (s, C=O), 1577 (vs), 1503 (vs), 1463 (s), 1412 (s), 1377 (m), 1311 (m), 1282 (s), 1193 (s), 1075 (m), 990 (w), 908 (m), 834 (m), 730 (v), 699 (m).

HRMS (EI): calculated for: C₁₅H₂₄N₂O [M+H]⁺ 249.1967, found: 249.1959.

N-Butyl-3-hexylpyridin-4-amine (**32**)



In a flame dried three necked Schlenk flask LiAlH₄ (62 mg, 1.63 mmol) were stirred in THF. Compound **31** (0.30 g, 1.21 mmol) was dissolved in THF and slowly added via a dropping funnel at 0 °C in 15 min. After stirring for additional 15 min at room temperature the reaction mixture was refluxed for three hours. The reaction was quenched with EtOAc and the solvent removed under reduced pressure. After addition of DCM to the residue it was filtered over Celite and directly subjected to column chromatography using silica (EtOAc 100 %). A yellow oily substance was obtained in 84 % (0.23 g) yield.

R_f: 0.17 (silica, EtOAc 100%).

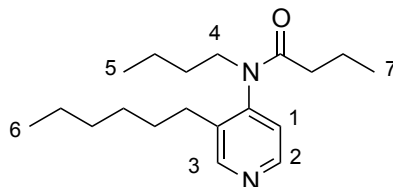
¹H NMR (300 MHz, CDCl₃): δ = 0.90 (s, 3H), 0.99 (t, ³*J* = 7.3 Hz, 3H), 1.18 – 1.76 (m, 12H), 2.35 – 2.48 (m, 2H), 3.19 (dd, ³*J* = 12.4 Hz, ³*J* = 7.0 Hz, 2H), 4.05 (s, br, 1H, NH), 6.45 (d, ³*J* = 5.7 Hz, 1H, H-1), 8.03 (s, 1H, H-3), 8.16 (d, ³*J* = 5.6 Hz, 1H, H-2).

¹³C NMR (75 MHz, CDCl₃): δ = 13.8, 14.0, 20.2, 22.6, 28.0, 28.3, 29.2, 31.3, 31.6, 42.5, 104.5, 120.6, 148.5, 148.7, 151.2.

IR (ATR): $\tilde{\nu}$ (cm⁻¹) = 3152 (w, br, NH), 3140 (w), 2955(m), 2926 (s), 2857 (m), 1596 (vs), 1573 (s), 1519 (s), 1464 (m) 1332(m), 1222 (w), 1189 (s), 1067 (m), 919 (w), 811 (s), 724 (m), 611 (m).

HRMS (EI): calculated for: C₁₅H₂₆N₂ [M]⁺ 234.2096, found: 234.2086.

N-Butyl-*N*-(3-hexylpyridin-4-yl)butyramide (**33**)



In an oven dried Schlenk tube the starting material **29** (0.28 g, 1.19 mmol) was dissolved in dry DCM. After the addition of NEt_3 (0.49 mL, 3.57 mmol) the slightly yellow reaction mixture was cooled to 0 °C and butyryl chloride (0.28 mL, 2.2 eq., 2.61 mmol) was added dropwise. The reaction mixture was stirred at room temperature over night. After the disappearance of starting material (TLC) the solvent was removed under reduced pressure and the orange residue was directly subjected to column chromatography (silica, IH/EtOAc/NEt_3 10:2:1) and yielded the product **30** in 59 % (0.21 g).

R_f : 0.52 (silica, IH/EtOAc/NEt_3 10:2:1).

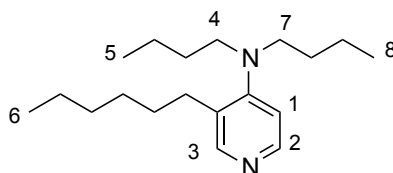
^1H NMR (300 MHz, CDCl_3): δ = 0.87 (ddd, 3J = 22.8 Hz, 3J = 11.0 Hz, 3J = 5.9 Hz, 10H), 1.15 – 1.72 (m, 13H), 1.72 – 2.00 (m, 2H), 2.44 – 2.61 (m, 2H), 2.95 – 3.10 (m, 1H), 4.04 – 4.23 (m, 1H), 7.00 (d, 3J = 5.1 Hz, 1H), 8.50 (d, 3J = 5.1, 1H), 8.63 (s, 1H).

^{13}C NMR (100 MHz, CDCl_3): δ = 13.7, 13.8, 13.9, 18.6, 20.1, 22.5, 28.2, 29.4, 29.8, 29.9, 31.5, 36.3, 48.4, 124.0, 135.7, 148.6, 148.7, 152.6, 171.9.

IR (ATR): $\tilde{\nu}$ (cm^{-1}) = 2958 (s), 2929 (s), 2872 (m), 1756 (w), 1663 (vs, C=O), 1583 (s), 1559 (m), 1491 (m), 1458 (m), 1397 (s), 1283 (m), 1214 (m), 1137 (m), 838 (w), 731 (w), 616 (w).

HRMS (EI): calculated for: $\text{C}_{19}\text{H}_{32}\text{N}_2\text{O}$ $[\text{M}]^+$ 304.2515, found: 304.2496.

N,N-Dibutyl-3-hexylpyridin-4-amine (**18**)



In an flame dried Schlenk flask $\text{BH}_3 \cdot \text{THF}$ (4.80 mL, 4.80 mmol) is stirred and **30** (0.30 g, 0.98 mmol) in 2 mL dry THF is added dropwise. The reaction mixture was refluxed for 16 hours and quenched by the slow addition of water. The mixture was poured onto 60 mL of 6M HCl and extracted with CHCl_3 . After making the aqueous phase under ice cooling slowly basic (pH=12) with NaOH, it was extracted again with CHCl_3 . After drying the organic phase over MgSO_4 the solvent was removed under reduced pressure and the crude mixture purified by column chromatography (silica, IH/EtOAc/NEt_3 10:2:1). The product was obtained as colorless oil in 18 % (51 mg) yield.

R_f : 0.68 (silica, $\text{CHCl}_3/\text{MeOH}$ 10:1).

^1H NMR (300 MHz, CDCl_3): δ = 0.86 (dd, 3J = 8.2 Hz, 3J = 6.4 Hz, 9H), 1.13 – 1.36 (m, 10H), 1.43 (ddd, 3J = 11.8 Hz, 3J = 8.4 Hz, 3J = 6.0 Hz, 4H), 1.60 (dd, 3J = 15.2 Hz, 3J = 7.5 Hz, 2H), 2.52 – 2.62 (m, 2H), 2.95 – 3.07 (m, 4H), 6.80 (d, 3J = 5.5 Hz, 1H), 8.21 (d, 3J = 5.5 Hz, 1H), 8.26 (s, 1H).

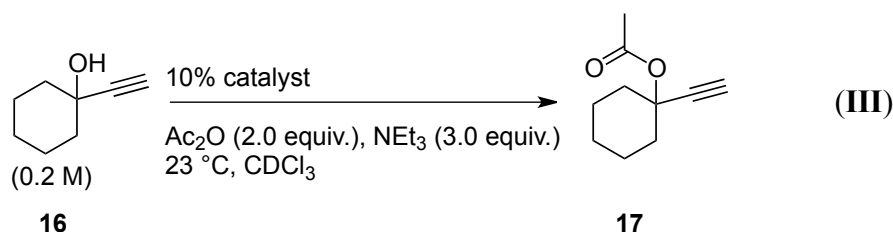
^{13}C NMR (75 MHz, CDCl_3): δ = 13.8, 14.0, 20.3, 22.6, 29.2, 29.3, 29.6, 29.7, 31.6, 52.2, 115.1, 131.3, 147.5, 151.5, 156.8.

IR (ATR): $\tilde{\nu}$ (cm^{-1}) = 2957 (s), 2930 (s), 2860 (m), 2354 (w), 1623 (w), 1585 (s), 1492 (m), 1465 (m), 1376 (m), 1166 (m), 1117 (m), 927 (m), 828 (m), 731 (m).

HRMS (EI): calculated for: $\text{C}_{19}\text{H}_{34}\text{N}_2$ $[\text{M}]^+$ 290.2722, found: 290.2711.

Conduction of Kinetic Measurements

The benchmark reaction (III) was carried out using stock solutions. The preparation of these stock solutions were carried out as follows: 3 mmol of the alcohol and 9 mmol triethylamine were mixed in a graduated 5 mL measurement flask. In the same way 6 mmol anhydride and 1.5 mmol dioxane (internal Standard) were mixed in another graduated 5 mL measurement flask. In a third graduated 5 mL measurement flask 0.3 mmol of the catalyst is weighed in. Every graduated 5 mL measurement flask is filled up to 5 mL with freshly distilled CDCl_3 and sealed with a septum. After shaking the 5 mL measurement flasks 200 μL of every stock solution is transferred into an oven-dried and degassed NMR-tube. The concentrations of the stock solutions are: alcohol **16**: 0.6 M; anhydride: 1.2 M; triethylamine: 1.8 M; dioxane: 0.3 M; catalyst: 0.06 M. Thus the concentrations used in the benchmark reaction (NMR tube) are: alcohol **16**: 0.2 M; acetic anhydride: 0.4 M; triethylamine: 0.6 M; dioxane: 0.1 M; catalyst: 0.02 M.



Scheme 3.12. ^1H NMR benchmark reaction (III); acylation of a tertiary alcohol **16** in CDCl_3 .

Evaluation Methods for Acylation Reaction Kinetics

There are two different approaches to calculate the conversion of this acylation reaction: 1. Calculation of conversion with respect to an internal standard (dioxane), and 2. Conversion determination without standard. The derivation for the formulas can be found in Larionov *et al.*, “Kinetics of reactions in homogeneous solution”.^[31]

- Calculation of conversion with respect to dioxane as internal standard (the meaning of the used abbreviations will be described below):

$$Conversion_{ester} = \left[\frac{4I_{ester}}{3I_{dioxane}} \right] * 100 \%$$

$$Conversion_{anhydride} = \left[1 - \frac{I_{anhydride}}{3I_{dioxane}} \right] * 200 \%$$

$$Conversion_{alcohol} = \left[1 - \left[\frac{4I_{alcohol}}{I_{dioxane}} \right] \right] * 100 \%$$

- Calculation of conversion without use of standard (used in this thesis):

$$Conversion_{ester \text{ without standard}} = \left[\frac{4I_{ester}}{I_{ester} + I_{anhydride} + I_{ammoniumacetate}} \right] * 100 \%$$

The data of acylation reactions within this thesis were evaluated with the $Conversion_{ester \text{ without standard}}$ method for reasons, which will be described in the next section.

The used abbreviations are as follows:

I_{ester} = Singlett of $-CH_3$ at 1.9 ppm; $I_{dioxane}$ = Singlett of 4 $-CH_2$ groups at 3.6 ppm;
 $I_{anhydride}$ = Singlett of $-CH_3$ at 2.1 ppm; $I_{alcohol}$ = Singlett of alkine proton at 2.3 ppm;
 $I_{ammoniumacetate}$ = Singlett of $-CH_3$ at 1.8 ppm.

Figure 3.13 shows a 1H NMR spectrum under reaction conditions with the different substrates designated to chemical shifts.

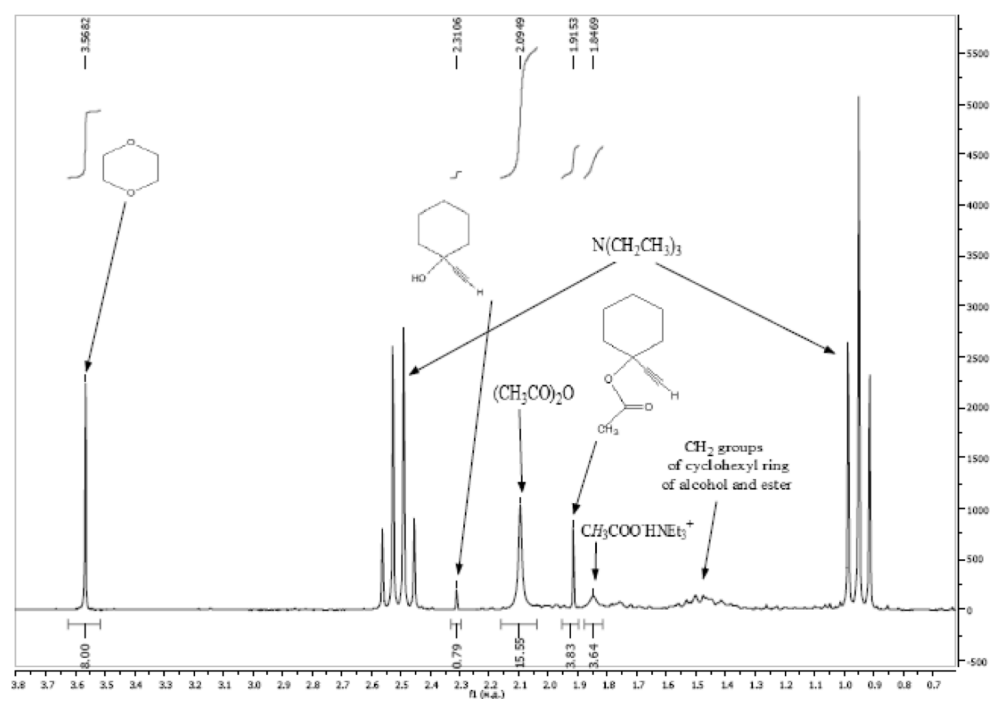


Figure 3.13. ^1H NMR (200 MHz) spectrum of the reaction mixture for the benchmark reaction.

The experimental data were fitted with a second order rate law:

$$\text{conversion} [\%] = c_1 * \left(1 - \frac{1}{2 \exp(k(t - t_0)) - 1} \right) * 100$$

The resulting plot is depicted in Figure 3.14 and the kinetic half-life time is calculated by:

$$t_{1/2} = \frac{\ln 1.5}{k_2[\text{ROH}]_0}$$

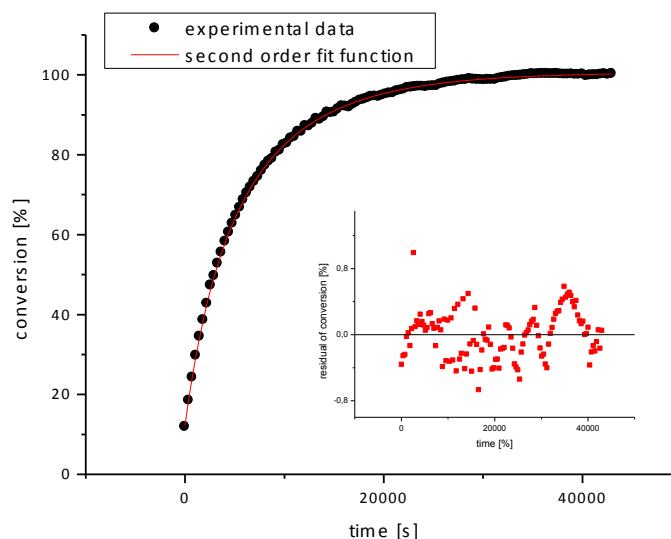


Figure 3.14. Results for the reaction of tertiary alcohol **16** and Ac₂O catalyzed by 10mol-% **2** in CDCl₃.

Effects of Different Evaluation Methods

The next section will show the effect of different evaluation methods applied for the kinetic measurement of acylation reaction (**III**). For that reason the conversion of a single dataset is evaluated in different ways as mentioned before. The effects of the different evaluation methods on the kinetic half-life time $t_{1/2}$ (time interval that is necessary for a given concentration to decrease to half of its initial value), maximum conversion y_0 and zero time t_0 (time when reaction starts by adding the catalyst to the reaction mixture) will be summarized. In comparison, the synthetic half-life time $t_{1/2(syn)}$ is the time interval between the start of a reaction and the time, when conversion is equal to 50% and differs from the kinetic half-life time in those cases, in which the maximum conversion of the reaction is different from 100%.

The first plot shows the conversion determined by the “*Conversion_{ester}*”-method (see above). On the right hand side of the plot the residuals are depicted.

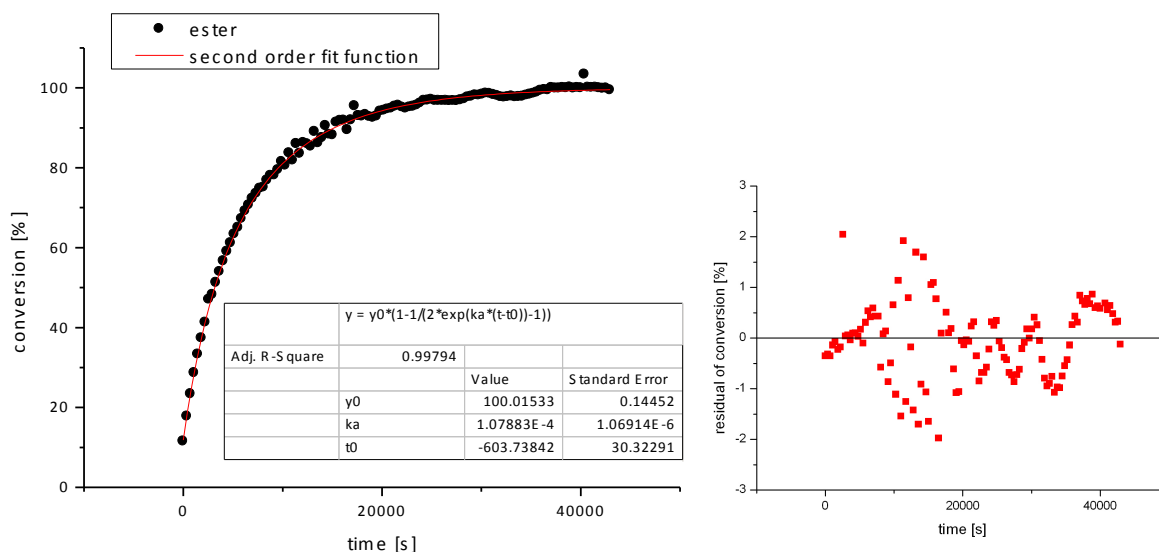


Figure 3.15. Fitting of kinetic data using the “*Conversion_{ester}*”-method. On the right hand side the residuals are depicted. The kinetic half-life time ($t_{1/2}$) is in this case 63 min.

Conversion determination by the “*Conversion_{anhydride}*”-method (see above) of the same dataset will lead to the following plot:

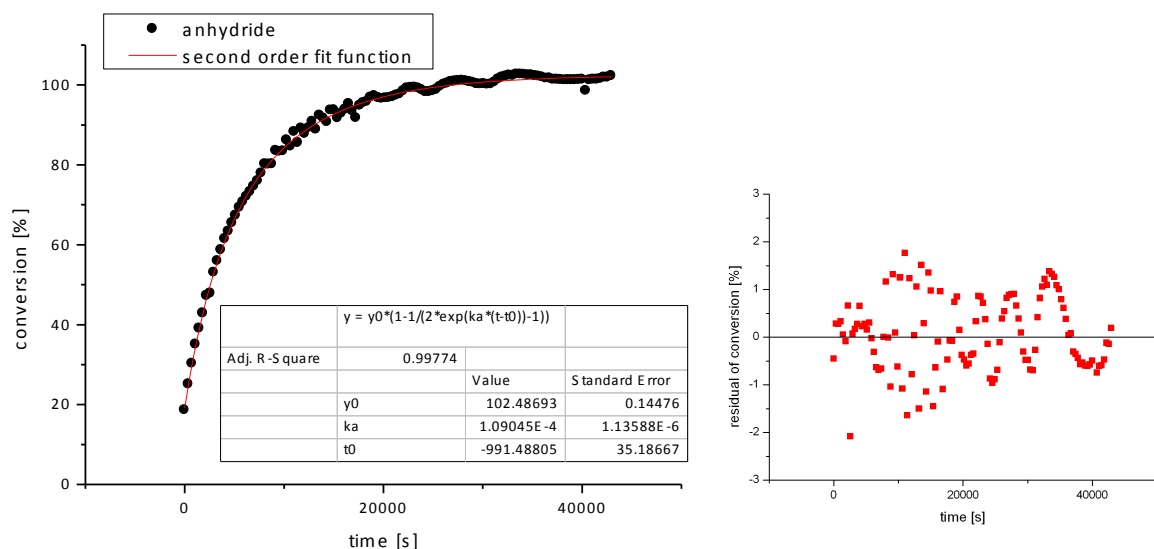


Figure 3.16. Fitting of the same kinetic data using the “*Conversion_{anhydride}*”-method. On the right hand side the residuals are depicted. The kinetic half-life time ($t_{1/2}$) is in this case 62 min.

By determination of conversion by the “*Conversion_{alcohol}*”-method (see above) the following will be obtained (the representing residual segment of -3 to 3 was in this case not sufficient):

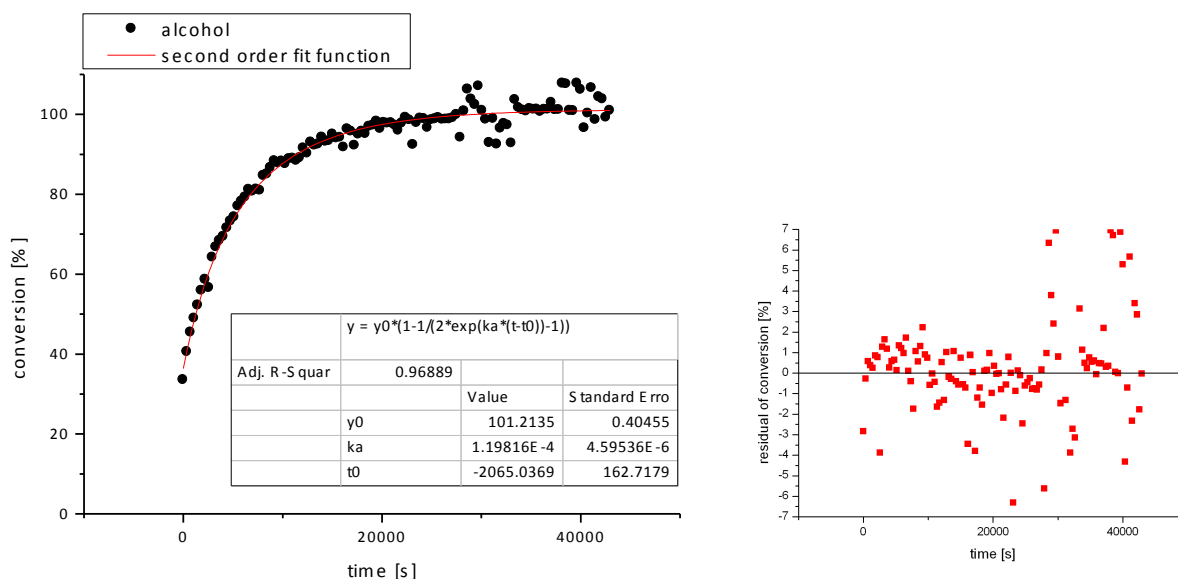


Figure 3.17. Fitting of the same kinetic data using the “*Conversion_{alcohol}*”-method. On the right hand side the residuals are depicted. The kinetic half-life time ($t_{1/2}$) is in this case 56 min.

Another possibility is the determination of the conversion by using the ammonium acetate-signal instead of the standard-integral (dioxane). This approach was introduced as: “*Conversion_{ester without standard}*” (see above):

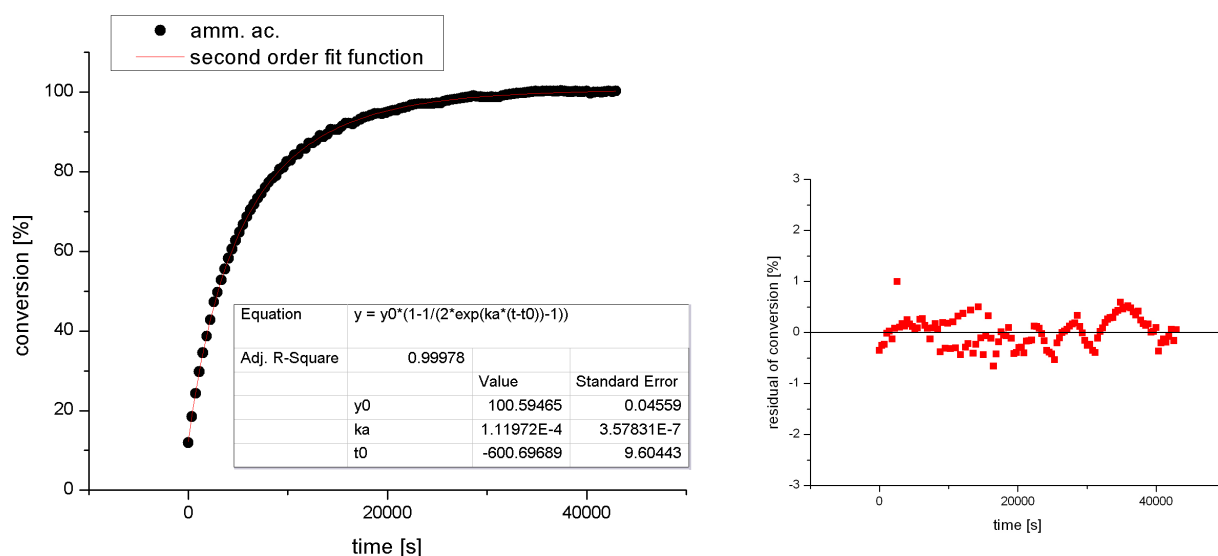


Figure 3.18. Fitting of the same kinetic data using the “*Conversion_{ester without standard}*”-method. On the right hand side the residuals are depicted. The kinetic half-life time ($t_{1/2}$) is in this case 60 min.

In Table 3.5 a comparison between the different evaluation methods and their effects of the mentioned parameters is given.

Table 3.5. Tabular comparison of the different evaluation methods.

	<i>Ester</i>	<i>Anhydride</i>	<i>Alkohol</i>	<i>Amm. ac</i>
$t_{1/2}$ [min]	63	62	56	60
y_0 [%]	100.0	102.4	101.2	100.6
k_a	1.08×10^{-4}	1.09×10^{-4}	1.20×10^{-4}	1.11×10^{-4}
$t_0^{[a]}$	10.06 min	16.52 min	34.14 min	10.01 min
Residuals ^[b] [%]	" -3 ; +3 "	" -2 ; +2 "	" -7; +7 "	" -0.6 ; +0.6 "

[a] t_0 Real = 10 min; [b] Most values.

For a validation of which is the best method of evaluation, all parameters have to be taken into account: $t_{1/2}$, y_0 , k_a , t_0 and the residuals. The residuals should vary statistically, not systematically, and the deviations should be rather small. In this case it can be seen that ‘*ester*’ and ‘*amm. ac*’ evaluation give the best and most reliable results. They have a t_0 -value that is in line with reality (in this case 10 min). They have maximum conversions (y_0) nearest to 100 % and residual values are best for the *amm. ac*-method.

Another possibility of how to handle data is to normalize the data to 100 % yield.

$$Conversion_{normalized} = \frac{y}{y_0} * 100 \%$$

This transformation will not change the half-life time (as the k_a values in the tables of the output parameters depicted in Figures 3.18 and 3.19 show). In both cases the obtained kinetic half-life time is 63 min. It should be added, that the parameter y_0 is still set as a variable during the fitting process and thus not fixed to 100. The data before normalization are depicted in Figure 3.18 and after normalization in Figure 3.19.

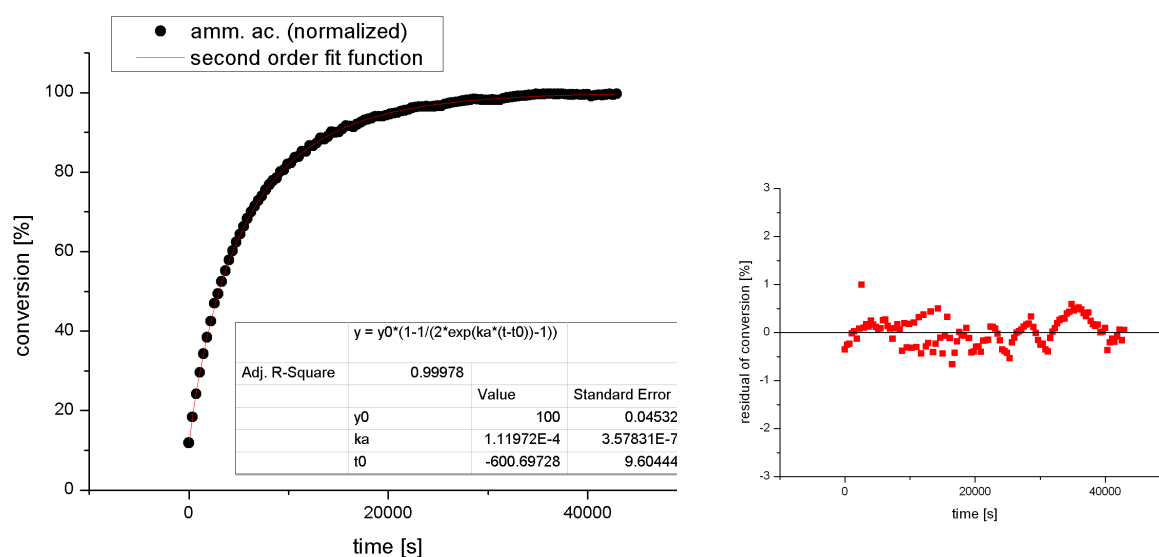


Figure 3.19. Data for *amm. ac.* for the same kinetic after normalisation. On the right hand side the residuals are depicted.

One more aspect of evaluation of reaction kinetics in general is to fit kinetic data up to different reaction times, given that the reaction proceeds to full conversion and the catalyst will not be deactivated during the catalytic process. Figure 3.18 shows a conversion time plot for a kinetic measurement containing data beyond 40000 sec although the reaction was essentially complete at around 30000 seconds. Figures 3.20 – 3.23 will show the effect of taking into account less reaction time (for the same test data set). The impact of the resulting fitted parameters will be summarized in Table 3.6.

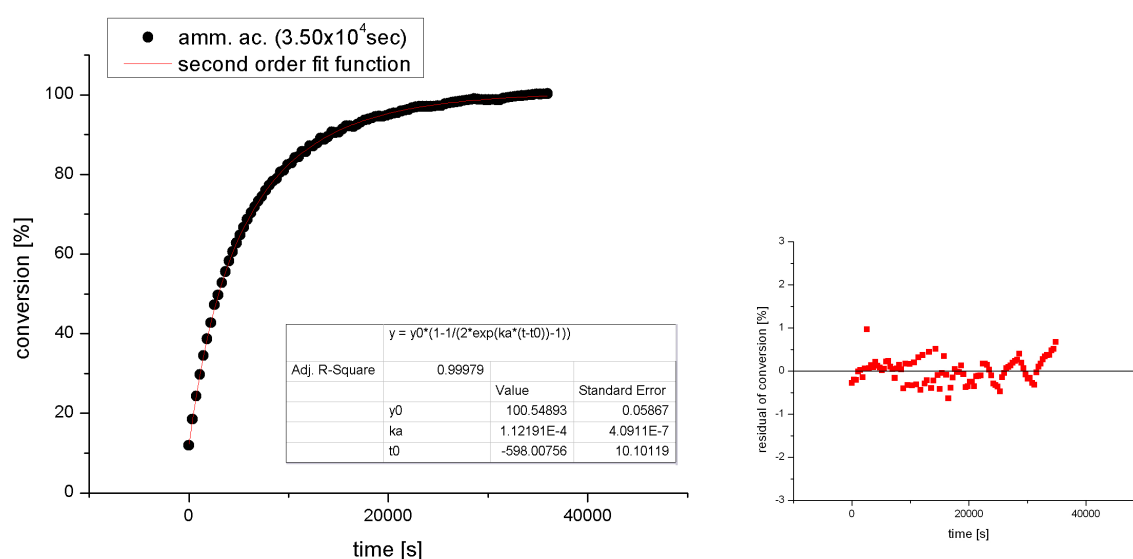


Figure 3.20. The same kinetic data as in Figure 3.18 (evaluated with the '*amm. ac.*'-method) fitted up to 35000 seconds. On the right hand side the residuals are depicted.

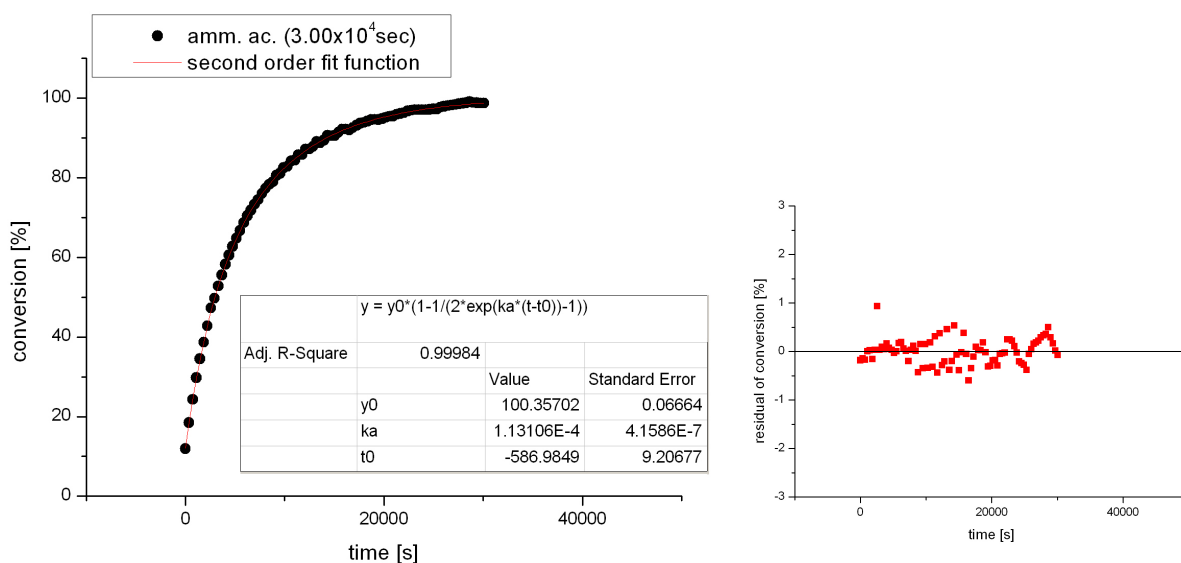


Figure 3.21. The same kinetic data as in Figure 3.18 (evaluated with the 'amm. ac'-method) fitted up to 30000 seconds. On the right hand side the residuals are depicted.

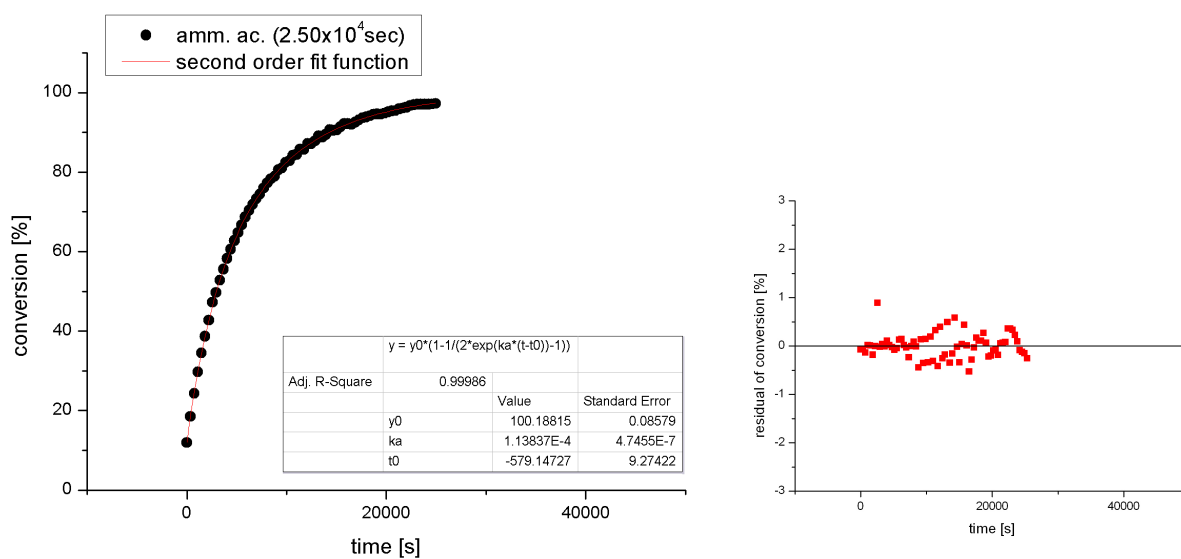


Figure 3.22. The same kinetic data as in Figure 3.18 (evaluated with the 'amm. ac'-method) fitted up to 25000 seconds. On the right hand side the residuals are depicted.

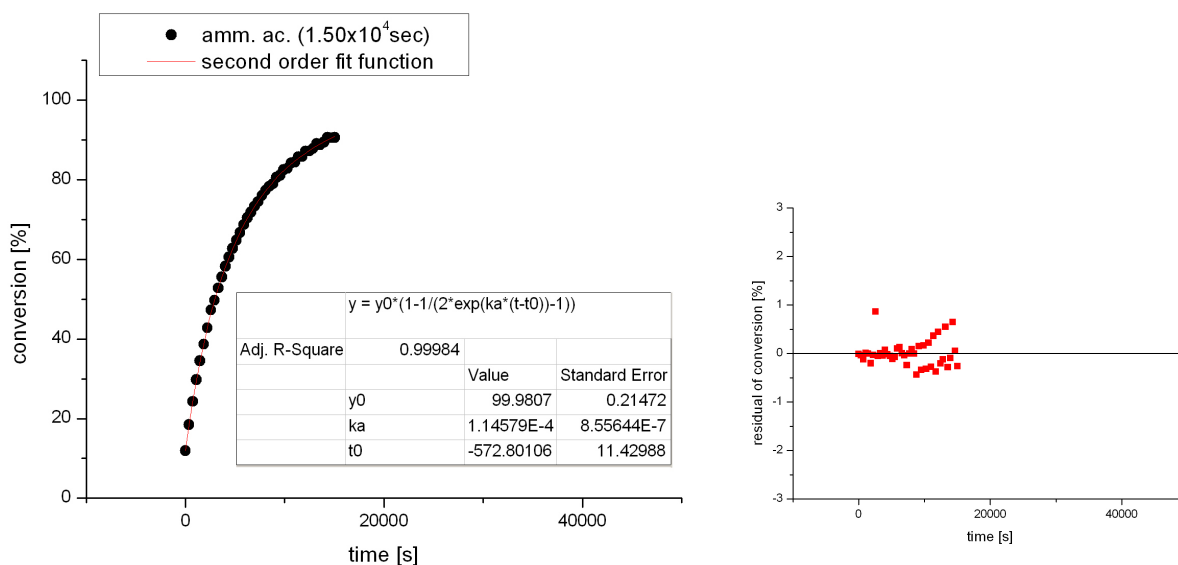


Figure 3.23. The same kinetic data as in Figure 3.18 (evaluated with the ‘*amm. ac*’-method) fitted up to 15000 seconds. On the right hand side the residuals are depicted.

In Table 3.6 the fitted output parameters are given for the test dataset fitted with the same second order rate law but taking into account different reaction times. For evaluation the “*amm. ac*”-method was used.

Table 3.6. Test dataset fitted up to different reaction times and resulting variations of obtained parameters $t_{1/2}$, y_0 , k_a , t_0 and maximum conversion of the last datapoint taken into account (conv.).

	4.00x10 ⁴ [sec]	3.50x10 ⁴ [sec]	3.00x10 ⁴ [sec]	2.50x10 ⁴ [sec]	1.50x10 ⁴ [sec]
$t_{1/2}$ [min]	60.4	60.2	59.8	59.4	59.0
y_0 [%]	100.59	100.54	100.37	100.18	99.98
k_a	1.12x10 ⁻⁴	1.12x10 ⁻⁴	1.13x10 ⁻⁴	1.14x10 ⁻⁴	1.15x10 ⁻⁴
t_0 [min] ^[a]	10.0	9.97	9.78	9.65	9.53
Conv. [%] ^[b]	100	100	98.7	97.2	90.6

[a] t_0 real = 10 min; [b] maximum conversion of the last datapoint.

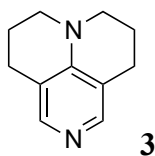
As Table 3.6 shows, the obtained half-life times do not depend on the reaction time taken into account as long as the reaction will finally proceed to full conversion and the catalyst does not decompose. It does not even matter if the last data point shows already full conversion as the last column (1.50x10⁴ [sec]) shows. In this special case the last data c show a conversion of just 90 %, nevertheless the fitting process predicts the reaction to proceed up to 99.98 %. The obtained half-life time in this special case differs only by 1 minute (59 minutes). From columns 2 (4.00x10⁴ [sec]) to 4 (2.50x10⁴ [sec]), in which the considered data show full conversion or almost full conversion, the obtained half-life times differ as well only within a 1 % margin. As could be seen in Table 3.6 the fitting process is quite robust in terms of

variation of reaction time used for the fitting process. One reason of this obtained ‘robustness’ of the dataset is the large amount of data points collected.

Data of kinetic runs

Kinetics of the reactions of catalysts **3**, **4a-c**, **5a-e** with alcohol **16**. All time specifications are in minutes if not stated differently. For every measurement the experimental data and the fit curve together with the residuals are depicted. The time window was chosen until the appearance of saturation at full conversion, depending on the speed of the catalyst. As the catalysts measured are too different in terms of activity it was not possible to compare the same time window for every catalyst. Every experiment was done at least twice and the resulting kinetic half-life times are given with standard deviations.

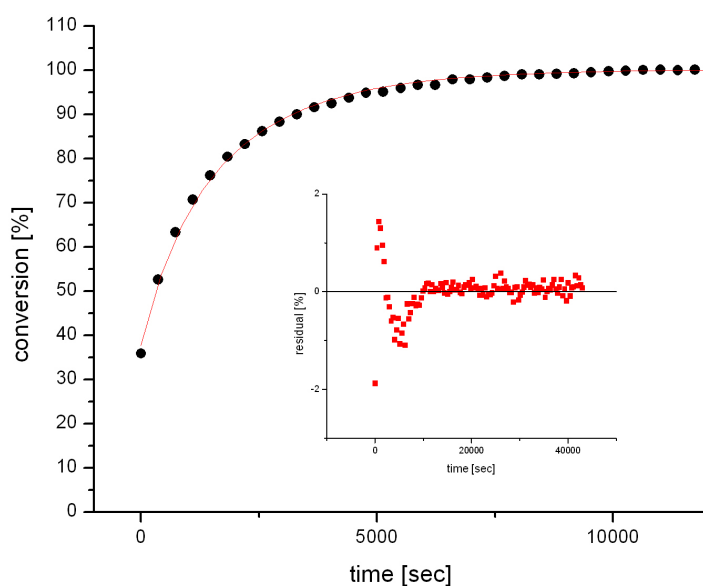
10 mol-% catalyst loading

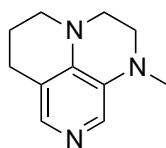


1) 15.1

2) 14.2

$= 14.7 \pm 0.5$



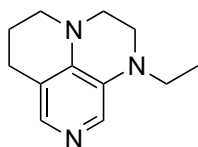
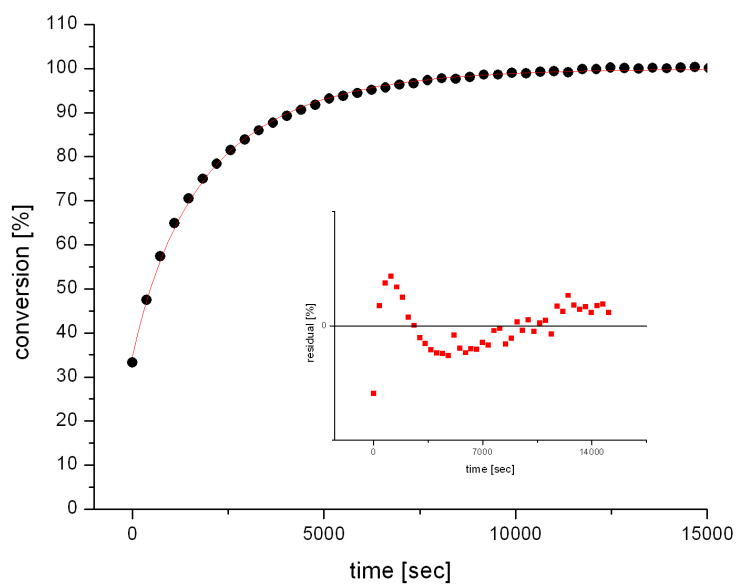


4a

1) 18.8

2) 17.1

$= 17.9 \pm 0.9$

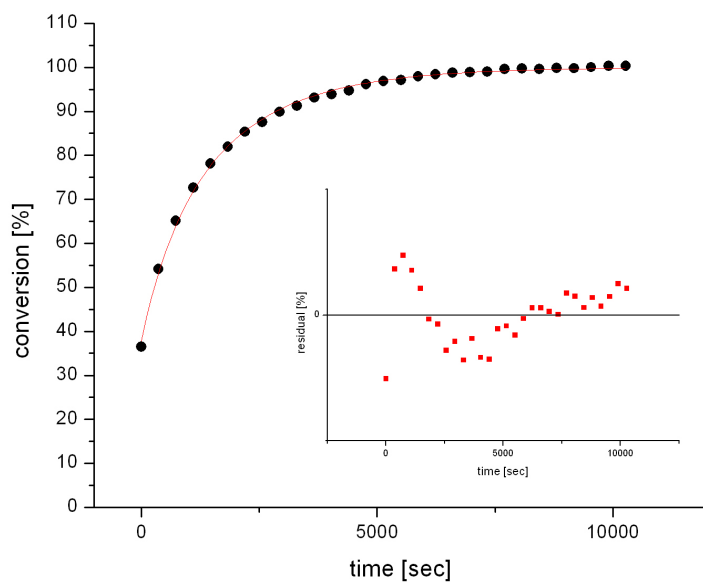


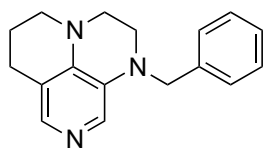
4b

1) 13.4

2) 14.1

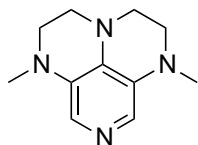
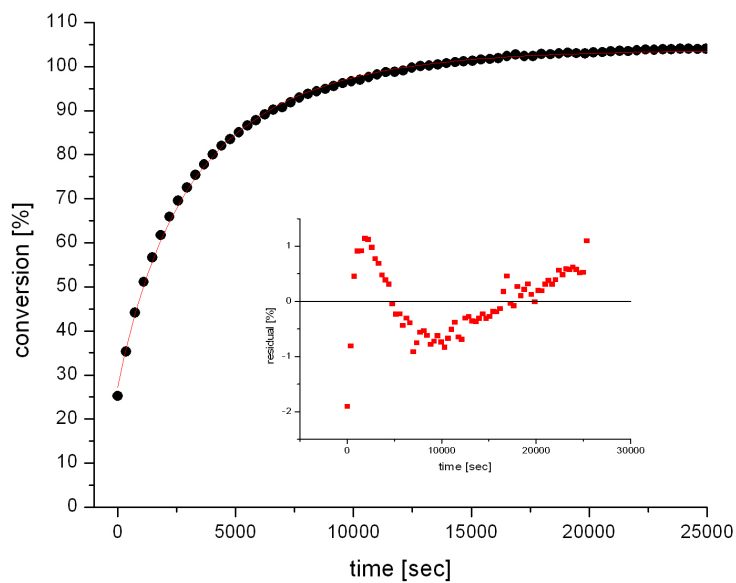
$= 13.8 \pm 0.4$





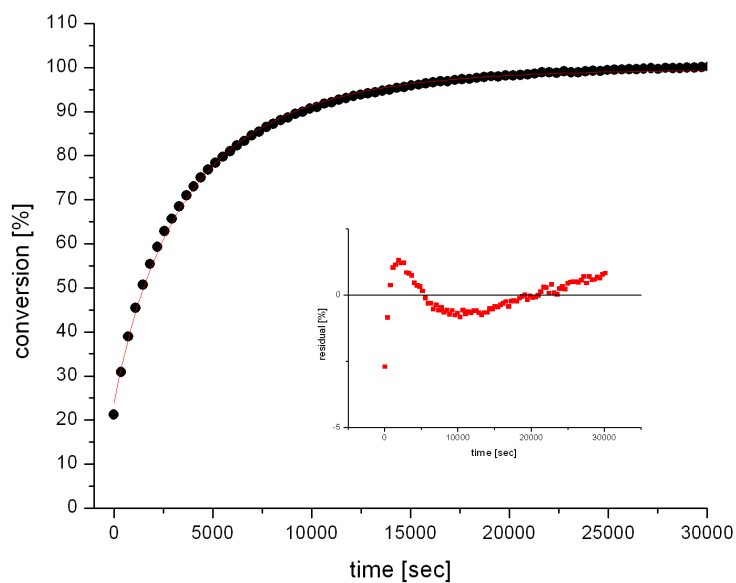
4c

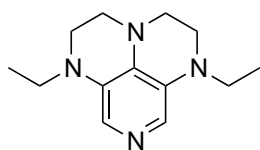
1) 34.1
2) 34.5
= 34.3 ± 0.2



5a

1) 36.1 3) 39.8
2) 38.1 = 38.0 ± 1.5





5b

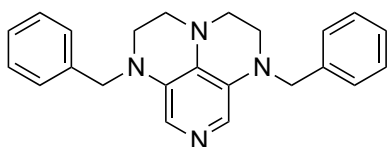
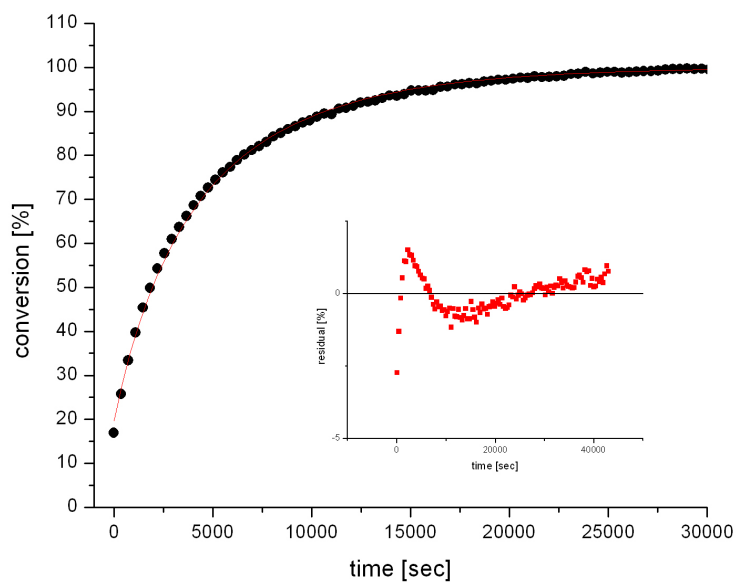
1) 44.9

3) 41.6

2) 44.9

4) 45.3

= 44.2 ± 1.5

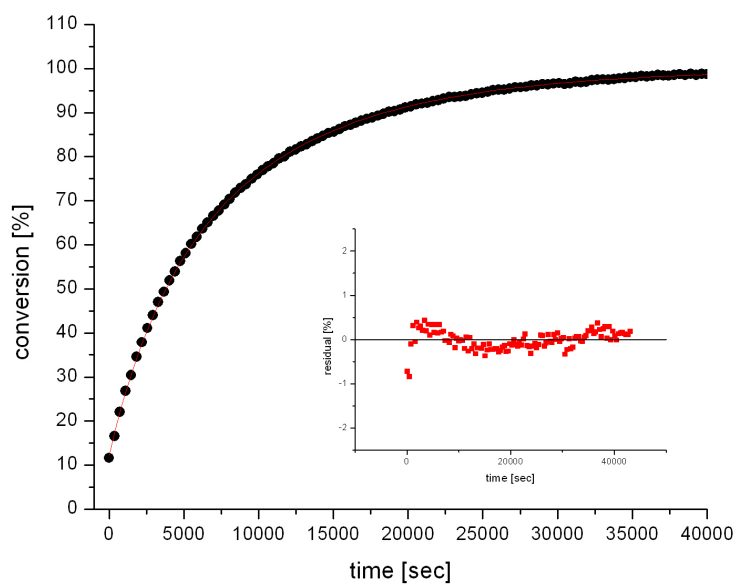


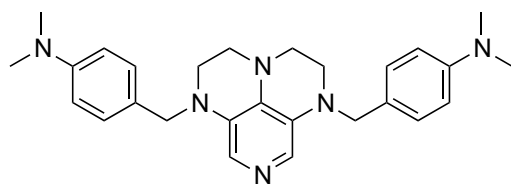
5c

1) 62.3

2) 68.5

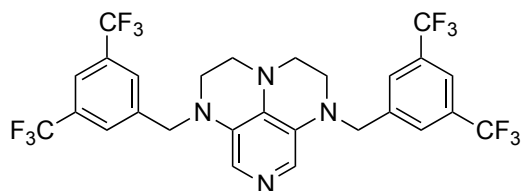
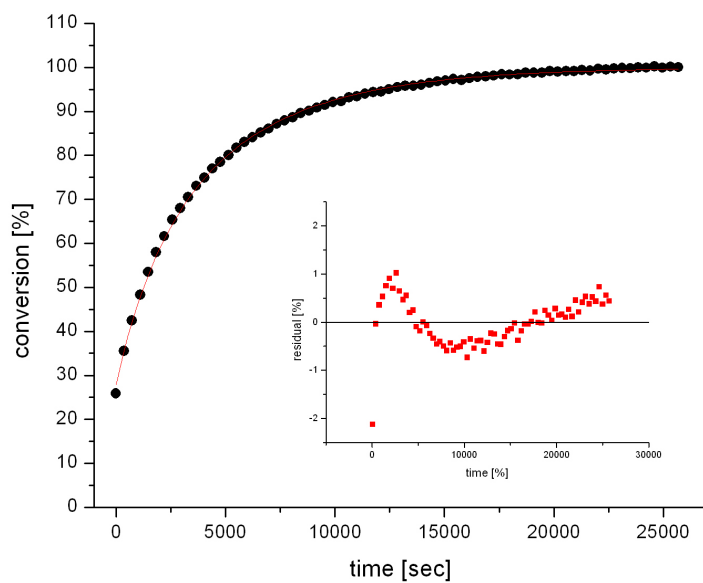
= 65.4 ± 3.1





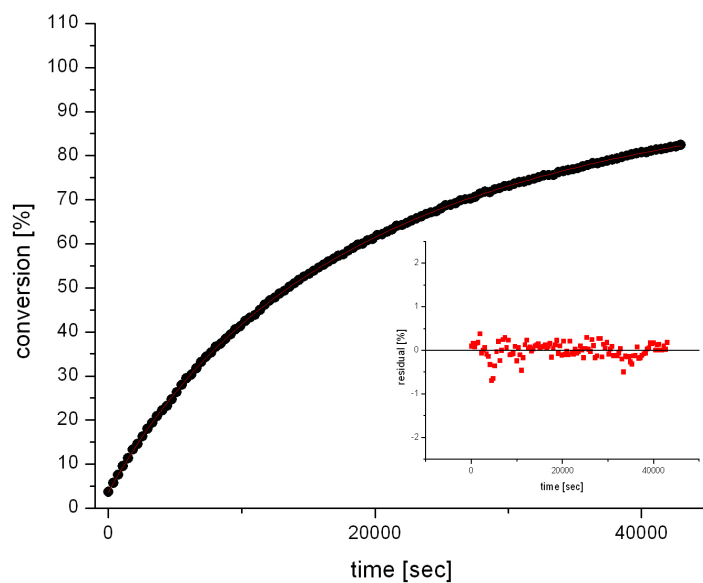
5d

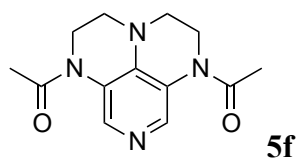
1) 39.4
2) 37.3
= 38.4 ± 1.0



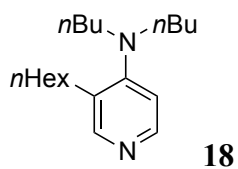
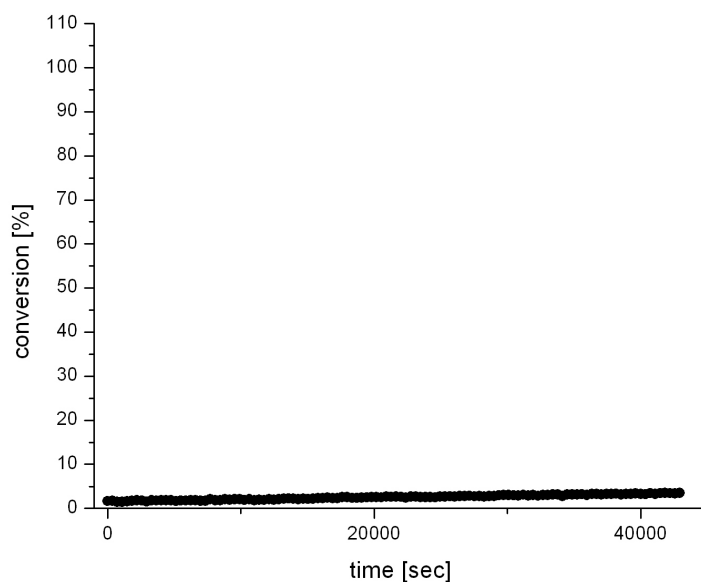
5e

1) 227.9
2) 226.8
= 227.3 ± 0.5

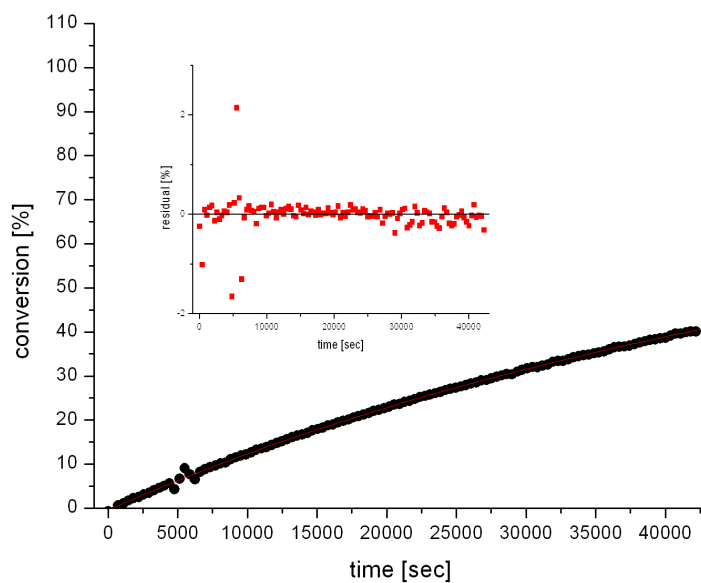


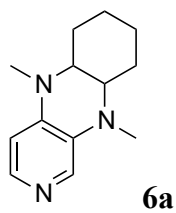


- 1) 13 % conversion after 12 h
- 2) 12 % conversion after 12 h
- ≥ 2880 min (extrapolated)

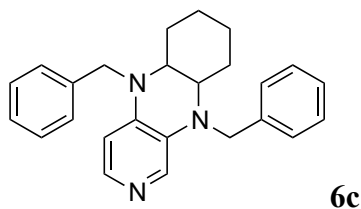
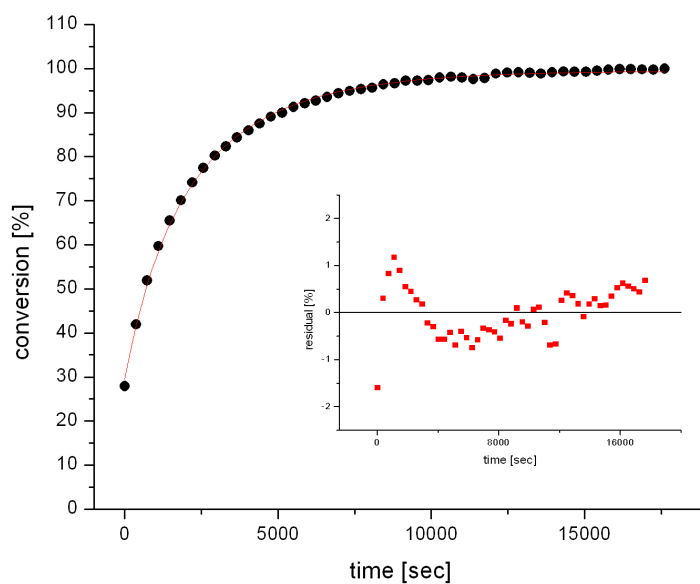


- 1) 818.2
- 2) 938.1
- $= 878.1 \pm 59.9$

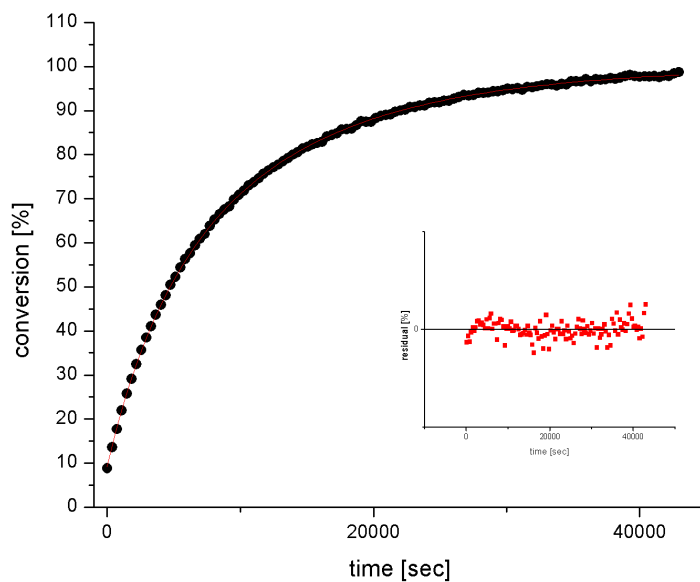




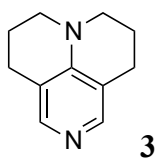
1) 19.5 3) 22.7
 2) 21.4 4) 21.6
 = 21.3 ± 1.1



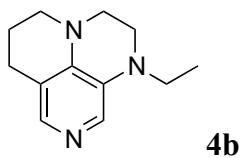
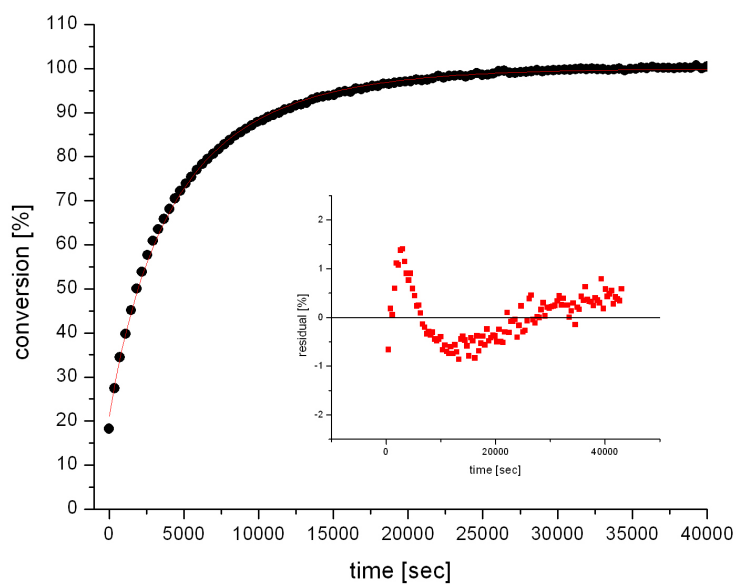
5) 89.9
 6) 98.1
 = 94.0 ± 4.1



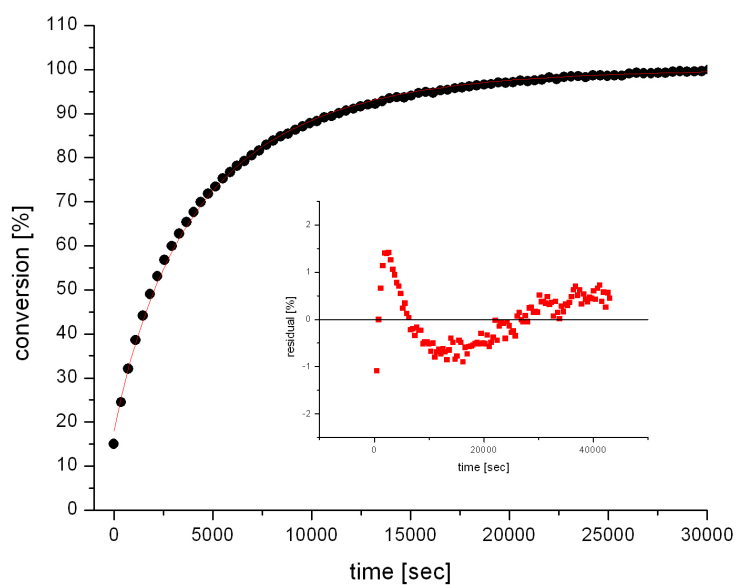
3 mol-% catalyst loading

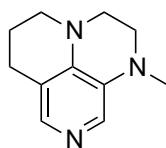


1) 46.7



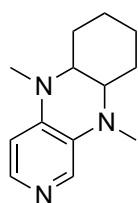
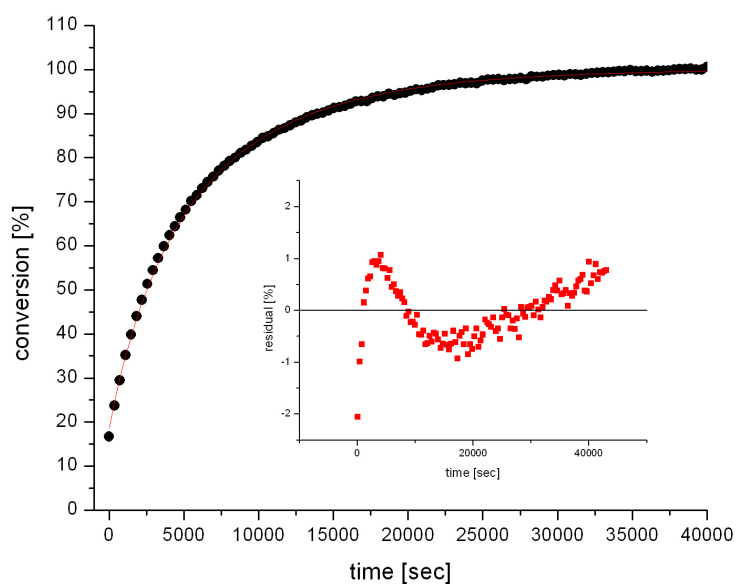
1) 45.9





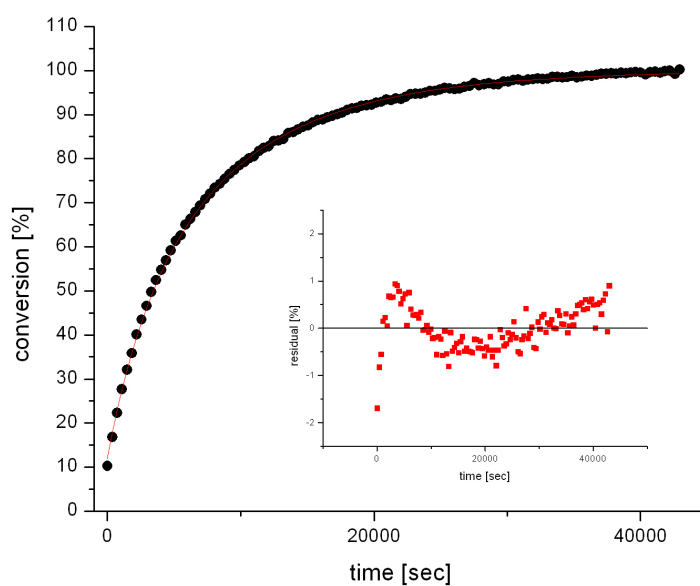
4a

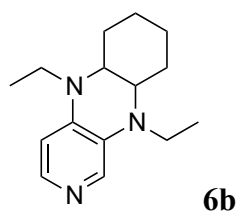
1) 57.4



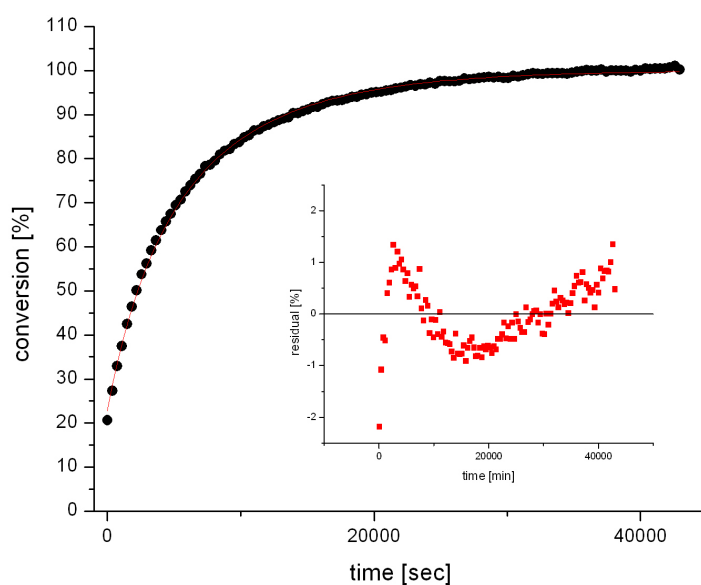
6a

1) 68.9





1) 68.9



Kinetics at 3 mol-% catalyst loading containing all surveyed catalysts:

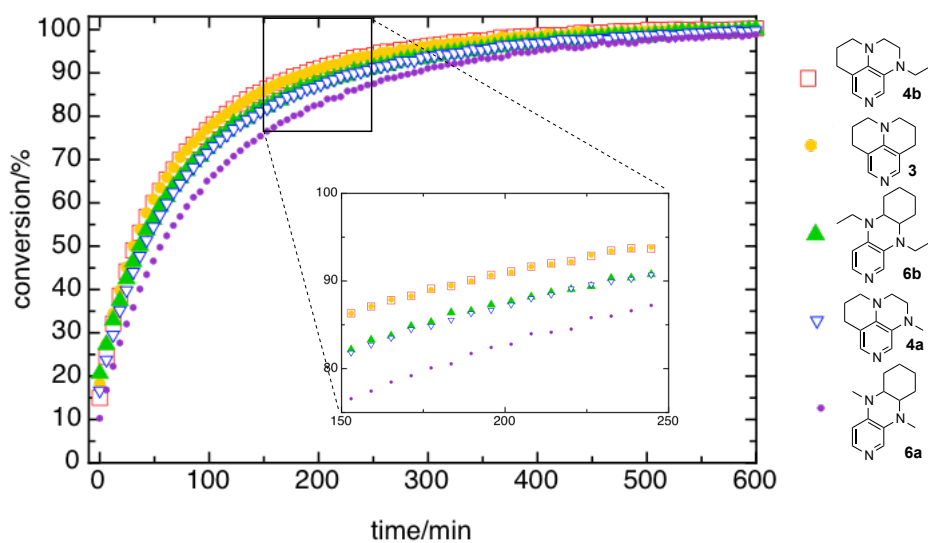
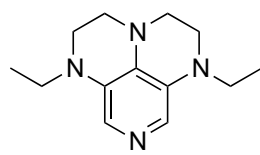


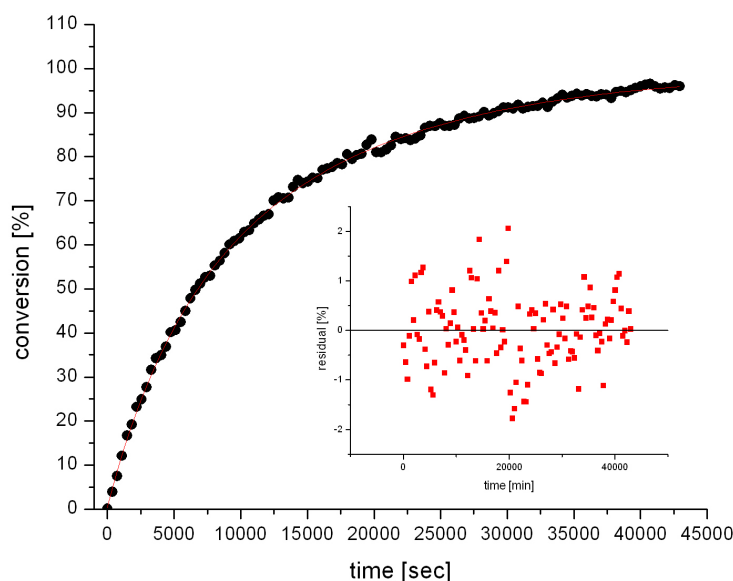
Figure 3.24. Conversion-time plots for catalysts **3**, **4a,b** and **6a,b** at 3 mol% catalyst loading.

Isobutyration



5b

1) 113.9



Solvent effects

We studied acylation reaction (**III**) in different solvents with commercially available **2** by means of ^1H NMR kinetics. The reaction of catalyst **2** in different solvents led with exception of THF and DMSO to full conversion for which the kinetic half-life times thus were extrapolated. For secondary non hindered alcohols Ishihara *et al.*^[16] found heptane being the best choice for running efficient and fast acylation reactions. We met solubility problems trying to perform the reaction in heptane leading to a tremendous increase in obtained half-life times. Additionally after some reaction time a precipitate formed, which was found to be triethyl ammonium acetate as identified by X-ray crystal structure analysis from the reaction mixture (cf. Figure 3.25). The same was true for pure CCl_4 . In order to achieve a better solubility without loosing too much of the solvent characteristics, we added 10 % CDCl_3 for the reaction in CCl_4 making it even possible to follow the reaction directly by ^1H NMR. Nevertheless the reaction mixture was still not 100 % homogeneous and thus it is not surprisingly that the reaction half-life time of **2** in 90/10 $\text{CCl}_4/\text{CDCl}_3$ is 1.5 times slower than in pure CDCl_3 (see Figure 3.26 and Table 3.7). In fact the solvent with the fastest turnover rates obtained in this study was CDCl_3 . The reaction in DCM is even 1.6 times slower although the solubility is here not a problem. For benzene we found an almost two-fold

decrease in reaction speed compared to chloroform. From all the solvents tested showing full conversion the worst performance in terms of reaction speed showed acetonitrile. Compared to chloroform we obtain a 2.8 fold decrease in activity. Unfortunately these results are not reflected by any of the solvent descriptors like ET30, AN (Gutmann acceptor number) and DN (Gutmann donor number).^[22,23]



Figure 3.25. Benchmark reaction (III) on large scale using heptane as solvent, catalyzed by 10 mol-% **2**. The pictures were taken at the beginning of the reaction (left, no precipitate), after 1 h (middle, yellow precipitate begins to form), and after 24 h (right, yellow precipitate).

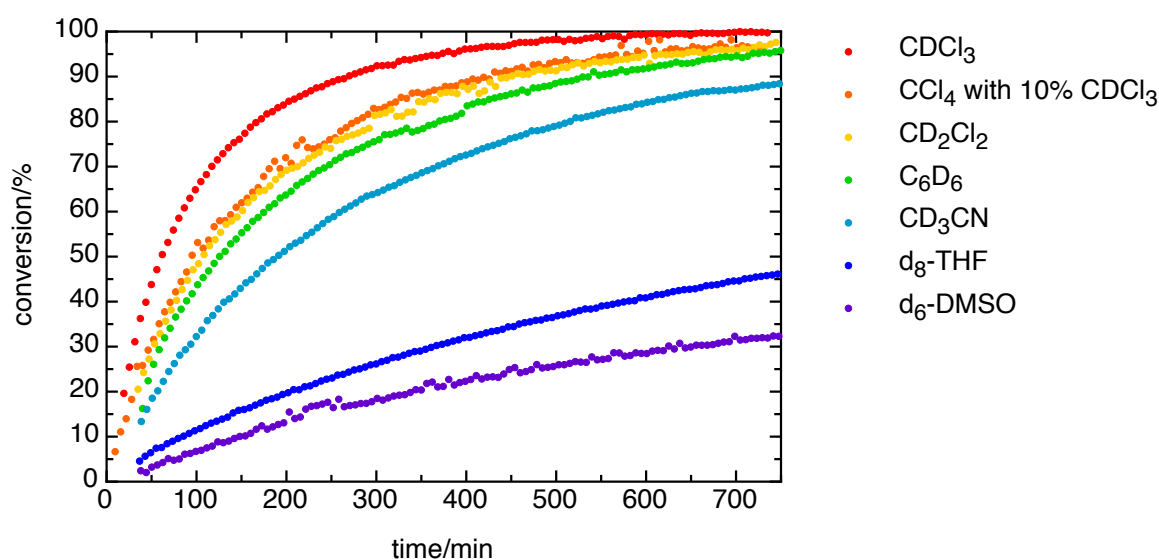


Figure 3.26. Conversion time plots using 10 mol-% **2** in benchmark reaction (III) in CDCl₃ (red), CCl₄ with 10 mol-% CDCl₃ (orange), CH₂Cl₂ (yellow), benzene (green), CH₃CN (light blue), THF (dark blue), DMSO (magenta).

Table 3.7. Kinetic half life times for acylation reaction (III) in different solvents with ET30, AN and DN.

solvent	$t_{1/2}^{[b]}$	ET30 ^[f] [kcal/mol]	AN ^[g] [kcal/mol]	DN ^[g] [kcal/mol]
CDCl ₃	67 ^[c]	39.1	23.1	4.0
CCl ₄ ^[a]	100.3	32.4	8.6	0.0
CD ₂ Cl ₂	109.2	40.7	20.4	1.0
C ₆ D ₆	128.6	34.3	8.2	0.1
CD ₃ CN	190.0	45.6	18.9	14.1
d ₈ -THF	800 ^[d]	37.4	8.0	20.0
d ₆ -DMSO	1125 ^[e]	45.1	19.3	29.8

[a] 90 % CCl₄ and 10 % CDCl₃; [b] Kinetic half-life times for benchmark reaction (III); [c] data from ref. 11; [d] linear extrapolation, 45 % conversion after 12 h; [e] linear extrapolation, 32 % conversion after 12 h. [f] data from ref. 23; [g] data from ref. 22.

Correlation plots

In addition to the correlations discussed in chapter 3.2 we surveyed additional correlations, which are depicted in Figures 3.27 – 3.31.

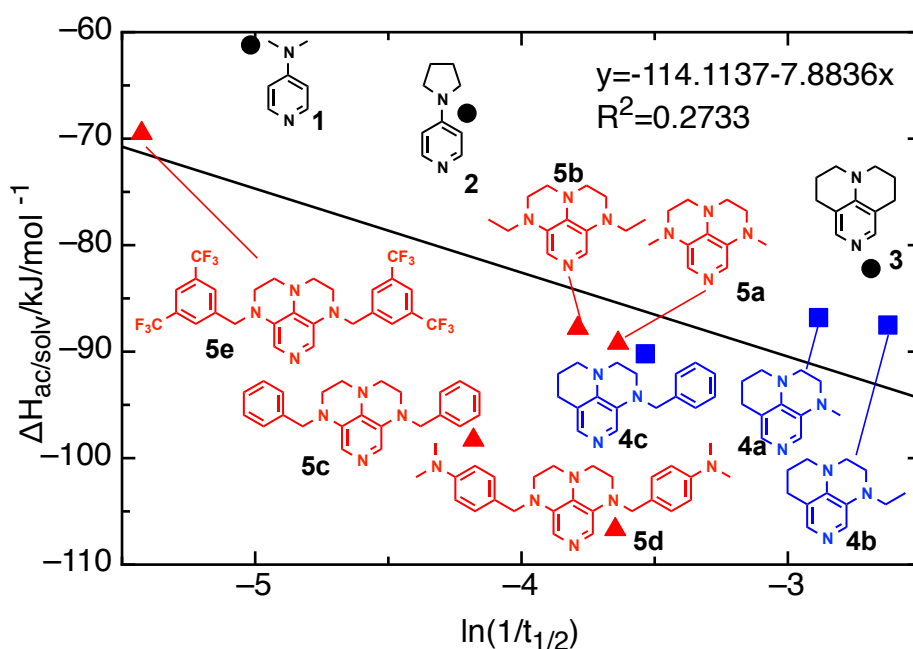


Figure 3.27. Correlation of affinity data (with PCM) with catalytic activity of 4-aminopyridines (black circles), 3,4-diaminopyridines (blue squares) and 3,4,5-triaminopyridines (red triangles).

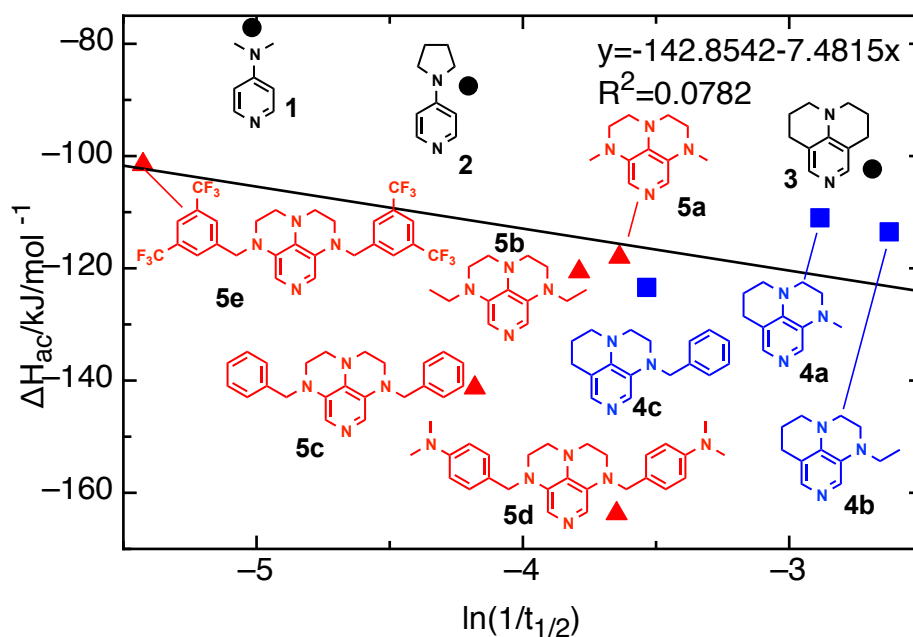


Figure 3.28. Correlation of affinity data (gas phase) with catalytic activity of 4-aminopyridines (black circles), 3,4-diaminopyridines (blue squares) and 3,4,5-triaminopyridines (red triangles).

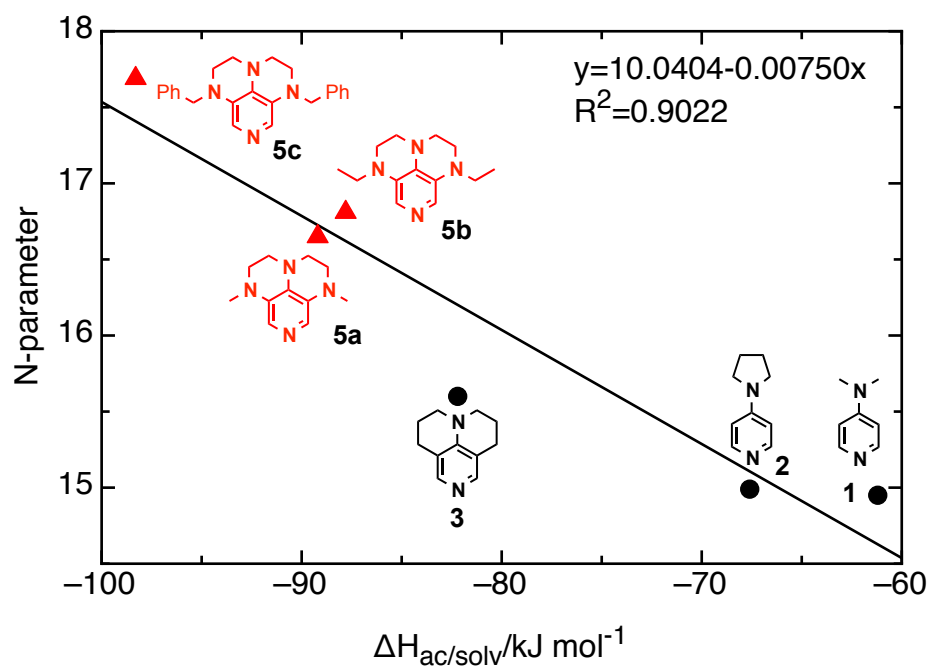


Figure 3.29. Correlation of N-parameters with acylation enthalpies ($\Delta H_{ac}/\text{solv}$) of 4-aminopyridines (black circles), and 3,4,5-triaminopyridines (red triangles).

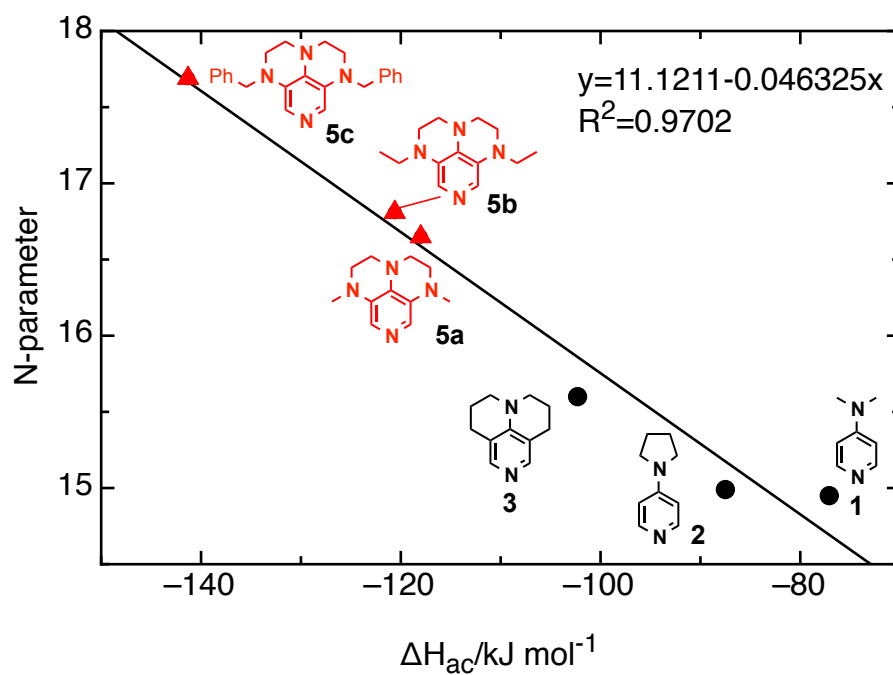


Figure 3.30. Correlation of N-parameters with acylation enthalpies in gas phase (ΔH_{ac}) of 4-aminopyridines (black circles), and 3,4,5-triaminopyridines (red triangles).

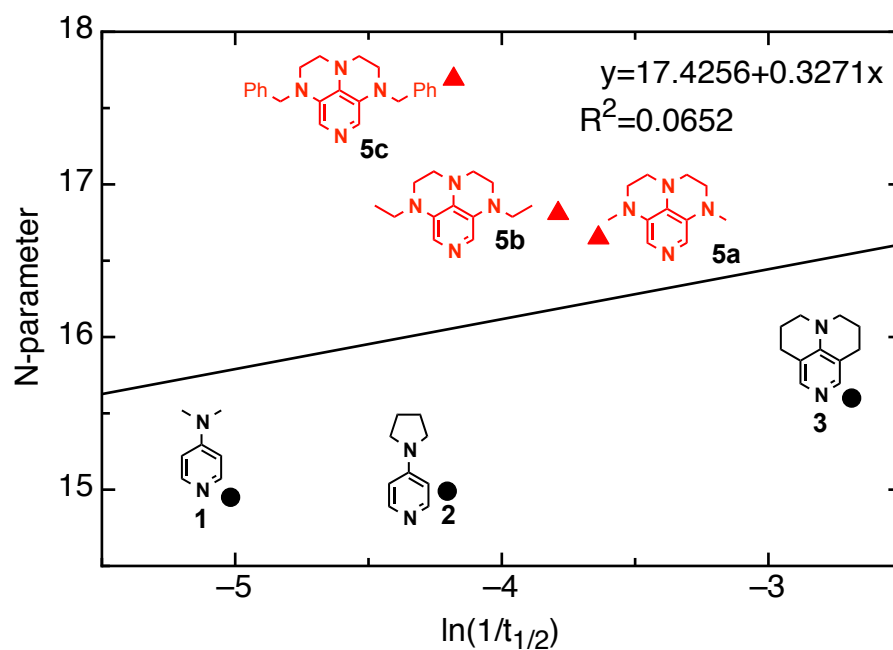


Figure 3.31. Correlation of N-parameters with kinetic data of 4-aminopyridines (black circles), and 3,4,5-triaminopyridines (red triangles).

Description of the QSAR parameters

Studies on the impact of input parameters for the QSAR program were tested with a larger set of catalysts depicted in Figure 3.32.

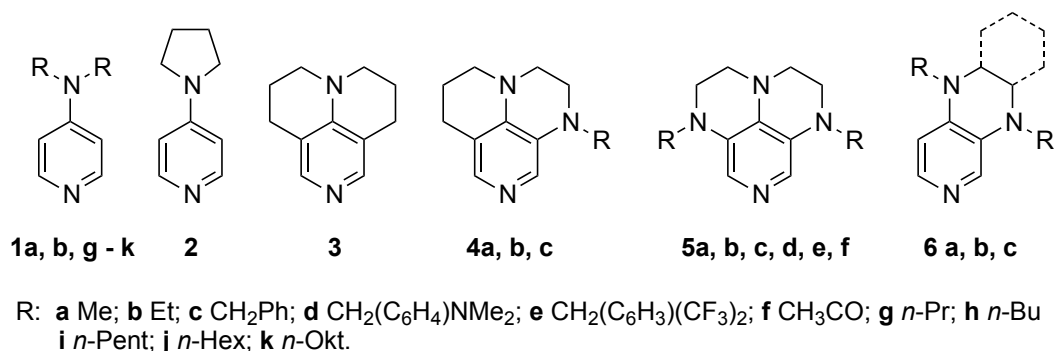


Figure 3.32. Catalysts used for the optimization of the QSAR model.

The surveyed parameters are depicted in Figure 3.33. As descriptors we used the gas phase acylation enthalpies (ΔH_{ac}), enthalpies including solvation terms in chloroform ($\Delta H_{ac/solv}$), the charge of the *ortho*-hydrogen atom of the free catalyst ($q_{ortho-H}$) and that of the pyridine nitrogen (q_N) and the bond distance ($dist_{N-C}$) between the nitrogen atom in 4-position and the pyridine carbon atom at the same position.

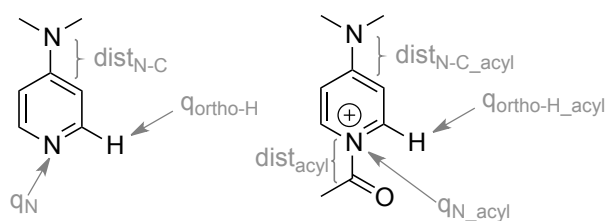


Figure 3.33. Depiction of the descriptors used for the QSAR models.

In Table 3.6 the number of input parameters was varied using ground state data of the free catalysts only. In one model the parameters of the free catalyst and that of the acylated catalyst according to Figure 3.33 were tested thus using 11 parameters (ΔH_{ac} , $\Delta H_{ac/solv}$, $q_{ortho-H}$, $dist_{N-C}$, q_N , $q_{ortho-H_acyl}$, $dist_{N-C_acyl}$, q_{N_acyl} and $dist_{acyl}$) in which the 2 $q_{ortho-H}$ charges of every catalyst were not averaged as usual, but taken separately ($R^2=0.916$, $Q^2=0.691$, (number of components: 4)). To understand the output parameters of the QSAR program these will be briefly described:

R^2 : Conventional R^2 value for the number of components used to create the model.

$$R^2 = 1 - \frac{SS_{err}}{SS_{tot}}$$

with: $SS_{tot} = \sum_i (y_i - y_{av})^2$; total sum of squares

$SS_{err} = \sum_i (y_i - f_i)^2$; sum of squares of residuals

and: $y_{av} = \frac{1}{n} \sum_i^n y_i$

f_i : predicted values

y_i : observed values

Q^2 : Crossvalidated R^2 value for the number of components used to create the model. To express the predictive power of the analysis, the cross-validated R^2 ($= Q^2$) is used. In cross-validation, one value is left out, a model is derived using the remaining data, and the model is used to predict the value originally left out. This procedure is repeated for all values, yielding Q^2 . Q^2 is normally (much) lower than R^2 and values greater than 0.5 already indicate significant predictive power.^[28]

$$Q^2 = 1.0 - \frac{\sum_y (y_{pred} - y_{actual})^2}{\sum_y (y_{actual} - y_{mean})^2}$$

y_{pred} : a predicted value (depending on model)

y_{actual} : an actual or experimental value

y_{mean} : the best estimate of the mean of all values that might be predicted
the summations are over the same set of y.

Number of components: the number of components that provided the largest value of Q^2 .

Table 3.8. Optimization of number of parameters used in the QSAR models.

Model-nr.	ΔH_{ac}	$\Delta H_{ac/solv}$	$q_{ortho-H}$	$dist_{N-C}$	q_N	R^2/Q^2 [a]
1 parameter						
1	✓					0.131/-0.047 (1)
2		✓				0.303/0.133 (1)
3			✓ ^{a2}			0.328/0.036 (1)
4			✓ ^{d3}			0.235/-0.065 (1)
5				✓		0.069/-0.109 (1)
2 parameters						
6	✓	✓				0.604/0.481 (2)
7	✓	✓ ^[b]				0.604/0.481 (2)
8		✓		✓		0.434/0.144 (2)
9		✓	✓ ^{a2}			0.705/0.604 (1)
10		✓	✓ ^{d3}			0.707/0.595 (2)
3 parameters						
11	✓	✓		✓		0.655/0.499 (3)
12	✓	✓	✓ ^{a2}			0.693/0.560 (2)
13	✓	✓	✓ ^{d3}			0.694/0.569 (2)
14		✓	✓ ^{a2}	✓		0.694/0.456 (2)
15		✓	✓ ^{d3}	✓		0.850/0.770 (3)
4 parameters						
16	✓	✓	✓ ^{a2}	✓		0.869/0.789 (3)
17	✓	✓	✓ ^{d3}	✓		0.852/0.764 (3)
5 parameters						
18	✓	✓	✓ ^{a2}	✓	✓ ^{a2}	0.917/0.861 (5)
19	✓	✓	✓ ^{d3}	✓	✓ ^{d3}	0.899/0.801 (5)

[a] in brackets the number of components is given; ✓^a: Mulliken charges; ✓^b: Chelpg charges; ✓^c: ESP charges from MOPAC; ✓^d: NPA charges; ¹: HF/6-31+G(2d,p); ²: HF/6-31G(d) with PCM model (PCM/UAHF/RHF/6-31G(d) solvation energies for chloroform); ³: HF/6-31G(d). [b] Only ΔG_{solv} was taken into account ((PCM/UAHF/RHF/6-31G(d) solvation energies for chloroform).

As noted before none of the descriptors for the pyridine nitrogen atom itself provided statistically significant predictive value.^[18] Thus we concentrated on the charge analysis of the *ortho*-hydrogen atom which plays a role in the transition state of DMAP catalyzed acetylation reactions due to the contacts to the acetate counterion.^[24] The analysis has been performed for the best conformers of the free catalysts at the HF/6-31G(d) level of theory. We surveyed Mulliken, CHELPG (charges from electrostatic potentials using a grid based method) and NPA (natural population analysis) charges at two levels of theory and additionally one model that accounts for solvent effects. In Table 3.9 the different types of charges (Mulliken, CHELPG and NPA) were surveyed in combination with different basis sets and solvent models. It was found that the NPA charges are the charges of choice considering PCM effects in chloroform. They show the best correlation with the experiment but with still acceptable effects towards changes in basis set and solvation model. A screening of the optimum choice of combination in terms of best correlating parameter set combinations for the QSAR model led us to the following ones: we use averaged NPA charges ($q_{ortho-H}$) of the *ortho*-hydrogen

atom to avoid getting too much parameters, as second we use the acylation enthalpies including a PCM solvation model ($\Delta H_{ac/solv}$) (= model-nr. 28a) and finally the N-C bond distance in 4-position ($dist_{N-C}$). It was found that having $\Delta H_{ac/solv}$ among the parameters the acylation enthalpies in the gas phase are redundant (compare models 6 and 7, Table 3.8). Finally model 28a was applied to the catalysts surveyed herein. The important catalyst characteristics for catalysts **1** – **5** can be found in Table 3.8.

Table 3.9. Variation of different basis sets and solvation model in the QSAR study.

Model-nr.	ΔH_{ac}	$\Delta H_{ac/solv}$	$q_{ortho-H}$	$dist_{N-C}$	R^2/Q^2 [a]
HF/6-31+G(2d,p)					
20	✓	✓	✓ ^{a1}	✓	0.662/0.250 (3)
21	✓	✓	✓ ^{b1}	✓	0.665/0.423 (4)
22	✓	✓	✓ ^{d1}	✓	0.846/0.759 (3)
HF/6-31G(d) with PCM model					
23	✓	✓	✓ ^{a2}	✓	0.869/0.789 (3)
24	✓	✓	✓ ^{b2}	✓	0.684/0.431 (4)
25	✓	✓	✓ ^{d2}	✓	0.839/0.746 (3)
HF/6-31G(d)					
26	✓	✓	✓ ^{a3}	✓	0.862/0.759 (3)
27	✓	✓	✓ ^{b3}	✓	0.674/0.417 (4)
28	✓	✓	✓ ^{d3}	✓	0.852/0.764 (3)
28a		✓	✓ ^{d3}	✓	0.850/0.770 (3)
28b	✓		✓ ^{d3}	✓	0.800/0.682 (3)
28c	✓	✓		✓	0.655/0.499 (3)
28d	✓	✓	✓ ^{d3}		0.694/0.569 (2)

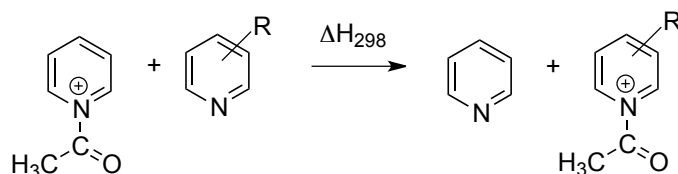
[a] in brackets the number of components is given; ✓^a: Mulliken charges; ✓^b: Chelpg charges; ✓^c: ESP charges from MOPAC; ✓^d: NPA charges; ¹: HF/6-31+G(2d,p); ²: HF/6-31G(d) with PCM model (PCM/UAHF/RHF/6-31G(d) solvation energies for chloroform); ³: HF/6-31G(d).

Table 3.10. QSAR input parameters of catalysts **1** – **5**.

Cat.	$\ln(1/t_{1/2})$	$\Delta H_{ac/solv}$ [kJ/mol]	$q_{ortho-H}$	$dist_{N-C}$ [Å]	$\ln(1/t_{1/2})$ exp.	$\ln(1/t_{1/2})$ pred.	residual
5d	-3.64806	-106.70	0.2227	1.4051	-3.6481	-3.6777	0.0297
5c	-4.18052	-98.30	0.2220	1.4044	-4.1805	-4.2015	0.0210
4c	-3.53515	-90.20	0.2162	1.3958	-3.5351	-3.5239	-0.0112
5a	-3.63759	-89.20	0.2137	1.3997	-3.6376	-3.3741	-0.2635
5b	-3.78872	-87.80	0.2112	1.4055	-3.7887	-3.3324	-0.4563
4b	-2.62467	-87.50	0.2109	1.3965	-2.6247	-2.9049	0.2802
4a	-2.88480	-86.80	0.2122	1.3939	-2.8848	-3.0640	0.1792
3	-2.68785	-82.20	0.2108	1.3884	-2.6879	-2.9600	0.2722
5e	-5.42627	-69.50	0.2171	1.4020	-5.4263	-5.6053	0.1790
2	-4.20469	-67.60	0.2150	1.3695	-4.2047	-3.9785	-0.2262
1	-5.01728	-61.20	0.2157	1.3787	-5.0173	-5.0132	0.0041

Theoretical Methods and Data

Acylation enthalpies



The conformational space of flexible pyridine derivatives has been searched using the MM3 force field and the systematic search routine implemented in MACROMODEL 9.7. Following a recently developed protocol for the calculation of cation affinity values,^[13] geometry optimizations have been performed in the gas phase at the B98/6-31G(d) level of theory. Thermal corrections to 289.15 K and 1 atm have been calculated at the same level of theory using the rigid rotor/harmonic oscillator model. Single point energies calculated at the MP2(FC)/6-31+G(2d,p) level have then been combined with thermal corrections obtained previously to calculate enthalpies (H_{298}) and free energies (G_{298}) at 298.15 K. In conformationally flexible systems enthalpies have been calculated as Boltzmann-averaged values over all available conformers within 30 kJ/mol. Solvent effects in chloroform have subsequently been determined through PCM (polarized continuum solvation model) single points at the RHF/6-31G(d) level with UAHF radii. All quantum mechanical calculations have been performed with Gaussian 03.^[27] In Figure 3.34 a graphical overview of acylation enthalpies in the gas phase is depicted and Figure 3.35 shows the calculated acylation enthalpies including solvent effects together with the *N*-parameters.

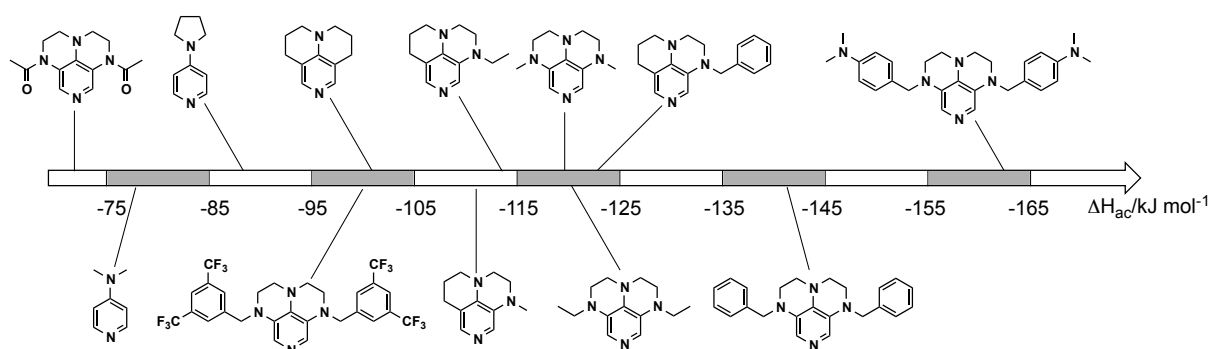


Figure 3.34. Acylation enthalpies in gas phase (ΔH_{ac}) for investigated catalyst.

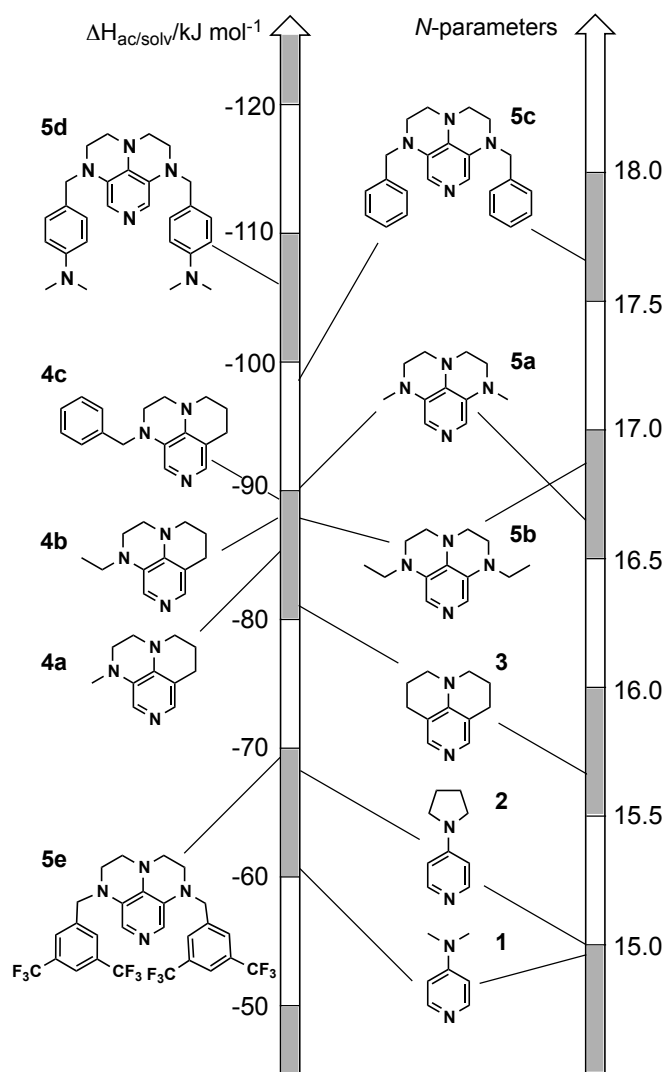


Figure 3.35. Acylation enthalpies with solvation effects ($\Delta H_{ac/solv}$) (left) and *N*-parameters for common pyridine based catalysts (right).

Chapter 3: Annelated Pyridines as Highly Nucleophilic and Lewis-Basic Catalysts for Acylation Reactions

Table 3.11. Calculated energies of conformers for catalysts **5d** and **5e**, as calculated at MP2/6-31+G(2d,p)//B98/6-31G(d) level with inclusion of solvent effects at PCM/UAHF/RHF/6-31G(d).

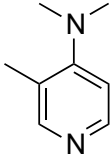
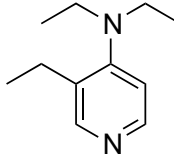
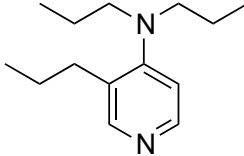
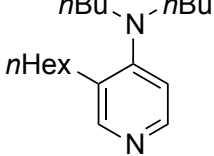
	B98/6-31G(d)		MP2(FC)/ 6-31+G(2d,p)	PCM/ UAHF/ RHF/ 6-31G(d)	MP2(FC)/ 6-31+G(2d,p)	"H ₂₉₈ " + ΔG_{solv}
Conf	E _{tot}	H ₂₉₈	E _{tot}	ΔG_{solv} [kJ/mol]	"H ₂₉₈ "	<H ₂₉₈ >
Pyr						
Pyr_1	-248.181767	-248.087628	-247.589433	-2.15	-247.495294	-247.498720
Pyr-Ac⁺						
Pyr-Ac ⁺ _1	-401.140005	-400.991697	-400.215517	-34.07	-400.067209	-400.121503
5d						
5d_5	-1377.273310	-1376.663857	-1373.974752	-4.1	-1373.365299	-1373.371832
5d_13	-1377.275202	-1376.665689	-1373.975470	-3.66	-1373.365957	-1373.371790
5d_6	-1377.274605	-1376.664862	-1373.975115	-3.86	-1373.365373	-1373.371524
5d_7	-1377.275834	-1376.665975	-1373.975495	-3.66	-1373.365636	-1373.371468
5d_4	-1377.273690	-1376.663737	-1373.974891	-3.87	-1373.364938	-1373.371105
5d_9	-1377.274707	-1376.664933	-1373.974696	-3.74	-1373.364922	-1373.370882
5d_17	-1377.273236	-1376.663538	-1373.974157	-3.95	-1373.364459	-1373.370754
5d_12	-1377.273230	-1376.663530	-1373.973692	-3.84	-1373.363991	-1373.370111
5d_16	-1377.271466	-1376.661683	-1373.973203	-4.19	-1373.363420	-1373.370097
5d_1	-1377.273796	-1376.663774	-1373.974318	-3.59	-1373.364296	-1373.370017
5d_14	-1377.273167	-1376.663416	-1373.973545	-3.79	-1373.363794	-1373.369834
5d_10	-1377.271339	-1376.661621	-1373.972685	-3.82	-1373.362967	-1373.369055
5d_11	-1377.271138	-1376.661331	-1373.971149	-3.97	-1373.361341	-1373.367668
5d-Ac⁺						
5d-Ac ⁺ _16	-1530.294965	-1529.630131	-1526.664562	-22.20	-1525.999728	-1526.035106
5d-Ac ⁺ _16_2	-1530.294965	-1529.630130	-1526.664559	-22.20	-1525.999724	-1526.035102
5d-Ac ⁺ _5_2	-1530.295110	-1529.630472	-1526.664628	-21.96	-1525.999990	-1526.034985
5d-Ac ⁺ _5	-1530.295110	-1529.630471	-1526.664631	-21.94	-1525.999992	-1526.034955
5d-Ac ⁺ _17	-1530.296435	-1529.631789	-1526.663844	-22.42	-1525.999198	-1526.034926
5d-Ac ⁺ _6	-1530.296646	-1529.632207	-1526.663833	-22.26	-1525.999395	-1526.034868
5d-Ac ⁺ _4	-1530.294758	-1529.629928	-1526.663378	-22.22	-1525.998548	-1526.033958
5d-Ac ⁺ _4_2	-1530.294058	-1529.629081	-1526.662531	-22.20	-1525.997554	-1526.032932
5d-Ac ⁺ _17_2	-1530.294001	-1529.629363	-1526.660669	-22.92	-1525.996031	-1526.032557
5d-Ac ⁺ _13	-1530.295345	-1529.631120	-1526.659805	-23.14	-1525.995580	-1526.032456
5d-Ac ⁺ _10	-1530.292983	-1529.628556	-1526.661485	-22.08	-1525.997058	-1526.032244
5d-Ac ⁺ _9_2	-1530.295304	-1529.630507	-1526.661509	-22.22	-1525.996712	-1526.032122
5d-Ac ⁺ _14_2	-1530.294637	-1529.630151	-1526.660755	-22.35	-1525.996269	-1526.031886
5d-Ac ⁺ _12	-1530.294709	-1529.629850	-1526.660820	-22.43	-1525.995961	-1526.031706
5d-Ac ⁺ _1	-1530.293105	-1529.628511	-1526.660863	-22.21	-1525.996269	-1526.031663
5d-Ac ⁺ _1_2	-1530.293106	-1529.628509	-1526.660850	-22.19	-1525.996252	-1526.031615
5d-Ac ⁺ _10_2	-1530.292720	-1529.627857	-1526.660741	-22.38	-1525.995878	-1526.031543
5d-Ac ⁺ _14_6	-1530.294302	-1529.629689	-1526.660586	-22.28	-1525.995973	-1526.031478
5d-Ac ⁺ _7_2	-1530.295415	-1529.630671	-1526.659513	-22.92	-1525.994769	-1526.031294
5d-Ac ⁺ _9	-1530.293625	-1529.628403	-1526.659251	-23.03	-1525.994028	-1526.030729

Chapter 3: Annelated Pyridines as Highly Nucleophilic and Lewis-Basic Catalysts for Acylation Reactions

5d-Ac ⁺ _11	-1530.292285	-1529.627430	-1526.659789	-22.34	-1525.994934	-1526.030535
5d-Ac ⁺ _14	-1530.291865	-1529.627252	-1526.657030	-23.27	-1525.992417	-1526.029500
5d-Ac ⁺ _12_2	-1530.291866	-1529.627225	-1526.657040	-23.28	-1525.992399	-1526.029498
5e						
5e_4	-2457.167590	-2456.680733	-2452.332600	3.2	-2451.845743	-2451.840643
5e_5	-2457.167844	-2456.680186	-2452.332439	3.36	-2451.844781	-2451.839426
5e_6	-2457.167475	-2456.679766	-2452.331402	3.23	-2451.843693	-2451.838545
5e_16	-2457.166341	-2456.678411	-2452.331395	3.21	-2451.843465	-2451.838349
5e_17	-2457.166909	-2456.678911	-2452.330841	3.13	-2451.842843	-2451.837855
5e_9	-2457.167235	-2456.679336	-2452.330594	3.29	-2451.842695	-2451.837452
5e_13	-2457.167124	-2456.679203	-2452.330138	3.22	-2451.842217	-2451.837086
5e_7	-2457.167440	-2456.679606	-2452.329809	3.17	-2451.841976	-2451.836924
5e_1	-2457.167009	-2456.679192	-2452.330928	4.02	-2451.843111	-2451.836705
5e_12	-2457.165605	-2456.677618	-2452.329303	3.25	-2451.841315	-2451.836136
5e_10	-2457.165057	-2456.677241	-2452.329585	3.69	-2451.841769	-2451.835888
5e_11	-2457.164568	-2456.676750	-2452.328251	3.38	-2451.840433	-2451.835047
5e_14	-2457.164693	-2456.676764	-2452.328819	4.31	-2451.840890	-2451.834022
5e-Ac⁺						
5e-Ac ⁺ _16_2	-2610.166251	-2609.623431	-2604.998864	-21.36	-2604.456044	-2604.490083
5e-Ac ⁺ _5	-2610.166298	-2609.623448	-2604.998542	-20.87	-2604.455693	-2604.488951
5e-Ac ⁺ _5_2	-2610.166297	-2609.623466	-2604.998567	-20.83	-2604.455737	-2604.488931
5e-Ac ⁺ _17	-2610.166226	-2609.623203	-2604.996205	-22.35	-2604.453182	-2604.488799
5e-Ac ⁺ _4	-2610.165544	-2609.622795	-2604.997395	-21.23	-2604.454646	-2604.488478
5e-Ac ⁺ _17_2	-2610.163792	-2609.620806	-2604.993838	-23.25	-2604.450853	-2604.487904
5e-Ac ⁺ _6	-2610.166176	-2609.623211	-2604.995963	-21.74	-2604.452999	-2604.487643
5e-Ac ⁺ _4_2	-2610.163876	-2609.621009	-2604.995773	-21.54	-2604.452905	-2604.487232
5e-Ac ⁺ _13_2	-2610.163538	-2609.620761	-2604.991138	-24.10	-2604.448361	-2604.486767
5e-Ac ⁺ _10_2	-2610.164630	-2609.621812	-2604.996347	-20.60	-2604.453529	-2604.486357
5e-Ac ⁺ _7_2	-2610.163406	-2609.620521	-2604.990748	-23.97	-2604.447863	-2604.486062
5e-Ac ⁺ _9	-2610.162859	-2609.619973	-2604.992293	-22.99	-2604.449407	-2604.486044
5e-Ac ⁺ _9_2	-2610.163525	-2609.620553	-2604.992841	-22.43	-2604.449869	-2604.485613
5e-Ac ⁺ _1	-2610.162845	-2609.620878	-2604.994296	-20.71	-2604.452329	-2604.485333
5e-Ac ⁺ _12_2	-2610.162355	-2609.619464	-2604.991647	-22.93	-2604.448756	-2604.485297
5e-Ac ⁺ _10	-2610.163287	-2609.620400	-2604.994743	-20.95	-2604.451856	-2604.485242
5e-Ac ⁺ _6_2	-2610.163733	-2609.620763	-2604.993542	-21.67	-2604.450573	-2604.485106
5e-Ac ⁺ _12	-2610.163094	-2609.620210	-2604.992336	-22.34	-2604.449453	-2604.485054
5e-Ac ⁺ _11_2	-2610.161781	-2609.619016	-2604.992997	-21.73	-2604.450232	-2604.484861
5e-Ac ⁺ _14_2	-2610.165660	-2609.622534	-2604.995442	-20.31	-2604.452316	-2604.484682
5e-Ac ⁺ _1_2	-2610.162704	-2609.619830	-2604.994320	-20.74	-2604.451446	-2604.484497

Extrapolation of acylation enthalpies for catalyst 18:

The calculation of the full conformational space of compound **18** would have included too many conformers for Boltzmann averaging. For that reason the acylation enthalpies in gas phase and in solvation (PCM model) were extrapolated (see Figure 3.36 and 3.37).

				
ΔH_{ac} MP2-5 [kJ/mol]:	-66.6	-74.8	-82.2	?
$\Delta H_{ac/solv}$ MP2-5/solv [kJ/mol]:	-50.3	-54.7	-54.6	?

Scheme 3.36. Extrapolation of enthalpies in gas phase (ΔH_{ac} MP2-5) and solvation ($\Delta H_{ac/solv}$ MP2-5/solv) for catalyst **18**.

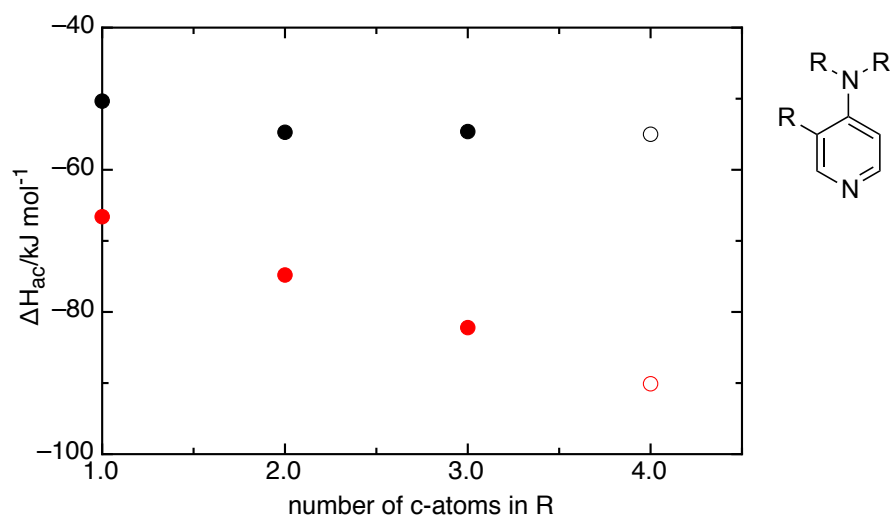
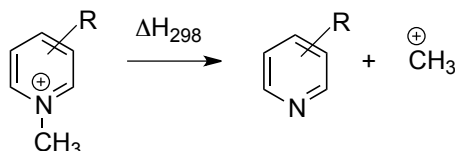


Figure 3.37. Extrapolation of ΔH_{ac} MP2-5 (red circles) and $\Delta H_{ac/solv}$ MP2-5/solv (black circles). The assumed values for the extrapolation are not filled.

Figure 3.37 shows that the gas phase enthalpies follow a rather linear correlation whereas the enthalpies with inclusion of the solvent model show a saturation effect. The gas phase enthalpy (ΔH_{ac} MP2-5) for **18** amounts up to -90.1 kJ/mol (after linear extrapolation) and the enthalpy in solution ($\Delta H_{ac/solv}$ MP2-5/solv) -55.0 kJ/mol (under the acceptance of a saturation effect; three data points were not sufficient to perform a non linear fit).

MCA values

Methyl cation affinities have been calculated as the reaction enthalpy at 298.15 K and 1 atm pressure for the methyl cation detachment reaction shown below. This is in analogy to the mass spectrometric definition of proton affinities.



The geometries of all species have been optimized at the B98/6-31G(d) level of theory. The conformational space of flexible pyridines and phosphanes and the corresponding cations has been searched using the MM3* force field and the systematic search routine implemented in MACROMODEL 9.7. All stationary points located at force field level have then been reoptimized at B98/6-31G(d) level as described before. Thermochemical corrections to 298.15 K have been calculated for all minima from unscaled vibrational frequencies obtained at this same level. The thermochemical corrections have been combined with single point energies calculated at the MP2(FC)/6-31+G(2d,p)//B98/6-31G(d) level to yield enthalpies H_{298} at 298.15 K. In conformationally flexible systems enthalpies have been calculated as Boltzmann-averaged values over all available conformers. This procedure has recently been found to reproduce G3 methyl cation affinity values of selected small and medium sized organocatalysts within 4.0 kJ mol⁻¹.^[12] All quantum mechanical calculations have been performed with Gaussian 03.^[27]

Table 3.12. Calculated energies of conformers for catalysts **5d** and **5e**, as calculated at MP2/6-31+G(2d,p)//B98/6-31G(d) level.

system	B98/6-31G(d)		MP2(FC)/6-31+G(2d,p)//B98/6-31G(d)	
	E_{tot}	H_{298}	E_{tot}	H_{298}
CH_3^+				-39.316929
CH_3^+	-39.462922	-39.427481	-39.352370	-39.316929
5d				-1373.365244
5d_13	-1377.275202	-1376.665689	-1373.975470	-1373.365957
5d_7	-1377.275834	-1376.665975	-1373.975495	-1373.365636
5d_6	-1377.274605	-1376.664862	-1373.975115	-1373.365373
5d_5	-1377.273310	-1376.663857	-1373.974752	-1373.365299
5d_4	-1377.273690	-1376.663737	-1373.974891	-1373.364938
5d_9	-1377.274707	-1376.664933	-1373.974696	-1373.364922
5d_17	-1377.273236	-1376.663538	-1373.974157	-1373.364459
5d_1	-1377.273796	-1376.663774	-1373.974318	-1373.364296

Chapter 3: Annelated Pyridines as Highly Nucleophilic and Lewis-Basic Catalysts for Acylation Reactions

5d_12	-1377.273230	-1376.663530	-1373.973692	-1373.363991
5d_14	-1377.273167	-1376.663416	-1373.973545	-1373.363794
5d_16	-1377.271466	-1376.661683	-1373.973203	-1373.363420
5d_10	-1377.271339	-1376.661621	-1373.972685	-1373.362967
5d_11	-1377.271138	-1376.661331	-1373.971149	-1373.361341
5d-Me⁺				-1412.934033
5d-Me ⁺ _5	-1417.002909	-1416.350286	-1413.587226	-1412.934602
5d-Me ⁺ _16	-1417.002349	-1416.348090	-1413.586624	-1412.932365
5d-Me ⁺ _	-1417.002907	-1416.349289	-1413.585385	-1412.931767
5d-Me ⁺ _4	-1417.002170	-1416.348015	-1413.585639	-1412.931484
5d-Me ⁺ _17	-1417.002443	-1416.348593	-1413.585095	-1412.931245
5d-Me ⁺ _1	-1417.000720	-1416.347191	-1413.583555	-1412.930026
5d-Me ⁺ _13	-1417.002459	-1416.349150	-1413.583296	-1412.929987
5d-Me ⁺ _9	-1417.001883	-1416.348114	-1413.583422	-1412.929653
5d-Me ⁺ _	-1417.002788	-1416.348782	-1413.583523	-1412.929516
5d-Me ⁺ _14	-1417.000886	-1416.347167	-1413.582263	-1412.928545
5d-Me ⁺ _12	-1417.000884	-1416.347151	-1413.582214	-1412.928480
5d-Me ⁺ _11	-1416.999406	-1416.345528	-1413.581532	-1412.927654
5e				-2451.844902
5e_4	-2457.167590	-2456.680733	-2452.332600	-2451.845743
5e_5	-2457.167844	-2456.680186	-2452.332439	-2451.844781
5e_6	-2457.167475	-2456.679766	-2452.331402	-2451.843693
5e_16	-2457.166341	-2456.678411	-2452.331395	-2451.843465
5e_1	-2457.167009	-2456.679192	-2452.330928	-2451.843111
5e_17	-2457.166909	-2456.678911	-2452.330841	-2451.842843
5e_9	-2457.167235	-2456.679336	-2452.330594	-2451.842695
5e_13	-2457.167124	-2456.679203	-2452.330138	-2451.842217
5e_7	-2457.167440	-2456.679606	-2452.329809	-2451.841976
5e_10	-2457.165057	-2456.677241	-2452.329585	-2451.841769
5e_12	-2457.165605	-2456.677618	-2452.329303	-2451.841315

5e_14	-2457.164693	-2456.676764	-2452.328819	-2451.840890
5e_11	-2457.164568	-2456.676750	-2452.328251	-2451.840433
5e-Me⁺				-2491.389131
5e-Me ⁺ _4	-2496.874252	-2496.342261	-2491.921708	-2491.389717
5e-Me ⁺ _5	-2496.873406	-2496.341419	-2491.920449	-2491.388463
5e-Me ⁺ _6	-2496.873089	-2496.341126	-2491.918499	-2491.386536
5e-Me ⁺ _16	-2496.871852	-2496.339686	-2491.915361	-2491.383195
5e-Me ⁺ _1	-2496.872148	-2496.340067	-2491.917211	-2491.385130
5e-Me ⁺ _17	-2496.871731	-2496.339779	-2491.915537	-2491.383585
5e-Me ⁺ _9	-2496.872230	-2496.341247	-2491.919008	-2491.388024
5e-Me ⁺ _13	-2496.872709	-2496.340778	-2491.918212	-2491.386281
5e-Me ⁺ _7	-2496.873773	-2496.341564	-2491.921623	-2491.389415
5e-Me ⁺ _10	-2496.871318	-2496.339150	-2491.916135	-2491.383967
5e-Me ⁺ _12	-2496.872168	-2496.340021	-2491.919073	-2491.386926
5e-Me ⁺ _14	-2496.873052	-2496.340681	-2491.918410	-2491.386039
5e-Me ⁺ _11	-2496.871037	-2496.338911	-2491.917312	-2491.385186

Crystallographic Data

The obtained crystal structure for compound **3** is in line with the already published one (CCDC 633500).

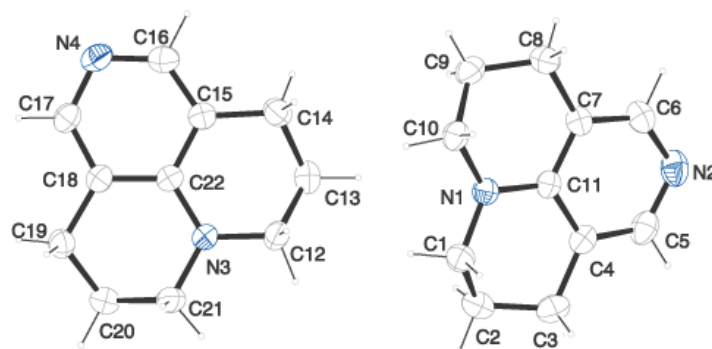


Figure 3.38. X-ray crystal structure for compound **3**.

The obtained crystal structure for compound **6a** is in line with the already published one (CCDC 622355).

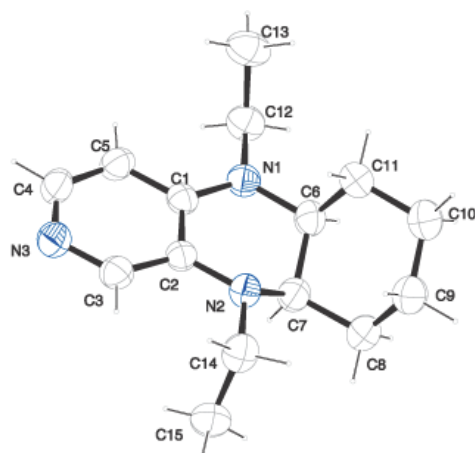


Figure 3.39. X-ray crystal structure for compound **6a**.

Table 3.13. Crystallographic data of **4a**.

	4a
net formula	C ₁₁ H ₁₅ N ₃
<i>M</i> _r /g mol ⁻¹	189.257
crystal size/mm	0.24 × 0.19 × 0.07
<i>T</i> /K	173(2)
radiation	MoKα
diffractometer	'KappaCCD'
crystal system	monoclinic
space group	<i>P</i> 2 ₁ / <i>c</i>
<i>a</i> /Å	9.0158(6)
<i>b</i> /Å	8.5738(6)
<i>c</i> /Å	25.5574(16)
α/°	90
β/°	94.298(4)
γ/°	90
<i>V</i> /Å ³	1970.0(2)
<i>Z</i>	8
calc. density/g cm ⁻³	1.27624(13)
μ/mm ⁻¹	0.079
absorption correction	none
refls. measured	5882
<i>R</i> _{int}	0.0770
mean σ(<i>I</i>)/ <i>I</i>	0.0942
θ range	3.28–24.15
observed refls.	1612
<i>x</i> , <i>y</i> (weighting scheme)	0.0956, 0
hydrogen refinement	constr
refls in refinement	3108
parameters	255
restraints	0
<i>R</i> (<i>F</i> _{obs})	0.0724
<i>R</i> _w (<i>F</i> ²)	0.1970
<i>S</i>	1.023
shift/error _{max}	0.001
max electron density/e Å ⁻³	0.329
min electron density/e Å ⁻³	−0.184

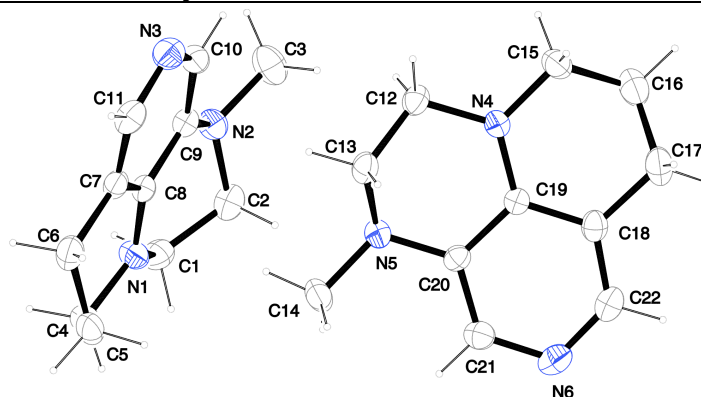


Table 3.14. Crystallographic data of **5c**.

	5c
net formula	C ₂₃ H ₂₄ N ₄
<i>M_r</i> /g mol ⁻¹	356.464
crystal size/mm	0.36 × 0.29 × 0.26
<i>T</i> /K	173(2)
radiation	MoKα
diffractometer	'Oxford XCalibur'
crystal system	triclinic
space group	<i>P</i> 1bar
<i>a</i> /Å	6.7771(7)
<i>b</i> /Å	10.1414(11)
<i>c</i> /Å	14.0005(14)
α/°	78.648(9)
β/°	77.902(9)
γ/°	83.399(9)
<i>V</i> /Å ³	919.74(17)
<i>Z</i>	2
calc. density/g cm ⁻³	1.2872(2)
μ/mm ⁻¹	0.078
absorption correction	'multi-scan'
transmission factor range	0.93079–1.00000
refls. measured	5113
<i>R</i> _{int}	0.0221
mean σ(<i>I</i>)/ <i>I</i>	0.0467
θ range	4.24–26.37
observed refls.	2885
<i>x</i> , <i>y</i> (weighting scheme)	0.0442, 0.2121
hydrogen refinement	constr
refls in refinement	3715
parameters	244
restraints	0
<i>R</i> (<i>F</i> _{obs})	0.0458
<i>R</i> _w (<i>F</i> ²)	0.1209
<i>S</i>	1.037
shift/error _{max}	0.001
max electron density/e Å ⁻³	0.173
min electron density/e Å ⁻³	-0.203

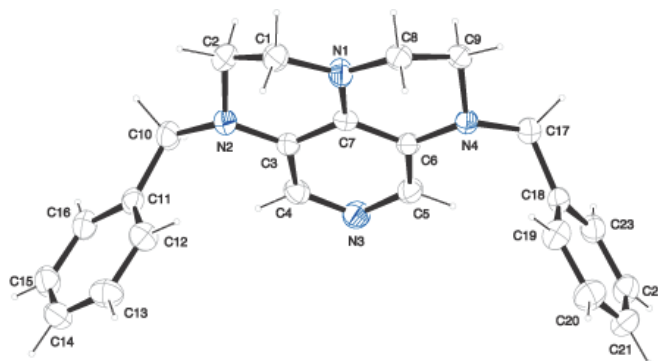


Table 3.15. Crystallographic data of **5d** with benzylalcohol.

	5d with benzylalcohol
net formula	C ₃₆ H ₄₇ N ₇ O
<i>M_r</i> /g mol ⁻¹	593.805
crystal size/mm	0.34 × 0.28 × 0.21
<i>T</i> /K	173(2)
radiation	MoKα
diffractometer	'KappaCCD'
crystal system	triclinic
space group	<i>P</i> 1bar
<i>a</i> /Å	10.7475(3)
<i>b</i> /Å	11.2640(3)
<i>c</i> /Å	15.6318(4)
α/°	96.177(2)
β/°	104.2366(18)
γ/°	114.7428(15)
<i>V</i> /Å ³	1617.53(7)
<i>Z</i>	2
calc. density/g cm ⁻³	1.21921(5)
μ/mm ⁻¹	0.076
absorption correction	none
refls. measured	10576
<i>R</i> _{int}	0.0293
mean σ(<i>I</i>)/ <i>I</i>	0.0402
θ range	3.37–25.52
observed refls.	4473
<i>x</i> , <i>y</i> (weighting scheme)	0.0701, 0.3613
hydrogen refinement	mixed
refls in refinement	5909
parameters	406
restraints	0
<i>R</i> (<i>F</i> _{obs})	0.0485
<i>R</i> _w (<i>F</i> ²)	0.1363
<i>S</i>	1.035
shift/error _{max}	0.001
max electron density/e Å ⁻³	0.203
min electron density/e Å ⁻³	–0.210

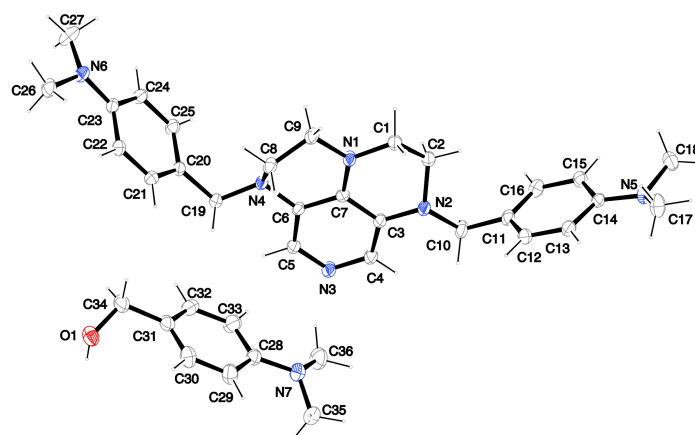


Table 3.16. Crystallographic data of **5e**.

	5e
net formula	C ₂₇ H ₂₀ F ₁₂ N ₄
<i>M_r</i> /g mol ⁻¹	628.456
crystal size/mm	0.31 × 0.18 × 0.13
<i>T</i> /K	173(2)
radiation	MoKα
diffractometer	'Oxford XCalibur'
crystal system	triclinic
space group	<i>P</i> 1bar
<i>a</i> /Å	8.7064(10)
<i>b</i> /Å	12.5447(14)
<i>c</i> /Å	13.4356(16)
α/°	63.787(11)
β/°	77.333(10)
γ/°	79.499(10)
<i>V</i> /Å ³	1278.3(3)
<i>Z</i>	2
calc. density/g cm ⁻³	1.6328(4)
μ/mm ⁻¹	0.159
absorption correction	'multi-scan'
transmission factor range	0.50690–1.00000
refls. measured	7083
<i>R</i> _{int}	0.0411
mean σ(<i>I</i>)/ <i>I</i>	0.0680
θ range	4.37–26.37
observed refls.	3382
<i>x</i> , <i>y</i> (weighting scheme)	0.1193, 1.1833
hydrogen refinement	constr
refls in refinement	5148
parameters	427
restraints	9
<i>R</i> (<i>F</i> _{obs})	0.0838
<i>R</i> _w (<i>F</i> ²)	0.2514
<i>S</i>	1.030
shift/error _{max}	0.002
max electron density/e Å ⁻³	0.642
min electron density/e Å ⁻³	−0.549

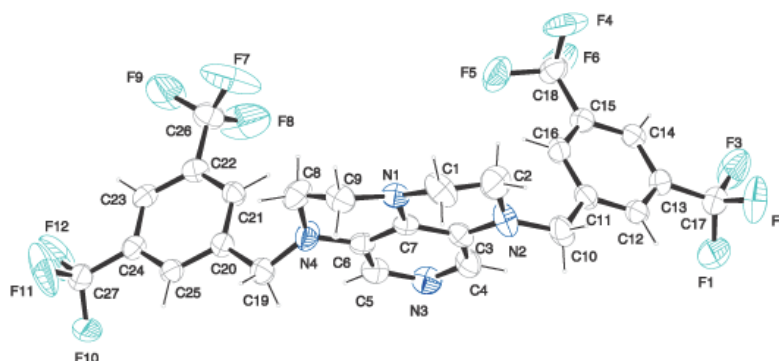
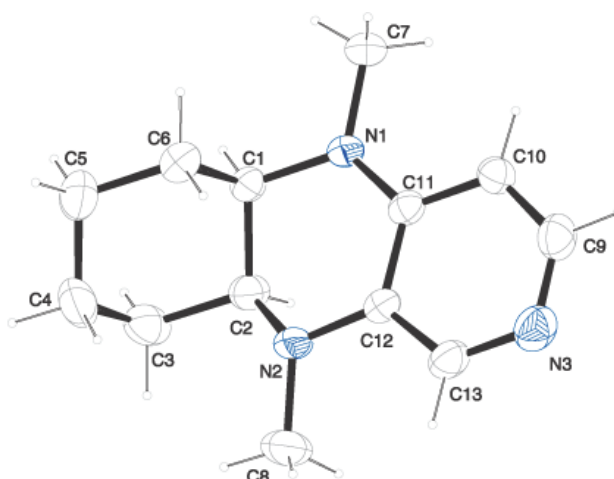


Table 3.17. Crystallographic data of **6a**.

	6a
net formula	C ₁₃ H ₁₉ N ₃
<i>M_r</i> /g mol ⁻¹	217.310
crystal size/mm	0.36 × 0.19 × 0.06
<i>T</i> /K	173(2)
radiation	MoKα
diffractometer	'Oxford XCalibur'
crystal system	monoclinic
space group	<i>P</i> 2 ₁ / <i>c</i>
<i>a</i> /Å	7.8737(11)
<i>b</i> /Å	23.409(3)
<i>c</i> /Å	6.5786(9)
α/°	90
β/°	109.346(17)
γ/°	90
<i>V</i> /Å ³	1144.1(3)
<i>Z</i>	4
calc. density/g cm ⁻³	1.2616(3)
μ/mm ⁻¹	0.077
absorption correction	'multi-scan'
transmission factor range	0.57256–1.00000
refls. measured	6139
<i>R</i> _{int}	0.0460
mean σ(<i>I</i>)/ <i>I</i>	0.0555
θ range	4.38–26.25
observed refls.	1574
<i>x</i> , <i>y</i> (weighting scheme)	0.0871, 0.1295
hydrogen refinement	constr
refls in refinement	2297
parameters	147
restraints	0
<i>R</i> (<i>F</i> _{obs})	0.0588
<i>R</i> _w (<i>F</i> ²)	0.1733
<i>S</i>	1.022
shift/error _{max}	0.001
max electron density/e Å ⁻³	0.223
min electron density/e Å ⁻³	–0.296



3.5 References

- [1] a) L. M. Litvinenko, A. I. Kirichenko, *Dokl. Akad. Nauk SSSR, Ser. Khim.* **1967**, 176, 97–100; b) W. Steglich, G. Höfle, *Angew. Chem.* **1969**, 81, 1001; *Angew. Chem. Int. Ed. Engl.* **1969**, 8, 981.
- [2] G. Höfle, W. Steglich, H. Vorbrüggen, *Angew. Chem.* **1978**, 90, 602 - 615; *Angew. Chem. Int. Ed. Engl.* **1978**, 17, 569 - 583.
- [3] Review: N. De Rycke, F. Couty, O. R. P. David, *Chem. Eur. J.* **2011**, 17, 12852 - 12871.
- [4] A. Hassner, L. R. Krepski, V. Alexanian, *Tetrahedron* **1978**, 34, 2069-2076.
- [5] M. R. Heinrich, H. S. Klisa, H. Mayr, W. Steglich, H. Zipse, *Angew. Chem.* **2003**, 115, 4975; *Angew. Chem. Int. Ed.* **2003**, 42, 4826 - 4828.
- [6] C. Lindner, R. Tandon, Y. Liu, B. Maryasin, H. Zipse, *Org. Biomol. Chem.* **2012**, 10, 3210 - 3218.
- [7] C. Lindner, R. Tandon, B. Maryasin, E. Larionov, H. Zipse, *Beilstein J. Org. Chem.* **2012**, 8, 1406 -1442.
- [8] N. De Rycke, G. Berionni, F. Couty, H. Mayr, R. Goumont, O. R. P. David, *Org. Lett.* **2011**, 13, 530 - 533.
- [9] a) I. Held, S. Xu, H. Zipse, *Synthesis* **2007**, 1185-1196. b) H. Zipse, I. Held, Bayer Material Science LLC, US 2008/0176747A1, **2008**.
- [10] I. Held, E. Larionov, C. Bozler, F. Wagner, H. Zipse, *Synthesis* **2009**, 2267 - 2277.
- [11] The problem using silica gel is that sometimes the catalyst sticks too much to the column to get it off again.
- [12] a) C. Lindner, B. Maryasin, F. Richter, H. Zipse, *J. Phys. Org. Chem.* **2010**, 23, 1036 – 1042. b) Y. Wei, G. N. Sastry, H. Zipse, *J. Am. Chem. Soc.* **2008**, 130, 3473 -3477. c) Y. Wei, T. Singer, H. Mayr, G. N. Sastry, H. Zipse, *J. Comp. Chem.* **2008**, 29, 291 - 297.
- [13] a) H. Mayr, B. Kempf, A. R. Ofial, *Acc. Chem. Res.* **2003**, 36, 66 -77. b) H. Mayr, M. Patz, *Angew. Chem., Int. Ed. Engl.* **1994**, 33, 938 - 957. c) H. Mayr, M. Patz, M. F. Gotta, A. R. Ofial, *Pure Appl. Chem.* **1998**, 70, 1993 - 2000. d) H. Mayr, A. R. Ofial, *Carbocation Chemistry*, G. A. Olah, G. K. S. Prakash, Wiley: Hoboken, NJ, 2004, Chapter 13, 331 - 358. e) H. Mayr, A. R. Ofial, *Pure Appl. Chem.* **2005**, 77, 1807 - 1821. f) R. Lucius, R. Loos, H. Mayr, *Angew. Chem., Int. Ed.* **2002**, 41, 91 - 95. g) M. Baidya, S. Kobayashi, F. Brotzel, U. Schmidhammer, E. Riedle, H. Mayr, *Angew. Chem., Int. Ed.* **2007**, 46, 6176 - 6179. h) H. Mayr, J. Bartl, G. Hagen, *Angew. Chem., Int. Ed. Engl.* **1992**, 31, 1613 - 1615.
- [14] T. A. Nigst, J. Ammer, H. Mayr, *J. Phys. Chem. A* **2012**, 116, 8494-8499.

- [15] S. Xu, I. Held, B. Kempf, H. Mayr, W. Steglich, H. Zipse, *Chem. Eur. J.* **2005**, *11*, 4751 - 4757.
- [16] A. Sakakura, K. Kawajiri, T. Ohkubo, Y. Kosugi, K. Ishihara, *J. Am. Chem. Soc.* **2007**, *129*, 14775 - 14779.
- [17] a) S. Singh, G. Das, O. V. Singh, H. Han, *Org. Lett.* **2007**, *9*, 401 - 404. b) S. Singh, G. Das, O. V. Singh, H. Han, *Tetrahedron Lett.* **2007**, *48*, 1983 - 1986.
- [18] E. Larionov, F. Achraier, J. Humin, H. Zipse, *ChemCatChem* **2012**, *4*, 559 - 566.
- [19] D. Könning, W. Hiller, M. Christmann, *Org. Lett.* **2012**, *14*, 5258–5261.
- [20] I. Held, A. Villinger, H. Zipse, *Synthesis* **2005**, 1425 - 1430.
- [21] A. C. Spivey, S. Arseniyadis, *Angew. Chem. Int. Ed.* **2004**, *43*, 5436 - 5441.
- [22] V. Gutmann, *Electrochimica Acta.* **1976**, *21*, 661.
- [23] a) C. Reichardt, *Chem. Rev.* **1994**, *94*, 2319 - 2358. b) C. Reichardt, G. Schäfer, *Liebigs Ann.* **1995**, 1579 - 1582. c) R. Eberhardt, S. Löbbecke, B. Neidhart, C. Reichardt, *Liebigs Ann. /Recueil* **1997**, 1195 - 1199. d) C. Reichardt, *Green Chem.* **2005**, *7*, 339 - 351.
- [24] (a) V. Lutz, J. Glatthaar, C. Würtele, M. Serafin, H. Hausmann, P. R. Schreiner, *Chem. Eur. J.* **2009**, *15*, 8548 - 8557. (b) C. B. Fisher, S. Xu, H. Zipse, *Chem. Eur. J.* **2006**, *12*, 5779 - 5784.
- [25] T. Sakamoto, N. Miura, Y. Kondo, H. Yamanaka, *Chem. Pharm. Bull.* **1986**, *34*, 2018 - 2023.
- [26] K.-T. Wong, S.-Y. Kua, F.-W. Yen, *Tetrahedron Lett.* **2007**, *48*, 5051.
- [27] Gaussian 03, Revision D.01, M. J. Frisch, G. W. Trucks, H.B. Schlegel, G. E. Scuseria, M. A. Robb, J. R. Cheeseman, J. A. Montgomery, Jr., T. Vreven, K. N. Kudin, J. C. Burant, J. M. Millam, S. S. Iyengar, J. Tomasi, V. Barone, B. Mennucci, M. Cossi, G. Scalmani, N. Rega, G. A. Petersson, H. Nakatsuji, M. S. Hada, M. Ehara, K. Toyota, R. Fukuda, J. Hasegawa, M. Ishida, T. Nakajima, Y. Honda, O. Kitao, H. Nakai, M. Klene, X. Li, J. E. Knox, H. P. Hratchian, J. B. Cross, V. Bakken, C. Adamo, J. Jaramillo, R. Gomperts, R. E. Stratmann, O. Yazyev, A. J. Austin, R. Cammi, C. Pomelli, J. W. Ochterski, P. Y. Ayala, K. Morokuma, G. A. Voth, P. Salvador, J. J. Dannenberg, V. G. Zakrzewski, S. Dapprich, A. D. Daniels, M. C. Strain, O. Farkas, D. K. Malick, A. D. Rabuck, K. Raghavachari, J. B. Foresman, J. V. Ortiz, Q. Cui, A. G. Baboul, S. Clifford, J. Cioslowski, B. B. Stefanov, G. Liu, A. Liashenko, P. Piskorz, I. Komaromi, R. L. Martin, D. J. Fox, T. Keith, M. A. Al-Laham, C. Y. Peng, A. Nanayakkara, M. Challacombe, P. M. W. Gill, B. Johnson, W. Chen, M. W. Wong, C. Gonzalez, and J. A. Pople, Gaussian, Inc., Wallingford CT, **2004**.
- [28] <http://www.cmbi.ru.nl/edu/bioinf4/comfa-Prac/comfa.shtml>, 26.10.2012, 14:02 CET.

- [29] K. Ko, K. Nakano, S. Watanabe, Y. Ichikawa, H. Kotsuki, *Tetrahedron Lett.* **2009**, 50, 4025 - 4029.
- [30] D. H. Ripin, D. A. Evans, http://daecr1.harvard.edu/pdf/evans_pKa_table.pdf
- [31] E. Larionov, H. Zipse “*Kinetics of reactions in homogeneous solution*” **2010**.

Chapter 4

Cation Affinity Numbers of Lewis Bases

C. Lindner, R. Tandon, B. Maryasin, E. Larionov, H. Zipse, Beilstein J. Org. Chem. 2012, 8, 1406–1442.

This Chapter is a modified version of the published manuscript (the affinity data for phosphanes obtained by C. Lindner are omitted and the “technical aspects” part is now represented by a pyridine) in order to keep the focus on obtained effects in pyridine derivatives. Data and results obtained by other authors are omitted in the Experimental Part.

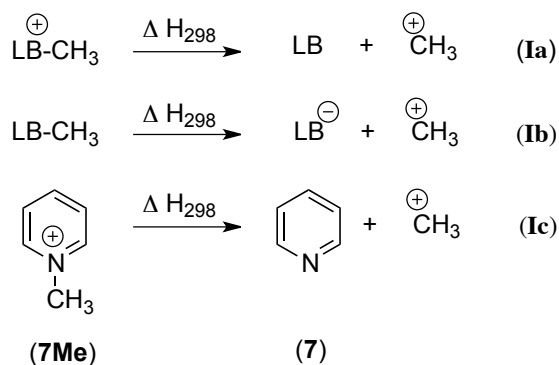
4.1 Introduction

Cation affinity values are important guidelines for the reactivity of Lewis and Brønsted bases.^[1-3] While proton affinity numbers (either as gas phase proton affinities or as solution phase pK_a values) have been used for a long time in quantitative approaches to describe base-induced or base-catalyzed processes, affinity data towards carbon electrophiles have only recently been adopted as tools for the assessment of Lewis base reactivity.^[4] This is mainly due to the scarcity of accurate experimentally measured or theoretically calculated data. The performance of various theoretical methods to provide accurate affinity data has recently been analyzed and a number of cost-efficient methods for the determination of precise gas phase values have been identified.^[5,6] Using these methods we now present a broad overview over the cation affinities of N-based nucleophiles.

4.2 Results and Discussion

Methyl Cation Affinities (MCA)

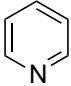
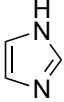
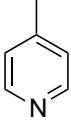
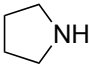
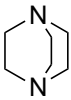
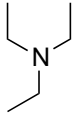
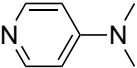
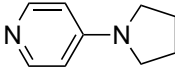
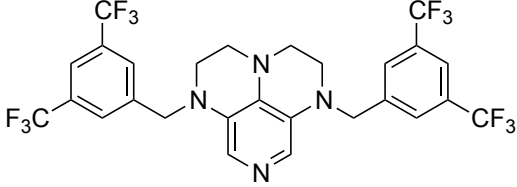
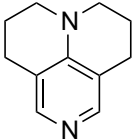
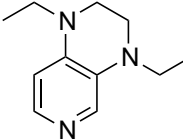
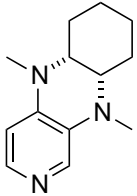
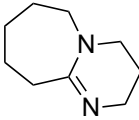
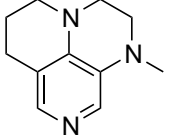
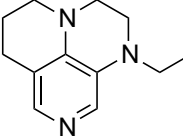
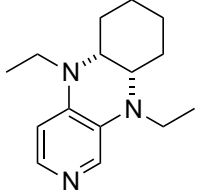
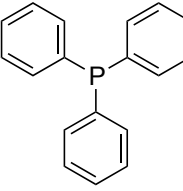
The methyl cation (CH_3^+) is the smallest carbocation useful as a chemical probe for Lewis bases. The respective methyl cation affinity (MCA) of a given Lewis base (LB) is obtained as the reaction enthalpy at 298.15 K and 1 bar pressure for the reaction shown in equation (Ia) for a neutral Lewis base and in equation (Ib) for an anionic base. This definition is in analogy to that for proton affinities (PA) and implies large positive energies for most of the P- and N-based Lewis bases used in catalytic processes. Using pyridine (**7**) as an example for a weak Lewis base, the methyl cation affinity corresponds to the enthalpy of the reaction in equation (Ic) and amounts to $\text{MCA}(\mathbf{7}) = +519.2 \text{ kJ/mol}$ at the G3 level of theory.^[5]

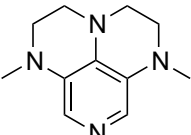
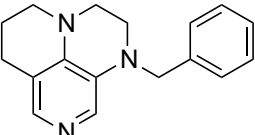
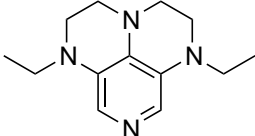
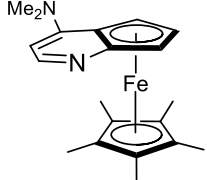
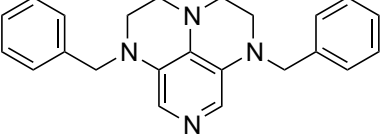
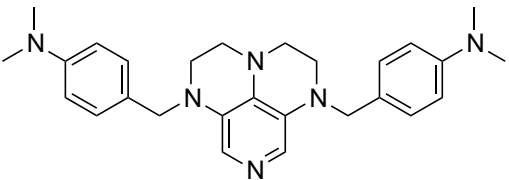


A recent analysis of theoretical methods found that calculations at MP2(FC)/6-31+G(2d,p)//B98/6-31G(d) level of theory (in short: "MP2-5") reproduce results obtained at G3 level within 4.0 kJ/mol for selected small and medium-sized organocatalysts.^[5] For pyridine (**7**) the MCA value obtained with this model amounts to $\text{MCA}(\mathbf{7}) = +518.7 \text{ kJ/mol}$, which is only 0.5 kJ/mol lower than the G3 value. The following discussion will thus be based on results obtained with the MP2-5 model, if not noted otherwise. Methyl cation affinity

(MCA) values obtained for N-centered Lewis bases using this approach are collected in Table 4.1.

Table 4.1. MCA values for surveyed Lewis bases, ordered by increasing MCA values.

System	Nr.	MCA [kJ/mol]	System	Nr.	MCA [kJ/mol]
	(7)	+518.7		(8)	+531.7 ^[a]
	(9)	+532.8		(10)	+539.8
	(11)	+562.2		(12)	+562.3
	(1)	+581.2 ^[b]		(2)	+590.1 ^[b]
	(5e)				+596.8
	(3)	+602.7		(13b)	+609.0
	(6a)	+609.1		(14)	+609.6 ^[c]
	(4a)	+611.0		(4b)	+613.3
	(6b)	+616.0		(15)	+618.7

	(5a)	+618.7		(4c)	+620.8
	(5b)	+621.6		(18)	+624.1 ^{[b], [d]}
	(5c)	+636.8			
	(5d)	+661.3			

[a] N3; [b] Pyridine nitrogen; [c] N(sp²); [d] See reference [7].

Pyridine (**7**) is a comparatively weak nucleophile as already mentioned above. This also applies to imidazole (**8**) and pyrrolidine (**10**), which have MCA values below 550 kJ/mol. In the case of pyridine it is possible to increase the Lewis basicity by introducing electron-donating groups in *para*-position. The key structure for this kind of catalysts is DMAP (**1**).

Raising the Lewis basicity of DMAP (**1**) can be accomplished by different means (Figure 4.1):

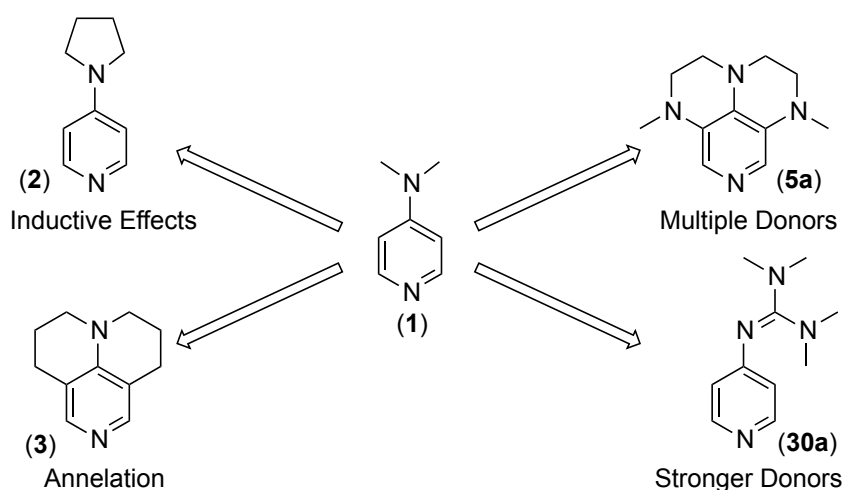


Figure 4.1. Increasing the Lewis basicity of DMAP (**1**).

The introduction of an alkyl group (**9**) gives a moderate increase in MCA-value compared to the just mentioned introduction of dialkylamino groups in 4-*N,N*-dimethylaminopyridine

(DMAP, **1**) or in 4-pyrrolidinopyridine (PPY, **2**). This is in accordance with the much higher catalytic efficiency of **1** and **2** for e.g. in acylation reactions.^[3,8-12] Conformational fixation is also accompanied by an increase in the MCA value comparing 4-pyrrolidinopyridine (PPY, **2**) and 9-azajulolidine (TCAP, **3**). The impact of multiple nitrogen donors can be obtained best by comparison of **3** (one *N*-Donor) with **6a** or **4a** (two *N*-Donors) and with **5a** (three *N*-Donors). Every nitrogen atom enhances the MCA by roughly 8 kJ/mol. The highest MCA value is obtained for triaminopyridine **5d**, in which the effect of three donors embedded in a cyclic framework is even increased by attachment of two dialkylaminogroups that donate their electrons through phenyl rings. The ferrocenyl group in DMAP-derivative **18** has great impact on the MCA value with MCA (**18**) = +624.1 kJ/mol.^[7] This is approximately 40 kJ/mol more than for DMAP with MCA (**1**) = +581.2 kJ/mol and may be the reason for the outstanding catalytic potential of **18**. For the chiral Lewis bases **6a**, **6b**, and **18** only one enantiomer is listed in Table 1. Affinity values towards achiral electrophiles such as the MCA values collected in Table 1 are, of course, exactly identical for both enantiomers, and we will therefore in the following report affinity values for only one of the enantiomers of a given chiral Lewis base. At last we want to compare the much smaller Lewis basicity of DABCO (**11**) as compared to DMAP (**1**), which has also been cited in experimental studies as the prime reason for the different catalytic profile of these two catalysts.^[13]

Acetyl Cation Affinities (ACA)

Reactions between carbon electrophiles and Lewis bases may also lead to the formation of a new common π -system. A well known example is the acyl transfer reaction catalyzed by pyridine bases, which involve acetylpyridinium cations as intermediates of the catalytic cycle.^[14-20] The acetyl cation may be considered to be a representative cationic probe for this type of situation and the corresponding acetyl cation affinities (ACA) of neutral Lewis bases thus reflect the enthalpies for the reaction shown in equation (II). Using pyridine again as a typical example, the acetyl cation affinity amounts to ACA(**7**) = +156.1 kJ/mol.

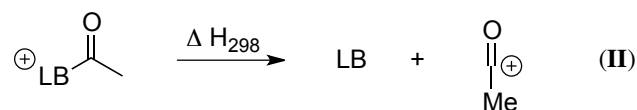
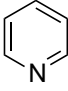
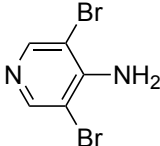
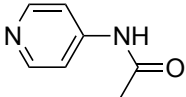
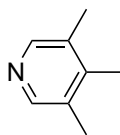
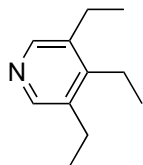
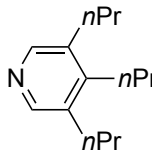
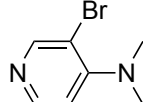
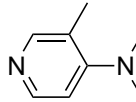
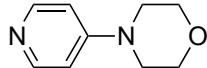
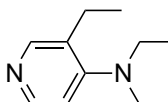
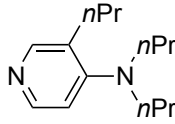
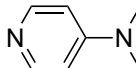
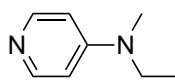
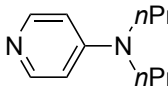
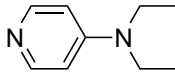
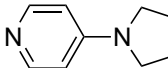
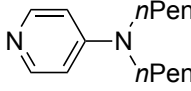
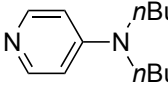
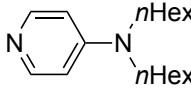
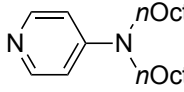
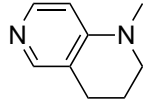
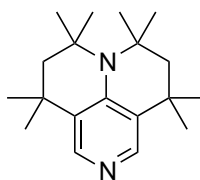
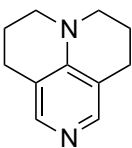
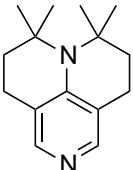
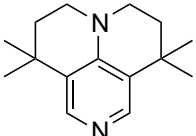


Table 4.2. ACA values of pyridines and 4-aminopyridines, ordered by increasing ACA values.

System	Nr.	ACA [kJ/mol]	System	Nr.	ACA [kJ/mol]
	(7)	+156.1		(19)	+164.7
	(20)	+175.0		(21)	+182.4 ^[b]
	(22)	+183.8 ^[b]		(23)	+183.5 ^[b]
	(24)	+184.1		(25)	+206.4
	(26)	+207.2		(27)	+210.7
	(28)	+211.4		(1)	+217.3
	(1b)	+219.4		(1d)	+222.2
	(1c)	+223.2		(2)	+223.7
	(1f)	+223.9 ^[a]		(1e)	+224.0 ^[a]
	(1g)	+224.2 ^[a]		(1h)	+224.6 ^[a]
	(29)	+227.8 ^[b]		(3d)	+230.0

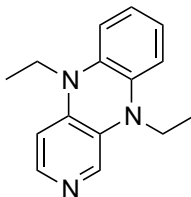
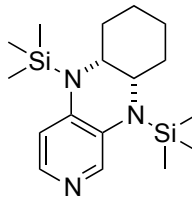
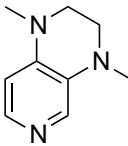
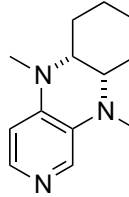
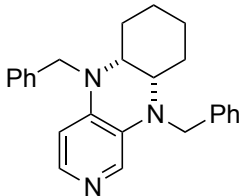
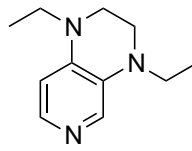
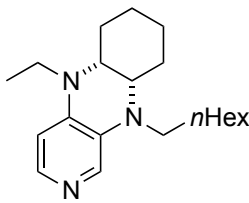
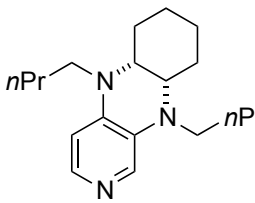
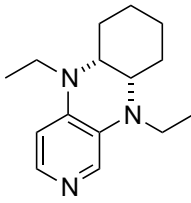
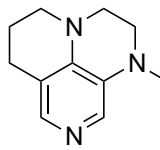
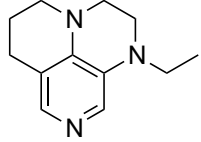
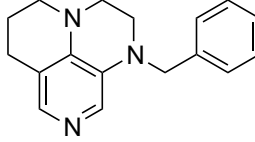
	(3)	+238.3		(3c)	+238.5
	(3b)	+239.1			

[a] The conformational space used is based on the minima found for system **1d** and elongation of alkyl groups using all-*trans* conformations; [b] Obtained by Dr. Evgeny Larionov.^[27]

For *N,N*-dialkyl-4-aminopyridines (**1**, **1b–1h**) it is interesting to see how elongation of the alkyl substituents leads to a rapid convergence of the ACA values. The two methyl groups in 4-dimethylaminopyridine (**1**) lead to an ACA value just 7 kJ/mol or 3 % below the two octyl groups (**1h**). The well-known catalyst PPY (**2**) has almost the same ACA like the dialkyl pyridines (**1e–1h**) and in fact the catalytic activity is very similar (see Chapter 5). Heteroatoms like bromine directly attached to the pyridine ring lower the ACA value dramatically (**1** vs. **24**). The impact of conformational fixation can be clarified best by comparing DMAP (**1**) and compound **29** where an alkyl chain is annelated to the pyridine ring. This effect raises the ACA by roughly 10 kJ/mol. This is not only a matter of inductive effects comparing with dialkyl derivative **1c** in which 4 carbon atoms donate their inductive effects, too, but without any conformational fixation. A doubly annelated ring system is present in the highly potent tricyclic pyridine **3**. The annelation has again an impact of almost 10 kJ/mol. The group of pyridines derived from the tricyclic moiety (**3**) can just slightly be modified towards higher affinity to the acetyl cation (**3c** and **3b**). Inclusion of too many methyl groups as in **3d** leads to disfavorable interactions and therefore to a decrease of the ACA value.

3,4-diaminopyridines have been shown to be particularly effective as acyl transfer catalysts.^[20] This is also visible in the respective ACA values (Table 4.3). Most of the 3,4-diaminopyridines (**13b**, **6a–e**) show ACA values roughly between 235 and 243 kJ/mol. Annelation of an additional six-membered ring to bicyclic 3,4-diaminopyridines leads to tricyclic diaminopyridines **4a–c** and is accompanied by an increase in acetyl cation affinities above 240 kJ/mol. Annelation of a carbocyclic ring thus has a comparable effect as already observed for DMAP (**1**) and its ring-extended forms **29** and **3**. This is in remarkable contrast to DMAP derivatives such as **25** carrying non-annelated alkyl substituents in 3- and/or 5-position with clearly lower ACA values. Comparison of pyridines **6b** and **6g** furthermore shows that alkyl groups directly attached to the amine substituents in 3- and 5-position are significantly more effective than aryl substituents in stabilizing the pyridinium ions formed through acetyl cation addition. Based on motif **6a** one can see that the elongation of methyl substituents to ethyl (**6b**) give roughly 5 kJ/mol whereas a further increase in chain length (**6d,e**) gives no increase at all. This shows that the motif itself is nucleophilic enough to overcome further inductive effects on that stage. Chapter 5 shows that 4-dialkylaminopyridines show a saturation of inductive effects for R = *n*Bu (**1e**).

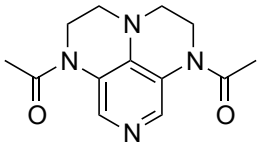
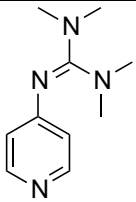
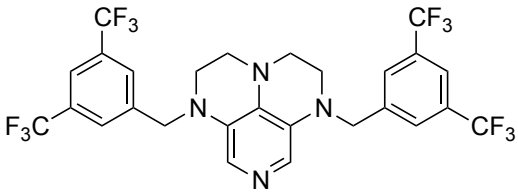
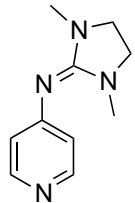
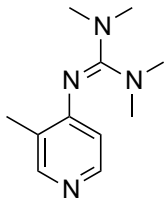
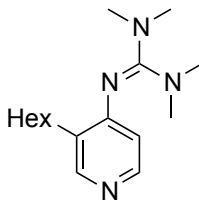
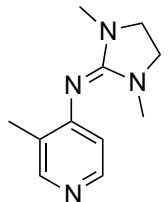
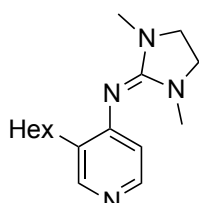
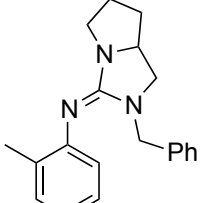
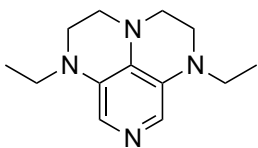
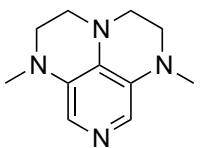
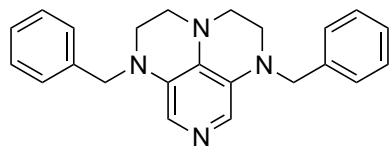
Table 4.3. ACA values of 3,4-diaminopyridines, ordered by increasing ACA values.

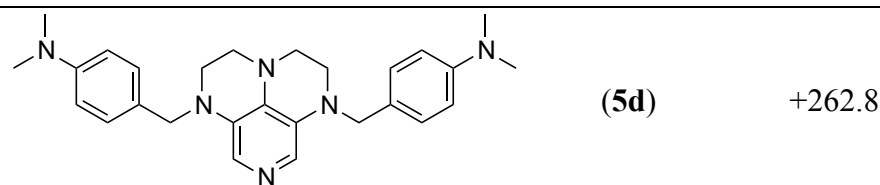
System	Nr.	ACA [kJ/mol]	System	Nr.	ACA [kJ/mol]
	(6g)	+216.2		(6f)	+225.9
	(13a)	+233.8		(6a)	+235.5
	(6c)	+236.0 ^[a]		(13b)	+237.5
	(6e)	+240.9 ^[a]		(6d)	+241.2 ^[a]
	(6b)	+241.3		(4a)	+242.9
	(4b)	+243.6		(4c)	+246.3

[a] Obtained by Dr. Evgeny Larionov.^[27]

Pyridine bases including a larger number of electron-donating substituents are highly interesting as Lewis base catalysts. ACA values for this class of compounds have been collected in Table 4.4.

Table 4.4. ACA values of 3,4,5-triaminopyridines and guanidines, ordered by increasing ACA values.

System	Nr.	ACA [kJ/mol]	System	Nr.	ACA [kJ/mol]
	(5f)	+204.3		(30a)	+223.6 ^[a]
	(5e)				+225.6
	(30b)	+226.2 ^[a]		(30c)	+229.1 ^[a]
	(30d)	+229.9 ^[a]		(30e)	+231.5 ^[a]
	(30f)	+231.6 ^[a]		(30g)	+232.8 ^[a]
	(5b)	+243.9		(5a)	+245.3
	(5c)	+254.4			



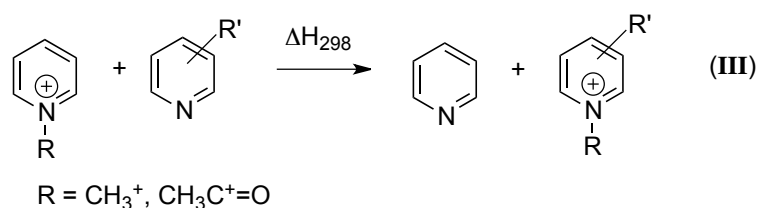
[a] Guanidines calculated by Dr. Evgeny Larionov.^[27]

The 3,4,5-triaminopyridines **5a–d** show the highest ACA values of all examined neutral Lewis bases with affinity values ranging from 225 to 263 kJ/mol. They exceed even the great donor abilities of the guanidine derivatives. These values parallel the impressively high nucleophilicity parameters N measured recently for these compounds and indicate that carbon basicities parallel the kinetics of base addition to carbocations for this class of compounds.^[48] Guanidinyl pyridines such as **30b–g** have, in contrast, surprisingly low ACA values around 230 kJ/mol. Structural changes in the guanidine motif have only a moderate influence on the affinity to acetyl cation. From an experimental side of view all these substances (3,4,5-triaminopyridines as well as the guanidinyl derivatives) are quite challenging in terms of handling due to their great nucleophilicity.

Technical aspects

It was shown recently that MCA values can be calculated with high accuracy with methods like G2, G3 or W1.^[5] Beside these expensive methods also some MP2 calculations can afford, slightly less, accurate results. For the MP2 calculations different combinations of polarization functions and diffuse functions were tested. In contrast, DFT methods such as B3LYP seem to be unsuitable for predicting MCA values in an adequate manner. A good compromise between computational effort and predictive value was found for the MP2(FC)/6-31+G(2d,p)//B98/6-31G(d) level of theory. Therefore all results described herein have been obtained using this approach.

Despite the fact that all affinity definitions in equations (I) – (II) use the separate reactants as the thermochemical reference state, it is for most applications in synthesis and catalysis fully sufficient to consider differences in cation affinities between two different Lewis bases. These differences can most easily be expressed as cation transfer reactions between two Lewis bases as described by eq. (III). The calculation of thermochemical data for isodesmic reactions is usually more accurate than for other defining equations due to the cancellation of numerous errors.



Additional practical challenges in calculating accurate affinity numbers concern the often large conformational space of Lewis bases and their cationic adducts. This can easily be demonstrated for **28** and its acylated form (**28Ac**). Depending on the strategy and the programs used for conformational searches, both species will have hundreds of conformations. Using systematic searches in combination with specifically selected force fields leads to 353 (**28**) and 798 (**28Ac**) conformations. Some of these conformations are eliminated in geometry optimizations at DFT level, but the final energy window of 25 kJ/mol for ‘good’ structures still contains 220 (**28**) and 443 (**28Ac**) structures (after the elimination of mirror-image conformers). A reliable calculation of Boltzmann-averaged thermochemical data and the identification of the best conformers thus requires frequency calculations and MP2 single point calculations for all of these structures. It should be added that the energetically best structure varies on moving from $E_{\text{tot}}(\text{DFT})$ to $H_{298}(\text{DFT})$ to $H_{298}(\text{MP2})$. At this last level of theory two close-lying all-*trans* conformations can be found for **28** as depicted in Figure 4.2.

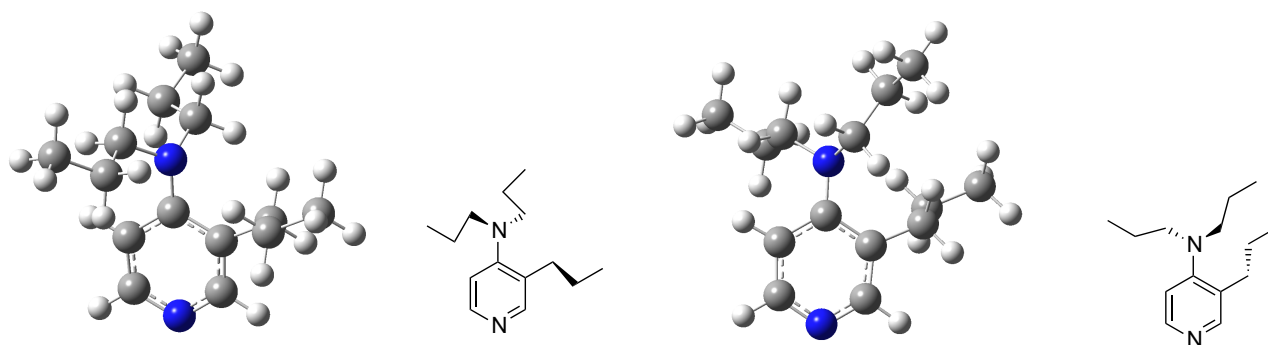


Figure 4.2. The energetically best conformations of **28** (**28_5**, left) and (**28_1**, right).

For the sake of clarity only the seven best conformations are shown in Figure 4.3.

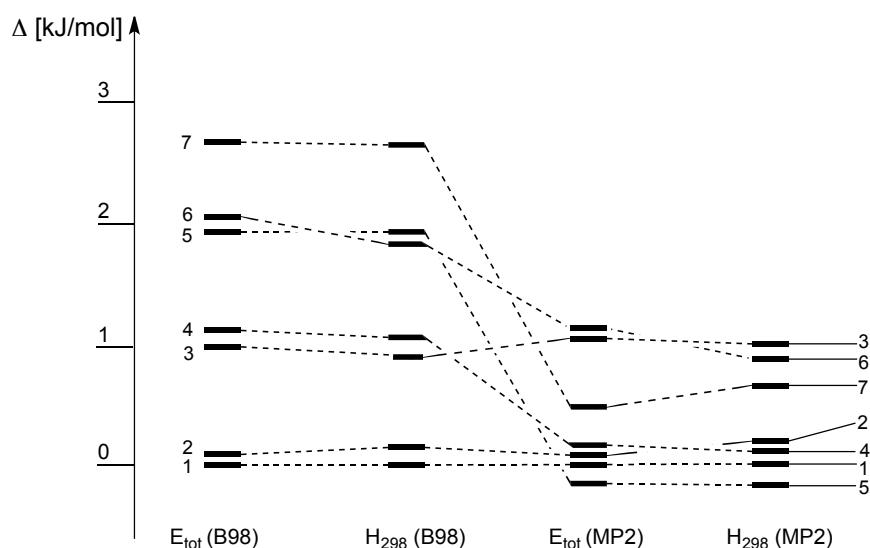


Figure 4.3. Relative order of the conformations 1 to 7 of compound **28** depending on the level of theory.

The eventually best conformation **28_5** is less favorable by 2 kJ/mol as compared to conformation **28_1** when using total energies (E_{tot}) or enthalpies at 298 K (H_{298}) obtained at B98/6-31G(d) level of theory. Moving to the MP2(FC)/6-31+G(2d,p)//B98/6-31G(d) energies or enthalpies the difference shrinks to 0.2 kJ/mol, now with **28_5** as the more stable structure. The reduction of energy differences on moving from DFT to MP2 single point energies is a rather general phenomenon observed in these studies. This implies that the definition of, for example, an energy window of 25 kJ/mol for conformational selection has different implications at these different levels of theory. Conformational preferences can, of course, also be quite different for the neutral Lewis base and its acylated adduct. For **28Ac** we find that conformation **28Ac_1** (Figure 4.4) has the lowest E_{tot} on both levels of theory as well as the lowest H_{298} .

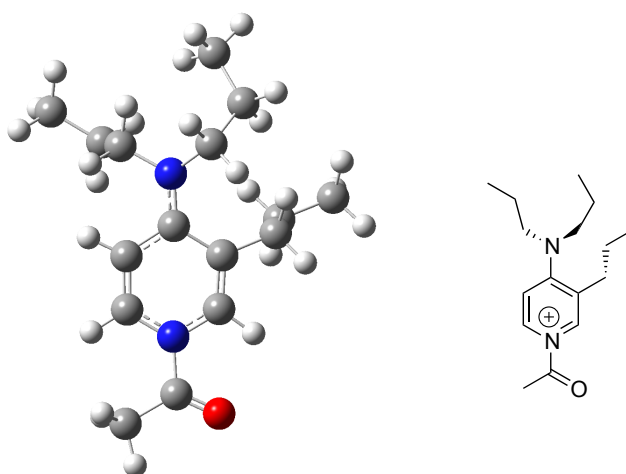


Figure 4.4. The structure of the energetically best conformation of **28Ac**.

All MCA values and acyl cation affinities employ Boltzmann-averaging over all available conformations within a 30 kJ/mol (25 kJ/mol for **28**) energy window. The Boltzmann-averaged MCA value of **28** thus amounts to +211.4 kJ/mol. Taking only the energetically best conformations in each case (**28** and **28Ac**) into account, the MCA value amounts to +212.6 kJ/mol. For this particular system the Boltzmann-averaging procedure thus offers no real benefit for the calculation of acyl cation affinities, but this can change depending on the systems under study. The most relevant role of extensive conformational searches is therefore that of the identification of the best conformation of the Lewis base as well as the cationic adduct (LB^+ -methyl, LB^+ -acetyl). Unfortunately, the actual conformational rank depends on the used level of theory, especially if dispersion interactions play a large role. This problem will gain in relevance when the steric demand is large. In the present study it can be neglected due to the use of MP2 single point calculations and the fact that the important minima could be found at the B98 level of theory.

4.3 Conclusion

Affinity data towards selected electrophiles provide the means to quantify Lewis bases with respect to their carbon basicity. This complements the limited amount of experimental affinity data and provides a quantitative guideline in catalyst development projects, in which the addition of Lewis bases to carbon electrophiles represent the key steps of the catalytic cycle.

4.4 Experimental Part

Computational Methods (MCA)

Methyl cation affinities of Lewis bases (LB) have been calculated as the reaction enthalpy at 298.15 K and 1 atm pressure for the methyl cation detachment reaction shown in equation (Ia). This is in analogy to the mass spectrometric definition of proton affinities.



The geometries of all species in equation (I) have been optimized at the B98/6-31G(d) level of theory. The conformational space of flexible Lewis bases and the corresponding cations has been searched using the MM3* force field and the systematic search routine implemented in MACROMODEL 9.7.^[21] All stationary points located at force field level have then been reoptimized at B98/6-31G(d) level as described before. Thermochemical corrections to 298.15 K have been calculated for all minima from unscaled vibrational frequencies obtained at this same level. The thermochemical corrections have been combined with single point energies calculated at the MP2(FC)/6-31+G(2d,p)//B98/6-31G(d) level to yield enthalpies H_{298} at 298.15 K. In conformationally flexible systems enthalpies have been calculated as Boltzmann-averaged values over all available conformers. This procedure has recently been found to reproduce G3 methyl cation affinity values of selected small and medium sized organocatalysts within 4.0 kJ/mol.^[5] All quantum mechanical calculations have been performed with Gaussian 03.^[22]

Table 4.5. Total energies and enthalpies (in Hartree) as calculated at the B98/6-31G(d) and MP2(FC)/6-31+G(2d,p)//B98/6-31G(d) level of theory for all systems (MCA). If more than one conformer exist at 298.15 K, the single values of the ten best conformers are denoted as well as the Boltzmann-averaged values for H_{298} at MP2(FC)/6-31+G(2d,p)//B98/6-31G(d) level of theory. Only conformers are included with a Boltzmann-weighting of at least 1 % (rounded) up to a maximum to ten conformers per system.

System	B98/6-31G(d)		MP2(FC)/6-31+G(2d,p)// B98/6-31G(d)	
	E_{tot}	H_{298}	E_{tot}	" H_{298} "
CH₃⁺	-39.462922	-39.427481	-39.352370	-39.316929
7	-248.181760	-248.087612	-247.589438	-247.495291
7-Me⁺	-287.856015	-287.718210	-287.147570	-287.009765
1	-382.100964	-381.928970	-381.179961	-381.007963
1-Me⁺	-421.801455	-421.585450	-420.762257	-420.546252
2	-459.498999	-459.289442	-458.383909	-458.174353
2-Me⁺	-499.203048	-498.949398	-497.969688	-497.716038
3	-536.905604	-536.658402	-535.602480	-535.355229
3-Me⁺	-576.614364	-576.322975	-575.192996	-574.901595
13b				-591.693361
13b_1	-593.418065	-593.130882	-591.981253	-591.694070
13b_2	-593.417089	-593.130032	-591.980205	-591.693148
13b_3	-593.416648	-593.129503	-591.979900	-591.692755
13b_4	-593.415838	-593.128722	-591.978867	-591.691751
13b_5	-593.415488	-593.128356	-591.979018	-591.691886
13b_6	-593.415277	-593.127873	-591.978972	-591.691568
13b_7	-593.414082	-593.126927	-591.977705	-591.690550
13b-Me⁺				-631.242261
13b-Me ⁺ _1	-633.129214	-632.797785	-631.574118	-631.242689
13b-Me ⁺ _2	-633.129077	-632.797925	-631.573803	-631.242651
13b-Me ⁺ _3	-633.128021	-632.796615	-631.572771	-631.241365
13b-Me ⁺ _4	-633.127946	-632.796535	-631.572692	-631.241281
13b-Me ⁺ _5	-633.127843	-632.796281	-631.572934	-631.241371
13b-Me ⁺ _6	-633.126370	-632.794816	-631.571168	-631.239614
13b-Me ⁺ _7	-633.125330	-632.793715	-631.570008	-631.238393
6a				-668.864138
6a_1	-670.810555	-670.485932	-669.188397	-668.863774
6a_2	-670.809955	-670.485240	-669.188192	-668.863477
6a_3	-670.809509	-670.485967	-669.188063	-668.864521
6a-Me⁺				-708.4130556
6a-Me ⁺ _1	-710.523274	-710.154417	-708.782257	-708.413400
6a-Me ⁺ _2	-710.521930	-710.153123	-708.781454	-708.412647
6a-Me ⁺ _3	-710.521960	-710.153186	-708.781416	-708.412642
4a				-590.538821
4a_1	-592.222726	-591.957797	-590.804005	-590.539076
4a_2	-592.221494	-591.956591	-590.802484	-590.537581
4a-Me⁺				-630.088475
4a-Me ⁺ _1	-631.93496	-631.625782	-630.397667	-630.088489
4a-Me ⁺ _2	631.935067	-631.625863	-630.397664	-630.088461
4b				-629.702332
4b_1	-631.521285	-631.226469	-629.997804	-629.702988

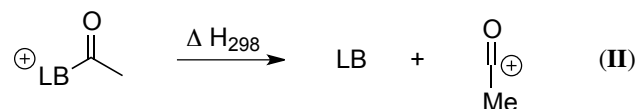
4b_2	-631.519929	-631.225072	-629.996450	-629.701594
4b_3	-631.519580	-631.224611	-629.995589	-629.700620
4b_4	-631.518936	-631.224066	-629.995691	-629.700821
4b_5	-631.518089	-631.223278	-629.994812	-629.700001
4b_6	-631.518347	-631.223563	-629.994767	-629.699983
4b-Me⁺				-669.252836
4b-Me ⁺ _1	-671.234101	-670.895069	-669.592430	-669.253399
4b-Me ⁺ _2	-671.232987	-670.893965	-669.591240	-669.252218
4b-Me ⁺ _4	-671.232612	-670.893380	-669.590990	-669.251757
4b-Me ⁺ _5	-671.232695	-670.893444	-669.591128	-669.251876
4b-Me ⁺ _6	-671.232675	-670.893535	-669.590966	-669.251826
6b				-747.191944
6b_1	-749.405682	-749.021776	-747.576377	-747.192470
6b_2	-749.407023	-749.022449	-747.576974	-747.192400
6b_3	-749.404877	-749.020263	-747.576944	-747.192329
6b_4	-749.405930	-749.021754	-747.576291	-747.192115
6b_5	-749.406234	-749.021772	-747.576561	-747.192098
6b_6	-749.404995	-749.020441	-747.576374	-747.191820
6b_7	-749.404598	-749.020095	-747.576157	-747.191654
6b_8	-749.404606	-749.020080	-747.576166	-747.191641
6b_9	-749.404830	-749.020098	-747.576215	-747.191483
6b_10	-749.406393	-749.021713	-747.576140	-747.191460
6b-Me⁺				-786.743479
6b-Me ⁺ _1	-789.121780	-788.692940	-787.173377	-786.744537
6b-Me ⁺ _2	-789.120016	-788.691557	-787.171915	-786.743456
6b-Me ⁺ _3	-789.120407	-788.691692	-787.172037	-786.743323
6b-Me ⁺ _4	-789.120407	-788.691688	-787.172038	-786.743319
6b-Me ⁺ _5	-789.119194	-788.690414	-787.171900	-786.743119
6b-Me ⁺ _6	-789.118810	-788.690096	-787.171405	-786.742691
6b-Me ⁺ _7	-789.118811	-788.690086	-787.171398	-786.742672
6b-Me ⁺ _8	-789.119475	-788.691090	-787.170972	-786.742587
6b-Me ⁺ _9	-789.119294	-788.690807	-787.170819	-786.742332
6b-Me ⁺ _10	-789.118385	-788.689728	-787.170896	-786.742240
4c				-820.851865
4c_1	-823.176622	-822.826137	-821.202780	-820.852295
4c_2	-823.176434	-822.825873	-821.202409	-820.851848
4c_3	-823.177128	-822.826607	-821.202518	-820.851997
4c_4	-823.176637	-822.826010	-821.201939	-820.851312
4c_5	-823.175198	-822.824733	-821.201087	-820.850621
4c_6	-823.174700	-822.824147	-821.199884	-820.849331
4c-Me⁺				-860.405256
4c-Me ⁺ _1	-862.890937	-862.496224	-860.799004	-860.404291
4c-Me ⁺ _2	-862.891864	-862.497139	-860.800363	-860.405638
4c-Me ⁺ _3	-862.890446	-862.495612	-860.798210	-860.403376
4c-Me ⁺ _4	-862.891273	-862.496634	-860.798320	-860.403681
4c-Me ⁺ _5	-862.891448	-862.496815	-860.798564	-860.403931
4c-Me ⁺ _6	-862.891753	-862.497047	-860.800381	-860.405675

4c-Me ⁺ ₇	-823.176622	-822.826137	-821.202780	-820.852295
4c-Me ⁺ ₈	-823.176434	-822.825873	-821.202409	-820.851848
4c-Me ⁺ ₉	-823.177128	-822.826607	-821.202518	-820.851997
4c-Me ⁺ ₁₀	-823.176637	-822.826010	-821.201939	-820.851312
5a				-645.721376
5a ₁	-647.539246	-647.256369	-646.004511	-645.721634
5a ₂	-647.537517	-647.254755	-646.002984	-645.720222
5a-Me ⁺				-685.273939
5a-Me ⁺ ₁	-687.253802	-686.926838	-685.601105	-685.274140
5a-Me ⁺ ₂	-687.253201	-686.926208	-685.600563	-685.273570
5b				-724.049255
5b ₁	-726.136622	-725.794008	-724.392585	-724.049971
5b ₂	-726.135261	-725.792675	-724.391022	-724.048436
5b ₃	-726.134093	-725.791344	-724.390368	-724.047619
5b ₄	-726.133773	-725.791105	-724.389136	-724.046468
5b ₅	-726.133843	-725.791423	-724.389524	-724.047104
5b ₆	-726.132311	-725.789756	-724.388635	-724.046080
5b ₇	-726.132623	-725.790069	-724.388834	-724.046280
5b ₈	-726.132578	-725.790061	-724.388529	-724.046012
5b ₉	-726.131575	-725.788592	-724.388232	-724.045249
5b ₁₀	-726.130711	-725.787685	-724.387694	-724.044668
5b-Me⁺				-763.602939
5b-Me ⁺ ₁	-765.851994	-765.465346	-763.990563	-763.603916
5b-Me ⁺ ₂	-765.850785	-765.463869	-763.989319	-763.602403
5b-Me ⁺ ₃	-765.850315	-765.463344	-763.989001	-763.602030
5b-Me ⁺ ₄	-765.849640	-765.463028	-763.988190	-763.601579
5b-Me ⁺ ₅	-765.850795	-765.463913	-763.989104	-763.602221
5b-Me ⁺ ₆	-765.849161	-765.462332	-763.987775	-763.600947
5b-Me ⁺ ₇	-765.849609	-765.462936	-763.988073	-763.601401
5b-Me ⁺ ₈	-765.849628	-765.462808	-763.988274	-763.601454
5b-Me ⁺ ₉	-765.848774	-765.461441	-763.987533	-763.600200
5b-Me ⁺ ₁₀	-765.848364	-765.461579	-763.986967	-763.600182
5c				-1106.348047
5c ₁	-1109.447043	-1108.993196	-1106.802424	-1106.348577
5c ₂	-1109.447132	-1108.993055	-1106.802354	-1106.348278
5c ₃	-1109.447628	-1108.993564	-1106.802303	-1106.348239
5c ₄	-1109.447585	-1108.993563	-1106.802088	-1106.348066
5c ₅	-1109.447026	-1108.992980	-1106.801891	-1106.347844
5c ₆	-1109.446406	-1108.992420	-1106.801637	-1106.347651
5c ₇	-1109.447786	-1108.993676	-1106.802326	-1106.348216
5c ₈	-1109.444983	-1108.991221	-1106.800827	-1106.347065
5c ₉	-1109.448248	-1108.994131	-1106.802136	-1106.348019
5c ₁₀	-1109.446099	-1108.991892	-1106.800767	-1106.346560
5c-Me⁺				-1145.907501
5c-Me ⁺ ₁	-1149.167468	-1148.669290	-1146.406434	-1145.908256
5c-Me ⁺ ₂	-1149.166518	-1148.668217	-1146.405837	-1145.907536
5c-Me ⁺ ₃	-1149.166429	-1148.668220	-1146.404848	-1145.906639
5c-Me ⁺ ₄	-1149.166725	-1148.668311	-1146.404532	-1145.906118
5c-Me ⁺ ₅	-1149.166180	-1148.667997	-1146.404041	-1145.905857
5c-Me ⁺ ₆	-1149.165179	-1148.666903	-1146.403228	-1145.904953
5c-Me ⁺ ₇	-1149.165420	-1148.667213	-1146.403135	-1145.904928
5c-Me ⁺ ₈	-1149.165655	-1148.667434	-1146.402799	-1145.904578
5c-Me ⁺ ₉	-1149.165740	-1148.667407	-1146.402253	-1145.903920

5c-Me ⁺ _10	-1149.166086	-1148.667599	-1146.402329	-1145.903842
5d				-1373.365244
5d_1	-1377.275202	-1376.665689	-1373.975470	-1373.365957
5d_3	-1377.274605	-1376.664862	-1373.975115	-1373.365373
5d_4	-1377.273310	-1376.663857	-1373.974752	-1373.365299
5d_5	-1377.273690	-1376.663737	-1373.974891	-1373.364938
5d_6	-1377.274707	-1376.664933	-1373.974696	-1373.364922
5d_7	-1377.273236	-1376.663538	-1373.974157	-1373.364459
5d_8	-1377.273796	-1376.663774	-1373.974318	-1373.364296
5d_9	-1377.273230	-1376.663530	-1373.973692	-1373.363991
5d_10	-1377.273167	-1376.663416	-1373.973545	-1373.363794
5d-Me⁺				-1412.934033
5d-Me ⁺ _1	-1417.002909	-1416.350286	-1413.587226	-1412.934602
5d-Me ⁺ _2	-1417.002349	-1416.348090	-1413.586624	-1412.932365
5d-Me ⁺ _3	-1417.002907	-1416.349289	-1413.585385	-1412.931767
5d-Me ⁺ _4	-1417.002170	-1416.348015	-1413.585639	-1412.931484
5d-Me ⁺ _5	-1417.002443	-1416.348593	-1413.585095	-1412.931245
5d-Me ⁺ _6	-1417.000720	-1416.347191	-1413.583555	-1412.930026
5d-Me ⁺ _7	-1417.002459	-1416.349150	-1413.583296	-1412.929987
5d-Me ⁺ _8	-1417.001883	-1416.348114	-1413.583422	-1412.929653
5d-Me ⁺ _9	-1417.002788	-1416.348782	-1413.583523	-1412.929516
5d-Me ⁺ _10	-1417.000886	-1416.347167	-1413.582263	-1412.928545
5e				-2451.844902
5e_1	-2457.167590	-2456.680733	-2452.332600	-2451.845743
5e_2	-2457.167844	-2456.680186	-2452.332439	-2451.844781
5e_3	-2457.167475	-2456.679766	-2452.331402	-2451.843693
5e_4	-2457.166341	-2456.678411	-2452.331395	-2451.843465
5e_5	-2457.167009	-2456.679192	-2452.330928	-2451.843111
5e_6	-2457.166909	-2456.678911	-2452.330841	-2451.842843
5e_7	-2457.167235	-2456.679336	-2452.330594	-2451.842695
5e_8	-2457.167124	-2456.679203	-2452.330138	-2451.842217
5e_9	-2457.167440	-2456.679606	-2452.329809	-2451.841976
5e_10	-2457.165057	-2456.677241	-2452.329585	-2451.841769
5e-Me⁺				-2491.389131
5e-Me ⁺ _1	-2496.874252	-2496.342261	-2491.921708	-2491.389717
5e-Me ⁺ _2	-2496.873406	-2496.341419	-2491.920449	-2491.388463
5e-Me ⁺ _3	-2496.873089	-2496.341126	-2491.918499	-2491.386536
5e-Me ⁺ _4	-2496.871852	-2496.339686	-2491.915361	-2491.383195
5e-Me ⁺ _5	-2496.872148	-2496.340067	-2491.917211	-2491.385130
5e-Me ⁺ _6	-2496.871731	-2496.339779	-2491.915537	-2491.383585
5e-Me ⁺ _7	-2496.872230	-2496.341247	-2491.919008	-2491.388024
5e-Me ⁺ _8	-2496.872709	-2496.340778	-2491.918212	-2491.386281
5e-Me ⁺ _9	-2496.873773	-2496.341564	-2491.921623	-2491.389415
5e-Me ⁺ _10	-2496.871318	-2496.339150	-2491.916135	-2491.383967

Computational Methods (ACA)

Acetyl cation affinity (ACA) of Lewis bases (LB) have been calculated as the reaction enthalpy at 298.15 K and 1 atm pressure including solvent effects (CHCl₃) for the detachment reaction shown in equation (II). This is in analogy to the mass spectrometric definition of proton affinities.



The geometries have been optimized at the B98/6-31G(d) level of theory. The conformational space of flexible Lewis bases and the corresponding cations has been searched using the MM3* force field and the systematic search routine implemented in MACROMODEL 9.7.^[21] All stationary points located at force field level have then been reoptimized at B98/6-31G(d) level as described before. Thermochemical corrections to 298.15 K have been calculated for all minima from unscaled vibrational frequencies obtained at this same level. The thermochemical corrections have been combined with single point energies calculated at the MP2(FC)/6-31+G(2d,p)//B98/6-31G(d) level to yield enthalpies H_{298} at 298.15 K. In conformationally flexible systems enthalpies have been calculated as Boltzmann-averaged values over all available conformers. In order to consider solvent effects in chloroform the PCM/UAHF/RHF/6-31G(d) approach was used. All quantum mechanical calculations have been performed with Gaussian 03.^[22]

Table 4.6. Total energies and enthalpies (in Hartree) as calculated at the B98/6-31G(d) and MP2(FC)/6-31+G(2d,p)//B98/6-31G(d) level of theory for all systems (ACA) as well as inclusion of solvent effects in chloroform at PCM/UAHF/RHF/6-31G(d). If more than one conformer exist at 298.15 K, the single values of each conformer are denoted as well as the Boltzmann-averaged values for H_{298} at MP2(FC)/6-31+G(2d,p)//B98/6-31G(d) level of theory. Only conformers are included with a Boltzmann-weighting of at least 1 % (rounded) up to a maximum to ten conformers per system. The systems are ordered by the sequence of appearance in Tables 4.2–4.4.

system	B98/6-31G(d)		MP2(FC)/ 6- 31+G(2d,p)	PCM/ UAHF/ RHF/ 6-31G(d)	MP2(FC)/ 6-31+G(2d,p)	"H ₂₉₈ " + ΔG _{solv}
	E _{tot}	H ₂₉₈	E _{tot}	ΔG _{solv} [kJ/mol]	"H ₂₉₈ "	<H ₂₉₈ >
CH ₃ -CO ⁺	-152.864773	-152.815435	-152.544414	-42.83	-152.495076	-152.563330
7	-248.181767	-248.087627	-247.589439	-9.00	-247.498727	-247.498727
7-Ac ⁺	-401.140004	-400.991691	-400.215516	-142.55	-400.121498	-400.121498
19	-5445.710391	-5445.615295	-5442.043341	-1.10	-5441.948244	-5441.949997
19-Ac ⁺	-5598.675003	-5598.525635	-5594.676214	-30.89	-5594.526846	-5594.576073
20						-454.947460
20_1	-456.123075	-455.969135	-455.094581	-4.29	-454.940642	
20_2	-456.117560	-455.963631	-455.089897	-3.84	-454.935967	
20-Ac ⁺						-607.577447
20-Ac ⁺ _1	-609.097006	-608.889040	-607.733281	-32.79	-607.525315	
20-Ac ⁺ _2	-609.096181	-608.888102	-607.732549	-33.14	-607.524470	
20-Ac ⁺ _3	-609.084790	-608.876809	-607.721457	-34.48	-607.513476	
20-Ac ⁺ _4	-609.085031	-608.876864	-607.721499	-34.37	-607.513331	
21	-366.086672	-365.904186	-365.181353	-7.11	-365.001576	-365.001576
21-Ac ⁺	-519.060128	-518.823483	-517.822649	-126.98	-517.634369	-517.634369
22						-482.485398
22_1	-483.975105	-483.702005	-482.758292	-1.67	-482.485830	
22_2	-483.973719	-483.700644	-482.756390	-1.92	-482.484048	
22_3	-483.972675	-483.699673	-482.755393	-2.64	-482.483395	
22_4	-483.972119	-483.699057	-482.753971	-3.77	-482.482344	
22-Ac ⁺						-635.118726
22-Ac ⁺ _1	-636.951414	-636.624166	-635.402799	-115.06	-635.119375	
22-Ac ⁺ _2	-636.949865	-636.622659	-635.400863	-115.14	-635.117513	
22-Ac ⁺ _3	-636.949773	-636.622428	-635.400705	-114.77	-635.117072	
22-Ac ⁺ _4	-636.949652	-636.622472	-635.399800	-115.27	-635.116523	
22-Ac ⁺ _5	-636.949816	-636.622611	-635.399914	-114.68	-635.116389	
22-Ac ⁺ _6	-636.948798	-636.621373	-635.399634	-114.89	-635.115970	
22-Ac ⁺ _7	-636.948571	-636.621367	-635.399474	-113.68	-635.115569	
23						-599.969258
23_1	-601.867333	-601.504627	-600.335730	8.66	-599.969725	
23_2	-601.866425	-601.503546	-600.335656	8.54	-599.969526	
23_3	-601.865755	-601.503017	-600.335223	8.95	-599.969075	
23_4	-601.866606	-601.503817	-600.335327	9.12	-599.969064	
23_5	-601.866109	-601.503417	-600.334732	7.95	-599.969012	
23_6	-601.864819	-601.501971	-600.334716	8.33	-599.968696	
23_7	-601.864972	-601.502256	-600.334668	9.00	-599.968526	
23_8	-601.865940	-601.503323	-600.333754	8.12	-599.968046	
23_9	-601.866884	-601.504187	-600.333874	8.45	-599.967958	
23-Ac ⁺						-752.602459
23-Ac ⁺ _1	-754.846894	-754.429794	-752.982879	-98.28	-752.603213	
23-Ac ⁺ _2	-754.845981	-754.428934	-752.982842	-97.49	-752.602926	
23-Ac ⁺ _3	-754.846060	-754.429106	-752.983008	-96.78	-752.602915	

23-Ac ⁺ ₄	-754.845109	-754.428275	-752.982213	-97.74	-752.602605	
23-Ac ⁺ ₅	-754.844513	-754.427544	-752.981423	-99.58	-752.602382	
23-Ac ⁺ ₆	-754.845179	-754.428012	-752.982244	-97.82	-752.602335	
23-Ac ⁺ ₇	-754.844582	-754.427449	-752.981463	-99.66	-752.602289	
23-Ac ⁺ ₈	-754.845169	-754.428013	-752.982907	-95.69	-752.602196	
23-Ac ⁺ ₉	-754.844386	-754.427448	-752.982380	-96.19	-752.602079	
24	-2953.188796	-2953.025593	-2950.788635	-1.79	-2950.625433	-2950.628285
24-Ac⁺						-3103.261734
24-Ac ⁺ ₁	-3106.165812	-3105.947834	-3103.431149	-30.62	-3103.213171	
24-Ac ⁺ ₂	-3106.166084	-3105.947897	-3103.431489	-30.07	-3103.213302	
25	-421.396615	-421.195314	-420.375062	-2.24	-420.173761	-420.177330
25-Ac⁺						-572.819276
25-Ac ⁺ ₁	-574.384977	-574.128494	-573.027529	-30.38	-572.771046	
25-Ac ⁺ ₂	-574.384774	-574.128179	-573.027195	-30.35	-572.770601	
26						-533.223855
26_1	-534.674094	-534.458445	-533.431574	-5.09	-533.215925	
26_2	-534.671639	-534.456042	-533.428547	-4.90	-533.212950	
26_3	-534.667855	-534.453746	-533.427916	-4.26	-533.213807	
26-Ac⁺						-685.866099
26-Ac ⁺ ₁	-687.661866	-687.391436	-686.082793	-33.72	-685.812363	
26-Ac ⁺ ₂	-687.661866	-687.391436	-686.082792	-33.72	-685.812362	
26-Ac ⁺ ₃	-687.661866	-687.391435	-686.082794	-33.72	-685.812363	
26-Ac ⁺ ₄	-687.661866	-687.391435	-686.082793	-33.72	-685.812362	
26-Ac ⁺ ₅	-687.661866	-687.391436	-686.082792	-33.72	-685.812362	
26-Ac ⁺ ₆	-687.661866	-687.391436	-686.082793	-33.72	-685.812363	
27						-537.664361
27_1	-539.288171	-538.997296	-537.955185	-0.43	-537.664310	
27_2	-539.286526	-538.995985	-537.955218	-0.12	-537.664677	
27_3	-539.287920	-538.996961	-537.954938	-0.33	-537.663979	
27_4	-539.287884	-538.996914	-537.954329	-0.46	-537.663359	
27_5	-539.287894	-538.996750	-537.953909	-0.78	-537.662765	
27_6	-539.287382	-538.996484	-537.953801	-0.51	-537.662903	
27_7	-539.287477	-538.996378	-537.953881	-0.43	-537.662782	
27_8	-539.287388	-538.996260	-537.953389	-0.58	-537.662261	
27_9	-539.287406	-538.996102	-537.952970	-0.93	-537.661667	
27_10	-539.286388	-538.994735	-537.952295	-1.12	-537.660642	
27-Ac⁺						-690.307930
27-Ac ⁺ ₁	-692.279948	-691.933358	-690.611664	-27.47	-690.265074	
27-Ac ⁺ ₂	-692.279758	-691.933333	-690.611476	-27.45	-690.265051	
27-Ac ⁺ ₃	-692.280672	-691.933848	-690.611320	-27.29	-690.264496	
27-Ac ⁺ ₄	-692.280672	-691.933849	-690.611318	-27.29	-690.264495	
27-Ac ⁺ ₅	-692.280366	-691.933609	-690.610929	-27.12	-690.264173	
27-Ac ⁺ ₆	-692.280366	-691.933609	-690.610925	-27.11	-690.264168	
27-Ac ⁺ ₇	-692.279420	-691.932822	-690.610141	-27.42	-690.263543	
27-Ac ⁺ ₈	-692.278087	-691.931753	-690.609443	-27.56	-690.263109	
27-Ac ⁺ ₉	-692.278087	-691.931752	-690.609442	-27.56	-690.263107	
27-Ac ⁺ ₁₀	-692.280012	-691.933306	-690.609490	-27.54	-690.262784	
28						-655.147892
28_5	-657.179874	-656.799109	-655.532221	2.13	-655.151455	
28_1	-657.180594	-656.799826	-655.532137	2.22	-655.151368	
28_4	-657.180147	-656.799415	-655.532067	2.32	-655.151334	
28_2	-657.180574	-656.799765	-655.532084	2.11	-655.151275	
28_7	-657.179610	-656.798757	-655.531938	2.54	-655.151084	
28_6	-657.179788	-656.799137	-655.531685	2.39	-655.151034	

28_3	-657.180216	-656.799494	655.531703	2.34	-655.150981	
28_8	-657.179605	-656.798688	-655.531032	2.45	-655.150114	
28_9	-657.179558	-656.798805	-655.530429	2.35	-655.149675	
28_10	-657.179512	-656.798671	-655.531991	2.12	-655.151150	
28-Ac⁺						-807.791735
28-Ac ⁺ _1	-810.174823	-809.738348	-808.191656	-23.18	-807.755181	
28-Ac ⁺ _2	-810.173846	-809.737642	-808.191448	-23.05	-807.755245	
28-Ac ⁺ _3	-810.172493	-809.736039	-808.191091	-23.28	-807.754638	
28-Ac ⁺ _4	-810.171537	-809.734888	-808.191328	-23.23	-807.754680	
28-Ac ⁺ _5	-810.172419	-809.736241	-808.190159	-23.65	-807.753981	
28-Ac ⁺ _6	-810.172419	-809.736241	-808.190159	-23.64	-807.753981	
28-Ac ⁺ _7	-810.174620	-809.738147	-808.191496	-22.95	-807.755023	
28-Ac ⁺ _8	-810.171541	-809.734866	-808.191351	-23.13	-807.754676	
28-Ac ⁺ _9	-810.174168	-809.737487	-808.191434	-23.01	-807.754754	
28-Ac ⁺ _10	-810.173784	-809.737454	-808.191606	-22.68	-807.755277	
1	-382.100962	-381.928959	-381.179977	-13.68	-381.013184	-381.013184
1-Ac⁺	-535.091159	-534.864305	-533.836116	-131.34	-533.659287	-533.659287
1b	-421.400415	-421.198543	-420.374849	-2.84	-420.172978	-420.177503
1b-Ac⁺						-572.824386
1b-Ac ⁺ _1	-574.392288	-574.135480	-573.032902	-30.37	-572.776094	
1b-Ac ⁺ _2	-574.392332	-574.135258	-573.032926	-30.37	-572.775852	
1d						-537.663074
1d_1	-539.292811	-539.001043	-537.954451	-0.71	-537.662683	
1d_2	-539.293771	-539.002066	-537.954231	-0.65	-537.662525	
1d_3	-539.288540	-538.997719	-537.952842	-0.86	-537.662021	
1d_4	-539.294761	-539.003085	-537.953964	-0.67	-537.662288	
1d_5	-539.292832	-539.001072	-537.953309	-0.82	-537.661549	
1d_6	-539.292832	-539.001067	-537.953310	-0.82	-537.661545	
1d_7	-539.294028	-539.002224	-537.953368	-0.62	-537.661564	
1d_8	-539.292137	-539.000246	-537.953085	-0.66	-537.661193	
1d_9	-539.291362	-538.999336	-537.952841	-0.86	-537.660814	
1d_10	-539.290465	-538.998527	-537.952504	-0.91	-537.660566	
1d-Ac⁺						-690.311051
1d-Ac ⁺ _1	-692.289974	-691.943339	-690.615729	-26.79	-690.269095	
1d-Ac ⁺ _2	-692.289974	-691.943337	-690.615730	-26.76	-690.269093	
1d-Ac ⁺ _3	-692.287303	-691.940567	-690.615189	-27.04	-690.268453	
1d-Ac ⁺ _4	-692.287303	-691.940567	-690.615188	-26.99	-690.268451	
1d-Ac ⁺ _5	-692.288154	-691.941357	-690.615007	-27.08	-690.268210	
1d-Ac ⁺ _6	-692.288154	-691.941361	-690.615006	-27.06	-690.268213	
1d-Ac ⁺ _7	-692.288154	-691.941360	-690.615006	-27.06	-690.268212	
1d-Ac ⁺ _8	-692.286569	-691.939824	-690.614546	-27.18	-690.267802	
1d-Ac ⁺ _9	-692.286568	-691.939820	-690.614543	-27.18	-690.267795	
1d-Ac ⁺ _10	-692.288187	-691.941145	-690.615072	-27.03	-690.268030	
1c						-459.340887
1c_1	-460.699626	-460.467717	-459.569493	-2.29	-459.337583	
1c_2	-460.698872	-460.467017	-459.568777	-2.39	-459.336921	
1c_3	-460.695706	-460.463514	-459.566589	-2.54	-459.334396	
1c_4	-460.695601	-460.463698	-459.566199	-2.53	-459.334296	
1c_5	-460.688598	-460.457621	-459.563361	-1.71	-459.332384	
1c-Ac⁺						-611.989239
1c-Ac ⁺ _1	-613.693223	-613.406531	-612.229788	-29.32	-611.943096	
1c-Ac ⁺ _2	-613.693223	-613.406527	-612.229789	-29.32	-611.943093	
1c-Ac ⁺ _3	-613.691702	-613.404882	-612.228221	-29.54	-611.941402	
1c-Ac ⁺ _4	-613.691702	-613.404881	-612.228221	-29.54	-611.941400	

1c-Ac ⁺ ₅	-613.691701	-613.404880	-612.228221	-29.54	-611.941399	
1c-Ac ⁺ ₆	-613.691702	-613.404879	-612.228221	-29.54	-611.941399	
1c-Ac ⁺ ₇	-613.691702	-613.404879	-612.228221	-29.54	-611.941399	
1c-Ac ⁺ ₈	-613.691701	-613.404879	-612.228221	-29.54	-611.941398	
1c-Ac ⁺ ₉	-613.688778	-613.401873	-612.225068	-29.50	-611.938163	
2	-459.499042	-459.289458	-458.383907	-16.90	-458.180759	-458.180760
2-Ac⁺	-612.493384	-612.228939	-611.043991	-130.58	-610.829281	-610.829281
1f						-694.309437
1f_1	-696.482340	-696.071133	-694.722029	0.33	-694.310821	
1f_2	-696.483260	-696.071916	-694.721441	0.15	-694.310098	
1f_3	-696.484181	-696.073018	-694.720709	-0.16	-694.309546	
1f_4	-696.482373	-696.071012	-694.720715	0.09	-694.309353	
1f_5	-696.482373	-696.071012	-694.720715	0.09	-694.309353	
1f_6	-696.483414	-696.072035	-694.720319	0.06	-694.308940	
1f_7	-696.480912	-696.069542	-694.720705	0.35	-694.309335	
1f_8	-696.480912	-696.069540	-694.720705	0.36	-694.309334	
1f_9	-696.481634	-696.070227	-694.720769	0.63	-694.309362	
1f_10	-696.480197	-696.068619	-694.721312	1.12	-694.309733	
1f-Ac⁺						-846.958049
1f-Ac ⁺ ₁	-849.480922	-849.014921	-847.384012	-25.62	-846.918011	
1f-Ac ⁺ ₂	-849.480922	-849.014921	-847.384012	-25.62	-846.918011	
1f-Ac ⁺ ₃	-849.478322	-849.012227	-847.384344	-25.35	-846.918249	
1f-Ac ⁺ ₄	-849.478322	-849.012228	-847.384346	-25.33	-846.918252	
1f-Ac ⁺ ₅	-849.478322	-849.012226	-847.384346	-25.33	-846.918250	
1f-Ac ⁺ ₆	-849.479604	-849.013299	-847.384208	-25.35	-846.917903	
1f-Ac ⁺ ₇	-849.479604	-849.013300	-847.384207	-25.35	-846.917902	
1f-Ac ⁺ ₈	-849.479582	-849.013234	-847.384164	-25.29	-846.917816	
1f-Ac ⁺ ₉	-849.479151	-849.012711	-847.383968	-25.46	-846.917528	
1f-Ac ⁺ ₁₀	-849.479151	-849.012711	-847.383968	-25.46	-846.917528	
1e						-615.985990
1e_1	-617.887497	-617.535936	-616.338253	-0.06	-615.986692	
1e_2	-617.888418	-617.536743	-616.337923	-0.12	-615.986248	
1e_3	-617.889328	-617.537918	-616.337281	-0.31	-615.985872	
1e_4	-617.887503	-617.536024	-616.337133	-0.27	-615.985654	
1e_5	-617.887503	-617.536023	-616.337133	-0.27	-615.985653	
1e_6	-617.886098	-617.534293	-616.336942	-0.17	-615.985137	
1e_7	-617.886098	-617.534293	-616.336942	-0.16	-615.985137	
1e_8	-617.888537	-617.536890	-616.336840	-0.09	-615.985194	
1e_9	-617.886754	-617.535081	-616.337112	0.17	-615.985439	
1e_10	-617.885263	-617.533778	-616.337062	0.30	-615.985577	
1e-Ac⁺						-768.634640
1e-Ac ⁺ ₁	-770.882953	-770.476564	-769.000087	-26.00	-768.593698	
1e-Ac ⁺ ₂	-770.882953	-770.476564	-769.000087	-26.00	-768.593698	
1e-Ac ⁺ ₃	-770.883688	-770.477305	-768.999787	-26.18	-768.593405	
1e-Ac ⁺ ₄	-770.885523	-770.479189	-769.000042	-25.98	-768.593708	
1e-Ac ⁺ ₅	-770.885523	-770.479188	-769.000042	-25.98	-768.593707	
1e-Ac ⁺ ₆	-770.883688	-770.477305	-768.999788	-26.09	-768.593406	
1e-Ac ⁺ ₇	-770.883688	-770.477305	-768.999787	-26.09	-768.593404	
1e-Ac ⁺ ₈	-770.883729	-770.477103	-768.999863	-26.18	-768.593236	
1e-Ac ⁺ ₉	-770.884158	-770.477758	-769.000061	-25.89	-768.593661	
1e-Ac ⁺ ₁₀	-770.884158	-770.477752	-769.000064	-25.89	-768.593658	
1g						-772.632535
1g_1	-775.077114	-774.606103	-773.105282	0.52	-772.634271	
1g_2	-775.078023	-774.606780	-773.104714	0.31	-772.633471	

1g_3	-775.078966	-774.607937	-773.103913	0.01	-772.632884	
1g_4	-775.077165	-774.605877	-773.103996	0.38	-772.632708	
1g_5	-775.077165	-774.605877	-773.103996	0.38	-772.632708	
1g_6	-775.078201	-774.607185	-773.103496	0.24	-772.632481	
1g_7	-775.075663	-774.604455	-773.103938	0.50	-772.632730	
1g_8	-775.075663	-774.604455	-773.103938	0.50	-772.632730	
1g_9	-775.076394	-774.605194	-773.104146	0.92	-772.632946	
1g_10	-775.075012	-774.604033	-773.105047	1.73	-772.634068	
1g-Ac⁺						-925.281271
1g-Ac ⁺ _1	-928.073514	-927.547654	-925.767944	-24.99	-925.242084	
1g-Ac ⁺ _2	-928.073508	-927.547619	-925.767969	-24.98	-925.242080	
1g-Ac ⁺ _3	-928.073384	-927.547455	-925.767939	-24.99	-925.242010	
1g-Ac ⁺ _4	-928.076042	-927.549910	-925.767587	-25.28	-925.241454	
1g-Ac ⁺ _5	-928.076042	-927.549910	-925.767586	-25.28	-925.241454	
1g-Ac ⁺ _6	-928.074230	-927.548259	-925.767633	-25.13	-925.241661	
1g-Ac ⁺ _7	-928.074229	-927.548225	-925.767629	-25.09	-925.241625	
1g-Ac ⁺ _8	-928.074229	-927.548115	-925.767627	-25.14	-925.241513	
1g-Ac ⁺ _9	-928.074752	-927.548676	-925.767664	-25.02	-925.241588	
1g-Ac ⁺ _10	-928.074718	-927.548335	-925.767783	-25.05	-925.241400	
1h						-929.278649
1h_1	-932.266633	-931.675706	-929.871618	0.86	-929.280691	
1h_2	-932.267584	-931.676735	-929.871007	0.62	-929.280157	
1h_3	-932.268490	-931.677826	-929.870241	0.30	-929.279577	
1h_4	-932.266627	-931.675837	-929.870194	0.55	-929.279404	
1h_5	-932.267523	-931.676782	-929.869797	0.55	-929.279056	
1h_6	-932.265849	-931.675225	-929.870497	1.29	-929.279873	
1h_7	-932.265275	-931.674129	-929.870283	0.86	-929.279138	
1h_8	-932.266627	-931.675837	-929.870194	1.11	-929.279404	
1h_9	-932.265275	-931.674129	-929.870284	1.25	-929.279138	
1h_10	-932.265691	-931.675106	-929.869398	1.30	-929.278813	
1h-Ac⁺						-1081.927528
1h-Ac ⁺ _1	-1085.265916	-1084.620141	-1082.534275	-24.83	-1081.888500	
1h-Ac ⁺ _2	-1085.265916	-1084.620140	-1082.534275	-24.83	-1081.888499	
1h-Ac ⁺ _3	-1085.264081	-1084.618509	-1082.534323	-24.59	-1081.888751	
1h-Ac ⁺ _4	-1085.264081	-1084.618507	-1082.534323	-24.59	-1081.888750	
1h-Ac ⁺ _5	-1085.264081	-1084.618503	-1082.534329	-24.58	-1081.888751	
1h-Ac ⁺ _6	-1085.264589	-1084.618904	-1082.534414	-24.52	-1081.888729	
1h-Ac ⁺ _7	-1085.263339	-1084.617439	-1082.534699	-24.45	-1081.888800	
1h-Ac ⁺ _8	-1085.263339	-1084.617439	-1082.534699	-24.45	-1081.888799	
1h-Ac ⁺ _9	-1085.263339	-1084.617439	-1082.534697	-24.45	-1081.888798	
1h-Ac ⁺ _10	-1085.264551	-1084.618863	-1082.534380	-24.49	-1081.888691	
29	-459.503374	-459.293804	-458.39138	-17.07	-458.1883116	-458.1883116
29-Ac⁺						-610.838384
29-Ac ⁺ _1	-612.49845	-612.234055	-611.052154	-132.51	-610.838229	
29-Ac ⁺ _2	-612.498722	-612.234281	-611.052535	-132.34	-610.838499	
3d						-848.669982
3d_1	-851.254112	-850.771763	-849.151412	-0.62	-848.669063	
3d_2	-851.250657	-850.768052	-849.147394	-0.95	-848.664789	
3d-Ac⁺						-1001.320907
3d-Ac ⁺ _1	-1004.257598	-1003.720341	-1001.821116	-23.35	-1001.283858	
3d-Ac ⁺ _2	-1004.257604	-1003.720441	-1001.820898	-23.37	-1001.283735	
3d-Ac ⁺ _3	-1004.256924	-1003.719222	-1001.820851	-23.64	-1001.283149	
3d-Ac ⁺ _4	-1004.256779	-1003.719155	-1001.820692	-23.59	-1001.283069	
3						-535.362849

3_1	-536.905604	-536.658613	-535.602351	-20.33	-535.3631033	
3_2	-536.904889	-536.657992	-535.601147	-20.75	-535.3621533	
3-Ac⁺						-688.016947
3-Ac ⁺ _1	-689.905522	-689.603408	-688.268359	-133.80	-688.0172068	
3-Ac ⁺ _2	-689.904728	-689.602521	-688.267441	-133.72	-688.0161653	
3c						-692.015254
3c_1	-694.077726	-693.713030	-692.375522	-2.88	-692.010827	
3c_2	-694.077773	-693.712773	-692.375016	-3.13	-692.010016	
3c-Ac⁺						-844.669415
3c-Ac ⁺ _1	-847.078527	-846.660001	-845.043576	-28.10	-844.625051	
3c-Ac ⁺ _2	-847.079945	-846.660004	-845.043578	-28.09	-844.623637	
3c-Ac ⁺ _3	-847.078585	-846.658988	-845.042365	-27.91	-844.622767	
3c-Ac ⁺ _4	-847.079945	-846.658938	-845.042332	-27.93	-844.621324	
3b						-692.027002
3b_1	-694.092217	-693.727548	-692.387481	-2.76	-692.022812	
3b_2	-694.091422	-693.726710	-692.386808	-2.83	-692.022096	
3b-Ac⁺						-844.681414
3b-Ac ⁺ _1	-847.095804	-846.676012	-845.057557	-27.56	-844.637765	
3b-Ac ⁺ _2	-847.095806	-846.676012	-845.057556	-27.55	-844.637763	
3b-Ac ⁺ _3	-847.094841	-846.674985	-845.056326	-27.56	-844.636470	
3b-Ac ⁺ _4	-847.094840	-846.674991	-845.056315	-27.54	-844.636466	
6f						-1405.990947
6f_1	-1409.421763	-1408.937279	-1406.486458	6.86	-1406.001973	
6f_2	-1409.421317	-1408.936855	-1406.486333	6.93	-1406.001871	
6f-Ac⁺						-1558.640320
6f-Ac ⁺ _1	-1562.425032	-1561.885771	-1559.154996	-15.69	-1558.615736	
6f-Ac ⁺ _2	-1562.424062	-1561.884777	-1559.154521	-15.55	-1558.615235	
6f-Ac ⁺ _3	-1562.424044	-1561.886128	-1559.153583	-14.92	-1558.615667	
6f-Ac ⁺ _4	-1562.422706	-1561.883431	-1559.152478	-14.84	-1558.613202	
13a	-514.820620	-514.593193	-513.593048	-4.48	-513.365621	-513.372761
13a-Ac⁺						-666.025137
13a-Ac ⁺ _1	-667.820735	-667.538347	-666.258398	-30.97	-665.976010	
13a-Ac ⁺ _2	-667.819559	-667.537128	-666.256714	-30.88	-665.974283	
6a						-668.869492
6a_1	-670.809509	-670.485967	-669.188063	-3.32	-668.864521	
6a_2	-670.810555	-670.485932	-669.188397	-3.47	-668.863774	
6a-Ac⁺						-821.522525
6a-Ac ⁺ _1	-823.814747	-823.434833	-821.857811	-28.39	-821.477897	
6a-Ac ⁺ _2	-823.813008	-823.433445	-821.856756	-28.39	-821.477193	
6a-Ac ⁺ _3	-823.812867	-823.433163	-821.856423	-28.36	-821.476719	
6a-Ac ⁺ _4	-823.813532	-823.433843	-821.856130	-28.25	-821.476441	
6a-Ac ⁺ _5	-823.811898	-823.432430	-821.855091	-28.21	-821.475623	
6a-Ac ⁺ _6	-823.811762	-823.432069	-821.854807	-28.22	-821.475114	
13b						-591.698885
13b_1	-593.418065	-593.130880	-591.981245	-14.56	-591.699606	
13b_2	-593.417088	-593.130024	-591.980224	-14.52	-591.698690	
13b_3	-593.416648	-593.129499	-591.979898	-14.18	-591.698150	
13b_4	-593.415838	-593.128722	-591.978867	-14.14	-591.697137	
13b_5	-593.415488	-593.128357	-591.979020	-15.06	-591.697625	
13b_6	-593.415277	-593.127870	-591.978978	-15.19	-591.697357	
13b_7	-593.414082	-593.126927	-591.977706	-14.56	-591.696097	
13b-Ac⁺						-744.352678
13b-Ac ⁺ _1	-746.420416	-746.078238	-744.649502	-121.08	-744.353441	

13b-Ac ⁺ ₂	-746.420285	-746.077937	-744.649302	-121.29	-744.353151	
13b-Ac ⁺ ₃	-746.419224	-746.076995	-744.648332	-121.13	-744.352239	
13b-Ac ⁺ ₄	-746.41917	-746.07687	-744.648337	-121.50	-744.352314	
13b-Ac ⁺ ₅	-746.419086	-746.076798	-744.648046	-121.17	-744.351909	
13b-Ac ⁺ ₆	-746.419086	-746.076799	-744.648047	-121.17	-744.351911	
13b-Ac ⁺ ₇	-746.419131	-746.076892	-744.64761	-120.12	-744.351122	
13b-Ac ⁺ ₈	-746.419131	-746.076893	-744.64761	-120.08	-744.351108	
13b-Ac ⁺ ₉	-746.418954	-746.076873	-744.647375	-120.33	-744.351125	
13b-Ac ⁺ ₁	-746.417975	-746.075703	-744.646556	-120.16	-744.350051	
4a						-590.547164
4a_1	-592.222726	-591.957797	-590.804005	-5.24	-590.539076	
4a_2	-592.221494	-591.956591	-590.802484	-5.38	-590.537581	
4a-Ac⁺						-743.202992
4a-Ac ⁺ ₁	-745.226542	-744.906419	-743.473561	-31.37	-743.153438	
4a-Ac ⁺ ₂	-745.226382	-744.906245	-743.473132	-31.35	-743.152996	
4a-Ac ⁺ ₃	-745.225730	-744.905688	-743.472321	-31.24	-743.152280	
4a-Ac ⁺ ₄	-745.225508	-744.905414	-743.471922	-31.19	-743.151829	
4b						-629.709795
4b_1	-631.521285	-631.226469	-629.997804	-4.71	-629.702988	
4b_2	-631.519929	-631.225072	-629.996450	-4.61	-629.701594	
4b_3	-631.518936	-631.224066	-629.995691	-4.90	-629.700821	
4b_4	-631.519580	-631.224611	-629.995589	-4.87	-629.700620	
4b_5	-631.518089	-631.223278	-629.994812	-4.96	-629.700001	
4b_6	-631.518347	-631.223563	-629.994767	-4.76	-629.699983	
4b-Ac⁺						-782.365897
4b-Ac ⁺ ₁	-784.525551	-784.175677	-782.668096	-30.39	-782.318222	
4b-Ac ⁺ ₂	-784.525570	-784.175622	-782.668009	-30.34	-782.318061	
4b-Ac ⁺ ₃	-784.524416	-784.174632	-782.666991	-30.42	-782.317207	
4b-Ac ⁺ ₄	-784.524425	-784.174211	-782.667069	-30.51	-782.316854	
4b-Ac ⁺ ₅	-784.524351	-784.174539	-782.666772	-30.33	-782.316960	
4b-Ac ⁺ ₆	-784.524123	-784.173948	-782.666624	-30.47	-782.316449	
4b-Ac ⁺ ₇	-784.524617	-784.174740	-782.666634	-30.16	-782.316757	
4b-Ac ⁺ ₈	-784.524536	-784.174700	-782.666386	-30.10	-782.316550	
4b-Ac ⁺ ₉	-784.523541	-784.173341	-782.665821	-30.37	-782.315621	
4b-Ac ⁺ ₁₀	-784.523397	-784.173384	-782.665597	-30.14	-782.315585	
4c						-820.858184
4c_1	-823.176622	-822.826137	-821.202780	-4.06	-820.852295	
4c_2	-823.176434	-822.825873	-821.202409	-3.98	-820.851848	
4c_3	-823.177128	-822.826607	-821.202518	-3.73	-820.851997	
4c_4	-823.176637	-822.826010	-821.201939	-3.80	-820.851312	
4c_5	-823.175198	-822.824733	-821.201087	-4.15	-820.850621	
4c_6	-823.174700	-822.824147	-821.199884	-4.11	-820.849331	
4c-Ac⁺						-973.515327
4c-Ac ⁺ ₁	-976.183761	-975.778069	-973.877242	-27.91	-973.471551	
4c-Ac ⁺ ₂	-976.182553	-975.776936	-973.875645	-28.64	-973.470028	
4c-Ac ⁺ ₃	-976.183497	-975.777791	-973.876811	-27.86	-973.471105	
4c-Ac ⁺ ₄	-976.182300	-975.776758	-973.875174	-28.58	-973.469632	
4c-Ac ⁺ ₅	-976.183266	-975.777572	-973.874516	-28.61	-973.468821	
4c-Ac ⁺ ₆	-976.181375	-975.776644	-973.873542	-28.46	-973.468811	
4c-Ac ⁺ ₇	-976.182902	-975.777316	-973.874028	-28.56	-973.468442	
4c-Ac ⁺ ₈	-976.181392	-975.775636	-973.873555	-28.62	-973.467799	
4c-Ac ⁺ ₉	-976.182231	-975.776621	-973.874677	-27.78	-973.469067	
4c-Ac ⁺ ₁₀	-976.182048	-975.776520	-973.874454	-27.80	-973.468926	
5f						-871.900890

5f_1	-874.162557	-873.856387	-872.199497	-4.90	-871.893327	
5f_2	-874.162566	-873.856218	-872.199425	-4.97	-871.893077	
5f_3	-874.158168	-873.852116	-872.194565	-6.34	-871.888513	
5f_4	-874.157849	-873.851751	-872.194119	-6.39	-871.888021	
5f_5	-874.155463	-873.849018	-872.194489	-5.12	-871.888044	
5f_6	-874.152544	-873.846564	-872.188499	-8.23	-871.882520	
5f_7	-874.152349	-873.845984	-872.191219	-6.53	-871.884854	
5f_8	-874.152381	-873.846253	-872.188009	-8.17	-871.881881	
5f-Ac⁺						-1024.542020
5f-Ac ⁺ _1	-1027.152078	-1026.791413	-1024.853242	-31.17	-1024.492577	
5f-Ac ⁺ _2	-1027.152078	-1026.791411	-1024.853244	-31.16	-1024.492576	
5f-Ac ⁺ _3	-1027.151914	-1026.791243	-1024.853053	-31.28	-1024.492382	
5f-Ac ⁺ _4	-1027.151914	-1026.791243	-1024.853053	-31.28	-1024.492382	
5f-Ac ⁺ _5	-1027.149460	-1026.788833	-1024.851236	-31.58	-1024.490609	
5f-Ac ⁺ _6	-1027.149354	-1026.788701	-1024.851159	-31.53	-1024.490506	
5f-Ac ⁺ _7	-1027.145691	-1026.785213	-1024.847850	-32.53	-1024.487372	
5f-Ac ⁺ _8	-1027.145689	-1026.785124	-1024.847908	-32.45	-1024.487343	
5f-Ac ⁺ _9	-1027.142172	-1026.781872	-1024.845140	-33.11	-1024.484840	
5f-Ac ⁺ _10	-1027.142172	-1026.781872	-1024.845140	-33.10	-1024.484840	
5b						-724.056335
5b_1	-726.136622	-725.794008	-724.392585	-4.50	-724.049971	
5b_2	-726.135261	-725.792675	-724.391022	-4.42	-724.048436	
5b_3	-726.134093	-725.791344	-724.390368	-4.72	-724.047619	
5b_4	-726.133773	-725.791423	-724.389136	-4.75	-724.046786	
5b_5	-726.133843	-725.791105	-724.389524	-4.33	-724.046786	
5b_6	-726.132311	-725.790069	-724.388635	-4.83	-724.046393	
5b_7	-726.132623	-725.790061	-724.388834	-4.62	-724.046272	
5b_8	-726.132578	-725.789756	-724.388529	-4.64	-724.045707	
5b_9	-726.131575	-725.788592	-724.388232	-4.92	-724.045249	
5b_10	-726.130711	-725.788734	-724.387694	-4.94	-724.045717	
5b-Ac⁺						-876.712556
5b-Ac ⁺ _1	-879.143513	-878.745843	-877.065732	-28.52	-876.668062	
5b-Ac ⁺ _2	-879.143513	-878.745843	-877.065732	-28.52	-876.668062	
5b-Ac ⁺ _3	-879.142627	-878.744948	-877.064824	-28.63	-876.667145	
5b-Ac ⁺ _4	-879.142627	-878.744947	-877.064824	-28.63	-876.667144	
5b-Ac ⁺ _5	-879.142268	-878.744719	-877.064513	-28.48	-876.666963	
5b-Ac ⁺ _6	-879.142094	-878.744165	-877.064457	-28.75	-876.666528	
5b-Ac ⁺ _7	-879.141653	-878.743747	-877.064156	-28.87	-876.666250	
5b-Ac ⁺ _8	-879.142238	-878.744608	-877.064431	-28.50	-876.666801	
5b-Ac ⁺ _9	-879.141397	-878.743848	-877.063798	-28.66	-876.666249	
5b-Ac ⁺ _10	-879.141959	-878.743942	-877.064138	-28.65	-876.666121	
5a						-645.730280
5a_1	-647.539246	-647.256369	-646.004511	-5.59	-645.721634	
5a_2	-647.537517	-647.254755	-646.002984	-5.76	-645.720222	
5a-Ac⁺						-798.387055
5a-Ac ⁺ _1	-800.544982	-800.207283	-798.676037	-30.69	-798.338338	
5a-Ac ⁺ _2	-800.544982	-800.207283	-798.676155	-30.59	-798.338457	
5a-Ac ⁺ _3	-800.545288	-800.207283	-798.676155	-30.58	-798.338150	
5a-Ac ⁺ _4	-800.545288	-800.206988	-798.676036	-30.69	-798.337736	
5c						-1106.352811
5c_1	-1109.447043	-1108.993196	-1106.802424	-3.16	-1106.348577	
5c_2	-1109.447132	-1108.993055	-1106.802354	-3.13	-1106.348278	
5c_3	-1109.447628	-1108.993564	-1106.802303	-2.81	-1106.348239	
5c_4	-1109.447585	-1108.993563	-1106.802088	-2.77	-1106.348066	

5c_5	-1109.447026	-1108.992980	-1106.801891	-2.88	-1106.347844	
5c_6	-1109.446406	-1108.992420	-1106.801637	-2.96	-1106.347651	
5c_7	-1109.447786	-1108.993676	-1106.802326	-2.59	-1106.348216	
5c_8	-1109.444983	-1108.991221	-1106.800827	-3.25	-1106.347065	
5c_9	-1109.448248	-1108.994131	-1106.802136	-2.51	-1106.348019	
5c_10	-1109.446099	-1108.991892	-1106.800767	-2.89	-1106.346560	
5c-Ac⁺						-1259.013024
5c-Ac ⁺ _1	-1262.458568	-1261.949602	-1259.483210	-24.72	-1258.974244	
5c-Ac ⁺ _2	-1262.458568	-1261.949602	-1259.483208	-24.72	-1258.974242	
5c-Ac ⁺ _3	-1262.459023	-1261.949814	-1259.483351	-24.48	-1258.974143	
5c-Ac ⁺ _4	-1262.459022	-1261.949815	-1259.483347	-24.48	-1258.974140	
5c-Ac ⁺ _5	-1262.459415	-1261.950243	-1259.481958	-24.77	-1258.972785	
5c-Ac ⁺ _6	-1262.459504	-1261.950296	-1259.481941	-24.63	-1258.972733	
5c-Ac ⁺ _7	-1262.458026	-1261.948997	-1259.481565	-24.51	-1258.972536	
5c-Ac ⁺ _8	-1262.456839	-1261.947632	-1259.480614	-24.88	-1258.971407	
5c-Ac ⁺ _9	-1262.457707	-1261.948591	-1259.481125	-24.47	-1258.972009	
5c-Ac ⁺ _10	-1262.457476	-1261.948463	-1259.479556	-25.14	-1258.970543	

4.4 References

- [1] E. Larionov, H. Zipse, *WIREs Comp. Mol. Sci.* **2011**, *1*, 601–619.
- [2] S.E. Denmark, G.L. Beutner, *Angew. Chem. Int. Ed.* **2008**, *47*, 1560–1638.
- [3] N. De Rycke, F. Couty, O.R.P. David, *Chem. Eur. J.* **2011**, *17*, 12852–12871.
- [4] Y. Wei, G.N. Sastry, H. Zipse, *J. Am. Chem. Soc.* **2008**, *130*, 3473–3477.
- [5] Y. Wei, T. Singer, H. Mayr, G.N. Sastry, H. Zipse, *J. Comp. Chem.* **2008**, *29*, 291–297.
- [6] Y. Wei, B. Sateesh, B. Maryasin, G.N. Sastry, H. Zipse, *J. Comp. Chem.* **2009**, 2617–2624.
- [7] C.E. Müller, P.R. Schreiner, *Angew. Chem. Int. Ed.* **2011**, *50*, 6012–6042.
- [8] a) C. Lindner, R. Tandon, Y. Liu, B. Maryasin, H. Zipse, *Org. Biomol. Chem.* **2012**, *10*, 3210 – 3218; b) R. Tandon, T. Unzner, T. A. Nigst, N. De Rycke, P. Mayer, H. Mayr, B. Wendt, O.R.P. David, H. Zipse, **2013**, *19*, 6435 – 6442; c) I. Held, S. Xu, H. Zipse, *Synthesis* **2007**, 1185–1196.
- [9] E. Larionov, F. Achrainer, J. Humin, H. Zipse, *ChemCatChem* **2012**, *4*, 559–566.
- [10] V. D'Elia, Y. Liu, H. Zipse, *Eur. J. Org. Chem.* **2011**, 1527–1533.
- [11] I. Held, P. von den Hoff, D.S. Stephenson, H. Zipse, *Adv. Synth. Catal.* **2008**, *350*, 1891–1900.
- [12] M.R. Heinrich, H.S. Klisa, H. Mayr, W. Steglich, H. Zipse, *Angew. Chem.* **2003**, *115*, 4975–4977. *Angew. Chem. Int. Ed.* **2003**, *42*, 4826–4828.
- [13] M. Baidya, S. Kobayashi, F. Brotzel, U. Schmidhammer, E. Riedle, H. Mayr, *Angew. Chem. Int. Ed.* **2007**, *46*, 6176–6179.
- [14] E. Vedejs, M. Jure, *Angew. Chem. Int. Ed.* **2005**, *44*, 3974–4001.
- [15] R. Wurz, *Chem. Rev.* **2007**, *107*, 5570–5595.
- [16] A.C. Spivey, S. Arseniyadis, *Top. Curr. Chem.* **2010**, *291*, 233.

- [17] C.E. Müller, P.R. Schreiner, *Angew. Chem. Int. Ed.* **2011**, *50*, 6012–6042.
- [18] I. Held, A. Villinger, H. Zipse, *Synthesis* **2005**, 1425–1426.
- [19] Y. Wei, I. Held, H. Zipse, *Org. Biomol. Chem.* **2006**, *4*, 4223–4230.
- [20] I. Held, E. Larionov, C. Bozler, F. Wagner, H. Zipse, *Synthesis* **2009**, 2267–2277.
- [21] Schrödinger, LLC., MacroModel 9.7, **2009**.
- [22] M. J. Frisch, G. W. Trucks, H. B. Schlegel, G. E. Scuseria, M. A. Robb, J. R. Cheeseman, J. A. Montgomery, Jr, T. Vreven, K. N. Kudin, J. C. Burant, J. M. Millam, S. S. Iyengar, J. Tomasi, V. Barone, B. Mennucci, M. Cossi, G. Scalmani, N. Rega, G. A. Petersson, H. Nakatsuji, M. Hada, M. Ehara, K. Toyota, R. Fukuda, J. Hasegawa, M. Ishida, T. Nakajima, Y. Honda, O. Kitao, H. Nakai, M. Klene, X. Li, J. E. Knox, H. P. Hratchian, J. B. Cross, V. Bakken, C. Adamo, J. Jaramillo, R. Gomperts, R. E. Stratmann, O. Yazyev, A. J. Austin, R. Cammi, C. Pomelli, J. W. Ochterski, P. Y. Ayala, K. Morokuma, G. A. Voth, P. Salvador, J. J. Dannenberg, V. G. Zakrzewski, S. Dapprich, A. D. Daniels, M. C. Strain, O. Farkas, D. K. Malick, A. D. Rabuck, K. Raghavachari, J. B. Foresman, J. V. Ortiz, Q. Cui, A. G. Baboul, S. Clifford, J. Cioslowski, B. B. Stefanov, G. Liu, A. Liashenko, P. Piskorz, I. Komaromi, R. L. Martin, D. J. Fox, T. Keith, M. A. Al-Laham, C. Y. Peng, A. Nanayakkara, M. Challacombe, P. M. W. Gill, B. Johnson, W. Chen, M. W. Wong, C. Gonzalez, J. A. Pople, Gaussian 03, Revision D.01, Gaussian, Inc., Wallingford CT, **2004**.

Chapter 5

Inductive Effects Through Alkyl Groups – How Long is Long Enough?

Raman Tandon, Tobias A. Nigst and Hendrik Zipse, Eur. J. Org. Chem. 2013, accepted.

Results obtained by Tobias A. Nigst are omitted in the Experimental Part. In this chapter homologues of DMAP (**1**) are discussed. In order to keep a consistent numbering, DMAP is specified in this chapter to be **1a**.

5.1 Introduction

The influence of alkyl groups of variable length on ground state properties of organic molecules and on their reaction rates in unimolecular and bimolecular transformations has been discussed in terms of steric and electronic substituent effects.^[1] The latter of these may be divided further into inductive (through-bond) and field (through-space) components, the strict separation of these components being difficult. In recent efforts to develop nucleophilic catalysts of enhanced reactivity and selectivity, we^[2] and others^[3] explored the performance of alkyl substituted aminopyridines of general formula **1**, **5**, and **6** in pyridine-catalyzed acylation reactions of tertiary alcohols (Figure 5.1). These compounds are highly active nucleophilic catalysts with small alkyl substituents such as R = methyl or ethyl, and the question thus arises whether the catalytic efficiency can be increased further by elongation of the alkyl groups.

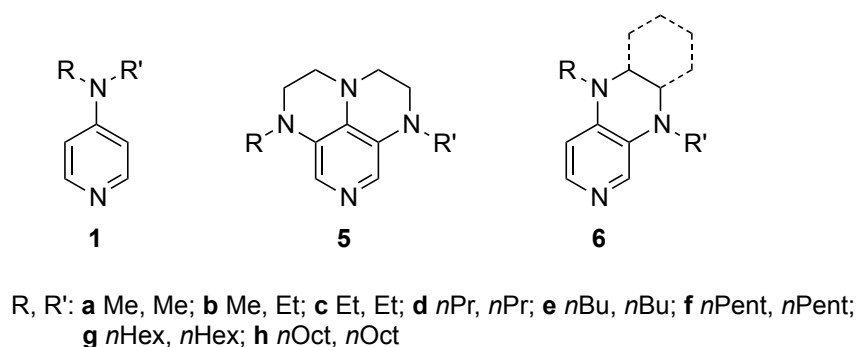
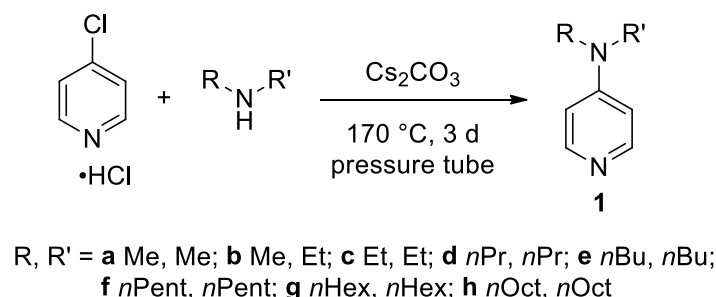


Figure 5.1. Structures of pyridine derivatives used as nucleophilic catalysts.

In more general terms this poses the question of the chain length dependence of inductive effects in alkyl substituents. We report here the effects of chain elongation of the alkyl groups in 4-alkylaminopyridines on the rates of pyridine-catalyzed acylations of alcohols, the benzylation of the pyridines, the reactions of *N*-benzoyl pyridinium ions with benzylamine, on their ¹H NMR properties, their theoretically calculated acetylation enthalpies, and on electronic and geometric properties of the respective acylated intermediates to provide a quantitative answer.

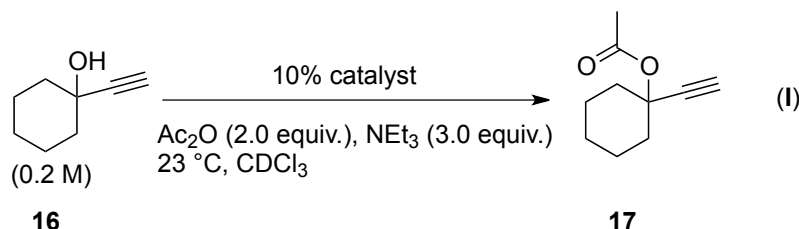
5.2 Results

The aminopyridines **1a–h** were synthesized by treatment of 4-chloropyridine with the corresponding dialkylamines following established literature procedures (Scheme 5.1).^[4]



Scheme 5.1. Synthesis of pyridine derivatives **1a–h**.

The catalytic potential of these catalysts has been explored in the acetylation of the tertiary alcohol **16** with acetic anhydride as followed by ^1H NMR spectroscopy (Scheme 5.2). All reactions eventually proceed to full conversion, and the rates of the reactions are thus characterized by the reaction half-life $t_{1/2}$ using the approach described previously (Table 5.1).^[2b]



Scheme 5.2. ^1H NMR benchmark reaction in CDCl_3 .

Table 5.1. Half-lives $t_{1/2}$ (in min) for the pyridine-catalyzed reaction of **16** with acetic anhydride in CDCl_3 .

Catalyst	$t_{1/2}$ [min]
1a	$151.0 \pm 1.7^{[a]}$
1b	110.3 ± 0.2
1c	74.9 ± 0.6
1d	65.5 ± 0.4
1e	58.7 ± 1.6
1f	60.8 ± 0.3
1g	61.0 ± 0.2
1h	59.1 ± 0.5

[a] From Ref. [2b].

In the above mentioned benchmark reaction, the catalytic activity increases with the chain length of the alkyl substituents on the amino group at C4 position by a factor of 2.6 from DMAP (**1a**) to 4-di-*n*-octylaminopyridine (**1h**), which has an activity comparable to that of 4-(pyrrolidino)pyridine (**2**).^[2d] Rates are fastest for R = butyl, which is thus the best compromise between chain length and activity, since elongation of the chain from butyl to octyl does not lead to increased activities. The results obtained for the unsymmetrically substituted pyridine **1b** blend rather well with those for the symmetrically substituted aminopyridines, which indicates that the inductive effects of the alkyl substituents are cumulative (Figure 5.2).

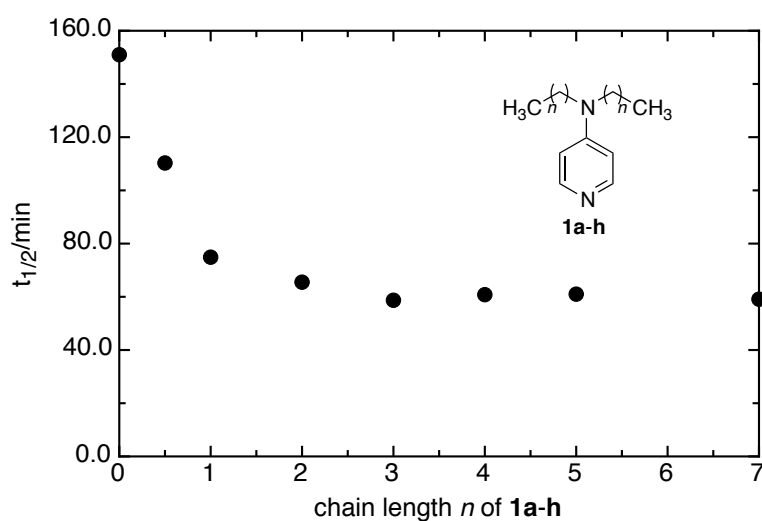
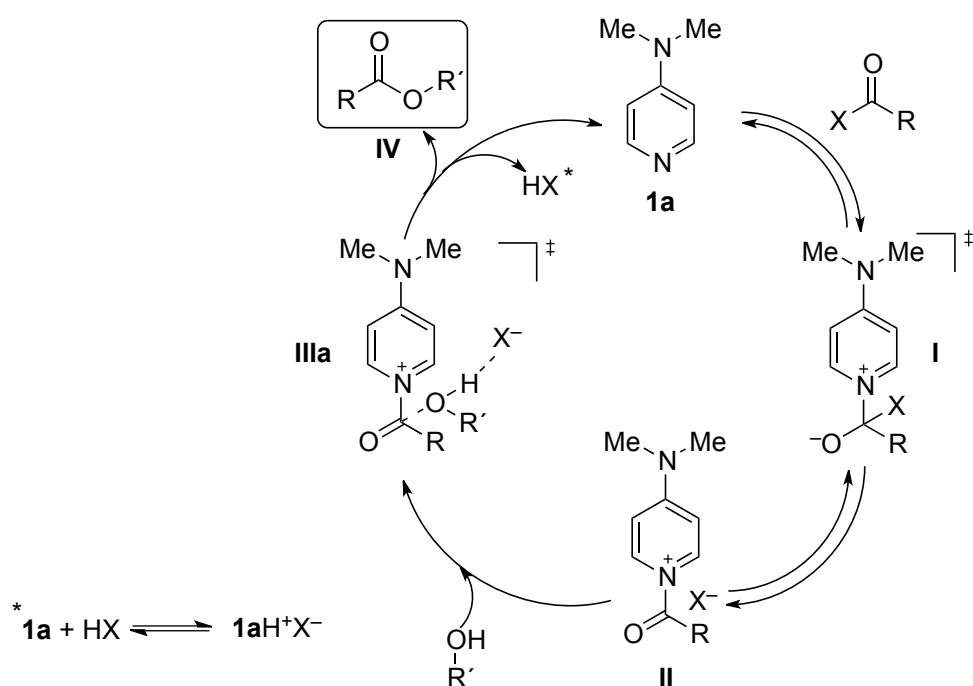


Figure 5.2. Correlation of half-life times $t_{1/2}$ (in min) with the length of the *N*-alkyl chains of **1a–1h**.

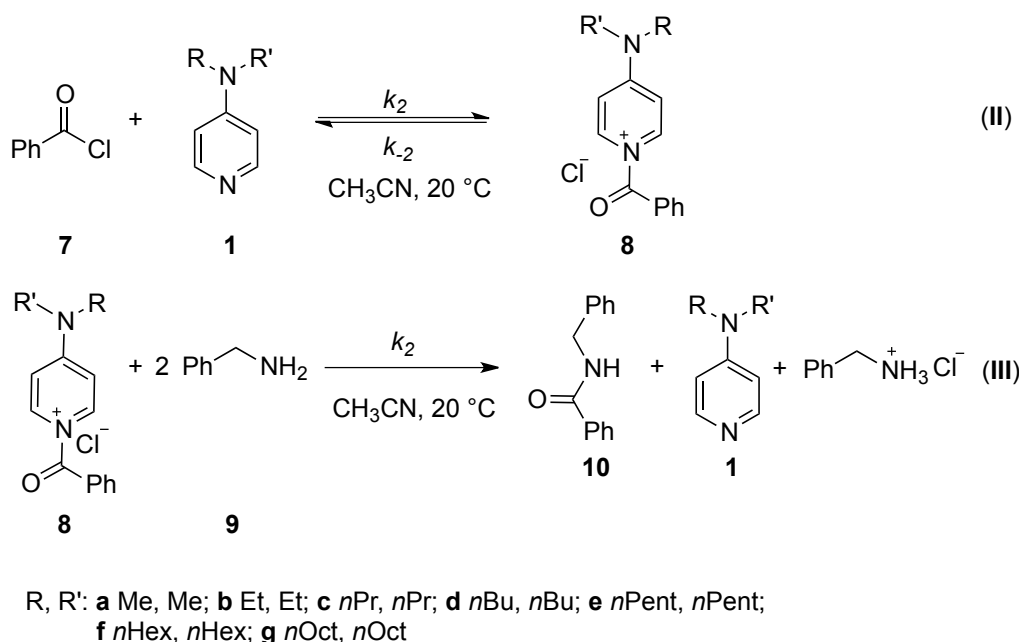
N-Acyl pyridinium ions have been proposed as the key intermediates of the catalytic cycle for the acylation reactions described above (Scheme 5.3).^[5]



Scheme 5.3. Simplified mechanism for the DMAP-catalyzed acylation of alcohols.

In a first step the nucleophilic catalyst (here pyridine **1a**) reacts with the acyl donor in a fast pre-equilibrium to form *N*-acyl pyridinium ion **II**. In the rate-determining, second step the acylated catalyst reacts with the alcohol to form the ester **IV** together with one equivalent acid as byproduct. In order to quantify the influence of the alkyl chain length on the first and the second step of the catalytic cycle separately, reaction rates for the two model reactions shown

in Scheme 5.4 have been measured. In the first of these reactions pyridines **1** react with benzoyl chloride **7** to yield the respective benzoylated pyridines **8**. These latter intermediates react in the second model reaction with benzyl amine **9**.



Scheme 5.4. Reaction of benzoyl chloride (**7**) with pyridines **1a–h** and aminolysis reactions of the thus formed *N*-benzoyl pyridinium chlorides **8a–h** with benzylamine (**9**) in acetonitrile.

The kinetics of both model reactions were followed by UV/Vis spectrophotometry under first order conditions monitoring the absorbances of the *N*-benzoyl pyridinium chloride **8a–h** as described previously.^[5b,c]

Table 5.2. Second-order rate constants k_2 for the reactions of benzoyl chloride (**7**) with pyridines **1a–h** and *N*-benzoyl pyridinium chlorides **8a–h** with benzylamine (**9**) in acetonitrile at 20 °C.

	k_2 [M ⁻¹ s ⁻¹]		k_2 [M ⁻¹ s ⁻¹]
1a	3.00×10^4 ^[a]	8a	4.78×10^2 ^[b]
1b	3.36×10^4	8b	4.11×10^2
1c	4.06×10^4	8c	3.78×10^2
1e	4.14×10^4	8e	3.68×10^2
1g	4.13×10^4	8g	3.53×10^2
1h	4.37×10^4	8h	3.69×10^2

[a] From Ref. [5b]; [b] From Ref. [5c].

For all reactions monoexponential increases or decays of the absorbances of **8a–h** were observed and the first-order rate constants k_{obs} were obtained by least-squares fitting of the exponential function $A = A_0 (1 - e^{-k_{\text{obs}}t}) + C$ or $A = A_0 e^{-k_{\text{obs}}t} + C$ to the time-dependent absorbances. Plots of k_{obs} versus the concentration of the compound in excess (**7** or **9**) were linear and the second-order rate constants k_2 (Table 5.2) were obtained as the slopes of these

plots. The intercepts of the plots were close to zero, in line with the quantitative courses of the reaction. While the reactivities of the pyridines **1a–h** towards benzoyl chloride (**7**) increase with the chain length of the alkyl groups by a factor of 1.5, a decrease of the reactivities of the *N*-benzoyl pyridinium ions **8a–h** by a factor of 1.3 was observed. Similar to the pyridine-catalyzed acylation reaction of **16**, saturation of the inductive effects of the alkyl groups are observed already at *R* = ethyl (Figure 5.3).

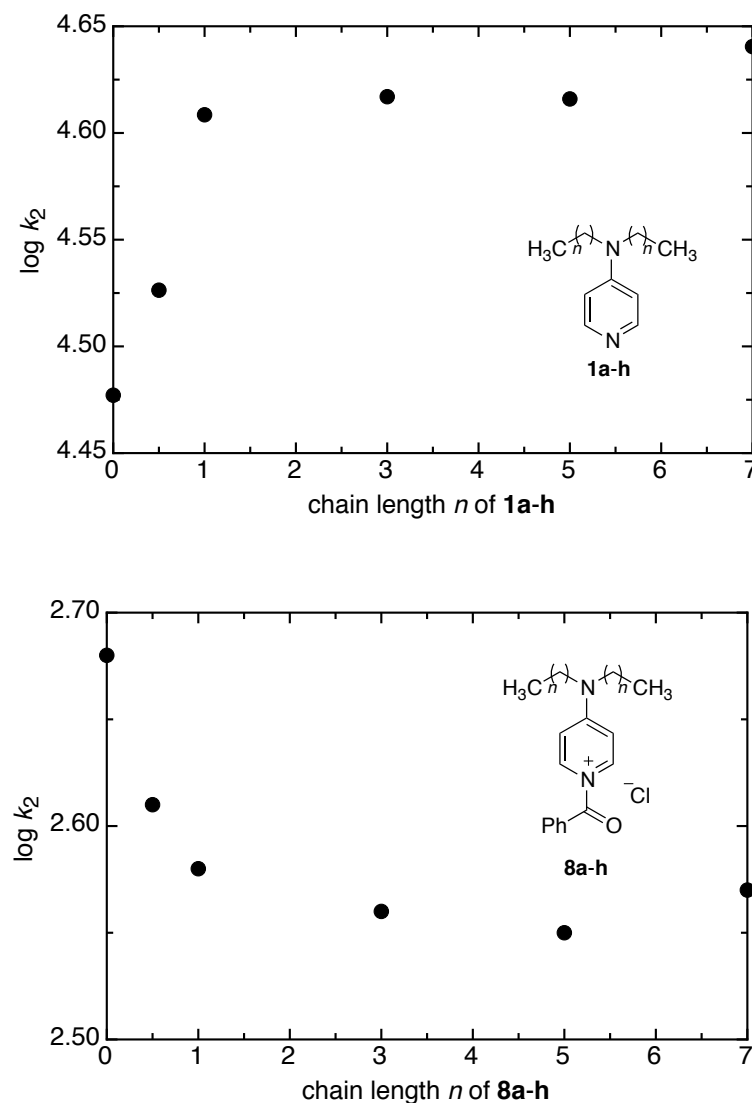
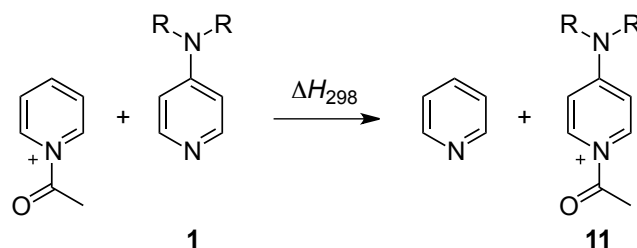


Figure 5.3. Correlation of the second-order rate constants k_2 for the reactions of **1a–h** with benzoyl chloride (**7**) with the length of the *N*-alkyl chains of **1a–h** (top) and the reactions of **8a–h** with benzylamine (**9**) with the length of the *N*-alkyl chains in **8a–h** (bottom).

It has been noted earlier that the stabilities of acylpyridinium ions serves as a quantitative indicator for the catalytic performance of the respective pyridines.^[2b] Thus, relative acetylation enthalpies for **1a–1h** were calculated at the MP2(FC)/6-31+G(2d,p)//B98/6-31G(d) level (in short MP2-5) according to the isodesmic reaction depicted in Scheme 5.5.



Scheme 5.5. Isodesmic reaction for the calculation of acetylation enthalpies of pyridines **1**.

For the catalysts **1a–d** all possible conformers within a range of 30 kJ/mol were taken into account. Conformers for catalysts **1e–1h** were generated from those for **1d** by adding the required number of terminal CH₂-groups in an *all-trans* conformation. The Boltzmann distribution was used to calculate the statistical weight of the individual conformers and averaged energies were used for the calculation of the acetylation enthalpies ($\Delta H_{298,\text{ave}}$). Additionally, acetylation enthalpies were computed using only the energetically best conformers of **1a–h** together with the best conformers of acylpyridinium ion **11a–h** ($\Delta H_{298,\text{best}}$), or those conformers of **11a–h** that match the best conformation of the parent pyridines **1a–h** ($\Delta H_{298,\text{sel}}$). How much these latter data depend on the theoretical level was tested by calculating acylation enthalpies at the MP2-5 and also the more expensive G3(MP2)B3 level of theory (see the Experimental Part).

Table 5.3 shows a summary of the calculated reaction enthalpies for catalysts **1a–h** for the Boltzmann-averaged conformers (second and third column) and the best conformers (fourth and fifth column, Figure 5.4).

Table 5.3. Acetylation enthalpies [kJ/mol] for pyridines **1a–h** according to Scheme 5.5 for the Boltzmann-averaged and best conformers calculated at MP2-5 level of theory in the gas phase and in CHCl₃ solution.

catalyst	$\Delta H_{298,\text{ave}}$		$\Delta H_{298,\text{best}}$	
	[kJ/mol]		[kJ/mol]	
	gas phase	CHCl ₃	gas phase	CHCl ₃
1a	−77.1	−61.2	−77.1	−61.2
1b	−81.6	−63.3	−81.9	−63.6
1c	−87.6	−67.1	−88.2	−67.8
1d	−90.1	−66.1	−90.6	−66.1
1e	−93.2	−67.9	−92.2	−67.1
1f	−94.1	−67.8	−93.2	−67.6
1g	−94.8	−68.1	−94.2	−67.4
1h	−96.7	−68.5	−95.0	−68.2

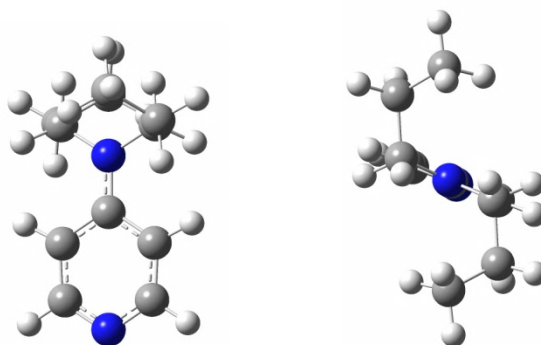


Figure 5.4. Best conformer of **1d** from front view (left) and top view (right).

The plots of Boltzmann-averaged and best acetylation enthalpies versus the number of C-atoms in the alkyl-substituents in pyridines **1a–h** show a steady increase in acylation enthalpies with increasing alkyl chain length, which is not yet saturated even for the octyl substituents (Figure 5.5). Due to the very large number of conformers in **1e–h** a significant part of the conformational space might not be covered due to the restrictions made for the generation of conformers. We note in passing that the trend observed here for selected conformers at MP2-5 level is also found when using significantly more accurate G3(MP2)B3 energies (see the Experimental Part). Recalculation of relative acylation enthalpies in the presence of the PCM continuum model for CHCl_3 leads to significantly reduced acylation enthalpies for all pyridines studied here (Figure 5.5). Moreover, the acylation enthalpies now level out at around -68 kJ/mol starting with an alkyl chain length of $n=2$, which is largely similar to the trend observed in the catalysis experiments. This latter trend is found in almost identical manner for both $\Delta H_{298,\text{ave}}$ and $\Delta H_{298,\text{best}}$.

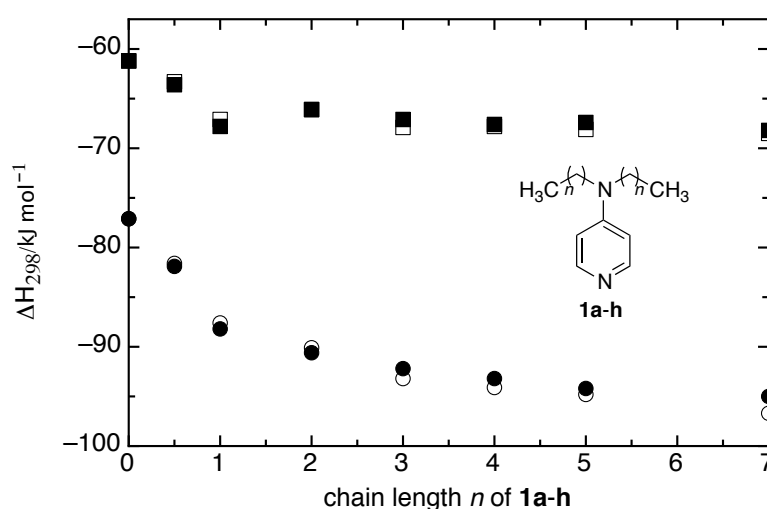


Figure 5.5. Correlation of acylation enthalpies in gas phase (circles) and CHCl_3 solution (squares) for the isodesmic reaction in Scheme 5.5 with the length of the *N*-alkyl chain of **1a–h** (open symbols: $\Delta H_{298,\text{ave}}$; closed symbols: $\Delta H_{298,\text{best}}$).

In order to further trace down the origin of this apparent "shielding" of the PCM solvent model on the calculated acylation enthalpies, the solvation energies were recalculated by only considering the electrostatic or only the non-electrostatic component of the overall solvation free energies (Table 5.4).

Table 5.4. Acetylation enthalpies in CHCl_3 [kJ/mol] for pyridines **1a–h** calculated at MP2-5 level according to Scheme 5.5 including only the electrostatic (second column) or the non-electrostatic (third column) component of the solvation energy.

catalyst	$\Delta H_{298,\text{best}}$	$\Delta H_{298,\text{best}}$
	[kJ/mol]	[kJ/mol]
	only electrostatic	only non-electrostatic
1a	-61.30	-77.08
1b	-63.04	-81.20
1c	-63.42	-83.92
1d	-65.50	-88.88
1e	-67.24	-91.96
1f	-67.30	-93.11
1g	-67.55	-94.07
1h	-67.49	-94.89

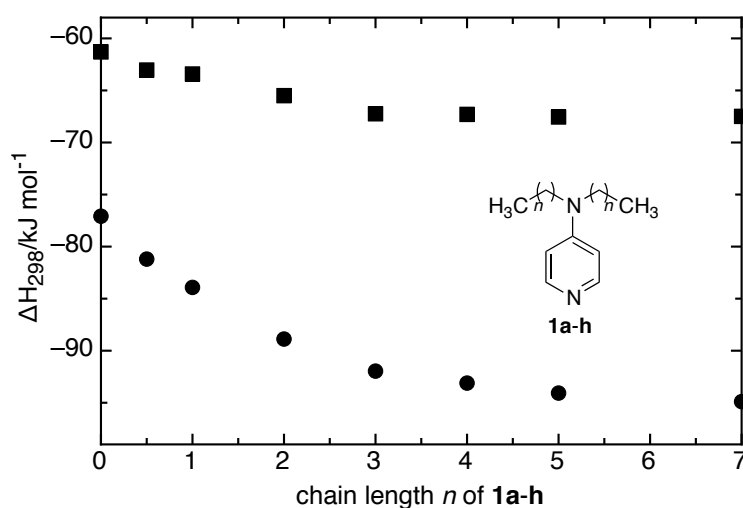


Figure 5.6. Acetylation enthalpies in CHCl_3 [kJ/mol] for pyridines **1a–h** calculated at MP2-5 level according to Scheme 5.5 including only the electrostatic (filled squares) or the non-electrostatic (filled circles) component of the solvation energy.

In the former case (electrostatics only) the calculated acylation enthalpies in CHCl_3 solution are numerically quite close to the data obtained for the full PCM model and display a saturation effect beyond $R=\text{butyl}$, whereas no such observation can be made when using only

the non-electrostatic component of the solvation energy (Figure 5.6). This implies that the electrostatic component of the solvation energy is essential in order to match the experimentally observed trends. Taking into account the electrostatic energies only reflect the obtained acylation enthalpies in CHCl_3 solution very well, which means that the non-electrostatic component has little influence on the reaction free energy.

Analysis of the structures of the best conformers of the acetylated pyridines shows that the inductive effects also impact the length of the amide bond, that is, the distance between the pyridine nitrogen and the carbonyl carbon atom (Table 5.5). Even though these changes are rather moderate in absolute terms, there is nevertheless a clear trend towards shorter bond distances for increasingly Lewis basic pyridines (Figure 5.7).

Table 5.5. N-C bond lengths $r(\text{N-C})$ of the acetylated catalysts **11a–h**.

Acetylated catalyst	$r(\text{N-C})$ [pm]
11a	148.29
11b	148.08
11c	147.86
11d	147.69
11e	147.64
11f	147.53
11g	147.54
11h	147.48

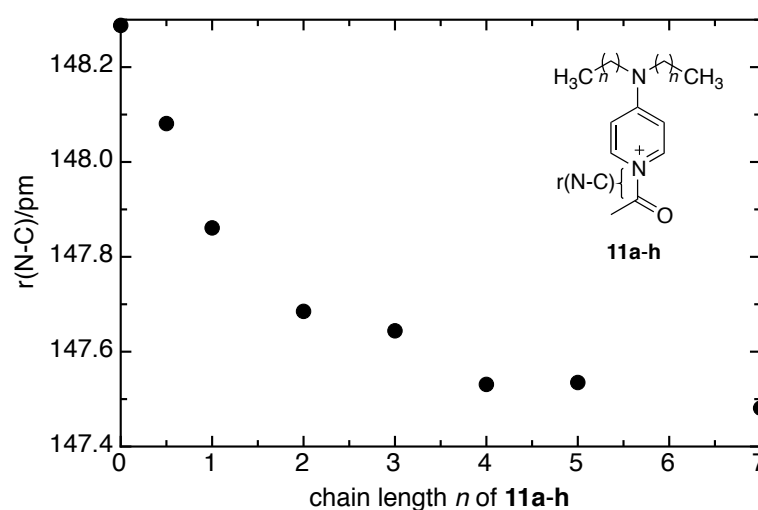


Figure 5.7. Correlation of the N-C bond length $r(\text{N-C})$ [pm] of the best conformers of **11a–h** with the length of the *N*-alkyl chains in **11a–h**.

Stronger electron donating effects of longer alkyl substituents may also be reflected in the overall charge of the pyridine nitrogen atom, which is often portrayed as the "formal" center of positive charge in acylpyridinium ions. Practically any population analysis method shows that the pyridine nitrogen atom in acylpyridinium ions **11** carry a negative partial charge and that the formal partial charge is not helpful in understanding the charge distribution in this type of system. However, the partial charge of the pyridinium nitrogen atom does vary with the size of the alkyl substituents in the expected manner, assuming slightly more negative values with longer alkyl substituents. The magnitude of these variations is, however, very small and does not lend itself to quantitative analysis (Figure 5.8). The same is true for analysis of the acyl group charge in acylpyridinium ions **11a–h**, even though the variations are slightly larger (see Experimental Part).

Table 5.6. Mulliken charges $q(N)$ on the pyridinium nitrogen atom of the acylated catalysts **11a–h**.

Acetylated catalyst	$q(N)$
11a	-0.781
11b	-0.782
11c	-0.783
11d	-0.783
11e	-0.783
11f	-0.783
11g	-0.783
11h	-0.783

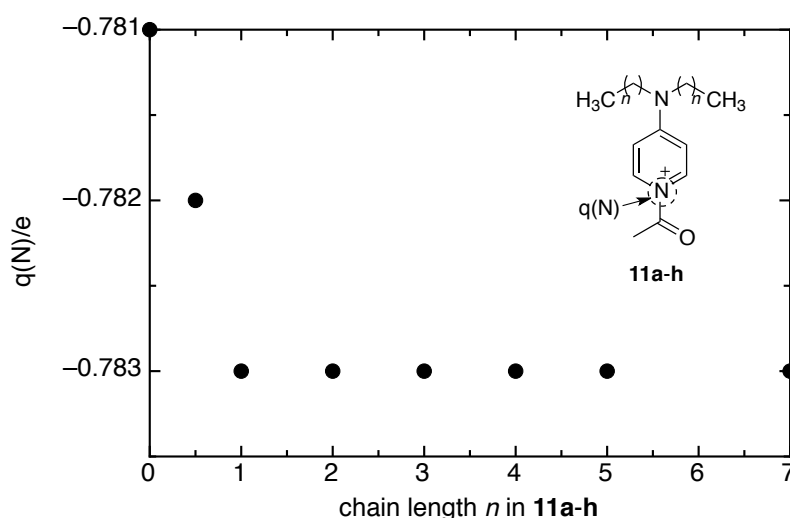


Figure 5.8. Mulliken charges $q(N)$ on the pyridinium nitrogen atom in the best conformers of **11a–h**.

The above mentioned metrics test the influence of inductive effects on the pyridine ring and its thermodynamic and kinetic properties. How much of the inductive effect arrives at the other (alkyl) terminus of the respective systems can quantitatively be assessed using the ^1H NMR resonances of the terminal methyl group protons.

Table 5.7. ^1H NMR shifts $\delta(^1\text{H}, \text{CH}_3)$ of the terminal CH_3 groups in pyridines **1a–h**.

Catalyst	$\delta(^1\text{H}, \text{CH}_3)$ [ppm]
1a	2.980
1b	2.020
1c	1.172
1d	0.912
1e	0.948
1f	0.908
1g	0.890
1h	0.859

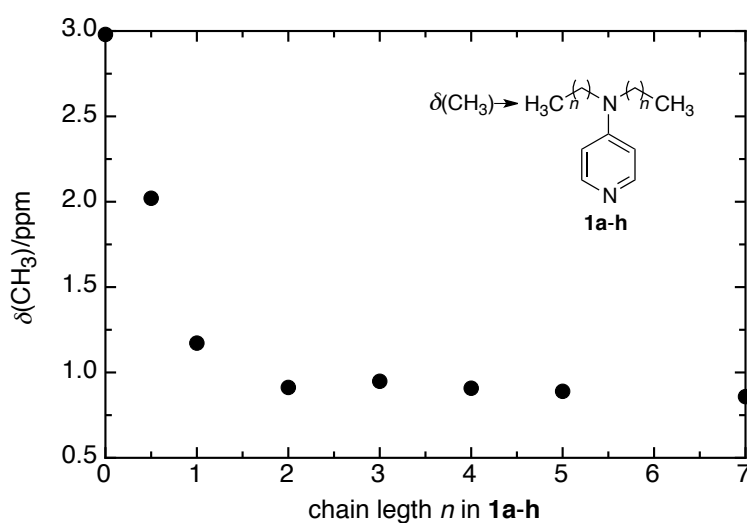


Figure 5.9. Correlation of ^1H NMR shifts of terminal CH_3 groups $\delta(^1\text{H}, \text{CH}_3)$ with the length of the N-alkyl chains in **1a–h**.

Figure 5.9 shows that the ^1H NMR chemical shift of the terminal CH_3 groups in pyridines **1a–h** represents a rather sensitive probe of the pyridine substitution pattern. The reason for the observed changes is primarily rooted in the distance between the probe nucleus (terminal hydrogen atom) and the significantly more electronegative nitrogen atom to which the alkyl substituent attaches.

5.3 Discussion

The impact of inductive effects in general^[1] and especially that of alkyl groups^[6] is not fully understood yet and thus still part of an ongoing discussion. This may also be due to the fact that the inductive effects of alkyl groups are often considered to be rather small,^[7] despite several examples that indicate the opposite.^[8] We test here the suitability of a model proposed by Galkin *et al.*^[6] in order to describe the chain length-dependent properties of pyridines **1a–h** in quantitative terms. One of the basic assumptions made here is that the increasingly large alkyl substituents influence the pyridine system only through electronic (inductive) effects and impart effectively no steric shielding on the reaction center (that is, the pyridine nitrogen atom). Under these conditions the effect of the N,N-dialkylamino substituent at C4 position of the pyridine ring can be expressed with a single substituent parameter σ^* , whose magnitude is derived using an inductive increment method. As shown in the quantitative expression (5.1) for the calculation of σ^* , the magnitude of the substituent effect depends on the distance between each center in the substituent and a point of reference r_j , a reference distance for a typical single bond length between such centers R_j , and the electronegativity difference between the respective center and the point of reference ΔX_j .

$$\sigma^* = 7.840 \cdot \sum_i \Delta \chi_i \frac{R_i^2}{r_i^2} \quad \text{Eq. (5.1)}$$

The proper topological "point of reference" for the systems under study is undoubtedly the pyridine nitrogen atom as the reaction center. Calculating σ^* substituent parameters (an exemplary calculation for the σ^* parameter for **1a** can be found in the Experimental Part) with respect to this center will in the following be referred to as "model 1". Relay of substituent effects between the nitrogen attached at C4 position and the pyridine nitrogen atom is, however, hardly well described using an inductive through-bond mechanism due to the presence of the common π system. An alternative "model 2" is therefore explored in which the point of reference is assumed to be the nitrogen atom holding the two alkyl substituents. Finally, a third model may be necessary in order to rationalize the results of the ^1H NMR studies, in which the points of reference are the hydrogen atoms of the terminal CH_3 groups (model 3). In all models the presence of two alkyl groups is taken into account by the summation of inductive effects of both alkyl groups and thus one σ^* is calculated for the overall obtained inductive effect (see example in the Experimental Part).

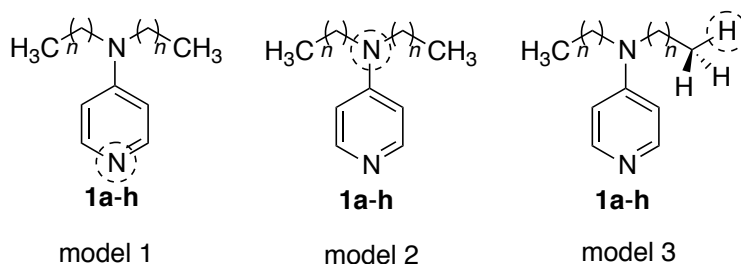


Figure 5.10. Overview of models 1–3 used for the calculation of σ^* values for **1a–h** according to Equation 5.1. The encircled atom illustrates the respective "center of reference" for each model.

The calculated σ^* values (Table 5.8) can subsequently be used together with a Hammett expression (5.2) to quantitatively describe the influence of alkyl chain length on experimentally observed or theoretically calculated data.

$$\log \frac{k_X}{k_H} = \rho \sigma^* \quad \text{Eq. (5.2)}$$

Table 5.8. Calculated σ^* values for **1a–h** for models 1, 2 and 3.

	σ^*	σ^*	σ^*
	model 1	model 2	model 3
1a	3.47	2.27	-2.23
1b	3.51	2.55	-2.13
1c	3.55	2.84	-2.01
1d	3.60	3.09	-1.93
1e	3.64	3.24	-1.89
1f	3.67	3.33	-1.87
1g	3.70	3.39	-1.87
1h	3.74	3.48	-1.85

Table 5.9 shows the R^2 values together with the values for ρ using the σ^* properties for model 2 with exception of the rationalization of the ^1H NMR shifts, in which the σ^* values for model 3 were used.

In general, the observed saturation effects are best reflected by model 3, in which the impact of a change in inductive effects is measured at the terminal methyl group protons in **1a–h** (for details see Experimental Part). This is most likely due to the well-marked saturation effect of the calculated σ^* -values obtained in model 3 (see Experimental Part). This method of analysis is in accordance to the determination of the ^1H NMR resonance experiment used for the correlation in Figure 5.9 and therefore only used to interpret the ^1H NMR shifts. Nevertheless the chemical background of the other metrics tested is different, and models 1 and 2 account for the surveyed properties therein. Model 1 yields in any case much lower R^2 -values as compared to model 2 (see Experimental Part). This may well be due to the large distance between reaction center and the growing alkyl chain in model 1. Therefore model 2 is subsequently used to determine the respective R^2 -values displayed in Table 5.9 in order to discuss the correlation analysis.

Table 5.9. R^2 -values together with the values for ρ using the σ^* properties for model 2 with exception of the ^1H NMR correlation in which the σ^* values for model 3 were used.

	σ^* (model 2)	R^2	ρ
1	$\log(k_2)^{[a]}$	0.9202	0.33
2	$\log(k_2(\text{benzoylation}))^{[b]}$	0.8752	0.12
3	$\log(k_2(\text{aminolysis}))^{[c]}$	0.8262	0.09
4	$\Delta H_{298,\text{ave}}$ gas phase ^[d]	0.9935	-15.91
5	$\Delta H_{298,\text{ave}}$ (CHCl_3) ^[e]	0.8968	-5.76
6	$\Delta H_{298,\text{best}}$ gas phase ^[f]	0.9809	-14.61
7	$\Delta H_{298,\text{best}}$ (CHCl_3) ^[g]	0.7955	-5.07
8	$\Delta H_{298,\text{best}}$ only electrostatic ^[h]	0.9599	-5.56
9	$\Delta H_{298,\text{best}}$ only non-electrostatic ^[i]	0.9911	-15.26
10	$r(\text{N-C})^{[j]}$	0.9925	-0.67
11	$\delta(^1\text{H}, \text{CH}_3)^{[k]}$	0.9236	-5.25

[a] Observed reaction rates in reaction (I) according to Scheme 5.2; [b] Observed reaction rates for benzoylation reaction (II) according to Scheme 5.4; [c] Observed reaction rates for aminolysis reaction (III) according to Scheme 5.4; [d] Boltzmann-averaged ΔH_{298} at MP2-5 level of theory: “MP2-5”: MP2/6-31+G(2d,p)//B98/6-31G(d); [e] Boltzmann-averaged ΔH_{298} at MP2-5 level of theory with PCM/UAHF/RHF/6-31G(d) solvation energies for chloroform; [f] Energetically best conformer used for the calculation of ΔH_{298} at MP2-5 level of theory; [g] Energetically best conformer used for the calculation of ΔH_{298} at MP2-5 level of theory with inclusion of solvent effects as described above; [h] Acetylation enthalpies for **1a–h** according to Scheme 5.5 including only the electrostatic term for the solvent contribution; [i] Acetylation enthalpies for **1a–h** according to Scheme 5.5 including only the non-electrostatic term for the solvent contribution; [j] N-C bond length of the pyridine nitrogen and the carbonyl group in **11a–h**; [k] ^1H NMR shifts of terminal CH_3 -group in **1a–h**, data displayed for model 3.

The data obtained in Table 5.9 can be divided into three groups as indicated by the dotted lines (entries 1–3, entries 4–9 and entries 10,11). As already mentioned before, the changes in charge of the pyridine nitrogen, as well as that of the whole acyl group in **11a–h** are too small to allow for a quantitative analysis (see Experimental Part).

The first group contains experimentally measured rate constants, which were correlated in a Hammett expression according to Equation 5.3.

$$\log(k_x) = \rho \sigma^* \quad \text{Eq. (5.3)}$$

According to the values for sensitivity parameter ρ , which is the slope of the linear correlation between $\log(k_x)$ and σ^* , the catalytic acylation reaction (I) shows the steepest increase with the most significant changes of inductive effects (*cf.* entry 1). This implies that the half-life times for benchmark reaction (I) show the largest variation in this particular dataset.

Furthermore, the reaction (I) is even better represented by the increment-based calculation of inductive effects ($R^2 = 0.9202$, entry 1) than the two single step model reactions (entries 2 and 3).

The second group of results contains energy data, which were correlated according to Equation 5.4.

$$\Delta H_{298} = \rho \sigma^* \quad \text{Eq. (5.4)}$$

The results displayed in Table 5.9 show the clear tendency, that inclusion of solvent effects (in chloroform) give significantly inferior correlations with the tested model proposed by Galkin *et al.* than the gas phase enthalpies themselves (*cf.* entries 4 and 5, and entries 6 and 7). The acetylation enthalpies in the gas phase are very much reflected by the acetylation enthalpies including only the non-electrostatic solvent contribution (*cf.* entries 6 and 9). This finding is not only supported by the very similar values for R^2 ($R^2 = 0.9809$ and 0.9911) but also on the basis of the slope of the correlation as indicated by ρ ($\rho = -14.61$ and $\rho = -15.26$).

The last group (entries 10,11) contains data, which describe structural parameters and therefore should not be correlated linearly according to the proposed increment model by Galkin *et al.* Still, employing the linear model used before for the acylation energies also for this last dataset yields very good linear correlations for $r(\text{N-C})$ ($R^2 = 0.9925$) and $\delta(^1\text{H}, \text{CH}_3)$ ($R^2 = 0.9925$, model 3 was used according to the ^1H NMR experiment). More complex relationships between σ^* and this last dataset were therefore not tested.

5.4 Conclusion

In summary, numerous properties of alkylaminopyridines show a saturation of substituent effects with the alkyl group chain lengths beyond four carbon atoms. We believe this to be a general result in situations lacking direct steric effects between alkyl substituents and the respective reaction centers. The fact that all observed saturation phenomena could be explained in a more than satisfactory way by aid of a simple increment-based prediction of through-bond inductive effects can be seen as strong support for this latter type of electronic substituent effect.

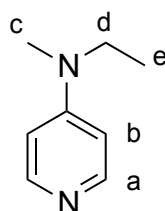
5.5 Experimental Part

All air and water sensitive manipulations were carried out under a nitrogen atmosphere using standard Schlenk techniques. Calibrated flasks for kinetic measurements were dried in the oven at $120\text{ }^\circ\text{C}$ for at least 12 hours prior to use and then assembled quickly while still hot, cooled under a nitrogen stream and sealed with a rubber septum. All commercial chemicals were of reagent grade and were used as received unless otherwise noted. CDCl_3 was refluxed for at least one hour over CaH_2 and subsequently distilled. ^1H and ^{13}C NMR spectra were

recorded on Varian 300 or Varian INOVA 400 machines at room temperature. All ^1H chemical shifts are reported in ppm (δ) relative to TMS (0.00); ^{13}C chemical shifts are reported in ppm (δ) relative to CDCl_3 (77.16). ^1H NMR kinetic data were measured on a Varian Mercury 200 MHz spectrometer at 23 °C. HRMS spectra (ESI-MS) were carried out using a Thermo Finnigan LTQ FT instrument. IR spectra were measured on a Perkin-Elmer FT-IR BX spectrometer mounting an ATR technology. Analytical TLC were carried out using aluminium sheets silica gel Si 60 F254.

Catalyst Synthesis

N-Ethyl-*N*-methylpyridin-4-amine (**1b**)



To 1.50 g (9.99 mmol) 4-chloropyridine hydrochloride was added 6.51 g (20 mmol) Cs_2CO_3 in an oven-dried pressure tube. After addition of 4.29 mL (50 mmol) *N*-methylethylamine, 0.23 g (0.20 mmol) $\text{Pd}(\text{PPh}_3)_4$ and 2 mL dest. water the pressure tube was closed and heated for 72 h at 120 °C in an oil bath. The brown suspension was poured into DCM, filtered and extracted three times with dist. water. After drying over MgSO_4 , filtration and evaporation of the solvent, the crude product was purified by column chromatography on silica ($\text{CHCl}_3/\text{MeOH}$, 10:1) yielding 870 mg (64 %) of a yellow liquid.

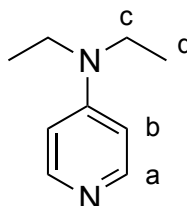
^1H NMR (400 MHz, CDCl_3): δ = 8.17 (dd, J = 5.0 Hz, 1.6 Hz, 2H, H_a), 6.45 (dd, J = 5.0 Hz, 1.6 Hz, 2H, H_b), 3.38 (q, J = 7.1 Hz, 2H, H_d), 2.91 (s, 3H, H_c), 1.12 (t, J = 7.1 Hz, 2H, H_e).

^{13}C NMR (101 MHz, CDCl_3): δ = 149.9 (C_a), 106.4 (C_b), 45.6 (C_d), 36.5 (C_c), 11.2 (C_e).

MS (EI) m/z (%): 136 (M^+ , 30), 121 ($\text{M}^+ - \text{CH}_3$, 100), 78 ($\text{C}_5\text{H}_4\text{N}^+$).

HRMS (EI): $\text{C}_8\text{H}_{12}\text{N}_2$ calc. 137.1037 g/mol $[\text{M} + \text{H}]^+$, found 137.0988 g/mol $[\text{M} + \text{H}]^+$.

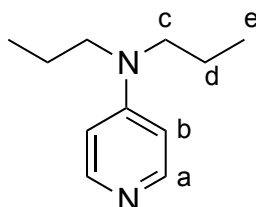
IR (ATR): $\tilde{\nu}$ = 2928 (w), 2850 (w), 1594 (vs), 1514 (vs), 1466 (w), 1371 (vs), 1230 (vs), 1210 (vs), 1110 (w), 1080 (w), 998 (vs), 799 (vs), 810 (vs), 736 (s).

N,N-Diethylpyridine-4-amine (**1c**)

To 1.50 g (9.99 mmol) 4-chloropyridine hydrochloride was added 6.51 g (20 mmol) Cs_2CO_3 in an oven-dried pressure tube. After adding 2.08 mL (20 mmol) diethylamine the pressure tube was closed and heated for 5 days at 170 °C in an oil bath. The brown solution was poured into DCM, filtered and the solvent was evaporated. Column chromatography (silica, EA/ NEt_3 , 20:1) followed by distillation of the brown crude product yielded 220 mg (20 %) of a pale yellow solid.

^1H NMR (300 MHz, CDCl_3): δ = 8.19 (dd, J = 5.0 Hz, 1.6 Hz, 2H, H_a), 6.47 (dd, J = 5.0 Hz, 1.6 Hz, 2H, H_b), 3.37 (q, J = 10.5 Hz, 4.5 Hz, 4H, H_c), 1.19 (t, J = 7.1 Hz, 6H, H_d).

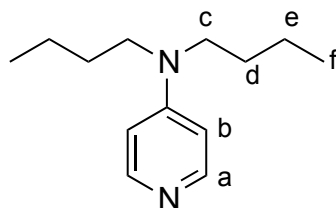
^{13}C NMR (75 MHz, CDCl_3): δ = 149.9 (C_a), 106.2 (C_b), 43.7 (C_c), 12.3 (C_d). (in agreement with literature^[9])

N,N-Dipropylpyridin-4-amine (**1d**)

To 1.00 g (6.66 mmol) 4-chloropyridine hydrochloride was added 3.25 g (9.99 mmol) Cs_2CO_3 into an oven-dried pressure tube. After adding 0.46 mL (3.33 mmol) dipropylamine the pressure tube was closed and heated for 3 days at 170 °C oil bath temperature. The warm brown solution was poured into DCM, filtered and the solvent was evaporated. Column chromatography (silica, EA/ NEt_3 , 20:1) of the brown crude mixture yielded 230 mg (38 %) of a pale yellow solid.

^1H NMR (300 MHz, CDCl_3): δ = 8.14 (dd, J = 5.0 Hz, 1.6 Hz, 2H, H_a), 6.40 (dd, J = 5.0 Hz, 1.6 Hz, 2H, H_b), 3.21 (t, J = 7.5 Hz, 4H, H_c), 1.70 – 1.48 (m, 4H, H_d), 0.91 (t, J = 7.4, 6H, H_e).

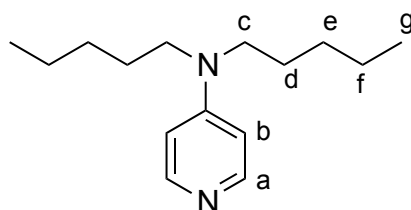
^{13}C NMR (75 MHz, CDCl_3): δ = 149.9 (C_a), 106.3 (C_b), 51.8 (C_c), 20.1 (C_d), 11.2 (C_e). (in agreement with literature^[10])

N,N-Dibutylpyridin-4-amine (**1e**)

To 1.00 g (6.66 mmol) 4-chloropyridin hydrochloride was added 2.49 mL (14.6 mmol) dibutylamine into an oven-dried microwave vial. After addition of 2.68 mL (33.3 mmol) pyridine the vial was closed with a septum cap and the reaction mixture was heated for 2h at 170 °C (200 W). The brown residue was taken up in DCM and was washed three times with sat. K_2CO_3 solution. The collected organic phase was dried over $MgSO_4$ and filtered. After evaporation of the solvent the crude mixture was purified two times by column chromatography (silica, EA/1H, 5:1) and yielded 240 mg (18 %) of a pale brown oil.

1H NMR (300 MHz, $CDCl_3$): δ = 8.16 (d, J = 3.3 Hz, 2H, H_a), 6.43 (d, J = 3.3 Hz, 2H, H_b), 3.26 (t, J = 7.6 Hz, 4H, H_c), 1.68 – 1.44 (m, 4H, H_d), 1.43-1.25 (m, 4H, H_e), 0.95 (t, J = 7.3 Hz, 6H, H_f).

^{13}C NMR (75 MHz, $CDCl_3$): δ = 149.9 (C_a), 106.3 (C_b), 49.9 (C_c), 29.0 (C_d), 20.2 (C_e), 13.9 (C_f). (in agreement with literature^[11])

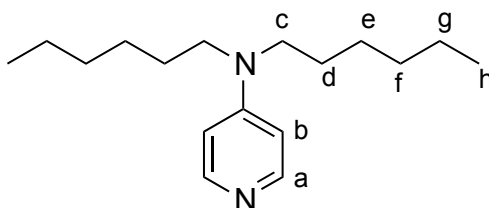
N,N-Dipentylpyridin-4-amine (**1f**)

To 2.00 g (13.3 mmol) 4-chloropyridine hydrochloride was added 3.75 mL (46.6 mmol) pyridine in an oven-dried pressure tube. After addition of 3.26 mL (15.98 mmol) dipentylamine the reaction mixture was heated for 22h at 185 °C. The brown crude mixture was taken up in DCM and washed with sat. K_2CO_3 solution. The collected organic phase was dried over $MgSO_4$, filtered and the solvent was evaporated under reduced pressure. After column chromatography (Silica, EA/ NEt_3 , 10:1) of the brown mixture the product was distilled three times at 140 °C (4 mbar) to give 190 mg (6 %) of a pale yellow viscous liquid.

^1H NMR (400 MHz, CDCl_3): δ = 8.15 (d, J = 6.6 Hz, 2H, H_a), 6.40 (d, J = 6.6 Hz, 2H, H_b), 3.26 (t, J = 7.6 Hz, 4H, H_c), 1.65 – 1.48 (m, 4H, H_d), 1.44 – 1.19 (m, 8H, H_e , H_f), 0.90 (t, J = 7.1 Hz, 6H, H_g).

^{13}C NMR (75 MHz, CDCl_3): δ = 149.8 (C_a), 106.4 (C_b), 50.1 (C_c), 29.1 (C_e), 26.6 (C_d), 22.5 (C_f), 14.0 (C_g). (in agreement with literature^[12])

N,N-Dihexylpyridin-4-amine (**1g**)

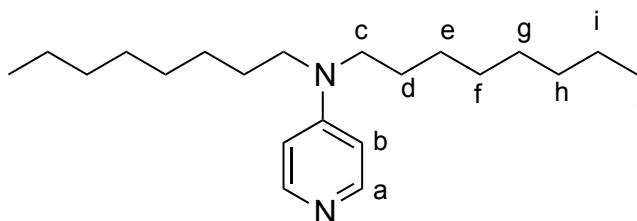


In a pressure tube 2.00 g (13.3 mmol) of 4-chloropyridine hydrochloride were suspended in 3.75 mL (46.6 mmol) pyridine. After addition of 6.21 mL (26.6 mmol) dihexylamine the pressure tube was closed and heated at 185 °C in an oil bath. After 22 h reaction time the residue was dissolved in DCM and washed three times with sat. K_2CO_3 -solution. After drying the organic layer over MgSO_4 and filtration, the solvent was evaporated at reduced pressure. Column chromatography (silica, EA/ NEt_3 10:1) followed by a distillation (130 °C, 10 mbar) gave 570 mg (16%) of a pale yellow viscous liquid.

^1H NMR (400 MHz, CDCl_3): δ = 8.15 (dd, J = 5.0 Hz, 1.6 Hz, 2H, H_a), 6.40 (dd, J = 5.0 Hz, 1.6 Hz, 2H, H_b), 3.26 (t, J = 7.5 Hz, 4H, H_c), 1.61 – 1.49 (m, 4H, H_d), 1.39 – 1.18 (m, 12H, H_e , H_f , H_g), 0.90 (t, J = 7.1 Hz, 6H, H_h).

^{13}C NMR (75 MHz, CDCl_3): δ = 149.8 (C_a), 106.4 (C_b), 50.1 (C_c), 31.6 (C_e), 26.9 (C_d), 26.7 (C_f), 22.6 (C_g), 14.0 (C_h). (in agreement with literature^[11])

N,N-Dioktylpyridin-4-amine (**1h**)



In a pressure tube 2.00 g (13.3 mmol) of 4-chloropyridine hydrochloride were suspended in 3.75 mL (46.6 mmol) pyridine. After addition of 8.10 mL (26.6 mmol) dioctylamine the pressure tube was sealed and heated at 160 °C in an oil bath. After 18 h the residue was

dissolved in DCM and washed three times with sat. K_2CO_3 -solution. After drying the organic layer over $MgSO_4$ and filtration, the solvent was evaporated at reduced pressure. Column chromatography on silica (EA/ NEt_3 10:1) and on basic $AlOx$. (EA/IH 1:10 \rightarrow 10:1) yielded 610 mg (14 %) of a brown viscous liquid.

1H NMR (300 MHz, $CDCl_3$): δ = 8.16 (dd, J = 5.0 Hz, 1.6 Hz, 2H, H_a), 6.40 (dd, J = 5.0 Hz, 1.6 Hz, 2H, H_b), 3.33 – 3.14 (t, J = 7.7 Hz, 4H, H_c), 1.72 – 1.41 (m, 4H, H_d), 1.41 – 1.18 (m, 20H, H_e , H_f , H_g , H_h , H_i), 1.01 – 0.76 (m, J = 6.0 Hz, 3H, H_j).

^{13}C NMR (75 MHz, $CDCl_3$): δ = 149.9 (C_a), 106.3 (C_b), 50.1 (C_c), 31.8 (C_e), 29.4 (C_f), 29.3 (C_g), 27.0 (C_d), 26.9 (C_h), 22.6 (C_i), 14.1 (C_j).

MS (EI) m/z (%): 318 (M^+ , 13), 219 ($C_{14}H_{23}N_2$, 100), 121 ($C_7H_9N_2$, 30).

HRMS (EI): $C_{21}H_{38}N_2$ calc. 318.3035 g/mol [M^+], found 318.3030 g/mol [M] $^+$.

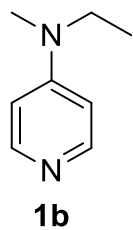
IR (ATR): $\tilde{\nu}$ = 2923 (vs), 2854 (s), 1593 (vs), 1512 (vs), 1466 (s), 1371 (s), 1228 (s), 1104 (w), 986 (s), 799 (vs), 734 (w).

Conduction and evaluation of kinetic measurements

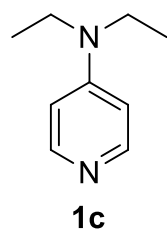
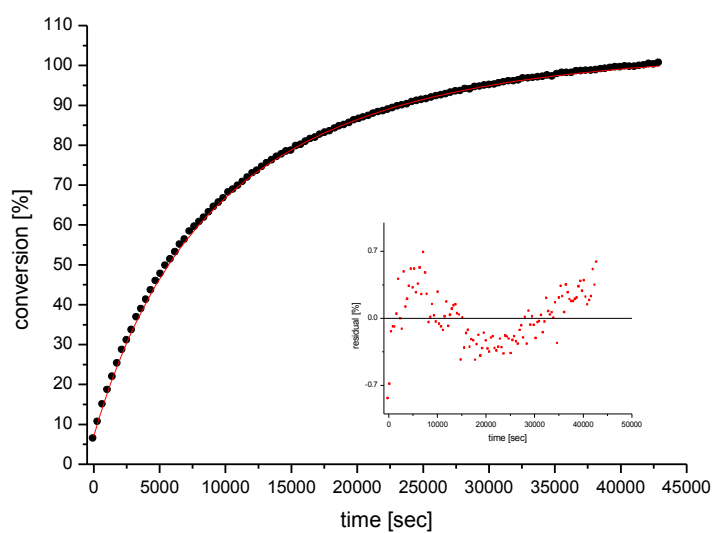
The kinetic measurements were conducted in the same way as described in Chapter 3.4.

Data of kinetic runs

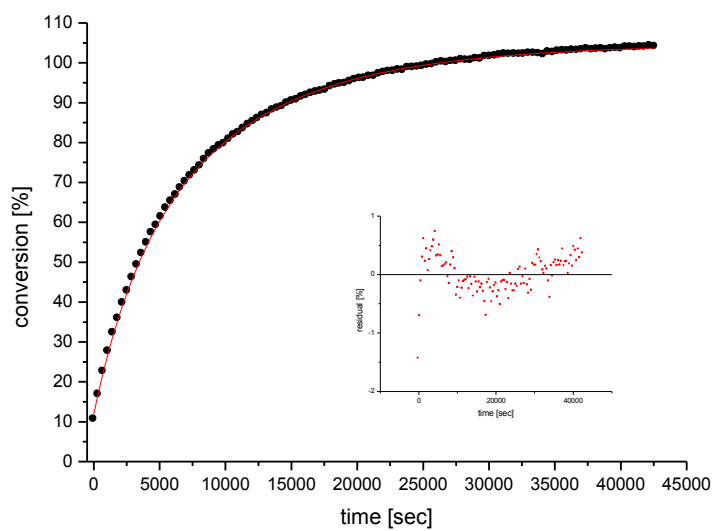
Kinetics of the reactions of catalysts **1a–h** with alcohol **16**. All time specifications are in minutes if not stated different. For every measurement the experimental data and the fit curve together with the residuals are depicted. Every experiment was done at least twice and the resulting kinetic half-life times are given with standard deviations.

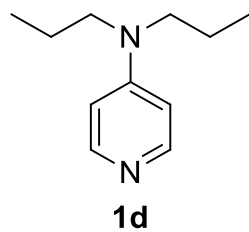


1) 110.1
 2) 110.4
 = 110.3 ± 0.2

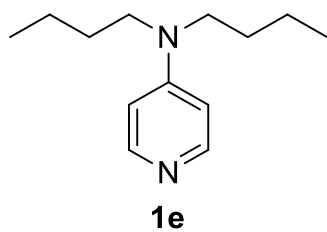
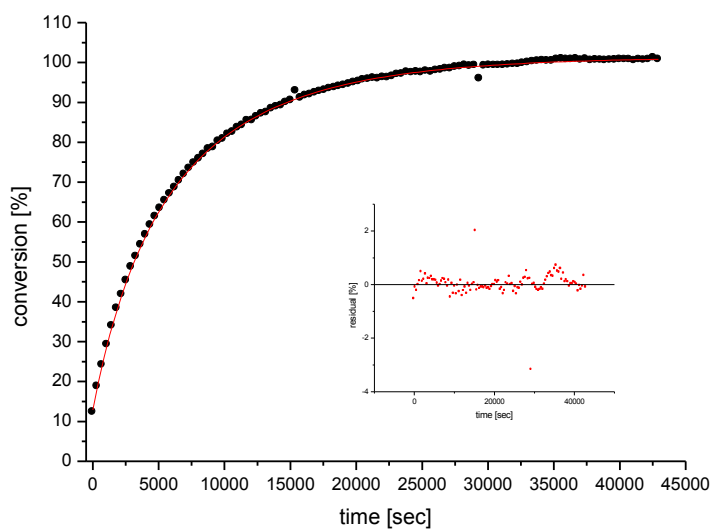


1) 74.3
 2) 75.4
 = 74.9 ± 0.6

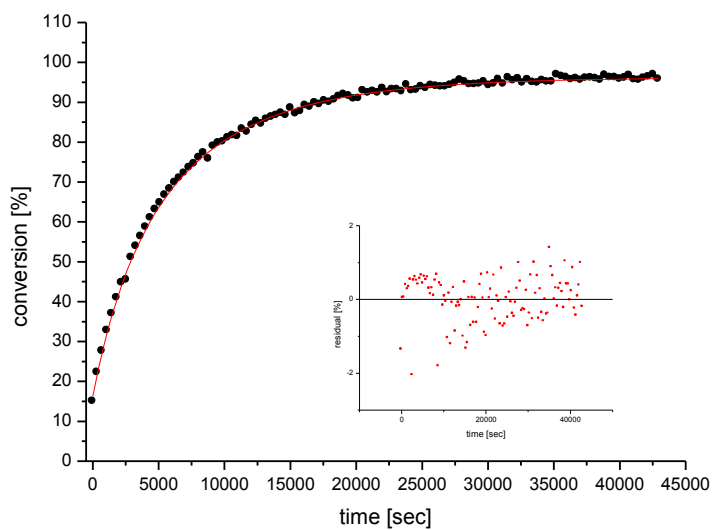


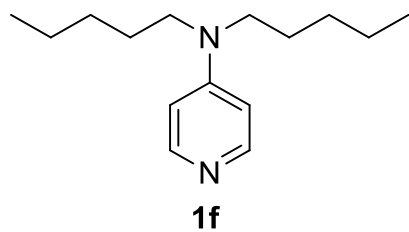


1) 65.1
2) 65.8
= 65.5 ± 0.4

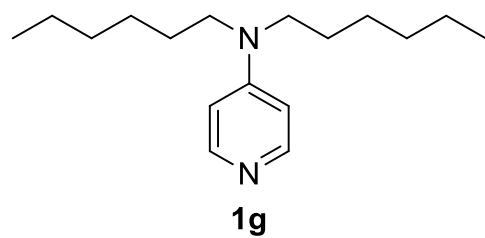
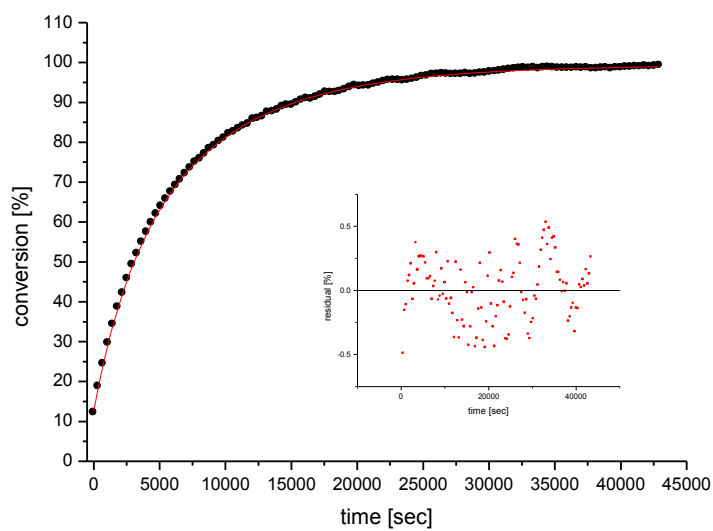


1) 57.1
2) 60.3
= 58.7 ± 1.6

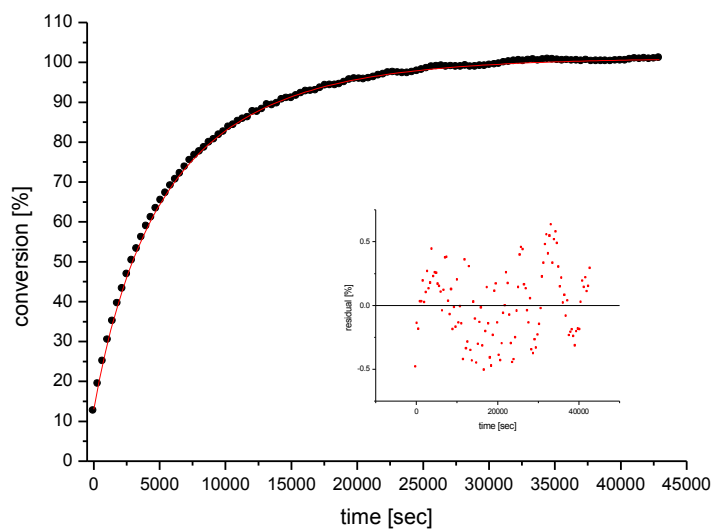


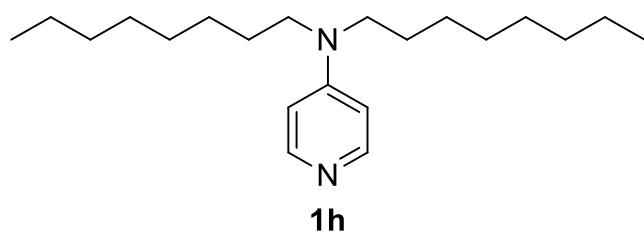


1) 61.1
2) 60.4
= 60.8 ± 0.3

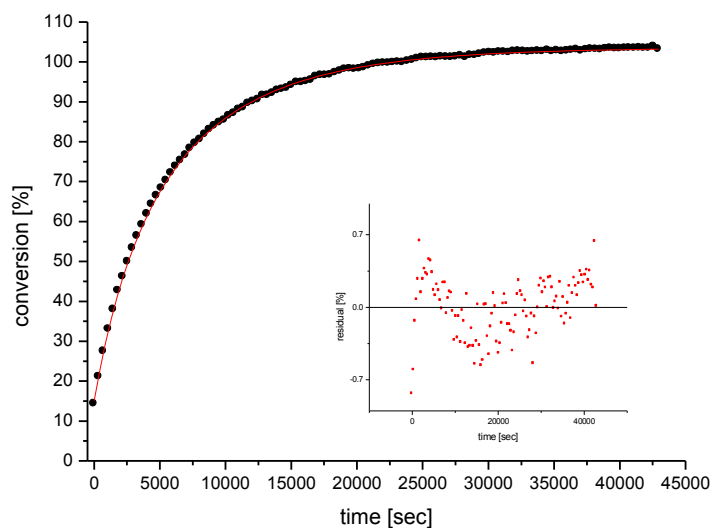


1) 60.8
2) 61.2
= 61.0 ± 0.2





1) 58.6
 2) 59.5
 = 59.1 ± 0.5



Additional correlations

Table 5.10. Mulliken charges $q(N)$ on the pyridinium nitrogen atom of the acylated catalysts **11a–h**.

Acetylated catalyst	$q(\text{COCH}_3)$ in 11a – 11h
11a	0.383
11b	0.381
11c	0.378
11d	0.377
11e	0.377
11f	0.375
11g	0.375
11h	0.375

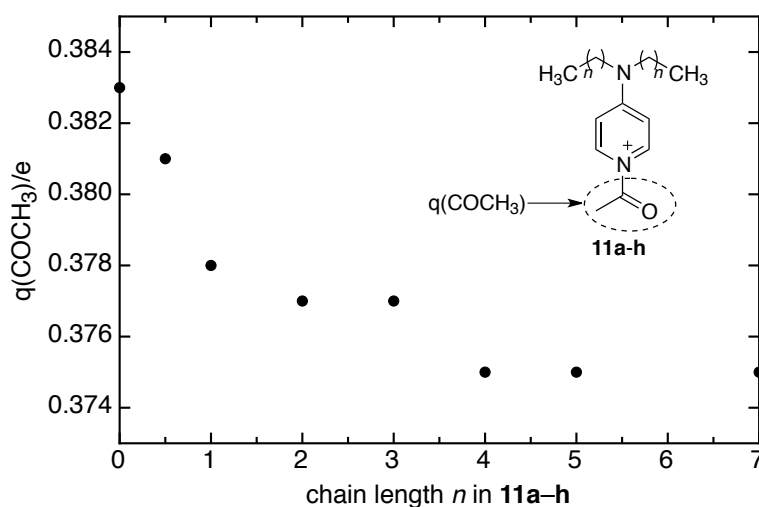


Figure 5.11. Mulliken charges $q(\text{COCH}_3)$ of the whole acyl group in **11a-h** for the best conformers.

Calculation of inductive effects by an increment-based method

Adapted method for calculation of σ^* values from Galkin et al.^[6] The calculation of σ^* values and $\log \frac{k_X}{k_H}$ was performed according to equations 5.1 and 5.2. The models surveyed can be found in Figure 5.10.

Table 5.11. Electronegativity χ and covalent radii R for nitrogen, carbon and hydrogen atoms.

	N	C	H
χ	3.04	2.55	2.20
R [pm]	71	sp ³ : 76 sp ² : 73 sp: 69	31

[a] Pauling scale^[13]; [b] data from Ref.^[14]

In the following part the σ^* value of **1a** for model 1 will be calculated exemplarily:

$$\sigma^* = 7.840 \cdot \sum_i \Delta\chi_i \frac{R_i^2}{r_i^2} \quad \text{Eq. (5.1)}$$

Point of reference in model 1 is the pyridine nitrogen. From there on the single contributions of every atom will be added. Since **1a** is symmetric, the summation will be done for one half of the molecule and the contributions can then be doubled.

$$\sigma^* = 7.840 \cdot \left(\left(0.49 \cdot \frac{73^2}{134.11^2} + 0.84 \cdot \frac{31^2}{243.18^2} + 0.49 \cdot \frac{73^2}{273.32^2} + 0.84 \cdot \frac{31^2}{381.76^2} \right. \right. \\ \left. \left. + 0.49 \cdot \frac{73^2}{415.11^2} + 0 \cdot \frac{71^2}{553.13^2} + 0.49 \cdot \frac{76^2}{699.32^2} + 0.84 \cdot \frac{31^2}{809.05^2} \right) \cdot 2 \right) \\ = 7.840 \cdot ((1.45 \cdot 10^{-1} + 1.37 \cdot 10^{-2} + 3.50 \cdot 10^{-2} + 5.54 \cdot 10^{-3} + 1.51 \cdot 10^{-2} + 0 \\ + 5.79 \cdot 10^{-3} + 1.23 \cdot 10^{-3}) \cdot 2) = 7.840 \cdot 0.443 = 3.47$$

$$\rightarrow \sigma^*_{(1a)} = 3.47$$

The bond lengths in **1a–h** necessary for the determination of r_i in Equation 5.1 are given in Figure 5.12.

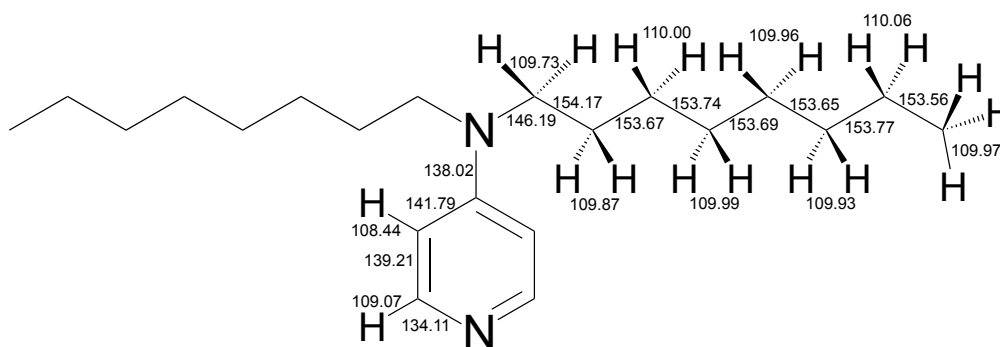


Figure 5.12. Bond length in **1a–1h**.

Plotting the σ^* -values from Table 5.8 vs. the alkyl chain length in **1a–h** for models 1–3 leads to Figures 5.13 – 5.15.

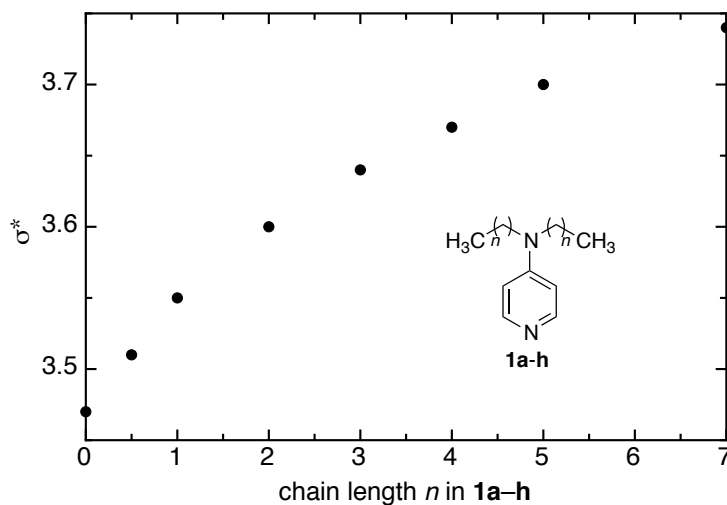


Figure 5.13. σ^* -values vs. chain length n in **1a–h** for model 1.

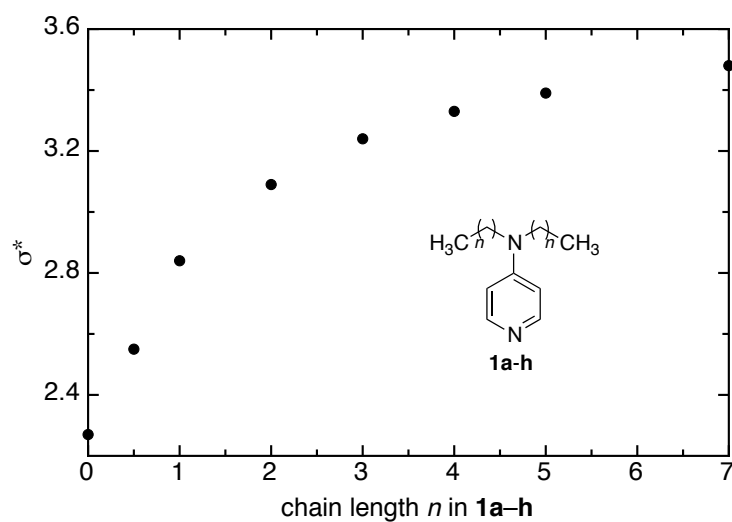


Figure 5.14. σ^* -values vs. chain length n in **1a-h** for model 2.

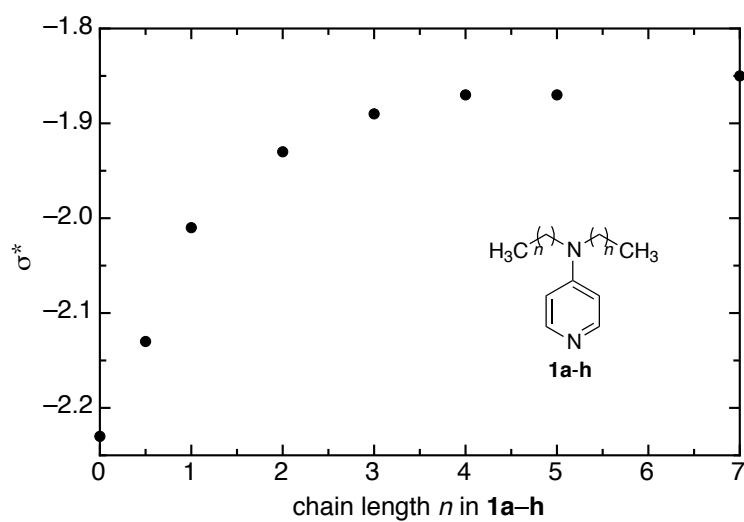


Figure 5.15. σ^* -values vs. chain length n in **1a-h** for model 3.

Table 5.12. R^2 -values together with the values for ρ using the σ^* properties for model 2 with exception of the ^1H NMR correlation in which the σ^* values for model 3 were used.

σ^* (model 2)		model 1		model 2		model 3	
		R^2	ρ	R^2	ρ	R^2	ρ
1	$\log(k_2)^{[a]}$	0.7727	1.42	0.9202	0.33	0.9731	1.07
2	$\log(k_{2(X)}/k_{2(1a)})^{[b]}$	0.7727	1.42	0.9202	0.33	0.9731	1.07
3	$\log(k_2(\text{benzoylation}))^{[c]}$	0.8664	0.51	0.8752	0.12	0.9655	0.40
4	$\log(k_2(\text{aminolysis}))^{[d]}$	0.9370	-0.29	0.8262	0.09	0.8217	-0.37
5	$\Delta H_{298,\text{ave}}$ gas phase $^{[e]}$	0.9333	-70.8	0.9935	-15.91	0.9889	-48.9
6	$\Delta H_{298,\text{ave}}$ solvation $^{[f]}$	0.7847	-24.7	0.8968	-5.76	0.9301	-18.0
7	$\Delta H_{298,\text{best}}$ gas phase $^{[g]}$	0.8892	-63.9	0.9809	-14.61	0.9942	-45.3
8	$\Delta H_{298,\text{best}}$ solvation $^{[h]}$	0.6663	-21.3	0.7955	-5.07	0.8488	-16.2
9	$\Delta H_{298,\text{best}}$ only electrostatic $^{[i]}$	0.9257	-25.0	0.9599	-5.56	0.9310	-16.8
10	$\Delta H_{298,\text{best}}$ only non-electrostatic $^{[j]}$	0.9620	-69.00	0.9911	-15.26	0.9622	-46.3
11	$r(\text{N-C})^{[k]}$	0.9216	-2.96	0.9925	-0.67	0.9923	-2.06
12	$q(\text{N})^{[l]}$	0.5856	-6.03×10^{-3}	0.7696	-1.51×10^{-3}	0.8538	-4.88×10^{-3}
13	$q(\text{COCH}_3)^{[m]}$	0.8887	-2.97×10^{-2}	0.9657	-6.74×10^{-3}	0.9691	-2.08×10^{-2}
14	^1H NMR shifts $^{[n]}$	0.6863	-6.75	0.8554	-1.64	0.9236	-5.25
		$\Delta\sigma^*$		$\Delta\sigma^*$		$\Delta\sigma^*$	
15	$\log(k_2)^{[a]}$	0.7727	1.42	0.9202	0.33	0.9731	1.07
16	$\log(k_{2(X)}/k_{2(1a)})^{[b]}$	0.7727	1.42	0.9202	0.33	0.9731	1.07

[a] Observed reaction rates in reaction (I) according to Scheme 5.2; [b] Observed reaction rates of **1a–h** in reaction (I) according to Scheme 5.2 in relation to the reaction rate obtained for **1a**; [c] Observed reaction rates for benzoylation reaction (II) according to Scheme 5.4; [d] Observed reaction rates for aminolysis reaction (III) according to Scheme 5.4; [e] Boltzmann averaged ΔH_{298} at MP2-5 level of theory: “MP2-5”: MP2/6-31+G(2d,p)//B98/6-31G(d); [f] Boltzmann averaged ΔH_{298} at MP2-5 level of theory with PCM/UAHF/RHF/6-31G(d) solvation energies for chloroform; [g] Energetically best conformer used for the calculation of ΔH_{298} at MP2-5 level of theory; [h] Energetically best conformer used for the calculation of ΔH_{298} at MP2-5 level of theory with inclusion of solvent effects as described above; [i] Acetylation enthalpies for **1a–h** according to Scheme 5.5 including only the electrostatic term for the solvent contribution; [j] Acetylation enthalpies for **1a–h** according to Scheme 5.5 including only the non electrostatic term for the solvent contribution; [k] N-C bond length of the pyridine nitrogen and the carbonyl group in **11a–h**; [l] Mulliken charges on N in **11a–h**; [m] Mulliken charges for the whole acyl cation in **11a–h**; [n] ^1H NMR shifts of terminal CH_3 -group in **1a–h**.

The plots for R^2 -values better than 0.90 in Table 5.12 are given in the following section.

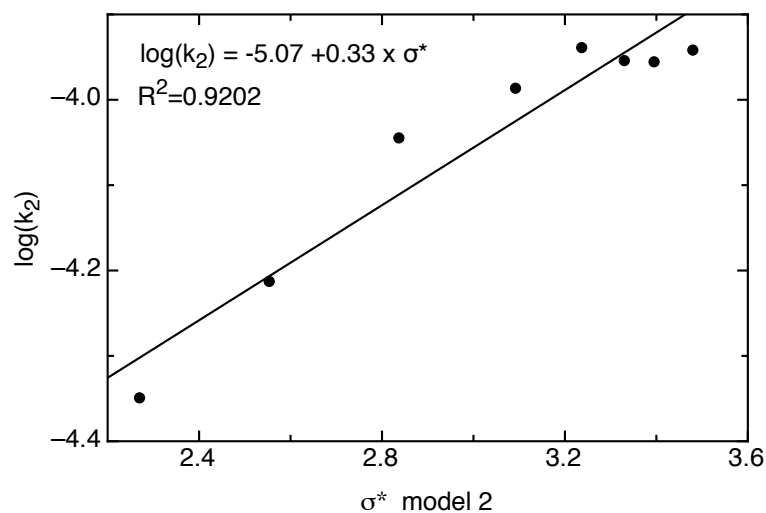


Figure 5.16. Observed $\log(k_2)$ values for acylation reaction (I) vs. σ^* -value determined for model 2.

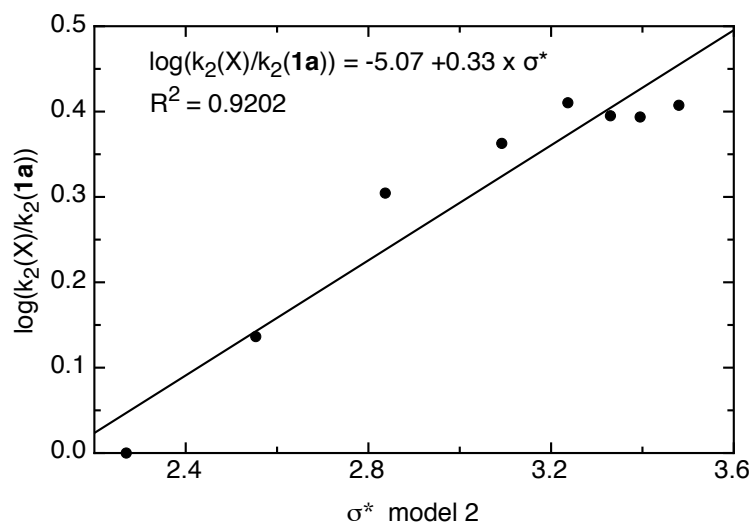


Figure 5.17. Observed $\log(k_2(X)/k_2(\mathbf{1a}))$ values for acylation reaction (I) vs. σ^* -value determined for model 2 with $X=\mathbf{1a-h}$.

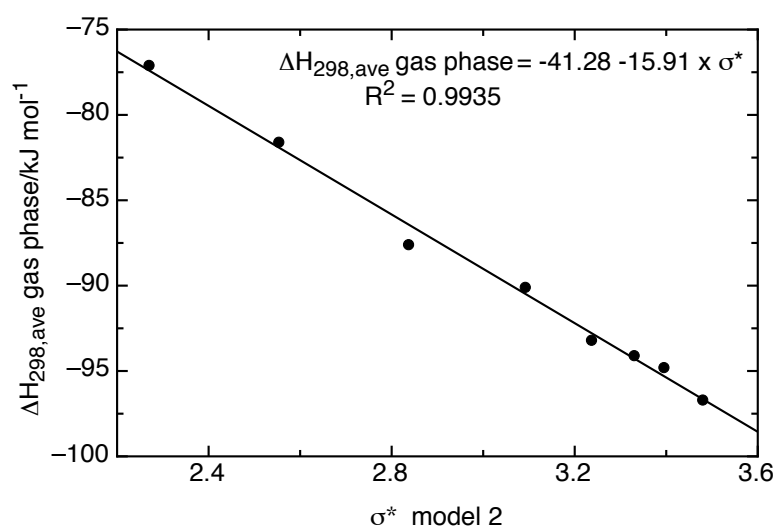


Figure 5.18. Boltzmann averaged ΔH_{298} in the gas phase at MP2-5 level of theory ($\Delta H_{298,\text{ave}}$ (gas phase)) vs. σ^* -value determined for model 2.

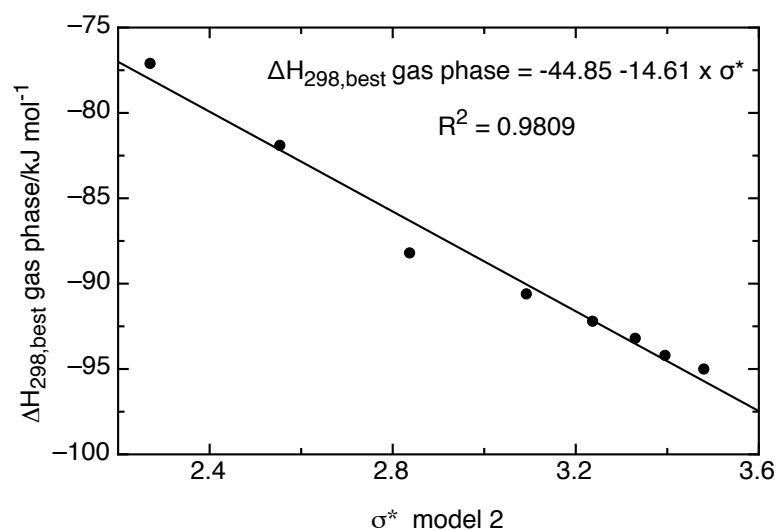


Figure 5.19. ΔH_{298} for the best conformer in the gas phase at MP2-5 level of theory ($\Delta H_{298,\text{best}}$ (gas phase)) vs. σ^* -value determined for model 2.

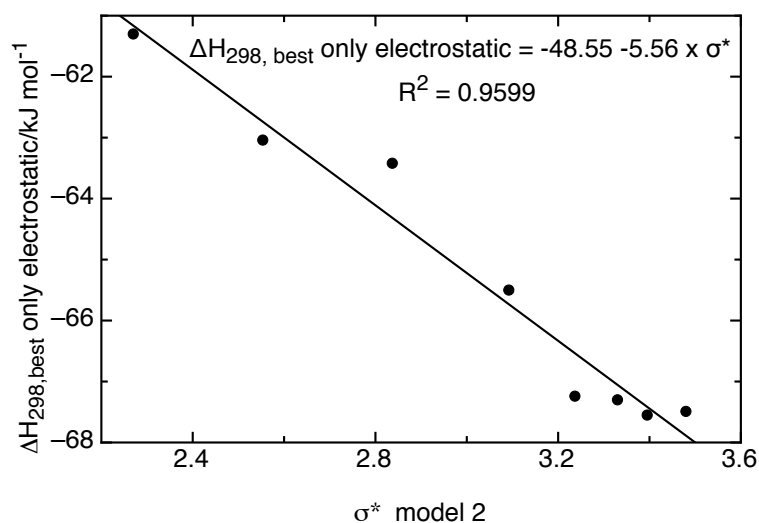


Figure 5.20. $\Delta H_{298, \text{best}}$ (only electrostatic) for **1a–h** according to Scheme 5 including only the electrostatic term for the solvent contribution at MP2-5 level of theory vs. σ^* -value determined for model 2.

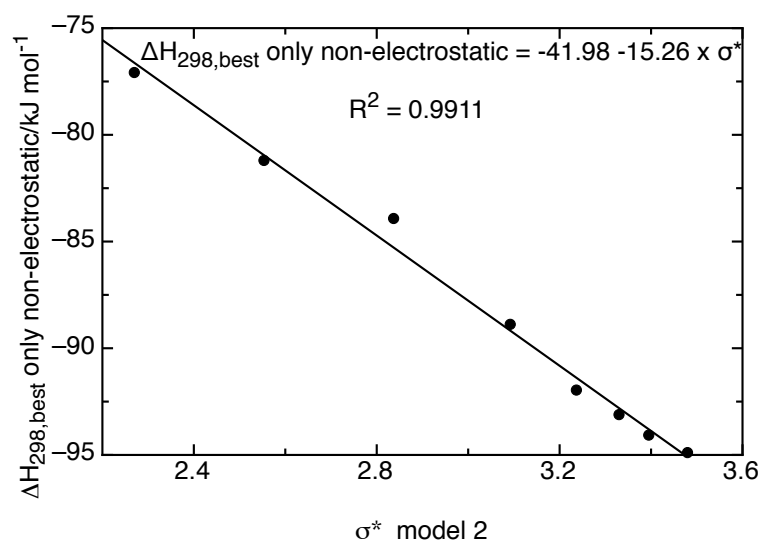


Figure 5.21. $\Delta H_{298, \text{best}}$ (only non-electrostatic) for **1a–h** according to Scheme 5 including only the non electrostatic term for the solvent contribution at MP2-5 level of theory vs. σ^* -value determined for model 2.

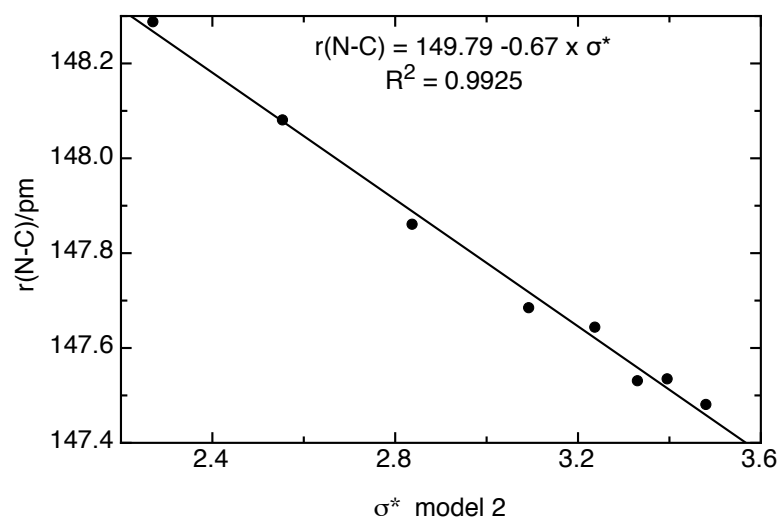


Figure 5.22. N-C bond length ($r(\text{N-C})$) of the pyridine nitrogen and the carbonyl group in **11a–h** in [pm] vs. σ^* -value determined for model 2.

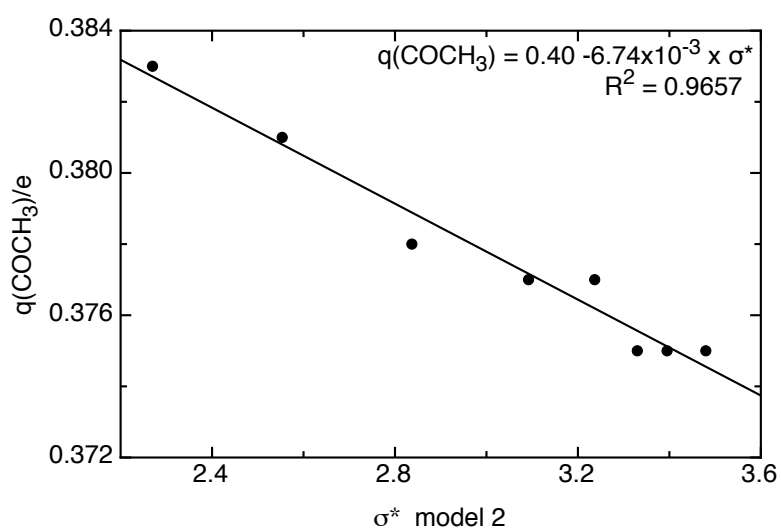


Figure 5.23. Charge of the whole acyl group ($q(\text{COCH}_3)$) in **11a–h** in [e] vs. σ^* -value determined for model 2.

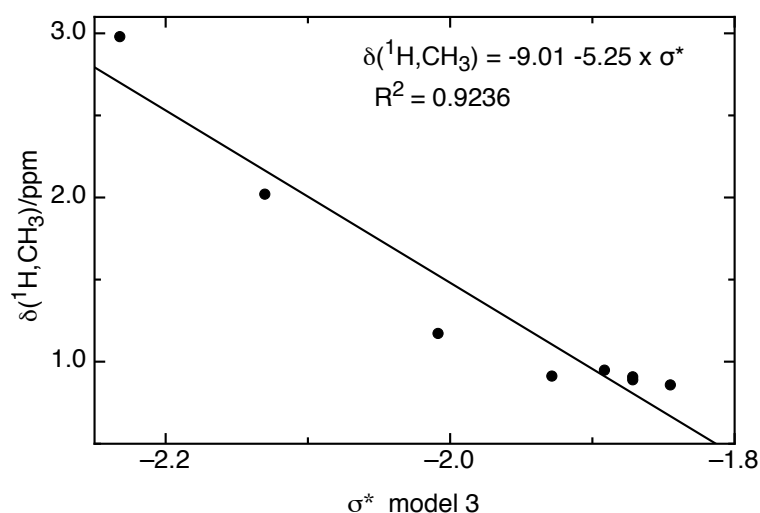


Figure 5.24. ^1H NMR shifts of terminal CH_3 -group ($\delta(^1\text{H},\text{CH}_3)$ in [ppm] vs. σ^* -value determined for model 2.

Theoretical procedures

Following a recently developed protocol for the calculation of cation affinity values,^[15,16,2b] geometry optimizations have been performed in the gas phase at B98/6-31G(d) level. Thermal corrections to 289.15 K and 1 atm have been calculated at the same level of theory using the rigid rotor/harmonic oscillator model. Single point energies calculated at the MP2(FC)/6-31+G(2d,p) level have then been combined with thermal corrections obtained previously to calculate enthalpies (H_{298}) and free energies (G_{298}) at 298.15 K. Solvent effects in chloroform have subsequently been determined through single point calculations with the PCM/UAHF/RHF/6-31G(d) continuum solvation model. Partial atomic charges have been calculated using the Mulliken population analysis at the B98/6-31G(d) level. For selected systems calculations have been repeated using the G3(MP2)B3 compound scheme developed by Curtiss *et al.*^[17,18] All quantum mechanical calculations have been performed with Gaussian 03.^[19]

Table 5.13. Acetylation enthalpies [kJ/mol] for pyridines **1a–h** according to Scheme 5.5 for the Boltzmann-averaged, selected and best conformers calculated at MP2-5 level of theory (columns 2–7) or G3MP2B3 (column 8) in the gas phase and in CHCl₃ solution.

catalyst	$\Delta H_{298,\text{ave}}$		$\Delta H_{298,\text{best}}$		$\Delta H_{298,\text{sel}}$		$\Delta H_{298,\text{sel}}$
	[kJ/mol]		[kJ/mol]		[kJ/mol]		G3MP2B3 [kJ/mol]
	gas phase	CHCl ₃	gas phase	CHCl ₃	gas phase	CHCl ₃	gas phase
1a	–77.1	–61.2	–77.1	–61.2	–77.1	–61.2	–81.8
1b	–81.6	–63.3	–81.9	–63.6	–81.3	–62.9	–86.6
1c	–87.6	–67.1	–88.2	–67.8	–88.2	–67.7	–92.6
1d	–90.1	–66.1	–90.6	–66.1	–88.9	–65.5	–93.9
1e	–93.2	–67.9	–92.2	–67.1	–92.1	–67.1	–97.3
1f	–94.1	–67.8	–93.2	–67.6	–93.2	–67.1	–98.6
1g	–94.8	–68.1	–94.2	–67.4	–94.2	–67.4	–99.6
1h	–96.7	–68.5	–95.0	–68.2	–95.0	–67.4	–

Table 5.14. Solvation energy data $\Delta G_{\text{solv.}}$ divided into electrostatic and non electrostatic terms for neutral catalysts **1a–h** and acylated catalysts **11a–h**.

catalyst	$\Delta G_{\text{solv.}}$					
	total		electrostatic		non electrostatic	
	1	11	1	11	1	11
a	–3.27	–31.39	–2.93	–32.10	–0.33	+0.71
b	–2.84	–30.37	–2.92	–31.51	+0.08	+1.14
c	–2.29	–29.32	–2.87	–30.93	+0.59	+1.61
d	–0.71	–26.78	–2.74	–29.97	+2.03	+3.19
e	–0.06	–26.00	–2.73	–29.73	+2.67	+3.74
f	+0.33	–25.62	–2.74	–29.40	+3.08	+3.78
g	+0.52	–25.00	–2.74	–29.32	+3.26	+4.32
h	+0.86	–24.84	–2.76	–29.10	+3.62	+4.26

Table 5.15 Calculated energies of conformers for catalysts **1a–1h**, as calculated at MP2/6-31+G(2d,p)//B98/6-31G(d) level with inclusion of solvent effects at PCM/UAHF/RHF/6-31G(d).

			E_{tot}	H_{298}	E_{tot}	H_{298}	E_{tot}	H_{298}
Conf			B98/6-31G(d)	B98/6-31G(d)	MP2(FC)/6-31+G(2d.p)	G_{solv} , kcal/mol	MP2-5 without solvation	MP2-5 with solvation
Pyr								
1			-248.181767	-248.087628	-247.589433	-2.15	-247.495294	-247.498720
Pyr-Ac ⁺								
1	ac		-401.140005	-400.991697	-400.215517	-34.07	-400.067209	-400.121503
1a								
1			-382.100962	-381.928960	-381.179975	-3.27	-381.007973	-381.013184
1a-Ac ⁺								
1	ac		-535.091159	-534.864305	-533.836114	-31.39	-533.609261	-533.659284
1b								
1			-421.400415	-421.198543	-420.374849	-2.84	-420.172978	-420.177503
1b-Ac ⁺								
1	ac1		-574.392288	-574.135480	-573.032902	-30.37	-572.776094	-572.824492
1	ac2		-574.392332	-574.135258	-573.032926	-30.37	-572.775852	-572.824249
1c								
4			-460.699626	-460.467717	-459.569493	-2.29	-459.337583	-459.341233
5			-460.698872	-460.467017	-459.568777	-2.39	-459.336921	-459.340730
2			-460.695706	-460.463514	-459.566589	-2.54	-459.334396	-459.338444
12			-460.695601	-460.463698	-459.566199	-2.53	-459.334296	-459.338328
10			-460.688598	-460.457621	-459.563361	-1.71	-459.332384	-459.335109
1c-Ac ⁺								
4	ac1		-613.693223	-613.406531	-612.229788	-29.32	-611.943096	-611.989821
4	ac2		-613.693223	-613.406527	-612.229789	-29.32	-611.943093	-611.989817
12	ac2		-613.691702	-613.404882	-612.228221	-29.54	-611.941402	-611.988477
12	ac1		-613.691702	-613.404881	-612.228221	-29.54	-611.941400	-611.988475
5	ac1		-613.691701	-613.404880	-612.228221	-29.54	-611.941399	-611.988474
10	ac2		-613.691702	-613.404879	-612.228221	-29.54	-611.941399	-611.988474
10	ac1		-613.691702	-613.404879	-612.228221	-29.54	-611.941399	-611.988474
5	ac2		-613.691701	-613.404879	-612.228221	-29.54	-611.941398	-611.988473
2	ac1		-613.688778	-613.401873	-612.225068	-29.50	-611.938163	-611.985174
2	ac2		-613.688797	-613.401760	-612.224973	-29.51	-611.937936	-611.984963
1d								
37			-539.292811	-539.001043	-537.954451	-0.71	-537.662683	-537.663814
34			-539.293771	-539.002066	-537.954231	-0.65	-537.662525	-537.663561
29			-539.288540	-538.997719	-537.952842	-0.86	-537.662021	-537.663391
7			-539.294761	-539.003085	-537.953964	-0.67	-537.662288	-537.663356
48			-539.292832	-539.001072	-537.953309	-0.82	-537.661549	-537.662856
49			-539.292832	-539.001067	-537.953310	-0.82	-537.661545	-537.662852
9			-539.294028	-539.002224	-537.953368	-0.62	-537.661564	-537.662552

64	-539.292137	-539.000246	-537.953085	-0.66	-537.661193	-537.662245
61	-539.291362	-538.999336	-537.952841	-0.86	-537.660814	-537.662185
111	-539.290465	-538.998527	-537.952504	-0.91	-537.660566	-537.662017
62	-539.291992	-539.000333	-537.952415	-0.69	-537.660756	-537.661856
85	-539.290007	-538.998114	-537.951373	-1.03	-537.659480	-537.661121
18	-539.288610	-538.996981	-537.951579	-0.50	-537.659950	-537.660747
3	-539.289875	-538.997982	-537.951279	-0.61	-537.659386	-537.660358
103	-539.288696	-538.996917	-537.950548	-0.85	-537.658770	-537.660124
15	-539.288720	-538.996971	-537.950657	-0.71	-537.658908	-537.660039
11	-539.290276	-538.998313	-537.950527	-0.87	-537.658564	-537.659950
24	-539.288889	-538.997060	-537.949759	-0.88	-537.657931	-537.659333
70	-539.287980	-538.996108	-537.949538	-0.96	-537.657666	-537.659196
90	-539.287099	-538.995070	-537.949661	-0.93	-537.657632	-537.659114
84	-539.287698	-538.995852	-537.949137	-0.86	-537.657291	-537.658661
39	-539.282774	-538.992967	-537.948055	0.48	-537.658248	-537.657483
60	-539.286580	-538.994778	-537.946978	-1.00	-537.655175	-537.656769
44	-539.283056	-538.991938	-537.947933	0.25	-537.656815	-537.656416
40	-539.283243	-538.992118	-537.947716	0.11	-537.656590	-537.656415
36	-539.283164	-538.992152	-537.946893	-0.16	-537.655882	-537.656137
78	-539.283972	-538.992085	-537.945907	-0.91	-537.654020	-537.655470
97	-539.284282	-538.992454	-537.945351	-1.04	-537.653523	-537.655180
1d-Ac⁺						
7 ac1	-692.289974	-691.943339	-690.615729	-26.79	-690.269095	-690.311787
7 ac2	-692.289974	-691.943337	-690.615730	-26.76	-690.269093	-690.311738
37 ac1	-692.287303	-691.940567	-690.615189	-27.04	-690.268453	-690.311544
37 ac2	-692.287303	-691.940567	-690.615188	-26.99	-690.268451	-690.311463
3 ac2	-692.288154	-691.941357	-690.615007	-27.08	-690.268210	-690.311365
49 ac1	-692.288154	-691.941361	-690.615006	-27.06	-690.268213	-690.311336
48 ac2	-692.288154	-691.941360	-690.615006	-27.06	-690.268212	-690.311335
61 ac1	-692.286569	-691.939824	-690.614546	-27.18	-690.267802	-690.311116
29 ac2	-692.286568	-691.939820	-690.614543	-27.18	-690.267795	-690.311109
48 ac1	-692.288187	-691.941145	-690.615072	-27.03	-690.268030	-690.311105
3 ac1	-692.288187	-691.941143	-690.615073	-27.03	-690.268028	-690.311103
49 ac2	-692.288187	-691.941143	-690.615072	-27.03	-690.268028	-690.311103
61 ac2	-692.286537	-691.939772	-690.614502	-27.21	-690.267736	-690.311098
29 ac1	-692.286537	-691.939773	-690.614501	-27.20	-690.267737	-690.311083
34 ac1	-692.288586	-691.941676	-690.615390	-26.73	-690.268480	-690.311077
34 ac2	-692.288597	-691.941614	-690.615430	-26.75	-690.268447	-690.311076
97 ac1	-692.288597	-691.941612	-690.615428	-26.75	-690.268444	-690.311073
64 ac1	-692.286900	-691.940493	-690.614412	-26.93	-690.268005	-690.310921
85 ac1	-692.285608	-691.938989	-690.613568	-27.40	-690.266949	-690.310614
85 ac2	-692.285608	-691.938989	-690.613565	-27.40	-690.266946	-690.310610
70 ac1	-692.286889	-691.940040	-690.614345	-26.97	-690.267496	-690.310475
64 ac2	-692.286889	-691.940039	-690.614344	-26.95	-690.267494	-690.310442
9 ac1	-692.288461	-691.941910	-690.614291	-26.75	-690.267740	-690.310369
9 ac2	-692.288461	-691.941902	-690.614291	-26.74	-690.267732	-690.310345

36	ac2	-692.288461	-691.941893	-690.614291	-26.74	-690.267723	-690.310336
36	ac1	-692.288461	-691.941884	-690.614290	-26.74	-690.267713	-690.310326
111	ac1	-692.283859	-691.937527	-690.611734	-27.65	-690.265401	-690.309465
111	ac2	-692.283916	-691.937315	-690.611746	-27.60	-690.265145	-690.309128
44	ac2	-692.285609	-691.938952	-690.612229	-27.13	-690.265572	-690.308806
84	ac2	-692.285610	-691.938929	-690.612235	-27.13	-690.265553	-690.308788
62	ac1	-692.285610	-691.938928	-690.612233	-27.13	-690.265550	-690.308785
39	ac2	-692.285610	-691.938927	-690.612233	-27.13	-690.265550	-690.308784
40	ac1	-692.285610	-691.938927	-690.612231	-27.13	-690.265548	-690.308782
40	ac2	-692.285608	-691.938916	-690.612201	-27.14	-690.265509	-690.308759
62	ac2	-692.285608	-691.938908	-690.612201	-27.14	-690.265501	-690.308751
39	ac1	-692.285608	-691.938914	-690.612201	-27.13	-690.265507	-690.308742
44	ac1	-692.285608	-691.938909	-690.612200	-27.13	-690.265501	-690.308736
90	ac2	-692.283154	-691.936353	-690.611439	-27.37	-690.264639	-690.308256
84	ac1	-692.285370	-691.938743	-690.611773	-27.05	-690.265146	-690.308253
103	ac1	-692.283154	-691.936350	-690.611439	-27.37	-690.264635	-690.308252
103	ac2	-692.283157	-691.936285	-690.611441	-27.38	-690.264569	-690.308202
90	ac1	-692.283158	-691.936290	-690.611437	-27.37	-690.264569	-690.308186
18	ac2	-692.282474	-691.936592	-690.610834	-27.00	-690.264952	-690.307980
11	ac2	-692.285079	-691.938428	-690.610697	-26.84	-690.264047	-690.306819
18	ac1	-692.282456	-691.935470	-690.610702	-27.03	-690.263717	-690.306792
11	ac1	-692.285122	-691.938269	-690.610738	-26.84	-690.263885	-690.306657
15	ac1	-692.283077	-691.936148	-690.610344	-27.05	-690.263414	-690.306521
24	ac2	-692.283507	-691.936583	-690.610270	-27.07	-690.263346	-690.306484
15	ac2	-692.283062	-691.936053	-690.610135	-27.11	-690.263126	-690.306329
24	ac1	-692.283544	-691.936533	-690.610128	-27.07	-690.263117	-690.306256
70	ac2	-692.282045	-691.936105	-690.608755	-27.15	-690.262815	-690.306081
60	ac2	-692.281448	-691.934966	-690.607755	-27.08	-690.261274	-690.304428
60	ac1	-692.281435	-691.934518	-690.607687	-27.07	-690.260770	-690.303909
97	ac2	-692.278860	-691.933027	-690.605483	-26.94	-690.259650	-690.302582
78	ac1	-692.278316	-691.931537	-690.605588	-27.33	-690.258809	-690.302362
78	ac2	-692.278300	-691.931328	-690.605602	-27.39	-690.258630	-690.302279
1e							
37		-617.887497	-617.535936	-616.338253	-0.06	-615.986692	-615.986788
34		-617.888418	-617.536743	-616.337923	-0.12	-615.986248	-615.986439
7		-617.889328	-617.537918	-616.337281	-0.31	-615.985872	-615.986366
49		-617.887503	-617.536024	-616.337133	-0.27	-615.985654	-615.986084
48		-617.887503	-617.536023	-616.337133	-0.27	-615.985653	-615.986083
61		-617.886098	-617.534293	-616.336942	-0.17	-615.985137	-615.985408
29		-617.886098	-617.534293	-616.336942	-0.16	-615.985137	-615.985392
9		-617.888537	-617.536890	-616.336840	-0.09	-615.985194	-615.985337
64		-617.886754	-617.535081	-616.337112	0.17	-615.985439	-615.985169
111		-617.885263	-617.533778	-616.337062	0.30	-615.985577	-615.985099
85		-617.884861	-617.533215	-616.335796	-0.34	-615.984151	-615.984693
62		-617.886578	-617.535001	-616.336191	0.10	-615.984614	-615.984455
18		-617.883333	-617.531687	-616.335538	0.22	-615.983892	-615.983542

3		-617.884456	-617.532879	-616.334928	-0.04	-615.983351	-615.983415
103		-617.883482	-617.531926	-616.335214	0.19	-615.983658	-615.983355
15		-617.883332	-617.532020	-616.334445	-0.05	-615.983134	-615.983213
11		-617.884930	-617.533132	-616.334057	-0.39	-615.982260	-615.982881
90		-617.881854	-617.530280	-616.334320	0.14	-615.982746	-615.982523
24		-617.883652	-617.532095	-616.333598	-0.24	-615.982042	-615.982424
70		-617.882691	-617.530994	-616.333345	-0.28	-615.981647	-615.982093
84		-617.882538	-617.530945	-616.333182	0.23	-615.981588	-615.981222
60		-617.881288	-617.529397	-616.331193	-0.17	-615.979302	-615.979573
44		-617.877742	-617.526908	-616.331997	1.18	-615.981163	-615.979282
40		-617.877946	-617.526987	-616.331377	0.74	-615.980418	-615.979239
39		-617.877946	-617.526986	-616.331375	0.78	-615.980415	-615.979172
36		-617.877798	-617.526769	-616.330099	0.20	-615.979070	-615.978751
78		-617.878773	-617.527280	-616.330025	-0.08	-615.978532	-615.978660
97		-617.879200	-617.527580	-616.329631	0.05	-615.978011	-615.977931
1e-Ac⁺							
37	ac2	-770.882953	-770.476564	-769.000087	-26.00	-768.593698	-768.635132
37	ac1	-770.882953	-770.476564	-769.000087	-26.00	-768.593698	-768.635132
49	ac1	-770.883688	-770.477305	-768.999787	-26.18	-768.593405	-768.635125
7	ac1	-770.885523	-770.479189	-769.000042	-25.98	-768.593708	-768.635110
7	ac2	-770.885523	-770.479188	-769.000042	-25.98	-768.593707	-768.635109
48	ac2	-770.883688	-770.477305	-768.999788	-26.09	-768.593406	-768.634983
3	ac2	-770.883688	-770.477305	-768.999787	-26.09	-768.593404	-768.634981
49	ac2	-770.883729	-770.477103	-768.999863	-26.18	-768.593236	-768.634957
97	ac2	-770.884158	-770.477758	-769.000061	-25.89	-768.593661	-768.634919
34	ac1	-770.884158	-770.477752	-769.000064	-25.89	-768.593658	-768.634916
3	ac1	-770.883729	-770.477103	-768.999865	-26.09	-768.593238	-768.634815
48	ac1	-770.883729	-770.477103	-768.999864	-26.09	-768.593238	-768.634815
97	ac1	-770.884205	-770.477612	-769.000120	-25.89	-768.593527	-768.634785
34	ac2	-770.884205	-770.477613	-769.000117	-25.89	-768.593525	-768.634784
29	ac2	-770.882224	-770.475606	-768.999500	-26.09	-768.592882	-768.634459
61	ac1	-770.882224	-770.475607	-768.999500	-26.06	-768.592883	-768.634412
78	ac1	-770.882224	-770.475609	-768.999496	-26.06	-768.592881	-768.634410
44	ac1	-770.882224	-770.475609	-768.999496	-26.06	-768.592881	-768.634410
29	ac1	-770.882223	-770.475542	-768.999468	-26.09	-768.592787	-768.634364
78	ac2	-770.882223	-770.475542	-768.999470	-26.06	-768.592789	-768.634319
61	ac2	-770.882223	-770.475542	-768.999468	-26.06	-768.592787	-768.634316
85	ac2	-770.881310	-770.474556	-768.998826	-26.31	-768.592072	-768.634000
85	ac1	-770.881310	-770.474553	-768.998825	-26.31	-768.592069	-768.633996
70	ac1	-770.882399	-770.475943	-768.999355	-25.67	-768.592899	-768.633807
64	ac2	-770.882399	-770.475940	-768.999358	-25.66	-768.592899	-768.633790
70	ac2	-770.882440	-770.475846	-768.999408	-25.67	-768.592814	-768.633722
64	ac1	-770.882440	-770.475846	-768.999410	-25.66	-768.592816	-768.633708
36	ac1	-770.883970	-770.477420	-768.998717	-25.82	-768.592167	-768.633314
9	ac2	-770.883970	-770.477391	-768.998717	-25.82	-768.592139	-768.633285
36	ac2	-770.883970	-770.477391	-768.998716	-25.82	-768.592138	-768.633284

9	ac1	-770.883969	-770.477367	-768.998703	-25.82	-768.592101	-768.633248
111	ac1	-770.879564	-770.472902	-768.997235	-26.00	-768.590573	-768.632007
111	ac2	-770.879594	-770.473007	-768.997110	-26.00	-768.590523	-768.631957
44	ac2	-770.881161	-770.474504	-768.997058	-26.06	-768.590400	-768.631930
84	ac1	-770.881092	-770.474569	-768.997012	-25.94	-768.590489	-768.631827
39	ac2	-770.881091	-770.474552	-768.997018	-25.93	-768.590479	-768.631801
62	ac2	-770.881092	-770.474565	-768.997014	-25.91	-768.590487	-768.631777
40	ac2	-770.881094	-770.474583	-768.997012	-25.90	-768.590501	-768.631775
84	ac2	-770.881161	-770.474504	-768.997032	-25.94	-768.590375	-768.631713
39	ac1	-770.881159	-770.474494	-768.997044	-25.93	-768.590380	-768.631702
62	ac1	-770.881159	-770.474492	-768.997047	-25.91	-768.590380	-768.631670
40	ac1	-770.881162	-770.474504	-768.997051	-25.90	-768.590393	-768.631668
103	ac1	-770.878753	-770.472094	-768.997007	-25.87	-768.590347	-768.631574
90	ac2	-770.878754	-770.472092	-768.997002	-25.83	-768.590340	-768.631503
103	ac2	-770.878818	-770.472181	-768.996826	-25.87	-768.590189	-768.631415
90	ac1	-770.878818	-770.472182	-768.996826	-25.83	-768.590190	-768.631353
18	ac2	-770.877930	-770.471492	-768.995613	-25.88	-768.589175	-768.630417
18	ac1	-770.877949	-770.471321	-768.995605	-25.88	-768.588977	-768.630219
15	ac1	-770.878637	-770.472070	-768.994911	-26.16	-768.588344	-768.630032
15	ac2	-770.878633	-770.471913	-768.994844	-26.16	-768.588124	-768.629813
11	ac2	-770.880689	-770.473966	-768.995119	-25.96	-768.588396	-768.629766
11	ac1	-770.880730	-770.473881	-768.995142	-25.96	-768.588293	-768.629663
24	ac2	-770.879108	-770.472413	-768.994858	-26.02	-768.588162	-768.629628
24	ac1	-770.879111	-770.472384	-768.994856	-26.02	-768.588128	-768.629594
60	ac2	-770.877088	-770.470609	-768.992628	-25.84	-768.586149	-768.627328
60	ac1	-770.877050	-770.470539	-768.992558	-25.84	-768.586047	-768.627226
1f							
37		-696.482340	-696.071133	-694.722029	0.33	-694.310821	-694.310295
34		-696.483260	-696.071916	-694.721441	0.15	-694.310098	-694.309858
7		-696.484181	-696.073018	-694.720709	-0.16	-694.309546	-694.309801
49		-696.482373	-696.071012	-694.720715	0.09	-694.309353	-694.309210
48		-696.482373	-696.071012	-694.720715	0.09	-694.309353	-694.309210
9		-696.483414	-696.072035	-694.720319	0.06	-694.308940	-694.308845
61		-696.480912	-696.069542	-694.720705	0.35	-694.309335	-694.308777
29		-696.480912	-696.069540	-694.720705	0.36	-694.309334	-694.308760
64		-696.481634	-696.070227	-694.720769	0.63	-694.309362	-694.308358
111		-696.480197	-696.068619	-694.721312	1.12	-694.309733	-694.307949
62		-696.481385	-696.070047	-694.719829	0.58	-694.308491	-694.307567
85		-696.479643	-696.068124	-694.719517	0.28	-694.307998	-694.307552
18		-696.478062	-696.066949	-694.719268	0.73	-694.308156	-694.306992
3		-696.479281	-696.067812	-694.718389	0.21	-694.306920	-694.306585
11		-696.479785	-696.068111	-694.717483	-0.23	-694.305809	-694.306176
103		-696.478244	-696.066897	-694.719325	1.20	-694.307978	-694.306066
15		-696.478181	-696.066749	-694.718044	0.39	-694.306612	-694.305990
90		-696.476792	-696.065473	-694.718583	0.97	-694.307264	-694.305718
70		-696.477485	-696.066199	-694.716876	0.07	-694.305590	-694.305478

24		-696.478507	-696.066812	-694.717192	0.19	-694.305496	-694.305194
84		-696.477414	-696.065926	-694.717468	1.17	-694.305980	-694.304115
60		-696.476117	-696.064578	-694.714720	0.36	-694.303182	-694.302608
39		-696.472716	-696.061987	-694.714791	1.00	-694.304062	-694.302468
40		-696.472716	-696.061987	-694.714791	1.00	-694.304062	-694.302468
36		-696.472619	-696.061808	-694.713426	0.33	-694.302615	-694.302089
44		-696.472569	-696.061847	-694.715684	1.88	-694.304962	-694.301966
78		-696.473556	-696.062231	-694.713777	0.51	-694.302452	-694.301639
97		-696.473976	-696.062556	-694.713476	0.72	-694.302056	-694.300909
1f-Ac⁺							
7	ac2	-849.480922	-849.014921	-847.384012	-25.62	-846.918011	-846.958839
7	ac1	-849.480922	-849.014921	-847.384012	-25.62	-846.918011	-846.958839
37	ac1	-849.478322	-849.012227	-847.384344	-25.35	-846.918249	-846.958646
97	ac1	-849.478322	-849.012228	-847.384346	-25.33	-846.918252	-846.958618
37	ac2	-849.478322	-849.012226	-847.384346	-25.33	-846.918250	-846.958616
34	ac1	-849.479604	-849.013299	-847.384208	-25.35	-846.917903	-846.958301
97	ac2	-849.479604	-849.013300	-847.384207	-25.35	-846.917902	-846.958300
34	ac2	-849.479582	-849.013234	-847.384164	-25.29	-846.917816	-846.958118
49	ac2	-849.479151	-849.012711	-847.383968	-25.46	-846.917528	-846.958102
48	ac1	-849.479151	-849.012711	-847.383968	-25.46	-846.917528	-846.958101
3	ac1	-849.479151	-849.012711	-847.383967	-25.46	-846.917527	-846.958100
49	ac1	-849.479198	-849.012736	-847.383889	-25.35	-846.917427	-846.957825
48	ac2	-849.479198	-849.012736	-847.383890	-25.34	-846.917428	-846.957810
3	ac2	-849.479198	-849.012735	-847.383890	-25.34	-846.917427	-846.957809
29	ac2	-849.477591	-849.011049	-847.383845	-25.29	-846.917302	-846.957605
78	ac1	-849.477591	-849.011044	-847.383846	-25.29	-846.917299	-846.957601
61	ac1	-849.477591	-849.011046	-847.383844	-25.29	-846.917299	-846.957601
29	ac1	-849.477612	-849.011094	-847.383736	-25.15	-846.917218	-846.957297
61	ac2	-849.477612	-849.011095	-847.383735	-25.14	-846.917218	-846.957282
78	ac2	-849.477612	-849.011094	-847.383735	-25.14	-846.917217	-846.957280
64	ac2	-849.477863	-849.011613	-847.383611	-24.88	-846.917361	-846.957009
70	ac1	-849.477864	-849.011604	-847.383602	-24.89	-846.917342	-846.957006
36	ac2	-849.479357	-849.012896	-847.382722	-25.44	-846.916261	-846.956802
36	ac1	-849.479355	-849.012858	-847.382709	-25.44	-846.916212	-846.956753
9	ac1	-849.479356	-849.012846	-847.382703	-25.44	-846.916193	-846.956735
9	ac2	-849.479355	-849.012844	-847.382701	-25.44	-846.916189	-846.956731
64	ac1	-849.477838	-849.011204	-847.383695	-24.87	-846.917060	-846.956693
70	ac2	-849.477838	-849.011206	-847.383692	-24.87	-846.917060	-846.956693
85	ac2	-849.476766	-849.010179	-847.383068	-25.18	-846.916481	-846.956608
85	ac1	-849.476769	-849.010196	-847.383059	-25.17	-846.916486	-846.956597
111	ac2	-849.475063	-849.008757	-847.382159	-24.85	-846.915853	-846.955454
111	ac1	-849.475134	-849.008906	-847.382069	-24.81	-846.915841	-846.955378
44	ac1	-849.476558	-849.010249	-847.381290	-25.19	-846.914981	-846.955124
62	ac2	-849.476558	-849.010245	-847.381291	-25.19	-846.914978	-846.955121
84	ac1	-849.476559	-849.010243	-847.381288	-25.19	-846.914972	-846.955115
40	ac2	-849.476560	-849.010215	-847.381298	-25.18	-846.914953	-846.955080

39	ac1	-849.476544	-849.010234	-847.381236	-25.19	-846.914926	-846.955069
62	ac1	-849.476544	-849.010235	-847.381234	-25.19	-846.914925	-846.955068
84	ac2	-849.476544	-849.010235	-847.381233	-25.19	-846.914924	-846.955067
40	ac1	-849.476544	-849.010234	-847.381233	-25.19	-846.914923	-846.955066
44	ac2	-849.476544	-849.010233	-847.381232	-25.19	-846.914921	-846.955064
39	ac2	-849.476561	-849.010206	-847.381294	-25.17	-846.914939	-846.955050
103	ac1	-849.474216	-849.007951	-847.381679	-24.26	-846.915415	-846.954075
90	ac2	-849.474215	-849.007957	-847.381686	-24.25	-846.915428	-846.954073
90	ac1	-849.474214	-849.007811	-847.381668	-24.35	-846.915265	-846.954070
103	ac2	-849.474214	-849.007809	-847.381669	-24.24	-846.915264	-846.953893
18	ac1	-849.473375	-849.006825	-847.379943	-25.08	-846.913394	-846.953361
18	ac2	-849.473359	-849.006705	-847.379932	-25.14	-846.913278	-846.953341
11	ac1	-849.476075	-849.009630	-847.379077	-25.53	-846.912632	-846.953317
11	ac2	-849.476115	-849.009448	-847.379123	-25.54	-846.912456	-846.953156
15	ac1	-849.474018	-849.007577	-847.378995	-25.46	-846.912554	-846.953127
15	ac2	-849.474042	-849.007690	-847.379043	-25.37	-846.912691	-846.953121
24	ac2	-849.474476	-849.007948	-847.378972	-25.32	-846.912444	-846.952794
24	ac1	-849.474493	-849.007961	-847.378971	-25.32	-846.912439	-846.952789
60	ac2	-849.472437	-849.006138	-847.376824	-25.00	-846.910525	-846.950365
60	ac1	-849.472476	-849.005898	-847.376888	-25.02	-846.910310	-846.950182
1g							
37		-775.077114	-774.606103	-773.105282	0.52	-772.634271	-772.633443
34		-775.078023	-774.606780	-773.104714	0.31	-772.633471	-772.632977
7		-775.078966	-774.607937	-773.103913	0.01	-772.632884	-772.632868
49		-775.077165	-774.605877	-773.103996	0.38	-772.632708	-772.632103
48		-775.077165	-774.605877	-773.103996	0.38	-772.632708	-772.632103
9		-775.078201	-774.607185	-773.103496	0.24	-772.632481	-772.632098
61		-775.075663	-774.604455	-773.103938	0.50	-772.632730	-772.631933
29		-775.075663	-774.604455	-773.103938	0.50	-772.632730	-772.631933
64		-775.076394	-774.605194	-773.104146	0.92	-772.632946	-772.631480
111		-775.075012	-774.604033	-773.105047	1.73	-772.634068	-772.631311
85		-775.074404	-774.603150	-773.102919	0.61	-772.631665	-772.630693
62		-775.076159	-774.605002	-773.103139	0.83	-772.631982	-772.630659
18		-775.072911	-774.601738	-773.102542	0.92	-772.631369	-772.629903
3		-775.074020	-774.602807	-773.101697	0.38	-772.630484	-772.629879
11		-775.074476	-774.603224	-773.100630	-0.05	-772.629378	-772.629457
15		-775.072893	-774.601748	-773.101289	0.56	-772.630144	-772.629252
103		-775.073017	-774.601979	-773.102846	1.68	-772.631808	-772.629131
24		-775.073221	-774.602233	-773.100450	0.38	-772.629462	-772.628857
70		-775.072215	-774.601113	-773.100151	0.28	-772.629049	-772.628603
90		-775.071637	-774.600371	-773.102270	1.63	-772.631004	-772.628406
84		-775.072132	-774.602009	-773.101007	1.58	-772.630884	-772.628366
60		-775.070936	-774.599473	-773.098304	0.68	-772.626841	-772.625757
40		-775.067548	-774.596946	-773.098038	1.22	-772.627436	-772.625492
39		-775.067548	-774.596946	-773.098038	1.22	-772.627436	-772.625492
36		-775.067379	-774.596759	-773.096633	0.51	-772.626013	-772.625200

1g-Ac ⁺	44	-775.067345	-774.596797	-773.098864	2.10	-772.628316	-772.624969
	78	-775.068356	-774.597283	-773.097051	0.73	-772.625977	-772.624814
	97	-775.068752	-774.597451	-773.096752	0.92	-772.625451	-772.623985
	37 ac2	-928.073514	-927.547654	-925.767944	-24.99	-925.242084	-925.281908
	37 ac1	-928.073508	-927.547619	-925.767969	-24.98	-925.242080	-925.281889
	97 ac2	-928.073384	-927.547455	-925.767939	-24.99	-925.242010	-925.281834
	7 ac1	-928.076042	-927.549910	-925.767587	-25.28	-925.241454	-925.281741
	7 ac2	-928.076042	-927.549910	-925.767586	-25.28	-925.241454	-925.281740
	3 ac1	-928.074230	-927.548259	-925.767633	-25.13	-925.241661	-925.281708
	49 ac2	-928.074229	-927.548225	-925.767629	-25.09	-925.241625	-925.281609
	48 ac1	-928.074229	-927.548115	-925.767627	-25.14	-925.241513	-925.281576
	34 ac1	-928.074752	-927.548676	-925.767664	-25.02	-925.241588	-925.281460
	34 ac2	-928.074718	-927.548335	-925.767783	-25.05	-925.241400	-925.281320
	29 ac2	-928.072730	-927.546791	-925.767454	-24.97	-925.241515	-925.281307
	48 ac2	-928.074306	-927.548057	-925.767565	-25.02	-925.241317	-925.281189
	3 ac2	-928.074305	-927.548052	-925.767562	-25.02	-925.241309	-925.281181
	78 ac2	-928.072748	-927.546815	-925.767348	-24.88	-925.241415	-925.281064
	29 ac1	-928.072748	-927.546814	-925.767347	-24.88	-925.241413	-925.281062
	61 ac2	-928.072748	-927.546812	-925.767348	-24.88	-925.241412	-925.281060
	44 ac1	-928.071729	-927.548258	-925.764802	-24.71	-925.241331	-925.280709
	64 ac1	-928.072887	-927.546931	-925.767365	-24.50	-925.241409	-925.280453
	70 ac2	-928.072879	-927.546848	-925.767396	-24.51	-925.241365	-925.280425
	64 ac2	-928.072979	-927.546932	-925.767368	-24.42	-925.241321	-925.280237
	85 ac1	-928.071891	-927.545536	-925.766876	-24.85	-925.240520	-925.280121
	85 ac2	-928.071891	-927.545534	-925.766875	-24.85	-925.240518	-925.280119
	70 ac1	-928.072993	-927.546779	-925.767378	-24.43	-925.241164	-925.280096
	78 ac1	-928.072730	-927.545520	-925.767456	-24.98	-925.240246	-925.280054
	9 ac1	-928.074473	-927.548127	-925.766283	-25.07	-925.239937	-925.279888
	36 ac1	-928.074473	-927.548126	-925.766282	-25.07	-925.239934	-925.279886
	36 ac2	-928.074473	-927.548126	-925.766281	-25.07	-925.239934	-925.279886
	9 ac2	-928.074474	-927.548126	-925.766280	-25.07	-925.239932	-925.279884
	61 ac1	-928.072730	-927.545326	-925.767458	-24.98	-925.240054	-925.279863
	62 ac1	-928.071692	-927.546914	-925.764769	-24.71	-925.239991	-925.279368
	60 ac1	-928.067640	-927.546755	-925.760630	-24.54	-925.239744	-925.278851
	111 ac2	-928.070298	-927.544162	-925.766203	-24.07	-925.240067	-925.278425
	103 ac1	-928.069379	-927.544135	-925.765584	-23.77	-925.240340	-925.278220
	111 ac1	-928.070327	-927.544162	-925.766027	-24.04	-925.239862	-925.278172
	84 ac1	-928.071729	-927.545520	-925.764817	-24.71	-925.238608	-925.277986
	62 ac2	-928.071729	-927.545518	-925.764815	-24.71	-925.238604	-925.277982
	40 ac2	-928.071728	-927.545516	-925.764810	-24.71	-925.238597	-925.277975
	39 ac2	-928.071730	-927.545510	-925.764810	-24.71	-925.238591	-925.277969
	39 ac1	-928.071692	-927.545327	-925.764771	-24.71	-925.238405	-925.277783
	84 ac2	-928.071692	-927.545324	-925.764766	-24.71	-925.238398	-925.277776
	44 ac2	-928.071692	-927.545330	-925.764775	-24.70	-925.238412	-925.277774
	40 ac1	-928.071692	-927.545327	-925.764766	-24.70	-925.238400	-925.277762

90	ac2	-928.069378	-927.543128	-925.765569	-23.77	-925.239319	-925.277199
90	ac1	-928.069396	-927.543037	-925.765641	-23.74	-925.239282	-925.277114
103	ac2	-928.069396	-927.543039	-925.765628	-23.74	-925.239270	-925.277102
11	ac2	-928.071192	-927.545119	-925.762680	-25.20	-925.236606	-925.276765
18	ac1	-928.068461	-927.542095	-925.763644	-24.74	-925.237277	-925.276703
11	ac1	-928.071158	-927.544845	-925.762607	-25.18	-925.236294	-925.276421
15	ac2	-928.069179	-927.542858	-925.762762	-25.04	-925.236441	-925.276345
15	ac1	-928.069150	-927.542761	-925.762708	-25.11	-925.236319	-925.276334
18	ac2	-928.068444	-927.542191	-925.763609	-24.34	-925.237356	-925.276144
97	ac1	-928.074725	-927.543136	-925.767795	-25.02	-925.236207	-925.276079
24	ac1	-928.069608	-927.543125	-925.762615	-24.97	-925.236132	-925.275924
24	ac2	-928.069611	-927.543079	-925.762599	-24.97	-925.236067	-925.275859
49	ac1	-928.074305	-927.541400	-925.767549	-25.02	-925.234645	-925.274517
60	ac2	-928.067594	-927.541540	-925.760564	-24.52	-925.234510	-925.273585
1h							
37		-932.266633	-931.675706	-929.871618	0.86	-929.280691	-929.279321
34		-932.267584	-931.676735	-929.871007	0.62	-929.280157	-929.279169
7		-932.268490	-931.677826	-929.870241	0.3	-929.279577	-929.279099
48		-932.266627	-931.675837	-929.870194	0.55	-929.279404	-929.278527
9		-932.267523	-931.676782	-929.869797	0.55	-929.279056	-929.278180
64		-932.265849	-931.675225	-929.870497	1.29	-929.279873	-929.277817
29		-932.265275	-931.674129	-929.870283	0.86	-929.279138	-929.277767
49		-932.266627	-931.675837	-929.870194	1.11	-929.279404	-929.277635
61		-932.265275	-931.674129	-929.870284	1.25	-929.279138	-929.277146
62		-932.265691	-931.675106	-929.869398	1.3	-929.278813	-929.276741
18		-932.262441	-931.671620	-929.868907	1.25	-929.278086	-929.276094
3		-932.263599	-931.672752	-929.867876	0.68	-929.277029	-929.275945
11		-932.264023	-931.673166	-929.866920	0.25	-929.276063	-929.275664
84		-932.261739	-931.671219	-929.867507	0.83	-929.276986	-929.275664
15		-932.262439	-931.671744	-929.867598	0.9	-929.276903	-929.275469
90		-932.259869	-931.668931	-929.868179	1.35	-929.277241	-929.275090
44		-932.256791	-931.666843	-929.865284	0.55	-929.275336	-929.274459
103		-932.262536	-931.671875	-929.869183	2.57	-929.278522	-929.274427
24		-932.262878	-931.671605	-929.866768	0.72	-929.275495	-929.274347
85		-932.263894	-931.673230	-929.869220	2.7	-929.278556	-929.274253
70		-932.261751	-931.670817	-929.866431	1.08	-929.275497	-929.273776
60		-932.260404	-931.669408	-929.864619	0.85	-929.273623	-929.272269
39		-932.256972	-931.666930	-929.864384	1.56	-929.274342	-929.271856
40		-932.256972	-931.666930	-929.864384	1.56	-929.274342	-929.271856
36		-932.256900	-931.666625	-929.862979	0.8	-929.272703	-929.271428
78		-932.257787	-931.667183	-929.863427	2.45	-929.272823	-929.268918
97		-932.258278	-931.667419	-929.863172	2.31	-929.272313	-929.268632
1h-Ac⁺							
7	ac1	-1085.265916	-1084.620141	-1082.534275	-24.83	-1081.888500	-1081.928069
7	ac2	-1085.265916	-1084.620140	-1082.534275	-24.83	-1081.888499	-1081.928068
49	ac1	-1085.264081	-1084.618509	-1082.534323	-24.59	-1081.888751	-1081.927938

48	ac2	-1085.264081	-1084.618507	-1082.534323	-24.59	-1081.888750	-1081.927937
78	ac2	-1085.264081	-1084.618503	-1082.534329	-24.58	-1081.888751	-1081.927922
34	ac2	-1085.264589	-1084.618904	-1082.534414	-24.52	-1081.888729	-1081.927804
97	ac1	-1085.263339	-1084.617439	-1082.534699	-24.45	-1081.888800	-1081.927763
37	ac2	-1085.263339	-1084.617439	-1082.534699	-24.45	-1081.888799	-1081.927763
37	ac1	-1085.263339	-1084.617439	-1082.534697	-24.45	-1081.888798	-1081.927761
97	ac2	-1085.264551	-1084.618863	-1082.534380	-24.49	-1081.888691	-1081.927718
34	ac1	-1085.264551	-1084.618858	-1082.534377	-24.49	-1081.888684	-1081.927711
61	ac2	-1085.262641	-1084.617019	-1082.534355	-24.34	-1081.888733	-1081.927521
29	ac1	-1085.262641	-1084.617013	-1082.534358	-24.34	-1081.888730	-1081.927519
49	ac2	-1085.264174	-1084.618364	-1082.534312	-24.47	-1081.888502	-1081.927497
48	ac1	-1085.264174	-1084.618370	-1082.534312	-24.46	-1081.888507	-1081.927487
3	ac1	-1085.264171	-1084.618396	-1082.534265	-24.47	-1081.888490	-1081.927485
78	ac1	-1085.264175	-1084.618355	-1082.534313	-24.46	-1081.888493	-1081.927472
29	ac2	-1085.262645	-1084.616861	-1082.534254	-24.24	-1081.888470	-1081.927099
61	ac1	-1085.262644	-1084.616852	-1082.534256	-24.24	-1081.888464	-1081.927093
64	ac1	-1085.262863	-1084.617245	-1082.534038	-23.88	-1081.888420	-1081.926476
64	ac2	-1085.262821	-1084.617029	-1082.534127	-23.90	-1081.888336	-1081.926423
36	ac1	-1085.264411	-1084.618581	-1082.533066	-24.59	-1081.887236	-1081.926423
70	ac1	-1085.262812	-1084.617025	-1082.534122	-23.90	-1081.888335	-1081.926422
36	ac2	-1085.264411	-1084.618578	-1082.533067	-24.59	-1081.887234	-1081.926421
9	ac1	-1085.264411	-1084.618578	-1082.533067	-24.59	-1081.887234	-1081.926420
9	ac2	-1085.264411	-1084.618578	-1082.533067	-24.59	-1081.887234	-1081.926420
85	ac1	-1085.261796	-1084.615900	-1082.533640	-24.23	-1081.887744	-1081.926357
85	ac2	-1085.261796	-1084.615900	-1082.533640	-24.23	-1081.887744	-1081.926357
70	ac2	-1085.262929	-1084.617058	-1082.534044	-23.79	-1081.888174	-1081.926085
40	ac1	-1085.261489	-1084.616993	-1082.531337	-24.12	-1081.886841	-1081.925279
39	ac1	-1085.261483	-1084.617035	-1082.531221	-24.10	-1081.886774	-1081.925179
62	ac1	-1085.261505	-1084.615887	-1082.531588	-24.15	-1081.885970	-1081.924456
11	ac2	-1085.260903	-1084.616703	-1082.529286	-24.69	-1081.885086	-1081.924432
40	ac2	-1085.260969	-1084.616419	-1082.530516	-24.03	-1081.885966	-1081.924260
62	ac2	-1085.261522	-1084.615725	-1082.531324	-24.14	-1081.885527	-1081.923997
39	ac2	-1085.261519	-1084.615716	-1082.531336	-24.13	-1081.885532	-1081.923986
44	ac1	-1085.260718	-1084.616142	-1082.530322	-23.84	-1081.885745	-1081.923737
44	ac2	-1085.260804	-1084.616039	-1082.530209	-23.90	-1081.885444	-1081.923531
18	ac2	-1085.258454	-1084.612666	-1082.530417	-24.20	-1081.884629	-1081.923194
18	ac1	-1085.258456	-1084.612395	-1082.530400	-24.21	-1081.884339	-1081.922920
103	ac2	-1085.259352	-1084.613363	-1082.532555	-22.75	-1081.886566	-1081.922820
11	ac1	-1085.261055	-1084.615165	-1082.529333	-24.70	-1081.883443	-1081.922805
15	ac2	-1085.259094	-1084.613288	-1082.529485	-24.54	-1081.883679	-1081.922786
15	ac1	-1085.259104	-1084.613472	-1082.529491	-24.42	-1081.883860	-1081.922775
103	ac1	-1085.259369	-1084.613313	-1082.532542	-22.72	-1081.886486	-1081.922693
3	ac2	-1085.259822	-1084.614063	-1082.529602	-24.37	-1081.883843	-1081.922679
90	ac1	-1085.258084	-1084.612235	-1082.531866	-22.82	-1081.886017	-1081.922383
24	ac1	-1085.259526	-1084.613586	-1082.529353	-24.42	-1081.883414	-1081.922329
24	ac2	-1085.259541	-1084.613451	-1082.529344	-24.42	-1081.883254	-1081.922170

90	ac2	-1085.258050	-1084.612082	-1082.531967	-22.69	-1081.886000	-1081.922158
60	ac2	-1085.257466	-1084.611582	-1082.527388	-23.92	-1081.881505	-1081.919623
60	ac1	-1085.257429	-1084.611476	-1082.527322	-23.91	-1081.881368	-1081.919472

Additional calculations on the G3MP2B3-level have been performed for the best conformations for every catalyst. The results are given in Table 5.15.

Table 5.16. Calculated energies of selected conformers for catalysts **1a** – **1h**, as calculated at G3MP2B3 level of theory.

Conf	MP2(FC)/G3MP2 Large	MP2(FC)/6-31G(d)	QCISD(T)/6-31G(d)	E _{tot} G3MP2B3	H ₂₉₈ G3MP2B3
Pyr					
1	-247.743288	-247.480917	-247.549940	-247.812311	-247.718172
Pyr-Ac⁺					
1.ac1	-400.461686	-400.042094	-400.145167	-400.564760	-400.416452
1a					
1	-381.426640	-380.994471	-381.105670	-381.537838	-381.365836
1a-Ac⁺					
1.ac1	-534.179287	-533.590508	-533.736587	-534.325366	-534.098512
1b					
1	-420.647244	-420.163547	-420.290752	-420.774449	-420.572577
1b-Ac⁺					
1.ac1	-573.401787	-572.761082	-572.923180	-573.563885	-573.307078
1.ac2	-573.401825	-572.761099	-572.923205	-573.563930	-573.306856
1c					
2	-459.864610	-459.328721	-459.471985	-460.007873	-459.778963
4	-459.867600	-459.332188	-459.475461	-460.010873	-459.778359
5	-459.866988	-459.331545	-459.474772	-460.010214	-459.775670
10	-459.859945	-459.326362	-459.468987	-460.002570	-459.775681
12	-459.864144	-459.328336	-459.471765	-460.007574	-459.771592
1c-Ac⁺					
2.ac1	-612.620092	-611.926956	-612.105155	-612.798291	-612.515775
2.ac2	-612.620139	-611.926978	-612.105177	-612.798338	-612.515775
4.ac1	-612.624426	-611.931767	-612.109807	-612.802466	-612.515770
4.ac2	-612.624427	-611.931767	-612.109807	-612.802467	-612.514142
5.ac1	-612.622920	-611.930223	-612.108264	-612.800961	-612.514141
5.ac2	-612.622920	-611.930223	-612.108264	-612.800961	-612.514139
10.ac1	-612.622920	-611.932233	-612.108265	-612.798952	-612.514138
10.ac2	-612.622920	-611.930223	-612.108265	-612.800962	-612.512129
12.ac1	-612.622919	-611.930223	-612.108265	-612.800961	-612.511385
12.ac2	-612.622920	-611.930223	-612.108265	-612.800962	-612.511301
1d					
37	-538.304079	-537.664430	-537.839791	-538.479440	-538.187672
1d-Ac⁺					
37.ac1	-691.061455	-690.264508	-690.474739	-691.271686	-690.924950

1e					
37	-616.739297	-615.996176	-616.204117	-616.947239	-616.595678
1e-Ac⁺					
37.ac1	-769.497867	-768.597309	-768.840086	-769.740644	-769.334256
1f					
37	-695.174685	-694.327902	-694.568382	-695.415165	-695.003958
1f-Ac⁺					
37.ac1	-847.933799	-846.929534	-847.204868	-848.209132	-847.743037
1g					
37	-773.609585	-772.659269	-772.932352	-773.882668	-773.411657
1g-Ac⁺					
37.ac1	-926.369072	-925.261247	-925.569174	-926.676999	-926.151110

In order to explore the similarities and differences of the preferred conformations in **1a** - **1h** the following part shows the conformational analysis of the five best conformations of these catalyst systems. Figure 5.25 shows the terminology for the evaluation of the different conformations whereas Table 5.17 shows the results of the evaluation.

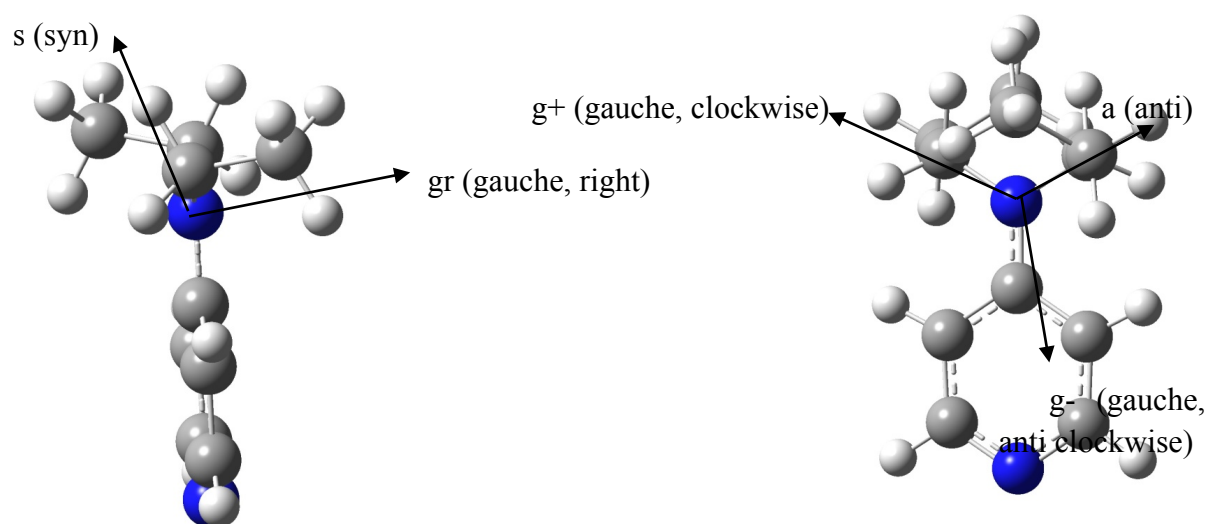


Figure 5.25. Terminology for the conformational analysis on the example of the preferred conformation for **1c** with tw = twisted; oop = out of plane.

As can be seen in Figure 5.25 the preferred conformation for longer alkyl groups in **1c** – **1h** is a “twisted” gauche conformation. As this is true for all catalyst conformations this conformation was named for reasons of simplicity “g” (=gauche). For the assignment of the conformers the pyridine ring was adjusted to a position shown in Figure 5.25 left where the pyridine ring heads out of the plane. If the alkyl group points to the right hand side the assignment is “gr” and in reverse “gl”. Afterwards the pyridine ring is turned like shown in Figure 5.25 right and the relative orientation of the alkyl chain towards the nitrogen in 4-position is determined. Finally the carbon-carbon bonds are analysed with g=gauche, a=anti and s=syn. Table 5.17 shows the results in that way, that every column show an additional C-atom beginning from the C-atom next to the nitrogen in 4-position.

Table 5.17. Conformational analysis of the DMAP-derivatives **1b** – **1h** and acylated derivatives **11b** – **11h**.

system	conformer	Orientation of C-atom							
		2		3	4	5	6	7	8
1b	1	gr							
11b	1ac1	gr							
	1ac2	gr							
1c	4	gr	gr						
	5	gr	gl						
	2	gl	s						
	12	gr	gl,s,tw						
	10	oop,a	oop,a						
11c	4ac1	gr	gr						
	4ac2	gr	gr						
	12ac2	gr	gl						
	12ac1	gr	gl						
	5ac1	gr	gl						
1d	37	gl	gl	g+	g+				
	34	gr	gr	g+	a				
	29	gr	gr	g-	g+				
	7	gl	gl	a	a				
	48	gr	gr	g+	a				
11d	7ac1	gl	gl	a	a				
	7ac2	gl	gl	a	a				
	37ac1	gl	gl	g+	g+				
	37ac2	gl	gl	g+	g+				
	3ac2	gl	gl	a	g-				
1e	37	gl	gl	g+	g+	a	a		
	34	gr	gr	g+	a	a	a		
	7	gl	gl	a	a	a	a		
	49	gl	gl	g-	a	a	a		
	48	gr	gr	a	g-	a	a		
11e	37ac2	gl	gl	g+	g+	a	a		
	37ac1	gl	gl	g+	g+	a	a		
	49ac1	gl	gl	a	g-	a	a		
	7ac1	gl	gl	a	a	a	a		
	7ac2	gl	gl	a	a	a	a		
1f	37	gl	gl	g+	g+	a	a	a	
	34	gr	gr	g+	a	a	a	a	
	7	gl	gl	a	a	a	a	a	
	49	gl	gl	g-	a	a	a	a	
	48	gr	gr	a	g-	a	a	a	
11f	7ac2	gl	gl	a	a	a	a	a	
	7ac1	gl	gl	a	a	a	a	a	
	37ac1	gl	gl	g+	g+	a	a	a	
	97ac1	gr	gr	g+	g+	a	a	a	

1g	37ac2	gl	gl	g+	g+	a	a	a		
	37	gl	gl	g+	g+	a	a	a	a	
	34	gr	gr	g+	a	a	a	a	a	
	7	gl	gl	a	a	a	a	a	a	
	49	gl	gl	g-	a	a	a	a	a	
11g	48	gr	gr	a	g-	a	a	a	a	
	37ac2	gl	gl	g+	g+	a	a	a	a	
	37ac1	gl	gl	g+	g+	a	a	a	a	
	97ac2	gl	gl	g+	g+	a	a	a	a	
	7ac1	gr	gr	a	a	a	a	a	a	
1h	7ac2	gl	gl	a	a	a	a	a	a	
	37	gl	gl	g+	g+	a	a	a	a	a
	34	gr	gr	g+	a	a	a	a	a	a
	7	gl	gl	a	a	a	a	a	a	a
	48	gr	gr	g-	a	a	a	a	a	a
11h	9	gl	gr	a	a	a	a	a	a	a
	7ac1	gl	gl	a	a	a	a	a	a	a
	7ac2	gl	gl	a	a	a	a	a	a	a
	49ac1	gl	gl	g-	a	a	a	a	a	a
	48ac2	gr	gr	g-	a	a	a	a	a	a
	78ac2	gl	gl	g-	a	a	a	a	a	a

Table 5.17 shows that the preferred conformation of all unacylated catalyst systems **1d** – **1h** is “gl, gl, g+, g+”. Figure 5.26 shows this conformation for **1d** from front view (left) and top view (right). Figure 5.27 shows the same preferred conformation for **1f** were now 5 C-atoms are on every side of the nitrogen atom.

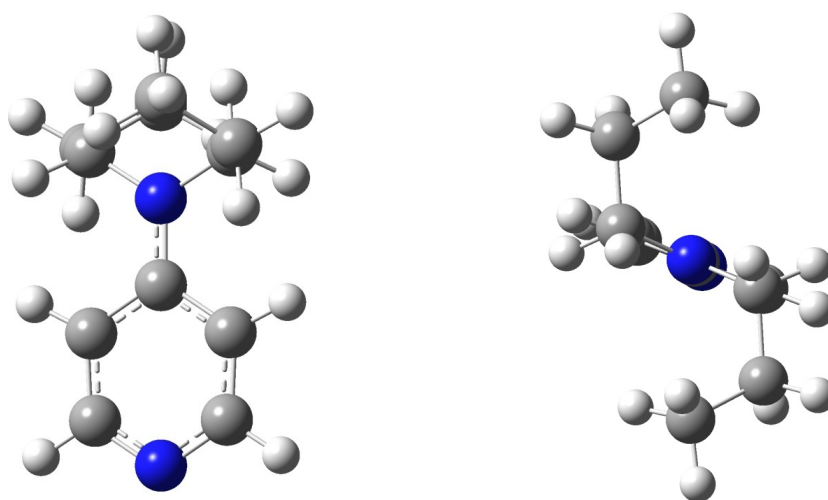


Figure 5.26. Preferred conformation for the unacylated catalyst **1d** from front view (right) and top view (left).

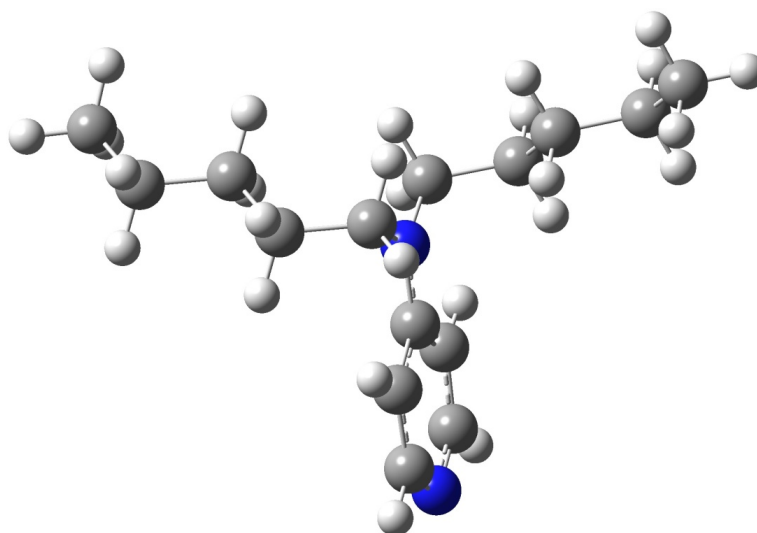


Figure 5.27. Another view for the preferred conformation now for **1f**.

5.6 References

- [1] a) O. Exner, *J. Phys. Org. Chem.* **1999**, *12*, 265 – 274; b) M. Charton, *J. Phys. Org. Chem.* **1999**, *12*, 275–282; c) V. Galkin, *J. Phys. Org. Chem.* **1999**, *12*, 283–288; d) O. Exner, M. Charton, V. Galkin, *J. Phys. Org. Chem.* **1999**, *12*, 289.
- [2] a) V. D'Elia, Y.-H. Liu, H. Zipse, *Eur. J. Org. Chem.* **2011**, 1527–1533; b) I. Held, E. Larionov, C. Bozler, F. Wagner, H. Zipse, *Synthesis* **2009**, 2267–2277; c) I. Held, P. von den Hoff, D. S. Stephenson, H. Zipse, *Adv. Synth. Catal.* **2008**, *350*, 1891–1900; d) I. Held, S. Xu, H. Zipse, *Synthesis* **2007**, 1185–1196; e) M. R. Heinrich, H. S. Klisa, H. Mayr, W. Steglich, H. Zipse, *Angew. Chem.* **2003**, *115*, 4975–4977; *Angew. Chem. Int. Ed.* **2003**, *42*, 4826–4828.
- [3] N. De Rycke, F. Couty, O. R. P. David, *Chem. Eur. J.* **2011**, *17*, 12852–12871 and references cited therein.
- [4] C. Pedersen, *Synthesis* **1978**, 844–845.
- [5] a) S. Xu, I. Held, B. Kempf, H. Mayr, W. Steglich, H. Zipse, *Chem. Eur. J.* **2005**, *11*, 4751–4757; b) T. A. Nigst R. Tandon, H. Mayr, H. Zipse, manuscript in preparation; c) T. A. Nigst, H. Mayr, *Eur. J. Org. Chem.* **2013**, accepted.
- [6] A.R. Cherkasov, V. I. Galkin, R. A. Cherkasov, *Russ. Chem. Rev.* **1996**, *65*, 641–656.
- [7] a) M. Charton, *J. Org. Chem.* **1979**, *44*, 903; b) M. Charton, *J. Am. Chem. Soc.* **1977**, *99*, 5687.
- [8] a) B. I. Istomin, V. A. Baranskii, *Russ. Chem. Rev.* **1982**, *52*, 223; b) M. I. Kabachnik, *Russ. Chem. Rev.* **1979**, *48*, 814.
- [9] J. Jerchel, *Chem. Ber.* **1958**, *91*, 1266.

- [10] C. Pedersen, *Synthesis* **1978**, 844.
- [11] D. J. Brunelle, D. A. Singleton, *Tetrahedron Lett.* **1984**, 25, 3383.
- [12] K. Ko, K. Nakano, S. Watanabe, Y. Ichikawa, H. Kotsuki, *Tetrahedron Lett.* **2009**, 50, 4025–4029.
- [13] L. Pauling, *J. Am. Chem. Soc.* **1932**, 54, 3570–3582.
- [14] B. Cordero, V. Gómez, A. E. Platero-Prats, M. Revés, J. Echeverría, E. Cremades, F. Barragán, S. Alvarez, *Dalton Trans.* **2008**, 21, 2832–2838.
- [15] Y. Wei, T. Singer, H. Mayr, G. N. Sastry, H. Zipse, *J. Comp. Chem.* **2008**, 29, 291–297.
- [16] Y. Wei, G. N. Sastry, H. Zipse, *J. Am. Chem. Soc.* **2008**, 130, 3473–3477.
- [17] L. A. Curtiss, K. Raghavachari, P. C. Redfern, V. Rassolov, J. A. Pople, *J. Chem. Phys.* **1998**, 109, 7764–7776.
- [18] A. G. Baboul, L. A. Curtiss, P. C. Redfern, K. Raghavachari, *J. Chem. Phys.* **1999**, 110, 7650–7657.
- [19] Gaussian 03, Revision D.01, M. J. Frisch, G. W. Trucks, H.B. Schlegel, G. E. Scuseria, M. A. Robb, J. R. Cheeseman, J. A. Montgomery, Jr., T. Vreven, K. N. Kudin, J. C. Burant, J. M. Millam, S. S. Iyengar, J. Tomasi, V. Barone, B. Mennucci, M. Cossi, G. Scalmani, N. Rega, G. A. Petersson, H. Nakatsuji, M. S3Hada, M. Ehara, K. Toyota, R. Fukuda, J. Hasegawa, M. Ishida, T. Nakajima, Y. Honda, O. Kitao, H. Nakai, M. Klene, X. Li, J.E. Knox, H. P. Hratchian, J. B. Cross, V. Bakken, C. Adamo, J. Jaramillo, R. Gomperts, R. E. Stratmann, O. Yazyev, A. J. Austin, R. Cammi, C. Pomelli, J. W. Ochterski, P. Y. Ayala, K. Morokuma, G. A. Voth, P. Salvador, J. J. Dannenberg, V. G. Zakrzewski, S. Dapprich, A. D. Daniels, M. C. Strain, O. Farkas, D. K. Malick, A. D. Rabuck, K. Raghavachari, J. B. Foresman, J. V. Ortiz, Q. Cui, A. G. Baboul, S. Clifford, J. Cioslowski, B. B. Stefanov, G. Liu, A. Liashenko, P. Piskorz, I. Komaromi, R. L. Martin, D.J. Fox, T. Keith, M. A. Al-Laham, C. Y. Peng, A. Nanayakkara, M. Challacombe, P. M. W. Gill, B. Johnson, W. Chen, M. W. Wong, C. Gonzalez, and J. A. Pople, Gaussian, Inc., Wallingford CT, 2004.

Chapter 6

Inductive Effects in DMAP–Polymers

In order to keep consistency in numbering, all catalysts and the supported variants will be titled as follows:

First the number of the catalyst ground structure is given, e.g. **1e** as mentioned in the section ‘General Comments’. To name the supported catalyst based on the motif of **1e**, the letter **p** (p = polymer) is added to the name of the catalyst making immobilized **1e** to **1ep**. If a clicked homogeneous phase catalyst based on the same motif exists, the letter **h** (h = homogeneous) is added making the clicked, but homogeneous phase catalyst derived from **1e** to **1eh** (see Figure 6.1).

6.1 Introduction

The aim of organocatalysis has always been to complement the options provided by conventional metal-based catalysts. However, the synthesis and production of organocatalysts is not just time consuming, but also expensive. Therefore recoverable catalysts are quite attractive. One way to ensure some degree of recoverability is the ‘immobilization’ of a catalyst on the surface of polymeric beads or inorganic particles through covalent binding. Since most catalytic processes take place in solution, polymerbound catalysts can easily be recovered through filtration, regenerated by washing with different solvents and successively reused.^[1] The copolymerization of DMAP-functionalized styrene is an established way to obtain polymer supported DMAP (**1p**), which is already commercially available.^[2,3] Usually the immobilized catalysts can be reused with no noteworthy detriment of activity for several times. Other variants of recoverable DMAP derivatives are e.g. microencapsulated DMAP polymer^[4], silica-coated magnetic nanoparticles^[5,6] or mesoporous silica nanospheres, in which DMAP is immobilized^[7]. Since the activity of DMAP polymer (**1p**) is dramatically decreased compared to the homogeneous catalyst, the area of application is restricted. It was, for example, reported that **1p** is not effective in the synthesis of *tert*-butyl esters using DCC^[2a]. But certainly it is still active enough to catalyze standard esterifications or the Baylis-Hillman reaction^[2,8].

6.2 Results and Discussion

Since it was already shown in Chapter 5 that the catalytic performance of DMAP (**1a**) can be increased by means of introducing additional inductive effects, we wanted to test if that is also true for DMAP polymer (**1p**). The dialkylated 4-aminopyridines show a saturation of substituent effects with alkyl group chain lengths beyond four carbon atoms (**1e**), thus our catalyst motif for the polymer supported catalyst **1ep** is based on catalyst **1e** (see Figure 6.1). The immobilization of highly active catalysts like **6b** was already performed by D’Elia *et al.*, whose immobilized variants (**6bp₁**, **bp₂**) show outstanding reactivity.^[9]

The synthesis of polymer supported catalyst **1ep** is realized by using a borane protection group, which facilitates the S_N2 reaction with **10** (Scheme 6.1). The copper-catalyzed Huisgen reaction was used to attach the catalytically active catalyst part to the polystyrene support. To perform the click reaction a 1% cross-linked Merrifield resin was modified with a terminal azide group. In parallel the homogeneous phase catalyst **1eh** was synthesized according to the same protocols.

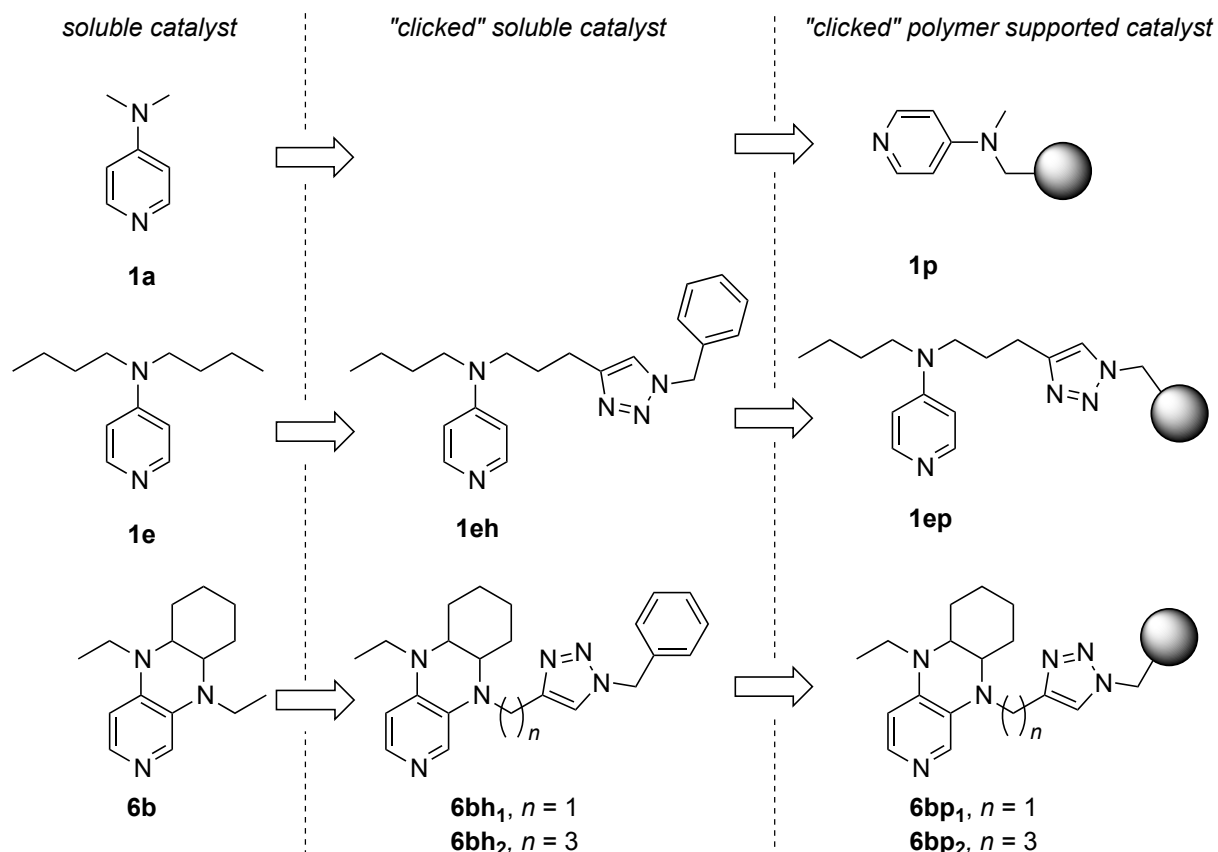
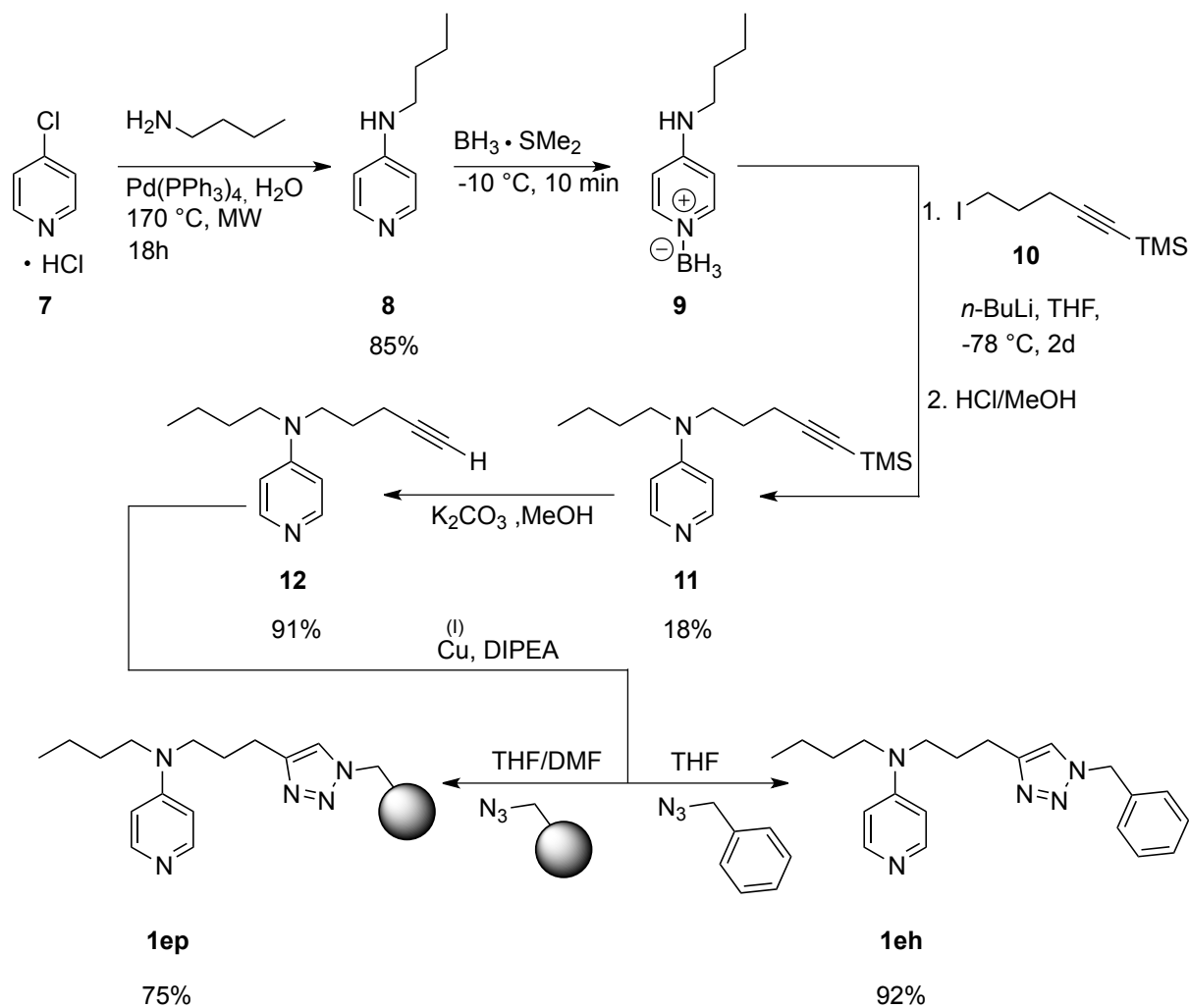


Figure 6.1. Polymer supported DMAP (**1p**) and synthesized DMAP polymer with increased chain length **1ep**.

The catalytic potential of the synthesized immobilized catalyst (**1ep**) as well as that of the soluble counterpart has been explored in the acetylation of tertiary alcohol **16** (reaction (I), Scheme 6.2). The reactions were followed by ^1H NMR spectroscopy in CDCl_3 as the solvent. All reactions eventually proceed to full conversion and the rate of reaction can thus be characterized by the reaction half-life $t_{1/2}$ using an approach described previously.^[10]



Scheme 6.1. Synthesis of immobilized catalyst and soluble counterpart.

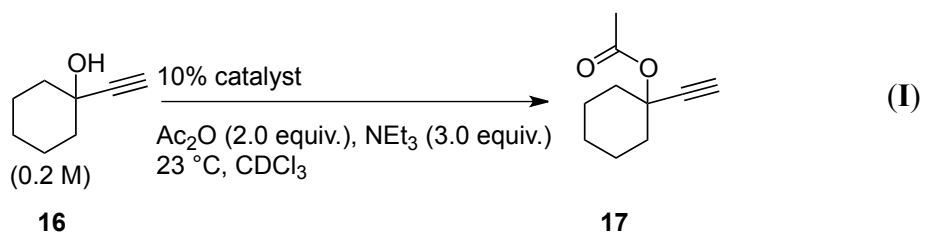
Scheme 6.2. ^1H NMR benchmark reaction in CDCl_3 .

Table 6.1. Catalytic activity of soluble and immobilized catalysts based on the DMAP-motif.

Entry	Catalyst	$t_{1/2}$ [min] ^[a]
<i>Soluble catalysts</i>		
1	1a	151.0 ± 1.7 ^[b]
2	1e	58.7 ± 1.6
3	6b	18.0 ± 0.5 ^[b]
4	1eh	91.9 ± 0.8
5	6bh₁	16.0 ± 0.1 ^[c]
6	6bh₂	18.0 ± 0.1 ^[c]
<i>Immobilized catalysts</i>		
7	1p	504.0 ± 8.0 ^[c]
8	1ep	452.0 ± 19.0
9	6bp₁	166.0 ± 3.0 ^[c]
10	6bp₂	58.0 ± 2.0 ^[c]

[a] Kinetic half-life times for benchmark reaction (**I**); [b] Data from ref. 10; [c] Data from ref. 9.

The data in Table 6.1 indicate that all immobilized catalysts are less reactive than their soluble counterparts. This common phenomenon is due to changes in the micro-environment of the catalyst and on the increased difficulty for the reactants to diffuse to the catalytically active center.^[10] A longer linker facilitates the substrate diffusion to the active site of the catalyst and has thus beneficial effects on the catalyst activity as entries 9 and 10 show. In case of **1ep** the linker length is equally to that of **6bp₂** and thus should be sufficient. Actually **1ep** shows dramatically increased (8-fold) half-life times (slowing the reaction down) compared to **6bp₂**. In comparison the ‘clicked’ soluble catalyst **1eh** is just 5-times less active than **6bh₂**. Interestingly the ‘clicked’ triazolyl residue has no effect on the activity on 3,4-diaminopyridine derived catalysts (comparing entries 3, 5 and 6) whereas the same residue causes a 1.5-fold loss in reactivity for **1e** (entries 2 and 4). Comparing the polymer supported **1ep** with the commercially available DMAP-polymer (**1p**) the increase in reactivity through inductive effects by means of additional alkyl groups is small (0.1 fold) compared to the effect obtained for the soluble counterparts in Chapter 5 (2.5 fold). With DMAP-polymer being commercially available and almost equally active, recyclability studies of the immobilized catalyst **1ep** show little promise. Catalysts **6bp₁**, **bp₂** were used repeatedly with no noteworthy reactivity loss.^[10]

6.3 Conclusion

DMAP-derivative **1e** was successfully immobilized on polystyrene support using a copper-catalyzed Huisgen reaction. Catalyst **1ep** showed only a 0.1 fold increased reactivity compared to DMAP polymer (**1p**). The additional inductive effects are thus not sufficient enough to obtain similar results like in the homogeneous catalysis, or diffusion control is too strongly restricted.

6.4 Experimental Part

General information

All air and water sensitive manipulations were carried out under a nitrogen atmosphere using standard Schlenk techniques. Calibrated flasks for kinetic measurements were dried in the oven at 120 °C for at least 12 hours prior to use and then assembled quickly while still hot, cooled under a nitrogen stream and sealed with a rubber septum. All commercial chemicals were of reagent grade and were used as received unless otherwise noted. CDCl₃ was refluxed for at least one hour over CaH₂ and subsequently distilled. ¹H and ¹³C NMR spectra were recorded on Varian 300 or Varian INOVA 400 and 600 machines at room temperature. All ¹H chemical shifts are reported in ppm (δ) relative to TMS (0.00); ¹³C chemical shifts are reported in ppm (δ) relative to CDCl₃ (77.16). ¹H NMR kinetic data were measured on a Varian Mercury 200 MHz spectrometer at 23 °C. HRMS spectra (ESI-MS) were carried out using a Thermo Finnigan LTQ FT instrument. IR spectra were measured on a Perkin-Elmer FT-IR BX spectrometer mounting ATR technology. Analytical TLC's were carried out using aluminum sheets silica gel Si 60 F254. For catalyst synthesis synthetic strategies according to D'Elia *et al.*^[10] were applied.

Conduction and Evaluation of Kinetic Measurements

Homogeneous phase catalysis

The kinetic measurements with soluble catalysts were performed according to the procedures described in Chapter 3.4.

Heterogeneous phase catalysis (according to D'Elia *et al.*^[10])

In dry CDCl₃ two stock solutions were prepared in calibrated 10 mL flasks. One containing the anhydride (1.2 M) and one containing the alcohol (0.6 M) and NEt₃ (1.8 M). In a dry 50 mL flask the two solutions were mixed under inert gas atmosphere and 10 mL of dry CDCl₃

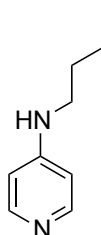
were added in order to adjust the concentration of the reagents to that used in the case of the soluble catalysts. Subsequently the appropriate amount of resin was added and the reaction vessel was shaken at room temperature at 480 turns/min with a rubber septum on top. The mechanical shaker was interrupted for about one minute in defined time intervals until the resin floated on top of the solution (see Figure 6.2), and 100 μL of a solid-free sample from the bottom of the reaction mixture were taken using a syringe. In a dry NMR tube 80 μL of this solution were placed and diluted with 0.8 mL of dry CDCl_3 . The sample was measured on a 200 MHz NMR spectrometer and the evaluation of kinetic data performed according to Chapter 3.4.



Figure 6.2. Resin floats on top of the reaction mixture in order to take a solid-free sample.

Catalyst Synthesis

N-Butylpyridin-4-amine (**8**)



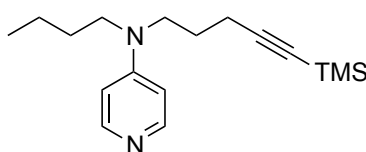
In a 10 mL microwave vial 4.00 g (26.66 mmol) **7** were dissolved in 2 mL of water. To that yellow solution 3.30 mL (133.30 mmol) butylamine were added together with 0.15 g (0.26 mmol) $\text{Pd}(\text{PPh}_3)_4$. The reaction mixture was heated at 170 $^{\circ}\text{C}$ for 18 hours in the microwave. After the reaction completed, NaOH was added until pH=12 was reached. Subsequently the mixture was extracted three times with DCM, the combined organic layers dried over MgSO_4 and the solvents removed under reduced pressure. Column chromatography of the crude reaction mixture using silica ($\text{CHCl}_3/\text{MeOH}$ 15:1) yields 3.40 g (85 %) of **8** as bright yellow solid.

^1H NMR (300 MHz, CDCl_3): δ = 8.19 (dd, 3J = 4.9 Hz, 3J = 1.5 Hz, 2H), 6.44 (dd, 3J = 4.9 Hz, 3J = 1.6 Hz, 2H), 4.24 (s, br, 1H, NH), 3.16 (td, 3J = 7.1 Hz, 3J = 5.6 Hz, 2H), 1.52 – 1.71 (m, 2H), 1.44 (dq, 3J = 13.9 Hz, 3J = 7.1 Hz, 2H), 1.06 – 0.78 (m, 3H).

^{13}C -NMR (75 MHz, CDCl_3): δ = 13.8, 20.2, 31.2, 42.4, 107.4, 149.8, 153.5.

HRMS (EI): calculated for: $\text{C}_9\text{H}_{14}\text{N}_2$ $[\text{M}]^+$ 150.1157, found: 150.1145.

N-Butyl-*N*-(5-(trimethylsilyl)pent-4-yn-1-yl)pyridin-4-amine (**11**)

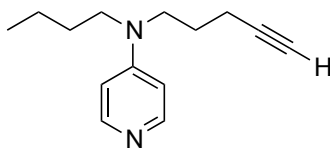


In a 50 mL Schlenk flask 2.00 g (13.3 mmol) **8** were dissolved in dry THF and cooled to -10 °C. To that solution 6.60 mL (13.30 mmol) of a 2 M $\text{BH}_3\text{Me}_2\text{S}$ solution in THF were added dropwise. After stirring the mixture for 10 minutes at room temperature it was cooled to -78 °C. At this temperature 5.87 mL (2.5 M, 14.63 mmol) *n*-BuLi were added dropwise and after 15 min the reaction was allowed to warm to 0 °C. At this temperature 3.18 mL of **10** (15.23 mmol) were added and the reaction was stirred at room temperature for 48 hours. The yellow solution was quenched by the careful addition of 3 mL EtOH. The solvent was removed under reduced pressure and the remaining material dissolved in 20 mL MeOH and 1.1 eq. of 12 M HCl (1.08 mL, 13.4 mmol) were added at 0 °C. The solvent was removed at reduced pressure and the residue dissolved in DCM and extracted with K_2CO_3 . The combined organic layers were dried over MgSO_4 , filtered and the solvent removed under reduced pressure. The raw material was purified by column chromatography on silica (EtOAc/TH/NEt₃ 20:20:1) and 0.65 g (18%) of **11** together with 0.53 g starting material was obtained.

^1H NMR (300 MHz, CDCl_3): δ = 8.19 (d, 3J = 6.6 Hz, 2H), 6.51 (d, 3J = 6.7 Hz, 2H), 3.53 – 3.41 (m, 2H), 3.38 – 3.24 (m, 2H), 2.30 (t, 3J = 6.7 Hz, 2H), 1.90 – 1.75 (m, 2H), 1.68 – 1.51 (m, 2H), 1.47 – 1.32 (m, 2H), 0.99 (t, 3J = 7.3 Hz, 3H, CH_3), 0.25 – 0.01 (s, 9H, SiMe_3).

^{13}C -NMR (75 MHz, CDCl_3): δ = 0.1, 13.9, 17.3, 20.2, 25.5, 29.1, 48.7, 49.9, 85.8, 105.9, 106.5, 149.8, 152.5.

HRMS (EI): calculated for: $\text{C}_{17}\text{H}_{28}\text{N}_2\text{Si}$ $[\text{M}]^+$ 288.2022, found: 288.2017.

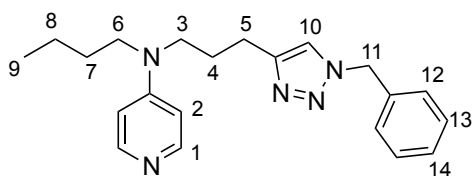
N-Butyl-*N*-(pent-4-yn-1-yl)pyridin-4-amine (**12**)

Compound **11** (0.42 g, 1.45 mmol) was dissolved in 7 mL MeOH and 0.30 g K₂CO₃ (2.18 mmol) were added. The reaction mixture was stirred at room temperature for 24 hours. After the reaction was complete (TLC), the solvent was removed under reduced pressure and the crude mixture partitioned between water (30 mL) and DCM (60 mL). The aqueous layer was washed three times with DCM (20 mL), and the combined organic layers were dried over MgSO₄, filtered, and concentrated under reduced pressure to afford the title compound (**12**) as a yellow oil in 91 % yield (0.29 g).

¹H NMR (300 MHz, CDCl₃): δ = 8.20 (d, ³*J* = 6.5 Hz, 2H), 6.50 (d, ³*J* = 5.1 Hz, 2H), 3.51 – 3.41 (m, 2H), 3.40 – 3.29 (m, 2H), 2.28 (td, ³*J* = 6.7 Hz, ³*J* = 2.6 Hz, 2H), 2.06 (t, ³*J* = 2.6 Hz, 1H), 1.83 (dt, ³*J* = 13.6 Hz, ³*J* = 6.8 Hz, 2H), 1.60 (dt, ³*J* = 11.8 Hz, ³*J* = 7.4 Hz, 2H), 1.38 (dq, ³*J* = 14.4 Hz, ³*J* = 7.3 Hz, 2H), 0.99 (t, ³*J* = 7.3 Hz, 3H).

¹³C-NMR (75 MHz, CDCl₃): δ = 13.9, 15.9, 20.2, 25.5, 29.0, 48.8, 50.0, 69.4, 83.1, 106.5, 149.5, 152.6.

HRMS (EI): calculated for: C₁₄H₂₀N₂ [M]⁺ 216.1628, found: 216.1616.

N-(3-(1-Benzyl-1*H*-1,2,3-triazol-4-yl)propyl)-*N*-butylpyridin-4-amine (**1eh**)

In an oven dried Schlenk tube 0.19 g (0.87 mmol) of compound **12** were dissolved in 5 mL dry THF and degassed. Subsequently benzylazide (0.15 g, 1.13 mmol), *N,N*-diisopropylethylamine (0.29 mL, 1.74 mmol) and Cu(PPh₃)₃Br (0.09 g, 0.09 mmol) were added and the resulting yellow solution was stirred for 24 hours. Then the solution was partitioned between 20 mL DCM and 10 mL saturated K₂CO₃ solution. The aqueous layer

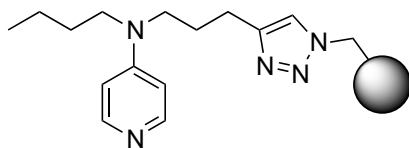
was washed with 10 mL DCM, and the combined organic layers dried over MgSO_4 , filtered, and concentrated under reduced pressure to yield an oil that was purified by column chromatography on silica gel ($\text{EtOAc}/\text{IH}/\text{NEt}_3$ 20:10:1) to afford 0.28 g of **1eh** (92%).

^1H NMR (300 MHz, CDCl_3): δ = 8.14 (d, 3J = 5.0 Hz, 2H, H-1), 7.49 – 7.34 (m, 3H, H-13, H-14), 7.32 – 7.25 (m, 2H, H-12), 7.21 (s, 1H, H-10), 6.39 (d, 3J = 5.0 Hz, 2H, H-2), 5.52 (s, 2H, H-11), 3.42 – 3.33 (m, 2H, H-3), 3.32 – 3.20 (m, 2H, H-6), 2.75 (t, 3J = 7.5 Hz, 2H, H-5), 2.09 – 1.91 (m, 2H, H-4), 1.63 – 1.48 (m, 2H, H-7), 1.45 – 1.22 (2H, H-8), 0.96 (t, 3J = 7.3 Hz, 3H, H-9).

^{13}C -NMR (75 MHz, CDCl_3): δ = 13.9, 20.2, 23.0, 26.5, 29.0, 49.3, 49.9, 54.1, 106.4, 120.6, 128.0, 128.8, 129.1, 134.8, 147.5, 149.9, 152.4.

HRMS (EI): calculated for: $\text{C}_{21}\text{H}_{27}\text{N}_5$ $[\text{M}]^+$ 349.2266, found: 349.2255.

Supported catalyst **1ep**



0.43 g (1.23 mmol) polystyrene-azide were suspended in an anhydrous THF/DMF mixture (7 mL/5 mL), and the suspension was degassed. Subsequently compound **12** (0.40 g, 1.85 mmol), 10 mol-% of $\text{Cu}(\text{PPh}_3)_3\text{Br}$ (0.18 g, 0.19 mmol) and *N,N*-diisopropylethylamine (0.63 mL, 3.70 mmol) were added. While keeping the reaction mixture under a constant flow of nitrogen, the reaction vessel was rotated in a water bath at 40 °C for 48 h. In that time the color of the suspension turned green. The resin was filtered and washed with DMF (80 mL), water/DMF (1:1; 80 mL), water (80 mL), water/MeOH (1:1; 80 mL), MeOH (80 mL), THF/MeOH (1:1; 80 mL), and finally THF (150 mL). The obtained green resin was dried under vacuum at 60 °C for 72 h to obtain **1ep** in 75% yield (0.51 g) as determined by elemental analysis. The FTIR spectrum showed the disappearance of the azide stretching band at 2091 cm^{-1} and the presence of new absorption bands at $\tilde{\nu} = 1595, 1514, 1366, 1223, 1016\text{ cm}^{-1}$, belonging to the backbone of the supported catalyst. Elemental analysis: found C 76.20, H 7.66, N 9.23. To verify the propriety of the elemental analysis the same sample was remeasured and gave: C 76.24, H 7.50, N 9.20. On the basis of the nitrogen content it was possible to calculate a loading of 1.31 mmol/g catalyst and an efficiency of 75% for the ‘click reaction’.

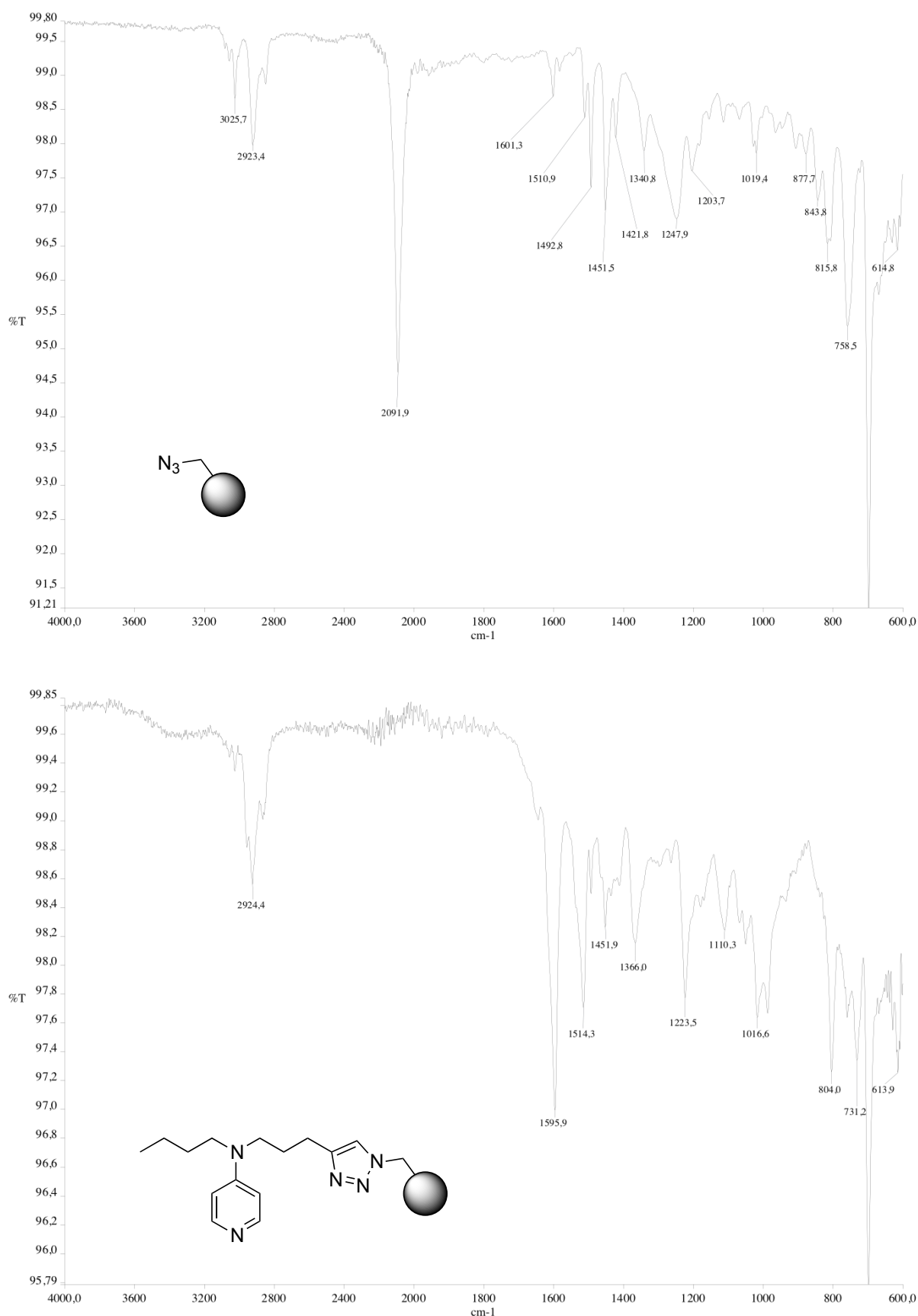
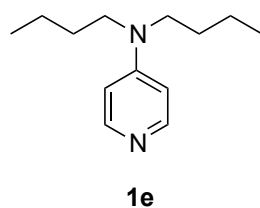


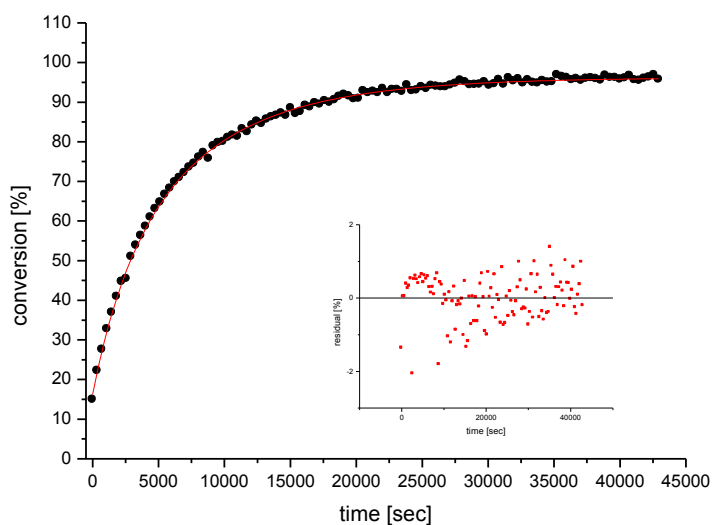
Figure 6.3. FTIR spectra of polystyrene-azide (top) and supported catalyst **1ep** (bottom).

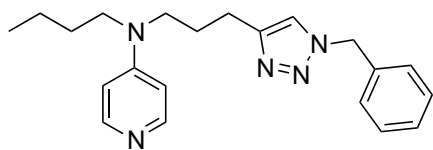
Data of Kinetic Runs

Kinetics of the reactions of catalysts **1e**, **1eh**, **1ep** with alcohol **16** at 10 mol-% catalyst loading. All time specifications are in minutes if not stated differently. For every measurement the experimental data and the fit curve together with the residuals are depicted. The time window was chosen until the appearance of saturation at full conversion, depending on the speed of the catalyst. As the catalysts measured are too different in terms of activity, it was not possible to compare the same time window for every catalyst. Every experiment was done at least twice and the resulting kinetic half-life times are given with standard deviations.



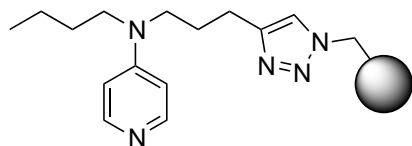
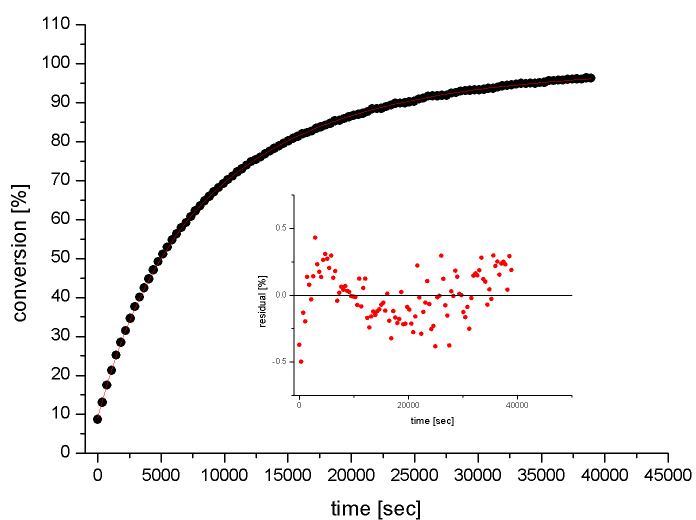
1) 57.1
2) 60.3
= 58.7 ± 1.6





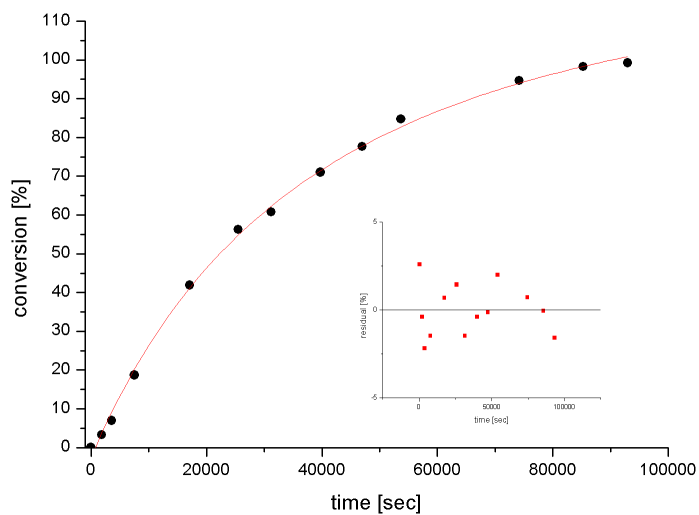
1eh

1) 91.1
2) 92.7
= 91.9 ± 0.8



1ep

1) 471
2) 433
= 452 ± 19



6.5 References

- [1] Benaglia, M. Editor, *Recoverable and Recyclable Catalysts*, John Wiley & Sons, **2009**.
- [2] a) S. Shinkai, H. Tsuji, Y. Hara, O. Manabe, *Bull. Chem. Soc. Jpn.* **1981**, *54*, 631. b) J. Yoshida, J. Hashimoto, N. Kawabata, *Bull. Chem. Soc. Jpn.* **1981**, *54*, 309.
- [3] a) E. J. Delaney, L. E. Wood, I. M. Klotz, *J. Am. Chem. Soc.* **1982**, *104*, 799. b) M. A. Hierl, E. P. Gamson, I. M. Klotz, *J. Am. Chem. Soc.* **1979**, *101*, 6020. c) F. M. Menger, D. J. McCann, *J. Org. Chem.* **1985**, *50*, 3928. d) A. Deratani, A., D. G. Darling, D. Horak, J. M. J. Frechet, *Macromolecules*, **1987**, *20*, 767. e) F. Guendouz, R. Jaquier, J. Verducci, *Tetrahedron* **1988**, *23*, 7095. f) M. Tomoi, Y. Akada, H. Kakiuchi, *Makromol. Chem. Rapid Commun.* **1982**, *3*, 537.
- [4] K. E. Price, P. B. Mason, A. R. Bogdan, S. J. Broadwater, J. L. Steinbacher, D. T. McQuade, *J. Am. Chem. Soc.* **2006**, *128*, 10376.
- [5] C. O. Dalaigh, S. A. Corr, Y. K. Gun'ko, S. J. Connon, *Angew. Chem. Int. Ed.* **2007**, *46*, 4329.
- [6] O. Gleeson, R. Tekoriute, Y. K. Gun'ko, S. J. Connon, *Chem, Eur. J.* **2009**, *15*, 5669.
- [7] H.-T. Chen, S. Huh, J. W. Wiench, M. Pruski, V. S.-Y. Lin, *J. Am. Chem. Soc.* **2005**, *127*, 13305.
- [8] A. Corma, H. Garcia, A. Leyva, *Chem. Commun.* **2003**, 2806.
- [9] V. D'Elia, Y. Liu, H. Zipse, *Eur. J. Org. Chem.* **2011**, 1527 – 1533.
- [10] I. Held, E. Larionov, C. Bozler, F. Wagner, H. Zipse, *Synthesis* **2009**, 2267 – 2277.

Chapter 7

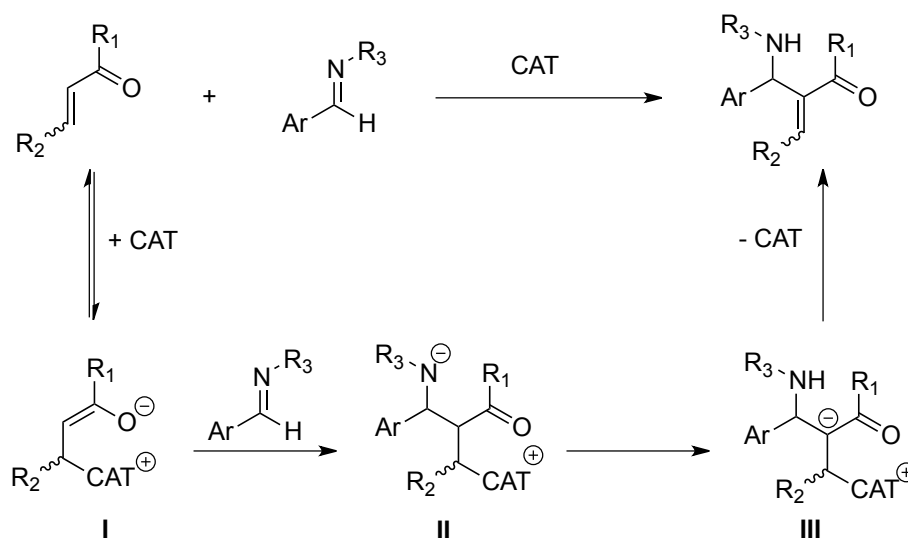
The *aza*-Morita-Baylis-Hillman Reaction of Electronically and Sterically Deactivated Substrates

Christoph Lindner, Raman Tandon, Yinghao Liu, Boris Maryasin, Hendrik Zipse, Org. Biomol. Chem. 2012, 10, 3210 – 3218.

To clarify my contributions in this Chapter the following should be mentioned: All kinetic measurements using phosphanes were conducted by C. Lindner and the kinetic studies of **6d–j**, **11** and **13b**, as well as the isolation of azaMBH products by Yinghao Liu. The calculation of zwitterionic intermediates was done by Boris Maryasin. Results obtained by co-authors are omitted in the Experimental Part.

7.1 Introduction

The *aza*-Morita-Baylis-Hillman (azaMBH) reaction is a synthetically useful C-C bond forming reaction involving the coupling of imines with Michael acceptors to form highly functionalized amines (Scheme 7.1).^[1,2,3,8] Despite the impressive development of various protocols for the enantioselective azaMBH reaction involving either chiral Lewis bases or combinations of achiral Lewis bases with chiral protic co-catalysts,^[4,5,6,7] the effective transformation of sterically and/or electronically deactivated Michael acceptors still provides an ambitious challenge. The azaMBH reaction is currently considered to involve initial attack of the Lewis base catalyst on the Michael acceptor,^[3c,3d,4] followed by addition of the resulting zwitterionic enolate **I** to the imine substrate. Subsequent intramolecular proton transfer within zwitterionic intermediate **II** and elimination of the nucleophilic catalyst close the catalytic cycle. Previous kinetic studies by Lloyd-Jones *et al.*^[11] indicate that reaction rates are most likely limited by the imine addition and/or the subsequent proton transfer step. The step most strongly affected by deactivated Michael acceptors is the initial nucleophilic addition step, and sluggish reaction rates for this class of substrates may simply derive from the reduced preequilibrium formation of zwitterionic enolate **I**. This implies that the use of Lewis base catalysts with increased carbon basicity will predictably lead to higher turnover rates. In the following we show that this is indeed the case.

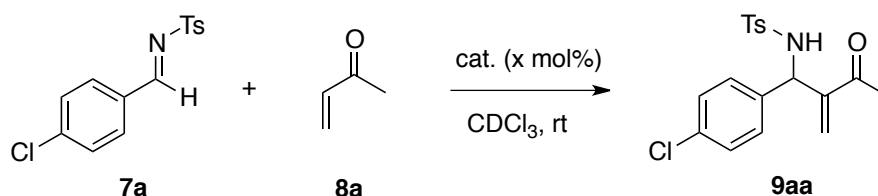


Scheme 7.1. The mechanism of the *aza*-Morita-Baylis-Hillman (azaMBH) reaction of imines with Michael acceptors.

7.2 Results and Discussion

Initial experiments were performed for the reaction of *p*-chlorotosylimine **7a** with methyl vinyl ketone (**8a**) using the nucleophilic catalysts depicted in Figure 7.2 in CDCl₃ as the

solvent (Scheme 7.2, Table 7.1). Methyl vinyl ketone (**8a**) has been selected here as a reference Michael acceptor of known high reactivity.



Scheme 7.2. The azaMBH reaction of N-tosylimine **7a** with MVK (**8a**) in CDCl_3 .

The reaction was conveniently monitored by ^1H NMR spectroscopy following the signals of imine **7a** and amine product **9aa**. Turnover curves were fitted using a simple kinetic scheme involving pre-equilibrium formation of zwitterionic enolate **I** and the followup addition/rearrangement step with imine. This kinetic model involving only three rate constants as variable parameters is closely similar to that used in previous studies,^[11] but does not include any type of co-catalysis by product molecules or other protic additives. More complex models involving a larger number of steps have also been explored, but not found to perform substantially better (see Experimental Part for further details). An example for the turnover curve with catalyst **2** is depicted in Figure 7.1.

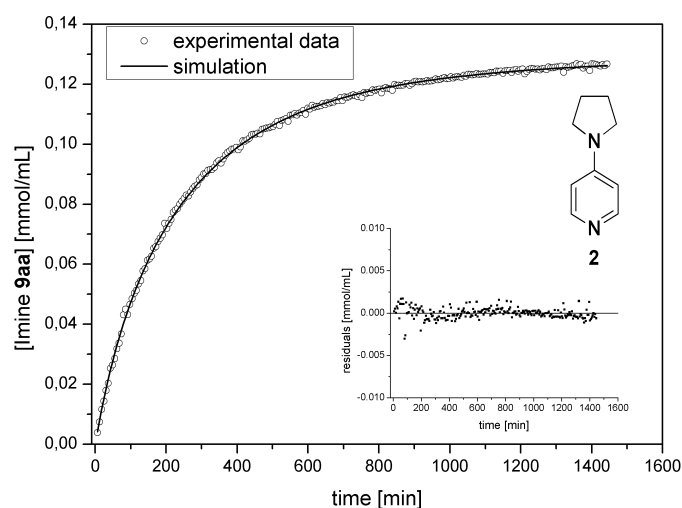


Figure 7.1. Results for the reaction of MVK (**8a**) with imine **7a** catalyzed by 10 mol% **2** in CDCl_3 .

The reaction half-life time $t_{1/2}$ listed in Table 7.1 as the most relevant kinetic parameter corresponds to the time required for 50% conversion of the initially used imine substrate and is obtained from the simulated turnover curve. Methyl cation affinity (MCA) values are available for most of the catalysts shown in Figure 7.2 and reflect the Lewis basicity of these species towards the methyl cation as the smallest carbon electrophile (Table 7.1).^[14]

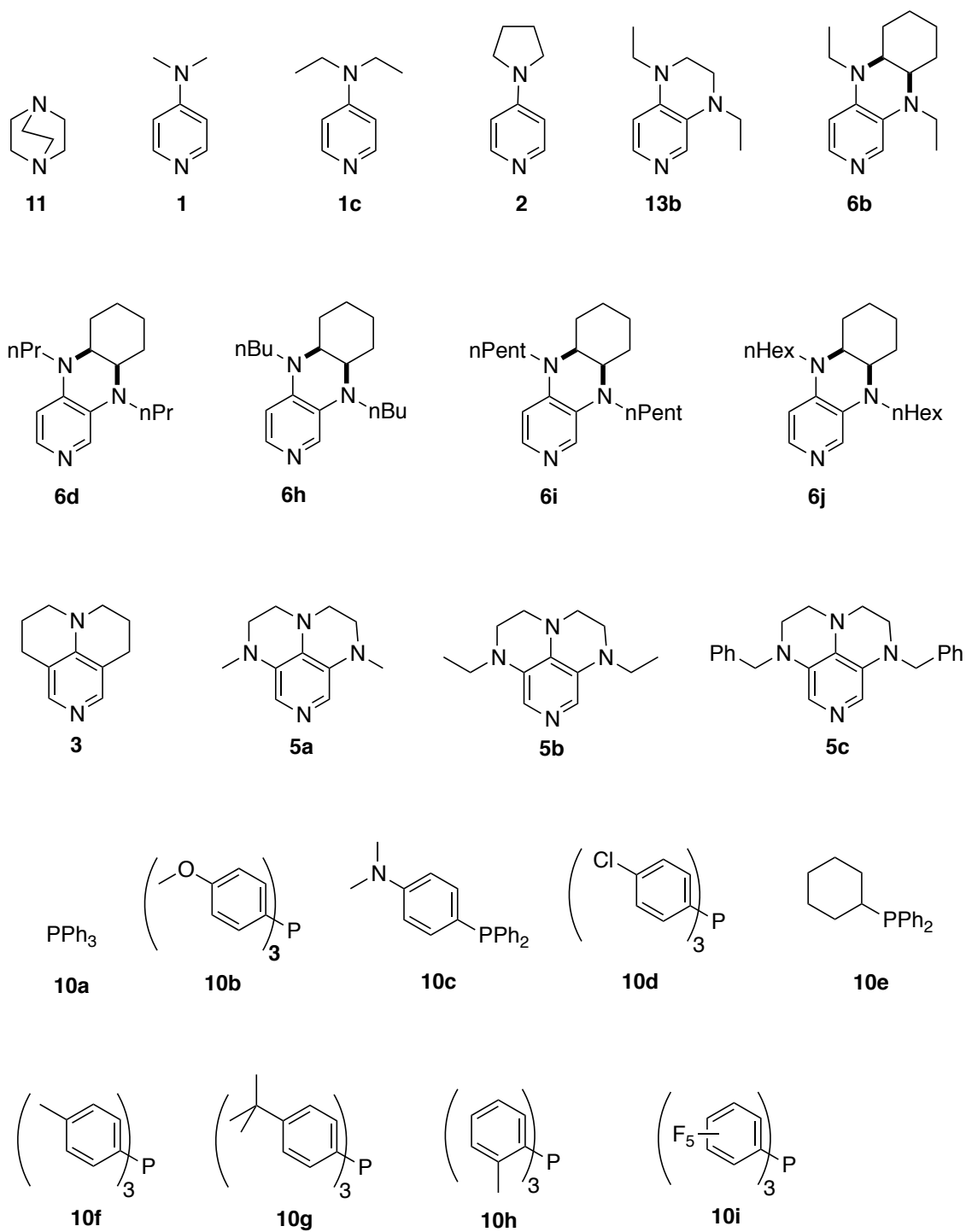


Figure 7.2. Catalysts used in the *aza*MBH reactions.

Table 7.1. Results for the azaMBH reaction with MVK (**8a**) shown in Scheme 7.2.

Entry	Catalyst	Time [h]	Conversion ^[a,c] [%]	<i>t</i> _{1/2} ^[c] [min]	MCA [kJ/mol]
using 10 mol% catalyst					
1	DABCO (11)	10	8	3750 ^[f]	+562.2
2	DMAP (1)	10	56	475	+581.2
3	1c	10	83	193	+589.1
4	PPY (2)	10	86	146	+590.1
5	5c	8	93	72	+636.8
6	13b	5	98	41	+609.0
7	5b	4	96	26	+621.6
8	5a	4	99	25	+618.7
9	6b	3	99(98) ^[b]	23	+616.0
10	3	3	98	20	+602.7
11	10i	-	-	nc ^[e]	+494.1
12	10h	-	-	nc ^[e]	+643.9
13	10d	34	95	271 ^[d]	+586.5
14	PPh ₃ (10a)	4	99	35	+618.4
15	10b	3	98	32	+651.0
16	10f	3	99	27	+637.2
17	10e	2	98	26	+630.2
18	10c	3	99	25	+646.7
19	10g	2	99	22	+643.9
using 5 mol% catalyst					
20	13b	10	97	75	+609.0
21	6j	10	99	55	-
22	6h	10	99	53	-
23	6i	10	99	53	-
24	6b	10	99(92) ^[b]	53	+616.0
25	6d	10	99	49	-
26	3	5	99	40	+602.7
27	PPh ₃ (10a)	8	98	69	+618.4
28	10c	7	98	64	+646.7
29	10b	9	95	60	+651.0
30	10f	5	99	46	+637.2
31	10e	4	99	45	+630.2
32	10g	4	99	41	+643.9
using 2.5 mol% catalyst					
33	PPh ₃ (10a)	13	95	146	+618.4
34	10g	10	92	80	+643.9
35	3	10	96	77	+602.7
36	10f	10	95	76	+637.2

[a] Determined by ¹H NMR; [b] Isolated yield; [c] 0.125 M imine, 1.2 equ. MVK; [d] 20 % catalyst; [e] No conversion; [f] Extrapolated value.

In the group of nitrogen-based catalysts the reaction is rather sluggish in the presence of catalysts of low Lewis basicity such as DABCO (**11**), yielding only 8 % turnover after 10 h reaction time. Extrapolating this rate in a linear fashion to 50 % turnover yields an approximate half-life time of 3750 minutes. Significantly higher rates are observed for pyridine catalysts such as DMAP (**1**) and PPY (**2**). Best results are obtained with the recently developed 3,4-diaminopyridine catalysts such as **6b**, with the tricyclic aminopyridine **3**, or with some of the phosphanes based on the PPh₃ motif. In all these latter cases complete turnover is achieved after 4 h. For catalyst **6b** it has been verified that this translates into an isolated yield of 98% after product isolation and purification. With respect to $t_{1/2}$ values the tricyclic pyridine **3** is found to be the fastest catalyst, closely followed by pyridine **6b**. This closely parallels recent results for the Lewis base-catalyzed acylation of tertiary alcohols.^[16] Phosphane **10g** is the most active phosphane catalyst studied here, but is only moderately faster than other triarylphosphanes carrying electron-donating substituents in *para* position such as **10c**. Replacing one of the phenyl groups in PPh₃ (**10a**) by a cycloalkyl substituent as in **10e** also enhances the catalytic activity, but also leads to a notable increase in phosphane oxidation (and thus deactivation). Rather poor results are obtained for phosphanes with electron-withdrawing substituents (such as **10i**) or with sterically demanding substituents in *ortho* position (as in **10h**).

With rate data for a larger number of systems in hand we can test for a possible quantitative correlation between catalyst basicity as quantified by MCA values and reaction rate. As can be seen in Figure 7.3 a linear correlation between basicity and reaction rate exists for catalysts of low Lewis basicity (that is, with MCA values less than 610 kJ/mol). For more Lewis basic compounds a saturation of the reaction rate at high level is found. The only catalyst not following this general trend is sterically hindered phosphane **10h**, whose rather large MCA value of 643.9 kJ/mol equals that of the most active phosphane **10g**, but whose very low reactivity did not allow for determining the reaction rate quantitatively. The intrinsically good Lewis basicity of catalyst **10h** is thus completely compensated by steric effects in reactions involving the substrate pair **7a/8a**.

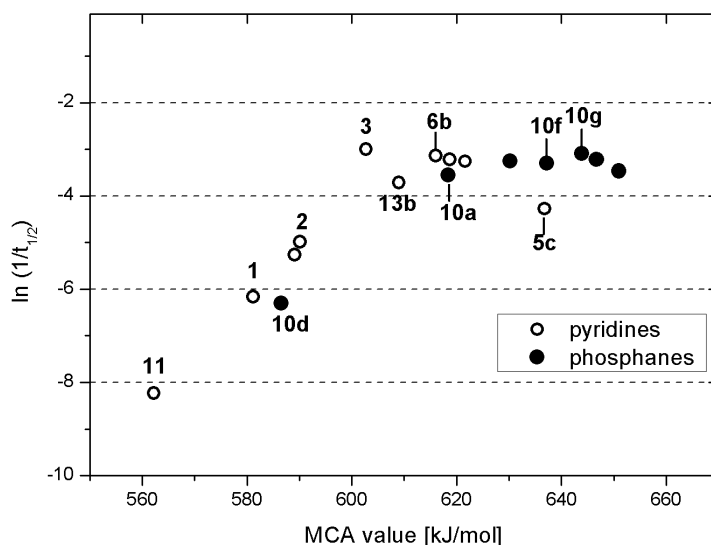


Figure 7.3. Correlation of reaction rates vs. MCA values for the reaction of MVK (**8a**) and **7a** with 10 mol% catalyst.

The absolute reaction rates obtained for electron-rich pyridines and phosphanes are somewhat too large at catalyst loadings of 10 mol% to obtain a precise picture of catalytic performance. To this end several of the reactions have been reinvestigated with a lower catalyst loading of 5 mol% (Table 7.1), now also including derivatives of catalyst **6b** with alkyl sidechains of variable lengths. The largely similar $t_{1/2}$ values determined for 3,4-diaminopyridines **6b** - **6j** imply, however, that the increasingly longer alkyl side chains in these compounds do not lead to an enhancement of the electron density of the pyridine ring (and thus not to an increase in catalytic performance). Tricyclic pyridine **3** thus remains the most effective catalyst found here, closely followed by phosphane **10g**.

For selected catalysts the reaction was also investigated at a loading of 2.5 mol%. Together with the results obtained at higher loadings this allows for an approximate analysis of the dependence of the reaction rate on the catalyst loading (Figure 7.4). Measurements at even lower loadings were accompanied by oxidation of the phosphane catalysts in a significant manner and were thus not pursued any further (see Experimental Part for details). The results for the most stable catalysts, e.g. **3** and **10a** indicate that reaction rates vary linearly with the catalyst concentration (cf. Figure 7.4). In mechanistic terms this implies the involvement of a single catalyst molecule in the rate limiting step. For both of these catalysts the interpolation curve is observed to pass through the intercept, reflecting minimal background reactivity. This latter point is also in line with rate measurements performed in the absence of catalysts.

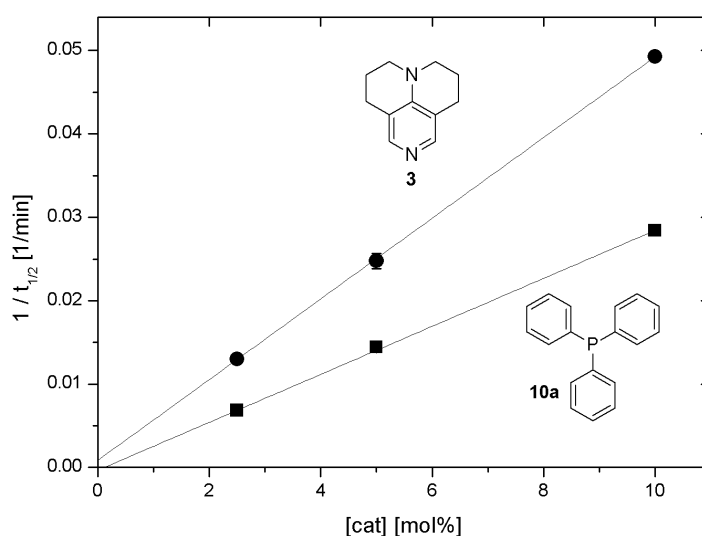
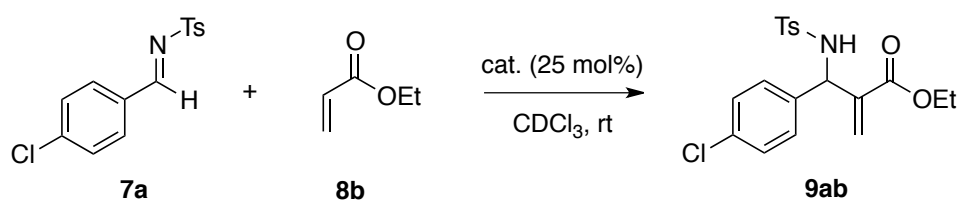


Figure 7.4. Correlation of the rates of reaction of MVK (**8a**) with **7a** vs. the concentration of the catalysts **3** (circles) and **10a** (squares).

Tosylimine **7a** was also used in benchmark reactions with ethyl acrylate (**8b**) as the Michael acceptor. Due to the much lower reactivity of this latter compound, reasonable turnover times require higher substrate concentrations and a catalyst loading of 25 mol% (Scheme 7.3, Table 7.2).



Scheme 7.3. The azaMBH reaction of N-tosylimine **7a** with ethyl acrylate (**8b**) in CDCl₃.

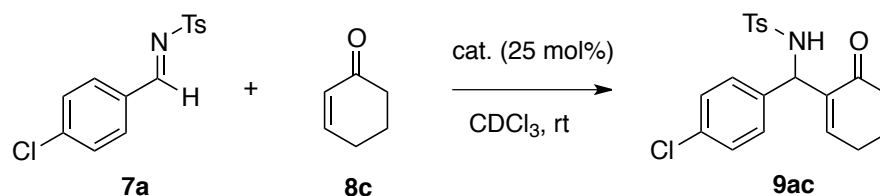
Table 7.2. Results for the azaMBH reaction with ethyl acrylate (**8b**) using 25 mol% catalyst as shown in Scheme 7.3.

Entry	Catalyst	Time [d]	Conversion ^[a,b] [%]	<i>t</i> _{1/2} [min]
1	10a	5	99	1384
2	6b	4	99	747
3	3	3	99	612
4	10f	2	99	595

[a] Determined by ¹H NMR; [b] 0.25 M imine, 4.0 equ. **8b**.

With these reaction conditions full conversion can be obtained after a maximum of five days. The phosphane catalyst **10f** turned out to be the most effective choice in this series with complete turnover after two days, although pyridine **3** is almost equally active. The half-life time of triphenylphosphane **10a** is more than two times longer than the two best catalysts.

In order to explore the effects of steric hindrance on the catalytic efficiency of pyridine and phosphane catalysts, the azaMBH reaction of cyclohexenone (**8c**) was studied under the same conditions used for acrylate **8b** (Scheme 7.4, Table 7.3).



Scheme 7.4. The azaMBH reaction of N-tosylimine **7a** with cyclohexenone (**8c**) in CDCl_3 .

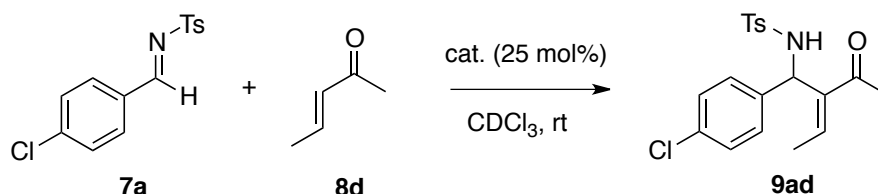
Table 7.3. Results for the azaMBH reaction with cyclohexenone (**8c**) using 25 mol% catalyst as shown in Scheme 7.4.

Entry	Catalyst	Time [h]	Conversion ^[a,c] [%]	$t_{1/2}$ ^[c] [min]
1	DABCO (11)	40	4	-
2	Quinuclidine	40	25	-
3	DMAP (1)	40	36	-
4	PPY (2)	30	43	-
5	6b	30	99(98) ^b	264
6	3	30	98	242
7	5a	40	95	456
8	5b	72	98	581
9	5c	72	97	758
10	PPh_3 (10a)	40	< 3	-
11	10f	40	< 3	-

[a] Determined by ^1H NMR; [b] Isolated yield; [c] 0.25 M imine, 4 equ. **8c**.

The reaction of cyclic ketone **8c** with DABCO (**11**) as catalyst shows almost no conversion. For the pyridine catalysts, in contrast, good turnover can be observed in particular for the 3,4-diaminopyridine catalyst **6b** and the tricyclic pyridine **3**. With these catalysts essentially complete turnover is achieved after 30 h reaction time, which translates into an isolated yield of adduct **9ac** of 98 % for **6b**. In surprising contrast to the result obtained for the acyclic Michael acceptors **8a** and **8b**, there is practically no turnover when using any of the phosphane catalysts for reaction with cyclohexenone **8c**. This unexpected result may indicate a generally larger sensitivity of triarylphosphanes to steric demands of the Michael acceptor, or may alternatively indicate the presence of stabilizing contacts between phosphane catalyst

and carbonyl oxygen atom in the zwitterionic enolates **I** formed in the initial addition steps (see Scheme 7.1). As indicated in Scheme 7.1 this latter type of interaction is only possible in acyclic Michael acceptors for geometric reasons. In order to differentiate between these two effects, additional measurements have been performed for acyclic Michael acceptor *trans*-3-penten-2-one (**8d**), in which the center of attack also carries an alkyl substituent.



Scheme 7.5. The azaMBH reaction of N-tosylimine **7a** with *trans*-3-penten-2-one (**8d**) in CDCl₃ solution.

Table 7.4. Results for the azaMBH reaction with *trans*-3-penten-2-one (**8d**) using 25 mol% catalyst as shown in Scheme 7.5.

Entry	Catalyst	Time [d]	Conversion ^[a,c] [%]	<i>t</i> _{1/2} ^[c] [h]
1	6b	29	92	164
2	3	29	98(93) ^b	120
3	PPh ₃ (10a)	5	< 2	-
4	10f	5	< 2	-

[a] Determined by ¹H NMR; [b] Isolated yield; [c] 0.125 M imine, 4 equ. **8d**.

Although the reaction of the sterically hindered ketone **8d** is the slowest of the four investigated azaMBH reactions, full conversion can be obtained for pyridine catalysts **6b** and **3** after 29 days. Product isolation and characterization indicates formation of a single stereoisomer **9ad** with (*E*)-configuration according to NOE experiments and X-ray analysis. In contrast to the two pyridine catalysts **6b** and **3**, there is no significant turnover for triarylphosphanes **10a** or **10f**. Since the acyclic nature of alkene **8d** does allow for contacts between carbonyl oxygen and phosphane catalysts in zwitterionic intermediate **I**, this latter result implies that triaryl phosphane catalysts are intrinsically more sensitive to the steric demands of Michael acceptors than pyridine catalysts.

The largely different reactivities of the four Michael acceptors **8a** - **8d** are already apparent from the conversion data in Tables 7.1 – 7.4. It was nevertheless desirable to compare the catalytic properties of pyridines (**3**) and phosphanes (**10a**) in transformations with these four substrates under strictly identical conditions. To this end an additional set of rate measurements was performed using tosylimine **7a** at 0.25 M concentration in combination with 4.0 eq. Michael acceptor and 25 mol% of catalyst. As can be seen from the turnover plot for catalysts **3** and **10a** in Figure 7.5 below, the reaction is now so fast for MVK (**8a**) as the substrate that the reaction is essentially complete within 3 min (**3**) and 20 min (**10a**)

respectively. For the *aza*MBH reaction with MVK (**8a**) and **3** as catalyst, the reaction half-life time is roughly one minute. The half-life times are dramatically increased for the electronically deactivated Michael acceptor **8b** (612 minutes), as well as for sterically hindered Michael acceptors (**8c**, 242 minutes; **8d**, 1890 minutes). The difference in the reactions of MVK (**8a**) and acrylate **8b** of 1 : 612 is significantly larger as compared to the ratio of 1 : 38 found in kinetic studies for the addition of DMAP (**1**) to MVK and methyl acrylate in aqueous solution.^[24] The half-life time in the case of phosphane **10a** as catalyst (cf. Figure 7.5) is four minutes (MVK (**8a**)) and 1384 minutes (ethyl acrylate (**8b**)) respectively. As already mentioned above the phosphanes are not catalytically active in the case of sterically hindered Michael-acceptors (**8c** and **8d**).

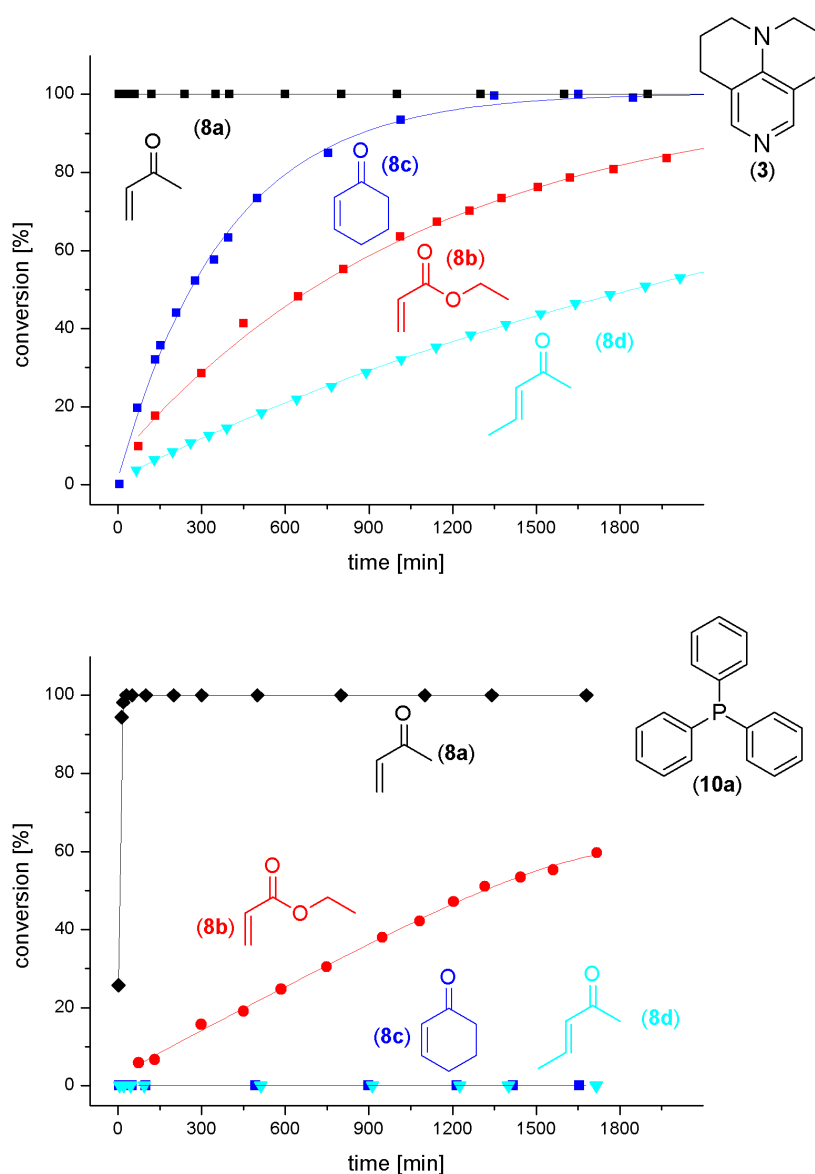
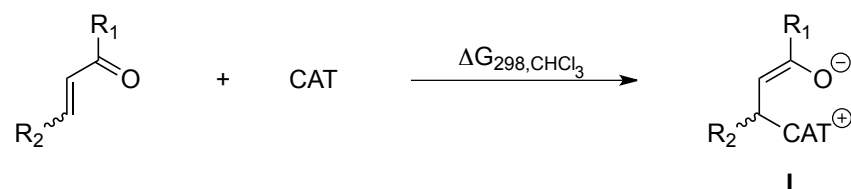


Figure 7.5. Turnover curves for **3** (top) and **10a** (bottom) for the *aza*MBH reactions of tosylimine **7a** (0.25 M) with 4 eq. of Michael acceptors **8a** (diamonds), **8b** (circles), **8c** (squares) or **8d** (triangles).

Suspecting that the largely different reaction rates for Michael acceptors **8a** - **8c** are, at least in part, due to the energetics of the first step of the catalytic cycle shown in Scheme 7.6, the reaction free energies for this step in CHCl₃ solution have been calculated for catalysts **6b** and **10a** using a theoretical protocol optimized for the description of zwitterionic species in organocatalytic reactions (Figure 7.6).^[21]



Scheme 7.6. Formation of adducts between catalyst and Michael-acceptors.

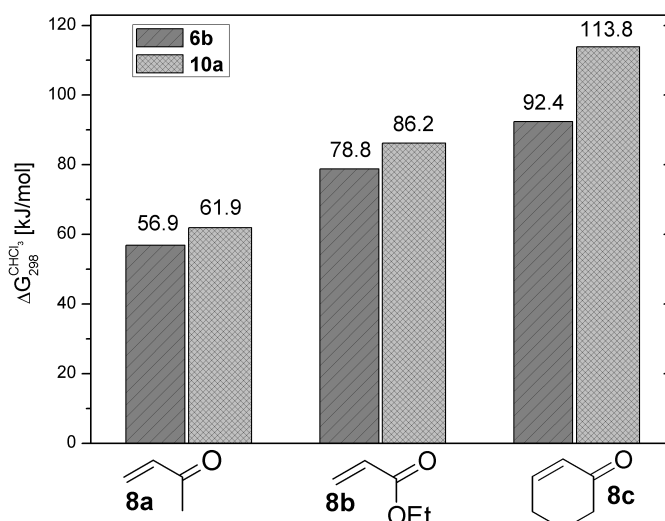


Figure 7.6. Reaction free energies $\Delta G_{298, \text{CHCl}_3}$ for the formation of zwitterionic enolates **I** involving catalysts **6b** and PPh₃ (**10a**) and different Michael acceptors (**8a** – **8c**) (obtained by Dr. B. Maryasin).

The reaction free energies for the addition of catalysts **6b** and **10a** to alkenes **8a** - **8c** are all large and positive, implying a rather unfavorable position of the preequilibrium. In qualitative agreement with the measured rate data, the most stable intermediate is calculated for the addition of **6b** to MVK (**8a**), closely followed by the adduct formed from the same alkene with **10a**. The zwitterionic intermediates **I** formed through reaction with the electronically deactivated acrylate **8b** are less favourable for both catalysts, again with a small preference for catalyst **6b**. This is again in agreement with available rate data. For sterically hindered alkene **8c** the agreement between calculated stabilities and measured rate data are less satisfactory in that the (comparatively fast) reaction with catalyst **6b** is not compatible with the very low calculated stability of the respective intermediate **I**. The least stable intermediate studied here is the adduct formed through reaction of alkene **8c** with phosphane **10a**, which is again in satisfactory agreement with the non-observation of product formation. The

energetically best conformations of the MVK-adducts with **6b** and **10a** are depicted in Figure 7.7.

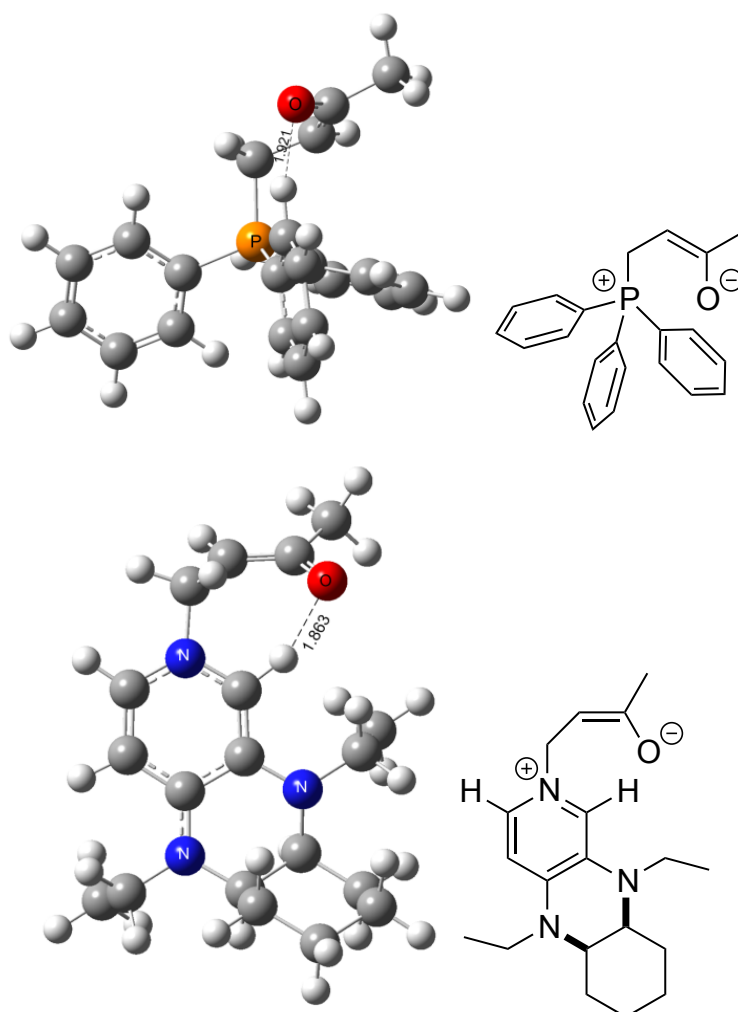
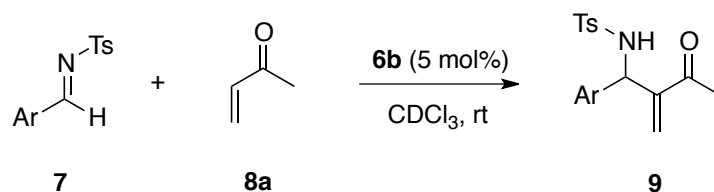


Figure 7.7. Structures of the best conformations of zwitterionic enolates **I** formed in the reaction of catalysts **6b** and **10a** with MVK (**8a**) (obtained by Dr. B. Maryasin).

In both structures we can identify a close contact between the enolate oxygen atom and one of the catalyst C-H bonds. In catalyst **6b** this interaction involves the α -C-H bond of the pyridine ring. This is closely similar to interactions identified between acylpyridiniumions and carboxylate counter ions in pyridine-catalyzed acylation reactions.^[22,23] In the adduct formed with PPh₃ (**10a**) the enolate oxygen atom is in direct contact with one of the phenyl *ortho*-C-H bonds.

In order to explore the synthetic scope of the protocols developed above, the reactions with MVK (**8a**) as the Michael acceptor were repeated with 3,4-diaminopyridine catalyst **6b** at 5 mol% loading for a number of different tosylimines (Scheme 7.7, Table 7.5). The entries in Table 7.5 are ordered by σ_{para} parameters.^[20,25]



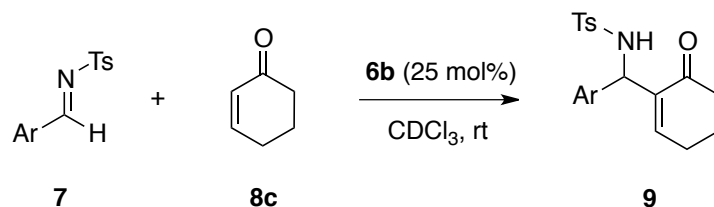
Scheme 7.7. The azaMBH reaction of MVK (**8a**) with various tosylimines and catalyst **6b** in CDCl_3 solution.

Table 7.5. Results for the azaMBH reaction with MVK (**8a**) using 5 mol% catalyst **6b** and selected tosylimines as shown in Scheme 7.7 (obtained by Dr. Y. Liu).

Entry	Ar	Tosyl-imine	Time [h]	Yield [%] ^[a,c]	Conv. [%] ^[b,c]	Prod.
1	<i>p</i> -NO ₂ -C ₆ H ₄	7c	1.5	90	99	9ca
2	<i>p</i> -NC-C ₆ H ₄	7b	1.5	94	99	9ba
3	<i>p</i> -Br-C ₆ H ₄	7e	14	86	93	9ea
4	<i>p</i> -Cl-C ₆ H ₄	7a	10	92	99	9aa
5	C ₆ H ₅	7f	15	73	99	9fa
6	<i>p</i> -Me-C ₆ H ₄	7g	20	80	89	9ga
7	<i>p</i> -MeO-C ₆ H ₄	7h	48	74	85	9ha

[a] Isolated yield; [b] Determined by ¹H NMR; [c] 0.125 M imine, 1.2 equ. MVK.

It is gratifyingly found that catalyst **6b** used at 5 mol% loading yields acceptable turnover times and good synthetic yields even for deactivated tosylimines carrying donor substituents such as **7h**. Reaction times are, of course, much shorter for acceptor substituted imines such as **7b** and **7c**. The latter are the fastest imines, which can also be found by their σ_{para} parameters. We note in passing that the variations in reaction times and yields observed here are fully compatible with, at least partially, rate-limiting addition of zwitterionic intermediates **I** to the imine substrates. A completely analogous set of experiments was performed with catalyst **6b** for the sterically hindered Michael acceptor cyclohexenone **8c** (Scheme 7.8, Table 7.6).



Scheme 7.8. The azaMBH reaction of cyclohexenone (**8c**) with various tosylimines and catalyst **6b** in CDCl_3 solution.

Table 7.6 Results for the azaMBH reaction with cyclohexenone (**8c**) using 25 mol% catalyst **6b** and selected tosylimines as shown in Scheme 7.8 (obtained by Dr. Y. Liu).

Entry	Ar	Tosyl-imine	Time [h]	Yield [%] ^[a,c]	Conv. [%] ^[b,c]	Prod.
1	<i>p</i> -NO ₂ -C ₆ H ₄	7c	24	85	99	9cc
2	<i>p</i> -NC-C ₆ H ₄	7b	24	88	99	9bc
3	<i>p</i> -Br-C ₆ H ₄	7e	60	90	99	9ec
4	<i>p</i> -Cl-C ₆ H ₄	7a	30	98	99	9ac
5	C ₆ H ₅	7f	60	83	95	9fc
6	<i>p</i> -MeO-C ₆ H ₄	7h	120	69	90	9hc
7	<i>o</i> -Cl-C ₆ H ₄	7d	48	84	95	9dc
8	<i>trans</i> -Ph-CH=CH	7i	54	87	96	9ic

[a] Isolated yield; [b] Determined by ¹H NMR; [c] 0.25 M imine, 4.0 equ. ketone **8c**.

Reactions with sterically hindered Michael acceptor **8c** are, even at the much higher catalyst and substrate concentrations used now, significantly slower as compared to those involving MVK (**8a**). After sufficiently long reaction times the corresponding azaMBH products **9** can, however, be isolated in good to excellent yields in all cases.

7.3 Conclusion

For all four Michael acceptors studied here an effective protocol for the azaMBH reaction could be developed. MVK (**8a**) is the most reactive of the studied substrates. Having no background reaction MVK (**8a**) and the tosylimine (**7a**) can be converted to the azaMBH product quantitatively in minutes. Most pyridine and phosphane catalysts tested in this reaction lead to full conversion in a short time. Using deactivated substrates the necessary reaction times for full conversion are significantly increased. For the electronically deactivated Michael acceptor (**8b**) pyridines as well as phosphanes can be used. In the case of sterically hindered substrates (**8c** and **8d**) only pyridines are catalytically active, which illustrates the synthetic value of this class of catalysts. All results found here are compatible with a reaction mechanism involving preequilibrium formation of zwitterionic intermediates from Michael acceptors and catalysts, and subsequent rate-limiting addition to the imine (followed by intramolecular proton transfer and elimination of catalyst). The high sensitivity of the azaMBH reaction rates to the steric and the electronic properties of the Michael acceptor substrate found here for the reaction in chloroform solution are, however, also compatible with a partially rate-limiting first addition step.

7.4 Experimental Part

General information

All air and water sensitive manipulations were carried out under a nitrogen atmosphere using standard Schlenk techniques. Calibrated flasks for kinetic measurements were dried in the oven at 120 °C for at least 12 hours prior to use and then assembled quickly while still hot, cooled under a nitrogen stream and sealed with a rubber septum. All commercial chemicals were of reagent grade and were used as received unless otherwise noted. CDCl₃ was refluxed for at least one hour over CaH₂ and subsequently distilled. ¹H and ¹³C NMR spectra were recorded on Varian 300 or Varian INOVA 400 machines at room temperature. All ¹H chemical shifts are reported in ppm (δ) relative to TMS (0.00); ¹³C chemical shifts are reported in ppm (δ) relative to CDCl₃ (77.16). ¹H NMR kinetic data were measured on a Varian Mercury 200 MHz spectrometer at 23 °C. HRMS spectra (ESI-MS) were carried out using a Thermo Finnigan LTQ FT instrument. IR spectra were measured on a Perkin-Elmer FT-IR BX spectrometer mounting ATR technology. All kinetic measurements with reaction times longer than 24 h were mechanically shaken; for each reaction the rotation speed was set at 480 turns/minute. Analytical TLC's were carried out using aluminium sheets silica gel Si 60 F254.

Conduction and evaluation of kinetic measurements

Experimental procedures for the kinetic measurements

General procedure of benchmark reactions of MVK **8a** with 10 % / 5 % catalyst: 0.5 mL from 5.0 mL of stock solution I (**7a** (220 mg, 0.75 mmol), MVK **8a** (63 mg, 0.90 mmol) and trimethoxybenzene (27 mg)) and 0.1 mL from 2 mL of stock solution II (0.15 mmol / 0.075 mmol of catalyst) were mixed in a NMR tube and sealed.

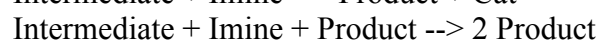
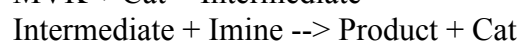
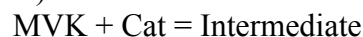
General procedure of benchmark reactions of **8b** and **8c** with 25% catalyst: 0.5 mL from 5.0 mL of stock solution I (**7a** (441 mg, 1.50 mmol), **8b** / **8c** (6.0 mmol) and trimethoxybenzene (67.2 mg)) and 0.1 mL from 2 mL of stock solution II (0.375 mmol of catalyst) were mixed in a NMR tube and flame-sealed.

General procedure of benchmark reactions of **8d** with 25 % catalyst: 0.5 mL from 5.0 mL of stock solution I (**7a** (220 mg, 0.75 mmol), **8d** (252 mg, 3.0 mmol) and trimethoxybenzene (67.2 mg)) and 0.1 mL from 2 mL of stock solution II (0.1875 mmol of catalyst) were mixed in a NMR tube and flame-sealed.

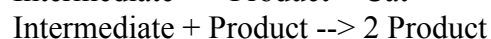
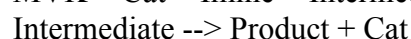
Details of the kinetic evaluation

Different models based on possible mechanisms were tested for the simulation in Copasi 4.7^[15] and the one with the least RMS deviation respectively best statistical spread was chosen. Following models were tested based on a selected number of catalysts and concentrations. The root mean square deviations were listed in Table 7.7. For equilibrium reactions '=' and for non reversible reactions '-->' was used. Model A and B were derived from Guy Lloyd Jones.^[11]

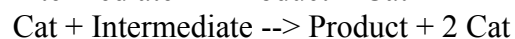
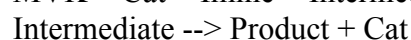
A)



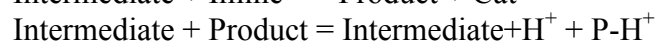
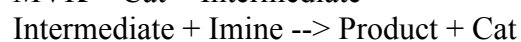
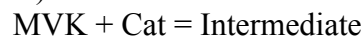
B)



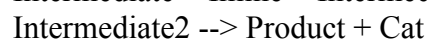
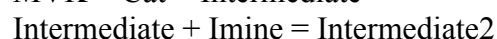
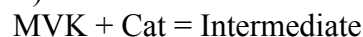
C)



D)



E)



F)

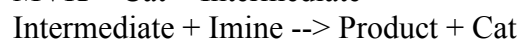
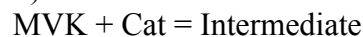


Table 7.7. Root mean square deviations of the tested models for simulation using different catalysts with varying concentration.

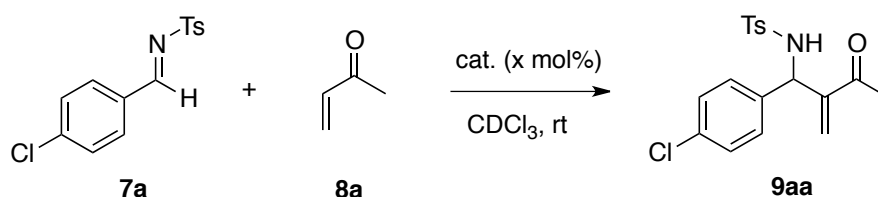
	A	B	C	D	E	F
3 10%	0.001112	0.001110	0.001253	0.001040	0.001153	0.000925
3 5%	0.000781	0.000812	0.001076	0.000946	0.000775	0.000775
2 10%	0.001650	0.001654	0.000980	0.000641	0.001480	0.001480
6b 10%	0.001409	0.001408	0.000921	0.000499	0.001511	0.001510
10a 10%	0.000455	0.000507	0.001076	0.000455	0.000468	0.000455
10a 5%	0.000564	0.000724	0.001037	0.000566	0.000567	0.000581
10a 2.5%	0.001009	0.001262	0.001333	0.000769	0.001157	0.000933
10f 10%	0.001429	0.001789	0.002065	0.001389	0.001440	0.001880
10f 5%	0.001003	0.001199	0.001660	0.000832	0.001025	0.001012
10f 2.5%	0.001306	0.001373	0.001277	0.000933	0.001380	0.001368
average	1.07E-03	1.18E-03	1.27E-03	8.07E-04	1.10E-03	1.09E-03

According to Table 7.7 model D was used due to the least averaged root mean square deviation.

Data of kinetic runs

The used data was normalized. All time specifications are in minutes if not stated differently. For every measurement the experimental data and the simulated curve together with the deviations are depicted. The resulting halflife times correspond to 50% conversion and are given with standard deviations if more than one measurement was done. The x-coordinate shows the time in minutes and the y-coordinate the concentration of product where $c(\text{imine})$ (which is given for every reaction) accounts for the maximum concentration of product.

Kinetic data for reactions of tosylimine (**7a**) and MVK (**8a**).



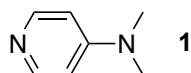
25 mol% catalyst

The following kinetic runs were performed with $c(\text{imine}) = 0.25 \text{ M}$ and $c(\text{MVK}) = 1.00 \text{ M}$.

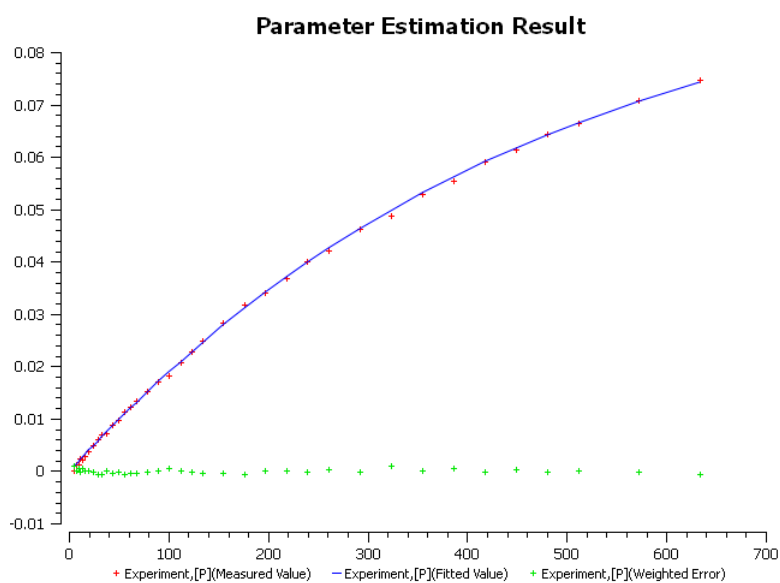
The kinetic measurement of **3** is not displayed due to the short reaction time and consequential few data points (see Figure 7.5).

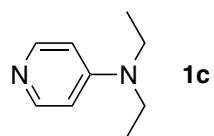
10 mol% catalyst

The following kinetic runs were performed with $c(\text{imine}) = 0.125 \text{ M}$ and $c(\text{MVK}) = 0.15 \text{ M}$.

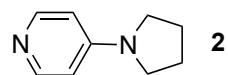
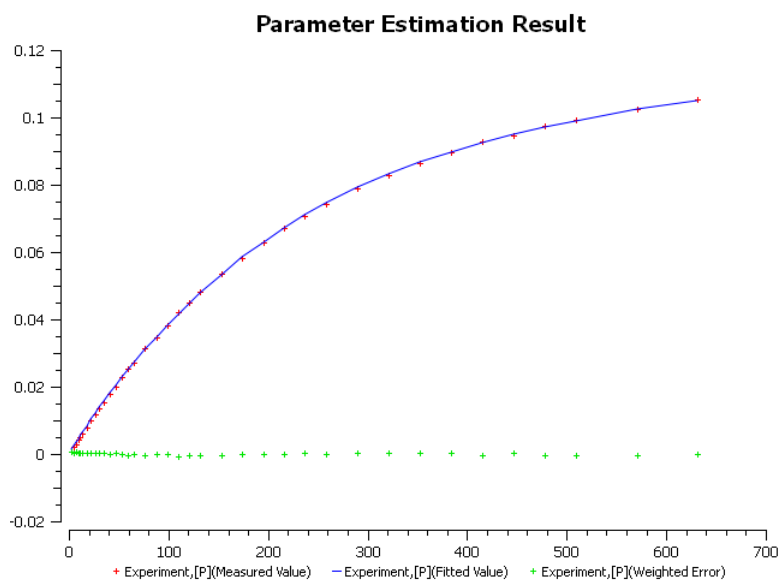


1) 458.6





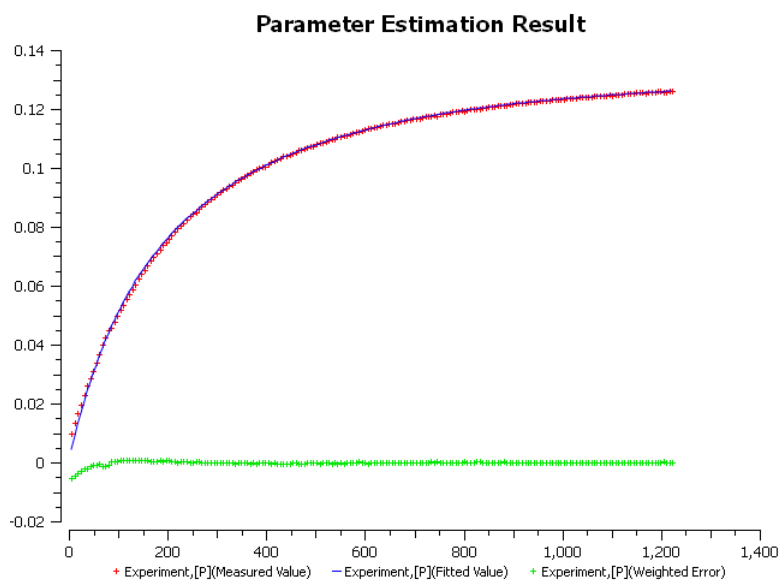
1) 192.7

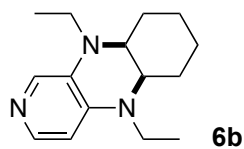


1) 138.6

2) 153.9

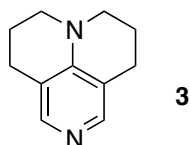
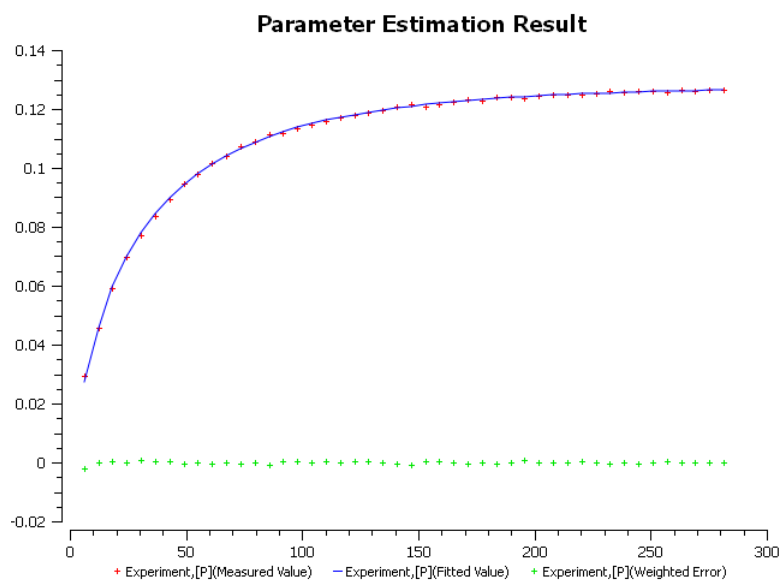
= 146.3 ± 7.7





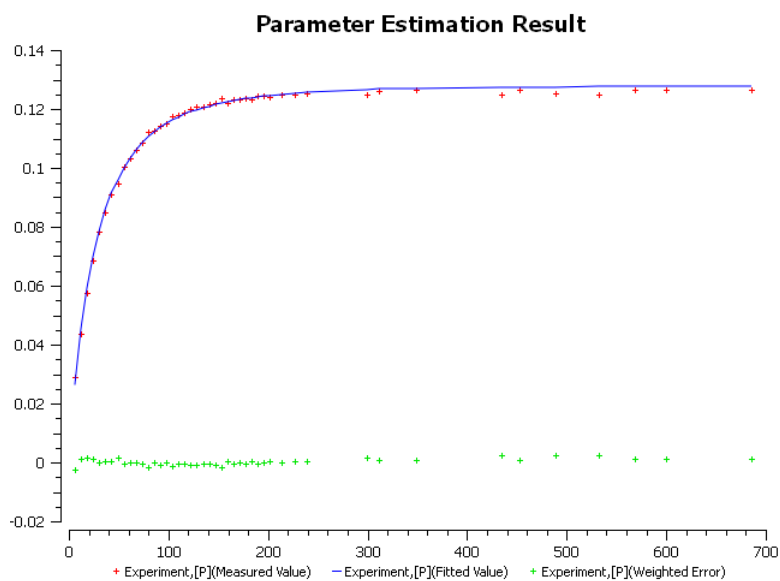
- 1) 20.2
- 2) 22.1
- 3) 26.3

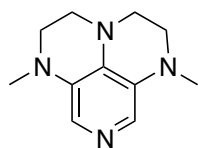
$$= 22.9 \pm 2.6$$



- 1) 20.3
- 2) 20.4

$$= 20.3 \pm 0.1$$



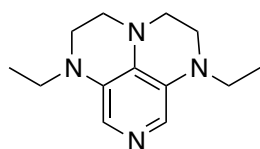
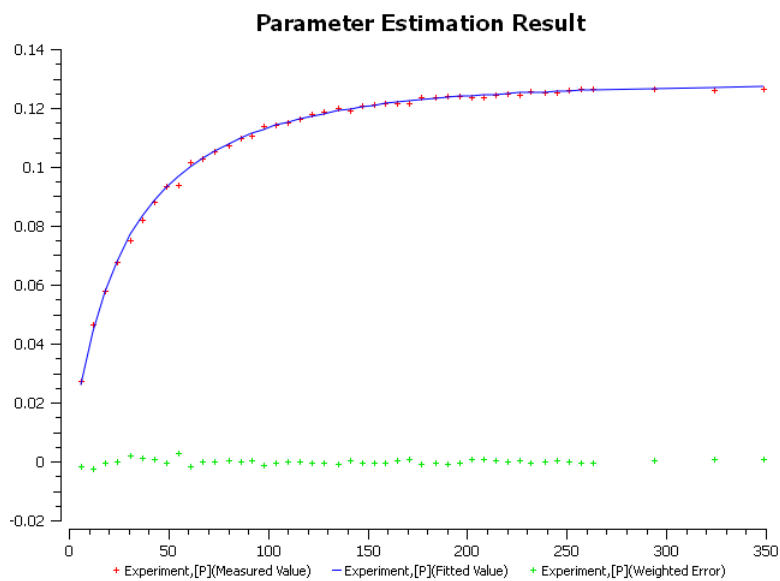


5a

1) 21.0

2) 29.0

$$= 25.0 \pm 4.0$$

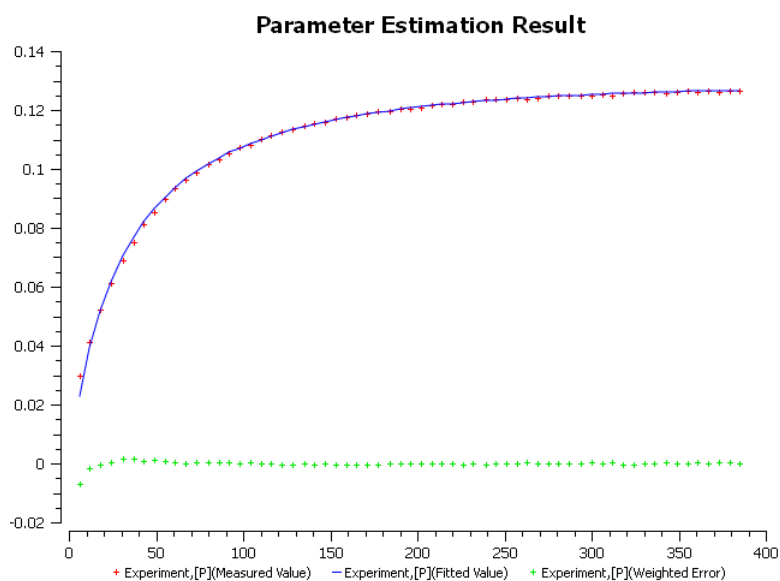


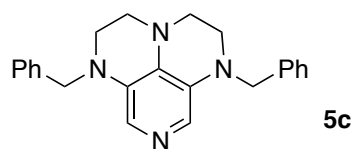
5b

1) 24.7

2) 27.5

$$= 26.1 \pm 1.4$$

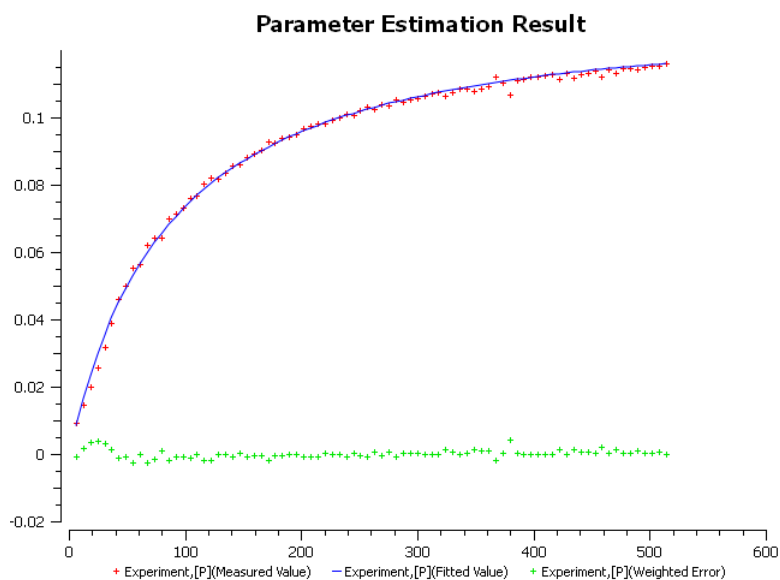




1) 72.6

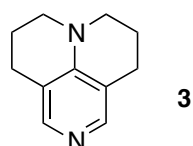
2) 71.8

$$= 72.2 \pm 0.4$$



5 mol% catalyst

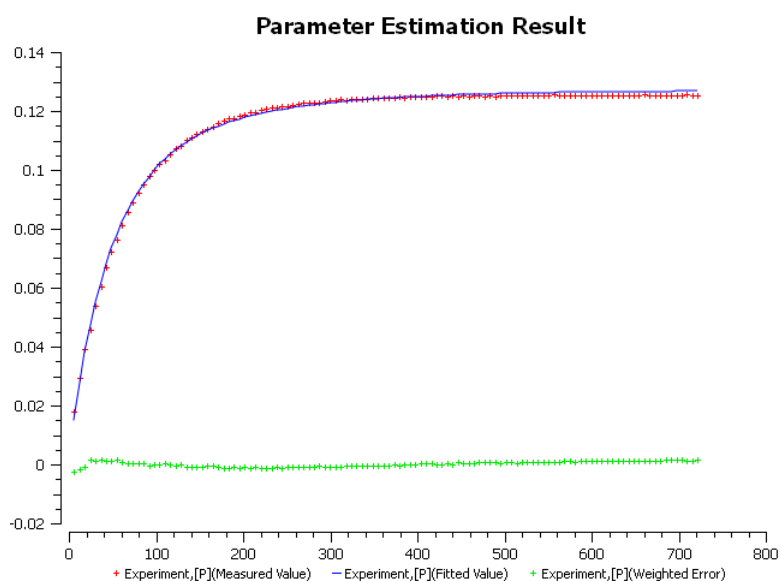
The following kinetic runs were performed with $c(\text{imine}) = 0.125 \text{ M}$ and $c(\text{MVK}) = 0.15 \text{ M}$.



1) 37.1

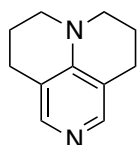
2) 43.6

$$= 40.4 \pm 3.2$$



2.5 mol% catalyst

The following kinetic runs were performed with $c(\text{imine}) = 0.125 \text{ M}$ and $c(\text{MVK}) = 0.15 \text{ M}$.

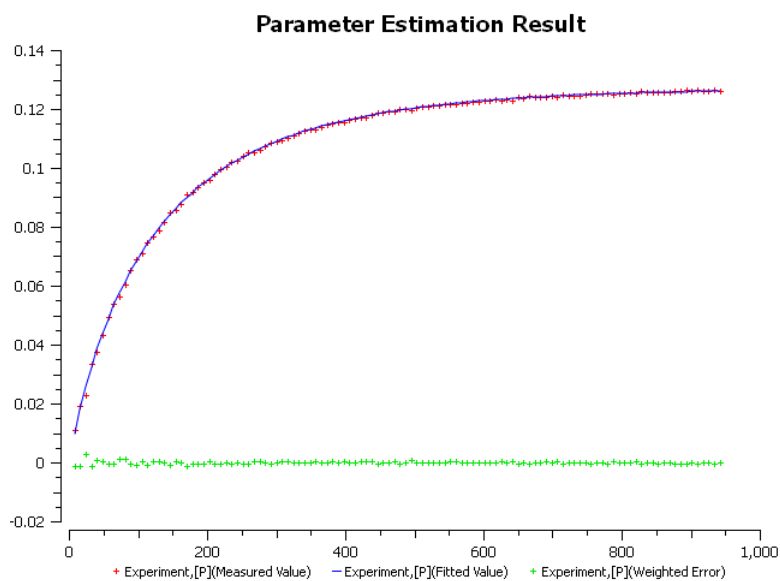


3

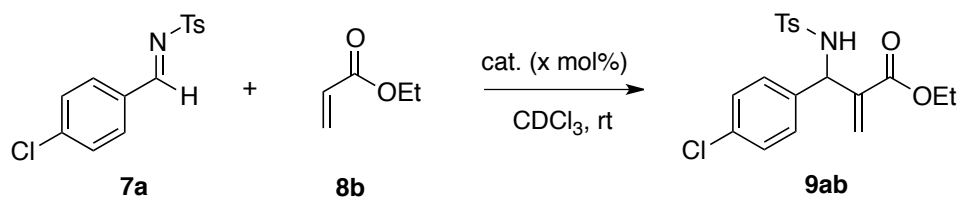
1) 83.59

2) 69.9

$= 76.8 \pm 6.9$

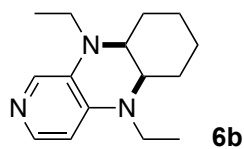


Kinetic data for reactions of tosylimine (**7a**) and ethyl acrylate (**8b**).

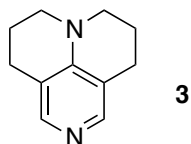
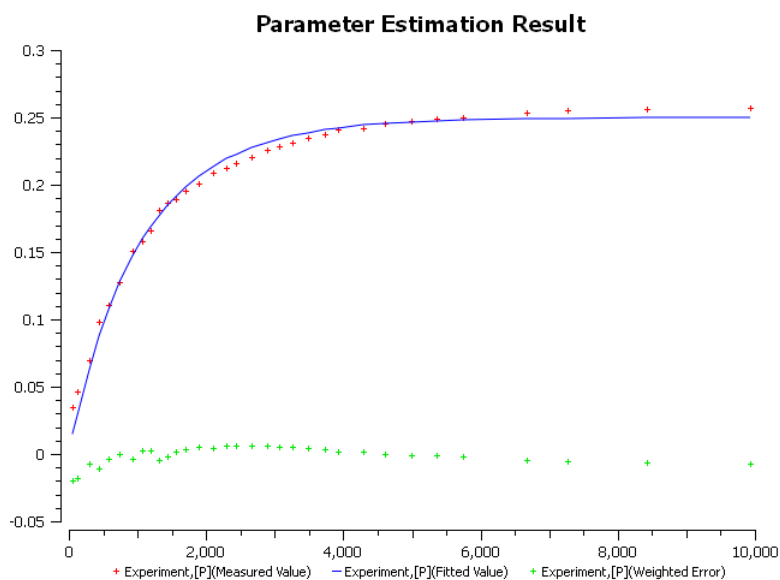


25 mol% catalyst

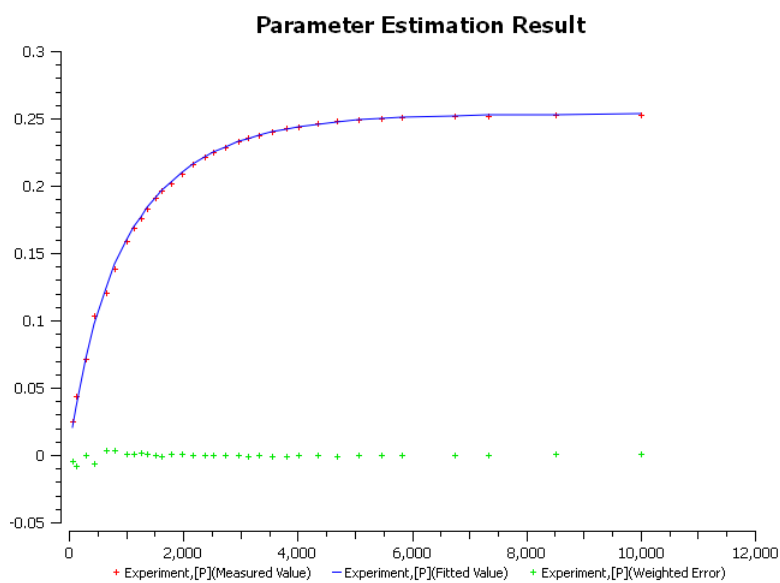
The following kinetic runs were performed with $c(\text{imine}) = 0.25 \text{ M}$ and $c(\text{ethyl acrylate}) = 1.00 \text{ M}$.



$$\begin{aligned} &1) 715.4 \\ &2) 729.8 \\ &3) 797.0 \\ &= 747.4 \pm 35.6 \end{aligned}$$



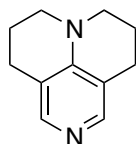
$$\begin{aligned} &1) 655.4 \\ &2) 568.3 \\ &= 611.9 \pm 43.6 \end{aligned}$$



12.5 mol% catalyst

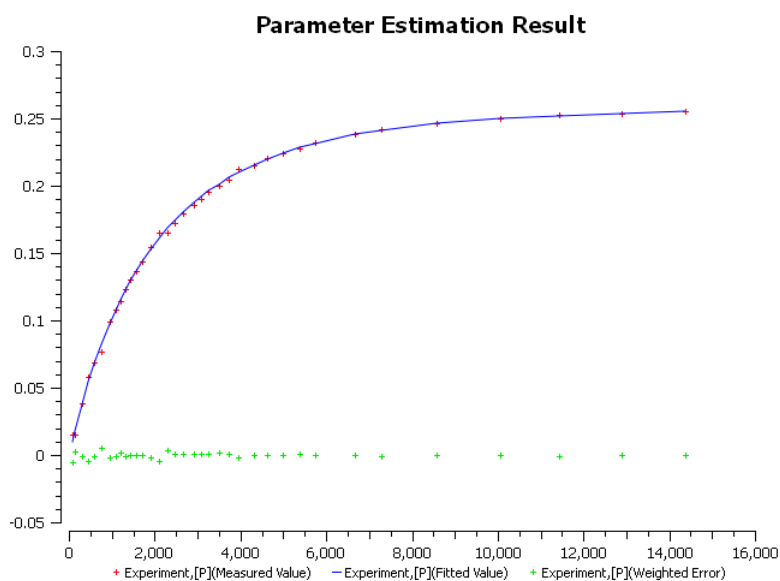
The measurements with 12.5 mol% catalyst loading were done in addition to the measurements with 25 mol%, but not discussed in the manuscript. The following kinetic runs were performed with $c(\text{imine}) = 0.25 \text{ M}$ and $c(\text{ethyl acrylat}) = 1.00 \text{ M}$.

Catalyst	Time [d]	Conversion ^[a,b] [%]	$t_{1/2}$ ^[c] [min]
10a	14	99	3113
3	6	99	1355

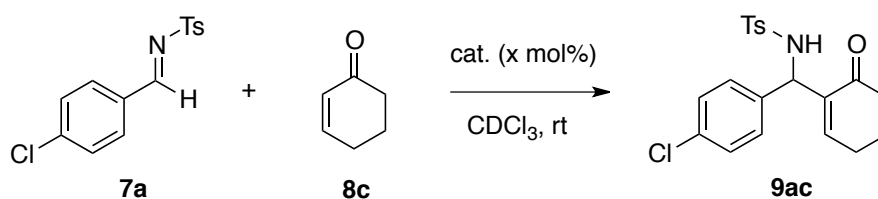


3

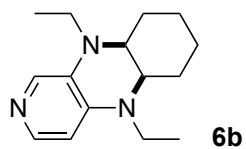
1) 1355



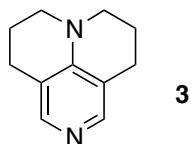
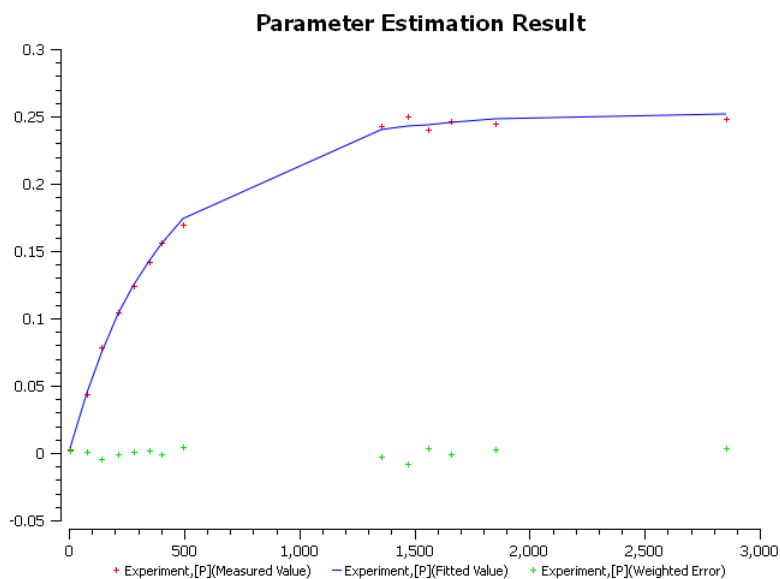
Kinetic data for reactions of tosylimine (**7a**) and cyclohexenone (**8c**).



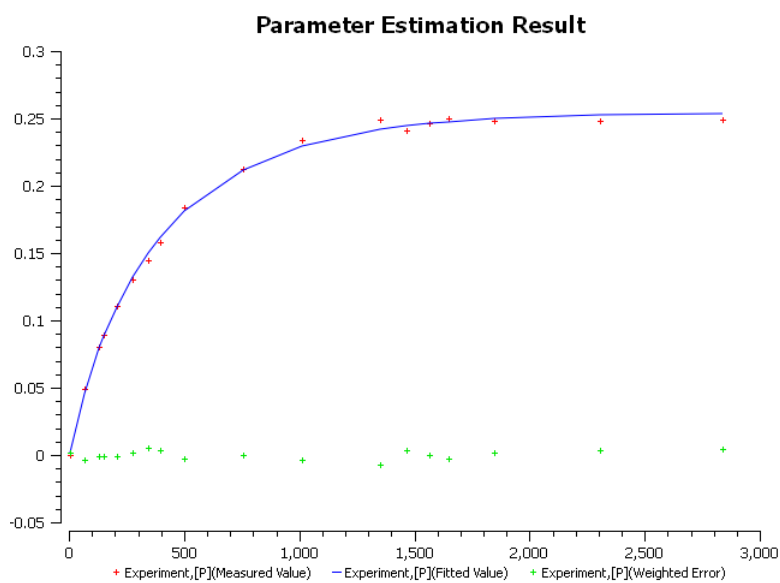
The following kinetic runs were performed with $c(\text{imine}) = 0.25 \text{ M}$ and $c(\text{cyclohexenone}) = 1.00 \text{ M}$.

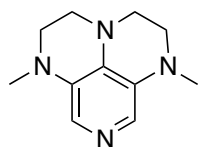


$$\begin{aligned} &1) \ 281.5 \\ &2) \ 247.3 \\ &= 264.4 \pm 17.1 \end{aligned}$$



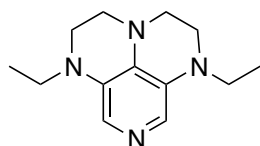
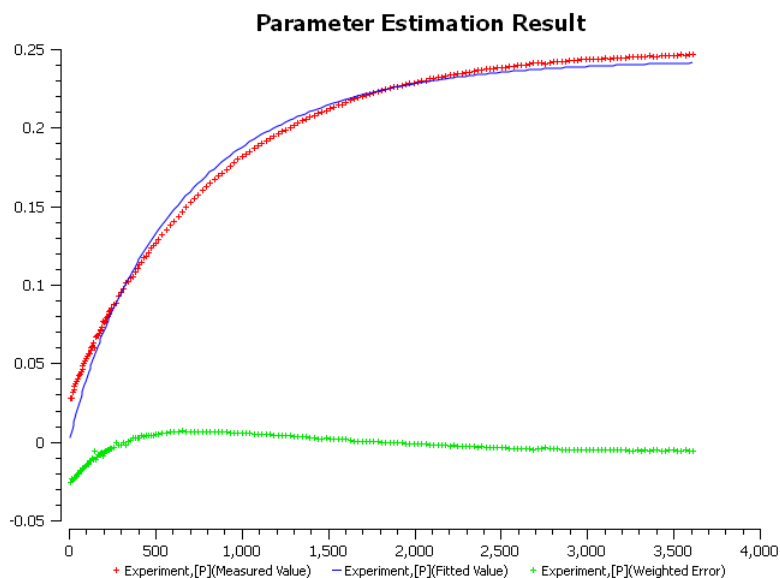
$$\begin{aligned} &3) \ 253.9 \\ &4) \ 230.6 \\ &= 242.3 \pm 11.7 \end{aligned}$$





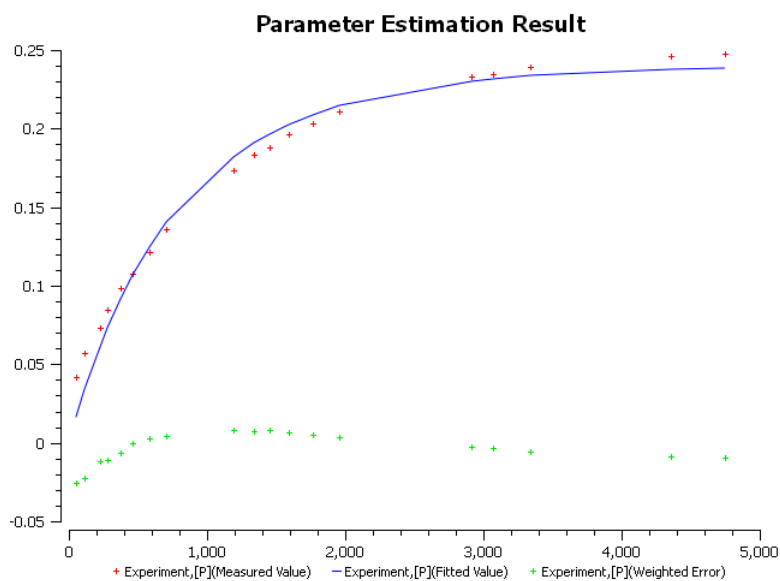
5a

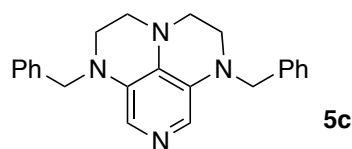
1) 456.6



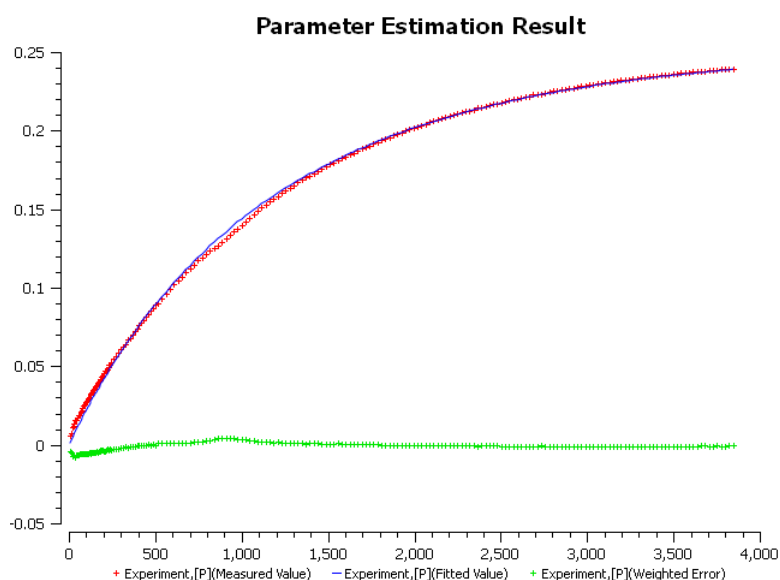
5b

1) 581.1

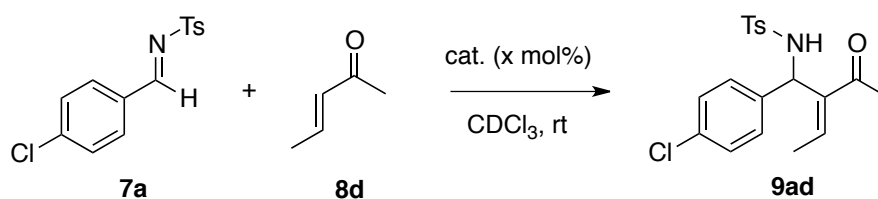




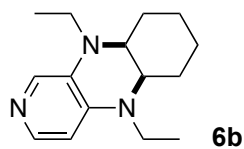
$$\begin{aligned} &1) \ 802.2 \\ &2) \ 713.6 \\ &= 757.9 \pm 44.3 \end{aligned}$$



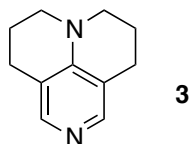
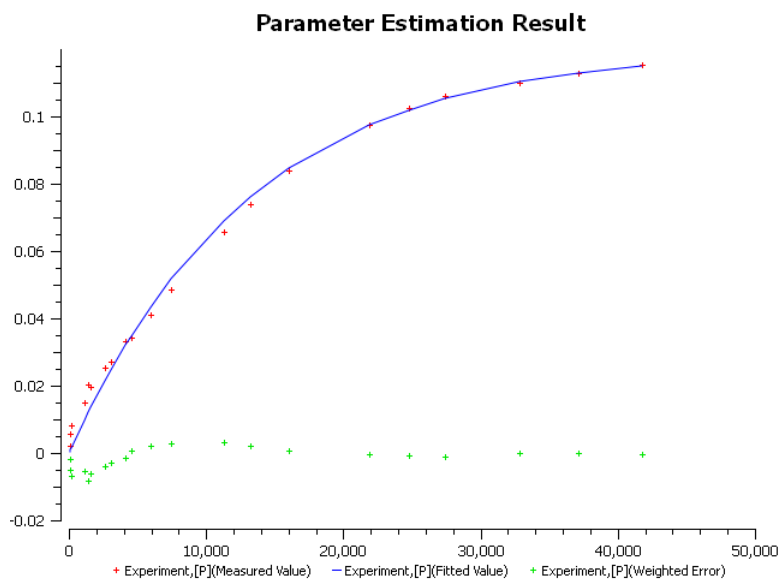
Kinetic data for reactions of tosylimine (**7a**) and *trans*-3-penten-2-one (**8d**).



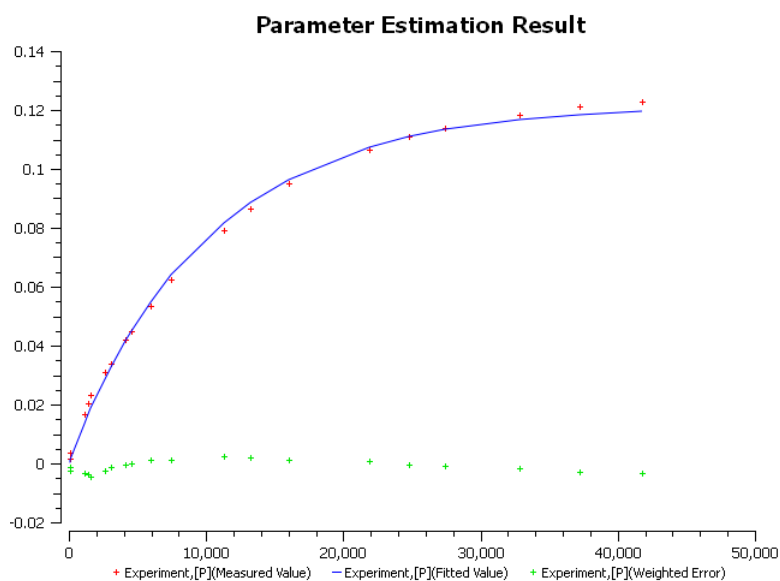
The following kinetic runs were performed with $c(\text{imine}) = 0.125 \text{ M}$ and $c(\text{trans-3-penten-2-one}) = 0.50 \text{ M}$.



1) 164 h



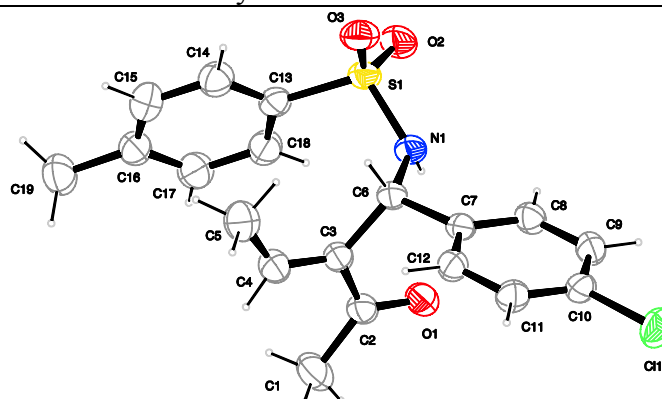
1) 120 h



X-ray analysis of 9ad

Table 7.8. Crystallographic data of **9ad**.

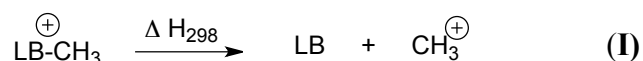
	9ad
net formula	C ₁₉ H ₂₀ ClNO ₃ S
$M_r/\text{g mol}^{-1}$	377.886
crystal size/mm	0.33 × 0.29 × 0.27
T/K	173(2)
radiation	MoK α
diffractometer	'KappaCCD'
crystal system	monoclinic
space group	$P2_1/n$
$a/\text{\AA}$	11.6299(2)
$b/\text{\AA}$	12.5750(3)
$c/\text{\AA}$	13.4433(2)
$\alpha/^\circ$	90
$\beta/^\circ$	103.9646(13)
$\gamma/^\circ$	90
$V/\text{\AA}^3$	1907.92(6)
Z	4
calc. density/ g cm^{-3}	1.31558(4)
μ/mm^{-1}	0.327
absorption correction	none
refls. measured	14916
R_{int}	0.0289
mean $\sigma(I)/I$	0.0245
θ range	3.24–27.42
observed refls.	3626
x, y (weighting scheme)	0.0456, 0.6132
hydrogen refinement	mixed
refls in refinement	4332
parameters	233
restraints	0
$R(F_{\text{obs}})$	0.0353
$R_w(F^2)$	0.0973
S	1.051
shift/error _{max}	0.001
max electron density/ e \AA^{-3}	0.305
min electron density/ e \AA^{-3}	−0.296



Computational methods and data

MCA values

Methyl cation affinities of pyridine and phosphane bases have been calculated as the reaction enthalpy at 298.15 K and 1 atm pressure for the methyl cation detachment reaction shown in eqn. (1). This is in analogy to the mass spectrometric definition of proton affinities.



The geometries of all species in eqn. (I) have been optimized at the B98/6-31G(d) level of theory. The conformational space of flexible pyridines and phosphanes and the corresponding cations has been searched using the MM3* force field and the systematic search routine implemented in MACROMODEL 9.7.^[16] All stationary points located at force field level have then been reoptimized at B98/6-31G(d) level as described before. Thermochemical corrections to 298.15 K have been calculated for all minima from unscaled vibrational frequencies obtained at this same level. The thermochemical corrections have been combined with single point energies calculated at the MP2(FC)/6-31+G(2d,p)//B98/6-31G(d) level to yield enthalpies H_{298} at 298.15 K. In conformationally flexible systems enthalpies have been calculated as Boltzmann-averaged values over all available conformers. This procedure has recently been found to reproduce G3 methyl cation affinity values of selected small and medium sized organocatalysts within 4.0 kJ mol⁻¹.^[14] All quantum mechanical calculations have been performed with Gaussian 03.^[16]

Table 7.9. Total energies and enthalpies (in Hartree) as calculated at the B98/6-31G(d) and MP2(FC)/6-31+G(2d,p)// B98/6-31G(d) level of theory for all systems. If more than one conformer exist at 298.15 K, the single values of each conformer are denoted as well as the Boltzmann-averaged values for H_{298} at MP2(FC)/6-31+G(2d,p)//B98/6-31G(d) level of theory. Only conformers are included with a Boltzmann-weighting of at least 1 % up to a maximum to ten conformations per system.

system	B98/6-31G(d)		MP2(FC)/6-31+G(2d,p)// B98/6-31G(d)	
	E_{tot}	H_{298}	E_{tot}	H_{298}
CH_3^+				-39.316929
CH_3^+	-39.462922	-39.427481	-39.352370	-39.316929
11				-344.154707
11_1	-345.194968	-345.003513	-344.346163	-344.154707
11-Me⁺				-383.685759
11-Me⁺_1	-384.879826	-384.643824	-383.921760	-383.685759

1				-381.007963
1_1	-382.100964	-381.928966	-381.179961	-381.007963
1-Me⁺				-420.546252
1-Me⁺_1	-421.801455	-421.585450	-420.762257	-420.546252
1c				-459.337226
1c_1	-460.699626	-460.467717	-459.569493	-459.337583
1c_2	-460.698872	-460.467017	-459.568777	-459.336921
1c_3	-460.695706	-460.463514	-459.566589	-459.334396
1c_4	-460.695601	-460.463698	-459.566199	-459.334296
1c_5	-460.688598	-460.457621	-459.563361	-459.332384
1c-Me⁺				-498.878535
1c-Me⁺_1	-500.402853	-500.126900	-499.155074	-498.879121
1c-Me⁺_2	-500.401457	-500.125500	-499.153700	-498.877743
1c-Me⁺_3	-500.401457	-500.125499	-499.153699	-498.877741
1c-Me⁺_4	-500.401452	-500.125503	-499.153680	-498.877730
1c-Me⁺_5	-500.398591	-500.122432	-499.150782	-498.874623
2				458.174353
2_1	-459.498999	-459.289442	-458.383909	-458.174353
2-Me⁺				-497.716038
2-Me⁺_1	-499.203048	-498.949398	-497.969688	-497.716038
13b				-591.693361
13b_1	-593.418065	-593.130882	-591.981253	-591.694070
13b_2	-593.417089	-593.130032	-591.980205	-591.693148
13b_3	-593.416648	-593.129503	-591.979900	-591.692755
13b_4	-593.415838	-593.128722	-591.978867	-591.691751
13b_5	-593.415488	-593.128356	-591.979018	-591.691886
13b_6	-593.415277	-593.127873	-591.978972	-591.691568
13b_7	-593.414082	-593.126927	-591.977705	-591.690550
13b-Me⁺				-631.242261
13b-Me⁺_1	-633.129214	-632.797785	-631.574118	-631.242689

13b-Me⁺_2	-633.129077	-632.797925	-631.573803	-631.242651
13b-Me⁺_3	-633.128021	-632.796615	-631.572771	-631.241365
13b-Me⁺_4	-633.127946	-632.796535	-631.572692	-631.241281
13b-Me⁺_5	-633.127843	-632.796281	-631.572934	-631.241371
13b-Me⁺_6	-633.126370	-632.794816	-631.571168	-631.239614
13b-Me⁺_7	-633.125330	-632.793715	-631.570008	-631.238393
6b				-747.191944
6b_1	-749.405682	-749.021776	-747.576377	-747.192470
6b_2	-749.407023	-749.022449	-747.576974	-747.192400
6b_3	-749.404877	-749.020263	-747.576944	-747.192329
6b_4	-749.405930	-749.021754	-747.576291	-747.192115
6b_5	-749.406234	-749.021772	-747.576561	-747.192098
6b_6	-749.404995	-749.020441	-747.576374	-747.191820
6b_7	-749.404598	-749.020095	-747.576157	-747.191654
6b_8	-749.404606	-749.020080	-747.576166	-747.191641
6b_9	-749.404830	-749.020098	-747.576215	-747.191483
6b_10	-749.406393	-749.021713	-747.576140	-747.191460
6b-Me⁺				-786.743479
6b-Me⁺_1	-789.121780	-788.692940	-787.173377	-786.744537
6b-Me⁺_2	-789.120016	-788.691557	-787.171915	-786.743456
6b-Me⁺_3	-789.120407	-788.691692	-787.172037	-786.743323
6b-Me⁺_4	-789.120407	-788.691688	-787.172038	-786.743319
6b-Me⁺_5	-789.119194	-788.690414	-787.171900	-786.743119
6b-Me⁺_6	-789.118810	-788.690096	-787.171405	-786.742691
6b-Me⁺_7	-789.118811	-788.690086	-787.171398	-786.742672
6b-Me⁺_8	-789.119475	-788.691090	-787.170972	-786.742587
6b-Me⁺_9	-789.119294	-788.690807	-787.170819	-786.742332
6b-Me⁺_10	-789.118385	-788.689728	-787.170896	-786.742240
3				-535.355098
3_1	-536.905604	-536.658613	-535.602351	-535.355360

3_2	-536.904889	-536.657992	-535.601147	-535.354250
3-Me⁺				-574.901592
3-Me⁺_1	-576.614364	-576.323195	-575.192993	-574.901824
3-Me⁺_2	-576.613741	-576.322527	-575.192298	-574.901084
5a				-645.721376
5a_1	-647.539246	-647.256369	-646.004511	-645.721634
5a_2	-647.537517	-647.254755	-646.002984	-645.720222
5a-Me⁺				-685.273939
5a-Me⁺_1	-687.253802	-686.926838	-685.601105	-685.274140
5a-Me⁺_2	-687.253201	-686.926208	-685.600563	-685.273570
5b				-724.049255
5b_1	-726.136622	-725.794008	-724.392585	-724.049971
5b_2	-726.135261	-725.792675	-724.391022	-724.048436
5b_3	-726.134093	-725.791344	-724.390368	-724.047619
5b_4	-726.133773	-725.791105	-724.389136	-724.046468
5b_5	-726.133843	-725.791423	-724.389524	-724.047104
5b_6	-726.132311	-725.789756	-724.388635	-724.046080
5b_7	-726.132623	-725.790069	-724.388834	-724.046280
5b_8	-726.132578	-725.790061	-724.388529	-724.046012
5b_9	-726.131575	-725.788592	-724.388232	-724.045249
5b_10	-726.130711	-725.787685	-724.387694	-724.044668
5b-Me⁺				-763.602939
5b-Me⁺_1	-765.851994	-765.465346	-763.990563	-763.603916
5b-Me⁺_2	-765.850785	-765.463869	-763.989319	-763.602403
5b-Me⁺_3	-765.850315	-765.463344	-763.989001	-763.602030
5b-Me⁺_4	-765.849640	-765.463028	-763.988190	-763.601579
5b-Me⁺_5	-765.850795	-765.463913	-763.989104	-763.602221
5b-Me⁺_6	-765.849161	-765.462332	-763.987775	-763.600947
5b-Me⁺_7	-765.849609	-765.462936	-763.988073	-763.601401
5b-Me⁺_8	-765.849628	-765.462808	-763.988274	-763.601454

5b-Me⁺_9	-765.848774	-765.461441	-763.987533	-763.600200
5b-Me⁺_10	-765.848364	-765.461579	-763.986967	-763.600182
5c				-1106.348047
5c_1	-1109.447043	-1108.993196	-1106.802424	-1106.348577
5c_2	-1109.447132	-1108.993055	-1106.802354	-1106.348278
5c_3	-1109.447628	-1108.993564	-1106.802303	-1106.348239
5c_4	-1109.447585	-1108.993563	-1106.802088	-1106.348066
5c_5	-1109.447026	-1108.992980	-1106.801891	-1106.347844
5c_6	-1109.446406	-1108.992420	-1106.801637	-1106.347651
5c_7	-1109.447786	-1108.993676	-1106.802326	-1106.348216
5c_8	-1109.444983	-1108.991221	-1106.800827	-1106.347065
5c_9	-1109.448248	-1108.994131	-1106.802136	-1106.348019
5c_10	-1109.446099	-1108.991892	-1106.800767	-1106.346560
5c-Me⁺				-1145.907501
5c-Me⁺_1	-1149.167468	-1148.669290	-1146.406434	-1145.908256
5c-Me⁺_2	-1149.166518	-1148.668217	-1146.405837	-1145.907536
5c-Me⁺_3	-1149.166429	-1148.668220	-1146.404848	-1145.906639
5c-Me⁺_4	-1149.166725	-1148.668311	-1146.404532	-1145.906118
5c-Me⁺_5	-1149.166180	-1148.667997	-114.640404	-1145.905857
5c-Me⁺_6	-1149.165179	-1148.666903	-1146.403228	-1145.904953
5c-Me⁺_7	-1149.165420	-1148.667213	-1146.403135	-1145.904928
5c-Me⁺_8	-1149.165655	-1148.667434	-1146.402799	-1145.904578
5c-Me⁺_9	-1149.165740	-1148.667407	-1146.402253	-1145.903920
5c-Me⁺_10	-1149.166086	-1148.667599	-1146.402329	-1145.903842

7.5 References

- [1] Recent reviews of MBH and *aza*MBH reactions: (a) D. Basavaiah, A. J. Rao, T. Satyanarayana, *Chem. Rev.* **2003**, *103*, 811–892. (b) D. Basavaiah, K. V. Rao, R. J. Reddy, *Chem. Soc. Rev.* **2007**, *36*, 1581–1588. (c) G. Masson, C. Housseman, J. Zhu, *Angew. Chem. Int. Ed.* **2007**, *46*, 4614–4628. (d) Y.-L. Shi, M. Shi, *Eur. J. Org. Chem.* **2007**, 2905–2916. (e) V. Singh, S. Batra, *Tetrahedron* **2008**, *64*, 4511–4574. (f) V. Declerck, J. Martinez, F. Lamaty, *Chem. Rev.* **2009**, *109*, 1–48. (g) J. Mansilla, J. M. Saa, *Molecules* **2010**, *15*, 709–734. (h) D. Basavaiah, B. S. Reddy, S. S. Badsara, *Chem. Rev.* **2010**, *110*, 5447–5674.
- [2] For selected examples, see: (a) M. Shi, Y.-M. Xu, *Chem. Commun.* **2001**, 1876–1877. (b) V. K. Aggarwal, A. M. M. Castro, A. Mereu, H. Adams, *Tetrahedron Lett.* **2002**, *43*, 1577–1581. (c) Y.-M. Xu, M. Shi, *J. Org. Chem.* **2004**, *69*, 417–425. (d) G.-L. Zhao, M. Shi, *J. Org. Chem.* **2005**, *70*, 9975–9984. (e) X. Tang, B. Zhang, Z. He, R. Gao, Z. He, *Adv. Synth. Catal.* **2007**, *349*, 2007–2017. For further examples see refs 1f and 1h.
- [3] For selected examples, see: (a) V. K. Aggarwal, A. Mereu, G. J. Tarver, R. McCague, *J. Org. Chem.* **1998**, *63*, 7183–7189. (b) S. Kobayashi, T. Busujima, S. Nagayama, *Chem. Eur. J.* **2000**, *6*, 3491–3494. (c) P. Buskens, J. Klankermayer, W. Leitner, *J. Am. Chem. Soc.* **2005**, *127*, 16762–16763. (d) I. T. Raheem, E. N. Jacobsen, *Adv. Synth. Catal.* **2005**, *347*, 1701–1708. Further examples can be found in references 1f and 1h.
- [4] T. Yukawa, B. Seelig, Y. Xu, H. Morimoto, S. Matsunaga, A. Berkessel, M. Shibasaki, *J. Am. Chem. Soc.* **2010**, *132*, 11988–11992.
- [5] (a) N. T. McDougal, S. E. Schaus, *J. Am. Chem. Soc.* **2003**, *125*, 12094–12095. (b) N. T. McDougal, W. L. Trevellini, S. A. Rodgen, L. T. Kliman, S. E. Schaus, *Adv. Synth. Catal.* **2004**, *346*, 1231–1240.
- [6] (a) K. Matsui, S. Takizawa, H. Sasai, *J. Am. Chem. Soc.* **2005**, *127*, 3680–3681. (b) K. Matsui, K. Tanaka, A. Horii, S. Takizawa, H. Sasai, *Tetrahedron: Asymmetry* **2006**, *17*, 578–583. (c) N. Abermil, G. Masson, J. Zhu, *J. Am. Chem. Soc.* **2008**, *130*, 12596–12597. (d) N. Abermil, G. Masson, J. Zhu, *Adv. Synth. Catal.* **2010**, *352*, 656–660.
- [7] (a) M. Shi, Y.-M. Xu, *Angew. Chem., Int. Ed.* **2002**, *41*, 4507–4510. (b) M. Shi, L.-H. Chen, *Chem. Commun.* **2003**, 1310–1311. (c) M. Shi, L.-H. Chen, C.-Q. Li, *J. Am. Chem. Soc.* **2005**, *127*, 3790–3800. (d) M. Shi, Y.-M. Xu, Y.-L. Shi, *Chem. Eur. J.* **2005**, *11*, 1794–1802. (e) M. Shi, L.-H. Chen, W.-D. Teng, *Adv. Synth. Catal.* **2005**, *347*, 1781–1789. (f) Y.-H. Liu, L.-H. Chen, M. Shi, *Adv. Synth. Catal.* **2006**, *348*, 973–979. (g) K. Matsui, S. Takizawa, H. Sasai, *Synlett* **2006**, 761–765. (h) K. Ito, K. Nishida, T. Gotauda, *Tetrahedron Lett.* **2007**, *48*, 6147–6149. (i) Z.-Y. Lei, X.-G. Liu, M. Shi, M. Zhao, *Tetrahedron: Asymmetry* **2008**, *19*, 2058–2062. (j) X.-Y. Guan, Y.-Q. Jiang, M. Shi, *Eur. J. Org. Chem.* **2008**, 2150–2155. (k) J.-M. Garnier, C. Anstiss, F. Liu, *Adv. Synth. Catal.* **2009**, *351*, 331–338. (l) J.-M. Garnier, F. Liu, *Org. Biomol.*

- Chem.* **2009**, *7*, 1272–1275. For multifunctional phosphane catalysts review: (m) Y. Wei, M. Shi, *Acc. Chem. Res.* **2010**, *43*, 1005–1018.
- [8] (a) C. Z. Yu, B. Liu, L. Q. Hu, *J. Org. Chem.* **2001**, *66*, 5413–5418. (b) R. Gausepohl, P. Buskens, J. Kleinen, A. Bruckmann, C. W. Lehmann, J. Klankermayer, W. Leitner, *Angew. Chem. Int. Ed.* **2006**, *45*, 3689–3692.
- [9] R. Robiette, V. K. Aggarwal, J. N. Harvey, *J. Am. Chem. Soc.* **2007**, *129*, 15513–15525.
- [10] J. S. Hill, N. S. Isaacs, *J. Phys. Org. Chem.* **1990**, *3*, 285–288.
- [11] V. K. Aggarwal, S. Y. Fulford, G. C. Lloyd-Jones, *Angew. Chem. Int. Ed.* **2005**, *44*, 1706–1708.
- [12] (a) U. Mayer, V. Gutmann, W. Gerger, *Monatsh. Chem.* **1975**, *106*, 1235–1257. (b) V. Gutmann, *Electrochem. Acta* **1976**, *21*, 661–670. (c) V. Gutmann, *Coord. Chem. Rev.* **1976**, *18*, 225–255.
- [13] (a) P. M. E. Mancini, R. D. Martinez, L. R. Vottero, N. S. Nudelman, *J. Chem. Soc., Perkin Trans.* **1984**, *2*, 1133–1138. (b) H. Kropt, M. R. Yazdanbachs, *Tetrahedron* **1974**, *30*, 3455–3459.
- [14] (a) C. Lindner, B. Maryasin, F. Richter, H. Zipse, *J. Phys. Org. Chem.* **2010**, *23*, 1036–1042. (b) Y. Wei, G. N. Sastry, H. Zipse, *J. Am. Chem. Soc.* **2008**, *130*, 3473–3477. (c) Y. Wei, T. Singer, H. Mayr, G. N. Sastry, H. Zipse, *J. Comp. Chem.* **2008**, *29*, 291–297.
- [15] (a) S. Hoops, S. Sahle, R. Gauges, C. Lee, J. Pahle, N. Simus, M. Singhal, L. Xu, P. Mendes, U. Kummer, *Bioinformatics* **2006**, *22*, 3067–3074. (b) Schrödinger, LLC., MacroModel 9.7, **2009**. (c) M. J. Frisch, G. W. Trucks, H. B. Schlegel, G. E. Scuseria, M. A. Robb, J. R. Cheeseman, J. A. Montgomery, Jr, T. Vreven, K. N. Kudin, J. C. Burant, J. M. Millam, S. S. Iyengar, J. Tomasi, V. Barone, B. Mennucci, M. Cossi, G. Scalmani, N. Rega, G. A. Petersson, H. Nakatsuji, M. Hada, M. Ehara, K. Toyota, R. Fukuda, J. Hasegawa, M. Ishida, T. Nakajima, Y. Honda, O. Kitao, H. Nakai, M. Klene, X. Li, J. E. Knox, H. P. Hratchian, J. B. Cross, V. Bakken, C. Adamo, J. Jaramillo, R. Gomperts, R. E. Stratmann, O. Yazyev, A. J. Austin, R. Cammi, C. Pomelli, J. W. Ochterski, P. Y. Ayala, K. Morokuma, G. A. Voth, P. Salvador, J. J. Dannenberg, V. G. Zakrzewski, S. Dapprich, A. D. Daniels, M. C. Strain, O. Farkas, D. K. Malick, A. D. Rabuck, K. Raghavachari, J. B. Foresman, J. V. Ortiz, Q. Cui, A. G. Baboul, S. Clifford, J. Cioslowski, B. B. Stefanov, G. Liu, A. Liashenko, P. Piskorz, I. Komaromi, R. L. Martin, D. J. Fox, T. Keith, M. A. Al-Laham, C. Y. Peng, A. Nanayakkara, M. Challacombe, P. M. W. Gill, B. Johnson, W. Chen, M. W. Wong, C. Gonzalez, J. A. Pople, Gaussian 03, Revision D.01, Gaussian, Inc., Wallingford CT, **2004**.Gaussian.
- [16] (a) V. D'Elia, Y. Liu, H. Zipse, *Eur. J. Org. Chem.* **2011**, 1527–1533. (b) I. Held, E. Larionov, C. Bozler, F. Wagner, H. Zipse, *Synthesis* **2009**, 2267–2277. (c) I. Held, P.

- von den Hoff, D. S. Stephenson, H. Zipse, *Adv. Synth. Catal.* **2008**, 350, 1891–1900.
(d) I. Held, S. Xu, H. Zipse, *Synthesis* **2007**, 1185–1196. (e) M. R. Heinrich, H. S. Klisa, H. Mayr, W. Steglich, H. Zipse, *Angew. Chem. Int. Ed.* **2003**, 42, 4826–4828.
- [17] V. S. Bryantsev, M. S. Diallo, W. A. Goddard III, *J. Phys. Chem. B* **2008**, 112, 9709–9719.
- [18] C. P. Kelly, C. J. Cramer, D. G. Truhlar, *J. Chem. Theory Comput.* **2005**, 1, 1133.
- [19] C. P. Kelly, C. J. Cramer, D. G. Truhlar, *J. Phys. Chem. B* **2006**, 110, 16066.
- [20] L. P. Hammett, *J. Am. Chem. Soc.* **1937**, 59, 96.
- [21] Y. Wei, B. Sateesh, B. Maryasin, G. N. Sastry, H. Zipse, *J. Comp. Chem.* **2009**, 2617–2624.
- [22] V. Lutz, J. Glatthaar, C. Würtele, M. Serafin, H. Hausmann, P. R. Schreiner, *Chem. Eur. J.* **2009**, 15, 8548–8557.
- [23] C. B. Fisher, S. Xu, H. Zipse, *Chem. Eur. J.* **2006**, 12, 5779–5784.
- [24] C. K. M. Heo, J. W. Bunting, *J. Org. Chem.* **1992**, 57, 3570–3578.
- [25] C. Hansch, A. Leo and R. W. Taft, *Chem. Rev.* **1991**, 91, 165–195.
- [26] Y. Liu, M. Shi, *Adv. Synth. Catal.* **2008**, 350, 122–128.
- [27] C. Anstiss, F. Liu, *Tetrahedron* **2010**, 66, 5486–5491.
- [28] Z.-Y. Lei, M. Shi, G.-N. Ma, *Eur. J. Org. Chem.* **2008**, 3817–3820.
- [29] M. Shi, Y.-M. Xu, G.L. Zhao, X.-F. Wu, *Eur. J. Org. Chem.* **2002**, 3666–3679.

Chapter 8

Polymerisation of Lactides Mediated by DMAP-Derivatives

8.1 Introduction

In the last decades a basic idea of an ecologically compatible economic management arose under catchphrases like “Green Chemistry”. These circumstances lead chemists to create environmentally reconcilable synthetic strategies and materials without detriment in terms of product characteristics and mechanical properties. One of these materials is polylactide (PLA), which is supplanting more and more petrochemical plastics.^[1] Polylactide is produced out of corn and sugar beets, which are cheap and renewable materials,^[2] and exhibits a better cost-benefit ratio not only due to its recyclability.^[3] It is compostable and decomposable through enzymes, thus minimizing the problem of waste management.^[4] It is not surprising that PLA already found its way into biomedical applications, packaging, fibres and e.g. microelectronics.^[5,6] One problem that occurs for the bulk synthesis are tin compounds, which are commonly used as initiators or catalysts.^[8,9] The catalysts are often too expensive or hard to remove from the polymer and thus accompanied by inadvertently accumulation effects.^[10] As a consequence these tin compounds are to be substituted by either non toxic metal based catalysts^[1,3,11] or organocatalysts.^[12] In the area of organocatalyzed lactide polymerization Hedrick *et al.* showed that DMAP (**1**) is a powerful organocatalyst yielding very narrow distributions of molecular weights. Moreover a linear relationship between molecular weight and monomer conversion was obtained.^[12b] DMAP (**1**) was found already in 1969 by Steglich and Höfle and is nowadays the catalyst of choice (in terms of cost-benefit ratio) for acylations of sterically demanding alcohols.^[13] The catalyst motif of DMAP (**1**) evolved during the years and even more powerful catalysts were found (see Figure 8.1).^[14-16]

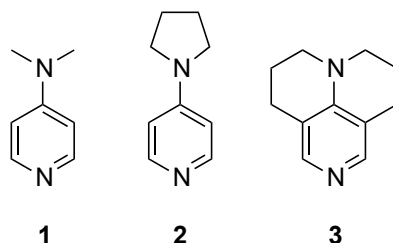


Figure 8.1. Catalysts based on the DMAP (**1**) motif.

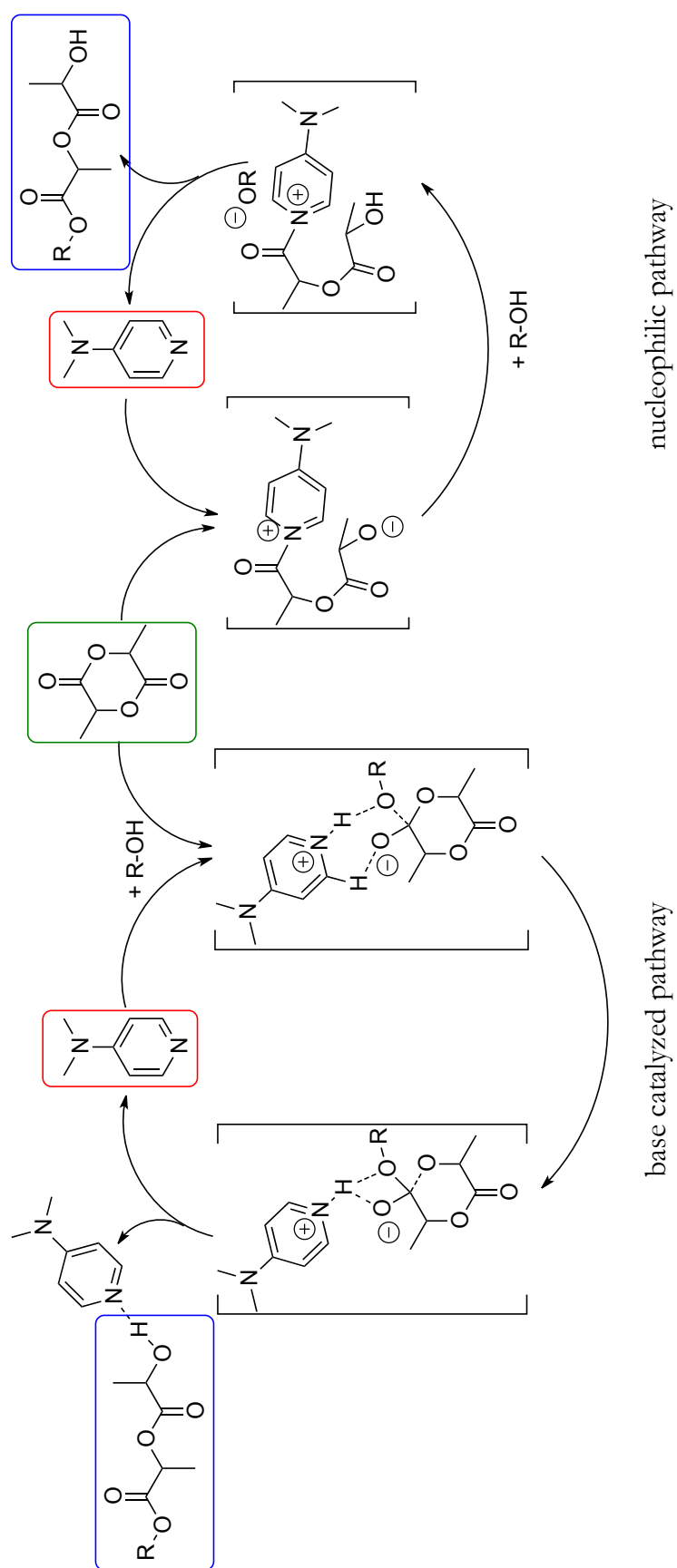
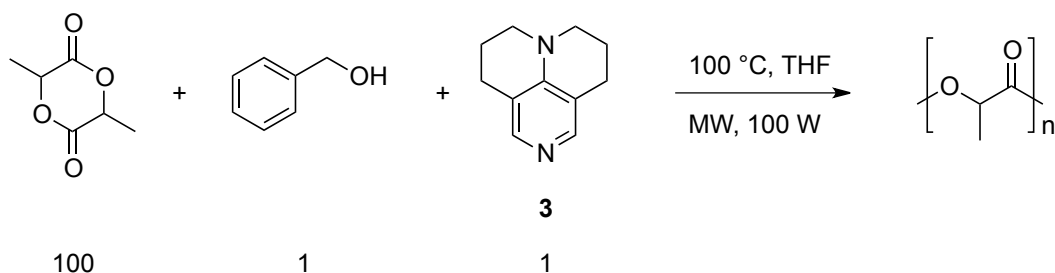


Figure 8.2. Accepted nucleophilic and base catalyzed mechanism for ROP using DMAP (1).

PPY (**2**) can catalyze the ROP of lactide only in the melt and is moreover substantial slower than DMAP (20 h vs. 20 min).^[5a,17,18] Concerning the mechanism of lactide polymerization using organocatalysts like DMAP (**1**) two different pathways are possible (Figure 8.2). On the one hand a nucleophilic pathway in which the organocatalyst itself reacts and activates the lactide monomer is discussed. On the other hand an alcohol activation mechanism where the organocatalyst serves as a base is possible. Computational studies predict the base-catalyzed pathway to be lower in energy (gas phase), but in solution, especially with an alcohol as initiator involved, things may change and the nucleophilic pathway could be predominant.^[19] More powerful catalysts than DMAP (**1**) like 9-azajulolidine (**3**) are already commercially available now. In this study we wanted to figure out if 9-azajulolidine (**3**) can show its superior catalytic behavior compared to **1** and **2** (which was already demonstrated in different other reactions)^[14, 20, 21, 22] also in the polymerization of lactide. Furthermore, we tried to utilize microwave technology as a source of heat. To the best of our knowledge no previous report exists yet on the ROP using microwave reactors and therefore we had to develop an optimized reaction protocol for the ROP using organocatalysts.

8.2 Results and Discussion

If not stated differently, polymerization studies were conducted with sublimated lactide, benzyl alcohol and catalyst **3** in a ratio of 100:1:1 in dry THF using stock solutions to minimize errors. The determination of yield was done by ¹H NMR, and number (M_n) and mass (M_w) averaged molar masses were analyzed by gel permeation chromatography (GPC) (details see Experimental Part 8.4).



Scheme 8.1. Standard reaction conditions for ring opening polymerization of lactide in the microwave using **3** as nucleophilic organocatalyst in THF.

In order to identify the best conditions for lactide polymerization using microwave technology several parameters like temperature, time, lactide to catalyst ratio, different catalysts and addition of co-catalysts were tested. In Table 8.1 the different reactions are listed (the entries are separated with horizontal lines according to the effects discussed in the text below).

Table 8.1. Optimization studies for ring opening polymerization of lactide with nucleophilic organocatalysts in a CEM microwave reactor.

Entry	Ratio ^[a]	Catalyst	Temp. [°C]	Time [h]	Conv. [%]	M _n [g/mol]	M _w [g/mol]	PD
1	100:1:1	3	150 ^[b]	24	98	1600	3800	2.38
2	100:1:1	3	150	4	98	1200	1900	1.58
3	100:1:1	3	150	8	98	600	3400	5.67
4	100:1:1	3	125	2	91	1200	1800	1.50
5	100:1:0.81	3	110	2	17			
6	100:1:0.81	3	90	8	23			
7	100:1:1	3	100	21	79			
8	100:1:1	3	100	45	94	1500	2900	1.93
9	200:1:1	3	100	24	74	2500	4300	1.72
10	200:1:1	3	100	48	89	3300	6500	1.96
11	100:1:1.03	3	100	0.3	9			
12	100:1:4.5	3	100	0.3	60			
13	100:1:1.3	3	100	24	93	3700	8400	2.27
14	100:1:1.3 ^[c]	3	100	24	87	1900	2800	1.47
15	100:1:1.3	3	100	24	93	3700	8400	2.27
16	100:1:1.3:1 ^[d]	3	100	24	93	1400	2100	1.50
17	100:1:1.3	1	100	24	62	2100	2900	1.38
18	100:1:1.3	2	100	24	84	2300	3100	1.35
19	100:1:1.3	3	100	24	93	3700	8400	2.27
20	100:1:1.3	1	100	48	83	2100	3400	1.62
21	100:1:1.3	2	100	48	94	1700	3000	1.76
22	100:1:1.3	3	100	48	93	2500	4800	1.92
23	100:1:1	3	100	4	23			
24	100:1:1	3	100	8	50			
25	100:1:1	3	100	21	79			
26	100:1:1	3	100	45	94	1500	2900	1.93
27	100:1:1	3	100	69	95	1100	2500	2.27
28	100:1:1	3	100	93	96	800	2000	2.50
29	100:1:1	3	100	117	97	700	1900	2.71
30	100:1:1	3	50 ^[e]	286	86	291	455	1.56

[a] Ratio of lactide/benzyl alcohol/catalyst; [b] Reaction performed in a standard chemical oven (not in the microwave reactor); [c] With freshly distilled benzyl alcohol; [d] One equivalent of co-catalyst 4-nitrophenol is added; [e] In CDCl₃, heated in a conventional oil bath.

The polymerization of lactide is often conducted in the melt in an oven.^[11] Running the reaction in bulk in an oven (melt) at 150 °C after 24 hours reaction time a conversion of 98 % was obtained for the reaction mixture of lactide/benzyl alcohol/**3** in the ratio of 100:1:1 (entry 1). The polymer distribution is broad (PD = 2.38) and the weight averaged molar mass amounts up to 3800 g/mol. Applying the same conditions with exception of the source of heat now being a microwave reactor, 4 hours reaction time are already enough to obtain the same yield with a better polymer distribution (PD=1.58), but the weight averaged molar mass drops by half (entry 2). In contrary to the melt in the oven, a black substance is observed (already after 25 min) in the microwave reactor, which is only possible to separate from the reaction vessel with great loss of product (Figure 8.4). Separate reference measurements with one single starting material in the reaction vial showed no decomposition.



Figure 8.4. Black reaction mixture obtained in melt in the microwave reactor at 150 °C.

Entries 2 and 3 in Table 8.1 show that doubling the reaction time (in melt) from 4 h to 8 h gives slightly better values for M_w , but the mass distribution within the polymer is about three times broader which is indicated by the PD value. Lowering the temperature to 125 °C and halve the reaction time to 2 hours changes almost nothing (entry 4). Since neat reactions were not applicable utilizing the microwave reactor, the following experiments were conducted in THF solution. At temperatures of 110 °C at slightly lower catalyst concentration the conversion after 2 hours amounted up to 17 % (entry 5). Lowering the temperature to 90 °C (entry 6) a reaction time of 8 hours was necessary to achieve similar yields which is also in accordance with the Arrhenius equation^[23]. The optimization of the lactide ratio was performed at 100 °C applying longer reaction times of 21 to 48 hours. It was found that a ratio of lactide/benzyl alcohol/**3** of 200:1:1 requires slightly longer reaction times, but gives much higher weight averaged molar masses with equal PD values (entries 7 to 10). Varying the catalyst concentration from lactide/benzyl alcohol/**3** 100:1:1.03 to 100:1:4.5, a dramatic increase in reaction speed is obtained. After 20 minutes a conversion of 60 % is obtained (entries 11 and 12). Does the purity of the initiator benzyl alcohol have any effect on the polymerization? To clarify this question we distilled the commercially available benzyl alcohol, which the supplier states to be of ≥ 99 % purity with the only impurity being < 0.005 % water. Water could actually lead to hydrolysis of the ester functionality already in small quantities, especially when having a catalyst like **3** in the reaction mixture. Entries 13 and 14 in Table 8.1 show, that using the purchased initiator much higher weight averaged molar masses are obtained whereas the distillation showed a more controlled polymerization, indicated by the much better PD value. The positive catalytic effects by addition of co-catalysts like 4-nitrophenol is already known from other reactions, like the Morita-Baylis-Hillman reaction^[24]. The addition of a mild Brønstedt acid accelerates usually the proton transfer step, which makes the combined acid base catalysis to a powerful tool for synthesis. In case of the lactide polymerization the co-catalyst 4-nitrophenol gives a much sharper polymer distribution (PD = 1.47) while the weight averaged molar mass drops to 2100 g/mol (entry 16), which is a 4-fold decrease compared to the reaction having no additives inside (entry 15). From the work of Steglich and Zipse *et al.* we know already that **3** is superior to **1** and **2** in terms of catalytic activity in acylation reactions by a factor of 10.^[14,25] The comparison of **1**, **2** and **3** regarding their ROP abilities of lactide were tested at reaction times of 24 and 48 hours. From the conversion of the three catalysts (Figure 8.5, the dashed lines in

Figure 8.5 are only included to guide the eye) it was observed, that not only for acylation or aza-Morita-Baylis-Hillman reactions **3** is superior to **2** and **1** (entries 17 to 22).^[14, 20, 21] Whereas catalyst **3** shows already 93 % conversion after 24 hours the yields of **2** and **1** are still increasing. After 48 hours **1** reached 83 % and **2** as well as **3** over 93 % yield.

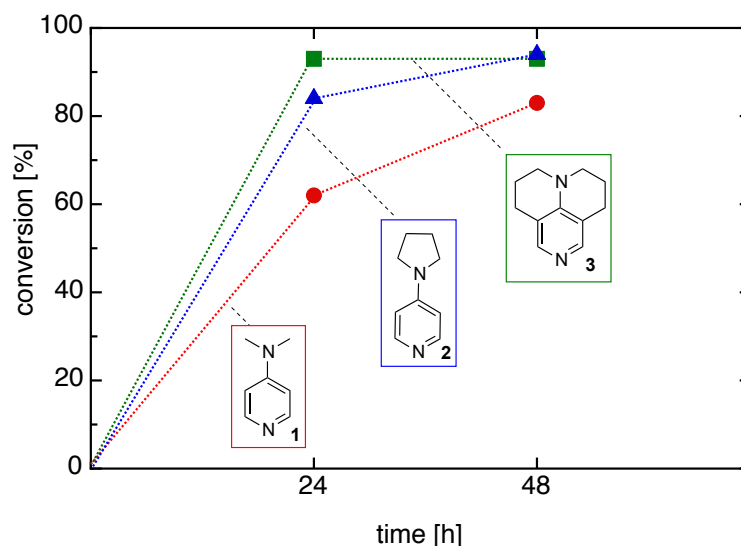


Figure 8.5. Conversion vs. time of **1** (red circles), **2** (blue triangles) and **3** (green squares) for a reaction mixture of lactide/benzyl alcohol/catalyst 100:1:1.3 at 100 °C in THF in the microwave.

A graphical comparison of the weight averaged molar masses at 24 and 48 hours reaction time (Figure 8.6) shows that **3** gives the biggest value of 8400 g/mol after 24 hours and decreases after 48 hours to 4800 g/mol. The weight averaged molar mass of DMAP (**1**) increases slightly from 2900 to 3400 g/mol whereas for **2** is seems almost constant comparing the results at 24 and 48 hours reaction time.

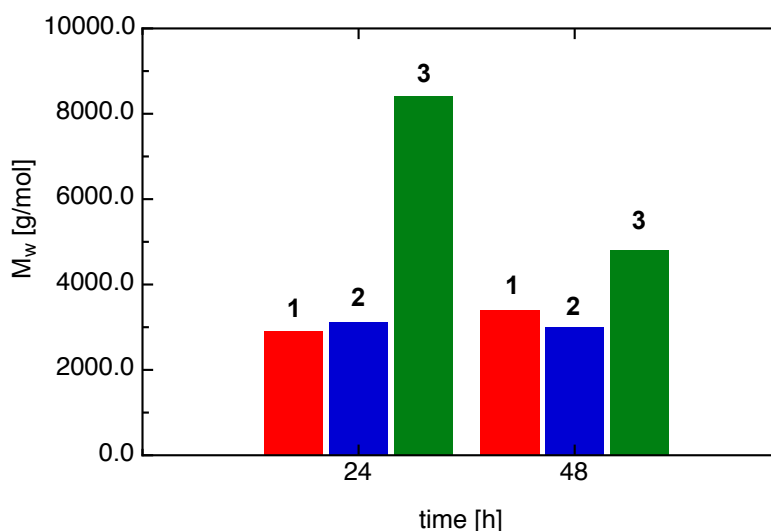


Figure 8.6. M_w vs. time of **1** (red bar), **2** (blue bar) and **3** (green bar) for a reaction mixture of lactide/benzyl alcohol/catalyst 100:1:1.3 at 100 °C in THF in the microwave.

Taking a closer look at the number averaged molar masses, that of **1** does not change after 24 and 48 hours. The number averaged molar mass of **2** is slightly decreasing and that of **3** after 48 hours amounts only up to 67 % compared to that of 24 hours.

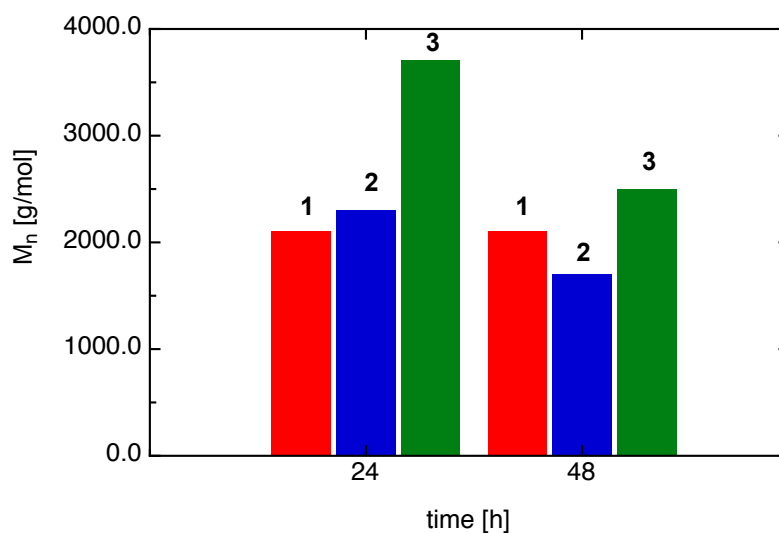


Figure 8.7. M_n vs. time of **1** (red bar), **2** (blue bar) and **3** (green bar) for a reaction mixture of lactide/benzyl alcohol/catalyst 100:1:1.3 at 100 °C in THF in the microwave.

The PD trend (Figure 8.8) shows for **1** and **2** an increase and for **3** a decrease, this could be evidence for the enhanced depolymerization of larger polymers.

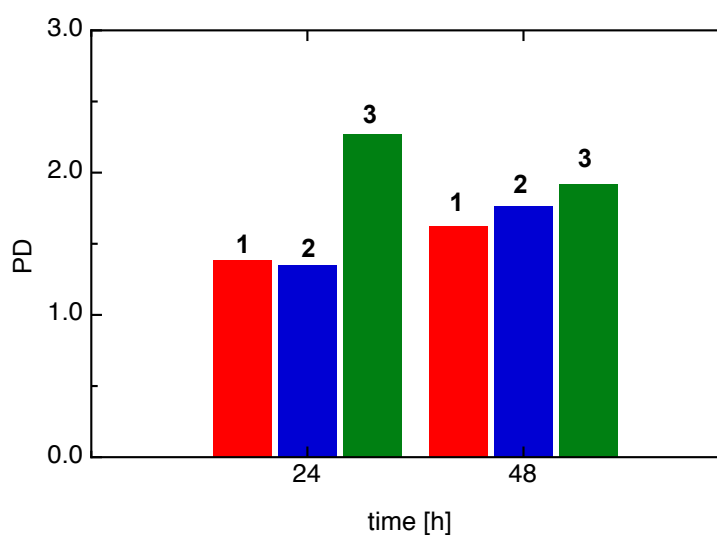


Figure 8.8. PD vs. time of **1** (red bar), **2** (blue bar) and **3** (green bar) for a reaction mixture of lactide/benzyl alcohol/catalyst 100:1:1.3 at 100 °C in THF in the microwave.

This observation was quite interesting because DMAP (**1**) as well as PPY (**2**) are already known to be effective in the ring opening polymerization (ROP) of lactide^[5a,17,18] without transesterification of the polylactide backbone.^[12] So why should 9-azajulolidine (**3**) catalyze the depolymerization? The pKa of **1** is known to be 9.2^[26] whereas the pKa of **3** is unknown but based on the increased nucleophilicity^[27] of 9-azajulolidine (**3**) compared to **1**, it should be more basic as well, making a chain scission more probable.^[28] Thus we pursued more detailed investigations onto the polymer length at different reaction times. To that end reaction kinetics were reasoned scaling the usual reaction conditions (10 mL reaction vessel) to a 80-mL reaction vessel up, which is also available for the microwave reactor. After distinct time intervals samples were taken, the solvent evaporated and the conversion verified by ¹H NMR spectroscopy. GPC measurements were only taken from samples above 80 % conversion. The conversion vs. time plot (black) is depicted in Figure 8.9 together with the weight and number averaged molar masses (red) (entries 23 - 29). For clarity, the left (black) y-axis belongs to the conversion vs. time plot and the right y-axis (red) belongs to the averaged molar masses vs. time plot. Figure 8.9 shows clearly that with ongoing reaction time and higher yields **3** is catalyzing the depolymerization of polylactide thus giving lower values for both M_w and M_n over time. The PD values indicate a broader mass distribution with increasing reaction time, too (from 1.93 to 2.71).

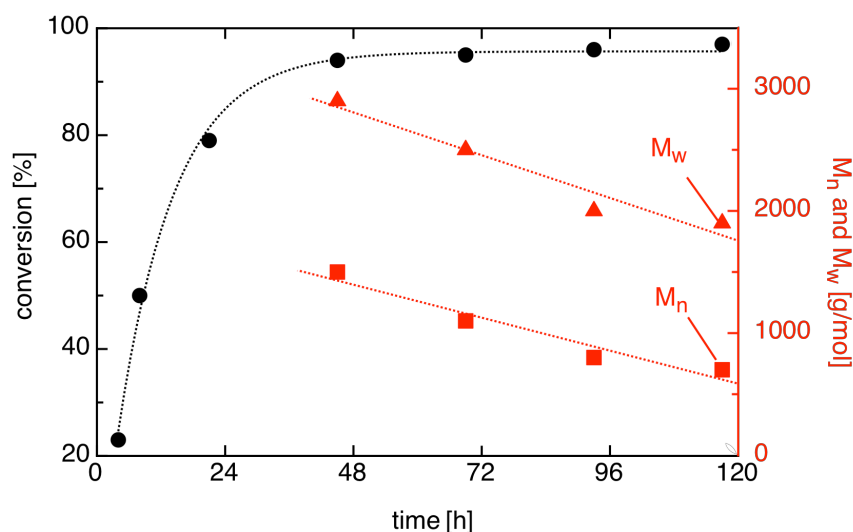


Figure 8.9. Conversion vs. time plot of **3** (black circles) for a reaction kinetic with lactide/benzyl alcohol/**3** at a ratio of 100:1:1 at 100 °C in THF in the microwave combined with the number (M_n , red squares) and mass (M_w , red triangles) averaged molar masses vs. time plot of the same reaction.

In Figure 8.10 the same kinetic data is plotted as $\ln(1/(100 - \text{conversion}))$. Presumably a second order rate law (black dotted line) gives a better approximation than a first order rate law (red dotted line), which is not only apparent from the shape of the curve but also from the R^2 values obvious. This would imply that a second molecule of catalyst **3** could be involved in the rate limiting step, which is not included in the mechanistic studies by Hedrick *et al.* yet.
[12,18,29]

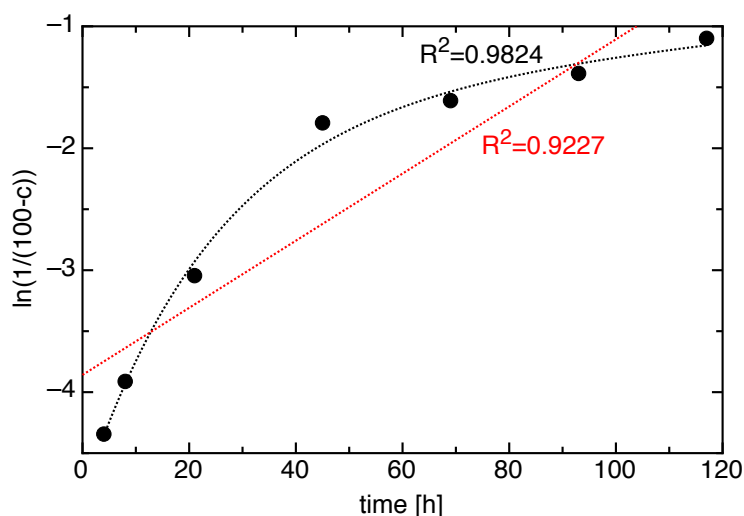


Figure 8.10. Reaction kinetics for reaction of lactide/benzyl alcohol/**3** at a ratio of 100:1:1 at 100 °C in THF in the microwave.

The same reaction kinetics were determined in CDCl_3 solution at 50 °C without microwave irradiation (Figure 8.11). After 286 h the reaction was stopped at 86 % conversion and the product analyzed by GPC (entry 30). It was found that the mass averaged molar mass is just 485 g/mol. These data suggest that not even oligomers were generated or they were depolymerized again.

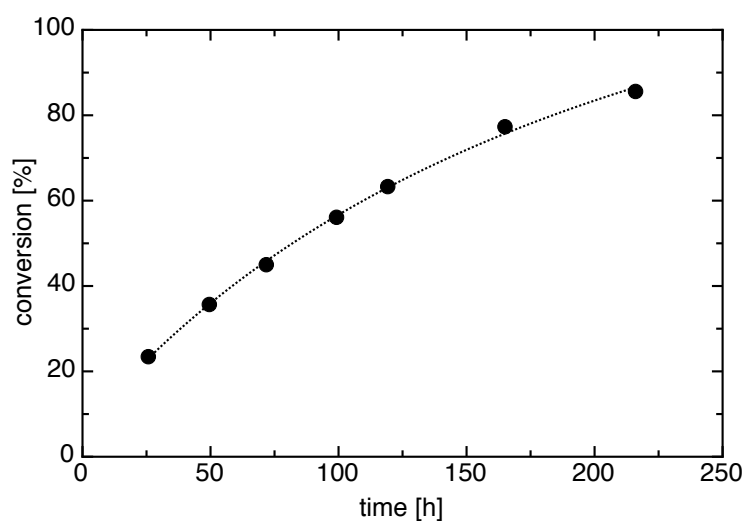


Figure 8.11. Conversion vs. time plot of **3** for a reaction kinetic with lactide/benzyl alcohol/**3** at a ratio of 100:1:1 at 50 °C in CDCl_3 heated in a conventional oilbath.

In Figure 8.12 the kinetic data is plotted as $\ln(1/(100-\text{conversion}))$ vs. time. Beyond any doubt a first order rate law is in this case better applicable ($R^2 = 0.9978$).

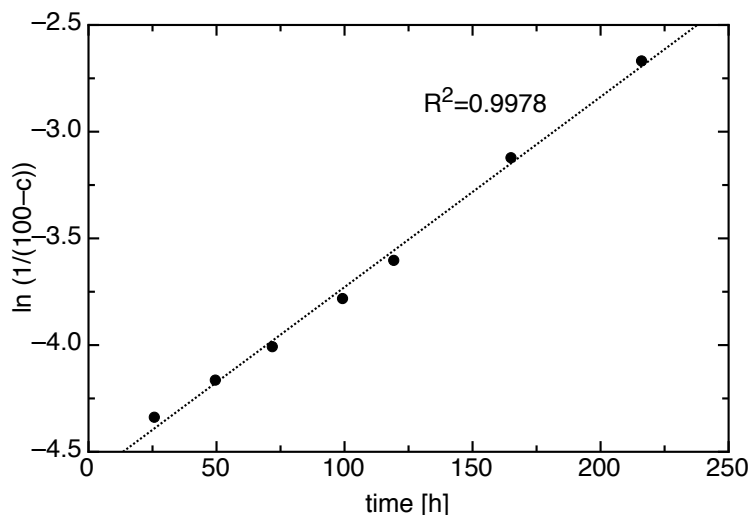


Figure 8.12. Reaction kinetic of **3** for a reaction kinetic with lactide/benzyl alcohol/**3** at a ratio of 100:1:1 at 50 °C in CDCl_3 heated in a conventional oilbath.

Going from THF as solvent to CDCl_3 and decreasing the reaction temperature to 50 °C not only the required reaction time is much higher, but also the $\ln(1/(100 - \text{conversion}))$ (Figures 8.10 and 8.12) plot changes dramatically from second to first order. A reason for that could either be the change in solvent or the change in temperature.

As another analytical method for the determination of polymer length ESI-MS and MALDI (anthracen matrix) spectroscopy were used. Conspicuously, in no case the masses detected were higher than 1800 although GPC measurements showed longer fragments for the same sample. Thus ESI-MS and MALDI measurements should be seen critical here. Longer polymer chains maybe only once ionized implying that a transfer into the gas phase is problematic.

8.3 Conclusion

In this study we surveyed different parameters concerning the polymerization of lactide in the microwave reactor using 9-azajulolidine (**3**) as organocatalyst. Utilizing microwave technology for the polymerization in melt we met problems, most likely due to uneven heat distribution leading to decomposed material. For the ROP of lactide in solution, microwave technology seems to be an attractive alternative to conventional heating in an oven due to dramatically reduced reaction times. The polymerization in THF solution in a microwave reactor was examined at 100 °C and did not show any decomposition of material. The ratio of lactide/benzyl alcohol/**3** 200:1:1 gave higher mass and number averaged molar masses and better polydispersity values as well. It has not been tested yet, but even better dispersities and

higher masses can potentially be reached using a ratio of 500:1:1. Water in the commercially available benzyl alcohol is not causing any problems in terms of hydrolysis. Distilled benzylic alcohol gives even smaller polymers but a better polydispersity. The addition of co-catalysts like 4-nitrophenol gives as well smaller averaged molar masses in the polymer. The comparison of different pyridines based on the DMAP-motif as catalysts showed that 9-azajulolidine (**3**) is in the ROP of lactide in terms of higher averaged molar masses (M_n , M_w) superior to DMAP (**1**) and PPY (**2**) but with the limitation of the first 24 hours of reaction time. While DMAP (**1**) keeps catalyzing the polymerization of lactide, **3** shows the strong tendency to catalyze not only the polymerization of lactide but also the depolymerization of polylactide at longer reaction times. Polymerization in $CDCl_3$ solution at 50 °C (without microwave) is not only time consuming but yields weight averaged masses below 500 g/mol. It can be stated that the use of organocatalysts in combination with microwave technology could be a very powerful combination for the ROP of lactides but conditions still need to be improved and optimized.

8.4 Experimental Part

General information

All air and water sensitive manipulations were carried out under a nitrogen atmosphere using standard Schlenk techniques. Calibrated flasks for kinetic measurements and microwave vials were dried in the oven at 120 °C for at least 12 hours prior to use and then assembled quickly while still hot, cooled under a nitrogen stream and sealed with a rubber septum. All commercial chemicals were of reagent grade and were used as received unless otherwise noted. $CDCl_3$ was refluxed for at least one hour over CaH_2 and subsequently distilled. 1H NMR spectra were recorded on Varian 300 or Varian INOVA 400 and 600 machines at room temperature. All 1H chemical shifts are reported in ppm (δ) relative to TMS (0.00); 1H NMR kinetic data were measured on a Varian Mercury 200 MHz spectrometer at 23 °C. HRMS spectra (ESI-MS) were carried out using a Thermo Finnigan LTQ FT instrument. Reactions utilizing microwave technology were conducted in a CEM Discover Benchmate microwave reactor (Model nr. 908010). 9-Azajulolidine (**3**) was obtained from TCI China (CAS.nr.: 6052-72-8), purity: > 97.0 % (GC) and benzyl alcohol from Sigma-Aldrich, purity \geq 99%.

Evaluation of kinetics and molar masses

All reactions utilizing microwave technology have been performed in a CEM Discover Benchmate microwave reactor. The progress of the reaction was monitored by 1H NMR spectroscopy following the signals of monomer (doublet at 1.6 – 1.7 ppm and quartet at 5.0 ppm) and polymer (multiplets at 1.5 – 1.6 ppm and 5.2 ppm) (see Figure 8.13).

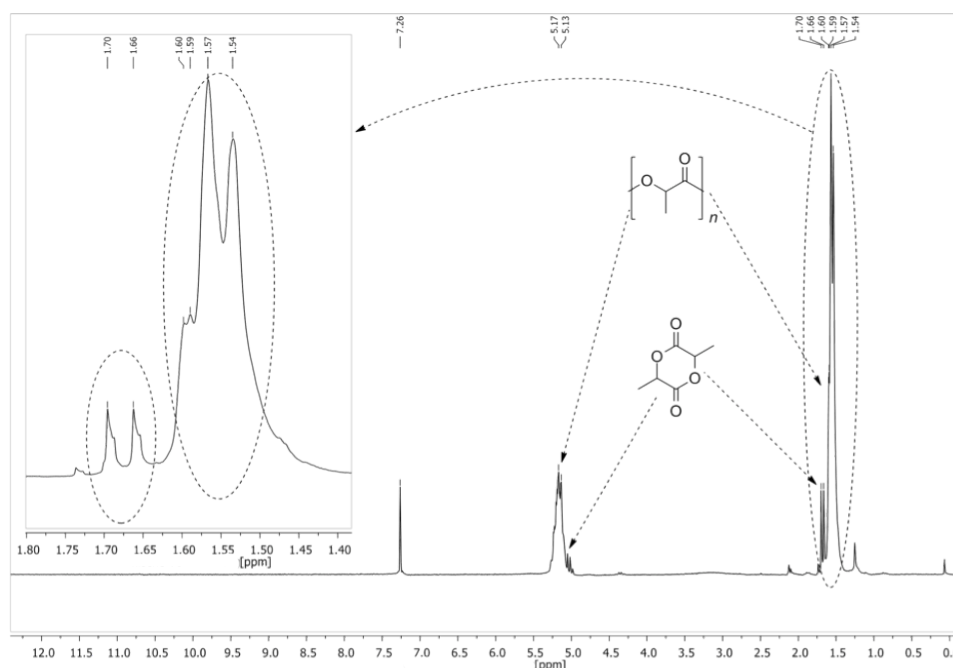


Figure 8.13. ¹H NMR spectrum of a reaction mixture showing 92 % conversion in CDCl₃.

The conversion was determined by the ratios of the according integral regions:

$$\text{conversion [\%]} = \frac{I_{\text{polymer}}}{I_{\text{polymer}} + I_{\text{monomer}}} \quad 8.1$$

Values of more importance in polymer chemistry than conversion are: the number averaged molar mass (M_n), the weight averaged molar mass (M_w) and the polydispersity (PD), which can be determined by means of GPC (gel permeation chromatography). The polydispersity shows how narrow the distribution of polymers is and is calculated by formula 8.2:

$$PD = \frac{M_w}{M_n} \quad 8.2$$

The measurements of molecular weight and molecular weight distribution via GPC with THF as mobile phase were conducted in the group of Prof. S. Herres-Pawlis by Ines dos Santos Vieira.

General procedure for microwave mediated ROP

If not stated differently, the reactions utilizing were conducted using the following stock solutions:

An oven-dried calibrated 20 mL flask was charged with 1.74 mg catalyst and 1.08 mg benzyl alcohol and filled with dry THF. In a new flame-dried microwave vial was added to 144.13 mg of the sublimated lactide 0.5 mL of the prepared stock solution. To work under inert conditions the setup depicted in Figure 8.14 was used.



Figure 8.14. Arrangement for working under inert gas with 10 mL microwave-vials.

The reaction mixture is sealed with a septum cap and placed in the microwave reactor and the respective program (100 °C, 100 W) is started. After completion of the reaction the solvent was removed under reduced pressure and a white to yellow solid or foam arose.

In the following part the MS-ESI data collected for different entries in Table 8.1 are given.

Entry 5:

MS (ESI): m/z (%) = 1817.5 $[\text{C}_{75}\text{H}_{101}\text{O}_{51}]^+$, 1745.5 $[\text{C}_{72}\text{H}_{97}\text{O}_{49}]^+$, 1601.5 $[\text{C}_{66}\text{H}_{89}\text{O}_{45}]^+$, 1313.4 $[\text{C}_{54}\text{H}_{73}\text{O}_{37}]^+$, 1169.3 $[\text{C}_{48}\text{H}_{65}\text{O}_{33}]^+$, 1025.3 $[\text{C}_{42}\text{H}_{57}\text{O}_{29}]^+$, 881.3 $[\text{C}_{36}\text{H}_{49}\text{O}_{25}]^+$, 737.2 $[\text{C}_{30}\text{H}_{41}\text{O}_{21}]^+$, 593.2 $[\text{C}_{24}\text{H}_{33}\text{O}_{17}]^+$, 305.1 $[\text{C}_{12}\text{H}_{17}\text{O}_9]^+$.

Entry 6:

MS (ESI): m/z (%) = 1745.5 $[\text{C}_{72}\text{H}_{97}\text{O}_{49}]^+$, 1601.5 $[\text{C}_{66}\text{H}_{89}\text{O}_{45}]^+$, 1457.4 $[\text{C}_{60}\text{H}_{81}\text{O}_{41}]^+$, 1169.3 $[\text{C}_{48}\text{H}_{65}\text{O}_{33}]^+$, 881.3 $[\text{C}_{36}\text{H}_{49}\text{O}_{25}]^+$, 737.2 $[\text{C}_{30}\text{H}_{41}\text{O}_{21}]^+$, 665.2 $[\text{C}_{28}\text{H}_{37}\text{O}_{19}]^+$, 377.1 $[\text{C}_{16}\text{H}_{21}\text{O}_{11}]^+$.

Entry 7:

MS (ESI): m/z (%) = 1817.5 $[\text{C}_{75}\text{H}_{101}\text{O}_{51}]^+$, 1745.5 $[\text{C}_{72}\text{H}_{97}\text{O}_{49}]^+$, 1601.5 $[\text{C}_{66}\text{H}_{89}\text{O}_{45}]^+$, 1457.4 $[\text{C}_{60}\text{H}_{81}\text{O}_{41}]^+$, 1025.3 $[\text{C}_{42}\text{H}_{57}\text{O}_{29}]^+$, 881.3 $[\text{C}_{36}\text{H}_{49}\text{O}_{25}]^+$, 737.2 $[\text{C}_{30}\text{H}_{41}\text{O}_{21}]^+$, 665.2 $[\text{C}_{28}\text{H}_{37}\text{O}_{19}]^+$, 521.2 $[\text{C}_{22}\text{H}_{29}\text{O}_{15}]^+$.

Entry 8:

MS (ESI): m/z (%) = 1745.5 $[\text{C}_{72}\text{H}_{97}\text{O}_{49}]^+$, 1601.5 $[\text{C}_{66}\text{H}_{89}\text{O}_{45}]^+$, 1457.4 $[\text{C}_{60}\text{H}_{81}\text{O}_{41}]^+$, 1025.3 $[\text{C}_{42}\text{H}_{57}\text{O}_{29}]^+$, 881.3 $[\text{C}_{36}\text{H}_{49}\text{O}_{25}]^+$, 809.2 $[\text{C}_{33}\text{H}_{45}\text{O}_{23}]^+$, 737.2 $[\text{C}_{30}\text{H}_{41}\text{O}_{21}]^+$, 665.2 $[\text{C}_{28}\text{H}_{37}\text{O}_{19}]^+$, 593.2 $[\text{C}_{24}\text{H}_{33}\text{O}_{17}]^+$, 521.2 $[\text{C}_{22}\text{H}_{29}\text{O}_{15}]^+$.

Entry 11:

MS (ESI): m/z (%) = 1169.3 $[\text{C}_{48}\text{H}_{65}\text{O}_{33}]^+$, 1025.3 $[\text{C}_{42}\text{H}_{57}\text{O}_{29}]^+$, 881.3 $[\text{C}_{36}\text{H}_{49}\text{O}_{25}]^+$, 737.2 $[\text{C}_{30}\text{H}_{41}\text{O}_{21}]^+$, 593.2 $[\text{C}_{24}\text{H}_{33}\text{O}_{17}]^+$, 305.1 $[\text{C}_{12}\text{H}_{17}\text{O}_9]^+$.

Entry 12:

MS (ESI): m/z (%) = 1889.6 $[\text{C}_{78}\text{H}_{105}\text{O}_{43}]^+$, 1745.5 $[\text{C}_{72}\text{H}_{97}\text{O}_{49}]^+$, 1601.5 $[\text{C}_{66}\text{H}_{89}\text{O}_{45}]^+$, 1457.4 $[\text{C}_{60}\text{H}_{81}\text{O}_{41}]^+$, 1169.3 $[\text{C}_{48}\text{H}_{65}\text{O}_{33}]^+$, 1025.3 $[\text{C}_{42}\text{H}_{57}\text{O}_{29}]^+$, 881.3 $[\text{C}_{36}\text{H}_{49}\text{O}_{25}]^+$, 737.2 $[\text{C}_{30}\text{H}_{41}\text{O}_{21}]^+$, 593.2 $[\text{C}_{24}\text{H}_{33}\text{O}_{17}]^+$, 305.1 $[\text{C}_{12}\text{H}_{17}\text{O}_9]^+$.

Entry 17:

MS (ESI): m/z (%) = 1673.5 $[\text{C}_{69}\text{H}_{93}\text{H}_{47}]^+$, 1601.5 $[\text{C}_{66}\text{H}_{89}\text{O}_{45}]^+$, 1529.4 $[\text{C}_{63}\text{H}_{85}\text{O}_{43}]^+$, 1025.3 $[\text{C}_{42}\text{H}_{57}\text{O}_{29}]^+$, 881.3 $[\text{C}_{36}\text{H}_{49}\text{O}_{25}]^+$, 809.2 $[\text{C}_{33}\text{H}_{45}\text{O}_{23}]^+$, 737.2 $[\text{C}_{30}\text{H}_{41}\text{O}_{21}]^+$, 449.1 $[\text{C}_{18}\text{H}_{25}\text{O}_{13}]^+$, 305.1 $[\text{C}_{12}\text{H}_{17}\text{O}_9]^+$.

Entry 23:

MS (ESI): m/z (%) = 1745.5 $[\text{C}_{72}\text{H}_{97}\text{O}_{49}]^+$, 1601.5 $[\text{C}_{66}\text{H}_{89}\text{O}_{45}]^+$, 1457.4 $[\text{C}_{60}\text{H}_{81}\text{O}_{41}]^+$, 1169.3 $[\text{C}_{48}\text{H}_{65}\text{O}_{33}]^+$, 1025.3 $[\text{C}_{42}\text{H}_{57}\text{O}_{29}]^+$, 881.3 $[\text{C}_{36}\text{H}_{49}\text{O}_{25}]^+$, 737.2 $[\text{C}_{30}\text{H}_{41}\text{O}_{21}]^+$, 593.2 $[\text{C}_{24}\text{H}_{33}\text{O}_{17}]^+$, 521.2 $[\text{C}_{21}\text{H}_{29}\text{O}_{15}]^+$.

Entry 25:

MS (ESI): m/z (%) = 1817.5 $[\text{C}_{75}\text{H}_{101}\text{H}_{51}]^+$, 1745.5 $[\text{C}_{72}\text{H}_{97}\text{O}_{49}]^+$, 1601.5 $[\text{C}_{66}\text{H}_{89}\text{O}_{45}]^+$, 1457.4 $[\text{C}_{60}\text{H}_{81}\text{O}_{41}]^+$, 1025.3 $[\text{C}_{42}\text{H}_{57}\text{O}_{29}]^+$, 881.3 $[\text{C}_{36}\text{H}_{49}\text{O}_{25}]^+$, 737.2 $[\text{C}_{30}\text{H}_{41}\text{O}_{21}]^+$, 665.2 $[\text{C}_{27}\text{H}_{37}\text{O}_{19}]^+$, 521.2 $[\text{C}_{21}\text{H}_{29}\text{O}_{15}]^+$.

Entry 26:

MS (ESI): m/z (%) = 1745.5 $[\text{C}_{72}\text{H}_{97}\text{O}_{49}]^+$, 1601.5 $[\text{C}_{66}\text{H}_{89}\text{O}_{45}]^+$, 1457.4 $[\text{C}_{60}\text{H}_{81}\text{O}_{41}]^+$, 1025.3 $[\text{C}_{42}\text{H}_{57}\text{O}_{29}]^+$, 881.3 $[\text{C}_{36}\text{H}_{49}\text{O}_{25}]^+$, 809.2 $[\text{C}_{33}\text{H}_{45}\text{O}_{23}]^+$, 737.2 $[\text{C}_{30}\text{H}_{41}\text{O}_{21}]^+$, 665.2 $[\text{C}_{27}\text{H}_{37}\text{O}_{19}]^+$, 593.2 $[\text{C}_{24}\text{H}_{33}\text{O}_{17}]^+$, 521.2 $[\text{C}_{21}\text{H}_{29}\text{O}_{15}]^+$.

8.5 References

- [1] J. Börner, I. dos Santos Vieira, M. Jones, A. Döring, D. Kuckling, U. Flörke S. Herres-Pawlis, *Eur. J. Inorg. Chem.* **2011**, 4441–4456.
- [2] A. P. Gupta, V. Kumar, *Eur. Polym. J.* **2007**, 43, 4053–4074.
- [3] I. dos Santos Vieira, S. Herres-Pawlis, *Eur. J. Inorg. Chem.* **2012**, 765–774.
- [4] J. Börner, I. dos Santos Vieira, M. Jones, A. Döring, D. Kuckling, U. Flörke S. Herres-Pawlis, *Eur. J. Inorg. Chem.* **2011**, 4441–4456.

- [5] a) J. Kadota, D. Pavlovic, J.-P. Desvergne, B. Bibal, F. Peruch, A. Deffieux, *Macromolecules* **2010**, *43*, 8874–8879. b) R. Langer, *Acc. Chem. Res.* **2000**, *33*, 94.
- [6] a) A. P. Gupta, V. Kumar, *Eur. Polym. J.* **2007**, *43*, 4053–4074. b) D. Garlotta, *J. Polym. Environ.* **2001**, *9*, 63–84.
- [7] H. R. Kricheldorf, *Chemosphere* **2001**, *43*, 49–54.
- [8] a) H. R. Kricheldorf, K. Bornhorst, H. Hachmann-Thiessen, *Macromolecules* **2005**, *38*, 5017. b) H. R. Kricheldorf, S. Rost, *Polymer* **2005**, *46*, 3248. c) H. R. Kricheldorf, H. Hachmann-Thiessen, G. Schwarz, *Biomacromolecules* **2004**, *5*, 492.
- [9] R. Mazarro, A. de Lucas, I. Garcia, J. F. Rodríguez, *J. Biomed. Mater. Res. Part B* **2007**, *85*, 196.
- [10] a) H. R. Kricheldorf, J. Meier-Haak, *Macromol. Chem.* **1993**, *194*, 715–725. b) M. Yuan, D. Liu, C. Xiong, X. Deng, *Eur. Polym. J.* **1999**, *35*, 2139–2145. c) H. R. Kricheldorf, D.-O. Damrau, *Macromol. Chem. Phys.* **1997**, *198*, 1753–1766.
- [11] a) J. Börner, U. Flörke, K. Huber, A. Döring, D. Kuckling, S. Herres-Pawlis, *Chem. Eur. J.* **2009**, *15*, 2362–2376. b) J. Börner, I. dos Santos Vieira, A. Pawlis, A. Döring, D. Kuckling, S. Herres-Pawlis, *Chem. Eur. J.* **2011**, *17*, 4507–4512. c) A. Hoffmann, U. Flörke, M. Schürmann, S. Herres-Pawlis, *Eur. J. Inorg. Chem.* **2010**, 4136–4144.
- [12] a) A. Chuma, H. W. Horn, W. C. Swope, R. C. Pratt, L. Zhang, B. G. G. Lohmeijer, C. G. Wade, R. M. Waymouth, J. L. Hedrick, J. E. J. Rice, *J. Am. Chem. Soc.* **2008**, *130*, 6749–6754. b) M. Kiesewetter, E. Shin, J. Hedrick, R. Waymouth, *Macromolecules* **2010**, *43*, 2093–2107. c) F. Nederberg, E. Connor, M. Möller, T. Glauser, J. Hedrick, *Angew. Chem. Int. Ed.* **2001**, *40*, 2712–2715.
- [13] W. Steglich, G. Höfle, *Angew. Chem.* **1969**, *81*, 1001; *Angew. Chem. Int. Ed. Engl.* **1969**, *8*, 981.
- [14] M. R. Heinrich, H. S. Klisa, H. Mayr, W. Steglich, H. Zipse, *Angew. Chem.* **2003**, *115*, 4975; *Angew. Chem. Int. Ed.* **2003**, *42*, 4826–4828.
- [15] G. Höfle, W. Steglich, H. Vorbrüggen, *Angew. Chem.* **1978**, *90*, 602–615; *Angew. Chem. Int. Ed.* **1978**, *17*, 569–583.
- [16] N. De Rycke, F. Couty, O. R. P. David *Chem. Eur. J.* **2011**, *17*, 12852–12871.
- [17] H. R. Kricheldorf, *Angew. Chem. Int. Ed.* **2006**, *45*, 5752–5784.
- [18] a) F. Nederberg, E. F. Connor, T. Glauser, J. L. Hedrick, *Chem. Commun.* **2001**, 2066–2067. b) F. Nederberg, E. F. Connor, M. Moller, T. Glauser, J. L. Hedrick, *Angew. Chem. Int. Ed.* **2001**, *40*, 2712–2715. c) H. R. Kricheldorf, N. Lomadze, G. Schwarz, *Macromolecules* **2008**, *41*, 7812–7816. d) H. R. Kricheldorf, N. Lomadze, G. Schwarz, *Macromolecules* **2007**, *40*, 4859–4864. e) H. R. Kricheldorf, C. Von Lossow, G. J. Schwarz, *Polym. Sci. Part A: Polym. Chem.* **2006**, *44*, 4680–4695.

- [19] C. Bonduelle, B. Martin-Vaca, F. P. Cossio, D. Bourissou, *Chem. Eur. J.* **2008**, *14*, 5304–5312.
- [20] I. Held, S. Xu, H. Zipse, *Synthesis* **2007**, 1185–1196. b) H. Zipse, I. Held, Bayer Material Science LLC, US 2008/0176747A1, **2008**.
- [21] C. Lindner, R. Tandon, Y. Liu, B. Maryasin, H. Zipse, *Org. Biomol. Chem.* **2012**, *10*, 3210–3218.
- [22] M. Yoshida, K. Saito, Y. Fujino, T. Doi, *Chem. Commun.* **2012**, *48*, 11796–11798.
- [23] E. Riedel, J. Janiak, *Anorganische Chemie*, Walter de Gruyter, Berlin, 7. Auflage, **2007**, 299.
- [24] M. Shi, Y. H. Liu, *Org. Biomol. Chem.* **2006**, *4*, 1468–1470.
- [25] I. Held, E. Larionov, C. Bozler, F. Wagner, H. Zipse, *Synthesis* **2009**, 2267–2277.
- [26] D. A. Evans, D. H. Ripin, http://daecr1.harvard.edu/pdf/evans_pKa_table.pdf.
- [27] compare chapter 1.
- [28] DMAP was shown to be able to perform chain scissions in polylactides under special preconditions, for more information see Ref. [18a].
- [29] a) L. Simon, J. M. Goodman, *J. Org. Chem.* **2007**, *72*, 9656–9662. b) A. Chuma, H. W. Horn, W. C. Swope, R. C. Pratt, L.; Zhang, B. G. G. Lohmeijer, C. G. Wade, R. M. Waymouth, J. L. Hedrick, J. E. Rice, *J. Am. Chem. Soc.* **2008**, *130*, 6749–6754. c) C.-L. Lai, H. M. Lee, C.-H. Hu, *Tetrahedron Lett.* **2005**, *46*, 6265–6270.

Chapter 9

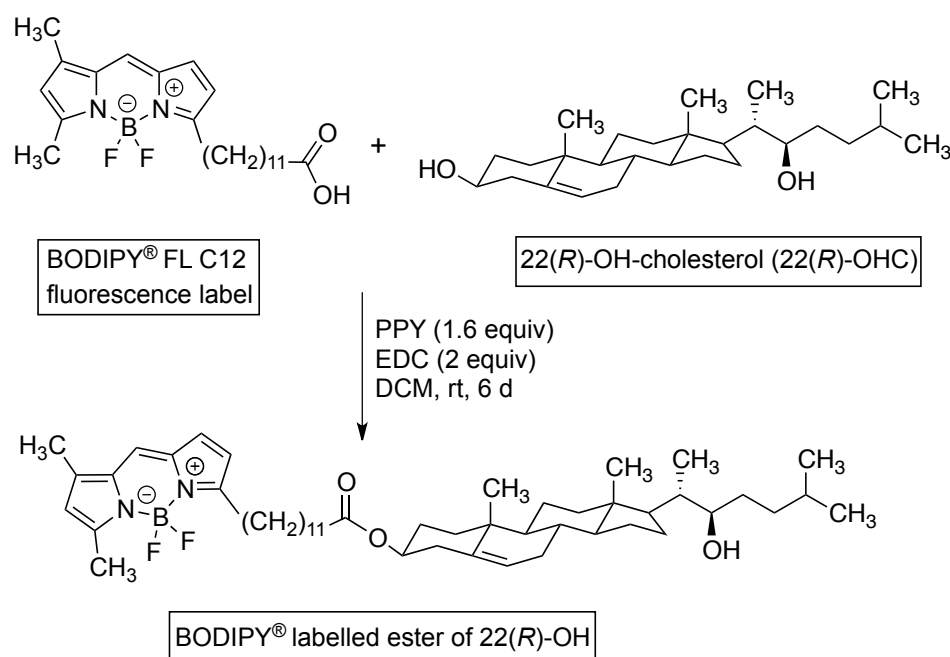
Platelet Inhibition by the Natural LXR Agonist 22(*R*)-OH-Cholesterol and its Fluorescence Labeling with Full Bioactivity

Stephanie Schaffer, Raman Tandon, Hendrik Zipse, Wolfgang Siess, Andreas Schmidt, Wolfgang Steglich, and Reinhard Lorenz, Biochem. Pharmacol. 2013, accepted.

Results obtained by S. Schaffer are omitted in the Experimental Part.

9.1 Introduction

Liver X receptors (LXRs) were first described as orphan nuclear transcription factors that dimerize with the retinoic acid receptor (RXR).^[1] LXRalpha is highly expressed in adipose tissue, liver, gut, macrophages and adrenals, whereas its close homologue LXRbeta is virtually ubiquitously expressed at lower levels. Several side chain oxycholesterols were identified as endogenous activating ligands of LXRs.^[2] LXRalpha activation and dimerization with RXR/RA in the nucleus results in binding to LXR recognition elements in the promoter of LXR target genes and up-regulation of their transcription. LXR agonists induce cellular and biliary cholesterol exporters and hepatic fatty acid synthesis and down-regulate sterol synthesis, triglyceride metabolism and gluconeogenesis.^[3] Meanwhile several non-metabolic functions of LXRalpha *e.g.* in inflammation and immune regulation were detected.^[4,5] Recently, two synthetic LXR agonists were shown to inhibit collagen-induced platelet aggregation and thrombus formation in mice by non-transcriptional interference with collagen receptor signalling.^[6] As only synthetic LXR agonists were tested, a non-LXR related side effect of these compounds could not be excluded and the relevance of natural LXR agonists for platelet activation remained to be established. Among the endogenous LXR agonists 22(*R*)-OH-cholesterol (22(*R*)-OHC, structure see Scheme 9.1) offers the unique opportunity to use its inactive isomer 22(*S*)-OHC as a negative control.



Scheme 9.1. Reaction of BODIPY[®] FL C12 with 22(*R*)-OH-cholesterol under optimized reaction conditions.

Stereospecificity of a 22(*R*)-OHC effect fits with a large body of experimental evidence on genomic LXR actions in diverse cells and renders unspecific cytotoxicity or interference with other pathways unlikely.^[2,3] We therefore used 22(*R*)-OHC and 22(*S*)-OHC to explore the effects of endogenous LXR agonists on platelet function. Furthermore, fluorescence labelled analogues of natural LXR agonists would be a valuable experimental tool to visualize intracellular LXR trafficking. We therefore synthesized the BODIPY-labelled esters of 22(*R*)- and 22(*S*)-OHC (structure see Scheme 9.1) by a PPY-catalyzed Steglich acylation adapted to the milligram scale. We then characterized the bioactivity, interaction, metabolic stability and cellular handling of these fluorescence labelled natural LXR ligand analogues in platelets and macrophages.

9.2 Results

Synthesis of Fluorescence Labelled 22-OHCs

The fluorescence labelled 22-OHC's were synthesized utilising a slightly modified variant of the Steglich reaction.^[7] Initially the esterification reaction of 22(*R*)OH-cholesterol and BODIPY[®] FL C3 resulted in just 4% yield under standard reaction conditions. As a model system for optimising the reaction conditions commercially available cholesterol and palmitic acid were used on a 100 mg scale. Among the tested parameters for optimising the reaction conditions were: working under inert gas atmosphere, solvent, coupling reagent, catalyst, and the reaction time and temperature. It was found that rigorous purification of the solvent (DCM) and working under an inert gas atmosphere increased the yields dramatically. In terms of the choice of solvent DCM gives better yields than THF or chloroform. Best yields were obtained when using EDC instead of DIC as the coupling reagent. With the latter choice (DIC) substantial amounts of N-acylurea byproducts were formed as characterized by mass spectroscopy. The formation of these byproducts can be avoided using the water-soluble activation reagent EDC. In terms of the catalyst PPY is superior to DMAP and best employed in amounts of 1.6 eq. and not in catalytic amounts. A reaction time of 4 days was sufficient to archive good to excellent yields, provided that the temperature is kept at room temperature. An increase in temperature is always problematic using DCM as solvent due to evaporation of the solvent. Using the optimized reaction conditions a yield of 83 % was obtained for the reaction on a 100 mg scale. With prices of over 100 € for 1 mg 22(*R*)-hydroxycholesterol an effort was made to scale the reaction down to milligram quantities of substrate. Using the optimized conditions on a 10 mg scale (with cholesterol) in a sealed NMR tube as the reaction vessel gave excellent yields (96 %), but required reaction times of 6 days. A further reduction of the reaction scale is plagued by rapid evaporation of the solvent into the NMR tube gas phase region. This problem was solved by using a purpose-built microreactor allowing the handling of substrate on the 0.5 - 1 mg scale under inert gas conditions (Figure 9.1).

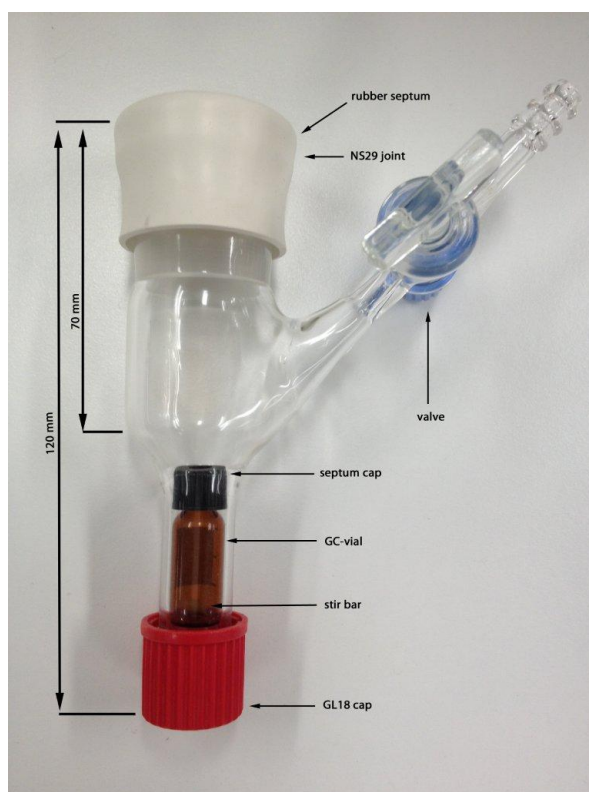


Figure 9.1. Microreactor for small scale esterification reactions under inert gas conditions.

Additionally, the use of Hamilton syringes is essential when handling stock solutions on this small scale in order to eliminate problems with plasticizers present in one-way plastic syringes. Utilising this microreactor setup and the optimized reaction conditions, the 22(*S*)- as well as the 22(*R*)-OH-cholesterols could be fluorescence labelled by a Steglich-type esterification reaction with BODIPY[®] FL C12 with yields up to 90 % (Scheme 9.1, determined by fluorescence spectrometry) on a 0.5 mg scale.

Effects of LXR ligands on collagen induced platelet aggregation

Overlays of representative aggregation curves are shown in Figure 9.2. The concentration-dependent inhibition of collagen-induced platelet aggregation by the pharmacologic LXR ligands was confirmed (Figure 9.2 A).

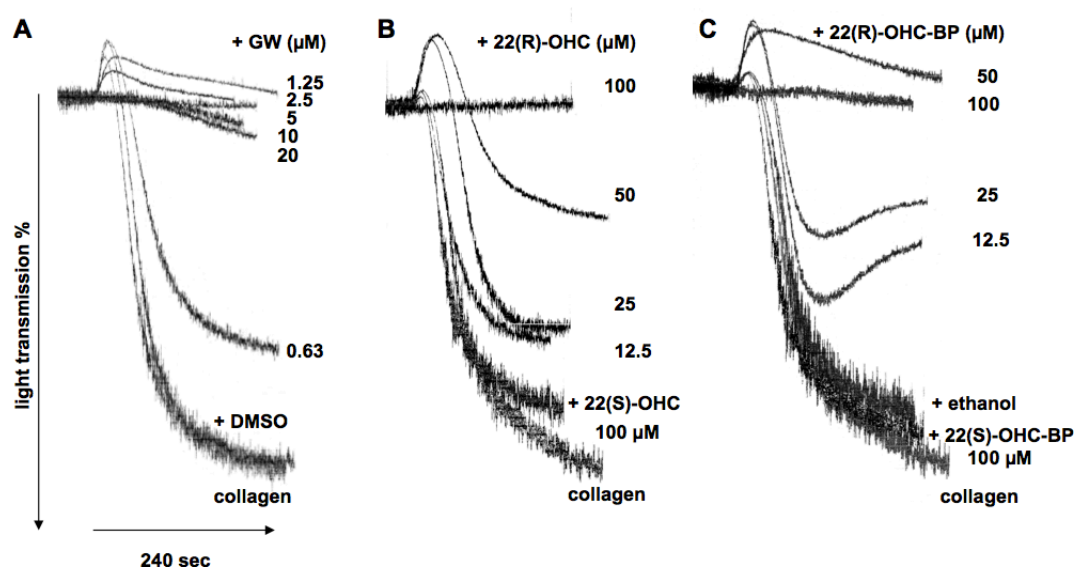
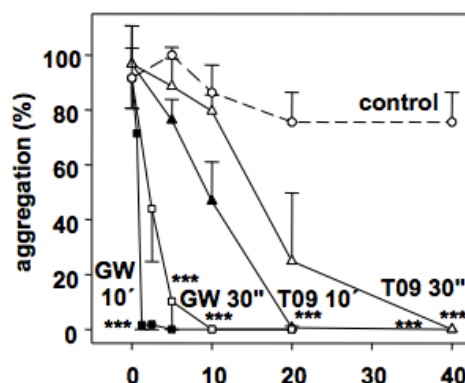


Figure 9.2. Overlays of aggregation curves of platelets preincubated for 10 min with indicated concentrations of (A) GW, (B) 22(*R*)-OHC or 22(*S*)-OHC and (C) their fluorescence labelled analogues 22(*R*)- or 22(*S*)-OHC-BP and stimulated with collagen (0.25 μg/ml). Controls with solvents (DMSO and ethanol) and maximal aggregation with collagen alone are included.

Next it was shown that also the natural LXR ligand 22(*R*)-OHC inhibited collagen induced platelet aggregation and shape change in a concentration-dependent manner, whereas its stereoisomeric 22(*S*)-OHC was completely inactive at least up to 100 μM (Figure 9.2 B). Third it was tested, whether the fluorescence labelling interfered with the biologic activity of 22(*R*)-OHC. The newly synthesized 22(*R*)-OHC-BP ester inhibited collagen-induced platelet aggregation and shape change even at lower concentrations than the native parent compound, whereas its stereoisomeric 22(*S*)-OHC-BP ester was inactive (Figure 9.2 C). The effects of the various LXR ligands on collagen-induced aggregation were quantified using platelets from six different donors. The inhibition of aggregation by the synthetic LXR agonists T09 and GW increased with their concentration and the preincubation time before stimulation with collagen (Figure 9.3 A). The newly synthesized fluorescence-labelled analogue, 22(*R*)-OHC-BP, inhibited platelet aggregation even more potently than 22(*R*)-OHC. In contrast, 22(*S*)-OHC was completely inactive and its fluorescence labelled stereoisomer, 22(*S*)-OHC-BP caused only a minor reduction of platelet aggregation not significantly different from solvent control (Figure 9.3 B). With a similar pattern of relative potencies T09 and GW, the natural agonist 22(*R*)-OHC and its analogue 22(*R*)-OHC-BP, but not the stereoisomers 22(*S*)-OHC and 22(*S*)-OHC-BP, prolonged platelet lag time or fully prevented platelet shape change at higher concentrations (data not shown).

A: Platelet inhibition by T09 and GW



B: Platelet inhibition by oxysterols

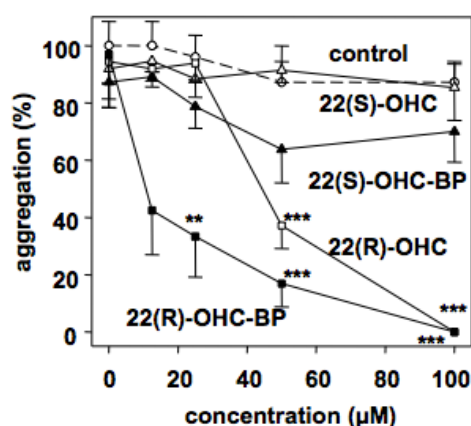
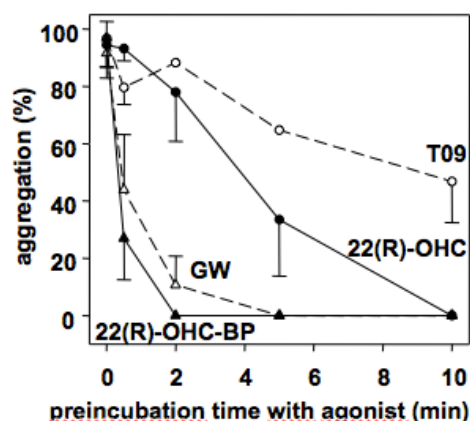


Figure 9.3. Concentration response curves of collagen (0.25 $\mu\text{g/ml}$) induced aggregation in platelets preincubated with (A): GW or T09 (10 min or 30 sec) and with (B) 22(*R*)-OHC-BP, 22(*R*)-OHC, their *S*-stereoisomers (10 min) compared to solvent control. means \pm SEM; ***: $p < 0.001$ by ANOVA on ranks with pair comparison to control.

Experiments varying the preincubation time of platelets with the LXR agonists before stimulation with collagen demonstrated a very fast onset of the effect of 22(*R*)-OHC-BP ester with 75% inhibition aggregation after 30 sec, a slightly slower action of GW and a more gradual onset of the inhibition by 22(*R*)-OHC and T09 (Figure 9.4 A). In coincubations the two stereoisomers of 22-OHC were tested for potential interference. If 22(*S*)-OHC was added to platelets immediately before 22(*R*)-OHC and platelets were stimulated with collagen 10 min later, isomolar 22(*S*)-OHC prevented the inhibition of platelet aggregation by 50 μM 22(*R*)-OHC alone and even the complete loss of platelet reactivity to collagen by 100 μM 22(*R*)-OHC was partially restored by 22(*S*)-OHC (Figure 9.4 B). In contrast, addition of 22(*S*)-OHC 10 min after 22(*R*)-OHC did not interfere with the inhibition of platelet aggregation by 22(*R*)-OHC (data not shown).

A: Kinetics of platelet inhibition via LXR



B: Interaction of 22(R)- and 22(S)-OHC

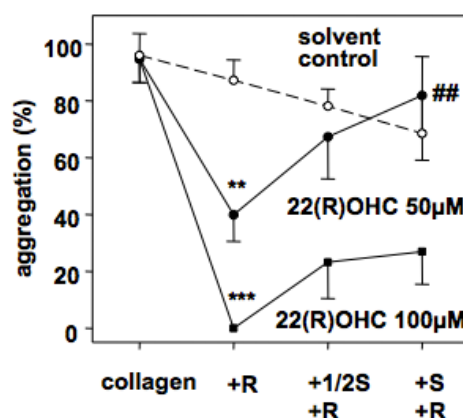


Figure 9.4. (A) Time course of inhibition of collagen induced aggregation by preincubation with 22(R)-OHC-BP, GW, 22(R)-OHC and T09. (B) Interaction of half- and isomolar 22(S)-OHC with inhibition of collagen induced aggregation by 22(R)-OHC. mean \pm SEM; **: $p < 0.01$ and ***: $p < 0.001$ by ANOVA on ranks with pair comparison of +R to collagen and +R+S.

Handling of labelled 22-OHCs by cells

Platelet suspensions were stained with 22(R)- or 22(S)-OHC-BP (10 μ M) for 10 min, allowed to attach to poly-L-lysine coated glass slides and evaluated by phase contrast and fluorescence microscopy. Platelets exposed to 22(S)-OHC-BP had spread on the glass surface, had formed aggregates and showed a diffuse weak fluorescence of their thinned cytoplasm. Platelets stained with 22(R)-OHC-BP had remained spherical, did not form aggregates and showed a more intense staining (Figure 9.5).

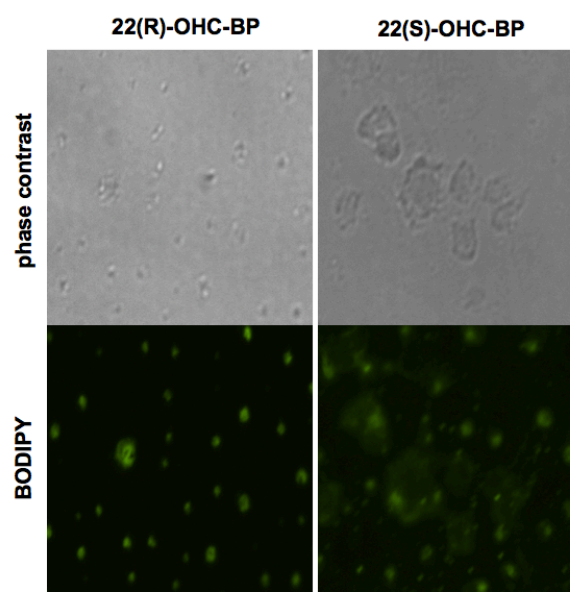


Figure 9.5. Phase contrast (top row) and fluorescence (bottom) microscopy of platelets suspensions life stained with 10 μ M 22(*R*)-OHC-BP (left) or 22(*S*)-OHC-BP (right) for 10 min and dropped on polylysine coated glass slides.

Differentiated U937 cells were incubated with 22(*R*)- or 22(*S*)-OHC-BP (1 μ M) for 8 and 24 h and evaluated by confocal laser microscopy. 22(*R*)-OHC-BP caused diffuse staining selectively concentrated in the nuclei already at 8 h, which was even intensified after 24 h exposure (Figure 9.6). In contrast, 22(*S*)-OHC-BP caused an exclusive accumulation of the staining in granular deposits in the cytoplasm of the macrophages at 8 h with only few residual spots remaining in the perinuclear cytoplasm after 24 h exposure to 22(*S*)-OHC-BP (Figure 9.6).

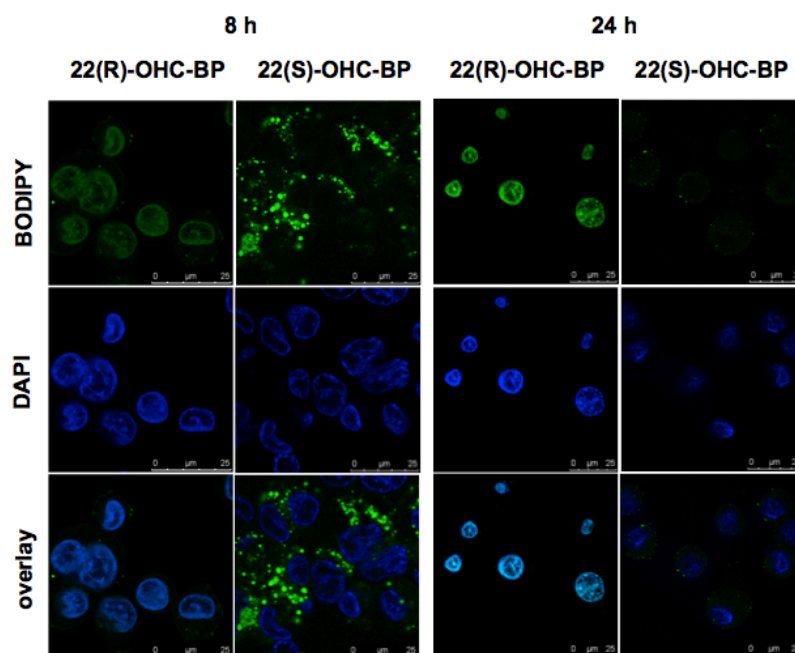


Figure 9.6. Confocal laser fluorescence microscopy of U937 cells incubated for 8 h (left) and 24 h (right) with 22(*R*)- or 22(*S*)-OHC-BP (1 μ M) as indicated and counterstained with DAPI. Top row: BODIPY (green). Middle row: DAPI (blue). Bottom row: overlay.

Macrophages that had been incubated with 22(*R*)- or 22(*S*)-OHC-BP, cholesterol-BP ester or free BP-duodecanoic acid (10 μ M) for 24 h were lysed, lipids were extracted, aliquots separated by TLC and fluorescent spots localized by UV. Virtually all the fluorescence extractable from cells incubated with 22(*R*)-, 22(*S*)-OHC-BP and -BP esters was still contained in a single spot that cochromatographed with the authentic 22(*R*)- or 22(*S*)-OHC-BP and cholesterol-BP esters as added to the cells. Extracts of cell supernatants revealed partial cleavage of 22(*R*)-OHC-BP, but not of 22(*S*)-OHC-BP. Laddering of the split-off BP-duodecanoic acid spot, also seen in control incubations with free BP-duodecanoic acid, was suggestive of partial beta-oxidation by cells. From stained and collagen-stimulated platelets all labelled compounds could be extracted unchanged (data not shown).

9.3 Discussion

LXRs were long regarded as metabolic master regulators of cellular cholesterol homeostasis. Very recently it was detected that LXRbeta is expressed in platelets and that two pharmacologic LXR agonists inhibit collagen-induced platelet aggregation and thrombus formation in mice obviously by enhancing Syk and PLCgamma2 association with LXRbeta. This interfered with their phosphorylation in the collagen receptor signalling pathway.^[6] We confirmed the antiaggregatory action of these synthetic LXR ligands and established the rapid kinetics of their effect on platelet aggregation. We first demonstrate that also the natural LXR agonist 22(*R*)-OHC inhibits collagen-induced platelet aggregation at concentrations that

stimulate genomic LXR effects in hepatocytes or macrophages.^[2,9] In contrast, its stereoisomer, 22(*S*)-OHC did not affect platelet aggregation even at high concentrations. This parallels the well established lack of genomic LXRalpha agonistic effects of 22(*S*)-OHC in macrophages, hepatocytes and cells transfected with LXRalpha reporter gene constructs.^[2,10] The stereospecificity of the 22(*R*)-OHC effect on collagen-induced platelet aggregation strongly supports LXR as the target molecule and argues against an undetected coincident mechanism of platelet inhibition by the synthetic compounds. The effects of 22(*R*)-OHC further demonstrate the potential of endogenous LXR ligands to modify platelet function. A recent study on plasma levels of LXR agonistic oxysterols reported levels in the range of 2 to 80 ng/ml, which is below the threshold levels that affected platelet reactivity *in vitro*.^[11] This does, however, not exclude a role of 22(*R*)-OHC or other more abundant oxysterols as local modifiers of platelet function. Plaques contain high amounts of LXR agonistic oxysterols generated by foam cells like 26-OHC.^[12,13] As collagen is a key trigger of platelet activation on endothelial denudation of plaques, simultaneously exposed endogenous LXR agonists may locally attenuate platelet reactivity to collagen. These non-transcriptional effects of LXR agonists on platelets could contribute to the benefit demonstrated in experimental atherosclerosis and primarily attributed to genomic LXR effects on lipid metabolism and inflammatory response in macrophages.^[14,15] At higher concentrations LXR agonists even prevented platelet shape change on collagen stimulation. This effectiveness against early steps of platelet activation and the fast kinetics of platelet inhibition by endogenous or synthetic LXR agonists could offer an additional relevant mechanism to counteract platelet deposition in plaque rupture. In coin incubations, isomolar 22(*S*)-OHC antagonized the effect of 22(*R*)-OHC and restored platelet reactivity to collagen. This further excludes an unspecific toxic inhibition of platelet function by 22(*R*)-OHC and suggests competition of 22(*R*)- and 22(*S*)-OHC for the same binding site on LXRbeta. Obviously, 22(*S*)-OHC is not a mere inactive stereoisomer, but (although lacking intrinsic activity) tightly binds to LXRbeta in platelets and blocks the non-genomic effects of 22(*R*)-OHC. It was concluded from computational molecular modelling that 22(*S*)-OHC fits into the binding pocket of LXRalpha and in fact, 22(*S*)-OHC partially down-regulated basal transcription of some LXR-inducible target genes.^[16] This fits with competitive displacement of endogenous agonists from LXRalpha.

The interaction at the level of binding to LXRs and the translocation between cytoplasm and nucleus in genomic LXR effects^[9] raised our interest to generate fluorescence-labelled LXR ligands for visualization. We chose the Steglich acylation^[7] to esterify 22(*R*)- and 22(*S*)-OHC with BP-3-duodecanoic acid as fluorescence label under mild conditions. It required optimization of several reaction parameters, changes in reagents and the design of a special microreactor to achieve a high yield at the milligram scale that is dictated by the availability and cost of 22-OH-sterols. The 22-OHC-BP esters were effectively purified from residual reagents and side products on minicolumns and no cell toxicity was detectable in subsequent experiments. The analogous cholesterol-BP ester has long been used as a non-cytotoxic, lipophilic fluorescent dye *in vitro*^[17] and BP-conjugates are regarded as non-toxic at labelling concentrations even *in vivo*.^[18] The modified Steglich acylation^[7] allowed selective 3-OH-esterification leaving the 22-hydroxy-function untouched. When the labelled 22(*R*)- and

22(*S*)-OHC-3-BP esters were tested in platelets, we found that the stereospecific bioactivity of their unlabelled parent compounds was fully preserved. This fits well with the localization of intrinsic activity to the 22(*R*)-hydroxy configuration of the sterol side chain^[2,10] and demonstrates that the bulky fluorescence label esterified to the sterol 3-hydroxy group does not hinder LXR binding and activation. Moreover, the concentration response curve of 22(*R*)-OHC was shifted to the left by esterification with BP and the kinetics of platelet inhibition was accelerated to the 30 sec range. This might be related to a faster transmembrane diffusion of the less polar 22(*R*)-OHC-BP ester into platelets rather than a truly enhanced intrinsic LXR-activity. It further demonstrates, that the signalling distal to LXR activation is not rate limiting for the very rapid and intense non-genomic antiplatelet effect. Consistent with preserved binding and intrinsic activity, the fluorescence-labelled esters 22(*R*)- and 22(*S*)-OHC-BP showed stereospecific differences when used for life cell staining in platelets and a human macrophage cell line. Platelets incubated with 10 μ M 22(*R*)-OHC-BP for staining preserved their resting spheroid shape despite exposure to an artificial surface, whereas platelets exposed to 10 μ M 22(*S*)-OHC-BP were activated. The morphologic differences after staining with 22(*R*)- and 22(*S*)-OHC-BP parallel the stereospecific inhibition of platelet reactivity to collagen, but extend the inhibition to early steps of platelet activation to the low staining concentration and to platelet activation by other surface stimuli.

Incubation of macrophages with 22(*R*)- or 22(*S*)-OHC-BP also showed characteristic differences in the time course, intracellular localization and structure of the staining. Whereas macrophage exposure to 22(*R*)-OHC-BP caused a sustained, diffuse, strictly nuclear localization of the label, 22(*S*)-OHC-BP resulted in a rapid but transient, granular, cytosolic accumulation of the label. This fits well with previous studies using indirect LXR localisation by immunoblot assays in nuclear extracts^[19] or unlabeled 22(*R*)-OHC in HEK293 cells transfected with fluorescent YFP-LXR constructs.^[9] The complementary evidence from both labelling methods suggests tight association of 22(*R*)-OHC-BP with LXRA in the nucleus and sustained binding of the complex to the LXR response elements in the promoter of target genes. In contrast, non-activating binding to LXR is known to dissociate LXR from genomic binding sequences and leads to translocation of LXR to the cytoplasm.^[9] Rapid clearance of 22(*S*)-OHC-BP from the cytoplasm fits also with the rapid secretion of endogenous oxysterols from macrophages, hepatocytes and enterocytes.^[13,20] There was no evidence for metabolic cleavage of the label from both 22-OHC-BP esters in platelets. Even in esterase rich macrophages the labelled esters were remarkably stable. Obviously steric hindrance by the bulky BP chromophore renders 22-OHC-BP esters resistant to lipases. Partial cleavage was only seen in extracts from macrophages incubated with 22(*R*)-OHC-BP, but not with 22(*S*)-OHC-BP. This may be related to the shorter retention of 22(*S*)-OHC-BP within cells. Free BP-duodecanoic acid cleaved from 22(*R*)-OHC-BP or directly added in control experiments may undergo beta-oxidation to some extent, but there was no evidence for transacylation and it was completely secreted by cells into the supernatant. This assures that the intracellular fluorescence reliably indicates the localization of intact labelled 22(*R*)- or 22(*S*)-OHC-BP esters and not of catabolites.

9.4 Conclusion

Using the microreactor and the optimised reaction conditions 22(*R*)- and 22(*S*)-OH-cholesterol could be fluorescence labelled by a Steglich-type acylation reaction with BODIPY[®] FL C12 with yields up to 90 % on a 0.5 mg scale. Synthesis and purification of the desired 22(*R*)- and 22(*S*)-OHC-BP esters were controlled by TLC with fluorescence- and ³H-detection and the structural identity demonstrated by ¹H NMR spectroscopy. The potent and rapid inhibition of collagen and foreign surface induced platelet activation by natural LXR agonists could attenuate platelet recruitment at sites of collagen exposure and high local accumulation of LXR agonistic oxysterols like in denuded plaques. 22(*R*)- and 22(*S*)-OHC could efficiently be fluorescence-labelled with even enhanced stereospecific LXR activity and high metabolic stability. Life staining with labelled 22(*R*)- and 22(*S*)-OHC-BP revealed characteristic differences in platelet morphology and in intracellular trafficking in macrophages, which reflects the LXR activity of the stereoisomers. Thus, 22(*R*)-OHC-BP and 22(*S*)-OHC-BP can be versatile tools for combined functional and microscopic studies of LXR related pathomechanisms and for current drug development of LXR modulators.^[21]

9.5 Experimental Part

Materials and Methods

Sterols, 22(*S*)-, 22(*R*)- and 25-hydroxycholesterol and 4-*N,N*-dimethylaminopyridine (DMAP, **1**), *N,N*-dicyclohexylcarbodiimide (DCC), T0901317 (T09) and GW3965 (GW) were purchased from Sigma Aldrich (Schnelldorf), 4,4-Difluoro-5,7-dimethyl-4-bora-3a,4a-diaza-s-indacene-3-duodecanoic acid (BODIPY[®] FL C12) from Molecular Probes (Leiden, NL), PPY (**2**) from Fluka chemicals (Buchs) and all solvents from Merck Chemicals (Darmstadt). All commercial chemicals were of reagent grade and used as received unless otherwise noted. CH₂Cl₂ was refluxed for at least one hour over CaH₂ and subsequently distilled. Aliquots of reaction samples were separated on silica TLC plates developed with cyclohexane/ethylacetate 80:20 (v/v). Spots were localized by UV light using a 480 nm filter screen, phosphomolybdate spraying for sterol staining or ³H-scanning on a Tracemaster 20 (Berthold) as needed. Compounds of interest were isolated from the reaction mixtures by application to silica SPE minicolumns conditioned with 4 ml hexane and eluted with a gradient of hexane/diethyl ether stepwise increased from 10:0 to 5:5 (v/v). Aliquots of fractions were checked for purity by TLC as described above and quantified by fluorescence spectrometry on a MITRAS LB940 (Berthold Technologies, Bad Wildbach) against a BODIPY standard curve. The products were identified by NMR spectroscopy using a Varian 600 MHz spectrometer and byproducts were identified by MS-ESI/HRMS measurements on a Thermo Finnigan LTQ FT instrument.

Platelet Preparation and Aggregation (conducted by S. Schaffer)

Blood from healthy fasting volunteer donors was drawn on acidic citrate dextrose (ACD, 1:6 v/v) and washed platelets were prepared as described^[6,8]. Briefly, blood was centrifuged at room temperature for 20 min at 200 g to obtain platelet-rich plasma. Prostacyclin (0.2 µg/ml) was added, platelets were centrifuged (1000 g, 10 min) and washed twice. The platelet pellet was resuspended in Tyrode-HEPES buffer (pH 7.4) (25 ml) and ACD (3 ml) in the presence of prostacyclin (0.2 µg/ml). Platelets were counted, adjusted to 400000/µl and rested for 30 min at 30 °C before experiments. Platelet aggregation was stimulated with collagen (0.25 µg/ml) and measured in a lumi-aggregometer (Chronolog, Haverton, PA) at 37°C whilst stirring (1000 rpm). If not indicated otherwise synthetic LXRalpha ligands, 22(R)- and 22(S)-OHC and BP-labelled 22-OHC esters or their solvent controls (DMSO or ethanol) were added 10 min before collagen. Inhibition of platelet aggregation by these compounds was expressed as the reduction in maximal change of light transmission caused by collagen. In addition the prolongation of lag time from addition of collagen until start of platelet shape change was determined.

Platelet and Macrophage Staining and Fluorescence Microscopy (conducted by S. Schaffer)

For microscopy 100 µl platelet suspension were stained with 10 µM 22(R)- or 22(S)-OHC-BP for 10 min at 37 °C, 5 µl were dropped on a poly-L-lysine-coated slide, allowed to adhere for 10 min in a humid Petri dish and washed with phosphate buffer and albumin (3 g/l) in a flow chamber at 20 sec⁻¹ shear rate for 2 min. Platelets were fixed with 3.7% formaldehyde in buffer and sealed between glasses for fluorescence microscopy (Eclipse TE 2000-E, 100 x Plan APO objective, Nikon) at 488 nm excitation and 535 nm emission. U937 cells were differentiated to macrophages with phorbol myristate (160 nM) for 4 days and allowed to adhere to cover slides placed in the wells. The medium was removed, cells were washed with PBS and incubated with 22(R)- or 22(S)-OHC-BP (1µM) for 8 or 24 h. Then cells were washed three times with PBS, fixed with methanol for 1 min, washed again, counterstained with DAPI and sealed between glasses for confocal laser microscopy (Leica TCS SP5 II, 63 x objective HCX PL APO CS) at 495 nm excitation and 519 nm emission for BODIPY and at 360/460 nm for DAPI.

Metabolic Stability of Labelled Compounds (conducted by S. Schaffer)

U937 cells grown in 6 well plates were incubated with 22(R)- or 22(S)-OHC-BP (1 µM) for 24 h and washed three times with PBS. Cells were detached by incubation with trypsin (0.05%) / EDTA (0.02%) for 20 min at 37 °C and cautiously scraped off from the wells. The cell suspension was diluted with fresh medium and centrifuged (300 g, 5 min). The cell pellet was resuspended, lysed by sonication and extracted with dichloromethane. Aliquots of the extracts were separated by silica TLC run with *n*-hexane/ethyl acetate (100/80) and screened

for fluorescent spots. Similarly, extracts from platelets incubated with 22(R)- or 22(S)-OHC-BP (10 μ M) for 10 min and stimulated with collagen were analysed.

Statistical Analysis (conducted by S. Schaffer)

Data are presented as means \pm SEM. Different experimental conditions were compared by analysis of variance on ranks and pair comparisons to control were made by Dunn's method.

General Procedure for the Esterification Reaction

The glassware is dried for at least 16 h in an oven (120 °C). The reactants 22-hydroxycholesterol, BODIPY[®] FL C12 and PPY (**2**) were dried under high vacuum for three hours. CH₂Cl₂ was freshly distilled over CaH₂ prior to use. Stock solutions of 22(R)- and 22(S)-hydroxycholesterol (1 mg/ 110 μ l), BODIPY[®] FL C12 (1 mg/ 40 μ l), 4-pyrrolidinopyridine (PPY, **2**) (1 mg/ 10 μ l) and 1-(3-dimethylaminopropyl)-3-ethylcarbodiimide (EDC) (10 μ l/ 50 μ l (v/v)) were prepared with distilled CH₂Cl₂. The stock solutions containing all reactants (see above) were combined in the reaction vessel (GC-vial). The BODIPY[®] FL C12 (1.00 equiv, 2.48 μ mol) followed by PPY (1.60 equiv, 3.97 μ mol), EDC (2.00 equiv, 4.97 μ mol) and 22-hydroxycholesterol (1.00 equiv, 2.48 μ mol) were added under inert gas atmosphere with a Hamilton syringe (25 μ l). After wrapping the microreactor and the enclosed GC-vial with parafilm the reaction was stirred at room temperature for 4 - 6 days. The solvent was then evaporated and the residue redissolved in 100 μ l CH₂Cl₂. The mixture was purified by chromatography on a SiO₂-cartridge and eluted with a *n*-hexane / diethylether gradient.

Description of the Microreactor

The micro reactor consists of an outer and an inner part. The outer part is a 120 mm long glass tube with NS29 joint and a diameter of 30 mm that narrows after 70 mm to a diameter of 15 mm. On the bottom of the narrowed part a screw thread is attached that fits for a GL18 cap. On the upper part of the glass tube after 50 mm (from the top) a valve is attached in order to connect to a vacuum and/or inert gas Schlenk-line. The inner part consists of a commercially available GC-vial (32x11.6 mm) with a screw cap (8 mm) and a septum. It is placed in the centre of the narrowed part of the glass tube above the GL18 screw and contains a micro stir bar. The whole micro reactor can be sealed with a NS29 rubber septum and wrapped with parafilm to avoid intrusion of air and moisture.

The glassware of the micro reactor (disassembled) is dried for at least 16 h in an oven (120 °C). After that the micro reactor is assembled quickly while still hot: the GL18 cap is screwed onto the bottom of the glass tube and the GC-vial (without cap but containing a micro stir bar) is inserted in the lower part of the glass-tube. The glass tube is then sealed with a NS29 rubber septum and the valve is connected to a Schlenk-line. After flame drying and

nitrogen purge of the whole micro reactor, the rubber septum is removed while keeping the nitrogen stream flowing. Now the cap of the GC-vial is screwed with tweezers. After closing the reactor with the NS29 septum again, the same procedure (flame drying and nitrogen purge) is repeated. After that the reactor can be used for reactions of 0.5 to 1 mg under inert gas atmosphere. The components are inserted in form of stock solutions with Hamilton syringes and long iron needles by piercing through both septums. After the addition has been finished, the rubber septum is removed again and the GC-vial is wrapped in parafilm, placed in the narrowed glass tube cavity again and the glass tube is sealed with the rubber septum and evacuated again. Finally the micro reactor is flushed with nitrogen, wrapped in parafilm and placed above a stirrer.

Product analysis

The products were identified by NMR spectroscopy using a Varian 600 MHz spectrometer.

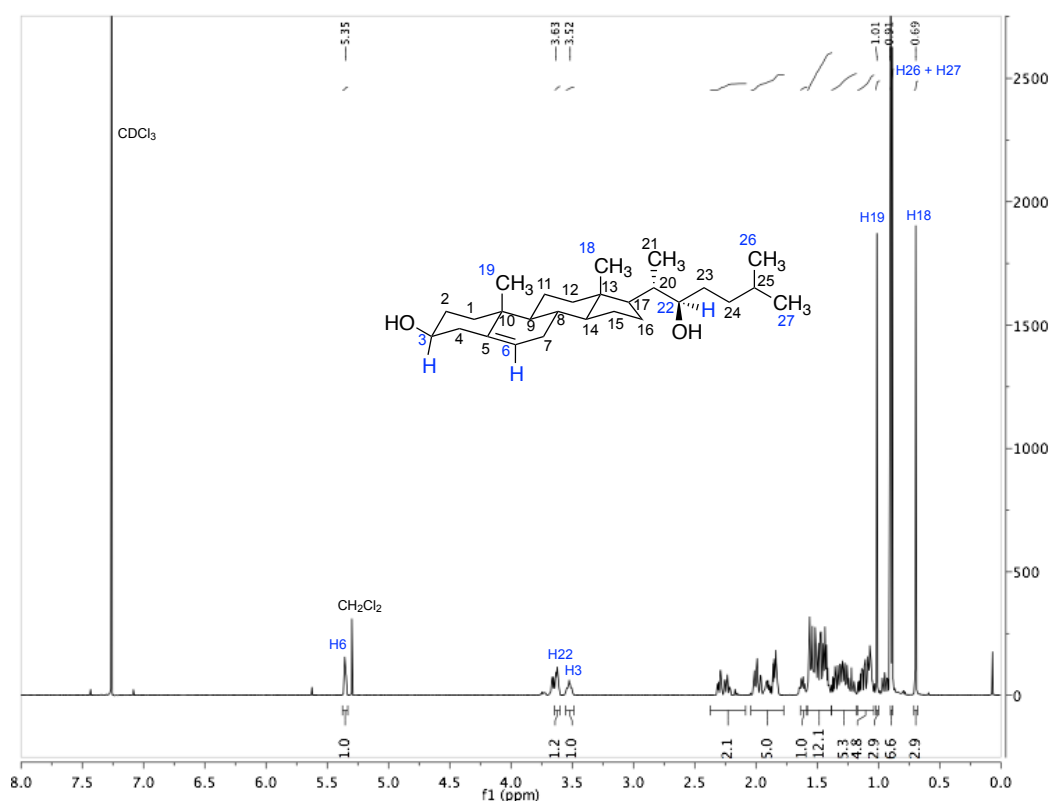


Figure 9.7. 600 MHz ¹H NMR spectrum of starting material 22(*R*)-OHC.

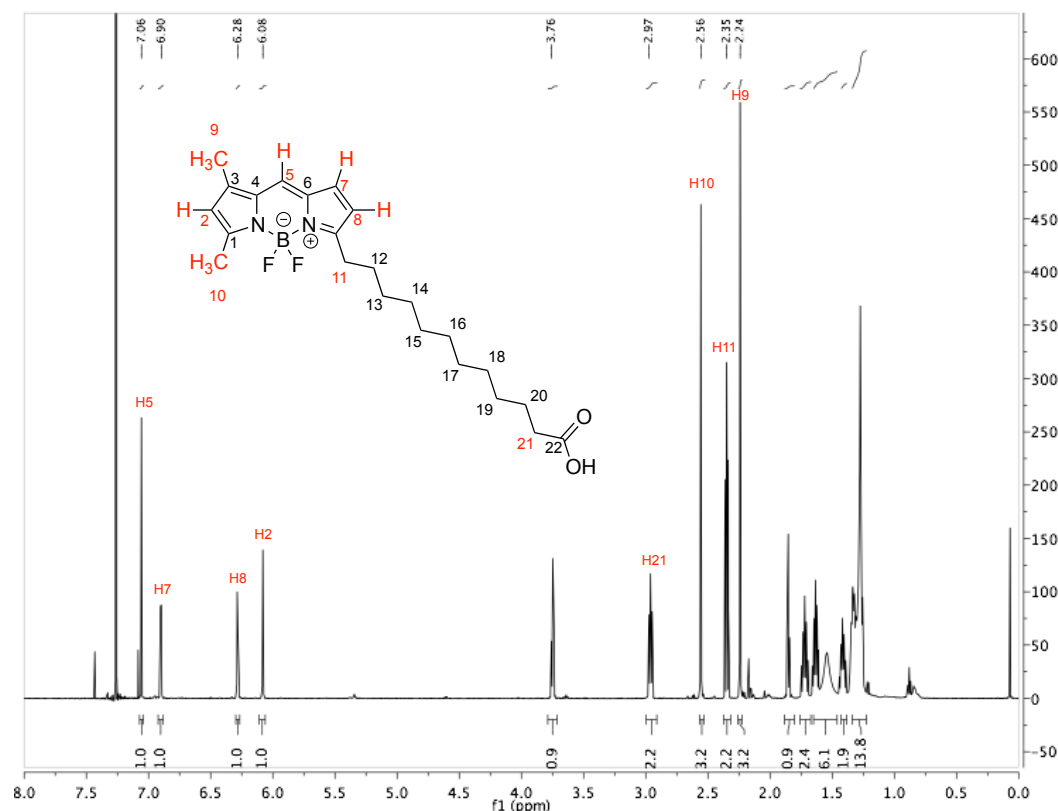


Figure 9.8. 600 MHz ^1H NMR spectrum of starting material BODIPY.

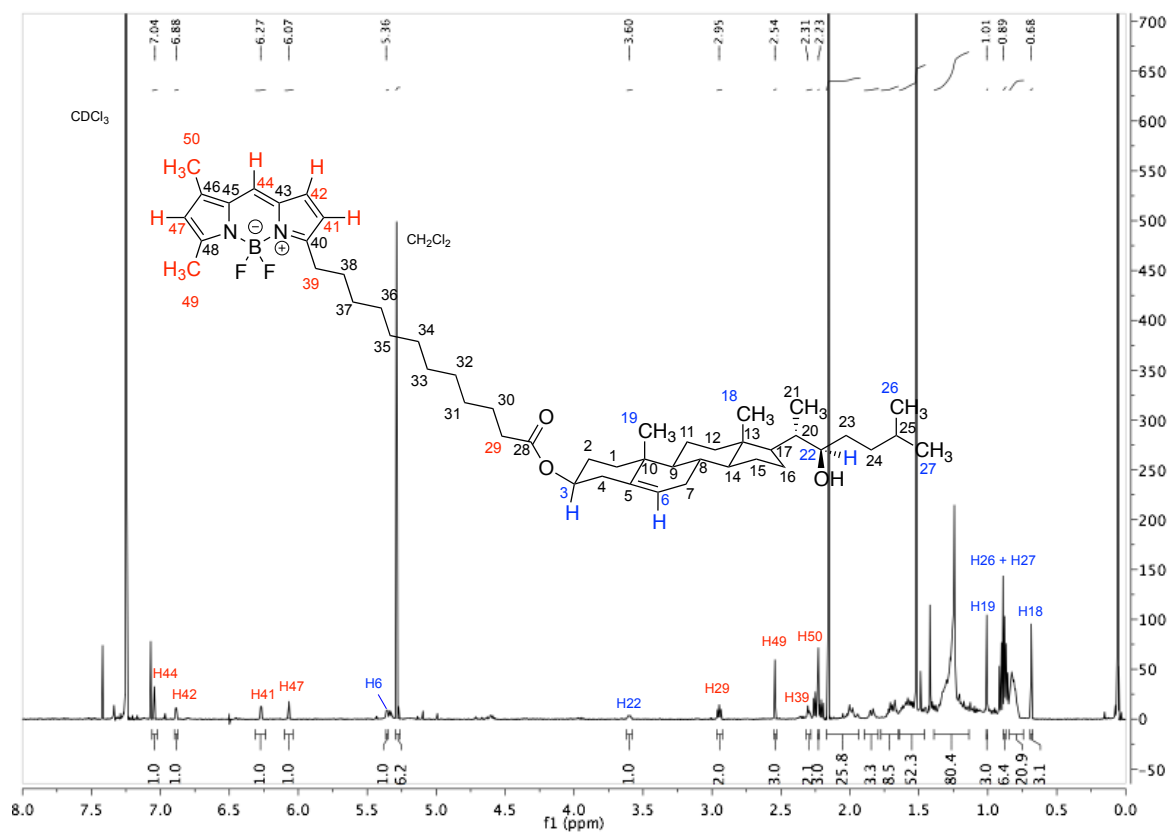
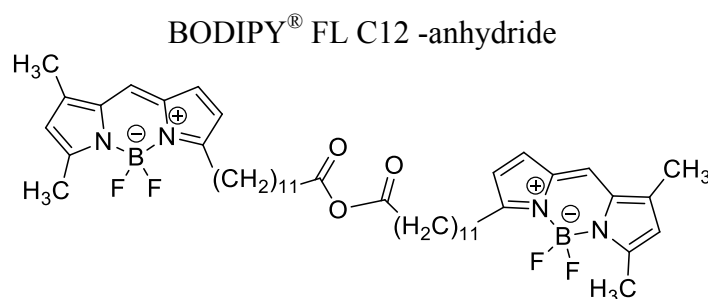


Figure 9.9. 600 MHz ^1H NMR spectrum of product BODIPY-22(*R*)-OHC.

The characteristic protons of the starting material 22(R)-hydroxycholesterol (blue) and that of the BODIPY[®] FL C12 (red) were aligned and both sets of signals were found in the obtained product in the right intensity relation. A proof for the regioselective acylation at the hydroxyl group in 3 position in the cholesterol moiety is that the product still contains the H22 signal whereas the signal of the H3 proton broadened up and is thus not easy to align.

Characterisation of Byproducts

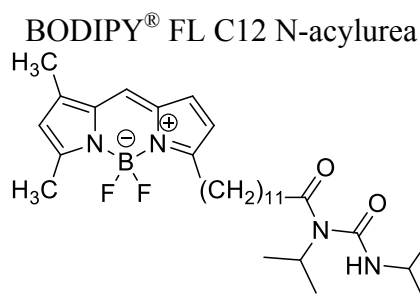
The side products of the esterification reaction were isolated and analysed by NMR and MS-ESI/HRMS spectroscopy using a Thermo Finnigan LTQ FT instrument.



This byproduct was isolated from the reaction of (S)-OHC and BODIPY[®] FL C12 according to the general procedure in chloroform. The chloroform was in that case not distilled, but used as purchased.

HRMS (ESI): $[M+Na^++Et_2O]^+$ calc. for $C_{50}H_{74}B_2F_4N_4NaO_4^+$: requires 915.5725, found: 915.5739.

MS (ESI): m/e 915 ($M+Na^++Et_2O$), 910, 764, 469, 464, 427, 425, 399.



This byproduct was isolated from the reaction of Sitosterol and BODIPY[®] FL C12 according to the general procedure with the use of DIC instead of EDC.

HRMS (ESI): $[M-H]^-$ calc. for $C_{30}H_{46}BF_2N_4O_2^-$: requires 543.3687, found: 543.3688.

MS (ESI): m/e 543 ($M-H$)⁻, 542, 458, 339, 288, 285.

9.6 References

- [1] P. J. Willy, K. Umesono, E. S. Ong, R. M. Evans, R. A. Heyman, D. J. Mangelsdorf, *Genes Dev.* **1995**, *9*, 1033–1045.
- [2] B. A. Janowski, P. J. Willy, T. R. Devi, J. R. Falck, D. J. Mangelsdorf, *Nature* **1996**, *383*, 728–731.
- [3] C. Fiévet, B. Staels, *Biochem. Pharmacol.* **2009**, *77*, 1316–1327.
- [4] S. J. Bensinger, P. Tontonoz, *Nature* **2008**, *454*–477.
- [5] T. Jakobsson, T. Treuter, J. A. Gustafsson, K. R. Steffensen, *Trends Pharmacol. Sci.* **2012**, *33*, 394–404.
- [6] M. Spyridon, L. A. Moraes, C. I. Jones, T. Sage, P. Sasikumar, G. Bucci, J. M. Gibbins, *Blood* **2012**, *117*, 5751–5761.
- [7] B. Neises, W. Steglich, *Angew. Chem. Int. Ed. Engl.* **1978**, *17*, 522–524.
- [8] J. Asselin, J. M. Gibbins, M. Achison, Y. H. Lee, L. F. Morton, R. W. Farndale, M. J. Barnes, S. P. Watson, *Blood* **1997**, *89*, 1235–1242.
- [9] K. Prufer, L. Boudreaux, *J. Cell Biochem.* **2007**, *100*, 60–85.
- [10] T. A. Spencer, D. Li, J. S. Russel, J. L. Collins, R. K. Bledsoe, T. G. Consler, L. B. Moore, C. M. Galardi, D. D. McKee, J. T. Moore, M. A. Watson MA, D. J. Parks, M. H. Lambert, T. M. Willson, *J. Med. Chem.* **2001**, *44*, 886–897.
- [11] W. J. Griffiths, P. J. Crick, Y. Wang, M. Ogundare, K. Tuschl, A. A. Morris, B. W. Bigger, P. T. Clayton, Y. Wang, *Free Rad. Biol. Med.* **2012**, asap.
- [12] K. L. H. Carpenter, S. E. Taylor, J. A. Ballantine, B. Fussel, B. Halliwell, M. J. Mitchinson, *Biochim. Biophys. Acta* **1993**, *1167*, 121–130.
- [13] I. Bjorkhem, O. Andersson, U. Diczfalussy, B. Sevastik, R. J. Xiu, C. Duan, E. Lund, *Proc. Natl. Acad. Sci.* **1994**, *91*, 8592–8596.
- [14] T. Claudel, M. D. Leibowitz, C. Fievet, A. Tailleux, B. Wagner, J. J. Repa, G. Torpier, J. M. Lobaccaro, J. R. Paterniti, D. J. Mangelsdorf, R. A. Heyman, J. Auwerx, *Proc. Natl. Acad. Sci.* **2001**, *98*, 2610–2615.
- [15] S. B. Joseph, E. McKilligin, L. Pei, M. A. Watson, A. R. Collins, B. A. Lafitte, M. Chen, G. Noh, J. Goodman, J. N. Hagger, J. Tran, T. K. Tippin, X. Wang, A. J. Lusis, W. A. Hsueh, R. E. Law, J. L. Collins, T. M. Willson, P. Tontonoz, *Proc. Natl. Acad. Sci.* **2002**, *99*, 7604–7609.
- [16] N. P. Hessvik, S. S. Bakke, R. Smith, A. W. Ravna, I. Sylte, A. C. Rustan, G. H. Thoresen, E. T. Kase, *J. Steroid Biochem. Mol. Biol.* **2012**, *128*, 154–164.
- [17] C. L. Bisgaier, L. L. Minton, A. D. Essenburg, A. White, R. Homan, *J. Lipid Res.* **1993**, *34*, 1625–1634.

- [18] R. Alford, H. M. Simpson, J. Duberman, G. C. Hill, M. Ogawa, C. Regino, H. Kobayashi, *Molecular Imaging* **2009**, 8, 341–354.
- [19] Y. Watanabe, T. Tanak, Y. Uchiyama, T. Takeno, A. Izum, H. Yamashita, J. Kumakura, H. Iwanari, J. Shu-Ying, M. Naito, D. J. Mangelsdorf, T. Hamakubo, T. Kodama, *Nuclear Receptor*, **2003**, 1, 1–7.
- [20] R. Brauner R, C. Johannes, F. Ploessl, F. Bracher, R. L. Lorenz, *J. Nutr.* **2012** 142, 981–989.
- [21] E. Viennois, K. Mouzat, J. Dufour, L. Morel, J. M. Lobaccaro, S. Baron, *Mol. Cell Endocrinol.* **2012**, 351, 129–141.

Chapter 10

Synthetic Studies Towards Derivatives of 9-Azajulolidine

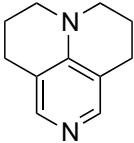
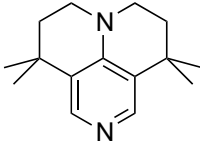
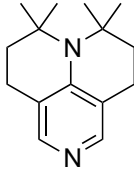
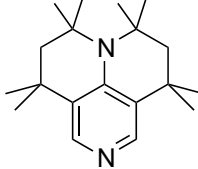
10.1 Introduction

Computational chemistry has always been a powerful tool for screening potential catalysts. The energetically most favored candidates could be synthesized and a trial and error approach can be avoided. Since 9-azajulolidine (**3**) is one of the most active catalysts in acylation reactions, structurally related compounds should be promising candidates. 9-Azajulolidine (**3**) bears no functional groups and synthetic transformations of **3** itself are therefore challenging.

10.2 Results and Discussion

For the search of more powerful catalysts based on the tricyclic 9-azajulolidine (**3**) motif, previous calculations^[1] were performed on the B3LYP/6-311+G(d,p)//B3LYP/6-31G(d) (B3LYP) level of theory in which the tetramethylated derivative **3b** showed to be a promising candidate (see Table 10.1). Calculations at a higher level of theory (MP2(FC)/6-31+G(2d,p)//B98/6-31G(d)) in gas phase and with inclusion of solvent effects (with PCM/UAHF/RHF/6-31G(d) solvation energies for chloroform) are confirming the previous work and are summarized in Table 10.1.

Table 10.1. Acylation enthalpies for 9-azajulolidine (**3**) and derivatives (**3b–d**) at different levels of theory based on the isodesmic model introduced in Chapter 3.

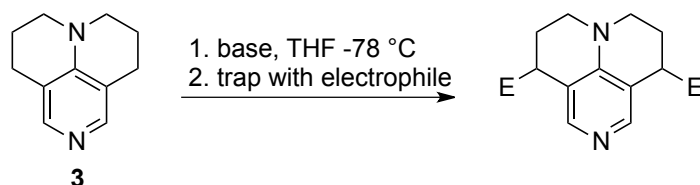
				
	3	3b	3c	3d
ΔH_{ac} (B3LYP) ^{[a][d]}	-108.9	-118.9		
ΔH_{ac} (MP2-5) ^[b]	-102.3	-113.0	-111.1	-112.6
ΔH_{ac} (MP2-5/solv) ^[c]	-82.3	-83.1	-82.4	-73.9

[a] B3LYP/6-311+G(d,p)//B3LYP/6-31G(d); [b] MP2(FC)/6-31+G(2d,p)//B98/6-31G(d); [c] MP2(FC)/6-31+G(2d,p)//B98/6-31G(d) with PCM/UAHF/RHF/6-31G(d) solvation energies for chloroform; [d] data from ref. [1, 2].

On the previously used B3LYP level of theory the energy differences between **3** and **3b** are quite large with 10 kJ/mol. The same results (11 kJ/mol) were observed for the more expensive method MP2-5 in gas phase. The inclusion of solvent effects change things dramatically and lead to an energy difference of only 1 kJ/mol between **3** and **3b**. By comparing derivatives **3b** and **3c** at MP2-5/solv level of theory it becomes clear that the positioning of the methyl groups in the carbocyclic framework is not important. The inductive effects are nearly the same and lead to an energy difference of 1 kJ/mol between these two compounds. Despite the fact that **3d** would be challenging to synthesize, the calculations

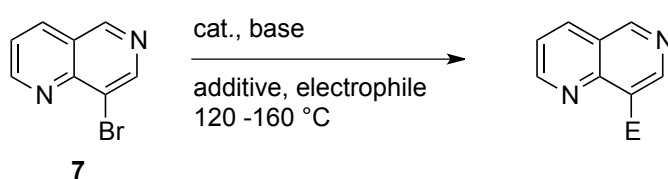
show that too many alkyl groups are unfavorable by 10 kJ/mol, which can be explained by solvation effects.

Held tried in 2007 already different synthetic methods to modify the 9-azajulolidine (**3**) core structure towards more potent alkylated derivatives of **3**. The following section briefly recapitulates what has been tested already. One of these approaches is based on experiments of Beak *et al.*^[3] to deprotonate **3** with strong bases like LDA, *n*-BuLi and *sec*-BuLi and trap the resulting species with an electrophile (Scheme 10.1). Among the tested electrophiles were ClSiEt₃, ClSiMe₃ and MeI. The desired product was not obtained in any of these attempts.



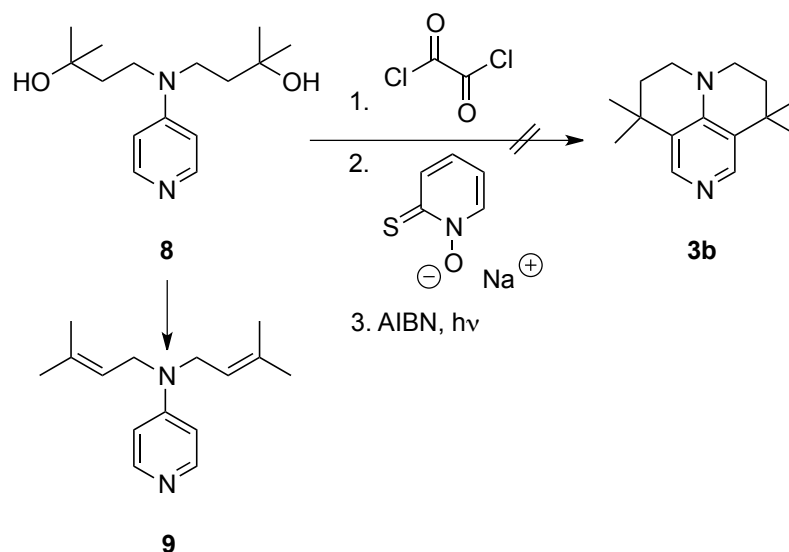
Scheme 10.1. Deprotonation of **3** and trapping with a nucleophile.

According to Yamanaka^[4] the keystone for the synthesis of **3** is the Heck coupling of **7** in order to build the tricyclic carbon framework. The basic idea was to modify the acceptor in the very same reaction in order to obtain structural diversity in the end product (Scheme 10.2). To this end different palladium-based catalysts were combined with variations in the base and solvent. The electrophile in most of these reactions was chosen to be ethyl crotonate. The only result which showed conversion (in low yield) to the desired product gave a mixture of regioisomers of the Heck coupling products using Pd₂(dba)₃, NEt₃ and Bu₄NBr in acetonitrile.



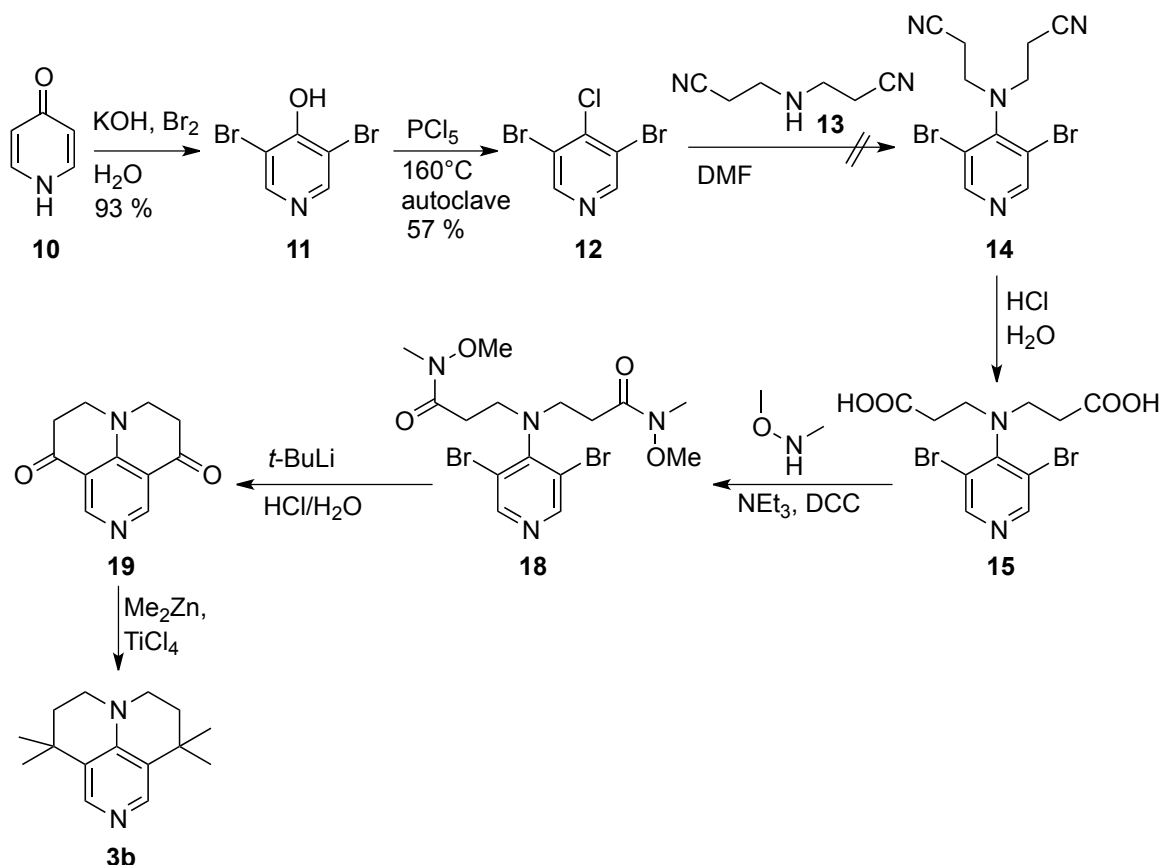
Scheme 10.2. Variations of the electrophile in the Heck coupling reaction.

The last approach of Held included a radical cyclisation of precursor **8** through an in-situ generated PTOC ester according to procedures of Newcomb *et al.*^[5] Instead of the desired product **3b** only elimination product **9** was found.



Scheme 10.3. PTOC ester mediated radical cyclization attempt of **8**.

Here we develop additional synthetic strategies towards the synthesis of **3b**. In the first route the key step is a nucleophilic aromatic substitution of **13** to trihalogenated **12** (Scheme 10.4). This strategy was already used by Spivey *et al.*^[6,7] to synthesize different chiral DMAP derivatives. Hydrolysis of the nitrile functionalities and formation of a Weinreb amide **18** are followed by the cyclization to **19**. Both Pearson^[8] and Selnick^[9a] made use of this strategy to build up complicated cyclic carbohydrates e.g. methyleneindanones. Recently Barriault *et al.*^[9b] showed in the synthesis of isofregenedol that the introduction of geminal methyl groups could be achieved by means of Me_2Zn and TiCl_4 . Using this procedure it would be possible to transform **19** in one single step into the desired **3b**.

Scheme 10.4. Suggested synthesis of **3b** via a S_NAr of **13** at **12**.

According to procedures known in the literature^[6] the first step proceeds smoothly in 93 % yield. For the second step quite harsh conditions in form of an autoclave and 160 °C have to be applied. **12** is obtained in 57 % yield. Indicated by GC-MS measurements a small amount of 3-bromo-4,5-dichloropyridine (regioisomer of **12**) is formed, which could not be separated by column chromatography nor by recrystallization. The mixture of **12** with its regioisomer was used to perform test reactions with dibutylamine according to procedures of Spivey *et al.*^[7] which resulted in 35 % yield. The use of **13** instead of dibutylamine with the same reaction conditions did not yield any product and a series of different reaction conditions was thus tested (Table 10.2, ordered by reaction vessel).

Table 10.2. Reaction conditions for the S_NAr of **12** and **13**.

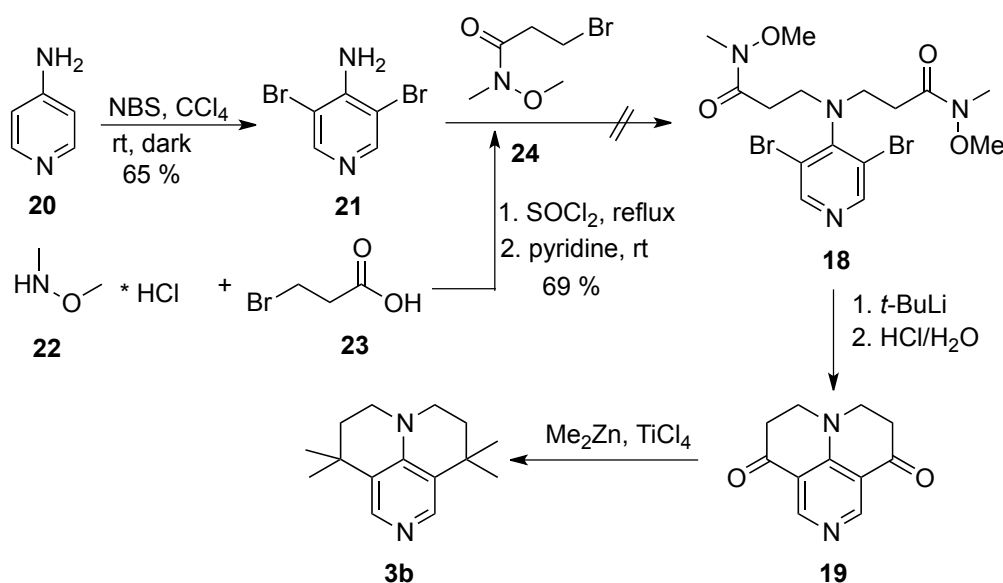
Entry	Reaction Vessel	Ratio 12 : 13	Time [h]	Temperature [°C]	Solvent	yield [%]
1	sealed tube	1 : 1.5	20	120	DMF	0
2	sealed tube	1 : 1.5	24	170	DMF	0
3	microwave	1 : 1.5	2	170	pyridine	0
4	microwave	1 : 1.5	2	200	-	0
5	microwave	1 : 3.1	4	170	DMF	0

Using a sealed tube after 20 hours at 120 °C only the starting material was recovered. Raising the temperature and reaction time to 170 °C and 24 hours no product was found, but a brown sticky substance that could not be further characterized. Using microwave technology we applied shorter reaction times, but all obtained products were almost not soluble in any solvent. All samples were hard to dissolve and showed polymeric character. Increasing the ratio of **12** to **13** (Table 10.2, entry 5) the substance could not be separated from the reaction vessel again. Using no solvent and 200 °C in the microwave also no desired product was obtained and most of the sample was decomposed to unidentified substances.

Since too many problems arose with the nitrile groups present in the molecule, we figured out another strategy to obtain compound **18**. The basic idea was to form the Weinreb-amide **18** through a S_N2 reaction of 3,5-dibromopyridin-4-amine (**21**) with **24** (Scheme 10.5). Investigations of Garcia-Ruan^[10] showed that the bromination of 4-aminopyridine (**20**) in 3 and 5 position is achieved best by using NBS in tetrachloromethane. In fact **21** was obtained without byproducts (other regioisomers) in moderate yields (65 %). In parallel **24** was synthesized from **22** and **23** in 69 % yield.^[11] The S_N2 reaction of **21** and **24** did not lead to the desired product under several conditions (Table 10.3). The use of a borane protection group on **21** did not succeed as well, maybe due to the elevated temperatures applied.

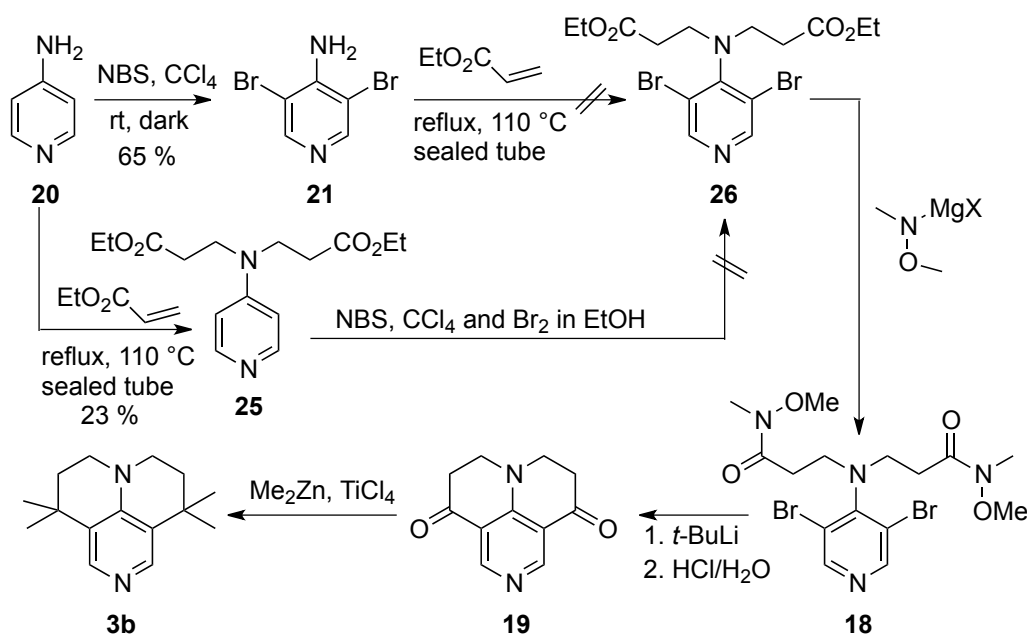
Table 10.3. Reaction conditions for the S_N2 reaction of **21** and **24**.

Base	Solvent	Temperature [°C]	Time [h]	Yield [%]
K ₂ CO ₃	CH ₃ CN	80	6	0
NaOMe	CH ₃ OH	65	23	0
NaH	THF	66	25	0



Scheme 10.5. Suggested synthesis of **3b** via Weinreb amide **18** through a S_N2 reaction of 3,5-dibromopyridin-4-amine (**21**) with **24**.

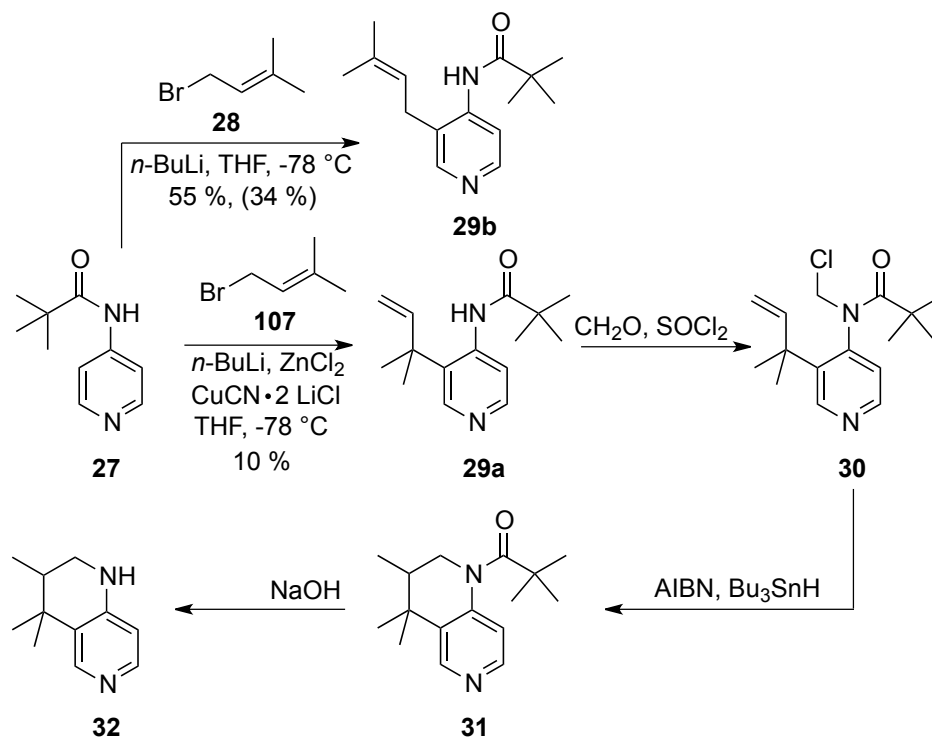
In the last approach a Michael addition of the 4-amino group of **21** to ethyl acrylate should give access to **26**, which could be easily transformed to **18**. Unfortunately, the steric hindrance present in **21** makes a Michael addition to ethyl acrylate impossible under different conditions. Performing the 1,4 addition with ethyl acrylate before the bromination, using 4-aminopyridine (**20**), the reaction was accomplished in 23 % yield. But the subsequent bromination of **25** afforded only a mono-bromination (**26a**) in 38 % yield (see Experimental Part). Using NBS in different solvents or longer reaction times, as well as bromine in ethanol did not achieve dibrominated substance **26**. The subsequent bromination of **26a** was as well not successful.



Scheme 10.6. Proposed synthesis of **3b** via Weinreb amide **18** through a Michael addition of ethyl acrylate to **21**.

Since the previous transformations all had in common that the geminal dimethyl groups are introduced in the end, a strategy was developed in which they were incorporated at the beginning of the reaction sequence. To this end **28** was meant to react with **27** in a S_N2' reaction (Scheme 10.7). The 4-aminogroup in **27** was protected by a pivaloyl group, which had the nice side effect to promote the directed ortho-metallation and thus ensuring the right center to react. Using *n*-BuLi as base for the deprotonation in THF, only product from a standard S_N2 reaction (**29b**) was obtained in 55 % yield (see Scheme 10.6). The transmetallation of lithium to zinc and subsequently to the less electropositive copper makes the resulting C-Cu bond less polarized and thus more selective. According to the accepted mechanism the reactive species is **27a** (Figure 10.1).^[12,13] Utilizing this strategy a product mixture of **29b** (34 %) and **29a** (10 %) was found, which could be separated by column chromatography. Using a borane protecting group on **27** a product mixture from **29a** and **29b** was found as well (TLC, GC-MS), which was not further purified due to the low overall yield of 24 %. The low yield comes presumably from additional protection/deprotection steps. In

consequence of the low yield and the fact that the product was obtained as a mixture of regioisomers we did not pursue this idea any further.



Scheme 10.7. $\text{S}_{\text{N}}2'$ reaction of 28 to 27 via transmetalation to Cu and subsequent radical cyclization of 30.

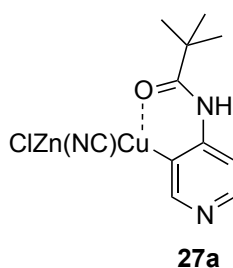
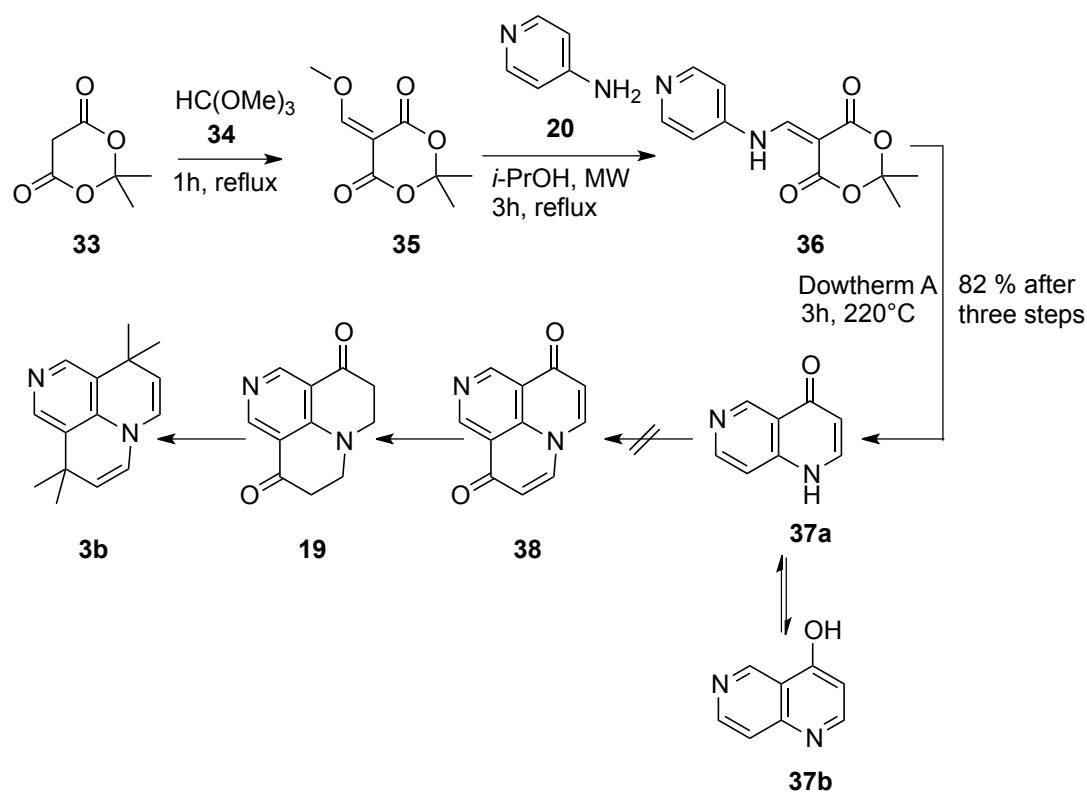


Figure 10.1. Functionalized copper reagent after transmetalation from Li to Zn to Cu.

The most promising synthetic approach until now was the use of a Meldrum's acid derivative to achieve the desired cyclisation (see Scheme 10.8). Starting from Meldrum's acid (33) the first two steps could be achieved within four hours (conventional heating) or 65 minutes (heating by microwave) and are easily conducted in a one pot reaction. If the second step (transformation of 35 to 36) was conducted in a microwave reactor the reaction time was dramatically decreased to 5 min with no detriment of yield. The product 36 is obtained as white solid and the only purification needed is filtration and washing with *i*-PrOH. The following thermochemically driven cyclization of 36 was conducted in the heat transferring solvent DowthermTM A. DowthermTM A consists of an eutectic mixture of biphenyl and

diphenyl oxide. Attempts to perform the reaction in the microwave were unsuccessful, most likely due to the lack of a dipole moment in the solvent (DowthermTM A) which is necessary for microwave-mediated heating. Carrying out the cyclization in a conventional oil bath the reactions proceeded smoothly and the cyclized product **37** was obtained in 82 % after three steps. A subsequent second addition of Meldrum's acid derivative **35** to **37** was not possible under different conditions. This could, maybe in part, be based on the pyridone (**37**) hydroxypyridine (**37a**) tautomerization (Scheme 10.8). To prevent the tautomerization different reducing agents like e.g. palladium on charcoal or zinc or iron in acetic acid were tested on **37** but none of them gave the desired product. The starting material was too stable and thus always recovered. Other transformations like deprotonation with a strong base and trapping with an electrophile like benzoylchloride did not succeed as well and in these cases starting material was recovered as well.



Scheme 10.8. Prospected synthesis of **3b** using Meldrum's acid derivative **35** for cyclization.

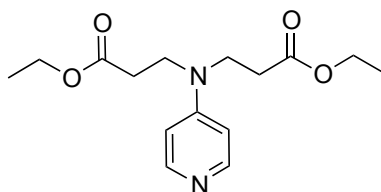
10.3 Conclusion

Since all of these synthetic studies failed at some stage it has to be concluded that the synthesis of derivatives of **3** is very challenging. Speaking with some experience about this compound class now, future synthesis strategies should aim at building up the carbocyclic framework first and the pyridine ring in the end. The pyridine nitrogen in aminopyridines acts as a strong base and a strong ligand, even if it is not supposed to. As a consequence most of the reactions on aminopyridines with transition metals or Lewis acids did not work well for this reason. In order to prevent the pyridine nitrogen from reacting, future efforts could use protecting groups like boranes as synthetic intermediates, which were already used herein and shown to have synthetic application.^[15] Unfortunately that adds additional steps for protection and deprotection reactions.

10.4 Experimental Part

Compounds **11** and **12** were prepared according to literature known procedures from Spivey^[7b]. Compounds **21** and **24** were synthesized by procedures of Garcia-Ruan^[10] and Aidhen^[11].

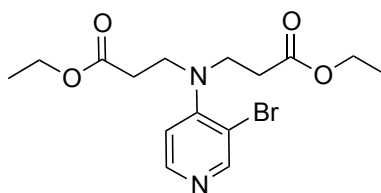
4-*N,N*-Diethylpropionateaminopyridine (**25**)



In a pressure tube 5.00 g (53.00 mmol) 4-aminopyridine (**20**) and 5 equivalents of freshly distilled ethyl acrylate (28.9 mL, 265.60 mmol) were heated for 4 days at 110 °C. After evaporation of excess ethyl acrylate the crude mixture was purified by column chromatography on silica (ETOAc/IH 1:4). The product **25** was obtained as brown oily substance in 23 % (3.64 g) yield.

¹H NMR (200 MHz, CDCl₃): δ = 8.12 (dd, ³*J* = 5.0 Hz, ³*J* = 1.6 Hz, 2H, CH_{Ar}), 6.40 (dd, ³*J* = 5.0 Hz, ³*J* = 1.6 Hz, 2H, CH_{Ar}), 4.03 (q, ³*J* = 7.1 Hz, 4H), 3.75 – 3.13 (m, 4H), 2.88 – 2.07 (m, 4H), 1.11 (dt, ³*J* = 12.7 Hz, ³*J* = 7.1 Hz, 6H, CH₃).

GC-MS (EI): RT 11.08 min, *m/z* (%) = 294 (M⁺), 249, 207, 193, 165, 107.

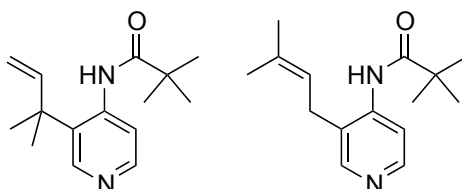
3-Bromo-4-*N,N*-diethylpropionateaminopyridine (**26a**)

To a solution of **25** (0.50 g, 1.69 mmol) in CCl_4 was added NBS (0.70 g, 3.91 mmol) in portions in the dark. The resulting mixture was stirred at room temperature over night. After evaporation of solvent the crude mixture was purified via column chromatography using silica (EtOAc/ NEt_3 20:1). The desired dibromination product **26** was not obtained, but **26a** in 38 % yield (0.24 g).

^1H NMR (300 MHz, CDCl_3): δ = 8.59 (s, 1H), 8.33 (d, 3J = 5.6 Hz, 1H), 6.90 (d, 3J = 5.6 Hz, 1H), 4.10 (q, 3J = 7.1 Hz, 4H), 3.64 (t, 3J = 7.1 Hz, 4H), 2.56 (t, 3J = 7.1 Hz, 4H), 1.22 (t, 3J = 7.1 Hz, 6H).

^{13}C NMR (75 MHz, CDCl_3): δ = 14.1, 29.6, 32.7, 47.4, 60.8, 116.4, 147.8, 153.1, 154.8, 171.5.

N-(3-(2-methylbut-3-en-2-yl)pyridin-4-yl)pivalamide (**29a**, left) and *N*-(3-(3-methylbut-2-en-1-yl)pyridin-4-yl)pivalamide (**29b**, right)



In a predried Schlenk flask 1.00 g (5.61 mmol) of **27** is dissolved in dry THF and cooled to -78°C . After addition of 2.2 eq. *n*-BuLi (4.93 mL, 12.3 mmol) the reaction mixture was stirred for 3 hours at -78°C . Subsequently 7.30 mL (7.30 mmol) of a 1 M solution of ZnCl_2 in THF were added and the solution stirred for 30 min. After the addition of $\text{CuCN}\cdot 2\text{LiCl}$ (1 M solution in THF, 4.93 mL, 4.93 mmol) the reaction was stirred for additional 30 min at -78°C . In the end the electrophile **28** was added (0.65 mL, 5.61 mmol) and the reaction mixture stirred over night at room temperature. After the addition of NH_4OH and NH_4Cl the reaction mixture was extracted three times with DCM and the combined organic layers dried over MgSO_4 . Column chromatography of the crude mixture on silica (EtOAc/ IH/NEt_3 20:15:1) gave 0.06 g (10 %) of **29a** and 0.22 g (34 %) of **29b**.

29a:

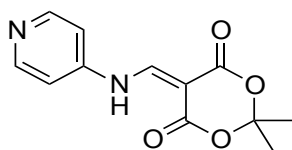
¹H NMR (200 MHz, CDCl₃) δ = 8.41 (d, ³*J* = 5.6 Hz, 1H), 8.33 (s, 1H), 8.23 (d, ³*J* = 5.6 Hz, 1H), 7.75 (s, 1H), 5.17 (s, 1H), 3.35 (d, ³*J* = 6.4 Hz, 2H), 1.85 – 1.67 (m, 6H), 1.26 (d, ³*J* = 0.6 Hz, 9H).

GC-MS (EI): RT 8.82 min, *m/z* (%) = 246 (M⁺), 231, 177, 161, 147, 132, 119, 57, 41.

29b:

¹H NMR (200 MHz, CDCl₃) δ = 8.77 – 8.30 (m, 2H), 8.11 (d, ³*J* = 35.7, 2H), 6.12 (dd, ³*J* = 17.7 Hz, ³*J* = 10.6 Hz, 1H), 5.24 (ddd, ³*J* = 18.5 Hz, ³*J* = 14.1 Hz, ³*J* = 0.9 Hz, 2H), 1.46 (s, 6H), 1.23 (d, ³*J* = 2.1 Hz, 9H).

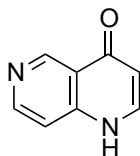
GC-MS (EI): RT 9.13 min, *m/z* (%) = 246 (M⁺), 190, 161, 147, 133, 119, 57.

2,2-Dimethyl-5-((pyridin-4-ylamino)methylene)-1,3-dioxane-4,6-dione (**36**)

To 5.00 g (34.7 mmol) Meldrum's acid **33** was added 50 mL (0.44 mol) trimethylorthoformate (**34**). The reaction mixture was heated at 125 °C oil bath temperature for one hour. After cooling to room temperature 3.26 g (34.7 mmol) 4-aminopyridine (**20**) was added together with 8 mL DMF and the reaction mixture was transferred to a microwave vial (80 mL). After refluxing the yellow solution for 5 minutes the white precipitate was filtered and washed with *i*-PrOH. The product **36** was obtained as a white solid in 90 % (7.73 g) yield.

¹H NMR (300 MHz, CDCl₃) δ = 11.65 – 10.54 (m, 1H, NH), 8.74 (s, 1H, CH_{Vinyl}), 8.71 – 8.59 (m, 2H, CH_{Ar}), 7.24 – 7.09 (m, 2H, CH_{Ar}), 1.79 (s, 6H, CH₃). (in line with literature data)^[14]

¹³C NMR (75 MHz, CDCl₃) δ = 27.2, 89.9, 105.7, 111.8, 143.9, 151.1, 151.8, 162.8, 165.2.

1,6-Naphthyridin-4(1H)-one (**37**)

In a 100 mL flask DowthermTM A (30 mL) was heated to 220 °C. The substrate **36** (0.46 mg, 1.85 mmol) was added in portions and the yellow solution is stirred at this temperature for 35 min. After cooling to room temperature isohexane was added and the precipitate filtered, washed with isohexane and dried. The product **37** was obtained as light brown solid in 91 % (0.23 g) yield.

Notice: this reaction should be conducted in high dilution ([0.06 M] DowthermTM A). The obtained product is soluble in DMSO and methanol but not in IH, EA, DCM.

¹H NMR (400 MHz, d₆-DMSO) δ = 12.07 – 11.77 (m, 1H), 9.15 (d, ³J = 0.8 Hz, 1H), 8.55 (d, ³J = 5.8 Hz, 1H), 7.94 (d, ³J = 7.6 Hz, 1H), 7.39 (dd, ³J = 5.9 Hz, ³J = 0.8 Hz, 1H), 6.13 (d, ³J = 7.6 Hz, 1H).

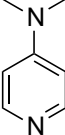
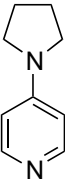
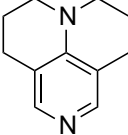
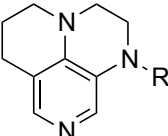
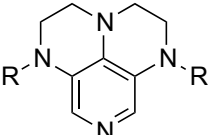
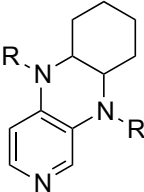
¹³C NMR (125 MHz, d₆-DMSO) δ = 112.5, 112.6, 121.4, 141.5, 145.4, 149.4, 150.2, 177.6.

10.5 References

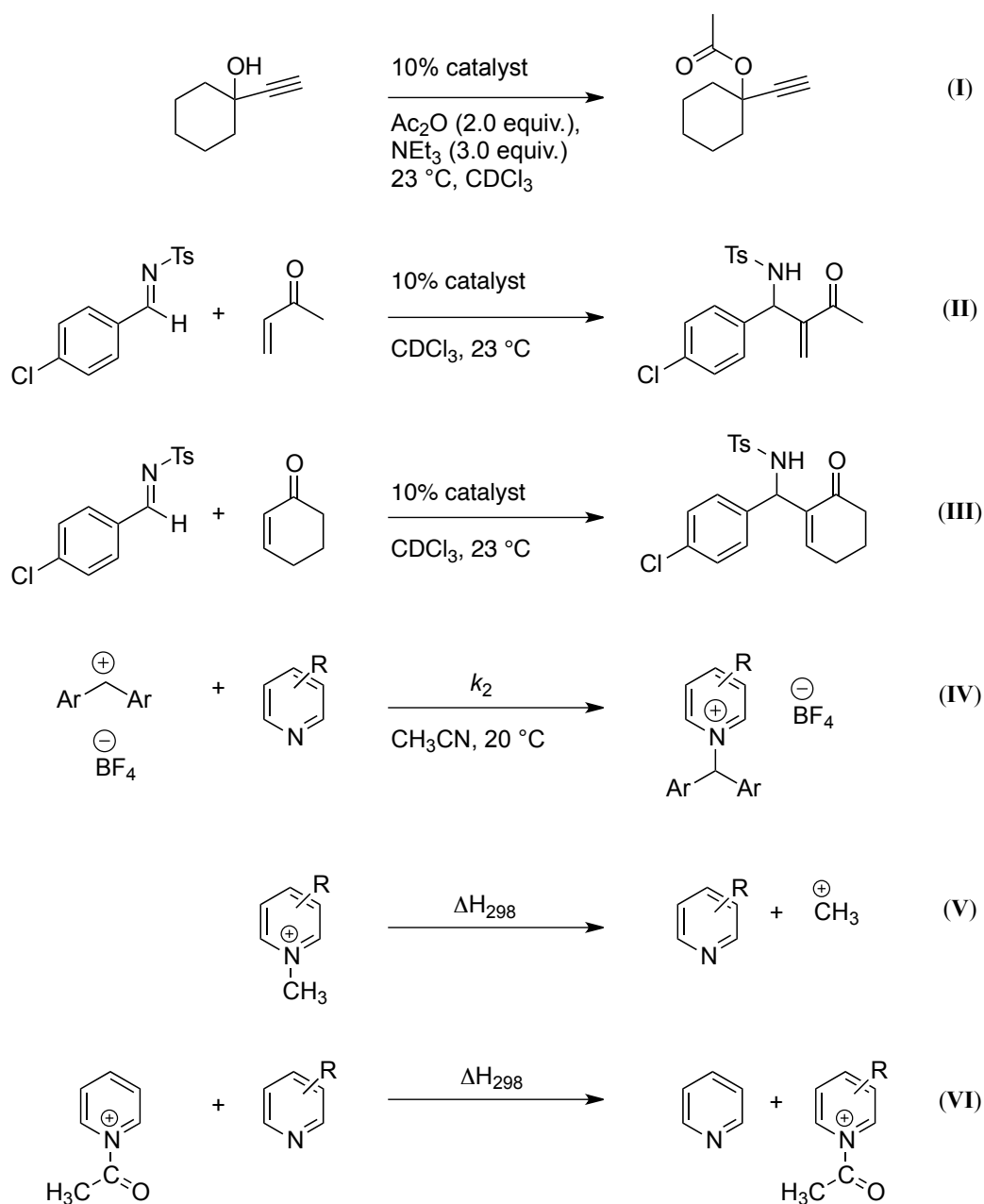
- [1] I. Held, *Dissertation*, Ludwig-Maximilians-Universität München, **2007**.
- [2] E. Larionov, F. Achraimer, J. Humin, H. Zipse, *ChemCatChem* **2012**, 4, 559 – 566.
- [3] P. Beak, W. J. Zajdel, D. B. Reitz, *Chem. Rev.* **1984**, 84, 471.
- [4] T. Sakamoto, N. Miura, Y. Kondo und H. Yamanaka, *Chem. Pharm. Bull.* **1986**, 5, 2018.
- [5] a) P. A. Simakov, F. N. Martinez, J. H. Horner, M. Newcomb, *J. Org. Chem.* **1998**, 63, 226. b) D. H. R. Barton, D. Crich, *J. Chem. Soc. Perkin Trans. I*, **1986**, 1603. c) B. Giese, J. Hartung, *Chem. Ber.* **1992**, 125, 1777.
- [6] A. C. Spivey, F. Zhu, M. B. Mitchell, S. G. Davey, R. L. Jarvest, *J. Org. Chem.* **2003**, 68, 7379-7385.
- [7] A. C. Spivey, D. P. Leese, F. Zhu, S. G. Davey, R. L. Jarvest, *Tetrahedron* **2004**, 60, 4513 –4525. b) A. C. Spivey, T. Fekner, S. E. Spey, *J. Org. Chem.* **2000**, 65, 3154 – 3159.
- [8] N. D. Pearson, N. J. P. Broom, P. J. O'Hanion, *Tet. Lett.* **1994**, 35, 3771 – 3774.

- [9] a) H. G. Selnick, E. M. Radzilowski, G. S. Ponticello, *Tet. Lett.* **1991**, 32, 721 – 724.
b) M. Riou, L. Barriault, *J. Org. Chem.* **2008**, 73, 7436 – 7439.
- [10] V. Canibano, J. F. Rodriguez, M. Santos, M. A. Sanz-Tejedor, M. C. Carreno, G. Gonzalez, J. L. Garcia-Ruano, *Synthesis* **2001**, 14, 2175 – 2179.
- [11] V. Selvamurugan, I. S. Aidhen, *Synthesis* **2001**, 15, 2239 – 2246.
- [12] a) P. Knochel, M. C. P. Yeh, S. C. Berk, J. Talbert, *J. Org. Chem.* **1984**, 53, 2390; b) S.C. Berk, P. Knochel, M. C. P. Yeh. *J. Org. Chem.* **1988**, 53, 5789; c) T.N. Majid, P. Knochel, *Tetrahedron Lett.* **1990**, 31, 4413.
- [13] D. Leonori, I. Coldham, *Adv. Synth. Catal.* **2009**, 351, 2619 – 2623.
- [14] N. A. Al-Awadi, I. Abdelhamid, A. Abdelshafy, A. M. Al-Etaibi, M. H. Elnagdi, *Synlett* **2007**, 16, 2205 – 2208.
- [15] V. D'Elia, Y. Liu, H. Zipse, *Eur. J. Org. Chem.* **2011**, 8, 1527 – 1533.

Kinetic and thermodynamic data of the most important pyridine based organocatalysts.

Catalyst	Nr.	$t_{1/2}^{[a]}$ [min]	$t_{1/2}^{[b]}$ [min]	$t_{1/2}^{[c]}$ [min]	$N (S_N)^{[d]}$	MCA ^[e]	ΔH_{ac} MP2-5 ^[f] [kJ/mol]	$\Delta H_{ac/solv}$ MP2-5/solv ^[g] [kJ/mol]
	1	151.0 ^[h]	475	nd ^[k]	15.51 (0.62) ^[m]	581.2	-77.1	-61.2
	2	67.0 ^[h]	146	nd ^[l]	14.99 (0.68)	590.1	-87.5	-67.6
	3	14.7 ^[i]	20	242	15.60 (0.68)	602.7	-102.3	-82.2
	4							
R = Me	4a	17.9				611.0	-111.0	-86.8
R = Et	4b	13.8				613.3	-113.5	-87.5
R = CH ₂ Ph	4c	34.3	33.7	338		620.8	-123.4	-90.2
	5							
R = Me	5a	38.0	32	456	16.65 (0.58) ^[n]	618.7	-118.0	-89.2
R = Et	5b	44.2	26	581	16.81 (0.60) ^[n]	621.6	-120.6	-87.8
R = CH ₂ Ph	5c	65.4	72	758	17.69 (0.57) ^[n]	636.8	-141.3	-98.3
R = CH ₂ Ph-4-NMe ₂	5d	38.4				661.3	-163.7	-106.7
R = CH ₂ Ph-3,5-CF ₃	5e	227.3	356			596.8	-101.5	-69.5
	6							
R = Me	6a	21.3				609.1	-108.2	-79.4
R = Et	6b	18.0 ^[h]	23	264	16.65 (0.64)	616.0	-118.2	-85.2
R = CH ₂ Ph	6c	94.0 ^[j]					-124.1	-81.4

[a] Kinetic half-life times for acylation reaction (**I**); [b] Kinetic half-life times for aza-MBH reaction (**II**); [c] Kinetic half-life times for aza-MBH reaction (**III**); [d] Nucleophilicity parameters in acetonitrile according to equation (**IV**); [e] Methyl cation affinity according to equation (**V**); [f] "MP2-5": MP2/6-31+G(2d,p)//B98/6-31G(d) according to equation (**VI**); [g] "MP2-5/solv": MP2/6-31+G(2d,p)//B98/6-31G(d) with PCM/UAHF/RHF/6-31G(d) solvation energies for chloroform according to equation (**VI**); [h] Data from ref.^[1]; [i] Remeasured and in line with published data (15 ± 0.1)^[1]; [j] The obtained data for the resynthesized catalyst are not in line with the published ones (116 ± 2.0)^[2]; [k] 36 % conversion after 40 h; [l] 43 % conversion after 40 h; [m] Data from ref.^[3], $N (S_N)=14.95 (0.67)$ published in ref.^[4]; [n] Data from ref.^[5].



-
- [1] I. Held, E. Larionov, C. Bozler, F. Wagner, H. Zipse, *Synthesis* **2009**, 2267–277.
- [2] E. Larionov, F. Achraimer, J. Humin, H. Zipse, *ChemCatChem* **2012**, 4, 559–566.
- [3] T. A. Nigst, J. Ammer, H. Mayr, *J. Phys. Chem. A* **2012**, 116, 8494–8499.
- [4] F. Brotzel, B. Kempf, T. Singer, H. Zipse, H. Mayr, *Chem. Eur. J.* **2007**, 13, 336–345.
- [5] N. De Rycke, G. Berionni, F. Couty, H. Mayr, R. Goumont, O. R. P. David, *Org. Lett.* **2011**, 13, 530–533.